

THE JOURNAL OF
PHYSICAL
CHEMISTRY

Volume 70

SEPTEMBER—DECEMBER 1966

PAGES 2709—4140

FREDERICK T. WALL, *Editor*

MARILYN H. PERRIN AND ROBERT G. LINCK, *Assistant Editors*

EDITORIAL BOARD

L. F. DAHL
B. P. DAILEY
F. S. DAINTON
J. R. FRESCO
G. J. HILLS
C. J. HOCHANADEL
C. KEMBALL

W. KLEMPERER
A. KUPPERMAN
F. A. LONG
J. L. MARGRAVE
J. P. McCULLOUGH
W. J. MOORE
W. A. NOYES, JR.

R. G. PARR
G. PORTER
B. S. RABINOVITCH
W. G. SCHNEIDER
S. I. WEISSMAN
W. WEST
B. ZIMM

CHARLES R. BERTSCH, *Senior Production Editor*

RICHARD H. BELKNAP
Assistant Director of Publications
Director of Research Journals

RICHARD L. KENYON
Director of Publications

JOSEPH H. KUNEY
Director of Business Operations
Director of Publications Research

EASTON, PA.
MACK PRINTING COMPANY
1966

THE JOURNAL OF
PHYSICAL CHEMISTRY

Volume 70, Number 9 September 1966

Energy Distribution of Photochemically Generated <i>t</i> -Pentoxy Radicals	Dennis Durant and G. R. McMillan	2709
The Steady-State Compliance of Dilute Polymer Solutions	Larry A. Holmes, Kazuhiko Ninomiya, and John D. Ferry	2714
The Infrared Absorption Spectrum of Oxygen-18-Labeled Glycine	I. Laulich, S. Pinchas, D. Samuel, and I. Wasserman	2719
The Association of Cadmium Ion and Bromide Ion in Molten Potassium Nitrate and in Molten Sodium Nitrate	Helen Braunstein, Jerry Braunstein, and Douglas Inman	2726
Polarographic and Potentiometric Evaluation of Association Constants in Low-Temperature Aqueous Melts	Jerry Braunstein, Alba Rosa Alvarez-Funes, and Helen Braunstein	2734
Infrared Study of the Nature of the Hydroxyl Groups on the Surface of Porous Glass	M. J. D. Low and N. Ramasubramanian	2740
Transport Numbers of Concentrated Sodium Chloride Solutions at 25°	L. J. M. Smits and E. M. Duyvis	2747
Coupling Constant and Chemical Shift of Tetrafluoroborate Ion in Mixed Solvents	R. Haque and L. W. Reeves	2753
Theory of Unidimensional Molecular Collisions. Broken Path Model	L. Blum	2758
The Vapor Pressure, the Evaporation Coefficient, and the Heat of Sublimation of Barium Fluoride	Patrick E. Hart and Alan W. Searcy	2763
The Study of Annelation Series of Benzenoid Hydrocarbons. I. The Influence of Annelation on the Changes of the Excitation Energy of the p Band	Jaroslav Koutecky, Petr Hochmann, and Miloš Titz	2768
A Chemical Kinetics Computer Program for Homogeneous and Free-Radical Systems of Reactions	Richard H. Snow	2780
The Flash Decomposition of Ethylene and Acetylene on Iridium	Robert S. Hansen, John R. Arthur, Jr., V. J. Mimeault, and R. R. Rye	2787
On the Importance of the Metastable Liquid State and Glass Transition Phenomenon to Transport and Structure Studies in Ionic Liquids. I. Transport Properties	C. Austen Angell	2793
Mass Spectrometric Study of the Rates of the Reactions of Nitrogen Atoms with Olefins	John T. Herron	2803
Nuclear Magnetic Resonance of Oxygen-17 and Chlorine-35 in Aqueous Hydrochloric Acid Solutions of Iron(III)	A. H. Zeltmann and L. O. Morgan	2807
The Buoyant Behavior of Bovine Serum Mercaptalbumin in Salt Solutions at Equilibrium in the Ultracentrifuge. II. Net Hydration, Ion Binding, and Solvated Molecular Weight in Various Salt Solutions	James B. Ifft and Jerome Vinograd	2814
Energy Transfer in Thermal Methyl Isocyanide Isomerization. Experimental Survey	F. J. Fletcher, B. S. Rabinovitch, K. W. Watkins, and D. J. Locker	2823
Correlation of Turbidity and Activity Data. III. The System Tungstosilicic Acid-Sodium Chloride-Water	J. P. Kratochvil, L. E. Oppenheimer, and M. Kerker	2834
The Obstruction Effect in the Self-Diffusion Coefficients of Sodium and Cesium in Agar Gels	A. Laird Slade, Adrien E. Cremers, and Henry C. Thomas	2840
Absorption Spectra of Octahedral Lanthanide Hexahalides	Jack L. Ryan and Chr. Klixbüll Jørgensen	2845
Studies of Acid-Base Equilibria in Molten Alkali Nitrates	L. E. Topol, R. A. Osteryoung, and J. H. Christie	2857
The Photochemistry of 1,3-Dioxolane	B. C. Roquette	2863



BOOKS OF PARTICULAR INTEREST TO RESEARCHERS

Positron Annihilation

PROCEEDINGS OF THE CONFERENCE ON POSITRON ANNIHILATION

edited by **A. T. Stewart**, *University of North Carolina, Chapel Hill* and **L. O. Roellig**, *Wayne State University, Detroit, Michigan*

This book contains a systematic and comprehensive review of positron annihilation in solids, liquids, and gases. Each paper is written by a specialist and active worker in the field. It is organized to serve as an introduction to the subject and an up-to-date summary for research workers.

November 1966, about 450 pp., \$16.50

Bromine and Its Compounds

edited by **Z. E. Jolles**, *Berk Ltd., London*

This monograph contains articles on the various commercial uses of bromine.

CONTENTS: Elemental Bromine. Inorganic Bromine Compounds. Organic Bromine Compounds. Radioactive Bromine and Bromine in Radiation Chemistry. Biological Aspects of Bromine and Some Bromine Compounds. Applications. Analytical. *Indexes.*

CONTRIBUTORS: A. Baniel, G. Booth, A. Demiel, H. Farkas-Himsley, M. Goldstein, D. H. O. John, M. D. Johnson, G. I. Jolles, Z. E. Jolles, A. Katchalsky, M. Lewin, S. J. Lyle, L. F. A. Mason, A. Mitzmager, E. F. Mooney, A. H. Oxtoby, M. L. Parker, C. T. Pumpelly, P. J. M. Radford, M. Schmeisser, E. Schuster, P. G. W. Scott, G. M. Segelman, F. Yaron.

June 1966, 940 pp., \$35.00

Available from Academic Press in the Americas with the exception of Canada.

Mechanism of Radiochemical Reactions

by **S. Ya. Pshezhetskiy**, *Moscow, Goskimizdat*

Provides an introduction to the growing field of radiochemistry.

CONTENTS: The Interaction of Radiation with Atoms and Molecules. Secondary Elementary Process. Some Laws Governing the Kinetics of Radiation-Chemical Reactions. The Mechanism of Some Simple Radiation-Chemical Reactions. Hydrocarbon Conversions Induced by Radiation. Radiation-Induced Conversions in Some Organic Compounds. Initiation of Chain Reactions. Some Features of Radiochemical Reactions in Condensed Phases. Reactions of Recoil Atoms.

November 1966, 360 pp., approx. \$14.50

A Logos Press Book

Molecular Relaxation Processes

CHEMICAL SOCIETY SPECIAL PUBLICATION NO. 20

This book is concerned with the rates of individual molecular processes. It provides an extension of classic molecular-kinetic studies, and the relaxation or correlation time, which is frequently a principal concern of the newer methods and is essentially the reciprocal of a molecular rate coefficient.

June 1966, 304 pp., \$10.50

Published jointly with *The Chemical Society.*

VOLUME 3

Advances in Physical Organic Chemistry

edited by **V. Gold**, *University of London, England*

CONTENTS: R. J. W. LE FÈVRE, *Molecular Refractivity and Polarizability.* ALLAN MACCOLL, *Gas-Phase Heterolysis.* DAVID SAMUEL and BRIAN L. SILVER, *Oxygen Isotope Exchange Reactions of Organic Compounds.* L. W. REEVES, N. M. R. *Measurements of Reaction Velocities and Equilibrium Constants as a Function of Temperature.* *Author Index. Cumulative Index of Authors. Cumulative Index of Titles.*

1965, 282 pp., \$10.00

Surface Chemistry

THE SECOND SCANDINAVIAN SYMPOSIUM ON SURFACE ACTIVITY

edited by **Per Ekwall, Kjell Groth, and Vera Runnström-Reio**

This volume bridges the gap between industrial applications of surface chemistry and the scientific research in the field. Emphasis is given to the technical use of surface active agents and of the principles of surface chemistry.

February 1966, 315 pp., \$15.50

Non-Stoichiometric Compounds

edited by **Lyon Mandelcorn**

Westinghouse Electric Corp., Pittsburgh, Pennsylvania

"...ten well written and beautifully illustrated chapters each written by an acknowledged expert who reviews a particular aspect of this broad subject..."

—*Journal of the Royal Institute of Chemistry*

Discusses in detail the non-stoichiometric compounds which include oxides, sulfides, selenides, and tellurides, and inclusion compounds of inorganic, organic, and solution types. Particular emphasis is placed on the structural features and physical properties of these systems.

1964, 674 pp., \$22.50

ACADEMIC PRESS NEW YORK AND LONDON
111 FIFTH AVENUE, NEW YORK, N. Y. 10003

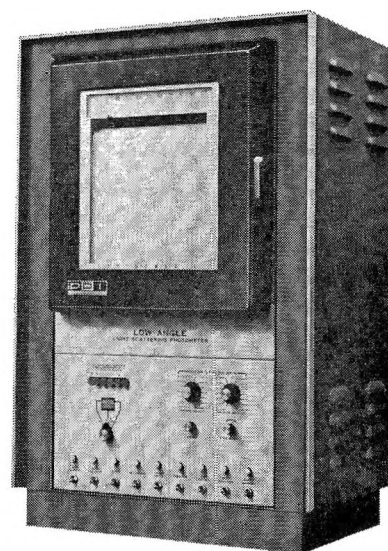
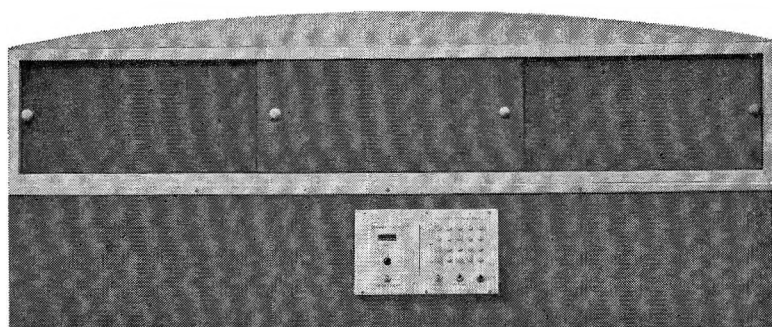
Dissociation Constant of Morpholinium Ion and Related Thermodynamic Quantities from 0 to 50° Hannah B. Hetzer, Roger G. Bates, and R. A. Robinson	2369
The γ Radiolysis of Liquid 2-Propanol. II. The Reaction of Solvated Electrons with Mono- and Disubstituted Benzenes Warren V. Sherman	2872
Temperature Dependence of Electrolytic Conductance: Tetrabutylammonium Fluoroborate in Phenylacetonitrile Ernesto J. del Rosario and John E. Lind, Jr.	2876
Multipulse Potentiodynamic Studies of the Competitive Adsorption of Neutral Organic Molecules and Anions on Platinum Electrodes. I. Competitive Adsorption of Carbon Monoxide and Chloride Ions S. Gilman	2880
The Interaction of Acridine Orange and Proflavine with Polyadenylic Acid Gordon G. Hammes and Colin D. Hubbard	2889
Henry's Law Studies of Solutions of Water in Organic Solvents W. L. Masterton and M. C. Gendrano	2895
Nuclear Magnetic Resonance Studies of Complexes Involving β -Diketones and Some Neutral Organophosphorus Esters George Pukanic, Norman C. Li, Wallace S. Brey, Jr., and George B. Savitsky	2899
Hydrogen-Deuterium Equilibration over Palladium Hydride R. J. Rennard, Jr., and R. J. Kokes	2905
Micellar Properties and Critical Opalescence of Dimethylalkylphosphine Oxide Solutions K. W. Herrmann, J. G. Brushmiller, and W. L. Courchene	2909
The Reaction of Isopropylbenzene on γ -Irradiated Silica Gels Enrique A. Rojo and Robert R. Hentz	2919
Pure Quadrupole Resonance of Halogens in Some Hexahalorhenates(IV) Ryuichi Ikeda, Akinobu Sasane, Daiyu Nakamura, and Masaji Kubo	2926
The Melting Point and Decomposition Pressure of Neptunium Mononitride W. M. Olson and R. N. R. Mulford	2932
The Americium-Hydrogen System W. M. Olson and R. N. R. Mulford	2934
Infrared Study of OH and NH ₂ Groups on the Surface of a Dry Silica Aerogel J. B. Peri	2937
Sedimentation Equilibrium of Ovalbumin in Concentrated Cesium Chloride Julie Hill and David J. Cox	2946
The Radiolysis of Ethyl Mercaptan J. J. J. Myron and R. H. Johnsen	2951
Multiple Knudsen Cell Effusion. Enthalpies of Vaporization of Indium and Gallium G. J. Macur, R. K. Edwards, and P. G. Wahlbeck	2956
Solubilization of a Water-Insoluble Dye as a Method for Determining Micellar Molecular Weights Hans Schott	2966
Interaction of the Tetraethanolammonium Ion with Water as Determined from Transport Properties D. Fennell Evans, G. P. Cunningham, and Robert L. Kay	2974
Lanthanum-Lanthanum Hydride Phase System D. T. Peterson and J. A. Straatmann	2980
The Vapor Pressure and Enthalpy of Vaporization of Molten Mercuric Chloride to the Critical Point J. W. Johnson, W. J. Silva, and D. Cubicciotti	2985
The Saturation Thermodynamic Functions for Mercuric Chloride from 298°K to the Critical Point Daniel Cubicciotti, H. Eding, and J. W. Johnson	2989
The Association of Bispyridinium Cations with Polycarboxylic Acids H. Morawetz and A. Y. Kandanian	2995

NOTES

Nitrogen Adsorption on Iridium and Rhodium V. J. Mimeault and Robert S. Hansen	3001
Catalysis over Supported Metals. VI. The Application of Magnetic Studies in the Interpretation of the Catalytic Properties of Nickel J. L. Carter and J. H. Sinfelt	3003
van der Waals Volumes and Radii of Metals in Covalent Compounds A. Bondi	3006
Studies on Solutions of High Dielectric Constant. VIII. The Cationic Transport Numbers of Potassium Bromide in N-Methylformamide at Different Temperatures and Concentrations Ram Gopal and O. N. Bhatnagar	3007
Photooxidation of Perfluoroethyl Iodide and Perfluoro- <i>n</i> -propyl Iodide Dana Marsh and Julian Hecklen	3008
Heats of Transport of the Rare Gases in a Rubber Membrane Mirion Y. Bearman and Richard J. Bearman	3010

designed to yield size and shape information on particles in the 0.2 to 200 micron diameter range...

**THE NEW PHOENIX
AUTOMATIC SCANNING
LOW-ANGLE
LIGHT-SCATTERING PHOTOMETER**



WRITE FOR INSTRUMENTATION DATA SHEET 1LA-265

PHOENIX PRECISION INSTRUMENT COMPANY

A Subsidiary of CENCO INSTRUMENTS CORP.

3803-05 NORTH 5TH STREET, PHILADELPHIA, PENNSYLVANIA. 19140, U.S.A.

World Wide Sales & Service



MAKERS OF **I** PRODUCTS

OWENS-ILLINOIS

a leading manufacturer of glass, plastics and forest products, has immediate need for:

**CHEMIST
TO
STUDY
SURFACES**

Join interdisciplinary group in surface phenomena and solid state inorganic chemistry, particularly interaction of liquids and gases with glass and glass-ceramic surfaces. MS or PhD, experience helpful but not mandatory.

Professional positions at Owens-Illinois, Inc., have an excellent salary range. Starting level commensurate with your education, experience and ability. Many plus benefits.

Send complete resume in confidence to:

Richard A. Duvall
Owens-Illinois Technical Center
Box 1035 B
Toledo, Ohio 43601

An Equal Opportunity Employer

**CONTACT ANGLE, WETTABILITY,
AND ADHESION**

ADVANCES IN CHEMISTRY SERIES 43

contains twenty-six papers given at the 1963 Kendall Award Symposium.

This is the largest and best collection of up-to-date papers giving both theoretical and practical approaches to wettability and adhesion—a subject important to many areas of science and technology.

In a sense this book is a tribute to the fundamental work of W. A. Zisman, 1963 recipient of the Kendall Award, who opens the symposium with a 48-page article which includes 107 references to other work

Some papers deal with the chemical structure of solid surfaces, solid-fluid interfacial tensions, and flow in capillaries as related to contact angle discussed in other papers. Still others explore adhesion theories, thermodynamics of wettability, chemisorption, coadsorption on metals, spreading of oils on surfaces and its prevention, a computer study of wettability, and other areas.

389 Pages, cloth bound \$8.00 postpaid in U. S. and Canada; plus 20 cents foreign and PUAS.

**Order from: Special Issues Sales
American Chemical Society
1155 Sixteenth St., N. W.
Washington, D. C. 20036**

The Methylene Blue-Ferrous Iron Reaction in a Two-Phase System	D. Fraçkowiak and E. Rabinowitch	3012
The First Ionization Potentials of Samarium, Europium, Gadolinium, Dysprosium, Holmium, Erbium, Thulium, and Ytterbium by the Electron-Impact Method	K. F. Zmbov and J. L. Margrave	3014

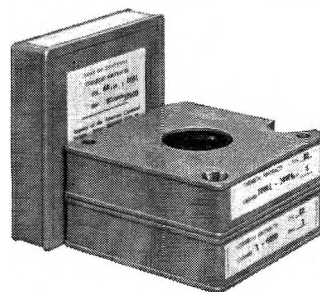
COMMUNICATIONS TO THE EDITOR

Comments on the Paper "Solubility of Hydrogen in Potassium Hydroxide and Sulfuric Acid; Salting-out and Hydration" by P. Ruetschi and R. F. Amlie	J. E. Desnoyers and B. E. Conway	3017
Ultrasonic Study of the Helix Coil Transition in Poly-L-lysine	R. C. Parker, K. Applegate, and L. J. Slutsky	3018
Geminate Recombination in Photochemistry: A First-Order Process	T. J. Sworski	3019
Reactivity of Electron-Donor-Acceptor Complexes. III. Hydrogen Exchange between Acetylene and Organic Electron-Donor-Acceptor Complexes	Masaru Ischikawa, Mitsuyuki Soma, Takaharu Onishi, and Kenzi Tamaru	3020
Electron Spin Resonance of Hydrocarbon Dianion Radicals	Edward G. Janzen, J. Grady Pacifici, and John L. Gerlock	3021
Pulse Radiolysis of the Aqueous Nitrate System. Formation of NO ₃ in Concentrated Solutions and the Mechanism of "Direct Action"	Malcolm Daniels	3022
The Magnetic Susceptibility of Palladium Hydride	Thomas R. P. Gibb, Jr., J. MacMillan, and R. J. Roy	3024
On the Validity of Single-Ion Activity in Polyelectrolyte Solution	Norio Ise and Tsuneo Okubo	3025

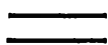
Note Editor's new address on page 1A



Think small!.....
**CHEMICAL
 ABSTRACTS on
 Microfilm**



1 Volume (13 Issues) of
 CHEMICAL ABSTRACTS



1 Volume (13 Issues) of
 CHEMICAL ABSTRACTS
 on Microfilm

If you would like to pack a lot into a small space, CHEMICAL ABSTRACTS on Microfilm will suit your needs. All 3.4 million abstracts published since 1907 are filmed on 16 mm microfilm to form a readily accessible file documenting 59 years of chemical progress.

You can find abstracts quickly and easily, using a variety of microfilm reader-printer equipment. Abstracts may be photocopied at the touch of a button, eliminating the need to make handwritten notes. As a consequence users report a substantial time saving and increasing use of CHEMICAL ABSTRACTS.

To find out how you can use this modern information tool in your program, write or telephone E. G. Johnson, Subscriber Information Department (614 293-5022).



Chemical Abstracts Service
 American Chemical Society



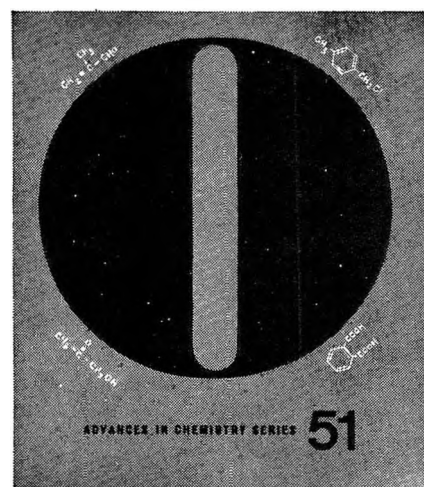
Columbus, Ohio 43216

AUTHOR INDEX

- Alvarez-Funes, A. R., 2734
 Angell, C. A., 2793
 Applegate, K., 3018
 Arthur, J. R., Jr., 2787
 Bates, R. G., 2869
 Bearman, M. Y., 3010
 Bearman, R. J., 3010
 Bhatnagar, O. N., 3007
 Blum, L., 2758
 Bondi, A., 3006
 Braunstein, H., 2726, 2734
 Braunstein, J., 2726, 2734
 Brey, W. S., Jr., 2899
 Brushmiller, J. G., 2909
 Carter, J. L., 3003
 Christie, J. H., 2857
 Conway, B. E., 3017
 Courchene, W. L., 2909
 Cox, D. J., 2946
 Cremers, A. E., 2840
 Cubicciotti, D., 2985, 2989
 Cunningham, G. P., 2974
 Daniels, M., 3022
 del Rosario, E. J., 2876
 Desnoyers, J. E., 3017
 Durant, D., 2709
 Duyvis, E. M., 2747
 Eding, H., 2989
 Edwards, R. K., 2956
 Evans, D. F., 2974
 Ferry, J. D., 2714
 Fletcher, F. J., 2823
 Fraçkowiak, D., 3012
 Gendrano, M. C., 2895
 Gerlock, J. L., 3021
 Gibb, T. R. P., Jr., 3024
 Gilman, S., 2880
 Gopal, R., 3007
 Hammes, G. G., 2889
 Hansen, R. S., 2787, 3001
 Haque, R., 2753
 Hart, P. E., 2763
 Heicklen, J., 3008
 Hentz, R. R., 2919
 Herrmann, K. W., 2909
 Herron, J. T., 2803
 Hetzer, H. B., 2869
 Hill, J., 2946
 Hochmann, P., 2768
 Holmes, L. A., 2714
 Hubbard, C. D., 2889
 Ifft, J. B., 2814
 Ikeda, R., 2926
 Inman, D., 2726
 Ischikawa, M., 3020
 Ise, N., 3025
 Janzen, E. G., 3021
 Johnsen, R. H., 2951
 Johnson, J. W., 2985, 2989
 Jørgensen, C. K., 2845
 Kandanian, A. Y., 2995
 Kay, R. L., 2974
 Kerker, M., 2834
 Kokes, R. J., 2905
 Koutecký, J., 2768
 Kratochvil, J. P., 2834
 Kubo, M., 2926
 Laulicht, I., 2719
 Li, N. C., 2899
 Lind, J. E., Jr., 2876
 Locker, D. J., 2823
 Low, M. J. D., 2740
 MacMillan, J., 3024
 Macur, G. J., 2956
 Margrave, J. L., 3014
 Marsh, D., 3008
 Masterton, W. L., 2895
 McMillan, G. R., 2709
 Mimeault, V. J., 2787, 3001
 Morawetz, H., 2995
 Morgan, L. O., 2807
 Mulford, R. N. R., 2932, 2934
 Myron, J. J. J., 2951
 Nakamura, D., 2926
 Ninomiya, K., 2714
 Okubo, T., 3025
 Olson, W. M., 2932, 2934
 Onishi, T., 3020
 Oppenheimer, L. E., 2834
 Osteryoung, R. A., 2857
 Pacifici, J. G., 3021
 Parker, R. C., 3018
 Peri, J. B., 2937
 Peterson, D. T., 2980
 Pinchas, S., 2719
 Pukanic, G., 2899
 Rabinovitch, B. S., 2823
 Rabinowitch, E., 3012
 Ramasubramanian, N., 2740
 Reeves, L. W., 2753
 Rennard, R. J., Jr., 2905
 Robinson, R. A., 2869
 Rojo, E. A., 2919
 Roquette, B. C., 2863
 Roy, R. J., 3024
 Ryan, J. L., 2845
 Rye, R. R., 2787
 Samuel, D., 2719
 Sasane, A., 2926
 Savitsky, G. B., 2899
 Schott, H., 2966
 Searcy, A. W., 2763
 Sherman, W. V., 2872
 Silva, W. J., 2985
 Sinfelt, J. H., 3003
 Slade, A. L., 2840
 Slutsky, L. J., 3018
 Smits, L. J. M., 2747
 Snow, R. H., 2780
 Soma, M., 3020
 Straatmann, J. A., 2980
 Sworski, T. J., 3019
 Tamaru, K., 3020
 Thomas, H. C., 2840
 Titz, M., 2768
 Topol, L. E., 2857
 Vinograd, J., 2814
 Wahlbeck, P. G., 2956
 Wasserman, I., 2719
 Watkins, K. W., 2823
 Zeltmann, A. H., 2807
 Zmbov, K. F., 3014

Selective Oxidation Processes

Do oxidation processes, products, and mechanisms interest you? "Selective Oxidation Processes" **ADVANCES IN CHEMISTRY SERIES No. 51** surveys a number of processes and details research on improving the range, selectivity, and mechanisms of such processes.



The book includes discussions of hydroxylating selected aromatics and olefins, pyrolysis of isobutylene—all of these by vapor phase processes. Among liquid phase processes are three general methods for oxidizing aromatics, sulfur dioxide as oxidant for a number of products, use of nitrogen dioxide catalyzed by selenium dioxide, and ozone as a selective oxidant. The last chapter is a broad survey of carbanion oxidation. The book is based on a symposium sponsored by the ACS Division of Petroleum Chemistry.

177 pages with index Cloth bound (1965) \$6.50

Other books in **ADVANCES IN CHEMISTRY SERIES** on topics of Industrial interest include:

No. 48 Plasticization and Plasticizer Processes. Seventeen papers survey recent studies on plasticizer action, properties, and production. Includes chapters on glass transition, plasticizer mobility, processes for phthalates and other plasticizers, and antiplasticizers.

200 pages with index Cloth bound (1965) \$7.00

No. 46 Patents for Chemical Inventions. What to do about your patentable idea before you call the attorney.

117 pages with index Cloth bound (1964) \$4.00

No. 38 Saline Water Conversion—II. Fourteen papers from two symposia; includes recovery of minerals from sea water, minimizing scale formation, wiped thin-film distillation, diffusion still, solar flash evaporation, osmosis, electrodialysis (3 papers), research in Israel, hydrate process.

199 pages Paper bound (1963) \$6.00

No. 34 Polymerization and Polycondensation Processes. An I&EC Division symposium with emphasis on unit processes. Twenty-one papers on addition polymerization, polycondensation reactions, commercial polymerization processes, and equipment design.

260 pages Paper bound (1962) \$8.00

No. 27 Saline Water Conversion. A Water and Waste Chemistry Division symposium; includes thermodynamics of desalting, solvent extraction, freezing, cen-

trifugal phase barrier recompression distillation, multi-stage flash evaporation, ion exchange, osmosis, and electrochemical demineralization.

246 pages Paper bound (1960) \$5.85

No. 24 Chemical Marketing in the Competitive Sixties. Twenty articles survey the challenge in marketing drugs, agricultural chemicals, industrial organics, inorganic and heavy chemicals, and plastics; the role of advertising; sales; delivering goods to the customer; monitoring sales performance; market research; technical service, and application research.

147 pages Paper bound (1959) \$3.50

No. 21 Ozone Chemistry and Technology. Sixty papers from the International Ozone Conference; includes ozone chemistry, high concentration ozone, ozone analysis and technology, formation in electrical discharge, toxicity, sterilization and water purification.

465 pages Cloth bound (1959) \$7.00

No. 19 Handling and Uses of Alkali Metals. Nineteen articles on the chemistry, manufacture, and use of the alkali metals; five are devoted solely or partly to lithium, two to potassium, the remainder to sodium.

177 pages Paper bound (1957) \$4.75

No. 10 Literature Resources for Chemical Process Industries. Information sources on market research (13 papers), resins and plastics (7 papers), textile chemistry (6 papers), food industry (10 papers), petroleum (10 papers), literature searching and language problems (13 papers).

582 pages with index Paper bound (1954) \$7.50

No. 5 Progress in Petroleum Technology. Survey of 25 years of progress at the ACS Diamond Jubilee. Thirty-two papers on all aspects of petroleum processing and products.

392 pages Cloth bound (1951) \$6.50

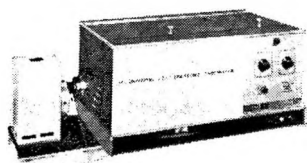
Order from **Special Issues Sales**
American Chemical Society
1155 Sixteenth St., N.W.
Washington, D. C. 20036

THE JOURNAL OF
PHYSICAL CHEMISTRY

Volume 70, Number 10 October 1966

Surface Viscosity of Polydimethylsiloxane Monolayers	N. L. Jarvis	3027
Zinc Oxide Sensitized Photochemical Reduction and Oxidation	Gerald Oster and Masahide Yamamoto	3033
Surface Tension of Liquid Uranium and Thorium Tetrafluorides and a Discussion on the Relationship between the Surface Tension and Critical Temperature of Salts	A. D. Kirshenbaum and J. A. Cahill	3037
Thermodynamics of Binary Alloys. II. The Lithium-Tin System	Melvin S. Foster, Carl E. Crouthamel, and Scott E. Wood	3042
Fluoranyl-Pyridine Charge-Transfer Complexes	W. R. Carper and R. M. Hedges	3046
The Choice of Reference Frame in the Treatment of Membrane Transport by Nonequilibrium Thermodynamics	D. C. Mikulecky and S. R. Caplan	3049
On the Temperature Coefficient of Unperturbed Dimensions of Atactic Polystyrene	Umberto Bianchi, Eligio Patrone, and Enrico Pedemonte	3057
An Electron Spin Resonance Study of Intermediates Formed during Photosensitized Oxidation of Alcohols	Peter J. Baugh, Glyn O. Phillips, and Jett C. Arthur, Jr.	3061
A Comparative Study of Adsorption by Ellipsometric and Radiotracer Methods	J. R. Miller and J. E. Berger	3070
Aberrations Peculiar to the Use of Rayleigh Optics with the Ultracentrifuge. Magnitude in Sedimentation Equilibrium	P. A. Charlwood and M. V. Mussett	3075
The Production of Perfluorocyclopropane in the Reaction of Oxygen Atoms with Tetrafluoroethylene	Norman Cohen and Julian Hecklen	3082
Photolysis of Methyl Iodide in the Presence of Nitric Oxide	Timothy Johnston and Julian Hecklen	3088
The Gas Phase Reaction of Sodium with Ethyl, <i>n</i> -Propyl, and Isopropyl Alcohols	E. M. Nemeth and J. F. Reed	3096
The Potential of the Ruthenium(II)-Ruthenium(III) Couple	R. R. Buckley and E. E. Mercer	3103
Determination of the Free Energy Change for the Reaction between Poly A and Poly U	Adiel Litan	3107
Hydrogen Sorption by Alumina at Low Pressures	M. J. D. Low and E. S. Argano	3115
Ion Association of Magnesium Sulfate in Water at 25°.	Gordon Atkinson and Sergio Petrucci	3122
Electron Spin Resonance Studies of Fundamental Processes in Radiation and Photochemistry. III. Aqueous Systems Containing Nitrate and Nitrite Ions	P. B. Ayscough and R. G. Collins	3128
Raman Spectra of Some Organic Solutes in Anhydrous Hydrogen Fluoride	Jacob Shamir and Herbert H. Hyman	3132
Reversing Intramolecular Kinetic Carbon Isotope Effect in the Gas-Phase Decomposition of Oxalic Acid	Gabriel Lapidus, Donald Barton, and Peter E. Yankwich	3135
A Torsion Effusion Study of the Reaction of Graphite with Hafnium and Uranium Dioxides	T. C. M. Pillay and N. W. Gregory	3140
Gas Phase Dipole Moments of a Series of Terminal 1-Bromoalkanes.	Shmuel Weiss	3146
Double-Layer Impedance of Electrodes with Charge-Transfer Reaction	Paul Delahay and Gilles G. Susbielles	3150
The (³ P ₁) Mercury-Photosensitized Decomposition of Monogermane	Yves Rousseau and Gilbert J. Mains	3158
Cohesive Energies in Polar Organic Liquids	Edwin F. Meyer and Robert E. Wagner	3162

NOW YOU CAN MEASURE
MOLECULAR WEIGHTS
 from **300 TO 1 BILLION***
 with **ONE INSTRUMENT . . .**



the BRICE-PHOENIX UNIVERSAL LIGHT SCATTERING PHOTOMETER

Sounds improbable, doesn't it? But it is true. And not only does it measure molecular and micellar weights from 300 to 1 Billion, but it also measures size, shape, mass, interactions in solutions, turbidity, dissymmetry, and depolarization. With features such as absolute calibration, wavelength selection, and temperature control one would expect to pay much more than the actual price of the BRICE-PHOENIX LIGHT-SCATTERING PHOTOMETER. As a matter of fact it is far below the cost of other instruments with more limited ranges.

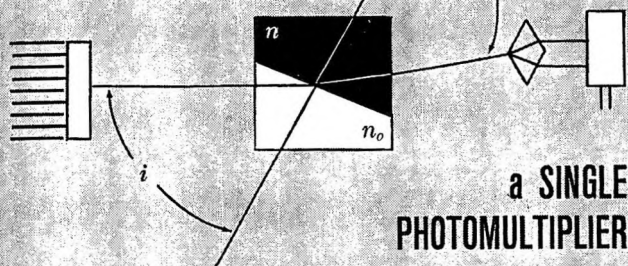
Certainly you will want more information. Send for Bulletin BP-2000.

*See DISSYMMETRIES, Anal. Chem. 36, 42A (1964); 36, 66A (1964); Science 143, 617 (1964) and 144, 449 (1964)



PHOENIX PRECISION INSTRUMENT COMPANY
 A Subsidiary of CENCO INSTRUMENTS CORP.
 3803-05 N. 5th Street, Phila., Penna. 19140, U.S.A.

WHY are MONOCHROMATIC
 LIGHT and



a SINGLE
 PHOTOMULTIPLIER

VITAL to AUTOMATIC DIFFERENTIAL REFRACTOMETRY?

MONOCHROMATIC LIGHT?

The use of monochromatic light eliminates the dispersion effect found in instruments employing polychromatic light. Only the use of monochromatic light permits differential refractometers to be calibrated in terms of absolute refractive index difference.

A SINGLE PHOTOMULTIPLIER?

Drift due to temperature changes, spectral shifts, and fatigue are eliminated with the use of a single photomultiplier tube. This also permits measurement of highly absorbing and turbid samples, a capability not provided by other photo-detectors.

The end result is an instrument with greater accuracy, more sensitivity, extended range and increased stability . . . the Phoenix Differential Refractometer. Want more reasons? Write for Bulletin R-2000.



PHOENIX PRECISION INSTRUMENT COMPANY
 A Subsidiary of CENCO INSTRUMENTS CORP.
 3803-05 N. 5th Street, Phila., Penna. 19140, U.S.A.

SELECTIVE OXIDATION PROCESSES

Do oxidation processes, products, and mechanisms interest you? "Selective Oxidation Processes" ADVANCES IN CHEMISTRY SERIES No. 51 surveys a number of processes and details research on improving the range, selectivity, and mechanisms of such processes.

The book includes discussions of hydroxylating selected aromatics and olefins, pyrolysis of isobutylene—all of these by vapor phase processes. Among liquid phase processes are three general methods for oxidizing aromatics, sulfur dioxide as oxidant for a number of products, use of nitrogen dioxide catalyzed selenium dioxide, and ozone as a selective oxidant. The last chapter is a broad survey of carbanion oxidation. The book is based on a symposium sponsored by the ACS Division of Petroleum Chemistry.

177 pages with index Cloth bound (1965) \$6.50

Order from

Special Issues Sales
 American Chemical Society
 1155 Sixteenth St., N.W.
 Washington, D. C. 20036

4754 p-Terphenyl, scint. \$9.00/100g.
 3917 Cobalt carbonyl, toluene susp. \$75.00/35g.abs.

RARE & FINE CHEMICALS

RARE

CHEMICALS

FINE

CATALOG NUMBER **5**

SEND FOR CATALOG #5

TELEPHONE
 AREA CODE 516
 GENERAL 3-6262

RARE & FINE CHEMICALS

TWX 516-433-8184
 TELEX 01-26464
 CABLE: KALABOR PLAINVIEWNEWYORK

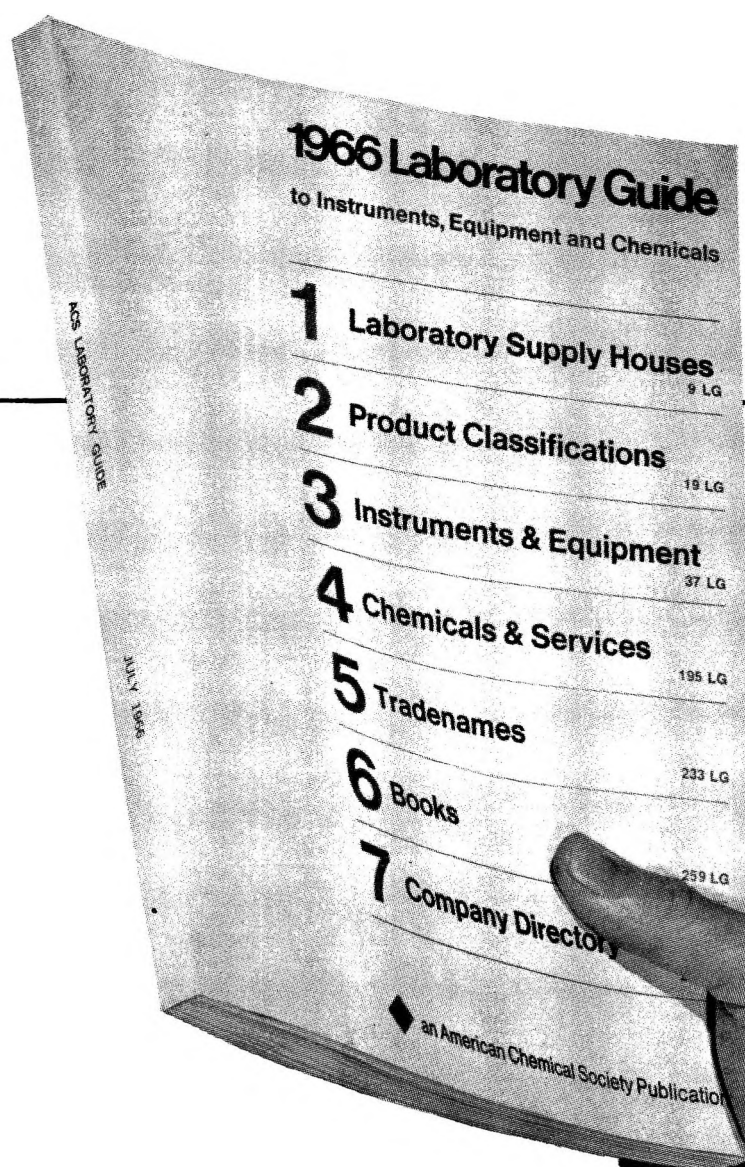
K&K LABORATORIES, INC.
 121 EXPRESS STREET, ENGINEERS HILL, PLAINVIEW, NEW YORK

Infrared Study of Adsorption of Carbon Dioxide, Hydrogen Chloride, and Other Molecules on "Acid" Sites on Dry Silica-Alumina and γ -Alumina	J. B. Peri	3168
Heats and Entropies of Dissociation of Sodium Salts of Aromatic Radical Anions in Tetrahydrofuran and Dimethoxyethane. The Limitation and Generalization of the Concepts of Contact and Solvent-Separated Ion Pairs	P. Chang, R. V. Slates, and M. Szwarc	3180
Vibrational Spectra of Organophosphorus Compounds. II. Infrared and Raman Spectra of CH_3POF_2 and CH_3POFCl	J. R. Durig, B. R. Mitchell, J. S. DiYorio, and F. Block	3190
Kinetics of the Solid-State Reaction between Magnesium Oxide and Ferric Oxide	Donald L. Fresh and J. Stuart Dooling	3198
On the Irradiation of <i>n</i> -Heptadecane	R. Salovey and W. E. Falconer	3203
Infrared Spectra of Some Alkaline Earth Halides by the Matrix Isolation Technique	Alan Snelson	3208
A New Isodielectric Method for Measurement of Dipole Moment in Solution	R. Thomas Myers and Viola M. L. Sun	3217
Rates of Hydrogen Abstraction from Methanol by CF_3 Radicals	Terry S. Carlton, J. Rodger Steeper, and Ronald L. Christensen	3222
Hydroxyl Group Stretching Frequency and Extinction Coefficient Studies on Aliphatic Alcohols	Izumi Motoyama and Charles H. Jarboe	3226
Self-Diffusion in Suspensions. Sodium in Montmorillonite at Equilibrium	Adrien Cremers and Henry C. Thomas	3229
Characterization of Graft Copolymers of Methylated Xylan and Polystyrene	James J. O'Malley and R. H. Marchessault	3235
The Hydrogen Fluoride Solvent System. IX. Potentiometric Study of the Systems: (1) $\text{Cu(s)} \text{CuF}_2\text{(s)} \text{TlF}(\text{HF}) \text{TlF}_3\text{(s)}(\text{Pt})$; (2) $\text{Ag(s)} \text{AgF},\text{TlF}(\text{HF}) \text{TlF}_3\text{(s)}(\text{Pt})$; (3) $\text{Ag(s)} \text{AgF}(\text{HF}) \text{AgF}_2\text{(s)}(\text{Pt})$	A. F. Clifford, W. D. Pardieck, and M. W. Wadley	3241
Kinetics of Diffusion-Controlled Reactions. An Experimental Test of the Theory as Applied to Fluorescence Quenching	William R. Ware and Joel S. Novros	3246
Decomposition of Silver Oxalate. I. Microscopic Observations of Partially Decomposed Crystals	Algird G. Leiga	3254
Decomposition of Silver Oxalate. II. Kinetics of the Thermal Decomposition	Algird G. Leiga	3260
Salt and Acid Effects in the Hydrolysis of <i>N</i> -Acylimidazolium Ions and the Role of Structured Water	James A. Fee and Thomas H. Fife	3268
Phase Separation of Poly-L-proline in Salt Solutions	A. Ciferri and T. A. Orofino	3277
A Method for the Determination of Protein Partial Specific Volumes	Margaret J. Hunter	3285
Spectroscopy and Franck-Condon Factors of Scandium Fluoride in Neon Matrices at 4°K	Donald McLeod, Jr., and William Weltner, Jr.	3293
The Double Layer at the Mercury-Formamide Interface	G. H. Nancollas, D. S. Reid, and C. A. Vincent	3300
Photochemistry of a Water-Soluble Polymeric Derivative of Chlorophyll	R. G. Jensen, G. R. Seely, and L. P. Vernon	3307
Solid-State Reactions between Picric Acid and Naphthols	R. P. Rastogi and N. B. Singh	3315
Structural Studies of Chelates by Ultrasonic Waves	Som Prakash and Satya Prakash	3325
The Lone-Pair Model and the Vibrational Force Constants of NF_3	E. C. Curtis and J. S. Muirhead	3330

NOTES

Estimated Activation Energies for the Four-Center Addition Reaction of H_2 , HX , and X_2 to Acetylenes	Sidney W. Benson and Gilbert R. Haugen	3336
On the Conductance of Symmetrical Electrolytes	W. Ebeling, W. D. Kraeft, and D. Kremp	3338
$\text{C}_3\text{F}_7 + \text{C}_2\text{H}_5$ and $\text{C}_2\text{F}_5 + \text{C}_2\text{H}_5$ Disproportionation/Combination and Cross-Combination Ratios. A Reexamination	G. O. Pritchard and R. L. Thommarson	3339
The Effect of Pressure on Liquid Miscibility	Donald B. Myers, Robert A. Smith, Jeffrey Katz, and Robert L. Scott	3341

ACS Laboratory Guide



The definitive directory to research instruments, chemicals, services, books, equipment and tradenames.

Issued annually in July, used daily to...

FIND WHO SELLS WHAT
INQUIRE ABOUT PRODUCTS
LOCATE SALES OFFICES
CREATE BIDDER'S LISTS
CONTACT VENDORS
PLACE ORDERS

Relationships between Electrode Potential and Related Functions, and the Hydrogen Content of Alloys of 40% Silver and 60% Palladium	A. W. Carson and F. A. Lewis	3343
The Self-Diffusion Coefficient of Sodium Dodecyl Sulfate Micelles	J. Clifford and B. A. Pethica	3345
A Correlative Treatment of the Heat of Adsorption with Coverage on the Monolayer Side	S. P. Moulik	3346
Vapor Species over Potassium Amalgams	John W. Reishus	3348
Spin Densities in Biphenylaminyl Network and Triphenylimidazolyl Network	Hisashi Ueda	3349
Volume-Energy Relations in Liquids at 0°K from Equations of State	S. T. Hadden	3351
Fluorine Bomb Calorimetry. XVII. The Enthalpy of Formation of Tungsten Hexafluoride	P. A. G. O'Hare and Ward N. Hubbard	3353
Interdiffusion and Self-Diffusion in Urea Solutions	P. C. Carman	3355
Effect of Inert Gas Pressure and Solubility on Fused Salt Conductance. II. Nitrogen with Sodium Nitrate	James L. Copeland and Steven Radak	3356
Pulse Radiolysis of Anhydrous Amines	Larry R. Dalton, James L. Dye, E. M. Fielden, and Edwin J. Hart	3358
The System Potassium Carbonate-Magnesium Carbonate	S. E. Ragone, R. K. Datta, Della M. Roy, and O. F. Tuttle	3360
Relative Determinations of Soret Coefficients of Electrolytes. III.	Toshio Ikeda and Hideo Miyoshi	3361
Instability Constants of Silver-Amine Complexes in Isopropyl Alcohol	J. L. Pauley and H. H. Hau	3363
Kinetics of the Gas Phase Pyrolysis of Tetranitromethane	J. M. Sullivan and A. E. Axworthy	3366
The Dissociation of Tetra- <i>n</i> -hexylammonium Iodide in Dichloromethane	R. A. Matheson	3368

COMMUNICATIONS TO THE EDITOR

An Activation Energy for the Transport of Carbon Dioxide through a Monolayer of Hexadecanol at the Air-Water Interface	J. G. Hawke and I. White	3369
Comments on the Effects of Nonbonded Electrons on Barriers to Internal Rotation	Albert B. Harvey	3370
A 2:1 Perylene-PMDA Molecular Complex	Ivor Ilmet and Lawrence Kopp	3371
Electron Spin Resonance of Thioketals. A Large Metal Ion Splitting	Edward G. Janzen and Coit M. DuBose, Jr.	3372
Intramolecular Energy Transfer in γ -Irradiated Alkylbenzenes	A. Zeman and H. Heusinger	3374
A Method for Predicting the Effect of Solvation on Hydrogen-Bonding Association Equilibria	Sherril D. Christian, James R. Johnson, Harold E. Affsprung, and Paul J. Kilpatrick	3376
Chemiluminescent Gas-Phase Reactions Involving Electronically Excited Oxygen Molecules. Trimethylaluminum and Diborane near 3 mtorr	Arthur Fontijn and Pieter H. Vree	3377

AUTHOR INDEX

- Affsprung, H. E., 3376
 Argano, E. S., 3115
 Arthur, J. C., Jr., 3061
 Atkinson, G., 3122
 Axworthy, A. E., 3366
 Ayscough, P. B., 3128

 Barton, D., 3135
 Baugh, P. J., 3061
 Benson, S. W., 3336
 Berger, J. E., 3070
 Bianchi, U., 3057
 Block, F., 3190
 Buckley, R. R., 3103

 Cahill, J. A., 3037
 Caplan, S. R., 3049
 Carlton, T. S., 3222
 Carman, P. C., 3355
 Carper, W. R., 3046
 Carson, A. W., 3343
 Chang, P., 3180
 Charlwood, P. A., 3075
 Christensen, R. L., 3222
 Christian, S. D., 3376
 Ciferri, A., 3277
 Clifford, A. F., 3241
 Clifford, J., 3345
 Cohen, N., 3082
 Collins, R. G., 3128
 Copeland, J. L., 3356
 Cremers, A., 3229
 Crouthamel, C. E., 3042
 Curtis, E. C., 3330

 Dalton, L. R., 3358
 Datta, R. K., 3360
 Delahay, P., 3150
 DiYorio, J. S., 3190
 Dooling, J. S., 3198
 DuBose, C. M., Jr., 3372
 Durig, J. R., 3190
 Dye, J. L., 3358

 Ebeling, W., 3338

 Falconer, W. E., 3203
 Fee, J. A., 3268
 Fielden, E. M., 3358
 Fife, T. H., 3268
 Fontijn, A., 3377
 Foster, M. S., 3042
 Fresh, D. L., 3198

 Gregory, N. W., 3140

 Hadden, S. T., 3351
 Hart, E. J., 3358
 Harvey, A. B., 3370
 Hau, H. H., 3363
 Haugen, G. R., 3336
 Hawke, J. G., 3369
 Hedges, R. M., 3046
 Heicklen, J., 3082, 3088
 Heusinger, H., 3374
 Hubbard, W. N., 3353
 Hunter, M. J., 3285
 Hyman, H. H., 3132

 Ikeda, T., 3361

 Ilmet, I., 3371

 Janzen, E. G., 3372
 Jarboe, C. H., 3226
 Jarvis, N. L., 3027
 Jensen, R. G., 3307
 Johnson, J. R., 3376
 Johnston, T., 3088

 Katz, J., 3341
 Kilpatrick, P. J., 3376
 Kirshenbaum, A. D., 3037
 Kopp, L., 3371
 Kraeft, W. D., 3338
 Kremp, D., 3338

 Lapidus, G., 3135
 Leiga, A. G., 3254, 3260
 Lewis, F. A., 3343
 Litan, A., 3107
 Low, M. J. D., 3115

 Mains, G. J., 3158
 Marchessault, R. H., 3235
 Matheson, R. A., 3368
 McLeod, D., Jr., 3293
 Mercer, E. E., 3103
 Meyer, E. F., 3162
 Mikulecky, D. C., 3049
 Miller, J. R., 3070
 Mitchell, B. R., 3190
 Miyoshi, H., 3361
 Motoyama, I., 3226
 Moulik, S. P., 3346

 Muirhead, J. S., 3330
 Mussett, M. V., 3075
 Myers, D. B., 3341
 Myers, R. T., 3217

 Nancollas, G. H., 3300
 Nemeth, E. M., 3096
 Novros, J. S., 3246

 O'Hare, P. A. G., 3353
 O'Malley, J. J., 3235
 Orofino, T. A., 3277
 Oster, G., 3033

 Pardieck, W. D., 3241
 Patrone, E., 3057
 Pauley, J. L., 3363
 Pedemonte, E., 3057
 Peri, J. B., 3168
 Pethica, B. A., 3345
 Petrucci, S., 3122
 Phillips, G. O., 3061
 Pillay, T. C. M., 3140
 Prakash, Satya, 3325
 Prakash, Som, 3325
 Pritchard, G. O., 3339

 Radak, S., 3356
 Ragone, S. E., 3360
 Rastogi, R. P., 3315
 Reed, J. F., 3096
 Reid, D. S., 3300
 Reishus, J. W., 3348
 Rousseau, Y., 3158
 Roy, D. M., 3360

 Salovey, R., 3203

 Scott, R. L., 3341
 Seely, G. R., 3307
 Shamir, J., 3132
 Singh, N. B., 3315
 Slates, R. V., 3180
 Smith, R. A., 3341
 Snelson, A., 3208
 Steeper, J. R., 3222
 Sullivan, J. M., 3366
 Sun, V. M. L., 3217
 Susbielles, G. G., 3150
 Szwarc, M., 3180

 Thomas, H. C., 3229
 Thommarson, R. L., 3339
 Tuttle, O. F., 3360

 Ueda, H., 3349

 Vernon, L. P., 3307
 Vincent, C. A., 3300
 Vree, P. H., 3377

 Wadley, M. W., 3241
 Wagner, R. E., 3162
 Ware, W. R., 3246
 Weiss, S., 3146
 Weltner, W., Jr., 3293
 White, I., 3369
 Wood, S. E., 3042

 Yamamoto, M., 3033
 Yankwich, P. E., 3135

 Zeman, A., 3374

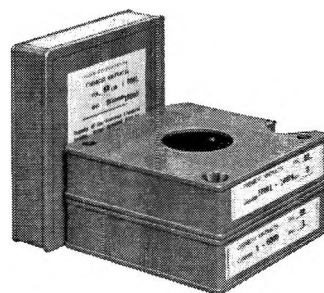
THE JOURNAL OF
PHYSICAL CHEMISTRY

Volume 70, Number 11 November 1966

Mass Spectrometric Studies at High Temperatures. XII. Stabilities of Dysprosium, Holmium, and Erbium Subfluorides	K. F. Zmbov and John L. Margrave	3379
Effect of Density on the Radiolysis of Propylene	M. Trachtman	3382
Reactivity of Some Cobalt(III) Complexes toward Photochemically Produced Hydrogen Atoms and Solvated Electrons in Aqueous Solution	John F. Endicott and Morton Z. Hoffman	3389
Mechanism of Solubilization of Water in Nonpolar Solutions of Oil-Soluble Surfactants: Effect of Electrolytes	Ayao Kitahara and Kijiro Kon-no	3394
The Temperature Dependence of Transport Properties of Ionic Liquids. The Conductance and Viscosity of Calcium Nitrate Tetrahydrate and Sodium Thiosulfate Pentahydrate	Cornelius T. Moynihan	3399
Biphasic Oxidation-Reduction Reaction with a Liquid Electron Exchanger of the Hydroquinone-Quinone Type	G. Scibona, P. R. Danesi, and F. Orlandini	3403
Thermodynamics of Binary Solutions of Nonelectrolytes with 2,2,4-Trimethylpentane. I. Volume of Mixing (25°) and Vapor-Liquid Equilibrium (35-75°) with Cyclohexane	Rubin Battino	3408
Thermodynamics of Binary Solutions of Nonelectrolytes with 2,2,4-Trimethylpentane. II. Phase Equilibrium Study with Cyclohexane and a New Cooling Curve Apparatus	Rubin Battino and George W. Allison	3417
The Unperturbed Dimensions of Polypropylene and Polyethylene	Hiroshi Inagaki, Takeaki Miyamoto, and Shigeyasu Ohta	3420
The Effect of Residual Abrasives on the Wettability of Polished Gold Surfaces	Malcolm L. White and J. Drobek	3432
Potentiometric Titration of a Nonionic-Cationic Surfactant in Aqueous Solution	Fumikatsu Tokiwa and Kenji Ohki	3437
A Study of the Equilibrium $\text{KNO}_3(\text{l}) \rightleftharpoons \text{KNO}_2(\text{l}) + \frac{1}{2}\text{O}_2(\text{g})$ over the Temperature Range 550-750°	Roger F. Bartholomew	3442
Electrochemistry of the Interface between Some Aluminosilicate Crystals and Salt Solutions. I. Surface Conductivity	S. D. James	3447
Electrochemistry of the Interface between Some Aluminosilicate Crystals and Salt Solutions. II. Electrokinetic Charge	A. S. Buchanan and S. D. James	3454
Nuances of the ECE Mechanism. I. Development of the Theoretical Relationships for Chronoamperometry	M. Dale Hawley and Stephen W. Feldberg	3459
An Electron Paramagnetic Resonance Study of Surface Defects on Magnesium Oxide	Jack H. Lunsford and John P. Jayne	3464
The Extraction of Hydrohalic Acids by Trilaurylamine	W. Müller and R. M. Diamond	3469
Photo-Fries Rearrangement of Aromatic Esters. Role of Steric and Electronic Factors	G. M. Coppinger and E. R. Bell	3479
Deuterium Oxide Solvent Isotope Effects on Fast Reactions of Substituted Malonic Acids	Melvin H. Miles, Edward M. Eyring, William W. Epstein, and Michael T. Anderson	3490
π -Complex Fluorescence. I. Room-Temperature Solution Studies of the Pyromellitic Dianhydride-Methylbenzene Complexes	H. M. Rosenberg and E. C. Eimutis	3494
Isomeric Variation Procedures for Physicochemical Properties of Alkanes	G. R. Somayajulu and B. J. Zwolinski	3498
The Effect of Added Alcohols on the Solubility and the Krafft Point of Sodium Dodecyl Sulfate	H. Nakayama, Kozo Shinoda, and E. Hutchinson	3502



Think small!.....
**CHEMICAL
ABSTRACTS on
Microfilm**



1 Volume (13 Issues) of
CHEMICAL ABSTRACTS



1 Volume (13 Issues) of
CHEMICAL ABSTRACTS
on Microfilm

If you would like to pack a lot into a small space, CHEMICAL ABSTRACTS on Microfilm will suit your needs. All 3.4 million abstracts published since 1907 are filmed on 16 mm microfilm to form a readily accessible file documenting 59 years of chemical progress.

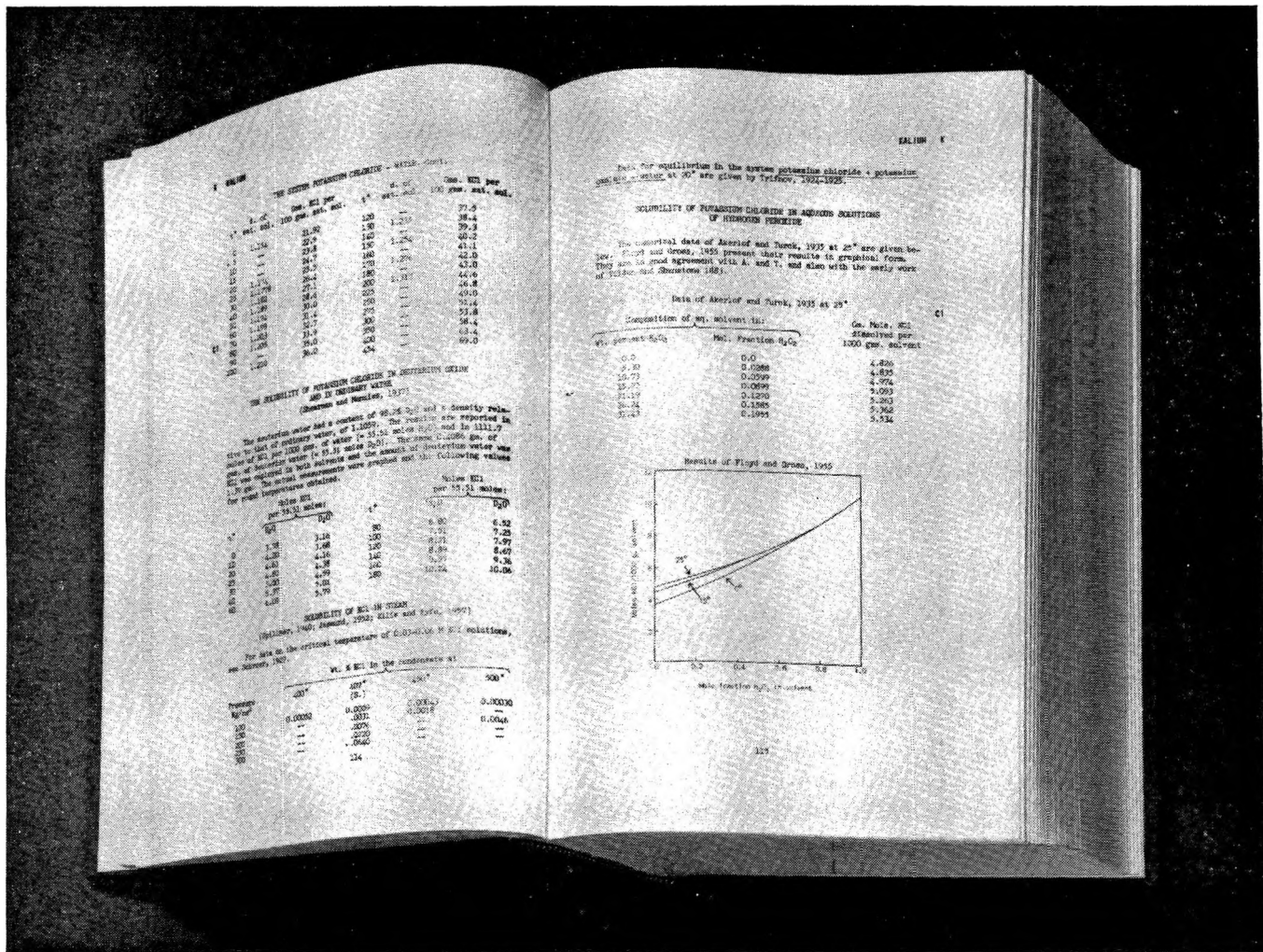
You can find abstracts quickly and easily, using a variety of microfilm reader-printer equipment. Abstracts may be photocopied at the touch of a button, eliminating the need to make handwritten notes. As a consequence users report a substantial time saving and increasing use of CHEMICAL ABSTRACTS.

To find out how you can use this modern information tool in your program, write or telephone E. G. Johnson, Subscriber Information Department (614 293-5022).



Columbus, Ohio 43216

The Nuclear Magnetic Resonance Spectra of Some 1,4-Disubstituted Naphthalenes	William B. Smith and Siram Chiranjeevi	3505
Study with Fast-Mixing Techniques of the Titanium(III) and Hydrogen Peroxide Reaction	Y. S. Chiang, J. Craddock, D. Mickewich, and J. Turkevich	3509
Specific Rearrangements in the Mass Spectra of Butyl Hexanoates and Similar Aliphatic Esters	W. H. McFadden, Lois E. Boggs, and R. G. Buttery	3516
Zinc Oxide-Photosensitized Photolysis of Lead Chloride	W. C. Tennant	3523
Molten Sulfur Chemistry. I. Chemical Equilibria in Pure Liquid Sulfur	T. K. Wiewiorowski and F. J. Touro	3528
Molten Sulfur Chemistry. II. The Solubility of Sulfur Dioxide in Molten Sulfur	F. J. Touro and T. K. Wiewiorowski	3531
Molten Sulfur Chemistry. III. The Sulfur-Carbon Disulfide System	F. J. Touro and T. K. Wiewiorowski	3534
Photodecomposition of Lead Chloride	A. Kaldor and G. A. Somorjai	3538
The Effect of Certain Salts on the Aqueous Solubilities of <i>o</i> -, <i>m</i> -, and <i>p</i> -Dinitrobenzene	Algird G. Leiga and James N. Sarmousakis	3544
Electron Paramagnetic Resonance Study of Cupric-Peptide Complexes	Graeme F. Bryce	3549
The Microcatalytic Hydrogenation of Benzene over Groups VIII and Ib Metals and Alloys	D. A. Cadenhead and N. G. Masse	3558
Dielectric Relaxation, Nuclear Magnetic Resonance, Infrared Absorption, and Hydrogen Bonding in Benzene Solutions of Phenols and Anilines	F. K. Fong, J. P. McTague, S. K. Garg, and C. P. Smyth	3567
Hydrogen Reduction of Nickel Oxide Doped and Mixed with Cupric Oxide	T. Yamashina and T. Nagamatsuya	3572
Energy Transfer in the Photo- and Radiation Chemical <i>cis-trans</i> Isomerization of Octene-2 in Benzene	Morton A. Golub and Curtis L. Stephens	3576
Electrical Double-Layer Measurements on Liquid Gallium, Indium-Gallium, and Mercury-Gallium Alloys	James N. Butler and Mary L. Meehan	3582
The Temperature Coefficient of the Unperturbed Dimensions of Polyisobutylene	J. E. Mark and G. B. Thomas	3588
Stereocomplex Formation in Solutions of Poly(methyl methacrylate)	R. Chiang, J. J. Burke, J. O. Threlkeld, and T. A. Orofino	3591
Combined Effects of Dose Rate and Temperatures in the Radiolysis of Liquid Chloroform. Application of Homogeneous Kinetics to the Radiolytic System	Fred P. Abramson and Richard F. Firestone	3596
The Enthalpies of Combustion and Formation of the 1-Alkanethiols. The Methylene Increment to the Enthalpy of Formation	W. D. Good and B. L. DePrater	3606
Structure of Organic Melts	John E. Lind, Jr., H. A. A. Abdel-Rehim, and S. W. Rudich	3610
The Voltammetric Characteristics and Mechanism of Electrooxidation of Hydroxylamine	Gadde Ramachandra Rao and Louis Meites	3620
Pure Quadrupole Resonance of Nitrogen-14 in Some Organic Thiocyanates	Ryuichi Ikeda, Daiyu Nakamura, and Masaji Kubo	3626
The Reactivity of Some High- and Low-Spin Iron(III) Complexes with Atomic Hydrogen in Aqueous Solution	Gil Navon and Gabriel Stein	3630
Crystal Field Studies on Vanadium and Chromium in Zirconium Oxide	John Meehan and R. E. Salomon	3642
On the Second Osmotic Virial Coefficient of Athermal Polymer Solutions	G. V. Schulz, H. Baumann, and R. Darskus	3647
An Electron Spin Resonance Study of the γ Radiolysis and the Photolysis of Frozen Ammonia-Water Systems	B. S. Al-Naimy, P. N. Moorthy, and J. J. Weiss	3654
On Diffusion-Controlled Particle Growth: the Moving Boundary Problem	F. C. Goodrich	3660
The Effect of Sulfiding a Nickel on Silica-Alumina Catalyst	G. E. Langlois, R. F. Sullivan, and Clark J. Egan	3666



NOW AVAILABLE FROM THE AMERICAN CHEMICAL SOCIETY

A valuable, new edition of an essential chemical reference—

Volume II of the Fourth Edition of Seidell's SOLUBILITIES OF INORGANIC AND METAL ORGANIC COMPOUNDS

Illustrated above are two of the 57 pages of data on solubilities of only *one* inorganic compound, potassium chloride, in various solvents and with various compounds. Volume II has a total of 1,914 pages of critically evaluated data, with tables, values at various temperatures, and melting point references . . . all systematically arranged for quick reference. And data are given for 1,281 other compounds besides potassium chloride and for 26 elements as well, covering the elements with symbols from K through Z.

Volume I appeared in 1959. With the appearance of Volume II in 1966 the data for inorganic and metal organic compounds in the Fourth Edition is now complete . . . a painstaking revision by Dr. William F. Linke, American Cyanamid

Company, continuing the compendium started by the late Dr. Atherton Seidell.

The book is a time-saving work aid, clearly indexed, and carefully cross-referenced with Volume I in terms of subject matter and literature cited in both volumes.

Seidell-Linke, "Solubilities of Inorganic and Metal Organic Compounds," Fourth Edition, Vol. II. iii 1,941 pages. Cloth bound. (1966) . . . \$32.50

Order from:

Special Issues Sales

AMERICAN CHEMICAL SOCIETY

1155 Sixteenth Street, N.W.

Washington, D. C. 20036

Thermal Degradation of Isotactic and Syndiotactic Poly(methyl methacrylate)	H. H. G. Jellinek and Ming Dean Luh	3672
The Kinetics of the Reaction at Low Temperatures between Sodium Films and Thermally Activated Hydrogen	J. R. Anderson and I. M. Ritchie	3681
Charge-Transfer Complexes of Mono- and Disubstituted Tetrazoles with π -Electron Acceptors	Thomas C. Wehman and Alexander I. Popov	3688
On the Location of Adsorbed Ethylene in a Zeolite	D. J. C. Yates	3693
A Thermodynamic Study of the Vaporization Behavior of the Substoichiometric Plutonium Dioxide Phase	R. J. Ackermann, R. L. Faircloth, and M. H. Rand	3698
Orientation of Free Radicals in Monoolefin Addition Reactions	J. B. Flannery, Jr.	3707
Ion-Exchange Membrane Potentials	A. S. Tombalakian and W. F. Graydon	3711
Electrical Conductances of Aqueous Solutions at High Temperatures and Pressures. III. The Conductances of Potassium Bisulfate Solutions from 0 to 700° and at Pressures to 4000 Bars	Arvin S. Quist and William L. Marshall	3714
Ultracentrifugal Studies of Barium Dinonylnaphthalenesulfonate-Benzene Systems. I. Sedimentation Velocity	T. Foster Ford, Samuel Kaufman, and Owen D. Nichols	3726

NOTES

Nuclear Magnetic Resonance of Hydrogen Polysulfides in Molten Sulfur	J. B. Hyne, E. Muller, and T. K. Wiewiorowski	3733
Dissociation of Palladium Oxide	Wayne E. Bell, R. E. Inyard, and M. Tagami	3735
Dissociation of Iridium Trichloride	Wayne E. Bell and M. Tagami	3736
Rotational Transitions in Neopentyl Alcohol and Neopentyl Glycol	J. A. Faucher, J. D. Graham, J. V. Koleske, E. R. Santee, Jr., and E. R. Walter	3738
Bond Angles and Bonding in Group IIa Metal Dihalides	Edward F. Hayes	3740
Gibbs Equation for Polyelectrolyte Adsorption	D. K. Chattoraj	3743
Spin-Spin Coupling in Di- <i>t</i> -butyl Carbinol	Larry K. Patterson and R. M. Hammaker	3745
Theoretical Study of Isoelectronic Molecules: Oxygen and Ethylene	Marvin Bishop and John Arents	3748
Consequences of the Proton Model for Hydrogen Absorption in the β Phase of the Hydrogen-Palladium System	Ted B. Flanagan and J. W. Simons	3750
The Heats of Formation of Acetyl Iodide and the Acetyl Radical	Robin Walsh and Sidney W. Benson	3751
X-Ray Diffraction Studies of the Effect of Traces of Hydrogen in Vanadium	Richard J. Roy and Thomas R. P. Gibb, Jr.	3753
Complexes of Azanaphthalenes with Iodine	Ivor Ilmet and Myron Krasij	3755
High-Temperature Enthalpy Studies of Bismuth Trisulfide and Antimony Triselenide	Alfred C. Glatz and Karen E. Cordo	3757

COMMUNICATIONS TO THE EDITOR

Electron Spin Resonance of O^{16} - O^{17} , O^{17} , O^{18} , and O^{18} - O^{16}	L. K. Keys	3760
The Role of Hydrogen Peroxide in the Reduction of Oxygen at Platinum Electrodes	A. Damjanovic, M. A. Genshaw, and J. O'M. Bockris	3761

AUTHOR INDEX

- Abdel-Rehim, H. A. A., 3610
 Abramson, F. P., 3596
 Ackermann, R. J., 3698
 Allison, G. W., 3417
 Al-Naimy, B. S., 3654
 Anderson, J. R., 3681
 Anderson, M. T., 3490
 Arents, J., 3748
 Bartholomew, R. F., 3442
 Battino, R., 3408, 3417
 Baumann, H., 3647
 Bell, E. R., 3479
 Bell, W. E., 3735, 3736
 Benson, S. W., 3751
 Bishop, M., 3748
 Bockris, J. O'M., 3761
 Boggs, L. E., 3516
 Bryce, G. F., 3549
 Buchanan, A. S., 3454
 Burke, J. J., 3591
 Butler, J. N., 3582
 Buttery, R. G., 3516
 Cadenhead, D. A., 3558
 Chattoraj, D. K., 3743
 Chiang, R., 3591
 Chiang, Y. S., 3509
 Chiranjeevi, S., 3505
 Coppinger, G. M., 3479
 Cordo, K. E., 3757
 Craddock, J., 3509
 Damjanovic, A., 3761
 Danesi, P. R., 3403
 Darskus, R., 3647
 DePrater, B. L., 3606
 Diamond, R. M., 3469
 Drobek, J., 3432
 Egan, C. J., 3666
 Eimutis, E. C., 3494
 Endicott, J. F., 3389
 Epstein, W. W., 3490
 Eyring, E. M., 3490
 Faircloth, R. L., 3698
 Faucher, J. A., 3738
 Feldberg, S. W., 3459
 Firestone, R. F., 3596
 Flanagan, T. B., 3750
 Flannery, J. B., Jr., 3707
 Fong, F. K., 3567
 Ford, T. F., 3726
 Garg, S. K., 3567
 Genshaw, M. A., 3761
 Gibb, T. R. P., Jr., 3753
 Glatz, A. C., 3757
 Golub, M. A., 3576
 Good, W. D., 3606
 Goodrich, F. C., 3660
 Graham, J. D., 3738
 Graydon, W. F., 3711
 Hammaker, R. M., 3745
 Hawley, M. D., 3459
 Hayes, E. F., 3740
 Hoffman, M. Z., 3389
 Hutchinson, E., 3502
 Hyne, J. B., 3733
 Ikeda, R., 3626
 Ilmet, I., 3755
 Inagaki, H., 3420
 Inyard, R. E., 3735
 James, S. D., 3447, 3454
 Jayne, J. P., 3464
 Jellinek, H. H. G., 3672
 Kaldor, A., 3538
 Kaufman, S., 3726
 Keys, L. K., 3760
 Kitahara, A., 3394
 Kon-no, K., 3394
 Koleske, J. V., 3738
 Krasij, M., 3755
 Kubo, M., 3626
 Langlois, G. E., 3666
 Leiga, A. G., 3544
 Lind, J. E., Jr., 3610
 Luh, M. D., 3672
 Lunsford, J. H., 3464
 Margrave, J. L., 3379
 Mark, J. E., 3588
 Marshall, W. L., 3714
 Masse, N. G., 3558
 McFadden, W. H., 3516
 McTague, J. P., 3567
 Meehan, J., 3642
 Meehan, M. L., 3582
 Meites, L., 3620
 Mickewich, D., 3509
 Miles, M. H., 3490
 Miyamoto, T., 3420
 Moorthy, P. N., 3654
 Moynihan, C. T., 3399
 Muller, E., 3733
 Müller, W., 3469
 Nagamatsuya, T., 3572
 Nakamura, D., 3626
 Nakayama, H., 3502
 Navon, G., 3630
 Nichols, O. D., 3726
 Ohki, K., 3437
 Ohta, S., 3420
 Orlandini, F., 3403
 Orofino, T. A., 3591
 Patterson, L. K., 3745
 Popov, A. I., 3688
 Quist, A. S., 3714
 Rand, M. H., 3698
 Rao, G. R., 3620
 Ritchie, I. M., 3681
 Rosenberg, H. M., 3494
 Roy, R. J., 3753
 Rudich, S. W., 3610
 Salomon, R. E., 3642
 Santee, E. R., Jr., 3738
 Sarmousakis, J. N., 3544
 Schulz, G. V., 3647
 Scibona, G., 3403
 Shinoda, K., 3502
 Simons, J. W., 3750
 Smith, W. B., 3505
 Smyth, C. P., 3567
 Somayajulu, G. R., 3498
 Somorjai, G. A., 3538
 Stein, G., 3630
 Stephens, C. L., 3576
 Sullivan, R. F., 3666
 Tagami, M., 3735, 3736
 Tennant, W. C., 3523
 Thomas, G. B., 3588
 Threlkeld, J. O., 3591
 Tokiwa, F., 3437
 Tombalakian, A. S., 3711
 Touro, F. J., 3528, 3531, 3534
 Trachtman, M., 3382
 Turkevich, J., 3509
 Walsh, R., 3751
 Walter, E. R., 3738
 Wehman, T. C., 3688
 Weiss, J. J., 3654
 White, M. L., 3432
 Wiewiorowski, T. K., 3528, 3531, 3534, 3733
 Yamashina, T., 3572
 Yates, D. J. C., 3693
 Zmbov, K. F., 3379
 Zwolinski, B. J., 3498

contents Nos. 12 1972

THE JOURNAL OF PHYSICAL CHEMISTRY

Registered in U. S. Patent Office © Copyright, 1966, by the American Chemical Society

VOLUME 70, NUMBER 9 SEPTEMBER 15, 1966

Energy Distribution of Photochemically Generated *t*-Pentoxy Radicals

by Dennis Durant and G. R. McMillan

Department of Chemistry, Western Reserve University, Cleveland, Ohio 44106 (Received May 9, 1966)

Previous studies on excited alkoxy radicals formed in photochemical processes were extended to the *t*-pentoxy species, which is well known to decompose by two parallel paths as shown in eq 1 and 2. The ratio of rate constants k_1/k_2 was estimated to be 104 at 114° from experiments on pyrolysis of *t*-pentyl nitrite. For radicals formed by photolysis of this compound, k_1/k_2 depends strongly on the absorbed wavelength but does not reach the expected limiting value of 104 at the longest wavelength which could be studied. The dependence of quantum yields at 3660 Å on pressure of an added scavenger, nitric oxide, showed that the k_1/k_2 obtained from photochemical experiments could be accounted for quantitatively by a contribution from excited radicals and a contribution identical with the ratio for unexcited radicals, obtained from pyrolysis experiments. These results provide limited justification for the "α method" often used in kinetic treatment of excited radical effects. Quantum-yield measurements at high pressures of added nitric oxide suggest preferential removal of excited radicals of lower energy and disclose a broad energy distribution of the excited radicals.

Introduction

A well-known complication in interpretation of photodecompositions is the formation of excited radicals in the primary process. To allow quantitative treatment in cases where the excitation leads to an abnormally high decomposition rate, it is often proposed that a fraction, α , of the radicals are excited and may only decompose, while the remainder are at thermal equilibrium but may or may not decompose. The usual kinetic arguments then yield information about the unexcited radicals.

Such a simple energy distribution, wherein it is assumed the radicals are either excited or strictly unexcited, is peculiar if the excitation of importance is

vibrational, as has been shown in the case of *t*-butoxy radicals in photolysis of *t*-butyl nitrite.¹ In most cases, it is not possible to decide if the unexcited radicals are truly at thermal equilibrium, a most important point if the results are to be used in discussion of other systems.

We have now studied the *t*-pentoxy radicals formed in photolysis of *t*-pentyl nitrite.² This radical decomposes by two paths. Measurement of the relative rates along these paths should give information about

(1) G. R. McMillan, *J. Am. Chem. Soc.*, **84**, 4007 (1962).

(2) P. Tarte, *Bull. Soc. Roy. Sci. Liege*, **22**, 226 (1953); B. G. Gowenlock and J. Trotman, *J. Chem. Soc.*, 4190 (1955).

the energy distribution of the radicals undergoing decomposition.

Experimental Section

t-Pentyl nitrite was prepared by reaction of *t*-pentyl alcohol with nitrous acid. The reaction mixture was fractionated and the product stored over mercury and K_2CO_3 in a cold, dark place. The last trace of acetone could not be removed from the compound, so conversion was kept above 1% in most experiments. Ethyl-*t*-pentyl peroxide was prepared as described previously.³ All pyrolyses and photolyses were carried out in a quartz vessel of diameter 50 cm and volume 240 cm³. The rate of thermal decomposition of the nitrite was measured both photometrically and by product analysis. A Hanovia Type A 550-w mercury arc was used in all illuminations. The desired wavelengths were isolated using filters. For 2537 and 3130 Å, the filters were those used in earlier work.¹ A 5-mm thickness of Corning 5860 was used for 3660 Å. This glass transmits some light at 3340 Å, but the nitrite absorbs very weakly at this wavelength. For 4047 Å, a solution of 4 M $Cu(NO_3)_2$ in water, 1.5-cm optical path, excluded $\lambda < 3750$ Å. The upper limit of absorption by the nitrite limited absorption to $\lambda > 4047$ Å. Quantum yields were measured at 3660 Å using the potassium ferrioxalate actinometer. The light beam was monitored with a G. E. 935 photocell and pen recorder so the intensity could be integrated over the course of an illumination.

Results

t-Pentyl nitrite at initial pressure 26 mm was pyrolyzed to conversions of about 20% over a range of temperature 157–183°. The yield ratio $Y_{CH_3COCH_3}/Y_{CH_3COC_2H_5}$ was 160 ± 4 in five experiments. Addition of small amounts of nitric oxide resulted in a linear decrease in the rate of acetone formation at $176 \pm 1^\circ$. At an initial pressure of 20 mm, the rate fell to one-third that obtained in the absence of added nitric oxide. $Y_{CH_3COCH_3}/Y_{CH_3COC_2H_5}$ fell to a constant value over a range of initial pressures (5–26 mm) of nitric oxide. In eight experiments, mixtures of *t*-pentyl nitrite (26 mm) and nitric oxide (14 mm) were pyrolyzed at temperatures 154–182°. $Y_{CH_3COCH_3}/Y_{CH_3COC_2H_5}$ was 104 ± 2 , not observably dependent on temperature. Ethyl-*t*-pentyl peroxide vapor (15 mm) was pyrolyzed at 114°. Addition of nitric oxide to an initial pressure of 75 mm reduced the acetone yield in the pyrolysis to <8% of that found in the absence of nitric oxide.

Table I summarizes the quantum yield ratios $\Phi_{CH_3COCH_3}/\Phi_{CH_3COC_2H_5}$ at different wavelengths meas-

ured in the photolysis of *t*-pentyl nitrite in the presence of nitric oxide. Only at 3660 Å is the ratio dependent on nitric oxide pressure in the ranges indicated. Constant absorbed intensity was not maintained at different wavelengths. By overlapping the range of conversion studied at various wavelengths, a total range of 6–55% was covered. The quantum yield ratio did not depend on extent of conversion. In a few experiments, the incident wavelength was 4047 Å. The quantum yield ratio was slightly higher than that at 3660 Å over the same range of nitric oxide pressure. Because of the prolonged exposures necessary to obtain even small conversion when the 4047-Å filter was used, we are not certain what wavelengths are actually responsible for the photolysis.

Table I: $\Phi_{CH_3COCH_3}/\Phi_{CH_3COC_2H_5}$ in the Photolysis of *t*-Pentyl Nitrite^a

Pressure of NO, mm	Wavelength, Å	$\Phi_{CH_3COCH_3}/\Phi_{CH_3COC_2H_5}$
0–85	2537	6.8
20–85	3130	11.3
26–105	3660	42–33 ^b

^a Pressure of *t*-pentyl nitrite = 26 mm; 114°. ^b Weak dependence of the ratio on NO pressure.

Figure 1 shows $\Phi_{CH_3COCH_3} + \Phi_{CH_3COC_2H_5}$ measured at 3660 Å at different nitric oxide pressures and temperatures. Figure 2 shows $\Phi_{CH_3COCH_3}/\Phi_{CH_3COC_2H_5}$ at the same wavelength. The conversion was kept constant at about 6%. A few experiments in the absence of added nitric oxide showed that the total ketone quantum yield increased as the per cent conversion decreased. A value of unity was measured at 3% conversion.

Discussion

*Relative Rates of the Decomposition Paths of the Unexcited *t*-Pentoxy Radical.* The *t*-pentoxy radical decomposes by two parallel paths



The relative rates are not known precisely, but studies in the liquid phase and fragmentary results from the gas phase show k_1/k_2 to be high.^{3,4} Both reactions are

(3) G. R. McMillan, *J. Am. Chem. Soc.*, **84**, 2514 (1962).

(4) J. K. Kochi, *ibid.*, **84**, 1193 (1962).

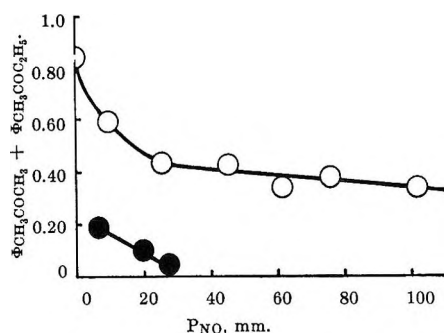


Figure 1. Dependence of quantum yield sum on nitric oxide pressure at 25 (●) and 114° (○).

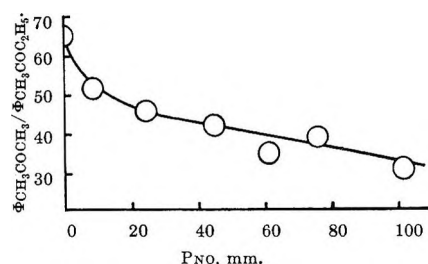
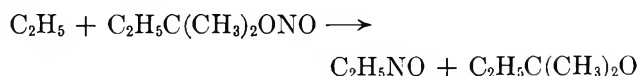


Figure 2. Dependence of quantum yield ratio on nitric oxide pressure at 114°.

slightly endothermic, and $\Delta H^\circ_1 - \Delta H^\circ_2 \sim -0.5$ kcal.^{5,6}

The initial step in the thermolysis of alkyl nitrites is considered to be scission of the RO-NO bond.⁷ Thermolysis of *t*-pentyl nitrite produced acetone and methyl ethyl ketone in a ratio 160:1. Upon addition of nitric oxide to an initial pressure of 5 mm, the rate of decomposition of nitrite and the yield ratio $Y_{\text{CH}_3\text{COCH}_3} / Y_{\text{CH}_3\text{COC}_2\text{H}_5}$ decreased. As the initial nitric oxide pressure was increased, the decomposition rate decreased further, but the yield ratio remained constant. These results suggest that the ketones are formed chiefly by (1) and (2) when nitric oxide is present in the system, but some additional step forms acetone when nitric oxide is not added. The decrease in rate due to nitric oxide is explained by direct scavenging of *t*-pentoxy and suppression, by scavenging of ethyl, of chain regeneration of *t*-pentoxy.^{7,8}



The ratio $Y_{\text{CH}_3\text{COCH}_3} / Y_{\text{CH}_3\text{COC}_2\text{H}_5}$ in the inhibited pyrolysis is thus associated with k_{1u} / k_{2u} , the subscripts signifying the unexcited, thermally equilibrated radicals expected in thermal decompositions. The value k_{1u} / k_{2u} was relatively insensitive to temperature over the range 154–182° so k_{1u} / k_{2u} may be taken as approxi-

mately 104 at 114°, the temperature of the photochemical experiments. Extensive work in solution on the β scission of *t*-alkoxy radicals leads to expectation of a considerable activation energy difference between steps 1 and 2.^{9,10} A value $k_{1u} / k_{2u} = 16$ at 114° was obtained previously from results on pyrolysis of ethyl-*t*-pentyl peroxide in the gas phase.³ We have repeated this work with the same results. We thus have two estimates of k_{1u} / k_{2u} , 16 and 104, with no satisfactory way of choosing between them, since no really detailed studies of the systems leading to the values have been made. The value 104 is consistent with the photochemical results and will be assumed correct.

*Ketone Formation in the Nitric Oxide Inhibited Photolysis of *t*-Pentyl Nitrite.* The most important primary process following absorption by simple alkyl nitrites in both the banded (λ 3200–4000 Å) and structureless (λ < 3000 Å) regions is believed to be decomposition to form alkoxy radicals and nitric oxide. For *t*-butyl nitrite, this is probably the sole primary process, with a primary quantum yield of one in both spectral regions.^{1,11} The ultraviolet absorption spectrum of *t*-pentyl nitrite is identical with that of the *t*-butyl compound;¹² furthermore, they are structurally similar in that they are both almost entirely the *trans* form.¹³ We therefore assume that the primary process in *t*-pentyl nitrite forms *t*-pentoxy radical and nitric oxide in unit primary yield.

The ratios $\Phi_{\text{CH}_3\text{COCH}_3} / \Phi_{\text{CH}_3\text{COC}_2\text{H}_5}$ observed in photolysis of *t*-pentyl nitrite–nitric oxide mixtures are much smaller than k_{1u} / k_{2u} , proving that the ketones are not entirely formed by decomposition of thermally equilibrated *t*-pentoxy radicals. The fact that the quantum yields are high (Figure 1 and ref 14) in the presence of large amounts of an efficient scavenger, nitric oxide, suggests that decomposition of equilibrated radicals makes negligible contribution to ketone formation under these conditions.

(5) P. Gray and A. Williams, *Chem. Rev.*, **59**, 239 (1959).

(6) Thermochemical data from J. G. Calvert and J. N. Pitts, Jr., "Photochemistry," John Wiley and Sons, Inc., New York, N. Y., 1965, Appendix, p 820.

(7) A recent study is that of J. M. Ferguson and L. Phillips, *J. Chem. Soc.*, 4416 (1965).

(8) P. Gray, *Chem. Ind. (London)*, 120 (1960).

(9) C. Walling and A. Padwa, *J. Am. Chem. Soc.*, **85**, 1593 (1963).

(10) J. D. Bacha and J. K. Kochi, *J. Org. Chem.*, **30**, 3272 (1965).

(11) G. R. McMillan, *J. Phys. Chem.*, **67**, 931 (1963).

(12) H. E. Ungnade and R. A. Smiley, *J. Org. Chem.*, **21**, 993 (1956).

(13) P. Gray and M. J. Pearson, *Trans. Faraday Soc.*, **59**, 347 (1963).

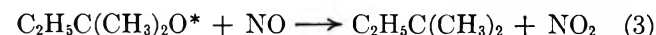
(14) Quantum yield measurements carried out at Celanese Chemical Co. showed $\Phi_{\text{CH}_3\text{COCH}_3} + \Phi_{\text{CH}_3\text{COC}_2\text{H}_5} = 1$ at 2537 Å and 25°; see ref 6, p 484.

The ratios $\Phi_{\text{CH}_3\text{COCH}_3}/\Phi_{\text{CH}_3\text{COC}_2\text{H}_5}$ are consistent with either a decomposition of excited radicals or a primary photoprocess in which the ketones are formed as finished products through scission of more than one bond. The apparent increased randomization in the bond breaking, that is, the increased relative rate of the more endothermic process following absorption of shorter wavelengths, is consistent with either view. On the basis of the previous studies, we accept the excited radical explanation and identify the $\Phi_{\text{CH}_3\text{COCH}_3}/\Phi_{\text{CH}_3\text{COC}_2\text{H}_5}$ ratios in Table I with k_{1e}/k_{2e} .

As the energy of the light quantum absorbed by the nitrite decreases, a vibrationally excited *t*-pentoxy should approach in behavior the unexcited radical, so that $k_{1e}/k_{2e} \rightarrow k_{1u}/k_{2u}$. In fact, even at the longest wavelength that could be studied, k_{1e}/k_{2e} is far from this limit. However, even at 3660 Å, the energy of the quantum is 40 kcal in excess of the bond-dissociation energy. Knight and Gunning found that an excess of energy of ~10 kcal is sufficient to produce excited *t*-butoxy radicals.¹⁵

A possible complication in these systems is the presence of nitrogen dioxide, formed in the chain conversion of NO to NO₂ and N₂, catalyzed by nitrosoalkanes. In the photolysis of *t*-butyl nitrite in the presence of nitric oxide at high pressures, Christie, Gilbert, and Voisey¹⁶ observed quantum yields of NO₂ up to 110. The reaction which forms NO₂ is second order with respect to nitric oxide. In view of the weak dependence on nitric oxide pressure of quantum yields and quantum yield ratios observed under most conditions in the present study, the presence of NO₂ probably has little effect on our conclusions.

Energy Distribution of t-Pentoxy Radicals Formed in Photolysis of t-Pentyl Nitrite at 3660 Å. Figure 1 shows that the quantum yield sum $\Phi_{\text{CH}_3\text{COCH}_3} + \Phi_{\text{CH}_3\text{COC}_2\text{H}_5}$ at first decreases rapidly, then slowly, as nitric oxide is added. The rapid decrease is due to efficient scavenging of unexcited *t*-pentoxy radicals by nitric oxide. At pressures of nitric oxide exceeding 35 mm, only excited radicals decompose. The slight decrease in ketone yield at the higher pressures may be due to deactivation or possibly some reaction such as (3), which would not lead to ketones.



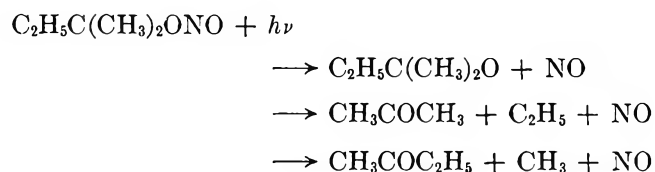
The dependence of the quantum yield ratio $\Phi_{\text{CH}_3\text{COCH}_3}/\Phi_{\text{CH}_3\text{COC}_2\text{H}_5}$ on nitric oxide pressure has the same form as the dependence of the quantum yield sum. Efficient scavenging of unexcited *t*-pentoxy lowers the ratio by removing those radicals for which k_1/k_2 is large. The high pressure, linear portions of the two curves can be extrapolated to give the contri-

tribution of the excited radicals to the lower pressure portions. It may then be calculated that $\Phi_{\text{CH}_3\text{COCH}_3}/\Phi_{\text{CH}_3\text{COC}_2\text{H}_5}$ comprises a contribution from excited radicals and a residual contribution with $\Phi_{\text{CH}_3\text{COCH}_3}/\Phi_{\text{CH}_3\text{COC}_2\text{H}_5} = 110$. The near equality with k_{1u}/k_{2u} confirms the bimodal energy distribution; the radicals are either excited or unexcited, with the unexcited radicals being identical with those formed in strictly thermal reactions.

The slow, linear decrease of $\Phi_{\text{CH}_3\text{COCH}_3}/\Phi_{\text{CH}_3\text{COC}_2\text{H}_5}$ at higher nitric oxide pressures reflects a decrease in k_{1e}/k_{2e} . This is accounted for by step 3 or any other process which would preferentially remove the less energetic excited radicals. Thus these results disclose a considerable breadth in the energy distribution of the excited radicals.

These results provide some justification for the use of the classical α method in systems in which excited alkoxy radicals are important, and thus perhaps give credence to certain rate constant ratios derived for unexcited radicals in such systems.¹⁷ The establishment of a bimodal distribution can be rationalized in several ways, but speculation is perhaps unjustified in a case where it is impossible to decide whether the phenomenon arises in or subsequent to the primary process.

Two alternative mechanisms deserve comment. Most of the kinetic results in this and other systems in which excited alkoxy radicals are postulated can be accounted for by primary processes which in the present instance would be



This mechanism cannot explain the pressure dependence of $\Phi_{\text{CH}_3\text{COCH}_3}/\Phi_{\text{CH}_3\text{COC}_2\text{H}_5}$ at high nitric oxide pressures, provided the excited nitrite molecule formed by light absorption has a lifetime too short to permit collisions at these pressures. A very short lifetime is consistent with the absence of rotational structure in the electronic spectra of nitrous acid and its alkyl esters,¹⁸ and with the high quantum yields observed in

(15) A. R. Knight and H. E. Gunning, *Can. J. Chem.*, **41**, 2849 (1963).

(16) M. I. Christie, C. Gilbert, and M. A. Voisey, *J. Chem. Soc.*, 3147 (1964).

(17) M. H. J. Wijnen, *J. Am. Chem. Soc.*, **82**, 1847 (1960); G. R. McMillan, *ibid.*, **83**, 3018 (1961).

(18) G. W. King and D. Moule, *Can. J. Chem.*, **40**, 2057 (1962). H. W. Thompson and C. H. Purkis, *Trans. Faraday Soc.*, **32**, 1466 (1936).

photolysis of alkyl nitrites in the gas and liquid phases, even at low temperature.^{1,11,19} A second possibility is that the excited alkoxy radicals in alkyl nitrite photolysis are in fact not alkoxy radicals at all, but α -hydroxyalkyls formed either through isomerization of alkoxy or perhaps in the primary process. The (excited?) α -hydroxyalkyl might then decompose into the *enol* form of the ketone plus an alkyl radical. Scavengers would be ineffective if the decomposition were fast enough. Such a mechanism is consistent with most results from these systems, but not with *in situ* infrared studies²⁰ of photolysis of *t*-butyl nitrite, wherein acetone is largely formed from excited alkoxy radicals. In another study in the same apparatus,

a half-life of about 2 min was observed for enol-acetone.²¹ Thus, an enol intermediate would lead to an induction period for keto-acetone in the *t*-butyl nitrite photolysis. No induction period is observed.²⁰

Acknowledgment. Grateful acknowledgment is made of partial support of this work by the Division of Air Pollution, Bureau of State Services, Public Health Service.

(19) P. Kabasakalian and E. R. Townley, *J. Am. Chem. Soc.*, **84**, 2711 (1962).

(20) G. R. McMillan, J. G. Calvert, and S. S. Thomas, *J. Phys. Chem.*, **68**, 116 (1964).

(21) G. R. McMillan, J. G. Calvert, and J. N. Pitts, Jr., *J. Am. Chem. Soc.*, **86**, 3602 (1964).

The Steady-State Compliance of Dilute Polymer Solutions

by Larry A. Holmes, Kazuhiko Ninomiya,¹ and John D. Ferry

Department of Chemistry, University of Wisconsin, Madison, Wisconsin 53706 (Received September 20, 1965)

In extremely dilute polymer solutions, the steady-state compliance J_e should be directly proportional to concentration; with increasing concentration, it should pass through a maximum and become inversely proportional to concentration. Experimental determinations from low-frequency dynamic mechanical measurements on solutions of a polystyrene ($M = 267,000$) in two chlorinated biphenyls, over a wide range of concentrations, confirm the presence of a maximum. The concentration dependence of J_e in the neighborhood of the maximum is calculated from the theories of Rouse and Zimm and a phenomenological theory of Ninomiya and Ferry. The latter conforms best to the shape observed experimentally; it predicts the maximum to be at a concentration of the order of the reciprocal of the intrinsic viscosity. With increasing concentration, the magnitude of J_e or of the low-frequency storage modulus shifts gradually from the Zimm prediction to the Rouse prediction; from this behavior, the concentration dependence of the hydrodynamic interaction parameter h can be obtained, and it agrees with previous conclusions from the form of the frequency dependence of dynamic properties. Values of J_e are calculated from the phenomenological theory and compared with experimental results on a number of solutions of polystyrene and polyisobutylene. Over a 200-fold range of J_e , the calculated values agree fairly well but are somewhat too small, a discrepancy which can be partly attributed to a slight degree of molecular weight heterogeneity.

Introduction

The steady-state compliance, J_e , is an important property of a viscoelastic material, being a measure of the stored energy in steady flow under small stresses. Its product with the shear stress is sometimes called the recoverable shear.² Besides its role in linear viscoelastic behavior, it has added importance through its close relation to normal stress phenomena.³ In concentrated macromolecular solutions of undiluted polymers, J_e can be obtained from measurements of creep or indirectly from stress relaxation,⁴ but these methods are not readily applicable to dilute solutions and the latter have therefore received little attention. However, quite dilute solutions can be subjected to sinusoidally varying deformations⁵ to measure the storage and loss components of the shear modulus, G' and G'' . At low frequencies, G'' is proportional to the circular frequency ω and G' is proportional to ω^2 . Thus, at very low frequencies, $G' \ll G''$. Since J_e is the low-frequency limit⁶ of $G'/(G'^2 + G''^2) = G'/G''^2$, it follows that

$$J_e = A\omega^2/(\omega\eta)^2 = A/\eta^2 \quad (1)$$

where A is the low-frequency limit⁷ of G'/ω^2 , and η , the steady-flow viscosity, is the corresponding limit of G''/ω . An alternative route to eq 1 is given in ref 3. Values of J_e obtained in this manner are reported

- (1) On leave from Japan Synthetic Rubber Co., Yokkaichi, Japan.
- (2) A. S. Lodge, "Elastic Liquids," Academic Press, New York, N. Y., 1964.
- (3) B. D. Coleman and H. Markovitz, *J. Appl. Phys.*, **35**, 1 (1964); H. Markovitz, *Proc. 4th Intern. Congr. Rheology*, **1**, 189 (1965).
- (4) A. V. Tobolsky, R. Schaffhauser, and R. Böhme, *J. Polymer Sci.* **B2**, 103 (1964).
- (5) M. H. Birnboim and J. D. Ferry, *J. Appl. Phys.*, **32**, 2305 (1961).
- (6) J. D. Ferry, "Viscoelastic Properties of Polymers," John Wiley and Sons, Inc., New York, N. Y., 1961, p 13.
- (7) Two statements in ref 6 should be corrected here. On p 172, it was suggested that for certain relaxation time distributions a limiting value of A may never be reached at low frequencies. Actually, it can be proved that for any distribution of finite times, G' will be proportional to ω^2 at sufficiently low frequencies—though this might be in a region where G' is too small to detect experimentally. On p 31, doubt was expressed that a limiting value of A had ever been obtained experimentally. Since then, however, many such measurements have been made.

here for a series of solutions of a polystyrene with sharp molecular weight distribution as well as a number of other dilute polymer solutions whose viscoelastic properties have been described previously.

Theory

The behavior of J_e in polymeric blends of different molecular weight species has evoked considerable interest since the original observations of Van Holde and Williams⁸ and Leaderman⁹ that J_e is strongly influenced by molecular weight distribution. If the molecular weight of component 1 in a binary mixture is much less than that of component 2, J_e goes through a large maximum as a function of composition where the proportion of component 2 is quite small. The location of this maximum is given by a phenomenological theory presented earlier¹⁰ as

$$v_2(\text{max}) = 1/N_{21} \quad (2a)$$

$$J_e(\text{max}) = J_{e2}N_{21}/4 \quad (2b)$$

where v_2 is the volume fraction of component 2, J_{e2} is its steady-state compliance in the pure state, and N_{21} is a parameter characteristic of the theory whose physical significance is the ratio of the energy dissipations in flow, per unit volume, of the two components. Equations 2 hold when $N_{21} \gg 1$.

A dilute polymer solution might be expected to resemble a binary polymeric blend with one component of very low molecular weight, so that at extremely low concentrations J_e would increase with concentration but would soon pass through a maximum. At moderate to high concentrations, J_e would be expected to be inversely proportional to polymer concentration,¹¹ and this relation has been confirmed in the range from 50 to 100% polymer.^{12,13} We develop here for dilute solutions the predictions of molecular theories and of the phenomenological theory described above, and compare them with experimental data, mostly on polystyrene.

Predictions of Molecular Theories. In the theories of Rouse,¹⁴ Zimm,¹⁵ and Tschoegl,¹⁶ the coefficient A is given by

$$A = (cRT/M)\tau_1^2S' \quad (3a)$$

$$\tau_1 = (\eta - v_1\eta_s)/(cRT/M)S \quad (3b)$$

$$S' = \sum(\tau_k/\tau_1)^2 \quad (3c)$$

$$S = \sum(\tau_k/\tau_1) \quad (3d)$$

where c is the polymer concentration in grams per milliliter, M is the polymer molecular weight, η_s is the solvent viscosity, and v_1 is its volume fraction in the solution; τ_1 is the terminal relaxation time and τ_k are the

other characteristic relaxation times specified by the respective theories. Although these theories are subject to modification to take into account a finite solute contribution to dynamic viscosity at very high frequencies,¹⁷⁻¹⁹ Peterlin's recent formulation²⁰ of this feature shows that at vanishing frequency the original equations are unaffected. (Otherwise, they would fail to reduce properly to the respective treatments of Debye and Kirkwood-Riseman for steady-state flow.) Thus eq 3 may be combined with eq 1 to obtain after rearrangement

$$J_e = (M/cRT)(1 - v_1/\eta_r)^2(S'/S^2) \quad (4)$$

where η_r , the relative viscosity, is η/η_s . For the Rouse theory, $S'/S^2 = 0.400$; for the Zimm, it is 0.206; for the intermediate cases of the Tschoegl theory, intermediate values may be obtained. At high concentrations, this reduces to $J_e = (M/cRT)(S'/S^2)$, as commonly used with the expectation that the Rouse value of S'/S^2 is applicable.¹¹⁻¹³ At extremely low concentrations, where $\eta_r = 1 + [\eta]c$, $[\eta]$ being the intrinsic viscosity in milliliters per gram, it reduces to

$$J_e = (M/RT)[\eta]^2c(S'/S^2) \quad (5)$$

so that J_e is directly proportional to c . For extremely low concentrations, the Zimm value of S'/S^2 should be applicable.²¹

Prediction of Phenomenological Theory. For a binary polymeric blend, the composition dependence of J_e is given¹⁰ by

$$J_e = \frac{J_{e1}v_1 + N_{21}^2J_{e2}v_2}{[1 + v_2(N_{21} - 1)]^2} \quad (6)$$

If component 1 is a solvent of low molecular weight, J_{e1} can be neglected, and $N_{21} \gg 1$, so this becomes

(8) K. E. Van Holde and J. W. Williams, *J. Polymer Sci.*, **11**, 243 (1953).

(9) H. Leaderman, R. G. Smith, and L. C. Williams, *ibid.*, **36**, 233 (1959).

(10) K. Ninomiya and J. D. Ferry, *J. Colloid Sci.*, **18**, 421 (1963).

(11) Reference 6, p 172.

(12) K. Ninomiya, J. R. Richards, and J. D. Ferry, *J. Phys. Chem.*, **67**, 327 (1963).

(13) Y. Öyanagi and J. D. Ferry, *J. Colloid Sci.*, **21**, 547 (1966).

(14) P. E. Rouse, Jr., *J. Chem. Phys.*, **21**, 1272 (1953).

(15) B. H. Zimm, *ibid.*, **24**, 269 (1956).

(16) N. W. Tschoegl, *ibid.*, **39**, 149 (1963); **40**, 473 (1964).

(17) J. Lamb and A. J. Matheson, *Proc. Roy. Soc. (London)*, **A281**, 207 (1964).

(18) W. Philippoff, *Trans. Soc. Rheology*, **8**, 117 (1964).

(19) J. D. Ferry, L. A. Holmes, J. Lamb, and A. J. Matheson, *J. Phys. Chem.*, **70**, 1685 (1966).

(20) A. Peterlin, *J. Polymer Sci.*, in press.

(21) J. E. Frederick, N. W. Tschoegl, and J. D. Ferry, *J. Phys. Chem.*, **68**, 1974 (1964).

$$J_e = N_{21}^2 J_{e2} v_2 / (1 + v_2 N_{21})^2 \quad (7)$$

At very low concentrations of component 2 (polymer), this reduces to

$$J_e = N_{21}^2 J_{e2} v_2 \quad (8)$$

There are several possible ways of estimating N_{21} for specific systems,^{10,22} but we shall do so by identifying eq 8 and 5. We assume that for the undiluted polymer $J_{e2} = (M/\rho_2 RT)(S'/S^2)_R$, where ρ_2 is the polymer density and the subscript R refers to Rouse; that in eq 5 the Zimm value of S'/S^2 is applicable; and we note that $c = v_2 \rho_2$. It follows that

$$N_{21} = [\eta] \rho_2 [(S'/S^2)_Z / (S'/S^2)_R]^{1/2} \cong [\eta] \rho_2 / \sqrt{2} \quad (9)$$

By a different derivation, involving the concentration dependence of the viscosity,²³ N_{21} can be identified with $[\eta] \rho_2 \sqrt{1 - 2k'}$, where k' is the Huggins constant. This is equivalent to eq 9 if $k' = 1/4$, which is in the range observed for good solvents.

The identification of N_{21} as closely related to $[\eta]$ is of course consistent with its interpretation¹⁰ as the ratio of flow energy dissipations, per unit volume, of solute and solvent. It cannot be expected that N_{21} will remain constant over a wide range of concentrations,^{10,22,23} but the above value deduced for extremely dilute solutions may be used tentatively in the moderately dilute range.

Experimental Section

Low-frequency measurements of the storage and loss shear moduli were made on 14 solutions of a polystyrene with sharp molecular weight distribution, S-108, generously provided by Dr. H. W. McCormick of the Dow Chemical Co., ranging in concentration from 0.75 to 10 wt %. The weight-average molecular weight, M_w , was 267,000; $M_w/M_n = 1.08$. The solvents were two chlorinated biphenyls, with the following viscosities (η) and densities (ρ) at 25°: A1248, $\eta = 2.62$ poises, $\rho = 1.452$ g/ml; A1232, $\eta = 0.143$ poise, $\rho = 1.269$ g/ml. Measurements were made on each solution at a single temperature, chosen between 0 and 35° to achieve the appropriate region of reduced frequency where G' and G'' are proportional to ω^2 and ω , respectively.

The Birnboim-Ferry apparatus⁵ with modifications previously described^{24,25} was used to cover the frequency range from 0.06 to 400 cps. Most measurements in recent years have been made with a combination of cell and driving rod with a gap of 0.0617 cm and a cell constant⁵ $A_c = 4846$ cm. (Previously⁵ denoted A , this constant is designated A_c here to avoid confusion with the coefficient used in eq 1.) For meas-

urements on solutions with lower viscosities, an alternative rod was fabricated which gives a gap of 0.0460 cm and $A_c = 22,540$ cm. It was necessary to determine the latter by calibration with Aroclor of known viscosity rather than from the apparatus dimensions, since calculation from the latter becomes numerically uncertain when the gap is small. The constants⁵ β and M are also changed somewhat. (A wide-gap combination with $A_c = 454.7$ is also available for solutions of much higher viscosity.)

Results

The low-frequency behavior is fully described by the two quantities η and A , which are given in Table I together with values for three other solutions of the same polymer S-108 previously studied.²⁴ The steady-state compliance J_e was calculated from eq 1 and then reduced to 25° (if the measurement was made at another temperature) by the equation $J_e(25^\circ) = J_e T \rho / T_0 \rho_0$, where $T_0 = 298^\circ\text{K}$ and ρ and ρ_0 are the solution densities at T and T_0 ; this reduction is a minor correction.

Log J_e is listed in Table I and plotted against concentration in Figure 1. The units are cm²/dyne. The

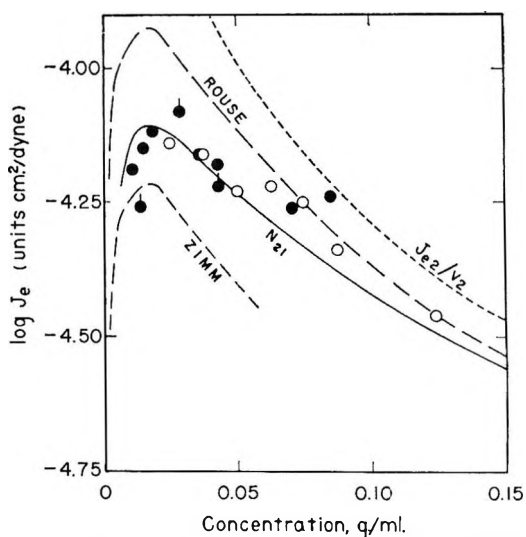


Figure 1. Log J_e for solutions of polystyrene S-108, plotted against concentration in g/ml (from Table I). Black circles, solutions in Aroclor 1248; open circles, in Aroclor 1232. Circles with pips from ref 24. Rouse and Zimm curves, from eq 4; N_{21} curve from eq 7 and 9.

(22) K. Ninomiya, J. D. Ferry, and Y. Oyanagi, *J. Phys. Chem.*, **67**, 2297 (1963).

(23) K. Ninomiya and J. D. Ferry, Abstracts, 12th Symposium on Polymers, Nagoya, Japan, 1963, p 178.

(24) R. B. DeMallie, Jr., M. H. Birnboim, J. E. Frederick, N. W. Tschoegl, and J. D. Ferry, *J. Phys. Chem.*, **66**, 536 (1962).

(25) N. W. Tschoegl and J. D. Ferry, *Kolloid-Z.*, **189**, 37 (1963).

Table I: Low-Frequency Parameters for Solutions of Polystyrene S-108, $M_w = 267,000$

Solvent	$c \times 10^2$, g/ml	Temp, °C	η , poises	Log A	Log J_e red. to 25°, cm ² /dyne	h from data of Figure 2
A1248	1.13	25.0	5.96	-2.64	-4.19	100
	1.44 ^a	25.0	6.47	-2.64	-4.26	...
	1.53	25.0	7.36	-2.41	-4.15	12
	1.84	25.0	8.88	-2.22	-4.12	6.3
	2.86 ^a	25.0	15.5	-1.70	-4.08	1.3
	3.60	25.0	20.8	-1.52	-4.16	1.6
	4.31	25.0	31.4	-1.18	-4.18	0.8
	4.30 ^a	25.0	28.8	-1.30	-4.22	3
	7.13	35.0	27.9	-1.38	-4.26	0
8.52	35.0	41.7	-1.02	-4.24	0	
A1232	2.53	0.6	4.51	-2.80	-4.14	1.3
	3.76	0.0	8.79	-2.22	-4.16	1.3
	5.04	0.0	15.19	-1.83	-4.23	1.6
	6.28	0.2	24.8	-1.39	-4.22	0
	7.50	0.0	39.7	-1.01	-4.25	0
	8.77	10.0	22.3	-1.60	-4.34	0
	12.40	0.1	241	0.36	-4.44	0

^a From ref 24; solvent viscosity 2.2 poises.

two solvents give closely similar results and the expected maximum is observed. The predictions of the Rouse and Zimm theories from eq 4 (using measured values of η_r) and the phenomenological theory from eq 7 are also plotted in Figure 1. For the latter calculation, J_{e2} was taken from a direct measurement from creep studies of the undiluted polymer at elevated temperatures,²⁶ reduced to 25°: $\log J_{e2} = -5.31$. Also included is the curve for J_{e2}/v_2 , often used as an estimate of J_e in very concentrated solutions.¹¹⁻¹³

The theories predict the maximum at about the observed location on the concentration scale. In magnitude, J_e appears to be approaching the Zimm prediction at low concentrations but closely conforms to the Rouse prediction at higher concentration; a similar transition from Zimm-like to Rouse-like behavior with increasing concentration is observed with respect to the frequency dependence of dynamic viscoelastic properties.²¹ In the neighborhood of the maximum, the concentration dependence is best described by the phenomenological theory.

Discussion

Magnitude of Low-Frequency Ratio G'/ω^2 as a Measure of Hydrodynamic Interaction. From eq 3, it is evident that

$$Ac/(\eta - v_1\eta_s)^2 = (M/RT)(S'/S^2) \quad (10)$$

which each theory specifies as a constant. This quantity is plotted against concentration in Figure 2 and is

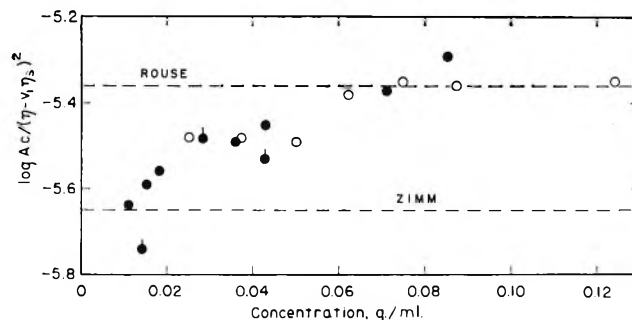


Figure 2. $\log (G'/\omega^2)_{\omega \rightarrow 0} c / (\eta - v_1\eta_s)^2$ plotted against concentration, for data of Table I. Key to points same as Figure 1.

seen to approach the Zimm value at low concentrations and the Rouse value at high concentrations.

The quantity S'/S^2 is denoted J_{eR} by Tschoegl,²⁷ who points out that it is a potential source of information for the hydrodynamic interaction parameter h which characterizes the transition from Zimm-like to Rouse-like behavior. For such an evaluation, we take Tschoegl's other parameter¹⁶ ϵ as zero in the expectation that in all but the most dilute solutions the coil configurations will be gaussian. Values of h calculated in this manner from the data of Figure 2, using Tschoegl's tables¹⁶ of S and S' , are also listed in Table

(26) G. Yasuda, E. Maekawa, T. Homma, and K. Ninomiya, *Gomu-Kyokaiishi*, 39, 177 (1966).

(27) N. W. Tschoegl, *J. Chem. Phys.*, 44, 2331 (1966).

Table II: Observed and Calculated Values of $\log J_e$ in Dilute Polymer Solutions (Temperature 25°, Units cm^2/dyne)

Sample	Mol wt $\times 10^{-3}$	Solvent	c , g/ml	$[\eta]$, ml/g	$\log J_e$, obsd	$\log J_e$, calcd ^a
Polystyrene						
S-102	82	A1248	0.0288	38.5	-4.94	-5.05
			0.0571		-4.76	-5.06
S-111	239		0.0288	78 ^b	-4.08	-4.29
			0.0571		-4.05	-4.40
S-1163	400		0.0288	100	-3.61	-4.00
			0.0568		-3.82	-4.14
MDP-1	1000	A1232	0.0127	205	-2.98	-3.27
MDP-2	1700	A1248	0.0072	205	-2.86	-3.00
			0.0144		-2.82	-3.06
			0.0286		-2.95	-3.20
		A1232	0.0127	270	-2.66	-2.96
			0.0253		-2.76	-3.12
Polyisobutylene						
HM	840	Primol D	0.0088	194	-3.08	-3.33
			0.0176		-3.23	-3.42

^a From eq 11. ^b Interpolated.

I. They show an essentially monotonic decrease from very high values to zero with increasing concentration. This conclusion was reached previously²¹ from the form of the frequency dependence of dynamic properties without regard to their magnitudes; the present deduction is entirely independent, being based solely on the magnitudes, and it avoids the as yet unexplained feature of the previous curve-matching procedure that the apparent molecular weights are always somewhat too large. It is, however, restricted to polymers of sharp molecular weight distribution; a similar treatment by Tamura, *et al.*²⁸ (who denote the quantity S'/S^2 as γ), showed how polydispersity can mask the distinction between high and low h .

Approximate Estimate of J_e from Intrinsic Viscosity by Phenomenological Theory. Predictions of J_e for any solution of a polymer homogeneous with respect to molecular weight can be made easily from the phenomenological theory, provided it can be assumed that $J_{e2} = (M/\rho_2 RT)(S'/S^2)_R$. The only additional information needed is the intrinsic viscosity in the solvent concerned. In terms of c , the relation can be written

$$J_e = \frac{cM[\eta]^2}{5RT(1 + c[\eta]/\sqrt{2})^2} \quad (11)$$

Values of $\log J_e$ calculated in this manner are compared in Table II with measured values for a number of other solutions of polystyrene²¹ and polyisobutylene,²⁹ derived from previous measurements. The comparison is shown graphically in Figure 3 together with the data for the solutions of Table I. Over a 200-fold range

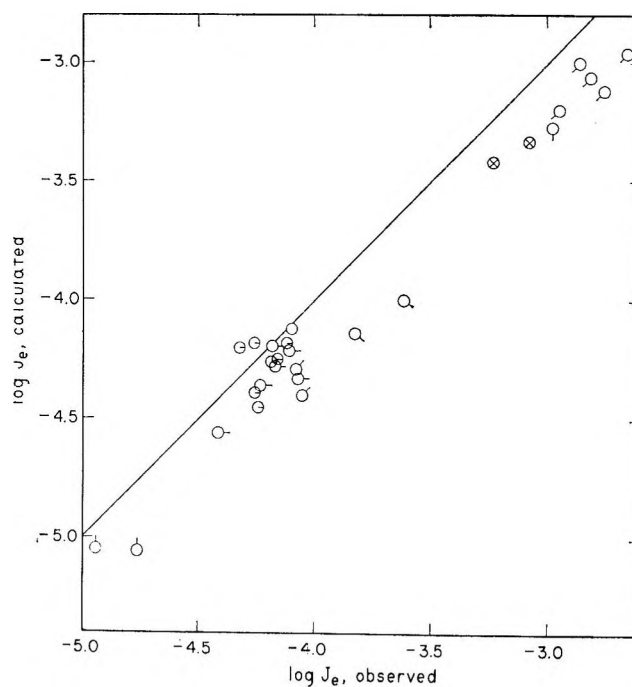


Figure 3. $\log J_e$ calculated from eq 11 plotted against observed values. Pip up, polystyrene S-102; successive 45° clockwise denote samples S-111, S-1163, MDP-2, and MDP-1. Internal pip denotes data from Table I. Crossed circles: polyisobutylene.

(28) M. Tamura, M. Kurata, K. Osaki, and K. Tanaka, *J. Phys. Chem.*, **70**, 516 (1966).

(29) N. W. Tschoegl and J. D. Ferry, *ibid.*, **68**, 867 (1964).

there is fair agreement, although most of the calculated values are somewhat too small, some by as much as a factor of 2. Some deviation in this direction is to be expected from a slight molecular weight heterogeneity, but it is doubtful whether more than a factor of about 1.3 can be attributed to this cause. The remainder can be attributed in a formal manner to an increase in N_{21} with concentration which has been neglected. However, the very simple formulation of

eq 11 is evidently useful for making estimates of J_0 in moderately dilute solutions over a considerable range of concentrations and molecular weights. In particular, eq 2 and 9 can provide an estimate of the location of the maximum.

Acknowledgment. This work was supported in part by grants from the National Science Foundation and the U. S. Public Health Service.

The Infrared Absorption Spectrum of Oxygen-18-Labeled Glycine

by I. Laulicht, S. Pinchas, D. Samuel, and I. Wasserman

The Weizmann Institute of Science, Rehovoth, Israel (Received October 26, 1965)

The infrared absorption of powdered 75 atom % ^{18}O α -glycine was measured in the 4000–400- cm^{-1} region in comparison with the absorption of the corresponding normal glycine. The assignment of the various glycine absorption bands is discussed in the light of the observed ^{18}O isotopic shifts. It is shown that the 1334–1324- cm^{-1} band attributed previously mainly to a CH_2 wagging has a pronounced C–C stretching character. The 894- cm^{-1} band of normal glycine, which was assigned to its C–C stretching, is now shown to be due probably to the CO_2^- scissoring. The 700–685- cm^{-1} band is assigned to the CO_2^- rocking while that about 502 cm^{-1} is attributed to an NH_3^+ group deformation.

The infrared absorption spectrum of glycine is of special interest since, obviously, its understanding is essential for the interpretation of the more complex spectra of peptides and proteins. This spectrum is also of importance in connection with the application of analytical infrared spectrophotometric methods to the problem of the composition and structure of various substances built up from amino acids. The infrared absorption of normal^{1,2} and variously deuterated^{1,3} glycine has therefore been investigated thoroughly along with the Raman spectrum of these substances^{2,4–6} and the infrared spectrum of ^{15}N glycine.¹ On basis of most of these measurements Suzuki, *et al.*,¹ calculated the potential energy distribution among the various elementary modes of vibration of glycine for each of its fundamental frequencies. The correctness of these calculations and the extent to which the respective

underlying assumptions hold were checked for those vibrations which affect mainly the hydrogen atoms or the nitrogen atom, by studying the effect of deuteration or ^{15}N labeling on the corresponding absorption frequencies of glycine. No such check, however, could be carried out up to now with respect to those vibrations which affect mainly the oxygen atoms.

(1) S. Suzuki, T. Shimanouchi, and M. Tsuboi, *Spectrochim. Acta*, **19**, 1195 (1963).

(2) M. Tsuboi, T. Onishi, I. Nakagawa, T. Shimanouchi, and S. Mizushima, *ibid.*, **12**, 253 (1958).

(3) K. Nakamura, *J. Chem. Soc. Japan*, **80**, 118 (1959).

(4) M. Takeda, R. E. S. Izvazzo, D. Garfinkel, I. H. Scheinberg, and J. T. Edsall, *J. Am. Chem. Soc.*, **80**, 3813 (1958).

(5) S. A. S. Ghazanfar, D. V. Myers, and J. T. Edsall, *ibid.*, **86**, 3439 (1964).

(6) K. Balasubramanian and R. S. Krishnan, *Proc. Indian Acad. Sci.*, **A59**, 115 (1964).

It was therefore interesting to measure the infrared absorption spectrum of ^{18}O -labeled glycine in comparison with that of normal glycine, in order to check the potential energy distribution calculated by Suzuki, *et al.*,¹ for the fundamental frequencies assigned by them to oxygen atoms centered normal modes of vibrations.

Such a study seems also to be of importance with respect to the possibility of applying spectrophotometric methods for the determination of ^{18}O glycine in the presence of normal glycine, as was done, *e.g.*, in the case of benzophenone.⁷

This paper thus reports the measured spectra of fine powders of 75 atom % ^{18}O -labeled and normal glycine in the 4000–400- cm^{-1} region. These powders gave very satisfactory spectra so that the use of a mulling agent or a potassium bromide pellet for obtaining good infrared spectra of glycine¹ could be left out altogether.

Glycine exists in three crystalline modifications, designated as α -, β -, or γ -glycine, respectively, which differ somewhat in their vibrational spectra.^{1,2,6,8} The samples used for this study were recrystallized from ethanol, and the X-ray powder diagram obtained from such a sample of normal glycine a few days after its crystallization showed⁹ it to be mainly in the β modification with a small part of it in the α form. About 10 days afterward, however, a second diagram taken on this sample showed that by then most of the glycine had already gone over into the α structure. The infrared absorption measurements which were carried out on the samples about 3 weeks after their crystallization were therefore made on practically pure α glycines.

If the very small isotopic effects on the kinetics of the exchange of ^{18}O for ^{16}O in glycine are overlooked, one can show statistically that the concentrations of $\text{NH}_3+\text{CH}_2\text{C}^{16}\text{O}_2^-$, $\text{NH}_3+\text{CH}_2\text{C}^{16}\text{O}^{18}\text{O}^-$, and $\text{NH}_3+\text{CH}_2\text{C}^{18}\text{O}_2^-$ of a 75 atom % ^{18}O glycine sample are related to each other as $0.25^2:(2)(0.25)(0.75):0.75^2$, respectively. This means that the labeled sample was composed of *ca.* 56% $\text{NH}_3+\text{CH}_2\text{C}^{18}\text{O}_2^-$, 38% $\text{NH}_3+\text{CH}_2\text{C}^{16}\text{O}^{18}\text{O}^-$, and 6% normal glycine.

Experimental Section

Normal Glycine. This material was a pure commercial product (Analar).

^{18}O Glycine. Normal glycine (2 g) was added to ^{18}O -enriched water (5 ml of 98 atom % ^{18}O), and gaseous hydrogen chloride was bubbled through the mixture until all of the glycine was dissolved.¹⁰ The solution was sealed in a tube and kept at 125° for 3 days. The water was then removed by vacuum, the residue dis-

solved in a small volume of water and neutralized with lithium hydroxide, and the free glycine precipitated by the addition of ethanol. After keeping the glycine several hours at 0°, it was filtered, washed with ethanol, and dried over calcium chloride *in vacuo*. The labeled glycine was analyzed for its oxygen-18 content according to Rittenberg, *et al.*,¹⁰ and found to contain 75.0 atom % ^{18}O .

Infrared Measurements. The absorption measurements in the 4000–630- cm^{-1} region were carried out using a Beckman IR-7 spectrophotometer, the frequency calibration of which seems to be correct within $\pm 1 \text{ cm}^{-1}$ in almost the whole of this region (for slow enough scanning). The absorption in the lower, 630–400- cm^{-1} , frequencies was investigated with a Perkin-Elmer, Model 12C, spectrophotometer equipped with a potassium bromide prism and calibrated with the help of the water vapor and 1,2,4-trichlorobenzene bands of this region. The maximum absorption frequencies thus obtained are believed to be correct well within $\pm 2 \text{ cm}^{-1}$.

The sample to be measured was ground in each case to a very fine powder and put between two proper salt plates in a demountable cell.

The thickness of the sample layer was, as a rule, unknown and was adjusted, by adding more material or removing part of it, according to its observed absorption.

Results

Figure 1 shows the absorption of the normal and ^{18}O glycine samples in the 1650–650- cm^{-1} region.

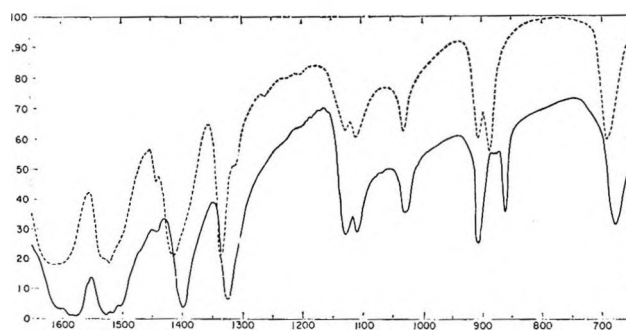


Figure 1. Infrared absorption of normal (---) and 75 atom % ^{18}O -labeled glycine (—) between 1650 and 650 cm^{-1} . Ordinate and abscissa scales represent per cent transmission and wavenumber, respectively.

(7) I. Laulicht and S. Pinchas, *Anal. Chem.*, **36**, 1980 (1964).

(8) P. Neelakantan and R. S. Krishnan, *Proc. Indian Acad. Sci.*, **A58**, 275 (1963).

(9) V. W. Hubig, *Z. Naturforsch.*, **13b**, 633 (1958).

(10) D. Rittenberg and L. Ponticorvo, *Intern. J. Appl. Radiation Isotopes*, **1**, 212 (1956).

Table I: The Absorption Bands (cm^{-1}) of Solid Normal and 75 Atom % ^{18}O Glycine^a

	Normal glycine powder	Normal glycine KBr pellets ¹	Labeled glycine powder	Assignment
a.	3180 m, sharp	3180 ^b	3180 sh	NH_3^+ antisym str
b.	2915 m, b	...	2915 m, b	CH_2 antisym str
c.	2830 m, b	2820 ^b	2840 m, b	CH_2 sym str
d.	2620 m, b	2610 ^b	2620 w	NH_3^+ sym str
e.	2130 w	2150 ^b	2180 w	f + s; f + r
f.	1604 s, b	1594	(1609 sh) 1586 s, b, 1574 s, b	CO_2^- antisym str ¹
g.	1527, 1514 s, b, 1502 sh	1527, 1518 1502	1527, 1519 s, 1502 sh	sym NH_3^+ deform ¹
h.	1443 w	1443	1442 w	CH_2 scissor ¹
i.	1413 s	1415	1401 s	CO_2^- sym str ¹
j.	1334 s	1334	1324 s	CH_2 wagging with a C-C str character
k.	1314 sh	1314		CH_2 twisting ¹
l.	1133 m	1131	1133 m	
m.	1114 m	1111	1114 m	NH_3^+ rocking ¹
n.	1035 m	1034	1034 m	C-N str ¹
o.	912 s	911	911 s	CH_2 rocking ¹
p.	894 s	893	870 s	CO_2^- scissor
q.	700 s	698	685 s	CO_2^- rocking
r.	608 s	608	601 m	CO_2^- wagging ¹
s.	502 s	503	501 s	NH_3^+ torsion

^a m, medium; sh, shoulder; b, broad; w, weak; s, strong. ^b Frequency read from the given absorption curve.

The frequencies of the observed absorption bands of normal and ^{18}O glycine in the 4000–400- cm^{-1} region are reported in Table I. The probable assignment of each band is added in the last column of this table.

It is evident from Table I that the agreement between the powder spectrum of normal glycine and that of an alkali halide pellet of this material is generally very good, the only real difference between them being in the broad f-band frequency. The value of 1604 cm^{-1} given for this band in Table I seems, however, to be more accurate than the value of¹ 1594 cm^{-1} since it agrees better with the value of 1610 cm^{-1} observed for it on a Nujol¹¹ mull.

The 3180- cm^{-1} frequency assigned in Table I to the NH_3^+ antisymmetrical stretching vibration is a little outside the (3130–3030- cm^{-1}) region usually attributed to this group.¹² This fact is probably the result of the absence of an alkyl substituent on the neighboring carbon atom in the case of glycine, in contradistinction to the case of all of the other amino acids, since such a substituent can be expected to decrease (sterically) the original HNH angle, thereby lowering somewhat the N–H stretching frequency of the other amino acids. That this vibration appears in the spectrum of the labeled glycine only as a shoulder seems to be connected with the f overtone (2×1586 minus an anharmonicity term) which falls in this case

on the lower frequency side of the N–H band and obliterates it to a certain extent.

Although Suzuki, *et al.*,¹ assign a calculated normal glycine band at 2960 cm^{-1} and an observed, glycine- d_3 , infrared band at 2940 cm^{-1} to a symmetrical CH_2 stretching, it seems to us that the band observed for powdered normal glycine at about 2915 cm^{-1} belongs to an *antisymmetrical* rather than to a *symmetrical* CH_2 stretching. This assignment is supported by the accepted attribution of the 2916–2936- cm^{-1} region to the *antisymmetrical* CH_2 stretching of hydrocarbons.¹³ The corresponding symmetrical CH_2 stretching¹³ seems to be responsible for the lower band at about 2830 cm^{-1} .

The reason for Suzuki's different assignment of the 2940- cm^{-1} band is no doubt the fact that the Raman spectrum of *aqueous* solutions of glycine shows⁵ two CH_2 stretching bands at about 2968 and 3011 cm^{-1} , the first of which is polarized and hence belongs to the *symmetrical* CH_2 stretching. It is, however, known that the presence of a free positive charge next to a

(11) "Documentation of Molecular Spectra Catalog," Butterworth and Co. Ltd., London, 1958, compound card No. 3707.

(12) See, *e.g.*, C. N. R. Rao, "Chemical Applications of Infrared Spectroscopy," Academic Press Inc., New York, N. Y., 1963, p 256.

(13) See ref 12, p 130.

CH₂ group in an *aqueous medium* (as in this case) leads to a compression of water molecules around the charged group, and this brings about a big increase in the neighboring CH₂ stretching frequencies.¹⁴ In the case of the antisymmetrical CH₂ stretching band of ethylenediamine in an aqueous acid solution this increase is from 2925 cm⁻¹ (for the liquid diamine) to 2990 cm⁻¹. This means that the *antisymmetrical* 3011-cm⁻¹ Raman band observed for the aqueous solution of the normal dipolar glycine molecule corresponds for crystalline glycine to a band at about 2940 cm⁻¹—very near the observed absorption of about 2915 cm⁻¹.

It is true that the Raman spectrum of crystalline glycine also shows a polarized band at about⁶ 2974 cm⁻¹ and a band at 3008 cm⁻¹. However, these bands do *not* seem to be directly related to the neighboring 2968- and 3011-cm⁻¹ bands of the aqueous solutions since the crystalline bands belong to the A_g and B_g species of the crystalline unit cell⁶ (which contains four glycine molecules). These species are symmetrical with respect to an inversion in the center of the unit cell and are therefore Raman active and infrared inactive while the solution bands do not belong to such symmetrical species since the solvated glycine dipolar ion does not possess a symmetry center.

The crystalline glycine infrared absorption bands observed at about 2830 and 2915 cm⁻¹ correspond, no doubt, to the weak Raman bands at about 2830 and 2895 cm⁻¹, respectively, and are very probably the A_u and B_u CH₂ stretching bands, accordingly, which as such should strictly be infrared active and Raman inactive. The fact that they appear at all in the Raman spectrum may be the result of the intermolecular hydrogen bonding which, probably, affects somewhat the selection rules of the glycine crystal.

It is thus seen that the CH₂ stretchings of the A_g and B_g species of α glycine are appreciably higher in frequency not only from the normal CH₂ bands of non-aqueous liquid samples but also from the corresponding A_u and B_u vibrations which are the only ones active in infrared absorption.

The d band falls in the middle of the 2760–2530-cm⁻¹ region, where most amino acids are known to exhibit at least one hydrogen-bound NH₃⁺ stretching band,¹⁵ and is therefore assigned in Table I to the symmetrical NH₃⁺ stretching which is strongly affected by the powerful hydrogen bonding existing in crystalline glycine, between the neighboring NH₃⁺ and CO₂⁻ groups.

The assignment of the 2130–2180-cm⁻¹ band as due to the f + s and f + r overtones seems more reasonable than that attributing this usual amino acid band again to some NH₃⁺ stretching vibration,¹⁵ since (a) its fre-

quency seems too low for it and (b) it is difficult to see why such a stretching would be affected so much by ¹⁸O labeling. With the overtones assignment, however, the effect of the ¹⁸O labeling on the e frequency is much easier to explain since it is then only the result of a difference in the relative intensities of the two overtone absorptions (composing this band, according to this assignment) between the case of ¹⁸O glycine and that of normal glycine.

The Isotopic Frequency Shifts

The CO₂⁻ antisymmetrical band of normal glycine at about 1604 cm⁻¹ (which probably masks the weaker antisymmetrical NH₃⁺ deformation band to be expected in this vicinity) can be seen from Table I to be split for the labeled glycine into a shoulder at about 1609 cm⁻¹ and two strong bands at about 1586 and 1574 cm⁻¹, respectively. Since the labeled sample was calculated above to contain 56 atom % of NH₃⁺-CH₂C¹⁸O₂⁻ and 38 atom % of NH₃⁺-CH₂C¹⁶O¹⁸O⁻, it is clear that the 1586-cm⁻¹ band belongs to the C¹⁶O¹⁸O⁻ stretching band while the 1574-cm⁻¹ band belongs to the C¹⁸O₂⁻ stretching band. The shoulder at about 1609 cm⁻¹ probably belongs to the NH₃⁺ antisymmetrical deformation band now partly uncovered by the isotopic shift of the CO₂⁻ band. This assignment gives isotopic shifts of about 18 and 30 cm⁻¹ for the C¹⁶O¹⁸O⁻ and C¹⁸O₂⁻ frequencies, respectively.

Assuming the CO₂⁻ oscillator to be harmonic and isolated from the rest of the glycine molecule, it is possible to estimate roughly the expected isotopic shift of the 1604-cm⁻¹ frequency for the C¹⁸O₂⁻ modification by using the equation¹⁶

$$(\omega^i)^2/1604^2 = m_x m_y (m_x + 2m_y^i \sin^2 \alpha) / m_x m_y^i (m_x + 2m_y \sin^2 \alpha)$$

where ω^i = the isotopic frequency,¹⁷ $m_x = 12$, $m_y = 16$, $m_y^i = 18$, and α = the OCO angle¹⁸ = 125.5°.

This equation thus gives $\omega^i = (1604)(0.9797) = 1571$ cm⁻¹, *i.e.*, an expected C¹⁸O₂⁻ isotope shift of about 33 cm⁻¹, which is in good agreement with the observed value of 30 cm⁻¹. Since the isotopic shift of the antisymmetrical stretching vibration of the C¹⁶O¹⁸O molecule is about half of the corresponding

(14) S. A. S. Ghazanfar, J. T. Edsall, and D. V. Myers, *J. Am. Chem. Soc.*, **86**, 564 (1964).

(15) See ref 12, p 257.

(16) G. Herzberg, "Infrared and Raman Spectra of Polyatomic Molecules," D. Van Nostrand Co., Princeton, N. J., 1945, p 228.

(17) Strictly, only the zero-order frequencies can be used in this equation; however, no appreciable error is to be expected if the observed absorption frequencies are substituted instead.

(18) R. E. Marsh, *Acta Cryst.*, **10**, 814 (1957).

$C^{18}O_2$ isotopic shift,¹⁹ the expected isotopic shift for the antisymmetrical stretching of the $C^{16}O^{18}O^-$ group is therefore about 16.5 cm^{-1} , very close to the observed value of 18 cm^{-1} .

These results show that the potential energy of the 1604-cm^{-1} vibration of normal glycine is centered in the CO_2 group, in harmony with the calculation of Suzuki, *et al.*,¹ according to which this vibration (calculated¹ to have an 1609-cm^{-1} frequency) has an 82% CO_2 stretching and 11% CO_2 rocking character.

The symmetrical CO_2^- stretching band of the labeled glycine can be seen from Table I to move from 1413 to 1401 cm^{-1} without splitting into two branches (for the two labeled modifications) as expected. The observed isotopic shift of this band being only 12 cm^{-1} strongly suggests that the 1401-cm^{-1} band belongs to the mixed (labeled) species although it amounts to only *ca.* 38% of the labeled sample. The expected isotopic shift of this band for the $C^{18}O_2^-$ group is about 25 cm^{-1} in analogy to (a) the value of 27 cm^{-1} observed for the similar symmetrical stretching vibration of the NO_2 group of nitrobenzene,²⁰ (b) the value of about 24 cm^{-1} observed for the symmetrical SO_2 stretching in diphenyl sulfone,²¹ and (c) the value of about 30 cm^{-1} of the $C^{18}O_2^-$ antisymmetrical stretching band. The expected shift for the symmetrical stretching of the $C^{16}O^{18}O^-$ group, however, is only about half of this value, *i.e.*, *ca.* 12 cm^{-1} , as observed. The corresponding frequency of $C_6H_5N^{16}O^{18}O$ was also observed²⁰ to decrease from 1349 to 1335 cm^{-1} giving an isotopic shift of about 14 cm^{-1} .

The symmetrical stretching absorption of the $NH_3^+CH_2C^{18}O_2^-$ species seems to be hidden in the low-frequency side of the 1401-cm^{-1} band which can be seen from Figure 1 to be clearly asymmetrical, being much less steep on the low-frequency side than on the other one. That 38% of the mixed modification here gives rise to a stronger absorption than 56% of the homogeneously labeled glycine might be the result of the appreciably higher transition moment of the symmetrical stretching of the heterogeneous, ionized $C^{16}O^{18}O$ group than that of the corresponding symmetrical $C^{18}O_2$ group.

The shift of 10 cm^{-1} reported in Table I for the j band of the labeled glycine is most unexpected since it was calculated¹ to consist of 81% CH_2 wagging and only about 2% CO_2 stretching. However, the large difference between its observed value of 1334 cm^{-1} and its calculated frequency¹ of 1278 cm^{-1} , as well as the fact that the respective Raman band of the dipolar glycine ion at 1327 cm^{-1} does not have a counterpart band in the Raman spectrum of the $NH_3^+CH_2COOH$

cation,⁵ shows that this calculation needs some correction.

It seems therefore that, as a result of the CH_2 wagging which gives rise to the 1334-cm^{-1} band of the dipolar glycine ion, the $C-CH_2$ bond itself is also set in vibration and is stretched considerably. This is opposed by the electrostatic attraction between the positive charge on the nitrogen atom and the negative charge on the oxygen atoms. The energy of this vibration is thus increased over the value calculated for it without taking into account this attraction, and this can explain the discrepancy between the calculated and observed frequency of this band. Since the glycine cation is devoid of such an effect, it is clear why it does not show a Raman band corresponding to the 1327-cm^{-1} Raman band of the dipolar glycine ion.⁵ The $C-C$ stretching character of the 1334-cm^{-1} infrared vibration (the small difference in frequency between the Raman and the corresponding infrared band stems no doubt from the different state of aggregation of the measured sample in each case) can also explain its considerable shifting on ^{18}O labeling since the latter appreciably affects the mass of the vibrating $C-COO^-$ group. Analogously, the similar $C-NO_2$ stretching frequency was also observed²⁰ to move significantly (from 1109 to about 1105 cm^{-1}) on the labeling of (one of) the NO_2 atoms by oxygen-18.

The band at 1324 cm^{-1} seems to be the result of the merging together of the two close bands expected in this region for the two labeled modifications of glycine. Its lower steepness on the long-wavelength side seems to be brought about, at least in part, by the nearby 1314-cm^{-1} CH_2 twisting absorption masked by it.

The fact that the 894-cm^{-1} band of normal glycine appears in the spectrum of ^{18}O glycine as a sharp band at 870 cm^{-1} is evidence against Suzuki's assignment of it as due to a $C-C$ stretching¹ since a vibration of this type cannot be expected to show such a big isotopic shift. Even if this stretching were centered only in the $C-CO_2$ bond, its expected isotopic shift on changing the $C^{16}O_2$ mass (44 units) for that of $C^{18}O_2$ (48 units) could not be more than about 0.01 of its frequency, *i.e.* (in this case), *ca.* 9 cm^{-1} , as can be calculated using Hooke's equation for a diatomic oscillator. It appears, therefore, that the 894-cm^{-1} band belongs to the $C^{16}O_2^-$ scissoring (which was assumed by Suzuki, *et al.*, to absorb at 698 cm^{-1}) while the 870-cm^{-1} band

(19) D. F. Eggers, Jr., and C. B. Arends, *J. Chem. Phys.*, **27**, 1405 (1956).

(20) S. Pinchas, D. Samuel, and B. L. Silver, *Spectrochim. Acta*, **20**, 179 (1964).

(21) S. Pinchas, D. Samuel, and M. Weiss-Brodsky, *J. Chem. Soc.*, 3968 (1962).

belongs to the corresponding bending of the $C^{18}O_2^-$ group.

The observed isotopic shift of this band amounting to 24 cm^{-1} is in good agreement with this assignment since it was found that the ^{18}O -induced shift of the corresponding bending of the very similar NO_2 group amounts to *ca.* 30 cm^{-1} in nitromethane while it is equal to about 26 cm^{-1} in the case of nitrobenzene.²⁰

The symmetrical bending frequency of the NO_2 group was observed to be 914 cm^{-1} for nitromethane and 850 cm^{-1} for nitrobenzene.²⁰ These values also support the assignment of the parallel 894-cm^{-1} glycine band to the similar scissoring of the CO_2^- group, rather than to the C-C stretching vibration, since the antisymmetrical and symmetrical CO_2^- stretching frequencies are also very near to the corresponding NO_2 values,²⁰ as can be seen from Table II.

Table II: Fundamental Frequencies of the CO_2^- Groups of Glycine and the NO_2 Groups of Nitrobenzene (cm^{-1})

	$C^{16}O_2^-$	$N^{14}O_2$	$C^{18}O^{18}O^-$	$N^{16}O^{18}O$	$C^{18}O_2^-$	$N^{18}O_2$
Antisym str	1604	1531	1586	1518	1574	1510
Sym str	1413	1349	1401	1335	?	1322
Sym bend	894	850	?	838	870	824

The spectrum of solid sodium formate²² shows a strong band at about 780 cm^{-1} which can be assigned only to its CO_2^- scissoring since it contains no C-C group at all and no other strong band appears between 1350 and 625 cm^{-1} . Since the C-H stretching frequencies are much higher than 780 cm^{-1} while the C-C frequencies are only a little higher,²³ one must look at the formate ion, HCO_2^- , bending as a bending of an XO_2 oscillator where X equals about 13 units of mass ($12 + 1$) while looking at the respective vibration of the glycine ion, $RH_2CCO_2^-$, as similar to a bending of an XO_2 molecule where X equals only *ca.* 12 units of mass. Hence, the frequency of this bending in glycine must be appreciably *higher* than in the formate ion, *i.e.*, *higher* than 780 cm^{-1} .

This bending must be higher in frequency in glycine than in sodium formate also as a result of the hydrogen bonding that exists in glycine, between the CO_2^- and NH_3^+ groups, since it is well known that such a bonding increases the *bending* frequencies of the groups involved in it. This conclusion supports again our assignment of the 894-cm^{-1} glycine band as due to this bending, rather than the 700-cm^{-1} band,¹ and explains the large discrepancy between the observed value of 894 cm^{-1} and the value of 941 cm^{-1} calculated for this

band on the assumption that it is due to a C-C stretching.¹

The $C^{16}O^{18}O^-$ bending absorption to be expected for the labeled sample at about 882 cm^{-1} can be seen in Figure 1 to be obliterated by its two strong neighbors on both sides, the 911-cm^{-1} CH_2 rocking band and the 870-cm^{-1} $C^{18}O_2^-$ bending absorption due to the major component of the labeled sample. Although the absorption curve of the labeled sample appears unexpectedly flat at about 880 cm^{-1} , it still seems that, without the band of the $C^{16}O^{18}O$ species, the per cent transmission at this point would have been *ca.* 80% as compared with the present value of *ca.* 55% .

The fact that the 896-cm^{-1} Raman band of the normal dipolar glycine ion is sensitive to its negative electrical charge and moves to 869 cm^{-1} when this charge is lost⁵ (in the glycine cation) is in harmony with the assignment of the corresponding 894-cm^{-1} infrared band to the CO_2^- bending since this vibration can be expected to lose some of its energy with the loss of the symmetry, the resonance energy, and the internal electrostatic repulsion of the ionized carboxyl group. That this shift is not larger can be ascribed to the effect of the hydrogen bonding existing in this case between the neighboring $COOH$ groups. Its shift to about 840 cm^{-1} for the $ND_3^+CH_2CO_2^-$ modification⁵ can be understood if it is remembered that the ionized carboxyl groups of glycine interact, *intermolecularly*, very strongly with the neighboring ionized amino groups. This means that the glycine CO_2^- bending effects also a deformation of its NH_3^+ bonds and as such is decreased considerably by the increase in mass of the ND_3^+ groups and by the decrease in the $O \cdots DN$ bonding strength.

The band observed for normal glycine at about 700 cm^{-1} can be seen from Table I to move in the case of the labeled sample to about 685 cm^{-1} . This band is now assigned to the CO_2^- rocking since the CO_2^- scissoring has already been shown above to be responsible for the $894\text{-}870\text{-cm}^{-1}$ band. The 685-cm^{-1} absorption seems to be the result of the merging together of the two branches of this band expected for the two labeled species of glycine. The relative high frequency of this band, as compared, *e.g.*, with the value of about 420 cm^{-1} , reported in the case of the NO_2 rocking vibration of nitrobenzene,²⁰ also appears to be brought about by the strong electrostatic interactions present in crystalline glycine (as evidenced, *e.g.*, by the short 2.76-\AA N-O distance between neigh-

(22) "National Research Council-National Bureau of Standards Spectral Absorption Data," National Bureau of Standards, Washington, D. C., compound card No. 1653.

(23) See ref 12, p 143.

boring molecules²⁴). This interaction makes the rocking of the CO_2^- group also a deformation of several intramolecular and intermolecular bonds and adds considerably to its frequency. That this is really the case here seems to be supported by the fact that the Raman band corresponding to the 700 cm^{-1} infrared band and measured on a water solution, rather than on crystals as for the infrared band, appears⁵ already at 665 cm^{-1} . It is noteworthy in this respect that for the case of the glycine anion, where no such interactions are possible, no band at all was observed in this region.

The shift of the 608-cm^{-1} band to 601 cm^{-1} , as a result of ^{18}O labeling, is in harmony with its assignment to the CO_2^- wagging.¹ The 601-cm^{-1} band is probably again the result of the absorption of both of the labeled glycine modifications.

The fact that the 502-cm^{-1} band was observed to be practically insensitive to ^{18}O labeling is evidence against its attribution to the CO_2^- rocking.¹ This band may be due to a torsionlike deformation of the NH_3^+ group

to which were also assigned the 516-cm^{-1} band of γ -glycine and the 545-cm^{-1} band¹ of $\text{NH}_3^+\text{CD}_2\text{CO}_2^-$. This vibration must, however, also affect very seriously other groups of the glycine dipolar ion because of the hydrogen bond coupling existing between its NH_3^+ and its CO_2^- groups. This conclusion is supported by the fact that its isotopic shift in the case of $\text{ND}_3^+\text{-CH}_2\text{C}^{16}\text{O}_2^-$ amounts to 9 cm^{-1} only although this low shift may also be the result of a close superposition of several vibrations.²⁵

Acknowledgment. The loan of a Beckman IR-7 spectrophotometer and financial support by the National Heart Institute, National Institutes of Health, are gratefully acknowledged. Thanks are also due to Dr. F. Hirshfeld of this institute for the X-ray examinations and the interpretation of their results.

(24) G. Albrecht and R. B. Corey, *J. Am. Chem. Soc.*, **61**, 1087 (1939).

(25) Pointed out by a referee.

The Association of Cadmium Ion and Bromide Ion in Molten Potassium Nitrate and in Molten Sodium Nitrate¹

by Helen Braunstein, Jerry Braunstein,^{2a} and Douglas Inman^{2b}

Department of Chemistry, University of Maine, Orono, Maine (Received November 1, 1966)

The electromotive force was measured of cells consisting of a Pd-PdO-CdO indicator electrode and a reference half-cell in solutions of Cd(NO₃)₂ and K(Na)Br in the molten solvents KNO₃, NaNO₃, and an equimolar mixture of KNO₃ and NaNO₃. The association constant of CdBr⁺, calculated from the activity coefficients (γ_M) of Cd(NO₃)₂, was K_1 (moles of solvent per mole): 650 in KNO₃ at 358°, 625 in NaNO₃ at 331°, and 1500 in (Na,K)NO₃ at 258°. The specific Helmholtz free energies of association, calculated from the association constant with the quasi-lattice model, were $-\Delta A$ (kcal per mole): 5.88 in KNO₃, 5.62 in NaNO₃, and 5.83 in (Na,K)NO₃. The results in (Na,K)NO₃ were shown to be consistent with previous measurements of the activity coefficients of (Na,K)Br using an Ag-AgBr indicator electrode. In the absence of dinuclear species formation and at low solute concentrations the thermodynamic association constant may be estimated (if insufficient data are available for extrapolation to infinite dilution) by the relation $K_1 \cong s_0/(1 - s_0R_M)$ where s_0 is the slope, at zero ligand concentration (R_L) and at the concentration R_M of solute cation, of a plot of $\ln 1/\gamma_M$ vs. R_L .

Introduction

Association constants and Helmholtz free energies of association of CdBr⁺ in molten nitrate are here reported as part of an investigation of solvent effects on association in molten salt solutions.^{3,4} A systematic study of the solvent effect requires the use of a number of different experimental methods and a self-consistent analysis of the data if significant results are to be obtained.^{5,6} Electromotive force methods are among the most accurate and convenient when suitable reversible electrodes are available. In molten nitrates, the silver electrode has been the only suitable electrode of the first kind and has been used extensively for the study of the association of silver ions.^{4,7} Silver-silver halide electrodes have been used for the study of associations of halide ions with lead or cadmium ions in solutions where the solubility of the silver halide is sufficiently low.⁸⁻¹⁰ Inman^{5,11} has demonstrated the applicability of an electrode of the third kind—palladium-palladium oxide-cadmium oxide—to the study of association equilibria of cadmium ion with halide ions in molten sodium nitrate-potassium nitrate eutectic.

In this paper, we present a detailed comparison of the evaluation of the association constant of CdBr⁺ in molten equimolar sodium nitrate-potassium nitrate

(1) Based on an M.S. thesis submitted by H. Braunstein, National Science Foundation Cooperative Fellow, to the Graduate School of the University of Maine. This work was supported in part under U. S. Atomic Energy Commission Contract No. AT(30-1)-2873 with the University of Maine; Report No. NYO-2873-11. The work was initiated during a stay at the Molten Salt Laboratory at Northampton College of Advanced Technology, London, by two of the authors (H. B. and J. B.).

(2) (a) To whom correspondence should be addressed at Reactor Chemistry Division, Oak Ridge National Laboratory, Oak Ridge, Tenn. (b) Department of Chemistry, Northampton College of Advanced Technology, London.

(3) J. Braunstein and A. S. Minano, *Inorg. Chem.*, **3**, 218 (1964).

(4) C. Thomas and J. Braunstein, *J. Phys. Chem.*, **68**, 957 (1964).

(5) (a) D. Inman, *Electrochim. Acta*, **10**, 11 (1965); (b) D. Inman, I. Regan, and B. Girling, *J. Chem. Soc.*, 348 (1964).

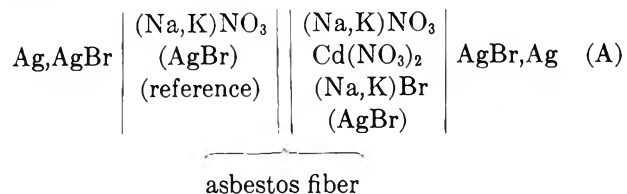
(6) J. Braunstein, M. Blander, and R. Lindgren, *J. Am. Chem. Soc.*, **84**, 1529 (1962).

(7) M. Blander, F. F. Blankenship, and R. F. Newton, *J. Phys. Chem.*, **63**, 1259 (1959).

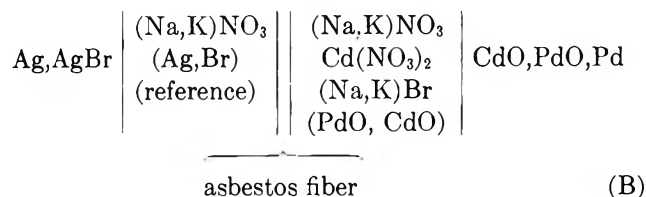
(8) J. Braunstein and R. M. Lindgren, *J. Am. Chem. Soc.*, **84**, 1534 (1962).

(9) R. W. Laity, "Electrodes in Fused Salt Systems," in D. J. G. Ives and G. J. Janz, "Reference Electrodes," Academic Press, New York, N. Y., 1961.

from earlier measurements of the emf of cell A with a silver-silver bromide indicator electrode and reference half-cell



and from measurements of the emf of cell B with a palladium-palladium oxide-cadmium oxide indicator electrode and a reference half-cell



In both cells, A and B, the reference half-cell consisted of a silver-silver bromide electrode dipping in the solvent under investigation contained in a Pyrex tube with an asbestos fiber providing a path for the transport of (solvent) ions. The difference between the emf of two cells A with differing cadmium concentrations but with the same bromide concentration corresponds to the emf of a "concentration" cell with two silver-silver bromide indicator electrodes in solutions containing $(\text{Na, K})\text{Br}$ at two different chemical potentials and leads to the activity coefficient of $(\text{Na, K})\text{Br}$. The difference between the emf of two cells B with differing bromide concentrations and the same cadmium concentration corresponds to the emf of a "concentration" cell with palladium-palladium oxide-cadmium oxide electrodes in solutions of cadmium nitrate at two different chemical potentials, and leads to the activity coefficient of $\text{Cd}(\text{NO}_3)_2$. We show that the association constant obtained from the activity coefficients of $\text{Cd}(\text{NO}_3)_2$ by measurements of cell B with the Pd-PdO-CdO indicator electrode is consistent with the association constant obtained from the activity coefficients of $(\text{Na, K})\text{Br}$ from previous measurements of cell A with the Ag-AgBr indicator electrode.

Cells with the palladium indicator electrode were used also to obtain the association constant of CdBr^+ in molten sodium nitrate and in molten potassium nitrate, whose higher melting points preclude the use of silver-silver bromide indicator electrodes without significant corrections for the solubility of silver bromide.^{3,8} The solubility of silver bromide does not interfere with the use of silver-silver bromide electrodes

in the reference half-cell since the chemical potential of AgNO_3 in the reference half-cell remains constant, as it is isolated from the indicator half-cell. In the indicator half-cell, however, dissolved silver ion would compete with cadmium ion in the formation of the associated species, and the analysis of the data for the association constants of cadmium with bromide would become more complicated.

The Helmholtz free energies of association are calculated from the association constants with the equations of a quasi-lattice model of molten salts¹² and are compared with values estimated by extrapolation of the Helmholtz free energies in mixed solvents. A simple method is presented for estimating the thermodynamic association constant from emf measurements at a single metal concentration in systems in which dinuclear species are absent.

Experimental Section

Description of Cell. The cell consisted of a 300-ml tall form beaker heated in a nichrome wire-wound electric furnace, a palladium wire electrode, a reference half-cell, and a thermocouple in a Pyrex well. The melt, containing solid PdO and CdO, was stirred vigorously with a Pyrex propeller. About 4-in. of the end of a 1.5-ft length of 0.016-in. diameter palladium wire was wound in the form of a helix about 5 mm in diameter and submerged in the melt. The asbestos fiber reference half-cell contained melt of the same composition as the solvent in the cell (in order to minimize junction potentials) and a silver-silver bromide electrode. It was inserted so that the surface of the solution in the cell was about 1 cm above the liquid in the reference half-cell. The temperature of the solution in the cell was measured with a calibrated chromel-alumel thermocouple in a 5-mm Pyrex well.

Chemicals. The solvent salts, KNO_3 and NaNO_3 , were Mallinckrodt analytical reagent grade chemicals used without further purification. The equimolar mixtures were fused under vacuum at 270° ; the pure solid nitrates were evacuated at 270° for at least 24 hr before use. Several KNO_3 melts fused without prior evacuation and then sparged with helium for 1 hr before oxide addition showed no noticeable difference in the experimental results. Anhydrous $\text{Cd}(\text{NO}_3)_2$ was prepared without fusion from Mallinckrodt analytical reagent grade $\text{Cd}(\text{NO}_3)_2 \cdot 4\text{H}_2\text{O}$. The tetrahydrate was crushed in an agate mortar and evacuated for at

(10) M. Blander, "Molten Salt Chemistry," Interscience Publishers, Inc., New York, N. Y., 1963.

(11) D. Inman, *Nature*, **194**, 279 (1962).

(12) (a) M. Blander, *J. Chem. Phys.*, **34**, 342 (1961); (b) M. Blander and J. Braunstein, *Ann. N. Y. Acad. Sci.*, **79**, 838 (1960).

least 24 hr at room temperature (the surface appeared white and opaque), 8–10 hr at 40°, 4–5 hr at temperatures between 40 and 100°, then 12–14 hr at 100°; slight decomposition was observed if the salt was heated under vacuum overnight above 150°. The $\text{Cd}(\text{NO}_3)_2$ was analyzed by ignition to CdO at 500–600°, and all samples prepared in the above manner agreed within 0.25% with the stoichiometric composition. Mallinckrodt analytical reagent grade KBr was crushed in an agate mortar and dried at 110° before use.

Fisher Certified reagent grade CdO was dried at 110°. PdO , obtained from Engelhard Industries, was pulverized by grinding for 30 sec in a stainless steel capsule on a Wig-L-Bug (Crescent Dental Manufacturing Co., Chicago, Ill.) and was stored at 400° in a muffle furnace until added to the melt since it appeared to adsorb moisture at room temperature, even in a desiccator.

Electrodes. The palladium wire was polished with jewelers' extra fine emery paper, moistened with analytical grade acetone, wiped dry, and brought to a bright polish by drawing it along a Pyrex glass rod. The surface of the wire showed no scratches or dull areas when inspected under a 10-power hand lens.

The silver–silver bromide electrode used in the reference half-cell was prepared by immersing a small helix of silver wire in a melt of the same composition as the solvent to be used, adding approximately 10^{-3} mole of AgNO_3 per mole of solvent, then sufficient KBr to produce a bright yellow precipitate of AgBr which was allowed to settle for 2–3 hr. One to two milliliters of the clear melt along with some solid AgBr and 10–20 mg of AgNO_3 were transferred to the reference half-cell tube (which was prepared by sealing an asbestos fiber into a Pyrex glass tube (about 9 mm) and testing for ionic conduction and low leakage of solution. The silver–silver bromide electrode was inserted through a centering tube and the reference half-cell was allowed to age in a solvent bath for at least 24 hr with frequent stirring to hasten equilibration.

Experimental Procedure. Three moles of KNO_3 (or of NaNO_3 , or of an equimolar mixture of KNO_3 with NaNO_3) in the cell was evacuated in a vacuum oven at room temperature for several hours, and at 270° for at least 24 hr. The cell was transferred to the furnace at atmospheric pressure, and the contents were fused (the equimolar mixture fused in the vacuum oven). Approximately 250 mg each of PdO and CdO were stirred into the molten solvent and allowed to equilibrate at least overnight. (In the earliest investigations, the first addition of $\text{Cd}(\text{NO}_3)_2$ was also made at this time; this was found to be unnecessary with the pure solvents, perhaps because of faster equilibration

at the higher temperatures with the pulverized oxide.) The temperature was adjusted and maintained manually with a Variac to within $\pm 0.1^\circ$.

At the start of the run, the emf of the cell was monitored with a Honeywell Electronik recorder until the emf was found to be constant for at least 15 min. The emf was then measured with a Keithley Model 660 differential potentiometric voltmeter. The limit of error of this instrument is $\pm 20 \mu\text{v}$ on the 1-mv scale which was used as the null indicator scale in all measurements. This is well within the precision of the measurement ($\pm 100 \mu\text{v}$). The cell emf often oscillated as much as $\pm 100 \mu\text{v}$, particularly at high bromide concentrations. At least one emf in each series of measurements was checked with a Rubicon Type B potentiometer to ensure adequate sensitivity and conduction through the asbestos fiber rather than the glass of the reference half-cell.

Weighed amounts of $\text{Cd}(\text{NO}_3)_2$ were added to the solvent and the emf of the cell was monitored until it remained constant within $\pm 0.1 \text{ mV}$ for 10 min or longer. This took from as long as 1 hr for the first addition to 10 min for succeeding additions. The emf has remained constant within $\pm 0.5 \text{ mV}$ for 3–4 hr and within 2–3 mV overnight. Except at very low final $\text{Cd}(\text{NO}_3)_2$ concentrations, at least five portions of $\text{Cd}(\text{NO}_3)_2$ were added and the emf values were plotted against the logarithm of the concentration of $\text{Cd}(\text{NO}_3)_2$ to determine whether the Nernst equation was being followed.

After checking the Nernst slope, several additions of KBr were weighed into the solution, and the emf of the cell was recorded after each addition. The comminution of the PdO with the Wig-L-Bug caused a marked improvement in the reproducibility and stability of the measurements, possibly since it permitted

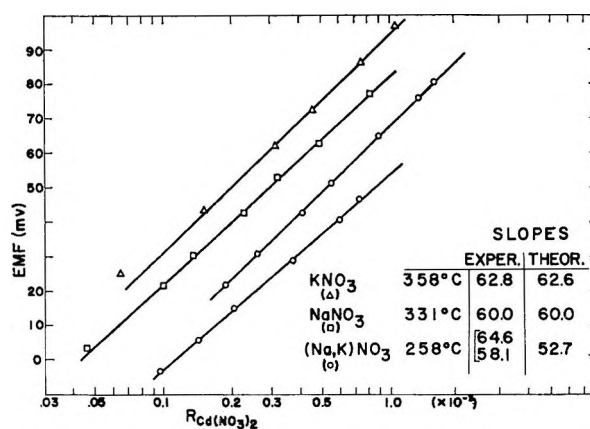


Figure 1. Electromotive force vs. the logarithm of the concentration (mole ratio) of cadmium nitrate in cells with Pd-PdO-CdO electrodes before bromide additions.

Table I

(a) Emf change in millivolts on addition of KBr to $\text{Cd}(\text{NO}_3)_2$ in equimolar mixture of NaNO_3 and KNO_3 , $T = 258^\circ$

$R_{\text{Cd}(\text{NO}_3)_2} = 2.075 \times 10^{-4}$			$R_{\text{Cd}(\text{NO}_3)_2} = 2.563 \times 10^{-4}$		
$R_{\text{KBr}} \times 10^3$	$-\Delta E, \text{mv}$	$\ln 1/\gamma_{\text{Cd}(\text{NO}_3)_2}$	$R_{\text{KBr}} \times 10^3$	$-\Delta E, \text{mv}$	$\ln 1/\gamma_{\text{Cd}(\text{NO}_3)_2}$
0.037	1.3	0.046	0.119	7.6	0.309
0.137	4.9	0.172	0.399	17.3	0.705
0.271	9.5	0.332	0.959	31.1	1.266
0.480	16.8	0.588	2.324	57.5	2.344
0.845	28.5	0.997			
2.073	54.8	1.918			

$R_{\text{Cd}(\text{NO}_3)_2} = 3.069 \times 10^{-4}$			$R_{\text{Cd}(\text{NO}_3)_2} = 4.283 \times 10^{-4}$		
$R_{\text{KBr}} \times 10^3$	$-\Delta E, \text{mv}$	$\ln 1/\gamma_{\text{Cd}(\text{NO}_3)_2}$	$R_{\text{KBr}} \times 10^3$	$-\Delta E, \text{mv}$	$\ln 1/\gamma_{\text{Cd}(\text{NO}_3)_2}$
0.036	2.1	0.064	0.078	1.3	0.045
0.094	4.1	0.124	0.238	4.4	0.153
0.166	5.1	0.154	0.466	9.8	0.341
0.300	10.6	0.320	0.638	13.0	0.453
0.486	16.3	0.493			
1.366	38.2	1.154			
2.551	62.2	1.879			

$R_{\text{Cd}(\text{NO}_3)_2} = 5.054 \times 10^{-4}$			$R_{\text{Cd}(\text{NO}_3)_2} = 7.185 \times 10^{-4}$		
$R_{\text{KBr}} \times 10^3$	$-\Delta E, \text{mv}$	$\ln 1/\gamma_{\text{Cd}(\text{NO}_3)_2}$	$R_{\text{KBr}} \times 10^3$	$-\Delta E, \text{mv}$	$\ln 1/\gamma_{\text{Cd}(\text{NO}_3)_2}$
0.166	4.7	0.173	0.068	2.0	0.079
0.416	10.7	0.394	0.184	4.4	0.174
0.950	22.5	0.829	0.352	7.7	0.305
1.801	37.0	1.363	0.648	10.6	0.420
3.145	55.7	2.052	1.378	22.9	0.907
			3.103	52.6	2.084

$R_{\text{Cd}(\text{NO}_3)_2} = 1.076 \times 10^{-3}$			$R_{\text{Cd}(\text{NO}_3)_2} = 1.219 \times 10^{-3}$		
$R_{\text{KBr}} \times 10^3$	$-\Delta E, \text{mv}$	$\ln 1/\gamma_{\text{Cd}(\text{NO}_3)_2}$	$R_{\text{KBr}} \times 10^3$	$-\Delta E, \text{mv}$	$\ln 1/\gamma_{\text{Cd}(\text{NO}_3)_2}$
0.091	1.6	0.060	0.382	4.5	0.182
0.225	3.7	0.140	0.839	11.6	0.470
0.577	8.5	0.320	1.405	12.6	0.509
1.182	16.3	0.615	2.263	19.5	0.787
1.850	23.7	0.893			
2.860	36.9	1.391			

$R_{\text{Cd}(\text{NO}_3)_2} = 1.544 \times 10^{-3}$			$R_{\text{Cd}(\text{NO}_3)_2} = 1.980 \times 10^{-3}$		
$R_{\text{KBr}} \times 10^3$	$-\Delta E, \text{mv}$	$\ln 1/\gamma_{\text{Cd}(\text{NO}_3)_2}$	$R_{\text{KBr}} \times 10^3$	$-\Delta E, \text{mv}$	$\ln 1/\gamma_{\text{Cd}(\text{NO}_3)_2}$
0.164	4.0	0.143	0.200	8.6	0.297
0.468	12.1	0.431	0.733	14.4	0.500
0.878	17.3	0.617	1.461	22.1	0.764
1.770	29.4	1.048	2.424	31.6	1.094
2.918	46.5	1.658			

(b) Emf change in millivolts on addition of NaBr to $\text{Cd}(\text{NO}_3)_2$ in NaNO_3 , $T = 331^\circ$

$R_{\text{Cd}(\text{NO}_3)_2} = 1.118 \times 10^{-4}$			$R_{\text{Cd}(\text{NO}_3)_2} = 2.938 \times 10^{-4}$		
$R_{\text{KBr}} \times 10^3$	$-\Delta E, \text{mv}$	$\ln 1/\gamma_{\text{Cd}(\text{NO}_3)_2}$	$R_{\text{KBr}} \times 10^3$	$-\Delta E, \text{mv}$	$\ln 1/\gamma_{\text{Cd}(\text{NO}_3)_2}$
0.038	0.3	0.011	0.184	2.9	0.103
0.084	0.8	0.030	0.464	7.2	0.257
0.210	3.0	0.113	0.682	10.6	0.378
0.372	6.1	0.230	1.009	15.2	0.542
0.721	10.8	0.408	1.393	20.7	0.738
1.225	18.7	0.706	2.071	29.7	1.059
			3.701	47.9	1.708

$R_{\text{Cd}(\text{NO}_3)_2} = 2.954 \times 10^{-4}$			$R_{\text{Cd}(\text{NO}_3)_2} = 4.992 \times 10^{-4}$		
$R_{\text{KBr}} \times 10^3$	$-\Delta E, \text{mv}$	$\ln 1/\gamma_{\text{Cd}(\text{NO}_3)_2}$	$R_{\text{KBr}} \times 10^3$	$-\Delta E, \text{mv}$	$\ln 1/\gamma_{\text{Cd}(\text{NO}_3)_2}$
0.206	2.6	0.098	0.176	1.9	0.072
0.438	6.1	0.230	0.542	6.5	0.245
0.997	13.5	0.510	1.090	13.5	0.510
1.459	20.2	0.763	1.936	24.2	0.914

$R_{\text{Cd}(\text{NO}_3)_2} = 8.097 \times 10^{-4}$			$R_{\text{Cd}(\text{NO}_3)_2} = 6.711 \times 10^{-4}$		
$R_{\text{KBr}} \times 10^3$	$-\Delta E, \text{mv}$	$\ln 1/\gamma_{\text{Cd}(\text{NO}_3)_2}$	$R_{\text{KBr}} \times 10^3$	$-\Delta E, \text{mv}$	$\ln 1/\gamma_{\text{Cd}(\text{NO}_3)_2}$
0.257	2.6	0.100	0.172	1.0	0.036
0.629	6.7	0.257	0.574	4.9	0.185
0.963	10.1	0.388	1.060	10.1	0.381
1.896	21.1	0.810	2.290	22.9	0.865

$R_{\text{Cd}(\text{NO}_3)_2} = 1.153 \times 10^{-3}$			$R_{\text{Cd}(\text{NO}_3)_2} = 7.756 \times 10^{-4}$		
$R_{\text{KBr}} \times 10^3$	$-\Delta E, \text{mv}$	$\ln 1/\gamma_{\text{Cd}(\text{NO}_3)_2}$	$R_{\text{KBr}} \times 10^3$	$-\Delta E, \text{mv}$	$\ln 1/\gamma_{\text{Cd}(\text{NO}_3)_2}$
0.120	0.7	0.025	0.322	2.8	0.105
0.576	4.8	0.169	0.602	4.7	0.176
1.045	10.1	0.357	1.168	9.3	0.348
1.951	19.1	0.674			

(c) Emf change in millivolts on addition of KBr to $\text{Cd}(\text{NO}_3)_2$ in KNO_3 , $T = 358^\circ$

$R_{\text{Cd}(\text{NO}_3)_2} = 1.346 \times 10^{-4}$			$R_{\text{Cd}(\text{NO}_3)_2} = 1.448 \times 10^{-4}$		
$R_{\text{KBr}} \times 10^3$	$-\Delta E, \text{mv}$	$\ln 1/\gamma_{\text{Cd}(\text{NO}_3)_2}$	$R_{\text{KBr}} \times 10^3$	$-\Delta E, \text{mv}$	$\ln 1/\gamma_{\text{Cd}(\text{NO}_3)_2}$
0.225	2.9	0.106	0.159	2.4	0.088
0.460	6.1	0.224	0.338	5.6	0.205
0.738	11.5	0.422	0.571	9.6	0.352
1.257	19.5	0.715	0.886	14.6	0.535

$R_{\text{Cd}(\text{NO}_3)_2} = 1.985 \times 10^{-4}$			$R_{\text{Cd}(\text{NO}_3)_2} = 2.067 \times 10^{-4}$		
$R_{\text{KBr}} \times 10^3$	$-\Delta E, \text{mv}$	$\ln 1/\gamma_{\text{Cd}(\text{NO}_3)_2}$	$R_{\text{KBr}} \times 10^3$	$-\Delta E, \text{mv}$	$\ln 1/\gamma_{\text{Cd}(\text{NO}_3)_2}$
0.168	3.3	0.121	0.213	3.0	0.110
0.462	9.2	0.337	0.505	7.2	0.264
1.073	17.1	0.627	0.846	11.1	0.407
			1.363	17.6	0.645

$R_{\text{Cd}(\text{NO}_3)_2} = 2.872 \times 10^{-4}$			$R_{\text{Cd}(\text{NO}_3)_2} = 5.339 \times 10^{-4}$		
$R_{\text{KBr}} \times 10^3$	$-\Delta E, \text{mv}$	$\ln 1/\gamma_{\text{Cd}(\text{NO}_3)_2}$	$R_{\text{KBr}} \times 10^3$	$-\Delta E, \text{mv}$	$\ln 1/\gamma_{\text{Cd}(\text{NO}_3)_2}$
0.087	0.5	0.018	0.179	2.0	0.073
0.244	1.7	0.062	0.464	6.2	0.227
0.491	5.4	0.198	0.781	10.8	0.396
			1.240	17.6	0.645
			1.829	25.2	0.924
			2.781	36.6	1.342

$R_{\text{Cd}(\text{NO}_3)_2} = 7.217 \times 10^{-4}$			$R_{\text{Cd}(\text{NO}_3)_2} = 1.058 \times 10^{-3}$		
$R_{\text{KBr}} \times 10^3$	$-\Delta E, \text{mv}$	$\ln 1/\gamma_{\text{Cd}(\text{NO}_3)_2}$	$R_{\text{KBr}} \times 10^3$	$-\Delta E, \text{mv}$	$\ln 1/\gamma_{\text{Cd}(\text{NO}_3)_2}$
0.118	1.1	0.036	0.245	1.5	0.055
0.266	3.0	0.099	0.769	6.5	0.238
0.460	5.8	0.191	1.618	13.7	0.502
0.877	11.7	0.385			
1.292	17.3	0.569			

$R_{\text{Cd}(\text{NO}_3)_2} = 1.428 \times 10^{-3}$			$R_{\text{Cd}(\text{NO}_3)_2} = 1.768 \times 10^{-3}$		
$R_{\text{KBr}} \times 10^3$	$-\Delta E, \text{mv}$	$\ln 1/\gamma_{\text{Cd}(\text{NO}_3)_2}$	$R_{\text{KBr}} \times 10^3$	$-\Delta E, \text{mv}$	$\ln 1/\gamma_{\text{Cd}(\text{NO}_3)_2}$
0.178	1.5	0.049	0.183	1.6	0.059
0.441	4.4	0.145	0.364	3.6	0.132
0.833	8.9	0.293	0.520	5.5	0.202
1.543	16.5	0.543	0.886	9.8	0.359
			1.286	14.2	0.521
			1.993	21.5	0.788

more rapid and complete equilibration of the melts with the oxides, and allowed less time for decomposition of $\text{Cd}(\text{NO}_3)_2$.

Results

The electromotive force of cell B was measured with the solvents NaNO_3 , KNO_3 , and equimolar NaNO_3 - KNO_3 at various concentrations of $\text{Cd}(\text{NO}_3)_2$ in the absence and in the presence of KBr .

In the absence of KBr , the variation of the emf with the concentration of $\text{Cd}(\text{NO}_3)_2$ was compared with the Nernst equation; typical data are presented in Figure 1. The concentrations are expressed as the mole ratios

$$R_{\text{Cd}(\text{NO}_3)_2} = \frac{n_{\text{Cd}(\text{NO}_3)_2}}{n_{\text{NaNO}_3} + n_{\text{KNO}_3}} \cong \frac{n_{\text{Cd}^{2+}}}{n_{\text{Na}^+} + n_{\text{K}^+} + n_{\text{Cd}^{2+}}}$$

$$R_{\text{Br}} = \frac{n_{\text{KBr}}}{n_{\text{NaNO}_3} + n_{\text{KNO}_3}} \cong \frac{n_{\text{Br}^-}}{n_{\text{NO}_3^-} + n_{\text{Br}^-}}$$

which are approximately equal to the ion fractions.^{6,7} The n are the stoichiometric numbers of moles of cadmium nitrate, cadmium ion, etc.

The use of ion fractions as concentration units in molten salts makes possible the interpretation of association constants in terms of a quasi-lattice model of molten salts.¹² Comparisons of association constants in different molten salt solvents can be interpreted in terms of the size and charge of the ions of the melt. In NaNO_3 and in KNO_3 , at the higher temperatures, the experimental slopes (in Figure 1) are in agreement with the theoretical Nernst slopes within the experimental error. At the lower temperature in NaNO_3 - KNO_3 the experimental slopes are constant but higher than the theoretical Nernst slopes, possibly because of a mixed potential involving oxygen at the palladium electrode as discussed by Inman.¹¹ While the deviation from the Nernst slope at the lower temperature is disturbing, the use of the experimental slope in place of the theoretical Nernst slope leads to association constants and other derived results in agreement with those determined previously with the Ag - AgBr indicator electrode, and it is believed that the cause of the mixed potential does not here interfere with the equilibria of the species in solution.

The change of emf of cell B on titration with KBr at several fixed concentrations of $\text{Cd}(\text{NO}_3)_2$ is presented in Table I. At solute concentrations low enough that the liquid junction potential is negligible, the emf of the cell may be written

$$E = \text{constant} + \frac{RT}{2F} \ln a_{\text{Cd}(\text{NO}_3)_2} \quad (1)$$

where $a_{\text{Cd}(\text{NO}_3)_2}$ is the activity of $\text{Cd}(\text{NO}_3)_2$. The stoichiometric activity coefficient is defined as $\gamma_{\text{Cd}(\text{NO}_3)_2} = a_{\text{Cd}(\text{NO}_3)_2}/R_{\text{Cd}(\text{NO}_3)_2}$.⁶⁻⁸ Agreement with the Nernst equation in the absence of bromide indicates that the activity coefficient is constant over the concentration range investigated and is unity if the reference state for the activity coefficient is infinite dilution of all solutes. The change of emf, ΔE , of cell B on addition of bromide at a fixed cadmium concentration leads to the activity coefficient

$$\ln \gamma_{\text{Cd}(\text{NO}_3)_2} = \frac{1}{k} \Delta E \quad (2)$$

where k is the "Nernst slope," RT/nF , for NaNO_3 and KNO_3 . In NaNO_3 - KNO_3 the experimental slope is used instead of the theoretical Nernst slope.¹¹ This is justified by agreement of the results with those obtained previously by titration of bromide with cadmium nitrate using silver-silver bromide indicator electrodes.⁸ The association constant for the formation of CdBr^+ was evaluated graphically by methods described previously.^{3,6} Plots of $\ln 1/\gamma_{\text{Cd}(\text{NO}_3)_2}$ and the extrapolation of the limiting slopes to infinite dilution of cadmium ion

$$\left(\frac{\partial \ln 1/\gamma_{\text{Cd}(\text{NO}_3)_2}}{\partial R_{\text{Br}}} \right)_{R_{\text{Cd}(\text{NO}_3)_2}, R_{\text{Br}}=0}$$

are presented in Figures 2a,b, 3a, and 4a. The extrapolated slopes are the thermodynamic association constants

$$K_1 = \lim_{\substack{R_{\text{Cd}} \rightarrow 0 \\ R_{\text{Br}} \rightarrow 0}} \left(\frac{\partial \ln 1/\gamma_{\text{Cd}(\text{NO}_3)_2}}{\partial R_{\text{Br}}} \right)_{R_{\text{Cd}(\text{NO}_3)_2}} \quad (3)$$

The specific Helmholtz free energy of association was calculated from the association constants by use of the relation of the quasi-lattice model

$$K_1 = Z(\exp(-\Delta A/RT) - 1) \quad (4)$$

The association constants and Helmholtz free energies are listed in Table II for Z , the lattice coordination number, equal to 6. Since the Helmholtz free energies of association of Cd^{2+} or Ag^+ with halide ions in nitrate melts have been shown to be nearly constant over appreciable ranges of temperature, they are useful for comparing data on association at different temperatures.^{3,10}

The Helmholtz free energy of association for CdBr^+ is more negative (as seen in Table II) in KNO_3 than in NaNO_3 by 0.30 kcal/mole. This is in the direction expected in view of the relative size of the two cations ($r_{\text{Na}^+} < r_{\text{K}^+}$) and the relative size of the two anions ($r_{\text{Br}^-} < r_{\text{NO}_3^-}$).^{3,13} The value of ΔA for CdBr^+ in

Table II: Association Constants, K_1 , and Helmholtz Free Energies of Association, $-\Delta A$

Solvent	Temp, °C	K_1 , moles of solvent/mole	$-\Delta A$, kcal/mole ($Z = 6$)
NaNO_3	331	625	5.58
KNO_3	358	650	5.88
KNO_3	240 ^a	...	5.80 ^a
$\text{NaNO}_3\text{-KNO}_3$	258	1500	5.83
$\text{NaNO}_3\text{-KNO}_3$	300	990 ^b	5.83 ^b
$\text{NaNO}_3\text{-KNO}_3$	240	1520 ^b	5.67 ^b

^a From ref 3, by extrapolation. ^b See ref 8.

KNO_3 obtained from direct measurements at 358° is 0.08 kcal/mole more negative than the value estimated by linear extrapolation of the values of ΔA obtained in mixtures of LiNO_3 and KNO_3 at solvent compositions between 0.2 and 0.74 mole fraction of KNO_3 .³ The difference is almost within the experimental error (~ 0.05 kcal/mole). The small discrepancy may be due in part to the difference of temperature of the measurements in KNO_3 (358°) and $\text{LiNO}_3\text{-KNO}_3$ mixtures (240°), since ΔA may not be entirely temperature independent, or to small uncertainties in the extrapolation.

Discussion

The emf of cells with a Pd-PdO-CdO indicator electrode has been shown to agree with the Nernst equation in the concentration of cadmium ion in molten NaNO_3 at 331° and in molten KNO_3 at 358°, and association constants of cadmium ion with bromide have been evaluated. At these temperatures the solubility of silver bromide is too high for reliable evaluation of the association constants with cells using silver-silver bromide indicator electrodes.

In $\text{NaNO}_3\text{-KNO}_3$ at 258°, although a higher slope than the theoretical Nernst slope is obtained for the Pd-PdO-CdO indicator electrode, the calculated value of the Helmholtz free energy of association, ΔA , of cadmium ion with bromide, using the "experimental Nernst slope" in the calculations, is found to agree with the value of ΔA obtained previously with the Ag-AgBr indicator electrode at 240 and 300°. (The solubility of AgBr is low enough, below 300°, to permit use of the Ag-AgBr indicator electrode to obtain the association constants.)⁸ A comparison of the emf data on activity coefficients from cell B (with the Pd-PdO-CdO indicator electrode) with the emf data from cell A (Ag-AgBr indicator electrode) using the thermodynamic consistency relations would be

desirable. A complete consistency test is not feasible because the two cells were not measured at the same temperature. It is possible, however, in this case to make a partial test by comparing values of the derivative function

$$s_0 = \lim_{R_{\text{Br}} \rightarrow 0} \left(\frac{\partial \ln 1/\gamma_{\text{Br}}}{\partial R_{\text{Cd}(\text{NO}_3)_2}} \right)_{R_{\text{Br}}}$$

which are obtained from measurements of cell A with the values of s_0 obtained indirectly from measurements of cell B. (s_0 is a function of the cadmium concentration, and the limit of s_0 at vanishing cadmium concentration is the association constant K_1 .)

Braunstein and Lindgren⁸ have reported activity coefficients of (Na,K)Br in the presence of $\text{Cd}(\text{NO}_3)_2$ in molten equimolar $\text{NaNO}_3\text{-KNO}_3$ at 240 and at 300°. At both temperatures, the plots of $1/\gamma_{\text{Br}}$ vs. $R_{\text{Cd}(\text{NO}_3)_2}$ were found to be straight lines at low bromide concentrations over the range of cadmium concentrations investigated.^{3,8} Thus the data corresponded, within the experimental error, to the equation

$$1/\gamma_{\text{Br}}|_{R_{\text{Br}}=0} = 1 + K_1 R_{\text{Cd}(\text{NO}_3)_2} \quad (5)$$

at zero bromide concentration, and the absence of curvature indicates the absence of dinuclear species.⁸ From the thermodynamic equation

$$\left(\frac{\partial \ln 1/\gamma_i}{\partial R_j} \right)_{R_i} = \left(\frac{\partial \ln 1/\gamma_j}{\partial R_i} \right)_{R_j}$$

we have

$$\left[\left(\frac{\partial \ln 1/\gamma_{\text{Cd}(\text{NO}_3)_2}}{\partial R_{\text{Br}}} \right)_{R_{\text{Cd}(\text{NO}_3)_2}} \right]_{R_{\text{Br}}, R_{\text{Cd}(\text{NO}_3)_2}} = \left[\left(\frac{\partial \ln 1/\gamma_{\text{Br}}}{\partial R_{\text{Cd}(\text{NO}_3)_2}} \right)_{R_{\text{Br}}} \right]_{R_{\text{Br}}, R_{\text{Cd}(\text{NO}_3)_2}} = s \quad (6)$$

Substitution of (5) in (6)

$$s_0 = \left[\left(\frac{\partial \ln 1/\gamma_{\text{Cd}(\text{NO}_3)_2}}{\partial R_{\text{Br}}} \right)_{R_{\text{Cd}(\text{NO}_3)_2}} \right]_{R_{\text{Br}}=0} = \frac{K_1}{1 + K_1 R_{\text{Cd}(\text{NO}_3)_2}} \quad (7)$$

The solid line in the upper left portion of Figure 2 is calculated from (7) using the extrapolated value of K_1 at 258°. This curve therefore represents the data from cells with Ag-AgBr indicator electrodes, which correspond to eq 5. The open circles in Figure 2c are the slopes

$$\left[\left(\frac{\partial \ln 1/\gamma_{\text{Cd}(\text{NO}_3)_2}}{\partial R_{\text{Br}}} \right)_{R_{\text{Cd}(\text{NO}_3)_2}} \right]_{R_{\text{Br}}=0}$$

(13) D. L. Manning, R. C. Bansal, J. Braunstein, and M. Blander, *J. Am. Chem. Soc.*, **84**, 2028 (1962).

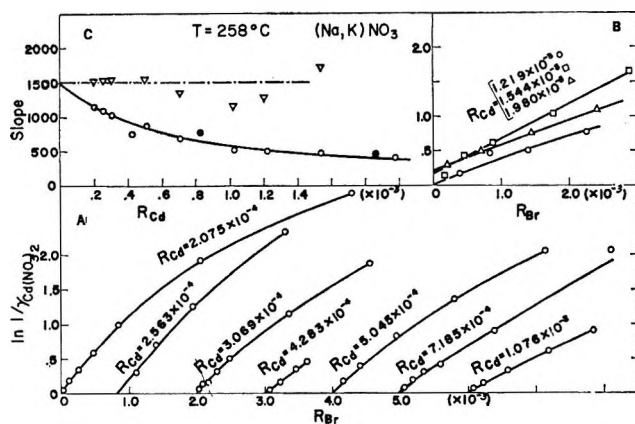


Figure 2. A and B: logarithm of the reciprocal of the activity coefficient of cadmium nitrate vs. the concentration (mole ratio) of bromide at several fixed cadmium concentrations in the solvent equimolar $\text{NaNO}_3\text{-KNO}_3$; C: solid line and open circles $\text{---}\circ\text{---}$, the slopes $s_0 = \lim_{R_{\text{Br}} \rightarrow 0} (\partial \ln 1/\gamma_{\text{Cd}(\text{NO}_3)_2} / \partial R_{\text{Br}})$ vs. the concentration (mole ratio) of cadmium nitrate; dash-dot line and inverted triangles $\text{---}\nabla\text{---}$, the estimated association constant for CdBr^+ , $s_0/1 - s_0 R_{\text{Cd}(\text{NO}_3)_2}$. The filled circles are slopes, s_0 , estimated from data in ref 5a.

obtained from the cells with Pd-PdO-CdO indicator electrodes using the experimental or "calibrated Nernst" slope.

The observed agreement of the concentration dependence of the derivatives s_0 obtained experimentally from cells with the Pd-PdO-CdO indicator electrode and indirectly, with (5) and (6), from cells with the Ag-AgBr indicator electrode is an even more stringent test of the consistency of the two sets of data than is just the agreement of the association constant, which is the limiting value of s_0 . Since the first derivatives with respect to the bromide concentration of $\ln 1/\gamma_{\text{Cd}(\text{NO}_3)_2}$ at zero bromide concentration are consistent over the entire range of cadmium concentrations investigated, it is suggested that the activity coefficients will be consistent at least in dilute solutions. This agreement appears to justify the use of the "experimental Nernst slope" in the evaluation of the association constants and suggests that the Pd-PdO-CdO electrode may lead to correct activity coefficients at higher bromide concentrations as well. That is, the agreement shows not only that the Pd-PdO-CdO electrode gives correct results at zero bromide, but at low bromide concentrations as well, since the derivatives $(\partial \ln 1/\gamma_{\text{Cd}} / \partial R_{\text{Br}})$ have the correct dependence on cadmium concentration.

Although independent proof of the absence of the dinuclear species $\text{Cd}_2\text{Br}^{3+}$ in KNO_3 and in NaNO_3 is not available, it is reasonable to assume that, as in the mixed solvent $(\text{Na,K})\text{NO}_3$, they are not important and that, therefore, equations of the form of (5) and

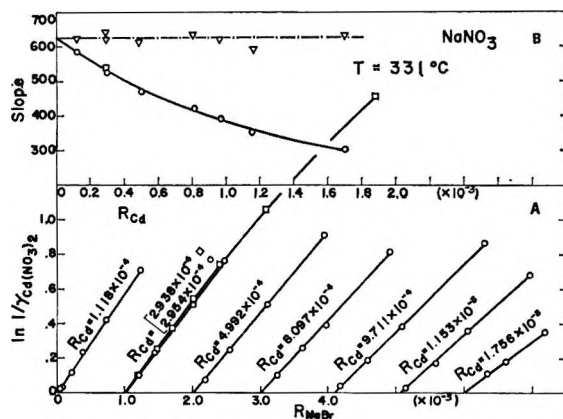


Figure 3. A: logarithm of the reciprocal activity coefficient of cadmium nitrate vs. the concentration of bromide in the solvent NaNO_3 ; B: solid line and open circles, $\text{---}\circ\text{---}$, the slopes $s_0 = \lim_{R_{\text{Br}} \rightarrow 0} (\partial \ln 1/\gamma_{\text{Cd}(\text{NO}_3)_2} / \partial R_{\text{Br}})$ vs. the mole ratio of cadmium nitrate; dash-dot line and inverted triangles, $\text{---}\nabla\text{---}$, the estimated association constant for CdBr^+ , $s_0/1 - s_0 R_{\text{Cd}(\text{NO}_3)_2}$ in the solvent NaNO_3 .

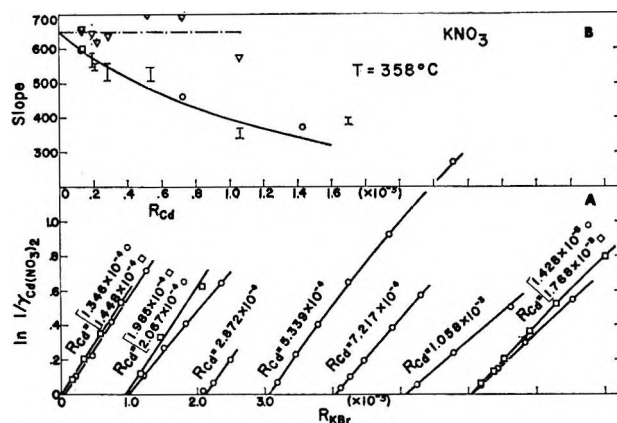


Figure 4. A: logarithm of the reciprocal activity coefficient of cadmium nitrate vs. the concentration of bromide in the solvent KNO_3 ; B: solid line and open circles, $\text{---}\circ\text{---}$, the slopes $s_0 = \lim_{R_{\text{Br}} \rightarrow 0} (\partial \ln 1/\gamma_{\text{Cd}(\text{NO}_3)_2} / \partial R_{\text{Br}})$ vs. the mole ratio of cadmium nitrate; dash-dot line and inverted triangles, $\text{---}\nabla\text{---}$, the estimated association constant for CdBr^+ , $s_0/1 - s_0 R_{\text{Cd}(\text{NO}_3)_2}$ in the solvent KNO_3 .

(7) are applicable in these solvents as well. The solid lines in Figures 3b and 4b are calculated from eq 7. The agreement with the experimental limiting slopes, particularly in the solvent sodium nitrate, confirms the absence of dinuclear species.¹⁴ Evaluation of the

(14) If the association constant for dinuclear species is not zero, eq 7 would take the form

$$\left[\left(\frac{\partial \ln 1/\gamma_{\text{Cd}(\text{NO}_3)_2}}{\partial R_{\text{Br}}} \right)_{R_{\text{Cd}(\text{NO}_3)_2}} \right]_{R_{\text{Br}}=0} = \frac{K_1 + 2K_1K_{12}R_{\text{Cd}(\text{NO}_3)_2} + \dots}{1 + K_1R_{\text{Cd}(\text{NO}_3)_2} + K_1K_{12}R_{\text{Cd}(\text{NO}_3)_2}^2 + \dots} \quad (7')$$

limiting second derivative

$$(2K_1K_{12} - K_1^2) = \lim_{\substack{R_{\text{Cd}} \rightarrow 0 \\ R_{\text{Br}} \rightarrow 0}} \left(\frac{\partial^2 \ln 1/\gamma_{\text{Cd}(\text{NO}_3)_2}}{\partial R_{\text{Br}} \partial R_{\text{Cd}(\text{NO}_3)_2}} \right) = \lim_{R_{\text{Cd}} \rightarrow 0} \left(\frac{\partial s_0}{\partial R_{\text{Cd}}} \right)$$

from the solid curves in Figures 3b and 4b also shows that K_{12} is zero within the experimental error. The solid circles in Figure 2c are the slopes of $\ln F_0 (= \ln 1/\gamma_{\text{Cd}(\text{NO}_3)_2})$ calculated from Inman's previously reported results⁵ in NaNO_3 - KNO_3 eutectic at 254° . The agreement with the results of the current study is well within the experimental error.

Higher association constants for species such as CdBr_2 , CdBr_3^- , etc., require the analysis of data at higher bromide concentrations and will be dealt with in subsequent work. The value of K_1 obtained here need not be modified in the calculation of higher association constants because the extrapolation procedure used here gives association constants which are invariant to the calculation of the successive higher association constants.¹⁵

A further potentially useful result for the estimation of association constants in systems where data over a

range of metal ion concentrations may be difficult to obtain follows from the rearrangement of eq 7 which leads to the result

$$K_1 = \frac{s_0}{1 - s_0 R_{\text{Cd}(\text{NO}_3)_2}} \quad (8)$$

Equation 8 is valid at low concentrations if the dinuclear association constant is nearly zero. Values of K_1 estimated from eq 8 are shown in Figures 2c, 3b, and 4b as dash-dot lines. In spite of some scatter, the estimates are closer to the extrapolated limits than are the slopes at finite cadmium concentrations. The averages of the values of K_1 estimated from eq 8 are 1465 in $(\text{Na,K})\text{NO}_3$, 625 in NaNO_3 , and 656 in KNO_3 , compared to the values 1500, 625, and 650 obtained by extrapolation to zero cadmium concentration.

The usefulness of the electrode of the third kind Pd-PdO-CdO in the evaluation of the association constant of cadmium ion with bromide in molten nitrates suggest the possibility that similar electrodes with oxides other than CdO may be feasible.

(15) The evaluation of only K_1 and K_{12} does not imply the absence of higher species. As distinct from a data-fitting procedure, our extrapolation does not require the assumption of a particular small set of species but leads successively to the coefficients in the Taylor's series expansion of the activity coefficients.⁶

Polarographic and Potentiometric Evaluation of Association Constants in Low-Temperature Aqueous Melts

by Jerry Braunstein,¹ Alba Rosa Alvarez-Funes, and Helen Braunstein

Department of Chemistry, University of Maine, Orono, Maine (Received February 21, 1966)

As part of an investigation of the effect of water on association in molten salt solutions, the association constant of cadmium with bromide was evaluated both polarographically and potentiometrically in fused calcium nitrate tetrahydrate at 50° as 3900 ± 200 (moles of bromide/mole of nitrate)⁻¹. Equations for the polarographic evaluation of successive association constants considering the change of ligand concentration at the cathode are modified for simple graphical analysis. The association constant of cadmium ion with chloride ion, here evaluated from polarographic measurements in a solvent consisting of 2 moles of water per mole of ammonium nitrate at 40°, is shown to agree with a previously reported potentiometric evaluation.

Introduction

As part of an investigation of the effect of water on association constants in molten salt solutions, association constants of cadmium ion with chloride ion, evaluated potentiometrically in a solvent consisting of 2 moles of water per mole of ammonium nitrate, have been reported previously.² Melts such as $\text{NH}_4\text{NO}_3 \cdot 2\text{H}_2\text{O}$ are intermediate between concentrated aqueous electrolyte solutions and molten salts, and it was shown that a quasi-lattice model of molten salts is useful in interpreting association equilibria in these melts. Measurements were made in a concentration cell with silver-silver chloride or cadmium amalgam electrodes. Data at low solute concentrations and extrapolation to infinite dilution of metal ions and ligand have been demonstrated previously to be necessary to obtain consistent thermodynamic association constants in molten salt solutions,^{2,3} but since stable reproducible values of the electromotive force of cells with amalgam electrodes are difficult to obtain at $\text{Cd}(\text{NO}_3)_2$ concentrations below 10^{-3} mole ratio (moles of cadmium per mole of ammonium nitrate), it is difficult to carry out the required extrapolation to infinite dilution of the slopes $\partial \ln 1/\gamma_{\text{Cd}(\text{NO}_3)_2} / \partial R_{\text{NH}_4\text{Cl}}$. ($\gamma_{\text{Cd}(\text{NO}_3)_2}$ is the activity coefficient of $\text{Cd}(\text{NO}_3)_2$ and $R_{\text{NH}_4\text{Cl}}$ is the mole ratio (moles NH_4Cl per mole of ammonium nitrate) of ligand.)

In this paper we report the results of potentiometric

and polarographic measurements of the association constant of cadmium ion with bromide ion at 50° in the solvent $\text{Ca}(\text{NO}_3)_2 \cdot 4\text{H}_2\text{O}$. Since polarographic measurements at low cadmium ion concentrations were found to be reproducible, the extrapolation to the thermodynamic association constants is facilitated. We extend the method of evaluation of successive association constants from polarographic measurements without a large excess of ligand to include polynuclear species and to obtain equations which lend themselves to simple graphical analysis. Polarographic measurements also are reported in the solvent $\text{NH}_4\text{NO}_3 \cdot 2\text{H}_2\text{O}$ at 39.9° at concentrations below those studied potentiometrically, and the measurements are shown to agree with the previously reported potentiometric measurements.

Evaluation of Association Constants

In order to evaluate thermodynamic association constants, it is necessary to extrapolate the data to a defined reference state, here infinite dilution of all solutes in the solvent $\text{Ca}(\text{NO}_3)_2 \cdot 4\text{H}_2\text{O}$ or $\text{NH}_4\text{NO}_3 \cdot$

(1) To whom correspondence should be addressed at Reactor Chemistry Division, Oak Ridge National Laboratory, Oak Ridge, Tenn.

(2) J. M. C. Hess, J. Braunstein, and H. Braunstein, *J. Inorg. Nucl. Chem.*, **26**, 811 (1964).

(3) (a) J. Braunstein, M. Blander, and R. M. Lindgren, *J. Am. Chem. Soc.*, **84**, 1529 (1962); (b) J. Braunstein and A. S. Minano, *Inorg. Chem.*, **3**, 218 (1964).

$2\text{H}_2\text{O}$.^{3a} For reliable extrapolations, data at low ligand concentrations are required; on the other hand, the frequently imposed polarographic condition of a large excess of ligand over metal ion to minimize relative changes of ligand concentration at the surface of the mercury drop (so that concentrations at the electrode surface may be approximated by bulk concentrations) has been shown to lead to appreciable errors in the calculated association constants.³ The change of ligand concentration at the surface of the dropping mercury electrode has been discussed by Tomes for the case where a single complex species is the predominant form.⁴ Ringbom and Eriksson⁵ have modified the equations of DeFord and Hume⁶ to take into account the change of ligand concentration at the cathode for the case of successive equilibria. However, the equations of Ringbom and Eriksson are expressed in the concentrations of associated and unassociated species at the surface of the mercury drop, neglect polynuclear complexes, and lead to equilibrium quotients rather than thermodynamic association constants since they do not include extrapolation to a defined reference state. Solution of their equations requires successive approximations and may be difficult if many species are present. Here we extend their treatment by deriving equations for the thermodynamic association constants, also taking into account the change of ligand concentration at the surface of the mercury drop. Our equations lend themselves to a simple graphical analysis since they are expressed in the stoichiometric concentrations of the components in the bulk solution rather than the concentrations of the unassociated species at the electrode surface.

We may write⁷ for the potential of a polarographic cell in which c_0^0 is the concentration of reducible metal ion of charge Z at the surface of the dropping mercury electrode and c_a^0 is the concentration of metal in the amalgam at the surface of the mercury drop

$$E = -\frac{RT}{ZF} \ln \frac{c_a^0}{c_0^0} \quad (1)$$

Denoting the concentration of unassociated ligand L as c_L , of unassociated metal ion M^{Z+} as c_0 , and of the associated species ML , ML_2 , M_2L , etc., as c_1 , c_2 , c_{12} , etc., respectively, the current along the polarographic wave may be written

$$i = k_0(c_0 - c_0^0) + k_1(c_1 - c_1^0) + k_2(c_2 - c_2^0) + 2k_{12}(c_{12} - c_{12}^0) + \dots = \bar{k}[(c_0 + c_1 + c_2 + 2c_{12} + \dots) - (c_0^0 + c_1^0 + c_2^0 + 2c_{12}^0 + \dots)] \quad (2)$$

where the superscript zero denotes concentrations at the surface of the mercury drop, the k are the products of the capillary constant by the diffusion current con-

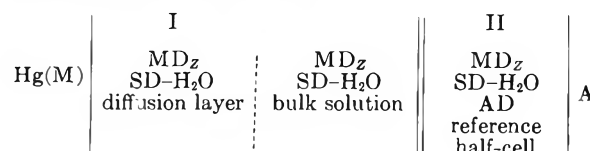
stants of the species, and \bar{k} is the weighted mean diffusion current constant multiplied by the capillary constant.⁶ Substituting the association constants

(4) J. Tomes, *Collection Czech. Chem. Commun.*, **9**, 81 (1937); J. J. Lingane, *Chem. Rev.*, **29**, 1 (1941); C. G. Butler and R. C. Kaye, *J. Electroanal. Chem.*, **8**, 463 (1964).

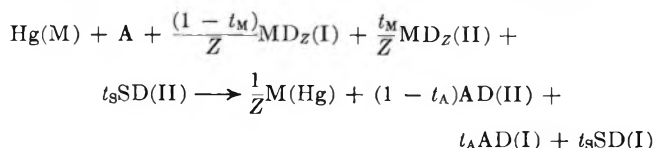
(5) A. Ringbom and L. Eriksson, *Acta Chem. Scand.*, **7**, 1105, 1146 (1953).

(6) D. D. DeFord and D. N. Hume, *J. Am. Chem. Soc.*, **73**, 5321 (1951).

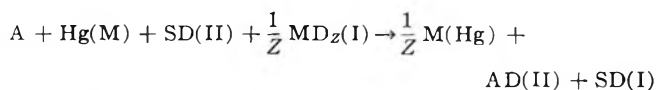
(7) We consider the polarographic cell to consist of the dropping mercury electrode at which reduction of a cation M^{Z+} to metal M takes place, a diffusion layer, the bulk solution, and a reference half-cell in the solvent $\text{SD-H}_2\text{O}$ where S^+ and D^- are the cation and anion of the supporting electrolyte.



The reference electrode A is considered to be reversible to the cation A^+ which is present at a low concentration. Reduction of 1 equiv of the cation M^{Z+} corresponds to the over-all process



if the transference numbers (t_M , t_A , and t_S) are independent of the concentrations through the diffusion region. If the concentrations of MD_Z and AD are very small so that the current is carried almost entirely by the ions of the supporting electrolyte, the transference numbers t_M and t_A will be negligible and the process may be approximated by



The potential of such a cell may be written

$$E' = E^\circ - \frac{RT}{F} \ln \frac{a^{1/Z} \text{M(Hg)}}{a^{1/Z} \text{MD}_Z(\text{I})} \frac{a_{\text{AD}(\text{II})} a_{\text{SD}(\text{I})}}{a_{\text{A}} a_{\text{Hg}(\text{M})} a_{\text{SD}(\text{II})}} \quad (i)$$

if the potential is assumed to have the same dependence on the activities of the components with the polarographic current flowing as in a reversible cell. The a_i are the activities of the reactant and product components; it is not necessary to resort to single-ion activities in the equations. If the transference numbers are not zero or constant, there will be an additional term in eq i

$$e = \frac{RT}{F} \int_{\text{I}}^{\text{II}} \left[t_A d \ln a_{\text{AD}} + t_S d \ln a_{\text{SD}} + \frac{t_M}{Z} d \ln a_{\text{MD}_Z} \right] \quad (ii)$$

In a dilute amalgam, the activity of the mercury, $a_{\text{Hg(M)}}$, is (nearly) equal to the activity of pure mercury. The activity of the metal A is constant (unity); the activity of SD (the supporting electrolyte) is constant, and the activity of AD in the reference half-cell is constant. The potential may therefore be written

$$E' = \text{constant} - \frac{RT}{ZF} \ln \frac{a_{\text{M(Hg)}}}{a_{\text{MD}_Z}}$$

or

$$E'' = -\frac{RT}{ZF} \ln \frac{a_{\text{M(Hg)}}}{a_{\text{MD}_Z}} \quad (iii)$$

The activity coefficient of the metal in the dilute amalgam is a constant (unity, if the reference state is infinite dilution in the amalgam).

$$\begin{aligned} K_1 &= \frac{c_1}{c_0 c_L} \\ K_2 &= \frac{c_2}{c_1 c_L} \\ K_{12} &= \frac{c_{12}}{c_1 c_0} \end{aligned} \quad (3)$$

etc., into (2)

$$i = \bar{k}c_0(1 + K_1c_L + K_1K_2c_L^2 + 2K_1K_{12}c_0c_L + \dots) - \bar{k}c_0^0(1 + K_1c_L^0 + K_1K_2c_L^{02} + 2K_1K_{12}c_0^0c_L^0 + \dots) \quad (4)$$

If the species do not follow Henry's law, the equations will also contain the activity coefficients of the species.^{3a} Since the diffusion current i_d is the current when the concentrations of the reducible species at the surface of the mercury drop are zero

$$i_d - i = \bar{k}c_0^0(1 + K_1c_L^0 + K_1K_2c_L^{02} + 2K_1K_{12}c_0^0c_L^0 + \dots) \quad (5)$$

The concentration of metal in the amalgam at the surface of the mercury drop is $c_a^0 = i/k_a$ where k_a is the product of the capillary constant by the diffusion current constant of metal in the amalgam. Substituting the expressions for c_a^0 and c_0^0 into the equation for the potential gives

$$E = -\frac{RT}{ZF} \ln \frac{i}{i_d - i} \frac{\bar{k}}{k_a} (1 + K_1c_L^0 + K_1K_2c_L^{02} + 2K_1K_{12}c_0^0c_L^0 + \dots) \quad (6)$$

When the current is half the diffusion current

$$E_{1/2} = -\frac{RT}{ZF} \ln \frac{\bar{k}}{k_a} (1 + K_1c_L^{01/2} + K_1K_2c_L^{01/22} + 2K_1K_{12}c_0^{01/2}c_L^{01/2} + \dots) \quad (7)$$

where the subscript $1/2$ indicates the potential and the concentrations at $i = i_d/2$. Subtracting $E_{1/2}^0$, the value of $E_{1/2}$ in the absence of ligand, from (7)

$$\Delta E_{1/2} = E_{1/2} - E_{1/2}^0 = -\frac{RT}{ZF} \ln \frac{\bar{k}}{k_0} (1 + K_1c_L^{01/2} + K_1K_2c_L^{021/2} + 2K_1K_{12}c_0^{01/2}c_L^{01/2} + \dots) \quad (8)$$

or, using the function F_0 of DeFord and Hume⁶

$$\ln F_0 = \left(-\frac{ZF}{RT} \Delta E_{1/2} - \ln \frac{\bar{k}}{k_0} \right) = \ln (1 + K_1c_L^{01/2} + K_1K_2c_L^{021/2} + 2K_1K_{12}c_0^{01/2}c_L^{01/2} + \dots) \quad (9)$$

Equation 9, which relates F_0 to the concentrations of the species at the surface of the dropping mercury electrode, is an extension of eq 7 of Ringbom and Eriksson which does not neglect the possibility of formation of polynuclear species. Solution of eq 9 for the association constants requires successive approximations. However, the evaluation of the constants can be greatly simplified and the need for successive approximations eliminated by considering the Taylor's series expansion of eq 9 in powers of the stoichiometric concentrations of the metal ion and ligand in the bulk solution, which we designate T_0 and T_L . The coefficients in the expansion

$$\lim_{\substack{T_L \rightarrow 0 \\ T_0 \rightarrow 0}} \left(\frac{\partial \ln F_0}{\partial T_L^{n-p} \partial T_0^p} \right)$$

are evaluated from eq 9 with the material balance of ligand and metal ion at the surface of the electrode and in the bulk solution. The coefficient of the constant term in the expansion is zero since

$$\lim_{\substack{T_0 \rightarrow 0 \\ T_L \rightarrow 0}} (\ln F_0) = 0$$

The coefficients of the stoichiometric concentrations in the Taylor's series are obtained by first expanding the right-hand side of eq 9 in the series $\ln(1+x) = -1/2x^2 + \dots$

$$\ln F_0 = K_1c_L^{01/2} + (K_1K_2 - 1/2K_1^2)c_L^{021/2} + 2K_1K_{12}c_0^{01/2}c_L^{01/2} + \dots \quad (10)$$

The first derivatives with respect to the stoichiometric concentrations are

(Reference 7 continued)

If the deviation from Henry's law (i.e., from the Nernst equation, which is observed to hold in these solutions for cadmium ion in the absence of halide, or halide in the absence of cadmium ion)² which are observed when ligand is added are due to the formation of associated species, and if the associated species as well as the unassociated metal ions and ligand follow Henry's law, we may write $a_{MDZ} = c_{MCD}^Z$. c_M is the concentration of "unassociated" metal ion and will be equal to the stoichiometric concentration of metal ion in the absence of ligand. Hence

$$E'' = -\frac{RT}{ZF} \ln \frac{c_{M(Hg)}}{c_{MCD}^Z} \quad (iv)$$

(If the species do not follow Henry's law, the species activity coefficients should be included.) Noting that c_D , the concentration of the anion of the supporting electrolyte, is virtually constant, and rewriting the concentrations of metal in the amalgam at the surface of the mercury drop and the concentration of M^{2+} in the solution at the surface of the mercury drop as $c_{M(Hg)} = c_a^0$ and $c_{M^{2+}} = c_0^0$, we have

$$E = -\frac{RT}{ZF} \ln \frac{c_a^0}{c_0^0} \quad (v)$$

$$\left(\frac{\partial \ln F_0}{\partial T_0}\right)_{T_L} = \left(\frac{\partial \ln F_0}{\partial c_{L^{0.5}}}\right)_{c_0^{0.5}} \left(\frac{\partial c_{L^{0.5}}}{\partial T_0}\right)_{T_L} + \left(\frac{\partial \ln F_0}{\partial c_0^{0.5}}\right)_{c_{L^{0.5}}} \left(\frac{\partial c_0^{0.5}}{\partial T_0}\right)_{T_L} \quad (11)$$

and

$$\left(\frac{\partial \ln F_0}{\partial T_L}\right)_{T_0} = \left(\frac{\partial \ln F_0}{\partial c_{L^{0.5}}}\right)_{c_0^{0.5}} \left(\frac{\partial c_{L^{0.5}}}{\partial T_L}\right)_{T_0} + \left(\frac{\partial \ln F_0}{\partial c_0^{0.5}}\right)_{c_{L^{0.5}}} \left(\frac{\partial c_0^{0.5}}{\partial T_L}\right)_{T_0} \quad (12)$$

Substitution of (10) in (11) and (12) and taking the limit as T_0 and T_L vanish gives

$$\lim_{\substack{T_0 \rightarrow 0 \\ T_L \rightarrow 0}} \left(\frac{\partial \ln F_0}{\partial T_0}\right)_{T_L} = K_1 \lim_{\substack{T_0 \rightarrow 0 \\ T_L \rightarrow 0}} \left(\frac{\partial c_{L^{0.5}}}{\partial T_0}\right)_{T_L} \quad (13)$$

and

$$\lim_{\substack{T_0 \rightarrow 0 \\ T_L \rightarrow 0}} \left(\frac{\partial \ln F_0}{\partial T_L}\right)_{T_0} = K_1 \lim_{\substack{T_0 \rightarrow 0 \\ T_L \rightarrow 0}} \left(\frac{\partial c_{L^{0.5}}}{\partial T_L}\right)_{T_0} \quad (14)$$

The concentration of unassociated ligand at the surface of the electrode may be related to the concentrations of unassociated species in the bulk solution and to the stoichiometric concentrations. If the current is carried through the solution only by the supporting electrolyte, a charge balance on all the solute species leads to the relation analogous to that of Tomes⁴ for one species

$$0 = i_{\oplus} - i_{\ominus} = ZJ_0 + (Z-1)J_1 + \dots + (2Z-1)J_{12} + \dots - J_L = Zk_0(c_0 - c_0^{0.5}) + (Z-1)k_1(c_1 - c_1^{0.5}) + \dots - k_L(c_L - c_L^{0.5}) - \dots \quad (15)$$

J_0, J_1 , etc., are fluxes of species of charge $Z, Z-1$, etc., and i_{\oplus} and i_{\ominus} are the current densities of the positive and negative solute species. Substituting eq 3 in (15), differentiating, and passing to the limit, we have

$$\lim_{\substack{T_0 \rightarrow 0 \\ T_L \rightarrow 0}} \left(\frac{\partial c_{L^{0.5}}}{\partial T_0}\right)_{T_L} = 0$$

$$\lim_{\substack{T_0 \rightarrow 0 \\ T_L \rightarrow 0}} \left(\frac{\partial c_{L^{0.5}}}{\partial T_L}\right)_{T_0} = 1$$

Hence

$$\lim_{\substack{T_0 \rightarrow 0 \\ T_L \rightarrow 0}} \left(\frac{\partial \ln F_0}{\partial T_0}\right)_{T_L} = 0$$

and

$$\lim_{\substack{T_0 \rightarrow 0 \\ T_L \rightarrow 0}} \left(\frac{\partial \ln F_0}{\partial T_L}\right)_{T_0} = K_1 \quad (16)$$

The coefficients of the higher terms in the expansion may be found in a similar manner (retaining the appropriate higher powers of the concentrations until passing to the limit). The resulting expansion, up to quadratic terms, is

$$\ln F_0 = K_1 T_L + (K_1 K_2 - \frac{1}{2} K_1^2) T_L^2 + (2K_1 K_{12} - K_1^2) T_0 T_L + \dots \quad (17)$$

Since eq 17 has the same form as the expansion of the stoichiometric activity coefficient $\ln 1/\gamma_0$ derived in an earlier paper, the same simple graphical analysis may be employed to calculate the association constants.^{3a} Only the stoichiometric concentrations are used in the calculations so that successive approximations are not required. Extrapolation to zero concentration leads to the thermodynamic association constants.

Experimental Section

Polarographic measurements were made with a controlled-potential and derivative voltammeter made by Indiana Instrument and Chemical Corp. (ORNL Model Q-1988)⁸ and a Sargent SR recorder with a 12.5-mv range plug. Initial and span potentials as well as some potentials along the polarographic wave were measured with a Keithley Model 660 differential voltmeter or a Leeds and Northrup Type K potentiometer. The polarographic cell consisted of a 100-ml Berzelius beaker clamped in a water bath controlled at 39.9 or 50.0°. The cell contained about 0.5 mole of ammonium nitrate in 1 mole of water or 0.5 mole of calcium nitrate tetrahydrate (which melts at 42.7°), the dropping mercury electrode, a platinum foil counter electrode (about 1 cm²), and a silver-silver chloride or silver-silver bromide reference half-cell. In order to minimize uncertainties due to liquid junction potentials, the reference half-cell was prepared with the same solvent as was used in the cell: either NH₄NO₃·2H₂O or Ca(NO₃)₂·4H₂O. The reference half-cell was prepared by a method similar to the method of preparation of reference half-cells used in molten salt investigations.^{3b} An asbestos fiber was sealed through the end of a length of 6-9-mm Pyrex tubing. The tubes were tested for leakage overnight in distilled water and then filled with solvent saturated with silver chloride

(8) M. T. Kelley, H. C. Jones, and D. J. Fisher, *Anal. Chem.*, **31**, 1262 (1960).

or silver bromide. A silver wire previously coated with silver halide was then inserted. The silver wire was coated with halide by first flaming the end to remove oxide and then quenching it in a dilute solution of KCl or KBr; a dilute solution of silver nitrate was then added. Groups of three to five reference half-cells prepared in this manner remained stable within several tenths of a millivolt over periods of several months when compared with each other and with similar electrodes in aqueous potassium chloride (bromide) solutions.

Cadmium nitrate was added to the cell either as the solid tetrahydrate or, with a micrometer syringe, as an aqueous solution. Ammonium chloride was added as weighed pellets of the dried salt. Potassium bromide was added as an aqueous solution by means of a micrometer syringe. The quantity of water added with the solute was insufficient to change the concentration or the half-wave potentials significantly. The solution in the cell was deoxygenated with nitrogen which was first bubbled through a large bulb of solution of the same composition as the solvent in the cell in order to prevent loss of water from the cell by evaporation. The half-wave potential was determined from plots of E vs. $\log i/(i_d - i)$ or by the method of Meites.⁹

The potentiometric measurements were made in the same cell used for the polarographic measurements and using the same silver-silver bromide reference half-cells. The cadmium amalgam electrode consisted of a J-tube of 9-mm Pyrex tubing containing enough cadmium amalgam, prepared as described previously,² to just fill the short arm of the J, which was immersed in the solution. Electrical contact was made by means of a platinum wire in the long arm of the J. Saturated nitrogen was passed through the solution which was stirred vigorously during the measurements. Solutes were added as described above.

Results

From the potentiometric measurements, the logarithm of the activity coefficient of $\text{Cd}(\text{NO}_3)_2$, $\ln \gamma_{\text{Cd}(\text{NO}_3)_2} = 2F/RT\Delta E$, was calculated from the cumulative change of emf, ΔE , on addition of bromide to the potentiometric cell containing a fixed concentration of cadmium nitrate¹ in the solvent $\text{Ca}(\text{NO}_3)_2 \cdot 4\text{H}_2\text{O}$ at 50° . In the absence of bromide, the emf of the cell followed the Nernst equation in the concentration of cadmium nitrate. At each cadmium concentration, the limiting slope

$$\left[\left(\frac{\partial \ln 1/\gamma_{\text{Cd}(\text{NO}_3)_2}}{\partial R_{\text{Br}}} \right)_{R_{\text{Cd}(\text{NO}_3)_2}} \right]_{R_{\text{Br}}=0}$$

was evaluated graphically and these slopes were then

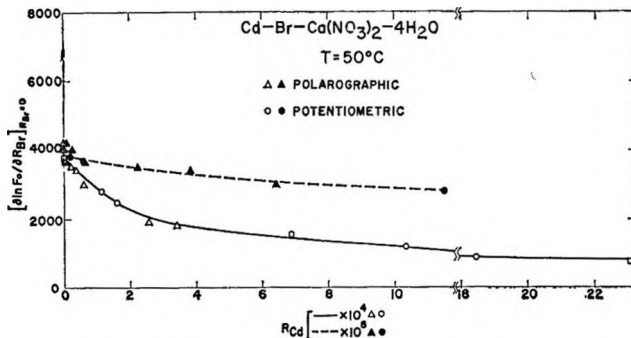


Figure 1. Extrapolation of the polarographic limiting slopes $[(\partial \ln F_0/\partial R_{\text{Br}})]_{R_{\text{Br}}=0}$ and the potentiometric limiting slopes $[(\partial \ln 1/\gamma_{\text{Cd}(\text{NO}_3)_2}/\partial R_{\text{Br}})]_{R_{\text{Br}}=0}$ to infinite dilution of cadmium nitrate to obtain the thermodynamic association constant.

plotted as a function of the concentration of cadmium ion as the circles in Figure 1 and extrapolated to the association constant.^{1,2} Concentrations are expressed as the mole ratios

$$R_{\text{Cd}(\text{NO}_3)_2} = \frac{n_{\text{Cd}(\text{NO}_3)_2}}{n_{\text{Ca}(\text{NO}_3)_2}}$$

and

$$R_{\text{Br}} = \frac{n_{\text{KBr}}}{2n_{\text{Ca}(\text{NO}_3)_2}}$$

where the n are numbers of moles of the components indicated by the subscripts.

The polarographic function $\ln F_0 = -(2F/RT)\Delta E_{1/2} + \ln(k_0/\bar{k})$, defined by eq 9, was calculated from the cumulative change, $\Delta E_{1/2}$, of the polarographic half-wave potential with successive bromide additions and from the diffusion currents;⁶ the slopes $(\partial \ln F_0/\partial R_{\text{Br}})_{R_{\text{Br}}=0}$ were evaluated graphically^{3a} and are plotted as the triangles in Figure 1. Extrapolation to zero cadmium concentration gives the thermodynamic association constant^{3a} for the formation of CdBr^+ in $\text{Ca}(\text{NO}_3)_2 \cdot 4\text{H}_2\text{O}$. In Figure 2 the polarographic slopes $(\partial \ln F_0/\partial R_{\text{Cl}})_{R_{\text{Cl}}=0}$ in $\text{NH}_4\text{NO}_3 \cdot 2\text{H}_2\text{O}$ at 40° are plotted together with the potentiometric slopes $(\partial \ln 1/\gamma_{\text{Cd}(\text{NO}_3)_2}/\partial R_{\text{Cl}})_{R_{\text{Cl}}=0}$ from the previously reported potentiometric measurements. In order to demonstrate the agreement of the polarographic and potentiometric results at the lowest concentrations, the slopes at the lowest cadmium concentrations have been plotted in Figures 1 and 2 on an expanded abscissa. The filled circles are potentiometric results and the filled triangles are polarographic results. It is seen that the slopes (and their extrapolation to the association constant, with eq 16) of the polarographic and potentiometric data are consistent.

(9) L. Meites, *J. Am. Chem. Soc.*, **72**, 2293 (1950).

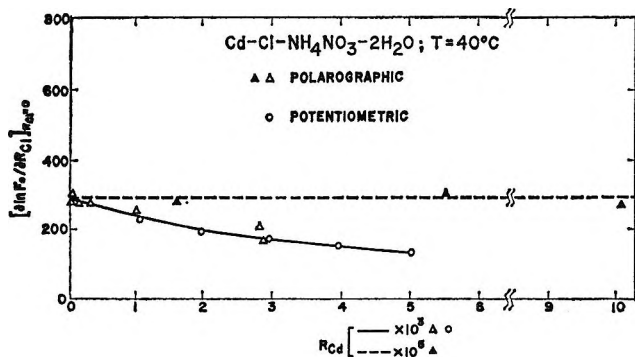


Figure 2. Extrapolation of the polarographic limiting slopes $[(\partial \ln F_0 / \partial R_{Cl})]_{R_{Cl} \rightarrow 0}$ and the potentiometric limiting slopes $[(\partial \ln 1/\gamma_{Cd(NO_3)_2} / \partial R_{Cl})]_{R_{Cl} \rightarrow 0}$ to infinite dilution of cadmium nitrate to obtain the thermodynamic association constant.

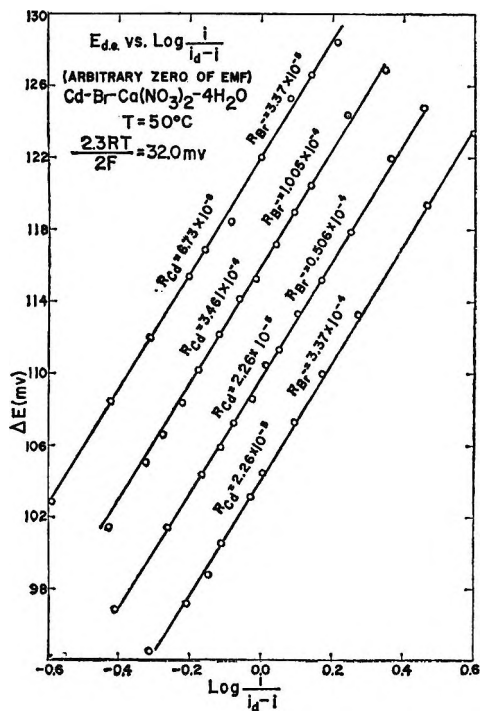


Figure 3. Potential of the dropping mercury electrode vs. $\log i/(i_d - i)$.

The association constant for the formation of $CdBr^+$ in the solvent $Ca(NO_3)_2 \cdot 4H_2O$ at 50° is 3900 ± 200 (moles of bromide/mole of nitrate) $^{-1}$. Using the graphical methods described previously,^{2,3a} the dinuclear association constant K_{12} is found to be 50 ± 200 , indicating the absence of dinuclear species. The association constant K_2 for the formation of $CdBr_2$ is

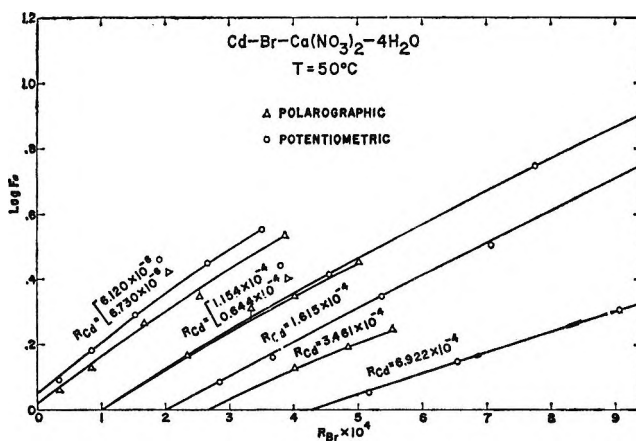


Figure 4. Plots of $\log F_0$ (polarographic, Δ) and $\log 1/\gamma_{Cd(NO_3)_2}$ (potentiometric, O) vs. the concentration of bromide at fixed concentrations of cadmium nitrate.

1500 ± 200 . The association constant for $CdCl^+$ in $NH_4NO_3 \cdot 2H_2O$ at 40° is 300 ± 15 , in agreement with the value reported previously, from emf measurements with cadmium amalgam electrodes, as 315 ± 20 .²

In Figure 3 it is seen that reversible waves were obtained with excess ligand or with excess metal ion. In Figure 4 are plotted some of the curves of $\ln F_0$ (polarographic) and $\ln 1/\gamma_{Cd}$ (potentiometric). The agreement between the polarographic and potentiometric results confirms that a large excess of ligand, which would vitiate the method for the evaluation of thermodynamic association constants, is not necessary in the polarographic measurements, but that extrapolation to infinite dilution of the solutes is required. The polarographic and potentiometric data are available as an ADI document.¹⁰

Acknowledgments. This work was supported under USAEC Contract No. AT-(30-1)-2873, Report NYO-2873-13. We are grateful to Dr. Douglas Inman for valuable discussions concerning the change of ligand concentration at the surface of the dropping mercury electrode.

(10) The data have been deposited as Document No. 8883 with the ADI Auxiliary Publications Project, Photoduplication Service, Library of Congress, Washington, D. C. A copy may be secured by citing the Document number and by remitting \$1.25 for photoprints, or \$1.25 for 35-mm microfilm. Advance payment is required. Make checks or money orders payable to: Chief, Photoduplication Service, Library of Congress.

Infrared Study of the Nature of the Hydroxyl Groups on the Surface of Porous Glass

by M. J. D. Low and N. Ramasubramanian

School of Chemistry, Rutgers, The State University, New Brunswick, New Jersey (Received November 1, 1965)

The slow dehydration and dehydroxylation of porous Vycor glass was followed by infrared spectroscopic techniques. Two sharp bands at 3748 and 3703 cm^{-1} and also two shoulders near 3850 and 3650 cm^{-1} were observed. Dehydroxylation, deuteration, fluoridation, and adsorption experiments showed all absorptions to be due to surface hydroxyl species. The 3748- cm^{-1} absorption is due to free surface silanol groups. The 3650- cm^{-1} shoulder is due to OH vibrations perturbed by hydrogen bonding. The 3703- cm^{-1} band has a half-width of 5 to 14 cm^{-1} and can only be observed at relatively low surface coverage. Impregnation of silica and porous glass with boric acid produced a band at 3703 cm^{-1} with the silica and enhanced that found with the glass, leading to the assignment of the 3703- cm^{-1} band to a B-OH surface structure. The nature of the species responsible for the 3850- cm^{-1} shoulder is uncertain.

Introduction

Porous Vycor glass has been studied extensively in recent years, emphasis being placed on obtaining information on the structure and properties of the glass surface, the nature of the surface hydroxyl groups, and on reaction of gases with the surface. The results of various studies involving infrared spectroscopic techniques are in general agreement, and the observation in the O-H region of a single asymmetric infrared band ascribed to isolated surface OH groups was reported in addition to a broad band due to hydrogen-bonded OH groups and adsorbed H_2O .¹⁻¹⁴ It was noticed, however, during a study of the interaction of activated hydrogen with glasses, that the surface of porous Vycor was unstable, contrary to the impression given by the literature. Small weight losses and changes in infrared spectra occurred over long periods of time on heating porous glass specimens *in vacuo*, and the asymmetric band ascribed to isolated surface OH groups was resolved. This led us to reexamine porous glass surfaces.

The existence of a second sharp band in the hydroxyl region has been mentioned previously. Sidorov,² working with a UR-10 spectrophotometer at a spectral slit width of 4 cm^{-1} , presented a spectrum of porous glass heated *in vacuo* at 650° for an unspecified time that

shows a small, sharp band marked to be at 3700 cm^{-1} . That band is not mentioned elsewhere in the paper, however. Also, Kozirovski and Folman,¹⁴ working with a Perkin-Elmer Model 21 spectrometer with CaF_2 optics, mention the formation of a 30- cm^{-1} spaced doublet when porous glass was evacuated for 1 hr at 900°. They state that the nature of the second,

- (1) T. H. Elmer, I. D. Chapman, and M. E. Nordberg, *J. Phys. Chem.*, **66**, 1517 (1962).
- (2) A. N. Sidorov, *Opt. Spectry. USSR*, **9**, 424 (1960).
- (3) I. D. Chapman and M. L. Hair, *J. Catalysis*, **2**, 145 (1963).
- (4) L. H. Little and M. V. Mathieu, *Actes Congr. Intern. Catalyse, 2^e, Paris*, **1**, 771 (1960).
- (5) N. W. Cant and L. H. Little, *Can. J. Chem.*, **42**, 802 (1964).
- (6) M. Folman, *Trans. Faraday Soc.*, **57**, 2000 (1961).
- (7) M. V. Mathieu, N. Sheppard, and D. J. C. Yates, *Z. Elektrochem.*, **64**, 734 (1960).
- (8) M. Folman and D. J. C. Yates, *Proc. Roy. Soc. (London)*, **A246**, 32 (1958).
- (9) M. Folman and D. J. C. Yates, *J. Phys. Chem.*, **63**, 183 (1959).
- (10) I. D. Chapman and M. L. Hair, *Trans. Faraday Soc.*, **61**, 1507 (1965).
- (11) A. V. Kieselev and V. I. Lygin, *Proc. Second Intern. Congr. Surface Activity*, **2**, 204 (1957).
- (12) T. H. Elmer, I. D. Chapman, and M. E. Nordberg, *J. Phys. Chem.*, **67**, 2219 (1963).
- (13) A. N. Sidorov, *Russ. J. Phys. Chem.*, **30**, 995 (1956).
- (14) Y. Kozirovski and M. Folman, *Trans. Faraday Soc.*, **60**, 1532 (1964).

sharp band of the doublet is uncertain, and also that the doublet was not always observed, but make the suggestion that a hydroxyl bonded to surface boron atoms may be responsible. The sharp band is not mentioned elsewhere in this paper. More recently, it was reported by Chapman and Hair¹⁰ that the reaction of ammonia with fluoridated glass at 200° produced a small band at 3700 cm⁻¹. The spectra were obtained with a Perkin-Elmer 221G spectrometer at unspecified spectral slit width. They noted that the position of this band was more suggestive of a hydroxyl stretching frequency (perhaps attached to a boron atom rather than a silicon atom), but proposed that it was due to a single N-H vibration where the nitrogen atom is bonded to two silicon atoms. No further discussion of the band is given.

It is interesting to note that in the above three studies, and also in subsequent ones by other workers, due consideration was not given to the existence of the second sharp hydroxyl band. The reason for this appears to be that much of the work was carried out with porous glass specimens that had been degassed at relatively low temperatures and/or for short periods of time, and that instruments not capable of resolving the band were used, as will be shown below. We have consequently studied the slow changes occurring on continuous evacuation leading to highly degassed surfaces systematically. The results of the present study agree with previous work in that the general trends of dehydration were confirmed, but differ significantly in the detail of all aspects.

Experimental Section

Samples of porous glass,¹⁶ Corning Code 7930, purchased from Corning Glass Co., were cut into rectangles 1 × 2 cm. For most infrared studies, a specimen of about 1-mm thickness was tied with thin platinum wire to a quartz carriage bearing a quartz-enclosed magnet. The carriage and specimen were then placed within the body of a Vycor cell similar to that described by Peri and Hannan.¹⁶ The specimen could be moved from the region of the cell windows to a furnace wound on the cell body by manipulating an externally applied magnet. Single and differential spectra obtained with such cells were run with the specimen at room temperature. In order to obtain spectra of the hot specimen, another type of cell was used. A piece of Vycor tube was closed off, and the sides were flattened to act as windows. The specimen was placed in the flattened region of this simple cell, which was then connected to a conventional vacuum system. The cell was surrounded by a furnace pierced by two holes directly opposite the cell windows to

permit passage of the infrared beam. The cell-furnace assembly was positioned in the sample space of a Perkin-Elmer Model 12C spectrometer, permitting spectra to be obtained at temperatures up to 850°.

The glass as received was clear and colorless. As we wished to observe the reactions over a wide range of temperatures, most of the work was done with the specimens as received. Some duplicate sets of experiments established that identical infrared results were obtained with untreated specimens and with specimens that had been heated in oxygen at 650°. Spectra were recorded at IX ordinate magnification with a Perkin-Elmer Model 521 spectrophotometer at theoretical slit widths of 3.9 and 2.4 cm⁻¹ at 3500 and 2500 cm⁻¹, respectively, or with a Perkin-Elmer Model 12C spectrometer equipped with CaF₂ optics. Two identical specimens and cells were used to obtain differential spectra.

Hydrogen and deuterium were purified by diffusion through hot palladium. Conventional vacuum systems capable of 10⁻⁶ torr were used. HF was prepared by the thermal decomposition of KHF₂ *in vacuo*. D₂O of 99.84% isotopic purity was freed from dissolved gases by alternate freezing and thawing *in vacuo*. In order to avoid the overlapping of spectra, the ordinates have been displaced for the spectra of several figures. When this was done, the % transmittance for a particular spectrum is indicated by a number next to the spectrum at the left ordinate.

Experiments and Results

Surface Areas. The degassing temperatures were kept below 900° in order to minimize sintering. Nitrogen BET surface areas,¹⁷ computed from data at six pressures, were 166, 173, 160, and 154 m²/g after heat treatment *in vacuo* for 3 hr at 300°, 19 hr at 500°, and 9 and 51 hr at 700°, respectively. The increase in area is considered to be brought about through the loss of water, small pores previously blocked by water becoming free and thus available for the penetration and adsorption of nitrogen. This agrees with the observation^{4,11} that degassing at 200° is necessary to remove physically adsorbed water and that some chemisorbed water remains at 500°. The decrease in area after the 51-hr, 700° treatment represents a loss of about one-tenth of the area at 500°, based on the initial weight of the specimen. If estimates of water loss per gram of starting weight are made, based on gravimetric measurements to be described elsewhere,

(15) M. E. Nordberg, *J. Am. Ceram. Soc.*, **27**, 299 (1944).

(16) J. B. Peri and R. B. Hannan, *J. Phys. Chem.*, **64**, 1526 (1960).

(17) S. Brunauer, P. H. Emmett, and E. Teller, *J. Am. Chem. Soc.*, **60**, 309 (1938).

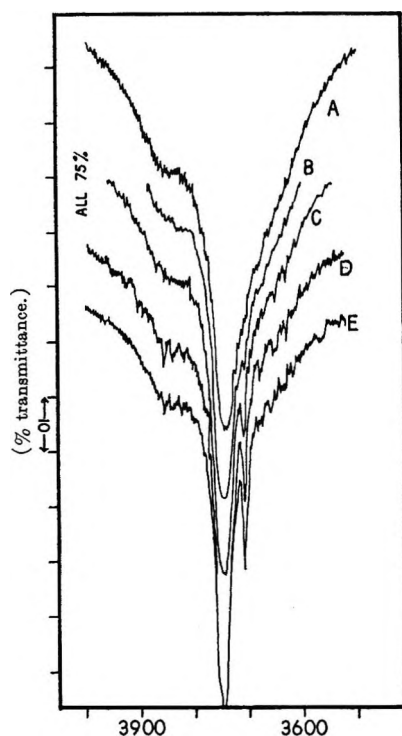


Figure 1. Dehydroxylation. Successive heat treatments, subsequent to 80 hr at 500°. The ordinates are displaced for clarity: at 600°, A, 25 hr; at 650°, B, 4 hr; C, 8 hr; D, 20 hr; at 700°, E, 2 hr.

a loss of area of similar magnitude results. This suggests that sintering was not drastic, so that possible effects of this were disregarded.

Dehydroxylation. The loss of water by porous glass specimens was followed from room temperature to 825° for long periods of time. Slow and continuous dehydration was found to occur even at 500° and below, but for present purposes only the later stages of degassing observed at high temperatures need be considered. Some results are shown in Figure 1. Spectrum A shows the general features previously reported, *i.e.*, an asymmetric band generally ascribed to surface silanol groups. Noticeable also is a distinct shoulder near 3850 cm^{-1} . On more severe degassing, the main band becomes sharper, as shown in the sequence A to E of Figure 1. Also, a second sharp band appears. A slow diminution of all bands and shoulders occurred at the higher temperature, as indicated by the successive spectra of Figure 2. Spectrum D of that figure shows a weak shoulder near 3850 cm^{-1} , the faint remnants of a band in the 3680–3550- cm^{-1} region, as well as the two prominent, sharp bands.

Various values have been quoted for the position of the hydroxyl band. The present experiments show that, besides the gross shift occurring during degassing

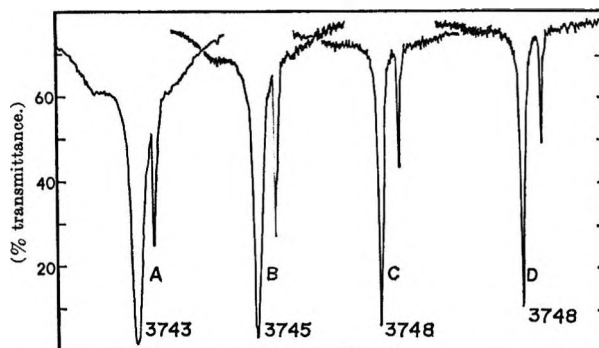


Figure 2. Dehydroxylation. Consecutive heat treatment following treatment at 750° for 24 hr: at 800°, A, 4 hr; at 825°, B, 20 hr; C, 68 hr; D, 92 hr.

at low temperatures or short times, there is a small shift of the free hydroxyl band until a very high degree of degassing is reached. For example, the position of the band changes from 3740 cm^{-1} (spectrum A, Figure 1) to 3743 cm^{-1} (spectrum E, Figure 1) at medium stages of degassing to a final value of 3748 cm^{-1} (spectra C and D, Figure 2) at high stages of degassing. The position of the free hydroxyl band is dependent on degassing conditions, *i.e.*, on the surface OH concentration. The value 3748 cm^{-1} will be used below to designate the free hydroxyl band.

During the heat treatments, a specimen was located within the furnace section of the cell and, at the end of a treatment, was moved to the window section of the cell. The spectrum was then measured with the specimen at room temperature. Heat treatments were also carried out without moving the specimens, spectra of the hot specimen being measured. Some of these spectra are shown in Figure 3. The resolution of those spectra and the degree of dehydration of that specimen were less than those shown in Figure 2. The sequence of spectra of Figure 3 serves to illustrate the slow process of dehydration. Of more importance is the fact that the spectra of hot and cold specimens showed similar structure, this indicating that the weak shoulders near 3850 and 3650 cm^{-1} were not artifacts caused by the readsorption of desorbed water as a specimen cooled to room temperature after a heat treatment. The shift in the broad band when the sample was cooled from 750 to 26° is similar to temperature-induced shifts of OH bands on alumina surfaces,¹⁸ and is attributed to the effects of temperature on hydrogen bonding.^{8,9,18}

The present spectra distinctly show the presence of a sharp band near 3703 cm^{-1} , in direct contrast to previous work¹⁻¹³ except for the instances noted

(18) J. B. Peri, *J. Phys. Chem.*, **69**, 211 (1965).

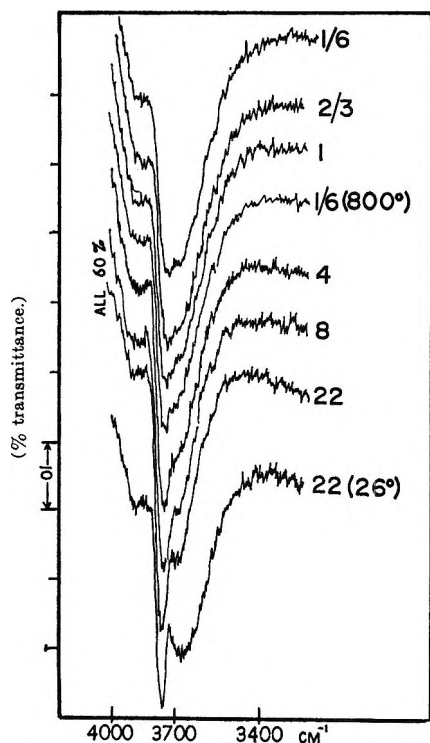


Figure 3. Spectra of hot specimen. Consecutive heat treatment for the times in hours indicated, at 750°. (The second 1/6-hr spectrum followed an 800° treatment.) The spectrum marked 22 (26°) was measured with the sample at room temperature. Other spectra were obtained at the temperature of heat treatment. The ordinates are displaced for clarity.

earlier.^{2,10,14} This discrepancy is brought about mainly by the difference in resolution of the spectrometers used and, to some extent, by the degassing conditions employed. Much of the previous work was done with Perkin-Elmer Model 21 instruments fitted with NaCl optics and occasionally with CaF₂ optics, whereas a Perkin-Elmer Model 521 grating instrument capable of higher resolution was used in this study, and instruments of suitable resolving power were used in the instances noted earlier.^{2,10,14} As the 3703-cm⁻¹ band has a half band width ranging from about 5 to 14 cm⁻¹ depending on the degree of degassing, instrument quality is important. However, the sharp 3703-cm⁻¹ band would not be detected unless degassing had proceeded beyond a stage such as that shown by spectrum A of Figure 1. The sharp band is completely obscured by the broad shoulder on the low-frequency side of the 3748-cm⁻¹ band, is barely detectable in spectrum B, but becomes prominent as in spectra C to E on further degassing of the sample. Kozirovski and Folman were not able to detect the hydroxyl doublet every time. They pointed out that Elmer,

Chapman, and Nordberg had not reported a doublet, and suggested that a cause for this could be a difference in the composition of the glass. We have, however, consistently detected the sharp band with samples taken from four different batches of glass obtained over a period of 2 years if degassing was sufficient and if an instrument capable of resolving the band was used.

Deuteration. The reaction with gaseous deuterium of specimens in various states of dehydration was examined at various temperatures and reaction times. The deuteration of a relatively poorly degassed specimen was not noticeable below 300°, but proceeded very slowly at 300°, the growth of bands in the OD region accompanying the decline of corresponding bands in the OH region. As the frequencies of the deuterio species fall in the region showing a broad band near 2700 cm⁻¹ attributed to boron oxide present in the solid, the growth of OD bands on top of this band is difficult to distinguish. Differential spectra were therefore made using identical cells and two specimens brought to similar stages of dehydration.

Figure 4 shows a sequence of differential spectra with specimens at a "medium" stage of dehydration. Negative bands appeared in the OH region as shown in plot A, because the specimens were not exactly matched at the beginning of the deuteration. Other differential spectra were obtained with specimens at high degrees of dehydration.

The bands and shoulders produced in the OD region by deuteration occurred near 2840, 2760, 2730, and 2700–2600 cm⁻¹. The relations between these and corresponding bands near 3850, 3740, 3703, and 3680–3550 cm⁻¹ in the OH region were 1.357, 1.357, 1.359, and about 1.38, respectively. For the spectra of highly degassed specimens the OH, OD positions and isomer shifts were, respectively, 3748 cm⁻¹, 2760 cm⁻¹,

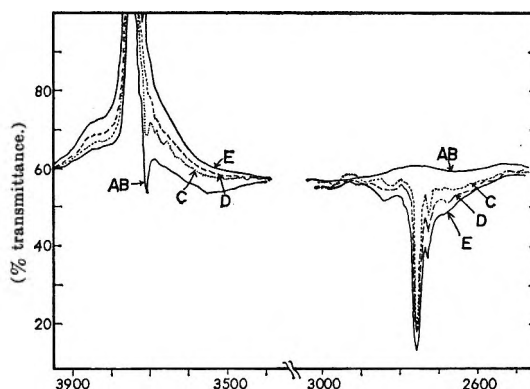


Figure 4. Differential spectra of deuteration. A: after the sequence of evacuations resulting in spectrum E of Figure 1. The sample was then heated in D₂ at 10 cm; B: 0.5 hr, 26°; C: 0.5 hr, 400°; D: 1.5 hr, 400°; E: 1 hr, 500°.

1.358₅, 3703 cm⁻¹, 2728 cm⁻¹, 1.358₉. This closely approximates the theoretical value of the isomer shift expected for identical OH and OD structures and, with the observation that the growth of a band in the OD region was accompanied by the decline of a corresponding band in the OH region, indicates that the four absorptions were brought about by surface OH groups, the deuteration involving the exchange of the hydrogen atom of an OH group by a deuterium atom.

The bands of the residual OH groups declined at different rates on heating *in vacuo*, shown, for example, by the sequence A, B, C, D of Figure 2. The exchange reactions similarly occur at different rates. For example, the ratio of peak heights of the sharp OD bands at 2760 and 2728 cm⁻¹ changed from about 0.6 after 2.5 hr at 500° to about 1.1 after 10 min at 600°, and to about 1.7 after 75 min at 600°. These differences indicate that a distinct surface OH species is responsible for each of the sharp bands.

The deuteration was accompanied by a frequency shift of the unexchanged silanol groups, except at very high stages of degassing. For the data of Figure 4, for example, the free OH band moved from an initial value of 3743 cm⁻¹ on the deuterium-free surface to a final value of 3748 cm⁻¹ for the residual OH groups. A similar small shift was observed for small and high OD surface concentrations.

Identical results could be produced by treating porous glass with D₂O, although deuteration of the surface occurred at lower temperatures than with D₂. For example, a sample was exposed to D₂O vapor at 2 cm pressure at 100° for 4 hr and was then degassed at 400° for 4 hr. Upon repetition of this cycle for five or six times about 90% of the surface OH species could be converted to the corresponding OD species.

HF Treatment. A porous glass specimen was degassed at 750° for 16 hr, was then exposed to HF at 1 cm pressure for 1 hr, and then was degassed at 500° for 4 hr. This successive HF treatment and degassing was repeated twice. The results are shown in Figure 5, the spectra showing that all bands could be removed completely by the HF treatment, thus indicating the sharp 3748- and 3703-cm⁻¹ bands to be caused by surface species. A slight shift to higher frequency in the Si-OH vibration can be seen as the removal of hydroxyls proceeds. The two sharp hydroxyl bands could be restored by adsorbing water on a fluoridated sample at room temperature and degassing at temperatures varying from 30 to 300°. Such experiments, which will be reported in detail elsewhere, indicate that the removal of surface boron through the formation of volatile BF₃ could not have occurred to an appreciable extent.

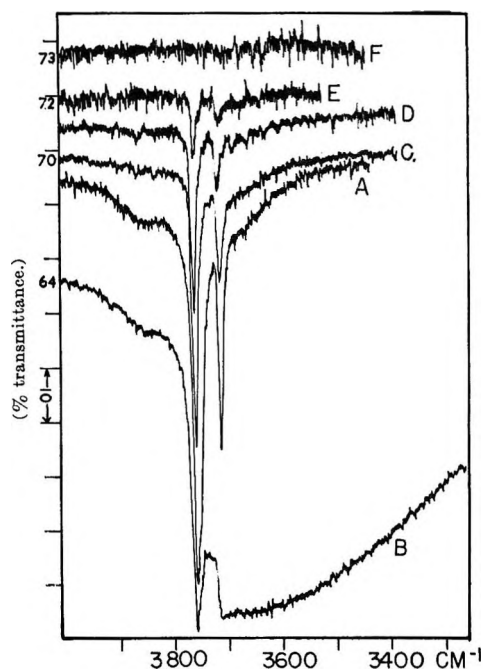


Figure 5. HF treatment: A, after 20 hr degassing at 750°; B, after 1 hr contact with 1 cm of HF at room temperature; C, after 0.5 hr degassing at 500°; D, after 4 hr degassing at 500°; E, after HF treatment as in B followed by 3 hr degassing at 500°.

HNO₃ Leaching. A porous glass specimen was leached with nitric acid following the procedure of Little, Klauser, and Amberg.¹⁹ They had shown the boron content of the glass to be unaffected by this treatment, but the aluminum and zirconium content as R₂O₃ changed from 0.89 to 0.36%. The spectra of the leached and unleached specimens, after identical degassing, were similar in the OH region and also in the 2700-cm⁻¹ region where bands attributed to the boric oxide in the glass occur. As the leaching did not affect the ratio of intensities of the sharp bands, this excludes the possibility that the 3703-cm⁻¹ band was caused by an OH associated with R₂O₃.

Boric Acid Impregnation. Cab-O-Sil²⁰ silica was impregnated with boric acid to result in a SiO₂-2% B₂O₃ sample approximating the chemical composition of the porous Vycor.

A slurry made from Cab-O-Sil and the required amount of an aqueous boric acid solution was air-dried at 135° for 2 hr. Self-supporting 1-in. diameter wafers of about 0.1 g of the pure and the impregnated Cab-O-Sil were prepared by pressing at 30 tons/in.². Spectra were recorded at different stages of degassing,

(19) L. H. Little, H. E. Klauser, and C. H. Amberg, *Can. J. Chem.*, **39**, 42 (1961).

(20) Cabot Co., Boston, Mass.

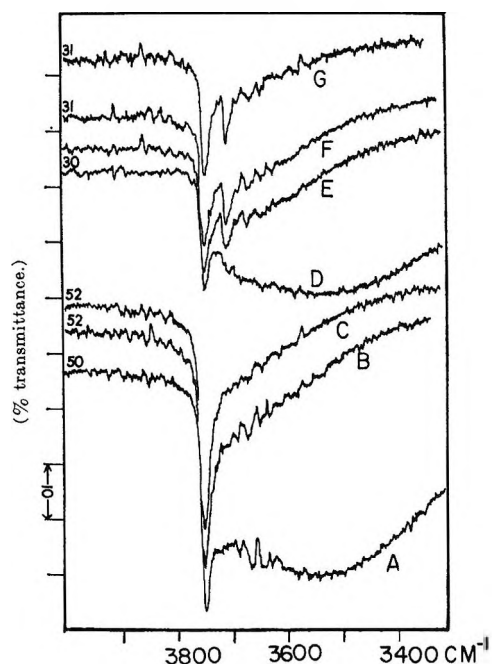


Figure 6. Boric acid treatments. Degassing of Cab-O-Sil: A, room temperature, 1 hr; B, 400°, 1 hr; C, 500°, 1 hr. Degassing of Cab-O-Sil + boric acid: D, room temperature, 0.25 hr; E, 300°, 0.5 hr; F, 400°, 0.25 hr; G, 400°, 1 hr. The ordinates are displaced.

examples being shown in Figure 6. The spectra of pure Cab-O-Sil show structure similar to that observed with other silica adsorbents,^{13,21,22} but a sharp band at 3703 cm^{-1} is evident in the spectra of the boric oxide-impregnated sample in addition to the hydroxyl band near 3745 cm^{-1} .

Another specimen was prepared by boiling a porous glass sample in 0.1% boric acid solution for 0.5 hr. The specimen was then air-dried and degassed. Comparison of the spectra of untreated and boric acid-treated specimens after identical degassing showed that the 3703- cm^{-1} band was enhanced by about 6%.

Discussion

The existence of four infrared absorptions in the O-H region has been shown. In concurrence with others, the 3748- cm^{-1} band is attributed to what are generally referred to as "free hydroxyls," *i.e.*, silanol groups so oriented that they do not react with their surroundings. The small frequency shifts from lower wavenumbers to 3748 cm^{-1} during the progress of deuteration or fluoridation of surfaces that have not been subjected to severe degassing, however, and also the small shifts to 3748 cm^{-1} on continued degassing of medium or highly degassed surfaces, indicate that the hydroxyl vibrations are not unperturbed except at very low degrees of surface coverage. A second band or shoulder

in the 3650- cm^{-1} region, responsible for the asymmetry of the low frequency side of the 3748- cm^{-1} band as in spectra A to C of Figure 1, and which gradually decreased in intensity to form a shoulder as in spectrum A of Figure 2, is similarly ascribed to the perturbation of the O-H stretching vibration through hydrogen bonding.

Spectrum A of Figure 1 shows a shoulder near 3850 cm^{-1} which declines in intensity but becomes somewhat more distinct in the sequence B to E, but which is still to be found in spectrum D of Figure 2 of a highly degassed specimen. Adams and Douglas²³ have assigned a band at 3846 cm^{-1} found with fused silicas to a combination of the bending vibration of OH within the fused silica and of a SiO_4 stretching vibration. The 3850- cm^{-1} shoulder of porous glass, however, changed in intensity on degassing and fluoridation in concert with other bands, showed an isomer shift. Other experiments not described here showed that the 3850- cm^{-1} shoulder decreased in intensity and disappeared completely when various amounts of acetone or methanol were adsorbed. The shoulder was restored on degassing the adsorbent at room temperature. Also, for spectra measured at various stages of degassing of the same sample as well as of different samples, the ratio of the area of the 3850- cm^{-1} shoulder and of the area of the rest of the absorption in the hydroxyl region remained constant, pointing to some relation of the 3850- cm^{-1} shoulder to surface hydroxyl concentration rather than to hydroxyls in the bulk of the glass. The exact nature of the species responsible for the 3850- cm^{-1} shoulder is uncertain, however.

The various degassing, fluoridation, and exchange experiments described above here indicated that the sharp 3703- cm^{-1} band is caused by an OH species, that the particular grouping is on the surface of the glass, and that the surface grouping is not the same as the silanol responsible for the 3748- cm^{-1} band. These experiments, as well as the results of the nitric acid leaching experiments which exclude the consideration of OH groups bonded to surface R_2O_3 , do not exclude the possibility of existence of a second silanol structure. However, the boric acid impregnation of silica, leading to the formation of a band at 3703 cm^{-1} , and the enhancement of the 3703- cm^{-1} band of porous glass by the boric acid treatment, lend strong support to the suggestion that the 3703- cm^{-1} band is brought about by surface B-OH groupings. That band is thus as-

(21) H. A. Benesi and A. C. Jones, *J. Phys. Chem.*, **63**, 179 (1959).

(22) R. S. McDonald, *J. Am. Chem. Soc.*, **79**, 850 (1957).

(23) R. V. Adams and R. W. Douglas, *Trans. Soc. Glass Techn.*, **43**, 147 (1959).

signed to OH groups bonded to surface boron atoms, and appears to be identical with bands mentioned previously.^{2,10,14} It seems likely that, with Chapman and Hair's work,¹⁰ the reaction of ammonia with the dehydroxylated porous glass surface had brought about the formation of some B-OH structures. The B-OH band is sharp and symmetrical and is observed at relatively high stages of degassing, indicating that the groups are not perturbed by hydrogen bonding. This assignment agrees with the observation that, for porous glass and for the synthetic SiO_2 -2% B_2O_3 sample, the ratios of the intensities of the 3748- and 3703- cm^{-1} bands are of similar magnitude. However, the boric oxide content of the glass is about 3%, so that an intensity ratio of Si-OH and B-OH of the order of 30 would be expected, for a homogeneous distribution of boron based on the assumption of identical absorptions of the two OH groups. As the boron of the synthetic sample is on the silica surface, this would imply that the surface boron concentrations of the glass and impregnated silica were similar, *i.e.*, that an appreciable fraction of the boron contained by the glass was on the glass surface. Such an enrichment could have occurred through the migration of boron to the surface

of the porous glass when heated above 500°¹³ as in the present study. It is interesting to note that absorption in the 3850- cm^{-1} region and the boron oxide bands near 2700 cm^{-1} found with porous glass were not observed with the SiO_2 -2% B_2O_3 sample. This indicates that the environment of the boron on the silica surface differed from that of the boron on or in the glass, and lends some support to the above assignment.

The present results indicate that the nature of the porous glass surface is more complex than had been supposed. If the surface hydroxyl groups play an active role in determining the characteristics of the surface, the existence of the B-OH groups in addition to the silanol species is of particular interest because the reactivity of the silica surface could be affected by their presence. The existence of multiple hydroxyl species should thus be taken into account in studies of adsorption and catalysis involving porous glass surfaces.

Acknowledgments. Support for this work through Contract No. DA36-039-AMC-02170(E) monitored by U.S.A.E.L., Contract Nonr-404 (19), and National Science Foundation Grant GP 1434, is gratefully acknowledged.

Transport Numbers of Concentrated Sodium Chloride Solutions at 25°

by L. J. M. Smits and E. M. Duyvis

*Koninklijke/Shell Exploratie en Productie Laboratorium, Rijswijk, The Netherlands
(Received November 19, 1965)*

Sodium transport numbers in NaCl solutions at 25°, from 0.024 *m* up to saturation (6.144 *m*), were obtained by measuring the emf of galvanic cells with transference. The values were higher than those obtained by Caramazza (up to 5 *m* using the emf method) and those of Currie and Gordon (up to 2.5 *m* using the adjusted indicator technique), the latter observations being corrected for volume changes. For this correction an equation was derived that differs from an approximate equation obtained by Bearman, Haase, and Spiro. Our results are in excellent agreement with Stokes' theory over the entire concentration range. The applicability of this theory in concentrated solutions is discussed. Incorporation in Stokes' equation of a recent theory of electrophoretic retardation of Fuoss and Onsager leads to physically impossible results at higher concentrations.

Introduction

To our knowledge, few data have been published on transport numbers for sodium chloride solutions at concentrations above 0.2 *m* (moles/kg of H₂O). Currie and Gordon,¹ using the adjusted indicator technique, which is a modification of the moving boundary method, obtained values of the sodium transport number up to a concentration of about 2.5 *m*. By measuring the emf of galvanic cells with liquid junction, Caramazza² obtained values of the sodium transport number for concentrations up to 5.0 *m*. No sets of data extending to saturated solutions are available. We therefore performed measurements of the sodium transport number in NaCl solutions at 25° over a concentration range from 0.024 *m* to saturation (6.144 *m*). Like Caramazza, we used the emf method, which is most convenient for very concentrated solutions.

Experimental Section

The cell used was of the flowing junction type, similar to that described by MacInnes and Yeh.³

It was difficult to obtain silver-silver chloride electrodes that were stable enough for measurements in very concentrated NaCl solutions. It was found that spongy electrodes with a large surface area performed satisfactorily. They were prepared in the following manner.

Platinum wires 0.5 mm in diameter were coated at one end with a pear-shaped sponge of silver by elec-

trolysis in a 0.4 *m* AgNO₃ solution, applying a current of 125–150 ma for 1 min. Every 5–10 sec the current was interrupted by lifting the electrode out of the solution. The silver sponge thus formed was then heated in a blue flame until it just glowed, to give more rigidity to the system. This procedure was repeated three times. The electrode was then heated in an oven at 350° to burn off all possible contamination introduced by the flame. About 15% of the silver was then converted to silver chloride electrolytically in an NaCl solution by applying a current of 2.5 ma. The electrodes were aged by short-circuiting several of them when immersed in the solution until they had an asymmetry potential of less than 0.01 mv. This was normally attained within 1 hr. The electrodes thus prepared gave stable and reproducible emf readings within a few hundredths of a millivolt over a period of at least 2 days.

For saturated NaCl solutions, however, the electrodes still deteriorated rapidly, unless the solution was also saturated with AgCl. A sufficient amount of silver chloride could be dissolved by gently heating under reflux a solution, saturated with NaCl at 25°, with an ex-

(1) D. J. Currie and A. R. Gordon, *J. Phys. Chem.*, **64**, 1751 (1960).

(2) R. Caramazza, *Gazz. Chim. Ital.*, **90**, 1839 (1960).

(3) D. A. MacInnes and Y. L. Yeh, *J. Am. Chem. Soc.*, **43**, 2563 (1921). For solutions of the same single electrolyte, a flowing junction is not required. However, this apparatus was already in use for experiments with more than one electrolyte.

cess of AgCl only. NaCl must not be present in excess, because then the silver ions in solution precipitate almost quantitatively during cooling, as NaCl and AgCl crystals are isomorphous.⁴ Saturation of the solution with silver by adding silver nitrate could not be applied here because the nitrate ion has a measurable effect on the emf.⁵

Regarding the reliability of silver-silver chloride electrodes in concentrated solutions, Lengyel, Giber, and Tamás⁶ discussed a possible effect of the presence of dissolved AgCl in LiCl solutions, up to 17 *m*, on the emf of galvanic cells with and without transference. They measured emf values of two kinds of cells with transference, one with silver-silver chloride electrodes and the other with lithium amalgam electrodes. Also, emf values of cells without transference were measured with the usual electrode arrangement of silver-silver chloride electrodes in the two electrolyte solutions and lithium amalgam separating the solutions. Combining the emf values of the different types of cells in three different ways and using isopiestic activities of LiCl, they calculated three sets of transport numbers. If all the electrodes used behave ideally and accurate values of activities at their measuring temperature of 15° are available, then the three sets of transport numbers calculated from either method should be identical. Lengyel, *et al.*, found this not to be the case at LiCl concentrations above 2.6 *m*. They concluded that this was due to the presence of dissolved AgCl in the neighborhood of the silver-silver chloride electrodes. Their experimental results, however, can equally well be explained by assuming that the lithium amalgam electrodes show deviations from ideal behavior. Moreover, Lengyel and Giber⁶ showed that silver-silver chloride electrodes behave satisfactorily in HCl solutions even at extremely high concentrations up to saturation (14.7 *m* at 25°), where the solubility of AgCl is also very high (more than 0.2 mole % of the HCl⁷). This proves that any possible deviation of silver-silver chloride electrodes in LiCl solutions does not necessarily mean failure in other solutions.

From the work of Harned and Nims,⁸ who measured the emf values of galvanic cells without transference with NaCl solutions up to 4 *m*, and isopiestic activity coefficients given by Robinson and Stokes,⁹ it appears that sodium amalgam electrodes and silver-silver chloride electrodes in NaCl solutions give emf readings that are correct within a few tenths of 1%. In view of these considerations, we believe that silver-silver chloride electrodes in NaCl solutions do not give appreciable errors.

In our experiments, we measured the emf of a succession of galvanic cells with liquid junction, keeping

the ratio of the molalities of the NaCl solutions at each side of the liquid junction at a constant value of 2, over a concentration range from 6.144 to 0.024 *m*. Each measurement was made with two electrodes on each side of the cell, the average of the four possible determinations of the emf being taken as the measured value. Two series of experiments were made; for the second one, freshly prepared electrodes and solutions were used.

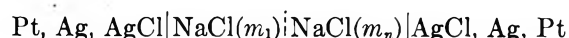
The cell potentials were measured with a compensator, accurate to 0.01 mv (Dr. C. E. Bleeker, N. V., Zeist, Holland, Type 2165). The measurements were carried out at a controlled temperature of 25 ± 0.2°.

Results

The measured values of the cell potentials were combined as

$$E_t(m_1|m_n) = E(m_1|m_2) + E(m_2|m_3) + \dots + E(m_{n-1}|m_n)$$

in which the *E* values are the emf values of the successive cells and *m*₁ = 0.02400. Thus for each concentration (*m*_{*n*}) a value of *E*_{*t*} was obtained. The potentials *E*_{*t*} are the emf values of galvanic cells with liquid junction of the type



The equation relating *E*_{*t*} to the mean ionic activity (*a*_±) of the electrolyte is^{10,11}

$$dE_t = -t_{\text{Na}}^h \frac{2RT}{F} \times 2.3026 \, d \log a_{\pm} \quad (1)$$

where *t*_{Na}^h is the sodium Hittorf transport number.

The experimental data of *E*_{*t*} vs. log *a*_± can be ac-

(4) C. Schierholz, *Sitzber. Kl. Akad. Wiss. Wien*, **101**, 2b, 4 (1892).

(5) This was shown by an increase of about 0.1 mv of the liquid junction potential between the saturated solution and a 3 *m* NaCl solution upon addition of NaNO₃ to the saturated solution, the number of moles of NaNO₃ added being equal to the number of moles of silver nitrate already present in the saturated solution.

(6) S. Lengyel, J. Giber, and J. Tamás, *Magy. Kem. Folyoirat*, **66**, 161 (1960); S. Lengyel and J. Giber, *Acta Chim. Acad. Sci. Hung.*, **32**, 235 (1962); S. Lengyel in "Electrolytes," B. Pesce, Ed., Pergamon Press Ltd., London, 1962, p 208.

(7) A. Seidell, "Solubilities of Inorganic and Metal Organic Compounds," Vol. I, 4th ed, W. F. Linke, Ed., D. van Nostrand Co., Princeton, N. J., 1958.

(8) H. S. Harned and L. F. Nims, *J. Am. Chem. Soc.*, **54**, 423 (1932).

(9) R. A. Robinson and R. H. Stokes, "Electrolyte Solutions," 2nd ed, Butterworth and Co. Ltd., London, 1959.

(10) The derivation of eq 1 has been given, for instance, by Guggenheim (ref 11, pp 456-458). It has to be noted that this derivation, especially the transition from his eq 14.06.5 to eq 14.06.11, is valid only if Hittorf transport numbers are used. These transport numbers are defined with ionic velocities taken with respect to the solvent.

(11) E. A. Guggenheim, "Thermodynamics," 4th ed, North-Holland Publishing Co., Amsterdam, 1959.

curately represented by a quadratic equation, the coefficients of which are calculated by the method of least squares

$$-E_t = 76.05 + 44.01 \log a_{\pm} - 0.6977 \log^2 a_{\pm} \quad (2)$$

The results of the measurements and the values calculated from the empirical eq 2 are given in Table I.

Table I: Potentials (E_t) of Galvanic Cells with Liquid Junction between NaCl Solutions at 25°. Comparison with Eq 2

Concn, moles/kg of H ₂ O, m_n	Log a_{\pm} ^a	- E_t , mv		
		First expt	Second expt	Calcd, eq 2
0.02400	-1.683	0	0	0.005
0.04800	-1.403	12.97	12.84	12.93
0.0960	-1.126	25.74	25.59	25.61
0.1920	-0.848	38.31	38.00	38.23
0.3840	-0.573	50.87	50.46	50.60
0.7680	-0.292	63.37	62.92	63.14
1.536	0.0036	76.35	76.06	76.21
3.072	0.3436	91.15	90.88	91.09
6.144	0.7897	110.59	110.21	110.37

^a The values of a_{\pm} were calculated from the mean ionic activity coefficients given in ref 9.

From eq 1 and 2 it follows for the concentration range from $m = 0.024$ to 6.144 that

$$t_{\text{Na}}^h = 0.3720 - 0.0118 \log a_{\pm} \quad (3)$$

In Figure 1, the values of t_{Na}^h are plotted against m for concentrations up to 0.2 m ; they show close agreement with the results obtained by Longworth (ref 9, p 158) and Allgood, *et al.* (ref 9, p 158). In Figure 2, the values of t_{Na}^h are plotted over the concentration range up to 6.144 m together with the values obtained by Currie and Gordon¹ and Caramazza.² We cannot evaluate the significance of the difference between our results and those of Caramazza as the accuracy of his measurements is not known to us. A closer examination (see next section) of the adjusted indicator technique, used by Currie and Gordon,¹ is required before a comparison with their results can be made.

Discussion of the Adjusted Indicator Technique

The adjusted indicator technique used by Gordon, *et al.*,^{1,12} is a variation of the moving boundary method for measuring transport numbers. In the latter method, the movement of a boundary between two electrolyte solutions having one ion in common (*e.g.*, KCl and NaCl) is measured while an electrical field is applied across this boundary. When p coulombs have

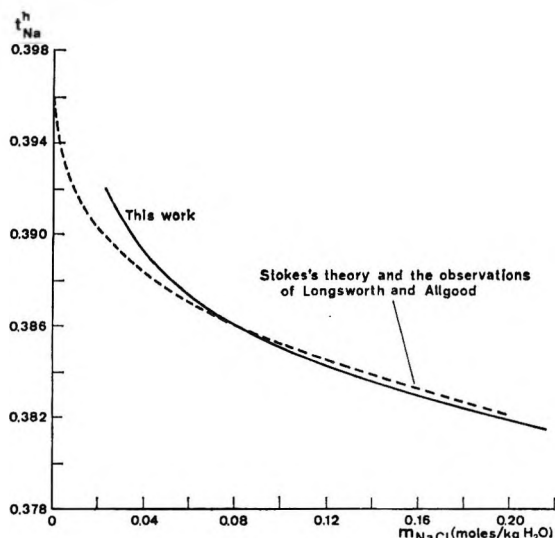


Figure 1. Hittorf transport numbers of the sodium ion in NaCl solutions at 25° (low concentrations).

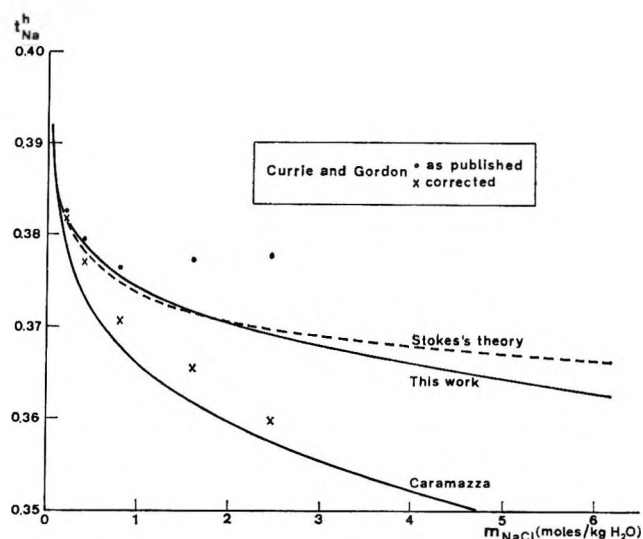


Figure 2. Hittorf transport numbers of the sodium ion in NaCl solutions at 25° (up to saturation).

passed, the boundary has passed a volume V liters of the cell.

The following equations then obtain

$$c_K V = p t_K^a / F \quad (4)$$

and

$$c'_{\text{Na}} V = p t_{\text{Na}}^a / F \quad (5)$$

where c_K denotes the normality of the K^+ ions in the KCl solution originally present in V ; c'_{Na} is the normality of the Na^+ ions present in V at the end of the

(12) D. R. Muir, J. R. Graham, and A. R. Gordon, *J. Am. Chem. Soc.*, **76**, 2157 (1954).

experiment which may differ from the initial Na^+ ion concentration. Thus

$$\frac{t_{\text{Na}}^{\text{a}}}{t_{\text{K}}^{\text{a}}} = \frac{c'_{\text{Na}}}{c_{\text{K}}} \quad (6)$$

The transport numbers in eq 4, 5, and 6 are apparent transport numbers (ref 13, p 218) and not Hittorf transport numbers, the movement of the boundary being taken with respect to the wall of the cell and not with respect to the water, which is also moving in the cell. Under the experimental conditions the concentration of the following solution (in this case NaCl) adjusts itself in such a way that eq 6, which is known as the Kohlrausch regulating function, is obeyed.

This adjusted concentration is measured in the adjusted indicator technique to determine the ratio of the two cation transport numbers. From this ratio and the known value of one of the cation transport numbers, the other cation transport number can be calculated. This technique has been improved by Gordon, *et al.*,^{1,12} to such an extent that accurate experimental results can be obtained.

Accurate values of potassium Hittorf transport numbers in KCl solutions up to 3 *N* were obtained by MacInnes and Dole¹⁴ using the Hittorf method. These values were employed by Currie and Gordon¹ to determine the sodium transport numbers in NaCl solutions. However, using eq 6, they actually obtained the ratio between the apparent transport numbers instead of the ratio between the Hittorf transport numbers. They tested their procedure at low concentration (0.1 *N* KCl) against the moving boundary method and found satisfactory agreement. However, at this low concentration the difference between apparent and Hittorf sodium transport numbers is very small and within their measuring accuracy. Application of eq 6 leads to erroneous results, however, at higher concentrations.

Bearman¹⁵ and Haase,¹⁶ treating the theory of the moving boundary technique, and Spiro,¹⁷ dealing with the adjusted indicator technique, corrected the Kohlrausch regulating function (eq 6). They arrived by different routes at the same equation for the ratio of Hittorf transport numbers, which can be written as

$$\frac{t_{\text{Na}}^{\text{h}}}{t_{\text{K}}^{\text{h}}} = \frac{c'_{\text{Na}}/c'_{\text{w}}\bar{v}'_{\text{w}}}{c_{\text{K}}/c_{\text{w}}\bar{v}_{\text{w}}} = \frac{P'_{\text{Na}}}{P_{\text{K}}} \quad (7)$$

where c_{w} and \bar{v}_{w} are the molar concentration and the partial molar volume of the water in the KCl solution, respectively, and c'_{w} and \bar{v}'_{w} are the corresponding quantities in the adjusted NaCl solution. Thus P'_{Na} and P_{K} are the electrolyte concentrations in moles per unit partial volume of water.

Spiro¹⁷ corrected Currie and Gordon's results¹ using eq 7 (see Table II).

Table II: Sodium Transport Numbers at 25° from the Adjusted Indicator Experiment¹

c_{NaCl} , moles/l.	m_{NaCl} , moles/kg of H ₂ O	t_{Na}^{h}		
		Currie and Gordon ¹ Eq 6	Spiro ¹⁷ Eq 7	Eq 8
0.201	0.2024	0.3825	0.3811	0.3815
0.388	0.3919	0.3794	0.3766	0.3767
0.771	0.7845	0.3762	0.3704	0.3706
1.550	1.6018	0.3771	0.3649	0.3654
2.333	2.4525	0.3776	0.3586	0.3596

Of the approximations made by the above-mentioned authors, the only one that influences the equation for the ratio of Hittorf transport numbers is the neglect of the change in partial molar volume of water when the water, upon passing the boundary, changes from being the solvent of KCl to that of NaCl. We have derived, however, a rigorous expression in which this change in partial molar volume of water is also taken into account.

In Figure 3, the situations at the beginning of the experiment (left) and at the end (right) are shown. Let us consider two reference planes I and II moving with a velocity such that the water transport through them is zero. During passage of p coulombs, these planes move from positions I and II to positions I' and II', respectively. The reference planes are chosen such that the boundary between the NaCl and KCl solutions is originally located in I and the final position of the boundary coincides with II'.

By definition, the transport numbers of the ions related to these reference planes are Hittorf transport numbers as no water passes through these planes.

During the passage of p coulombs, $pt_{\text{Na}}^{\text{h}}/F$ moles of sodium ions pass through the first reference plane into the volume between the reference planes and $pt_{\text{K}}^{\text{h}}/F$ moles of potassium ions are swept out of this volume through the second reference plane. By definition, the amount of water between the two reference planes remains constant. If this amount is equal to G kg, then

(13) H. S. Harned and B. B. Owen, "The Physical Chemistry of Electrolytic Solutions," 3rd ed, Reinhold Publishing Corp., New York, N. Y., 1958.

(14) D. A. MacInnes and M. Dole, *J. Am. Chem. Soc.*, **53**, 1357 (1931).

(15) R. J. Bearman, *J. Chem. Phys.*, **36**, 2432 (1962).

(16) R. Haase, *Z. Physik. Chem. (Frankfurt)*, **39**, 27 (1963).

(17) M. Spiro, *J. Chem. Phys.*, **42**, 4060 (1965).

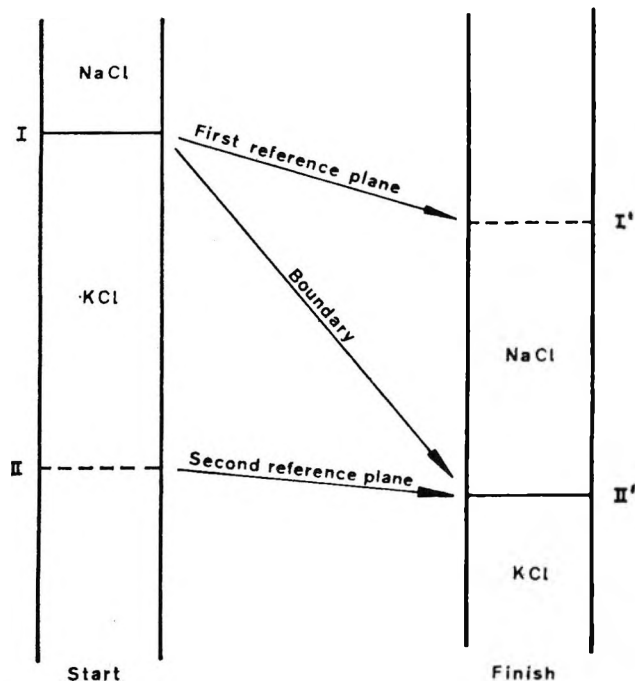


Figure 3. Movement of boundary and reference planes, the latter moving at water velocity.

the initial molal concentration of potassium ions, m_K , is given by

$$m_K = \frac{pt_K^h}{FG}$$

and the final molal concentration of sodium ions, m'_{Na} , in the following solution is given by

$$m'_{Na} = \frac{pt_{Na}^h}{FG}$$

Thus

$$\frac{t_{Na}^h}{t_K^h} = \frac{m'_{Na}}{m_K} \quad (8)$$

Thus the ratio of the Hittorf transport numbers is given by the ratio of the molal concentrations (moles/kg of H_2O) of NaCl and KCl.

From the molar concentrations of KCl and NaCl reported by Currie and Gordon (ref 1, Table I), we calculated the corresponding molal concentrations using the densities of the solutions given in the "International Critical Tables" (Vol. III, 79, 87). The sodium Hittorf transport numbers were then calculated from eq 8 and are shown in Figure 2 and in Table II.

As can be seen in Table II, the approximation in the derivation of eq 7 gives rise to an error that increases with increasing concentration. Up to a concentration of 2.5 m NaCl, this error does not exceed 0.3%.

Figure 2 shows that our observations are higher than those of Caramazza and the corrected data of Currie and Gordon.

Comparison with Stokes' Theory

On the basis of the Fuoss-Onsager theory of the conductance of electrolyte solutions, Stokes (ref 9, p 156 and ref 18) developed a theoretical expression for transport numbers. Stokes found that for 1:1 electrolytes his equation is in excellent agreement with observed data. Generally, however, these observations were made up to moderate concentrations only, but for some concentrated solutions too (HCl, up to 3 N , and LiCl, and KCl, up to 1 N), Stokes found excellent agreement. It is interesting to know how far his equation applies in concentrated NaCl solutions.

Simplified for 1:1 electrolytes, Stokes' equation is

$$t_+ = \frac{\lambda_+^0 - \frac{1}{2}B_2\sqrt{c}/(1 + \kappa\alpha)}{\Lambda^0 - B_2\sqrt{c}/(1 + \kappa\alpha)} \quad (9)$$

where α is the mean ionic diameter and Λ^0 and λ_+^0 are the limiting equivalent conductivities of the electrolyte and of the cation, respectively. B_2 is the coefficient of the electrophoretic term in the theory of conductance of electrolyte solutions; this coefficient is inversely proportional to the viscosity and to the square root of the dielectric constant. The Debye-Hückel parameter, κ , is inversely proportional to the square root of the dielectric constant. For the calculation of transport numbers from eq 9, it is of little importance for dilute solutions whether the viscosity and dielectric constant of the pure solvent or those of the solution are used to calculate B_2 and κ . In concentrated solutions, however, this remains a problem. By calculation, we found that the variation of the dielectric constant in aqueous sodium chloride solutions affected the results only slightly, but that variations in viscosity produced significant effects.¹⁹ The value of α used in our calculations was taken to be 5.2 Å, as Stokes found that this value gave excellent agreement between observed and calculated transport numbers for dilute NaCl solutions up to 0.2 N .

The transport numbers calculated with the viscosities of the appropriate solutions are higher than the experimental data. They show a minimum of 0.376 at a concentration of about 1.5 m , and curve upward to a value of 0.383 for the saturated solution (6.144 m). The results of the calculations when using the viscosity of pure

(18) R. H. Stokes, *J. Am. Chem. Soc.*, **76**, 1988 (1954).

(19) Values of dielectric constants of NaCl solutions were taken from J. B. Hasted, D. M. Ritson, and C. H. Collie, *J. Chem. Phys.*, **16**, 1 (1948). The viscosities of NaCl solutions were taken from L. L. Ezrokhi, *J. Appl. Chem. USSR*, **25**, 917 (1952).

water agree closely with our experimental data (see Figure 2).

For 3 *N* HCl and 1 *N* LiCl, the viscosity of the solutions ("International Critical Tables," Vol. III) is such that their use instead of pure water viscosity in Stokes' equation does not appreciably influence the calculated transport numbers.²⁰

If we apply Stokes' equation to concentrated solutions, however, some questions arise. The Fuoss-Onsager theory of conductance of electrolyte solutions underlying Stokes' equation is known to fail even at moderate concentrations. This failure may be due mainly to the treatment of the relaxation effect, which does not appear in the theoretical expression for the transport number. However, it is hard to see how the electrophoretic effect can be described up to saturation by a theory that regards the medium in which the ions move as a continuum with properties independent of the electrolyte concentration.

Regarding the influence of the viscosity of the solution on the calculated transport numbers, it does not seem justifiable to use this viscosity in the electrophoretic retardation terms and still use the limiting equivalent conductivities at infinite dilution. In the theory of electrolyte conductance, the velocity of an ion is regarded as composed of two elements: (a) the velocity of the unhindered ion and (b) the velocity of the ionic atmosphere surrounding the ion (electrophoretic retardation). Both constituent velocities are affected by variations in the viscosity of the surroundings. If these velocities are both affected to the same extent as a result of varying concentration, all terms on the right-hand side of eq 9 will vary by the same factor (*cf.* ref 18). This may be the reason why a close fit is obtained when the viscosity of pure water is used in B_2 , the limiting equivalent conductivities (λ_{+}^0 and Λ^0) being determined at infinite dilution.

At the higher concentrations, the question becomes important whether the transport numbers calculated with Stokes' equation are in fact Hittorf transport numbers, *i.e.*, whether the velocities of the ions are taken with respect to the solvent. In the theory of electrolyte conductance, the velocities of the ions and of the ionic atmospheres are considered with respect to their "surroundings" and it is not certain that water is not moving in this coordinate system. This question is irrelevant, of course, when conductivities of electrolyte solutions are calculated from the ionic mobilities.

Recently, Fuoss and Onsager²¹ published a revised treatment of the electrophoretic retardation in solutions of symmetrical electrolytes. With the aid of their eq 61, we modified Stokes' equation for the transport number of 1:1 electrolytes accordingly.

$$t_+ = \frac{\lambda_{+}^0 - 1/2S}{\Lambda^0 - S} \quad (10)$$

where $S = B_2\sqrt{c}\{1 - (\kappa ab/4)F(b)\}$ in which $b = e^2/\alpha\epsilon kT$, e is the protonic charge, and ϵ is the dielectric constant. S is the term describing the electrophoretic retardation of the ions.

It turned out, however, that cation transport numbers calculated with eq 10 for NaCl solutions at 25° showed very large deviations from the observed values at concentrations higher than 0.11 *m* (Table III). Beyond this concentration, the calculated transport numbers start to increase very sharply.

Table III: Comparison of Calculated and Observed Transport Numbers of NaCl Solutions at 25°

c , moles/l.	m , moles/kg of H ₂ O	$\kappa\alpha$	S , mho cm ² / equiv	t_+		
				Eq 10	Obsd ^a	Eq 9
0.01	0.01	0.171	5.14	0.3918	0.3918	0.3918
0.1095	0.110	0.566	10	0.387	0.385	0.385
0.434	0.440	1.13	0	0.396	0.378	0.378
1.00	1.02	1.71	-31	0.417	0.375	0.374
5.416	6.144	3.98	-354	0.473	0.363	0.366

^a For $m = 0.01$, ref 9; above 0.01 *m*, this work (eq 3).

For these calculations we used the viscosity and dielectric constant of pure water and the same mean ionic diameter ($\alpha = 5.2$ Å) as before.²² However, when other reasonable values of these constants are used, the general behavior of the transport numbers calculated with eq 10 is not changed.

Table III shows that at concentrations above 0.11 *m* the electrophoretic retardation as represented by S decreases with concentration and even goes through zero at 0.440 *m*. Since the latter represents a physical impossibility, eq 10 does not apply at concentrations above 0.440 *m*. This is because Fuoss and Onsager considered only cases with $\kappa\alpha$ negligible compared with unity. In particular, in their approximation of the Debye-Hückel expression for the electrical potential, a factor $e^{\kappa\alpha}/(1 + \kappa\alpha)$ was omitted. This renders their final

(20) KCl was omitted from this comparison. The agreement between observed and calculated transport numbers in KCl solutions cannot provide evidence for the correctness of the electrophoretic retardation term. This is because λ_{K}^0 is about equal to $1/2\Lambda_{KCl}^0$ and, as can be seen in eq 9, t_K is then about 0.5, practically independent of concentration and of the magnitude of the electrophoretic retardation.

(21) R. M. Fuoss and L. Onsager, *J. Phys. Chem.*, **67**, 628 (1963).

(22) For these values $b = 1.33$; the corresponding value of $F(b)$ is 2.57. This value was obtained by graphical extrapolation over a very short range of Table I of ref 21.

results applicable to very dilute solutions only. In Table III it can be seen that at NaCl concentration of 0.11 *m*, where $\kappa\alpha = 0.566$, the comparison between observed transport numbers and those calculated with eq 10 is already less satisfactory.

In the two other cases where Stokes' original eq 9 has been verified at high concentrations (3 *N* HCl and 1 *N* LiCl), *S* is negative and eq 10 again does not apply.

It thus appears that the older Fuoss-Onsager theory underlying eq 9 describes the electrophoretic retarda-

tion effect in aqueous solutions much better than the recent revised treatment. The refinements in this revised treatment of electrolyte conductance will show up to full advantage if the restriction $\kappa\alpha \ll 1$ can be removed.

Acknowledgments. The authors wish to thank C. Koole, who took a great part in developing the preparation technique of the electrodes and performed the measurements. The authors are also grateful to Shell Research N.V. for permission to publish this paper.

Coupling Constant and Chemical Shift of Tetrafluoroborate

Ion in Mixed Solvents¹

by R. Haque and L. W. Reeves

*Department of Chemistry, University of British Columbia, Vancouver 8, British Columbia, Canada
(Received November 30, 1965)*

The coupling constant J_{B-F} and the chemical shift δ_F of the BF_4^- ion have been measured as a function of concentration and solvent composition in water-acetone, water-dioxane, and water-DMSO mixtures. The coupling constant and chemical shift at infinite dilution depends on the solvent mixture as does the variation with concentration. We interpret the results in water, dioxane-water, and acetone-water mixtures in terms of changes in the hydrogen bonding of water to the BF_4^- anion. No inner-sphere ion-pair complex is indicated. In DMSO-water mixtures the behavior of the coupling constant and chemical shift changes are unique. A preferential solvation of the BF_4^- ion by the protolysis product of DMSO in water is suggested. The chemical-shift changes except at the highest concentrations are proportional to the coupling-constant changes, suggesting that variations have a common origin.

Introduction

The ^{11}B - ^{19}F coupling constant in sodium tetrafluoroborate was first reported by Reeves and co-workers² to be 4.8 cps. Later studies showed that this coupling constant is strongly dependent on the concentration and the cation.³ The value of the coupling constant *J* is low compared to the isoelectronic species of the series BeF_4^{2-4} and CF_4 ,⁵ and it does not follow the correlation suggested by Reeves.⁶ Kuhlmann and

Grant³ interpreted these changes in *J* in terms of ion-pair formation between Na^+ and BF_4^- ions and con-

(1) This research was supported by the National Research Council of Canada and the Petroleum Research Fund of the American Chemical Society.

(2) R. D. Chambers, H. C. Clark, L. W. Reeves, and C. J. Willis, *Can. J. Chem.*, **39**, 258 (1961).

(3) K. Kuhlmann and D. M. Grant, *J. Phys. Chem.*, **68**, 3208 (1964).

cluded that the measured coupling constant is an average for the ion pair $[\text{Na}^+\text{BF}_4^-]$ and BF_4^- with respective values 11 ± 2 and 1.13 ± 0.07 cps. They reported the value of equilibrium constant for (i) to be 0.22 ± 0.07 mole $^{-1}$ l. If ion-pair formation is the only factor responsible for this change, the coupling constant



of NaBF_4 should increase appreciably in solvents of low dielectric constant where ion-pair formation is more extensive, since the expression for equilibrium constant derived by Bjerrum⁷ involves dielectric constant ϵ in the denominator. The expression is given as (ii), where $Q(b) = \int \exp(y)y^{-4} dy$, $y = Z^2e^2/\gamma\epsilon RT$,

$$K = \frac{4\pi N}{1000} \left(\frac{Z^2e^2}{\epsilon kT} \right) Q(b) \quad (\text{ii})$$

and $b = Z^2e^2/a\epsilon kT$, and where N is number of ions, γ is distance between ions, a is distance of closest approach, e is electronic charge, Z is ionic charge, k is the Boltzmann constant, and T is the temperature. The measurements reported here show that the coupling constants in a (50/50 v/v) mixture of water and liquids of lower dielectric constant like acetone, dioxane, and dimethyl sulfoxide (DMSO) gave a different ∞ dilution intercept and have a larger slope. These observations suggest a modification of the interpretation of Kuhlmann and Grant.³ We have made a systematic investigation of the problem in mixed solvents. The present paper deals with changes in chemical shift and coupling constant as a function of concentration of sodium fluoroborate and the composition of the solvent.

Experimental Section

Materials. Reagent grade NaBF_4 was provided by Allied Chemical and Dye Corp. Acetone, dioxane, and DMSO were either AR or Spectrograde quality. Solutions of NaBF_4 were prepared by dissolving a known weight in either double-distilled water or a mixture of (50/50 v/v) water and the above solvents.

Apparatus and Technique. ^{19}F spectra were taken on a Varian H-R 60 spectrometer at an observing frequency of 56.4 Mc/sec. Chemical shifts were measured by side-band technique. The side bands were generated by a Hewlett-Packard audiooscillator monitored by a Hewlett-Packard 522B frequency counter. Samples were kept in a 3-mm i.d. Pyrex nmr tube, and a capillary of saturated NaBF_4 was used as an external standard. No susceptibility corrections were applied owing to the fact that these corrections are small compared to the changes in chemical shift. For each sample an average of five or six spectra were recorded and the mean chemical shift and coupling constant

taken. The experiments were performed at room temperature ($\sim 25^\circ$). In solutions less than 1 M, the coupling constant is always 1 cps or less, and so measurements were repeated at 94.1 Mc/sec on a Varian HA100 spectrometer. Samples were made up in concentric tubes with the electrolyte solution in the inner tube. The cylindrical annular space between the two tubes was filled with a solution of perfluorobenzene in carbon tetrachloride. It was possible to use the favorable dilution shift of perfluorobenzene in carbon tetrachloride to bring the fluorine signal within 1000 cps of the tetrafluoroborate ion and thus achieve a suitable peak for locking the magnetic field while scanning the tetrafluoroborate ion spectrum in a frequency sweep mode.

Results and Discussion

The variations of coupling constant and chemical shifts as a function of concentration of NaBF_4 and composition of electrolyte are shown in Figures 1 and 2. From these results it is clear that the coupling constant $J_{11\text{B}-19\text{F}}$ and ^{19}F chemical shift of tetrafluoroborate ion are dependent on the concentration and composition of the solvent.

Both the concentration dependence of $J_{11\text{B}-19\text{F}}$ and the absolute value are quite unusual. The reduced coupling constants $|j_{\text{Be-F}}|$ [$= |(J_{\text{BeF}}/\gamma_{\text{Be-F}})|^8$], $|j_{\text{B-F}}|$ (infinite dilution in water), and $|j_{\text{C-F}}|$ are 8.16, 0.16, and 34.9, respectively.

The dependence of coupling constant on s character is well established.⁹ While changes in coupling constant with temperature are well known when an unsymmetrical conformational time averaging is involved,¹⁰ the intrinsic dependence of geminal or directly bonded spin coupling on temperature or concentration is rare. Watts, Reddy, and Goldstein¹¹ noticed proton coupling constant changes from 1.96 to 3.24 cps due to concentration and different solvents in α -chloroacrylonitrile. Simultaneously, similar changes were observed by Shapiro and co-workers¹² in the case

(4) (a) P. E. Francis and I. J. Lawrenson, *J. Inorg. Nucl. Chem.*, **26**, 1462 (1964); (b) L. W. Reeves, J. Feeney, and R. Haque, to be published.

(5) N. Muller and D. T. Carr, *J. Phys. Chem.*, **67**, 112 (1963).

(6) L. W. Reeves, *J. Chem. Phys.*, **40**, 2423 (1964).

(7) C. W. Davies, "Ion Association," Butterworths, London, 1962.

(8) We express γ as (μ/I) , where μ 's are nuclear magnetons and I is merely the maximum observable quantum number.

(9) (a) C. Juan and H. S. Gutowsky, *J. Chem. Phys.*, **37**, 2198 (1962); (b) E. R. Malinowski, *J. Am. Chem. Soc.*, **83**, 4479 (1961).

(10) L. W. Reeves, *Advan. Phys. Org. Chem.*, **3**, 187 (1965).

(11) V. S. Watts, G. S. Reddy, and J. H. Goldstein, *J. Mol. Spectry.*, **11**, 325 (1963).

(12) B. L. Shapiro, S. J. Ebersole, and R. M. Kopchik, *ibid.*, **11**, 326 (1963).

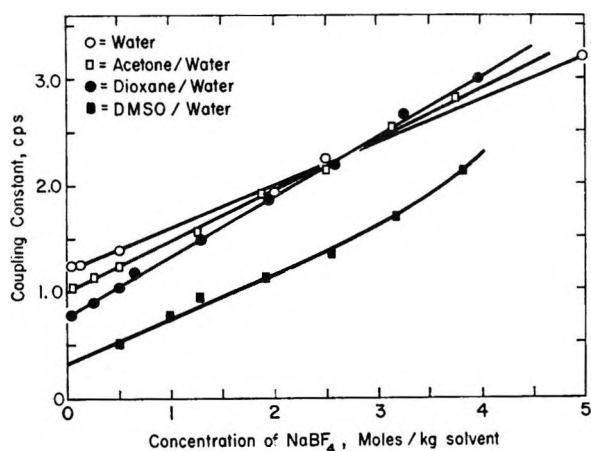


Figure 1. Concentration dependence of ^{11}B - ^{19}F coupling constant of NaBF_4 in different solvents.

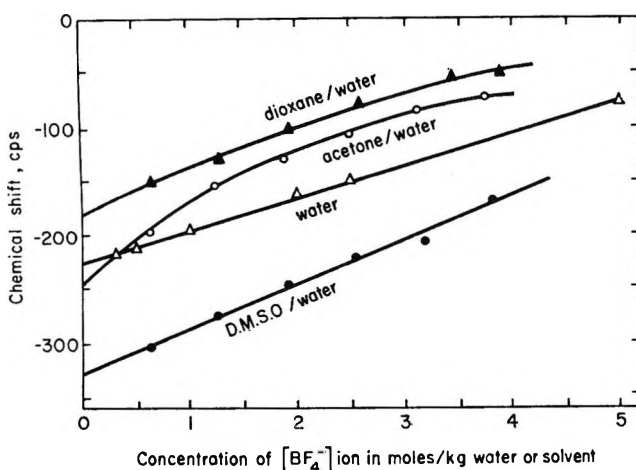


Figure 2. Concentration dependence of ^{19}F chemical shift of NaBF_4 in different solvents.

of formaldoxime and its methyl ether. Similar other cases have been reported by Schneider and co-workers¹³ in the case of molecules involving heavy nuclei. These studies have been extended by Bates, Cawley, and Danyluk¹⁴ for the geminal H-C-H coupling in different vinylsilanes. Other solvent studies of J include the recent work of McLauchlan, Reeves, and Schaefer,¹⁵ who varied both solvent and temperature, and of Cyr and Reeves¹⁶ on trimethyltin bromide in different organic solvents. All these investigations have been interpreted in terms of association or molecular complexes. In the case of organosilicon and tin compounds, there is a vacant d orbital so that a change in hybridization can be responsible for such variations of J . However, the case of the BF_4^- ion is different. Boron cannot change its coordination number. The coupling constant changes in NaBF_4 from 1 to 4 cps with con-

centration in water. The other interesting feature of these changes noted by Kuhlmann and Grant³ is effect of nature of cation. For example, the coupling constant increases by the addition of NaNO_3 , NaClO_4 , and LiNO_3 in a 0.5 M solution of NaBF_4 . However, the value of J is almost constant when HNO_3 is added, and it decreases in NH_4NO_3 solutions. An ion-pair mechanism was suggested by Kuhlmann and Grant.³ The ^{19}F spectrum of NaBF_4 is a sharp quartet in spite of the fact that a ^{11}B nucleus with spin $3/2$ has a small quadrupole moment. Quadrupole relaxation has been observed in BF_3 by Gillespie and co-workers.¹⁷ The preservation of the point group symmetry T_d at all concentrations of NaBF_4 is indicated, so that external electric field gradients introduced by solvation effects must be small or of symmetry T_d . An inner-sphere ion pair would certainly introduce distortions of other symmetry and increase the rate of quadrupolar relaxation of the ^{11}B nucleus.¹⁸ The quadrupole coupling constant of KBF_4 measured in the solid state for ^{11}B is quite small¹⁹ (0.23 Mc/sec). In heavy metal fluoroborate solutions such broadening effects in the ^{19}F spectra have been observed.²⁰ We have studied and will report elsewhere some work on fluoroborates of Sn^{2+} , Cd^{2+} , Sb^{3+} , and Pb^{2+} cations. Ion-pair effects on the inner-sphere type are much more probable with these large polarizable cations. Recent work of Ryss and Radchenko²¹ on NaBF_4 solutions by X-rays disclosed that in this solution in the concentration range 2-9 M, Na^+ ion is hexacoordinated with water, and showed that there is no direct contact between the Na^+ ion and BF_4^- ion. The hydrolysis of NaBF_4 to NaBF_3OH is very small³ and the BF_4^- ion itself is a stable ion. The possibility of exchange between $\text{BF}_3\text{-OH}^-$ and BF_4^- would lead to a line broadening. No appreciable broadening occurs. The coupling measured is therefore the true one and not an effect modified by chemical exchange.

We suggest the possibility that this change in coupling constant is due to hydrogen bonding between the BF_4^- ion and the surrounding water in the

(13) J. V. Hatton, W. G. Schneider, and W. Siebrand, *J. Chem. Phys.*, **39**, 1330 (1963).

(14) P. Bates, C. Cawley, and S. S. Danyluk, *ibid.*, **40**, 2415 (1964).

(15) K. A. McLauchlan, L. W. Reeves, and T. Schaefer, *Can. J. Chem.*, **44**, 1473 (1966).

(16) N. Cyr and L. W. Reeves, to be published.

(17) J. Bacon, R. J. Gillespie, and J. W. Quail, *Can. J. Chem.*, **41**, 3063 (1963).

(18) K. J. Packer and E. L. Muetterties, *Proc. Chem. Soc.*, 147 (1964).

(19) P. J. Bray and A. H. Silver, *Bull. Am. Phys. Soc.*, **1**, 323 (1956).

(20) R. Haque and L. W. Reeves, to be published.

(21) A. I. Ryss and I. V. Radchenko, *J. Struct. Chem.*, **5**, 489 (1964).

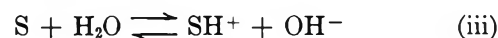
form of a hydration sphere. It is sensible on the basis of electronegativity of participating atoms that the hydrogen bond $[F_3B-F]^- \cdots H-O-$ should be quite strong though not previously encountered.

The values of J_{B-F} at infinite dilution are 1.19 cps in water, 1.0 cps in acetone-water, 0.76 cps in dioxane-water, and 0.32 cps in DMSO-water, respectively.²² It is clear that the environmental change of the isolated BF_4^- ion in these solvents is reflected in both coupling constant and chemical shift changes (Figures 1 and 2). The rate of change of coupling constant with concentration is also a function of solvent. It is 0.4 cps mole⁻¹ kg of solvent in water, 0.48 in acetone-water, 0.56 in dioxane-water, and 0.44 in DMSO/water. It is reasonable that changes in coupling constant should reflect changes in the number and strength of hydrogen bonds between water and the BF_4^- ion. Evans²³ noted that the ¹³C-H coupling constant in $CHCl_3$ is a function of solvent. A change of ~10% is observed between inert and strong donor solvents indicating a variation with hydrogen bond strength $C-H \cdots X$. Evans suggests that the electrostatic repulsion leads to an increase in s character in the -CH bond and thus J_{C-H} increases. Although variations in coupling constant between liquid and vapor hydrides for J_{17O-1H} , J_{14N-1H} , and J_{1H-19F} have not been noted yet, it is anticipated that they will be larger than the 10% change in $CHCl_3$. It is in order to expect a considerable change in the B-F coupling constant when a $[B-F \cdots H-O]$ hydrogen bond is formed.

If the coupling constant variations are to be explained largely on the basis of changes in the number and/or strength of hydrogen bonds $[B-F \cdots H-O]$, then the following facts need rational explanation: (a) the lack of dependence of J in NH_4BF_4 solutions on concentration in contrast to sodium salt;³ (b) the influence of added electrolytes on J ;³ (c) the collapse of spin coupling, probably a quadrupolar relaxation effect, in salts with the ions Sn^{2+} , Cd^{2+} , Sb^{3+} , and Pb^{2+} (this has been observed in this work²⁰); (d) the changes in the ∞ dilution values of J and changes in J with concentration in mixed solvents; (e) measurements of $(NH_4)_2BeF_4$ solutions showing J_{Be-F} to be independent of concentration (but so far the limited solubility of Na_2BeF_4 in water has precluded a study of the J_{Be-F} dependence in this salt);⁵ (f) the lack of coupling constant variations in all soluble salts of PF_6^- , SiF_6^{2-} , and AsF_6^- ^{19, 24} with changes in concentration.

The peculiarity of the sodium salt in (a) or the effect of added salts with small ionic radius in (b), Na^+ and Li^+ , is probably due to the strong ion-dipole forces present which disrupt the hydrogen-bonded structure of water and effectively remove from the

solution water molecules which in dilute solution are available to form the weaker hydrogen bonds $[B-F \cdots H-O]$. This polarization effect has been noted by Shoolery and Alder.²⁵ The NH_4^+ salt which causes only very small changes in J does not similarly affect the surrounding water structure. The effect of large polarization ions (c) is related to the observations of Packer and Muetterties,¹⁸ and the increased rate of quadrupolar relaxation of the ¹¹B nucleus may be due to ion-pair formation or changes in field gradient due to solvation or both. It is known from previous nmr studies that the diffusion effect or chemical shift changes in the solvent resonances²⁶ in dioxane-water mixtures can be explained in terms of preferential solvation of the cation by the water molecules. Hydrogen bond formation with the anion then becomes a competitive process with hydrogen bond formation with the donor solvent component. In these mixed solvents, the following protolytic equilibrium exists²⁷⁻³⁰



where S is the solvent molecule (acetone, dioxane, or DMSO). This reaction is negligible in the case of acetone and dioxane. The lowering in coupling constant in DMSO-water could be due to interaction of the SH^+ species with the BF_4^- ion. There also may be a strong tendency of DMSO to form solvated species with the Na^+ ion. However, reaction iii together with hydrogen bonding is probably responsible for the low value of the coupling constant. At infinite dilution in any solvent mixture the low concentration of BF_4^- ion allows favorable competition for the water molecules in hydrogen bond formation.

We have measured the coupling constant J_{Be-F} in the BeF_4^{2-} ion for solutions of the ammonium salt^{4b} and found it to be independent of concentration like NH_4BF_4 solution. The sodium salt is quite insoluble and we have been unable to measure J_{Be-F} for this salt. It should vary with concentration in company with salts of small cations if our suggestions here are to be consistent. The $[Be-F \cdots H-O]$ hydrogen bond should also be quite a strong hydrogen bond.

(22) We thank a referee for encouraging us to make these measurements.

(23) D. F. Evans, *J. Chem. Soc.*, 5575 (1963).

(24) K. J. Packer, private communication.

(25) J. N. Shoolery and B. J. Alder, *J. Chem. Phys.*, **23**, 805 (1955).

(26) A. Fratiello and D. C. Douglass, *ibid.*, **39**, 2017 (1963).

(27) J. R. Holmes, D. Kivelson, and W. C. Drinkard, *J. Am. Chem. Soc.*, **84**, 4677 (1962).

(28) G. Mavel, *Compt. Rend.*, **248**, 1505 (1959).

(29) G. Mavel, *ibid.*, **249**, 1753 (1959).

(30) G. Mavel, *J. Chim. Phys.*, **57**, 649 (1960).

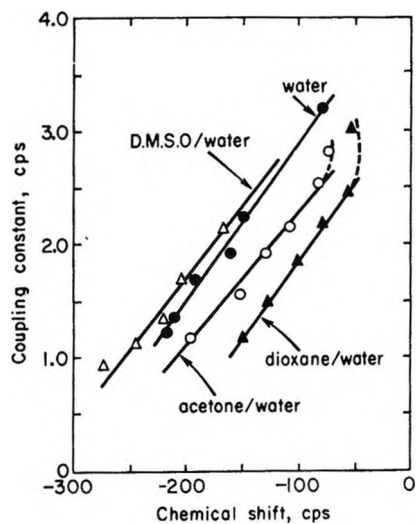


Figure 3. Graph showing dependence of ^{19}F chemical shift and ^{11}B - ^{19}F coupling constants of NaBF_4 in different solvents.

The lack of variation which has been observed for couplings of central atom to fluorine in PF_6^- , SiF_6^{2-} , and AsF_6^- ions (although a detailed study has not yet been made for couplings in SiF_6^{2-} and AsF_6^- ion) may be associated with a very much weaker hydrogen bond $[\text{X}-\text{F}\cdots\text{H}-\text{O}]$ when X is electronegative. The strongest hydrogen bond occurs when the X-F bond is completely ionic, *i.e.*, the F^- ion.

For a good portion of the concentration range studied in dioxane-water and acetone-water mixtures the chemical shift change is linearly dependent on the coupling constant. This last statement is true for the whole range of concentrations available in aqueous solution and DMSO-water mixtures (Figure 3).

The chemical shift is a sensitive function of solvent and cation; it is difficult to use it as a reliable measure of any single interaction. In fact, the infinite dilution chemical shift is not the same for the BF_4^- ion in water or any of the solvent mixtures. The second solvent component plays some role, therefore, in the environment of the BF_4^- ion. This effect does not seem to

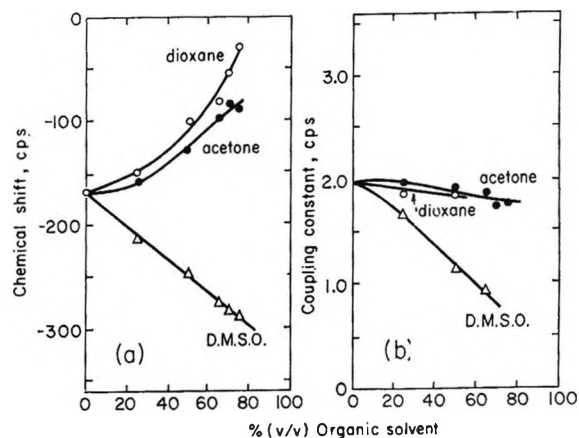


Figure 4. (a) Dependence of ^{11}B - ^{19}F coupling constant in NaBF_4 on solvent composition. (b) Dependence of ^{19}F chemical shift in NaBF_4 on solvent composition.

be simply a reduction in the mean distance of the nearest cation, since we would then expect the order of the infinite dilution shift to depend on the dielectric constant of the medium. The order of δ_∞ is dioxane- H_2O > H_2O \sim acetone- H_2O > DMSO- H_2O from high field to low field.

The effect of the organic solvent component is more clearly seen in Figure 4. We have maintained the concentration of BF_4^- ion in moles/1000 g of solvent constant but varied the ratio of water-organic solvent. As the organic solvent component increases in concentration, widely divergent chemical shift changes are observed. DMSO causes a large low-field shift and $J_{\text{B-F}}$ also decreases on adding DMSO. The behavior in DMSO-water mixture is unique and cannot be explained on the basis of hydrogen-bonded interactions at the BF_4^- ion. We suggest as before the specific solvation of the protolysis product of DMSO²⁷⁻³⁰ at the BF_4^- ion.

Acknowledgments. We thank Professor D. M. Grant for sending us the relevant parts of the Ph.D. Thesis of Dr. K. F. Kuhlmann.

Theory of Unidimensional Molecular Collisions. Broken Path Model

by L. Blum

Facultad de Ciencias Exactas y Naturales, Buenos Aires, Argentina (Received December 17, 1965)

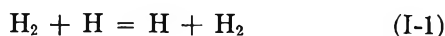
A harmonic oscillator model for reactive chemical collisions is proposed. The model is solved rigorously for the reaction $\text{H}_2 + \text{H} = \text{H} + \text{H}_2$. The results show the appearance of quite narrow resonance peaks for the reaction cross sections.

I. Introduction

The theoretical study of chemical reactions from the standpoint of the general collision theory¹ requires the knowledge of the cross sections involved in the reaction. Recently, a number of experiments have been conducted on this subject.² From the theoretical point of view, the problem of the reaction cross sections is a very difficult one, and not as much has been done. However, classical approaches have been explored recently.³ Also, a quantum mechanical solution for a reasonable potential surface has been attempted.⁴

Even in the simplest case, the solution of the problem is very difficult. For this reason, it seems worthwhile to study a model with an interaction potential which only roughly approximates the real one, but which is exactly solvable. The model will be described in section II. It is similar to the model discussed by Eyring.⁵

Section III is devoted to the discussion of some features of the cross section of the reaction



in the case of a head on collision.

II. The Broken Path Model

Let us take the simple case of reaction I-1 in one dimension. Using Born-Oppenheimer's approximation,^{3,4} we write the Schroedinger equation of the system as (see Figure 1)

$$-\frac{\hbar^2}{2M_{\text{H}}} \left[\frac{\partial^2}{\partial r_{12}^2} + \frac{\partial^2}{\partial r_{23}^2} - \frac{\partial^2}{\partial r_{12} \partial r_{23}} \right] \Psi + V\Psi = E\Psi \quad (\text{II-1})$$

The solutions for $r_{23} > q_{\alpha}$ (reactants or entrance channel) are of the form

$$\phi_{\alpha} = [A_{\alpha}' e^{ik_{\alpha} r_{\alpha}} + B_{\alpha}' e^{-ik_{\alpha} r_{\alpha}}] \varphi_{\alpha} \quad (\text{II-2})$$

and for $r_{12} > q_{\beta}$ (products or exit channel)

$$\phi_{\beta} = A_{\beta}' e^{ik_{\beta} r_{\beta}} \varphi_{\beta} \quad (\text{II-3})$$

where $r_{\alpha} = r_{23} + 1/2 r_{12}$ and $r_{\beta} = r_{12} + 1/2 r_{23}$. B_{α} is the amplitude of the ingoing wave. A_{α} and A_{β} are the amplitudes of the outgoing waves for channels α and β . B_{β} is zero because there are no ingoing waves in channel β . q_{α} and q_{β} are the smallest distances of no interaction.

In the region where all three atoms interact, the function V (eq II-1) has a complicated form.⁶ The solution of eq II-1 in this region is extremely difficult; in principle, one could either search for approximate solutions of the exact equation, using variation or perturbation methods, or look for an approximate potential which is exactly solvable. In this paper we choose the latter approach.

The exact potential V is thus replaced by two (or eventually more) "cut parabolic saddles" (Figures 2 and 3). The approximation also replaces the usually curved reaction path by a broken line.

Analytically, in region I, we have

$$V_1 = -k'x^2 + ky^2 + V^0 \quad (\text{II-4})$$

with x and y defined in eq II-5.

(1) M. A. Eliason and J. Hirschfelder, *J. Chem. Phys.*, **30**, 1426 (1959).

(2) See, for example, D. Beck, E. F. Greene, and J. Ross, *ibid.*, **37**, 2895 (1962); S. Datz, D. R. Herschbach, and E. H. Taylor, *ibid.*, **35**, 1549 (1961).

(3) M. Karplus, R. N. Porter, and R. D. Sharma, *ibid.*, **43**, 3259 (1965).

(4) K. Pitzer and E. M. Mortensen, Special Publication No. 16, The Chemical Society, London, 1962.

(5) H. Eyring, J. Walter, and G. E. Kimball, "Quantum Chemistry," John Wiley and Sons, Inc., New York, N. Y., 1954.

(6) S. Sato, *J. Chem. Phys.*, **23**, 592 (1955).

$$\begin{aligned} x &= r_{12} \cos \theta_1 - r_{23} \sin \theta_1 \\ y &= r_{12} \sin \theta_1 + r_{23} \cos \theta_1 \end{aligned} \quad (\text{II-5})$$

where x is the distance along the reaction path, with y the distance perpendicular to the reaction path. That is

$$\begin{aligned} V_1 &= V^0 + r_{12}^2(k \cos^2 \theta_1 - k' \sin^2 \theta_1) + \\ &\quad r_{23}^2(k \sin^2 \theta_1 - k' \cos^2 \theta_1) + \\ &\quad 2r_{12}r_{23}(k + k') \cos \theta_1 \sin \theta_1 \end{aligned} \quad (\text{II-6})$$

Similarly, in region II

$$\begin{aligned} V_2 &= V^0 + r_{12}^2(k \cos^2 \theta_2 - k' \sin^2 \theta_2) + \\ &\quad r_{23}^2(k \sin^2 \theta_2 - k' \cos^2 \theta_2) + \\ &\quad 2r_{12}r_{23}(k + k') \cos \theta_2 \sin \theta_2 \end{aligned} \quad (\text{II-7})$$

Equation II-1 is now solvable in each of the regions of configuration space (Figure 3). Let us then find the solutions for region I. Using normal coordinates⁷

$$\begin{aligned} Q_{11} &= h_1 r_{12} + h_2 r_{23} \\ Q_{21} &= h_3 r_{12} + h_4 r_{23} \end{aligned} \quad (\text{II-8})$$

eq II-1 splits into two equations

$$\frac{d^2 \phi_{11}}{dQ_{11}^2} + \frac{2}{\hbar^2} \left[E_{11} - \frac{\lambda_{11}}{2} Q_{11}^2 \right] \phi_{11} = 0 \quad (\text{II-9})$$

and

$$\frac{d^2 \phi_{21}}{dQ_{21}^2} + \frac{2}{\hbar^2} \left[E_{21} + \frac{\lambda_{21}}{2} Q_{21}^2 \right] \phi_{21} = 0 \quad (\text{II-10})$$

Equation II-9 is the usual Hermite equation for harmonic oscillators. Equation II-10 is a confluent hypergeometric equation, which has two linearly independent solutions known as the parabolic cylinder or Weber functions⁸

$$\begin{aligned} D_{-(1/2) - (i\epsilon/2)}(Q_{21} \sqrt{2i\gamma_{21}}); \\ D_{-(1/2) + (i\epsilon/2)}(Q_{21} \sqrt{-2i\gamma_{21}}) \end{aligned} \quad (\text{II-11})$$

where $\epsilon = 2E_{21}/\hbar \sqrt{\lambda_{21}}$ and $\gamma_i = \sqrt{\lambda_i/\hbar}$. The complete solution for region I is then

$$\begin{aligned} \Psi_1 &= \exp \left\{ -\frac{\gamma_{11}}{2} Q_{11}^2 \right\} H_n(Q_{11} \sqrt{\gamma_{11}}) \times \\ &\quad [A_1 D_{-(1/2) - (i\epsilon/2)}(Q_{21} \sqrt{2i\gamma_{21}}) + \\ &\quad B_1 D_{-(1/2) + (i\epsilon/2)}(Q_{21} \sqrt{-2i\gamma_{21}})] \end{aligned} \quad (\text{II-12})$$

For region II, we have, similarly

$$\begin{aligned} \Psi_2 &= \exp \left\{ -\frac{\gamma_{12}}{2} Q_{12}^2 \right\} H_n(Q_{12} \sqrt{\gamma_{12}}) \times \\ &\quad [A_2 D_{-(1/2) - (i\epsilon/2)}(Q_{22} \sqrt{2i\gamma_{22}}) + \\ &\quad B_2 D_{-(1/2) + (i\epsilon/2)}(Q_{22} \sqrt{-2i\gamma_{22}})] \end{aligned} \quad (\text{II-13})$$

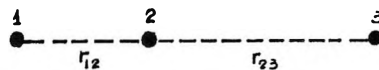


Figure 1. Activated complex.

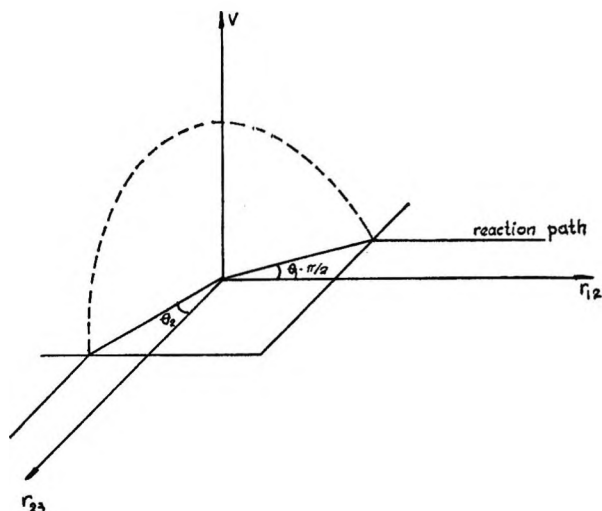


Figure 2. Potential energy.

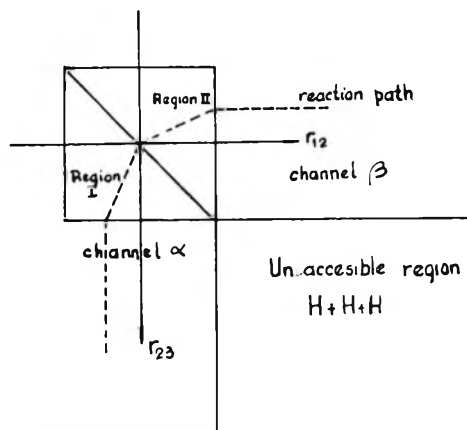


Figure 3. Configuration space.

Let us now specialize in cases in which all oscillators are in their fundamental levels. For reaction I-1 this is not a bad assumption since the activation energy is about 7 kcal/mole, whereas the energy needed to excite the first vibrational level is *ca.* 12 kcal/mole.

Now the problem is reduced to that of finding the values of the different A 's and B 's. This is done using the conditions of continuity of the functions and the first derivatives at the boundaries of the regions.

(7) E. B. Wilson, J. C. Decius, and P. C. Cross, "Molecular Vibrations," McGraw-Hill Book Co., Inc., New York, N. Y., 1959.

(8) P. M. Morse and H. Feshbach, "Methods of Theoretical Physics," McGraw-Hill Book Co., Inc., New York, N. Y., 1953.

Four boundary channel α -region I

$$\varphi_\alpha(A'e^{ik_\alpha r_\alpha} + B_\alpha'e^{-ik_\alpha r_\alpha})|_\alpha = \Psi_1|_\alpha \quad (\text{II-14})$$

$$ik_\alpha\varphi_\alpha(A_\alpha'e^{ik_\alpha r_\alpha} - B_\alpha'e^{-ik_\alpha r_\alpha})|_\alpha = \Psi_1'|_\alpha \quad (\text{II-15})$$

For boundary region I-region II

$$\Psi_1|_0 = \Psi_2|_0 \quad (\text{II-16})$$

$$\Psi_1'|_0 = \Psi_2'|_0 \quad (\text{II-17})$$

For boundary region II-channel β

$$\Psi_2|_\beta = A_\beta'e^{ik_\beta r_\beta}\varphi_\beta|_\beta \quad (\text{II-18})$$

$$\Psi_2'|_\beta = ik_\beta A_\beta'e^{ik_\beta r_\beta}\varphi_\beta|_\beta \quad (\text{II-19})$$

Using conditions of orthogonality of the wave functions of the stable oscillators, we get simpler relations.

For boundary channel α -region I

$$A_\alpha e^{ik_\alpha r_\alpha} + B_\alpha e^{-ik_\alpha r_\alpha} = A_1\chi_\alpha + B_1\chi_\alpha^* \quad (\text{II-20})$$

$$ik_\alpha(A_\alpha e^{ik_\alpha r_\alpha} - B_\alpha e^{-ik_\alpha r_\alpha}) = A_1\chi_\alpha' + B_1\chi_\alpha'^* \quad (\text{II-21})$$

For boundary region I-region II

$$A_1\kappa_1 + B_1\kappa_1^* = A_2\kappa_2 + B_2\kappa_2^* \quad (\text{II-22})$$

$$A_1\kappa_1' + B_1\kappa_1'^* = A_2\kappa_2' + B_2\kappa_2'^* \quad (\text{II-23})$$

For boundary region II-channel β

$$A_\beta e^{ik_\beta r_\beta} = A_2\chi_\beta + B_2\chi_\beta^* \quad (\text{II-24})$$

$$ik_\beta A_\beta e^{ik_\beta r_\beta} = A_2\chi_\beta' + B_2\chi_\beta'^* \quad (\text{II-25})$$

Here, we used the definitions

$$\chi_\alpha = \left(\frac{\nu_\alpha}{\pi}\right)^{1/2} \int_{-\infty}^{\infty} dr_{12} \exp\{-1/2[\nu_\alpha(r_{12} + q_\alpha t g \theta_1)^2 + \gamma_{11}Q_{11}^2]\} D_{-(1/2)-(i\epsilon/2)}(Q_{21}\sqrt{2i\gamma_{21}}) \quad (\text{II-26})$$

$$A_\alpha = A_\alpha' \exp\left(-\frac{k_\alpha^2}{8\nu_\alpha}\right)$$

$$B_\alpha = B_\alpha' \exp\left(-\frac{k_\alpha^2}{8\nu_\alpha}\right)$$

and similar expressions for χ_β and A_β' .

Also

$$\kappa_1 = \int_{-\infty}^{\infty} dx \exp\{-1/2(\gamma_{12}Q_{12}^2 + \gamma_{11}Q_{11}^2)\} \times D_{-(1/2)-(i\epsilon/2)}(Q_{21}\sqrt{2i\gamma_{21}}) \quad (\text{II-27})$$

$$\kappa_2 = \int_{-\infty}^{\infty} dx \exp\{-\gamma_{12}Q_{12}^2\} D_{-(1/2)-(i\epsilon/2)}(Q_{22}\sqrt{2i\gamma_{22}}) \quad (\text{II-28})$$

with $\nu_\alpha = \sqrt{0.5M_H F_{HH}}$ and $x = (1/\sqrt{2})(r_{12} + r_{23})$.

Integration of these expressions gives (see Appendix)

$$\chi_\alpha = (1/h_3)\left(\frac{\nu_\alpha}{\gamma_{21}}\right)^{1/2} \exp(-q_\alpha^2 c_\alpha) \frac{1}{(4a_\alpha^2 + 1)} \times \left(\frac{2a_\alpha + i}{2a_\alpha - i}\right)^{i\epsilon/4} D_{-(1/2)-(i\epsilon/2)}(-b_\alpha q_\alpha \sqrt{2i}) \quad (\text{II-29})$$

and a similar expression for χ_β

$$\kappa_1 = \frac{\sqrt{2\pi}}{(h_3 + h_4)\sqrt{\gamma_{21}}(4a_1^2 + 1)^{1/4}} \times \left(\frac{2a_1 + i}{2a_1 - i}\right)^{i\epsilon/4} D_{-(1/2)-(i\epsilon/2)}(0) \quad (\text{II-30})$$

and a similar expression for κ_2 . a_α , b_α , c_α , etc., are numerical constants which depend on the parameters of the potential energy, and are defined in the Appendix.

Upon solving eq II-20-25, we obtain

$$A_\alpha/B_\alpha = (\Omega_1/\Omega_2)e^{-2ik_\alpha r_\alpha} \quad (\text{II-31})$$

$$A_\beta/B_\alpha = \frac{2ik_\alpha \Delta_1 \Delta_\beta}{\Omega_2} e^{-ik_\alpha r_\alpha - ik_\beta r_\beta} \quad (\text{II-32})$$

where

$$\Omega_1 = -C_1(D_1C_3 - D_2C_4) + C_2(D_2^*C_3 - D_1^*C_4) \quad (\text{II-33})$$

$$\Omega_2 = -C_1(D_1C_5 - D_2C_6) + C_2(D_2^*C_5 - D_4^*C_6) \quad (\text{II-34})$$

and

$$\begin{aligned} \Delta_\beta &= \chi_\beta\chi_\beta'^* - \chi_\beta'\chi_\beta^*; \quad \Delta_1 = \kappa_1\kappa_1'^* - \kappa_1'\kappa_1^* \\ D_1 &= \kappa_2\kappa_1'^* - \kappa_2'\kappa_2^*; \quad D_2 = \kappa_2\kappa_1 - \kappa_2'\kappa_2^* \\ C_1 &= \chi_\beta'^* - ik_\beta\chi_\beta^*; \quad C_2 = \chi_\beta' - ik_\beta\chi_\beta \\ C_3 &= ik_\alpha\chi_\alpha + \chi_\alpha'; \quad C_4 = ik_\alpha\chi_\alpha^* + \chi_\alpha^* \\ C_5 &= ik_\alpha\chi_\alpha - \chi_\alpha'; \quad C_6 = ik_\alpha\chi_\alpha^* - \chi_\alpha^* \end{aligned} \quad (\text{II-35})$$

If some of the oscillators are in excited states, then the matching procedure described here is not sufficient. In that case a more general theory, the R -matrix theory⁹, may be used. The use of this theory will be discussed in separate papers.

III. Discussion of Results

In this section we discuss the coefficients

$$T = |A_\beta|^2/|B_\alpha|^2 \quad (\text{III-1})$$

$$R = |A_\alpha|^2/|B_\alpha|^2 \quad (\text{III-2})$$

where T is the probability of reactive scattering and R is the probability of elastic scattering.

(9) A. M. Lane and R. G. Thomas, *Rev. Mod. Phys.*, **30**, 257 (1958).

The parameters of the interaction potential V varied with the range of physically reasonable values. The results of some calculations for different values of the parameters are shown in Table I. In all the cases we

Table I: Position and Width of First Resonances^a

k	k'	θ_1 , deg	θ_2 , deg	Reduced width	First reso- nance, ϵ
5	-0.20	50	40	10^{-8}	0.8
5	-0.20	60	30	5×10^{-3}	0.27
5	-0.20	70	20	2×10^{-3}	1.1
3	-0.20	60	30	10^{-3}	0.6
7	-0.20	60	30	10^{-2}	0.9

^a Force constants are given in mdynes/A; $q_c = 0.1 \text{ \AA} - \epsilon$ is defined by eq II-11.

observed the presence of resonances (see Figure 4). Just at the top of the resonance peaks, II-31 and -32 are not very accurate (estimated error at the top, <15).

Though all the cases of Table I were computed using eq II-31 and -32, Breit and Wigner's resonance formula¹⁰ gives a more accurate estimate at the top of the peak. Also, the functional dependence on the parameters c_α (which is a function of the interaction potential parameters) and q_α (the range of the potential) is better seen in that formula.

$$T_\alpha \frac{\Gamma_\alpha \Gamma_\beta}{(E - E_r)^2 + 1/4 \Gamma^2} \quad (\text{III-3})$$

where

$$\Gamma_\alpha \propto k_\alpha |\chi_\alpha|^2; \quad \Gamma_\beta \propto k_\beta |\chi_\beta|^2; \quad \Gamma = \Gamma_\alpha + \Gamma_\beta \quad (\text{III-4})$$

is the total width of the level. In our case

$$\Gamma \approx \exp(-2c_\alpha q_\alpha^2) \quad (\text{III-5})$$

as may be seen from (II-29). The estimated widths of Table I are given using this formula. It is clear that the dependence on the parameters of the potential, particularly q_α , is very strong. For this reason, more accurate calculations are needed to prove the existence of such a behavior.

In particular, we are studying the unidimensional reaction with a Eyring-Sato⁶ potential, using a variational method. Our preliminary results indicate that for $q_\alpha = 0.35$, c_α is of the order of 7; that is, the levels are relatively broad.

Resonances in molecular collisions have been discussed in several cases.¹¹⁻¹³ The influence of these resonances in chemical reactions is to reduce the steric

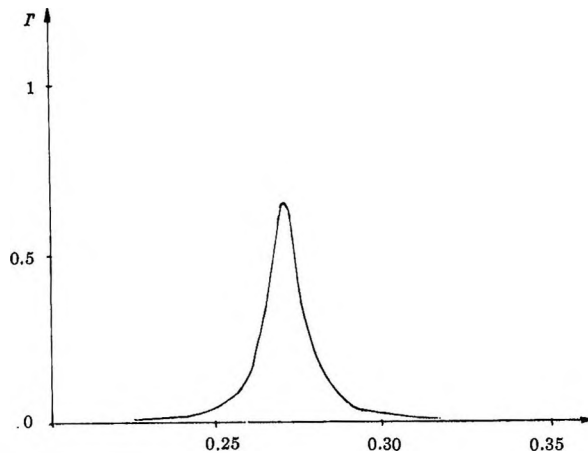


Figure 4. First resonance: $k = 5.0$, $k' = -0.2$; $\theta_1 = 60^\circ$, $\theta_2 = 30^\circ$; $q_\sigma = q_\beta = 0.1 \text{ \AA}$; cf. eq II-11 for ϵ .

factor.¹⁴ The precise nature of these resonances will be discussed in forthcoming papers. They may be due to some kind of dynamical matching between the motion of the atoms, but they may also be due to a poor overlap of the internal wave function with the channel wave functions. This overlap would be greater in a "curved reaction path."

Acknowledgments. The author is indebted to Dr. R. Ch. de Guber for her kind permission to use the Mercury Ferranti computer of this university.

Appendix

After some elementary transformations we may write (II-26) in the form

$$\chi_\alpha = \left(\frac{\nu_\alpha}{\pi}\right)^{1/2} \frac{e^{-c\alpha' r_{21}^2}}{h_3 \sqrt{\gamma_{21}}} \int_{-\infty}^{\infty} dx \times e^{-a\alpha x^2 - b\alpha' x r_{21}} D_{-(1/2) - (i\epsilon/2)}(x\sqrt{2i}) \quad (\text{A-1})$$

where

$$a_\alpha = \frac{1}{2h_3^2 \gamma_{21}} (\nu_\alpha + \gamma_{11} h_\epsilon^2) \quad (\text{A-2})$$

$$b_\alpha' = \frac{1}{h_3 \sqrt{\gamma_{21}}} [\gamma_{11} h_1 (h_2 - h_1 h_4 / h_3) - \nu_\alpha (h_4 / h_3 - t g \theta_1)] \quad (\text{A-3})$$

$$c_\alpha' = 1/2 [\nu_\alpha (h_4 / h_3 - t g \theta_1)^2 + \gamma_{11} (h_2 - h_1 h_4 / h_3)^2] \quad (\text{A-4})$$

(10) See, for example, T. Y. Wu and T. Ohmura, "Quantum Theory of Scattering," Prentice-Hall Inc., Englewood Cliffs, N. J., 1962.

(11) S. Matthies and V. G. Neudachin, *Soviet Phys. JETP*, **18**, 95 (1964).

(12) A. M. Brodskii and A. Y. Temkin, *Dokl. Akad. Nauk SSSR*, **152**, 127 (1963).

(13) L. Blum, *Bull. Am. Phys. Soc.*, **9**, 42 (1964).

(14) L. Blum, *Nuovo Cimento*, **35**, 1164 (1964).

Using the integral representation of the Weber function¹⁵

$$D_{-(1/2)-(i\epsilon/2)}(x\sqrt{2i}) = \frac{e^{-ix^2/2}}{\Gamma\left(\frac{1}{2} + \frac{i\epsilon}{2}\right)} \times \int_0^\infty dt e^{-(t^2/2)-(xt\sqrt{2i})} t^{-(1/2)+(i\epsilon/2)} \quad (\text{A-5})$$

we get

$$\chi_\alpha = \left(\frac{\nu_\alpha}{\pi\gamma_{21}}\right)^{1/2} \frac{e^{-c\alpha'r_{23}^2}}{h_3\Gamma\left(\frac{1}{2} + \frac{i\epsilon}{2}\right)} \int_{-\infty}^\infty dx e^{-a_\alpha x^2 - b\alpha'x r_{23}} \times \int_0^\infty dt e^{-t^2/2 - xt\sqrt{2i}} t^{-(1/2)+(i\epsilon/2)} \quad (\text{A-6})$$

Changing the order of integration

$$\chi_\alpha = \left(\frac{\nu_\alpha}{\pi\gamma_{21}}\right)^{1/2} \frac{e^{-c\alpha'r_{23}^2}}{h_3\Gamma\left(\frac{1}{2} + \frac{i\epsilon}{2}\right)} \int_0^\infty dt e^{-t^2/2} t^{-(1/2)+(i\epsilon/2)} \times \int_{-\infty}^\infty dx e^{-x^2(a_\alpha + i/2) - x(b\alpha'r_{23} + t\sqrt{2i})} \quad (\text{A-7})$$

$$\chi_\alpha = (1/h_3) \left(\frac{\nu_\alpha}{\pi\gamma_{21}}\right)^{1/2} \frac{e^{-c\alpha'r_{23}^2}}{\Gamma\left(\frac{1}{2} + \frac{i\epsilon}{2}\right)} \frac{\sqrt{\pi}}{(a_\alpha + i/2)^{1/2}} \times \int_0^\infty dt e^{-t^2/2} t^{-(1/2)+(i\epsilon/2)} \exp\left[\frac{(b\alpha'r_{23} + t\sqrt{2i})^2}{2(2a_\alpha + i)}\right] \quad (\text{A-8})$$

$$= (1/h_3) \left(\frac{\nu_\alpha}{\pi\gamma_{21}}\right)^{1/2} \frac{e^{-c\alpha'r_{23}^2}}{\Gamma\left(\frac{1}{2} + \frac{i\epsilon}{2}\right)} \frac{e^{-b\alpha'^2 r_{23}^2/2(2a_\alpha + i)}}{(a_\alpha + i/2)^{1/2}} \times \int_0^\infty dt e^{-r^2/2[(2a_\alpha - i)/2a_\alpha + i] + \{(b\alpha'\Gamma_{23}t\sqrt{2i})/(2a_\alpha + i)\}} t^{-(1/2)+(i\epsilon/2)} \quad (\text{A-9})$$

and changing variables to

$$t' = t \left(\frac{2a_\alpha - i}{2a_\alpha + i}\right)^{1/2} \quad (\text{A-10})$$

we get

$$\chi_\alpha = 1/h_3 \left(\frac{\nu_\alpha}{\gamma_{21}}\right) \frac{e^{-c\alpha'r_{23}^2}}{\Gamma\left(\frac{1}{2} + \frac{i\epsilon}{2}\right)} \frac{e^{-b\alpha'r_{23}^2/2(2a_\alpha + i)}}{(a_\alpha + i/2)^{1/2}} \times \left(\frac{2a_\alpha + i}{2a_\alpha - i}\right)^{1/4(i+i\epsilon)} \int_0^\infty dt' e^{-t'^2/2 + t'\sqrt{2i}b\alpha'r_{23}} t'^{-(1/2)+(i\epsilon/2)} \quad (\text{A-11})$$

where

$$b_\alpha = \frac{b\alpha'}{4a_\alpha^2 + 1} \quad (\text{A-12})$$

Recalling the definition of the Weber function A-5, we get, after some simplifications

$$\chi_\alpha = 1/h_i \left(\frac{\nu_\alpha}{\gamma_{21}}\right)^{1/2} e^{-c\alpha'q\alpha^2} \frac{1}{(4a_\alpha^2 + 1)^{1/4}} \left(\frac{2a_\alpha + i}{2a_\alpha - i}\right)^{i\epsilon/4} \times D_{-(1/2)-(i\epsilon/2)}(-b_\alpha q_\alpha \sqrt{2i}) \quad (\text{A-13})$$

with $c_\alpha = c\alpha' - a_\alpha b_\alpha^2$.

To find κ_1 and κ_2 we note that (II-27) and (II-28) can be written as

$$\frac{1}{\sqrt{2}\gamma_{2j}(h_3 + h_4)} \int_{-\infty}^\infty dx e^{-a_j x^2} D_{-(1/2)-(i\epsilon/2)}(x\sqrt{2i}) \quad (\text{A-14})$$

with $j = 1, 2$ and

$$a_1 = \frac{1}{2(h_3 + h_4)^2 \gamma_{21}} [\gamma_{12}(h_5 + h_6)^2 + \gamma_{11}(h_1 + h_2)^2] \quad (\text{A-15})$$

$$a_2 = \frac{\gamma_{12}(h_5 + h_6)^2}{\gamma_{22}(h_7 + h_8)^2} \quad (\text{A-16})$$

Using (A-13) we get

$$\kappa_j = \frac{\sqrt{\pi}}{\sqrt{2}\gamma_{2j}(h_3 + h_4)} \frac{1}{(4a_j^2 + 1)^{1/4}} \times \left(\frac{2a_j + i}{2a_j - i}\right)^{i\epsilon/4} D_{-(1/2)-(i\epsilon/2)}(0) \quad (\text{A-17})$$

(15) I. S. Gradshteyn and I. M. Ryzhik, "Tablitsii Integralov Summi Riadov i Proizvedenii," Moscow, 1962.

The Vapor Pressure, the Evaporation Coefficient, and the Heat of Sublimation of Barium Fluoride

by Patrick E. Hart and Alan W. Searcy

Inorganic Materials Research Division, Lawrence Radiation Laboratory, and Department of Mineral Technology, College of Engineering, University of California, Berkeley, California (Received December 21, 1965)

The vapor pressure of barium fluoride was measured in the temperature range 1261 to 1548°K by the torsion-effusion method. The free-surface sublimation pressure from the [111] faces of single crystals was measured by the torsion-Langmuir method in the range 1315 to 1492°K. Comparison of the torsion-effusion and torsion-Langmuir data indicates a sublimation coefficient of 0.9 ± 0.1 . Extrapolation of the data in the Langmuir experiments yields a heat of sublimation at 298°K of 90.6 ± 3 kcal/mole and for the Knudsen experiments yields 90.3 ± 3 kcal/mole by the third-law method and 90.3 ± 3 kcal/mole and 88.8 ± 3 kcal/mole by the second-law method. The second-law Knudsen value should be given greatest weight until supporting thermochemical data are better established.

Introduction

Measurements of the vapor pressure of barium fluoride have been made by Ruff and LeBoucher¹ between 1960 and 2206°F by use of a dynamic method, by Green, *et al.*,² by means of a Knudsen effusion study with a mass spectrometer between 1232 and 1505°K, by Hildenbrand, *et al.*,³ by means of a torsion-effusion study between 1300 and 1550°K, and by Bautista and Margrave⁴ by means of a weight-loss study on single crystals between 1167 and 1250°K.

From a comparison of various effusion and free-surface evaporation studies, Bautista and Margrave⁴ suggest that the evaporation coefficient for alkaline earth fluorides and chlorides are in the range 0.1 to 0.3.

However, the free-surface and effusion experiments compared were in no case performed in both the same apparatus and in the same temperature range, so that the apparent differences in measured pressures could arise from systematic experimental errors. It therefore seemed desirable to measure the vapor pressure of some alkaline earth difluoride by an effusion and by a Langmuir method in a single apparatus. Since one of these authors⁵ had already obtained some torsion-effusion data for barium fluoride and since single crystals of barium fluoride were available, barium fluoride was chosen as the substance for study by the torsion-effusion^{6,7} and torsion-Langmuir⁸ methods.

Experimental Section

Barium fluoride in the form of powder of optical quality and of single crystals was obtained from Semi Elements, Inc.

The torsion apparatus that was used in this work is described by Hammer and Pask.⁹ The apparatus makes use of the interaction of an electric field with a small permanent magnet to balance the torque produced by effusion of vapor from orifices or surfaces which are offset from the center of support. Calibration of the apparatus was effectuated in the manner described by Hammer and Pask. For the present study, the torsion cells were made of National Carbon ZT-101 graphite

- (1) O. Ruff and L. LeBoucher, *Z. Anorg. Chem.*, **219**, 376 (1934).
- (2) J. W. Green, G. D. Blue, T. C. Ehlert, and J. L. Margrave, *J. Chem. Phys.*, **41**, 2245 (1964).
- (3) D. L. Hildenbrand, E. Murad, N. D. Potter, L. P. Thread, and W. F. Hall, Aeronutronics Report U-3183 W. O. 2253, June 30, 1965.
- (4) Z. G. Bautista and J. L. Margrave, *J. Phys. Chem.*, **69**, 1770 (1965).
- (5) P. E. Hart, Lawrence Radiation Laboratory Report, UCRL-11124, Berkeley, Calif., Jan 16, 1964.
- (6) H. Mayer, *Z. Physik*, **67**, 240 (1931).
- (7) M. Vollmer, *Z. Physik. Chem. (Bodenstein Festband)*, 863 (1931).
- (8) Z. A. Munir and A. W. Searcy, *J. Chem. Phys.*, **42**, 4223 (1965).
- (9) R. R. Hammer and J. A. Pask, *J. Am. Ceram. Soc.*, **47**, 264 (1964).

in box shape. Pairs of orifices with three different areas¹⁰ were used in the Knudsen experiments. Corrections for the finite orifice lengths¹¹ were made in calculations from the data. Before effusion holes were machined in the cell walls, each cell was heated with barium fluoride inside. No observable deflection was found when the cells and samples were heated to 1450°K. Therefore, it was assumed that measured deflections during the experiment were due only to effusion of vapor through the orifices.

In the Langmuir free-surface evaporation experiments, cleaved [111] faces of barium fluoride single crystals were placed behind graphite washers mounted in the vertical cell walls. Two sets of washers were used, set 4 with orifices of 1.98-mm diameter, set 5 with 0.98- and 0.99-mm diameters. The angle of taper of the orifices outward through the 1.6 mm thick washer was 60° with the normal. Force correction factors were used for the orifices as calculated by Freeman.¹² Cells had moment arms 9.5 cm in length.

Microscopic examination at 250× of single crystals heated at 1450°K for 45 min showed no roughening of the [111] surface near the center of the region exposed for evaporation. Toward the edges of the exposed surfaces, successive edges of [111] surfaces rose from the flat central region toward the original crystal surface. The correction for molecules reflected or condensed near the edges of the exposed surface are demonstrated to be negligible by the fact that data obtained from surfaces whose areas differed by a factor of 4 were in excellent agreement.

The furnace heating elements were of hairpin-shaped tungsten wires connected in parallel. Electromagnetic repulsion of the torsion assembly which was noted in other torsion-effusion work¹³ was not observed because of the self-cancelling of the induced field in the hairpin elements. Temperatures were measured by a thermocouple placed in a reference graphite cell located below the effusion cell in the furnace hot zone. To calibrate the effusion cell temperature against the reference cell temperature, a thermocouple was mounted in an effusion cell. This thermocouple was calibrated by a gold-point determination when both cells were in the vapor pressure apparatus. The relative temperatures of thermocouples in the reference and effusion cells were measured at a series of power settings. With the furnace geometry used for the first two sets of effusion studies, the effusion cell was 15° hotter than the reference cell at the gold point. For the third set of effusion studies and the Langmuir studies the difference was 45°. The vaporization cells were reproducibly mounted in a region of the furnace in which cell temperatures were demonstrated by experiment to be

changed less than 2° by vertical displacements of the cell by 3.0 cm. Horizontal gradients in the cell when mounted in this section of the furnace should be correspondingly small.

The equilibrium vapor pressure of tin was measured by the torsion-effusion method to check for any systematic errors that would affect pressure readings. The third-law heat of sublimation of tin at 298°K was determined as $\Delta H^\circ_{298} = 71.79 \pm 0.27$ kcal/mole. In an exhaustive study of tin by the same method, Schulz¹⁴ found $\Delta H^\circ_{298} = 71.8$ kcal/mole compared with $\Delta H^\circ_{298} = 72.2$ kcal, the value suggested by Hultgren, *et al.*,¹⁵ from earlier studies.

Prior to a run, the cell and sample were heated some 50° higher than the highest temperature to be reached during the run and until the ambient pressure in the furnace was no higher than 5×10^{-5} torr. In any particular run from two to six points were taken with at least 15 min being allowed after each temperature change in order to ensure that equilibrium was reached.

Results and Discussion

The results of this study are shown in Figure 1 and in Tables I and II. The lines of the graph are the least-squares fit to the data collected.

Molecular flow equations for low-pressure gas flow through an orifice have been shown to apply only when the mean free path of the vapor species is greater than some critical value that depends on the dimensions of the effusion orifice.^{16,17} Mean free path to diameter ratios were calculated using the hard-spheres approximation¹⁸ with the molecular diameter of barium fluoride taken as 8.14 Å, the sum of ionic diameters at room temperature, assuming a linear molecule. This value of λ/d can be used only for relative comparison. Recent

(10) Orifice set 1: diameter 1.07 mm, length 1.30 mm, moment arm length 11.6 mm; diameter 1.05 mm, length 1.30 mm, moment arm length 11.9 mm. Orifice set 2: diameter 2.36 mm, length 1.30 mm, moment arm length 11.6 mm; diameter 2.34 mm, length 1.30 mm, moment arm length 11.9 mm. Orifice set 3: diameter 0.92 mm, length 0.75 mm, moment arm length 12.9 mm; diameter 0.92 mm, length 0.77 mm, moment arm length 12.8 mm.

(11) R. D. Freeman and A. W. Searcy, *J. Chem. Phys.*, **22**, 762 (1954).

(12) R. D. Freeman, Oklahoma State University Technical Documentary Report No. ASD-TDR-63-754, Aug 1963.

(13) D. A. Schulz and A. W. Searcy, *J. Phys. Chem.*, **67**, 103 (1963).

(14) D. A. Schulz, Ph.D. Thesis, University of California, Berkeley, Calif., 1961.

(15) R. Hultgren, R. L. Orr, P. D. Anderson, and K. K. Kelley, "Values of Thermodynamic Properties of Metals and Alloys," John Wiley and Sons, Inc., New York, N. Y., 1963.

(16) A. W. Searcy and D. A. Schulz, *J. Chem. Phys.*, **38**, 772 (1963).

(17) K. D. Carlson, P. W. Gilles, and R. J. Thorn, *ibid.*, **38**, 2064 (1963).

(18) S. Dushman, "Scientific Foundations of Vacuum Technique," John Wiley and Sons, Inc., New York, N. Y., 1949.

Table I: Torsion-Effusion Sublimation Pressures for Barium Fluoride^a

T , °K	P , atm	$-\left(\frac{\Delta F^\circ_T - \Delta H^\circ_{298}}{T}\right)$, cal/deg	ΔH°_{298} , kcal/mole
1491	3.32×10^{-6}	39.77	89.81
1459	1.69×10^{-6}	39.96	90.17
1440	1.03×10^{-6}	40.07	90.57
1414	5.83×10^{-6}	40.22	90.74
1388	3.56×10^{-6}	40.35	90.61
1548	1.24×10^{-4}	39.42	88.71 ^b
1520	6.90×10^{-6}	39.57	89.09 ^b
1358	1.59×10^{-6}	40.46	90.99
1378	2.56×10^{-6}	40.39	90.92
1395	3.95×10^{-6}	40.32	90.70
1425	8.77×10^{-6}	40.10	90.21
1358	2.18×10^{-6}	40.47	90.55
1448	1.44×10^{-6}	40.03	90.03
1526	7.55×10^{-6}	39.57	89.17 ^b
1401	5.27×10^{-6}	40.28	90.27
1305	6.10×10^{-7}	40.69	90.22
1430	9.90×10^{-4}	40.13	90.13
1388	3.80×10^{-6}	40.37	90.46
1402	5.22×10^{-6}	40.27	90.33
1293	4.68×10^{-7}	40.74	90.13
1308	6.76×10^{-7}	40.67	90.13
1318	8.70×10^{-7}	40.64	90.12
1375	3.08×10^{-6}	40.41	90.25
1359	2.13×10^{-6}	40.48	90.28
1277	3.47×10^{-7}	40.82	89.87
1261	2.52×10^{-7}	40.89	89.64
1375	3.10×10^{-6}	40.41	90.22
1384	4.20×10^{-6}	40.37	89.92
1370	2.53×10^{-6}	40.43	90.48
1350	1.73×10^{-6}	40.52	90.29
1336	1.19×10^{-6}	40.58	90.43
1455	1.44×10^{-6}	39.98	90.40
1390	4.04×10^{-6}	40.33	90.36
1431	9.22×10^{-6}	40.12	90.39
1486	2.70×10^{-6}	39.80	90.21
1486	2.95×10^{-6}	39.80	90.05
1506	3.73×10^{-6}	39.69	90.29
1535	5.86×10^{-6}	39.53	90.41
1394	4.76×10^{-6}	40.32	90.24
1413	7.52×10^{-6}	40.22	89.96
1440	1.13×10^{-6}	40.07	90.30
1464	1.99×10^{-6}	39.93	89.95
1473	2.34×10^{-6}	39.88	89.95
1548	7.11×10^{-6}	39.45	90.45
1360	2.02×10^{-6}	40.48	89.49
1523	4.93×10^{-6}	39.58	90.30
1395	4.51×10^{-6}	40.32	90.37
1501	3.66×10^{-6}	39.72	90.09
1529	5.29×10^{-6}	39.55	90.39

$$\bar{A}_v = 90.25 \pm 0.28$$

^a First 14 points taken with orifice set 1; middle 17 points with orifice set 2; last 18 points with orifice set 3. ^b Indicates where λ/d was calculated to be less than 1.0.

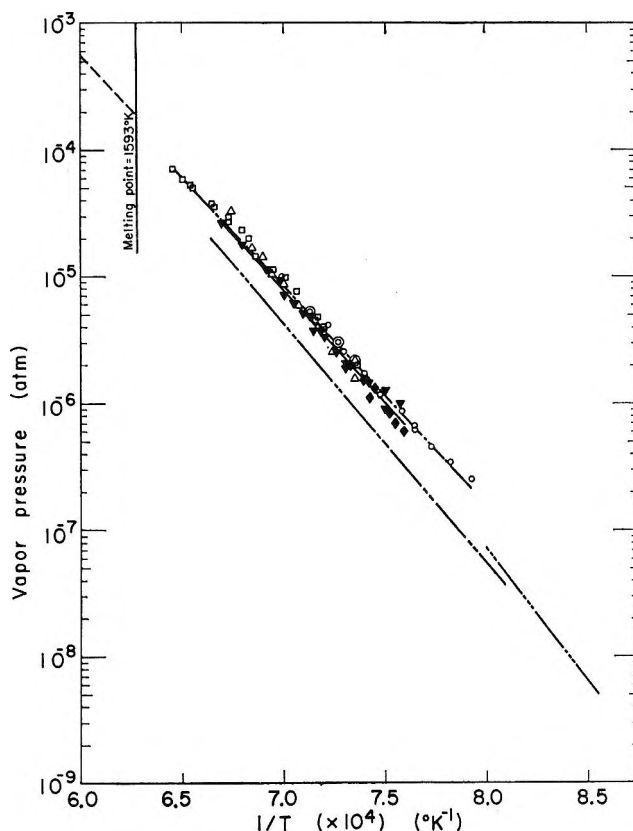


Figure 1. Vapor pressure of barium fluoride: ---, Knudsen experiment (this work) $\lambda/d > 1.0$; Δ , orifice 1, O, orifice 2, \square , orifice 3; —, Langmuir experiment (this work); ∇ , orifice 4, \diamond , orifice 5; - - - -, Buff and LeBouche (extrapolated); - · - · -, Green, *et al.*; - - - -, Bautista and Margrave.

experiments¹⁹ indicate barium fluoride may be a bent molecule and thus would have a slightly smaller effective molecular diameter than assumed. Knudsen pressures for which calculated λ/d values are less than 1.0 are excluded in the final calculations of the heats of sublimation and are not shown in Figure 1 because systematic deviations in calculated values, presumably arising from failure of the molecular flow approximation, are apparent for measurements at lower λ/d values. For orifice 1 when λ/d was less than 1.0, ΔH°_{298} values of 1.54 to 1.28 kcal/mole below the average were found. Schulz and Searcy¹³ also found substantial deviation in ΔH°_{298} values when λ/d became less than a critical value near unity.

Least-squares calculations from Knudsen data where $\lambda/d > 1.0$ yield for the vapor pressure in atmospheres $\log P = -[(79.73 \pm 0.77)/4.576] \times (10^3/T) + 7.15 \pm 0.12$ between 1261 and 1548°K and $\log P = -[(80.53$

(19) L. Warton, R. A. Berg, and W. Klemperer, *J. Chem. Phys.*, **39**, 2023 (1963).

Table II: Torsion-Langmuir Sublimation Pressure for Barium Fluoride^a

T , °K	P , atm	$-\left(\frac{\Delta F^\circ_T - \Delta H^\circ_{298}}{T}\right)$, cal/deg	ΔH°_{298} , kcal/mole
1445	1.11×10^{-6}	40.05	90.61
1470	1.79×10^{-6}	39.90	90.59
1492	2.67×10^{-6}	39.75	90.52
1318	9.72×10^{-7}	40.63	89.90
1394	3.65×10^{-6}	40.31	90.88
1425	7.16×10^{-6}	40.16	90.78
1395	4.11×10^{-6}	40.31	90.61
1390	3.33×10^{-6}	40.34	90.91
1331	1.28×10^{-6}	40.59	89.85
1347	1.48×10^{-6}	40.53	90.52
1365	2.09×10^{-6}	40.45	90.68
1417	6.09×10^{-6}	40.20	90.71
1365	2.00×10^{-6}	40.45	90.74
1408	5.06×10^{-6}	40.24	90.78
1377	2.53×10^{-6}	40.40	90.89
1430	9.05×10^{-6}	40.12	90.37
1402	4.93×10^{-6}	40.28	90.45
1331	9.00×10^{-7}	40.59	90.85
1328	8.43×10^{-7}	40.60	90.83
1315	6.27×10^{-7}	40.65	90.77
1345	1.13×10^{-6}	40.53	91.11
1323	7.20×10^{-7}	40.62	90.92
1340	1.32×10^{-6}	40.55	90.38
1361	2.06×10^{-6}	40.48	90.49
1350	1.56×10^{-6}	40.52	90.56

$$\text{Av} = 90.62 \pm 0.30$$

^a First 18 points with orifice set 4; last 7 points with orifice set 5.

$\pm 1.8)/4.576] \times (10^3/T) + 7.22 \pm 0.29$ between 1315 and 1492°K for the Langmuir experiment. The errors are the standard deviations from least-squares fits.

The heats of sublimation of barium fluoride at 298°K for the Knudsen and Langmuir data were calculated by both the second-law and third-law methods. In all calculations, BaF₂ was considered to be the major vapor species² because thermodynamic calculations indicate that the pressures produced by the reactions BaF₂(s) + C(s) = BaF(g) + CF(g), BaF₂(s) + C(s) = Ba(g) + CF₂(g), and BaF₂(s) + 1/2C(s) = BaF(g) + 1/2CF₂(g), would be several orders of magnitude below the observed pressures.

The same heat capacity equations and free-energy functions for solid barium fluoride²⁰ and the same estimated heat capacity and free-energy functions for barium fluoride gas²¹ were used in calculating heats of sublimation as were used by Green, *et al.*,² and by Bautista and Margrave.⁴ The free-energy functions used are expected to be as reliable as can presently be

estimated²¹ whether or not the BaF₂(g) molecule is linear or bent as suggested by recent electric dipole studies.¹⁹ The second-law treatment yielded $\Delta H^\circ_{298} = 88.78 \pm 1.26$ kcal/mole from the Knudsen experiments and $\Delta H^\circ_{298} = 90.29 \pm 1.81$ kcal/mole from the Langmuir experiments. The third-law calculations for the 46 Knudsen measurements for which $\lambda/d > 1.0$ yielded $\Delta H^\circ_{298} = 90.25 \pm 0.28$ kcal/mole and for the 25 Langmuir measurements yielded $\Delta H^\circ_{298} = 90.62 \pm 0.30$. The indicated errors are the standard deviations. The free-energy functions could be in error by enough to contribute a 4 kcal error to the calculated heats at 298°K; however, the heat of sublimation calculated by the third-law method is probably correct to within ± 3 kcal/mole. Assuming a $+5^\circ$ error at the high end of measurements and a -5° error at the lower end (correspondingly $\pm 10\%$ errors in pressures) yields an estimated maximum error of 2.8 kcal for the second-law calculation.

Brewer, *et al.*,²¹ concluded from the early work of Ruff and LeBoucher¹ that the heat of sublimation of barium fluoride is about 88 kcal/mole at 298°K. Green, *et al.*,² in the mass spectrometer study found $\Delta H^\circ_{298} = 92.3$ kcal/mole by the third-law method and $\Delta H^\circ_{298} = 93.8$ kcal/mole by the second-law method. Torsion-effusion studies of Hildenbrand, *et al.*,³ yield $\Delta H^\circ_{298} = 88.6$ kcal when recalculated with the same free-energy functions used by the other investigators. The Langmuir measurements of Bautista and Margrave⁴ yield $\Delta H^\circ_{298} = 92.3$ kcal/mole from third-law analysis and $\Delta H^\circ_{298} = 94.7$ kcal/mole by second-law analysis.

Hildenbrand and co-workers³ believe their experimental results indicate that barium fluoride is bent. We will not comment further on this point because the work of Hildenbrand, *et al.*, is not yet published except in company reports. The second- and third-law measurements of the present work agree well when Brewer's²¹ free-energy functions are used. The second-law Knudsen measurements should be given greatest weight until supporting thermochemical data for third-law calculations are better established.

Since the same free-energy functions were used by Green, *et al.*,² by Bautista and Margrave,⁴ and by us and since the measurements were made in approximately the same temperature ranges, the differences in calculated heats of sublimation at 298°K reflect the systematic differences of approximately a factor of 2 in measured pressures and not possible errors in the free-energy functions. Mass spectrometer pressure measure-

(20) K. K. Kelley, U. S. Bureau of Mines Bulletin, 584, U. S. Government Printing Office, Washington, D. C., 1960, p 23.

(21) L. Brewer, G. Somayajulu, and E. Brackett, *Chem. Rev.*, **63**, 111 (1963).

ments are usually expected to be uncertain by a factor of 2 or more. Presumably, it was in recognition of the inherent uncertainty in mass spectrometer measurements that Bautista and Margrave did not draw the conclusion from the excellent agreement of their Langmuir results for barium fluoride with mass spectrometer measurements in their laboratory that $\alpha = 1$.

Instead, they concluded from comparison of the Langmuir data with effusion measurements of other investigators that evaporation coefficients for alkaline earth halides probably generally lie in the range 0.1 to 0.3. For barium fluoride specifically, comparison of Bautista's results to our effusion results would lead to the conclusion that the value of α is about 0.5.

A recent paper of Loehman, Kent, and Margrave²² does describe both Knudsen measurements (above the melting point) and Langmuir measurements (below the melting point) for strontium chloride. The Langmuir experiments were performed on single crystals suspended in the furnace. Extrapolation of Knudsen data into the range below the melting point clearly indicates an evaporation coefficient of 0.3 for the solid.

Comparison of our own free-surface and effusion data for barium fluoride yields $\alpha = 0.9 \pm 0.1$. The *relative* error in our measurements of free surface and effusion data probably should not exceed 10% because most sources of systematic error are common to the free-surface and effusion measurements. The most prob-

able source of serious error in determination of α is a discrepancy between measured temperature and true temperature of the evaporating surface of a Langmuir sample. In this research the Langmuir specimens were mounted in the same position as the orifices of the effusion cells in a chamber of demonstrated uniform temperature. If the true value of α were 0.5, our free-surface temperatures would have to be approximately 35° higher than the temperature inside an effusion cell placed in the same positions in order to account for the results presented in this paper. An actual temperature difference of more than 5° is very unlikely.

The 111 faces of the barium fluoride surfaces remained smooth when examined at 240 magnifications; surface roughening did not, therefore, significantly increase the effective rate of evaporation. The evaporation coefficient for this face of a barium fluoride crystal is near unity within a small probable experimental error, and the evaporation coefficients for other alkaline earth fluorides are probably also near unity.

Acknowledgments. We extend our thanks to Dr. Reuben Hammer and Professor Joseph Pask, who designed and constructed the apparatus used in this research. This work was done under the auspices of the U. S. Atomic Energy Commission.

(22) R. E. Loehman, R. A. Kent, and J. L. Margrave, *J. Chem. Eng. Data*, **10**, 296 (1965).

The Study of Annellation Series of Benzenoid Hydrocarbons. I. The Influence of Annellation on the Changes of the Excitation Energy of the p Band

by Jaroslav Koutecký,¹ Petr Hochmann, and Miloš Titz

*Institute of Physical Chemistry, Czechoslovak Academy of Sciences, Prague, Czechoslovakia
(Received January 10, 1966)*

For the group of 86 catacondensed and pericondensed benzenoid hydrocarbons, the theoretical estimates of the excitation energy of the p band, calculated by the Hückel method and by the semiempirical method of the limited configuration interaction, as well as the experimental values of the same quantity, are plotted against the number of atoms of the respective molecules. In the plots thus obtained, the influence of the topology and size of the molecules on the changes of the theoretical and experimental values of the p-band excitation energy may be traced. A surprising similarity of plots for the three quantities mentioned has been found, and the importance of the molecular topology as the molecule characteristics is shown. Approximate rules based on the distribution of the "nodal points" in the highest occupied molecular orbital of the parent hydrocarbon have been derived, predicting the direction of the p-band shift with benzene ring annellation.

Introduction

When comparing the differences in energy of the lowest unoccupied and the highest occupied molecular orbital in Hückel approximations ($E(N \rightarrow V_1)$) with the experimental value of the excitation energy corresponding to the p band according to Clar's classification² (ϵ_{exptl}), a statistically significant correlation is found for benzenoid hydrocarbons³ as well as for other types of hydrocarbons.⁴ However, the dependence of ϵ_{exptl} on $E(N \rightarrow V_1)$ shows a considerable scattering. This scattering is connected with the decomposition of the dependence in question into partial dependences for narrower structural types. *E.g.*, the benzenoid hydrocarbons arising from 1,2-benzopyrene or 3,4-benzopyrene by a linear annellation, *i.e.*, hydrocarbons of the Pa[0,*n*] or Pb[0,*n*] type, respectively (see Table I), show systematic deviations from the regression line of dependence ϵ_{exptl} on $E(N \rightarrow V_1)$ (*cf.* Table II). If, however, the decomposition of the dependence in still finer subclasses is considered, the amount of information contained in every dependence is lowered, which results in a reduced predictability.

This is the reason why this work has not been limited to the study of the dependence ϵ_{exptl} on $E(N \rightarrow V_1)$ as a superposition of partial dependences. The en-

deavor has been made to differentiate the influence of the size of the conjugated system from the influence of its topology. For hydrocarbons where the use of the conventional Hückel method does not depend on the choice of parameters, the matrix of the effective Hamiltonian is identical with the topological matrix which represents in a unique way the structural formula belonging to the carbon skeleton of the molecule considered as an unweighted graph.^{5,6} The connection of the Hückel eigenproblem with the diagonalization of the topological matrix is very well known.⁷⁻⁹ It was

(1) Department of Chemistry, The John Hopkins University, Baltimore, Md. 21218.

(2) E. Clar, "Polycyclic Hydrocarbons," Academic Press Inc., New York, N. Y., 1964.

(3) (a) A. Streitwieser, Jr., "Molecular Orbital Theory for Organic Chemists," John Wiley and Sons, Inc., New York, N. Y., 1961; (b) J. Koutecký, J. Paldus, and R. Zahradník, *J. Chem. Phys.*, **36**, 3129 (1962).

(4) D. Meuche, K. Strauss, and E. Heilbronner, *Helv. Chim. Acta*, **41**, 57, 414 (1958).

(5) C. Berge, "Théorie des Graphes et ses Applications," Dunod, Paris, 1958.

(6) J. Sedláček, "Kombinatorika v theorii a praxi," Nakladatelství ČSAV, Praha, 1964.

(7) M. M. Gunthardt and H. Primas, *Helv. Chim. Acta*, **39**, 1645 (1956).

(8) K. Ruedenberg, *J. Chem. Phys.*, **22**, 1828 (1954).

used also to establish important relationships between the Hückel and the one-dimensional free electron theory on one hand¹⁰ and between the Hückel and valence-bond method on the other hand.¹¹ The resonance energies of the π -electron systems were discussed recently in terms of topological concepts.¹²

Even if the importance of the topology is generally understood, the quantitative aspects of the influence of the topology seem to be not fully exhausted. Therefore, the dependence of the quantity $E = 2e$, where e designates the lowest eigenvalue in the absolute sense (*e.g.*, regardless the sign) of the topological matrix, on the number of carbon atoms (N) of the relevant hydrocarbon is studied. The first quantity, being a characteristic of the topological matrix, is in relation with the graph representing the π -electronic system, *i.e.*, with the structural formula of the molecule. This quantity represents the estimate of the lowest excitation energy for alternant hydrocarbons in Hückel's scheme (*i.e.*, $E(N \rightarrow V_1) = E$). On the other hand, the number of carbon atoms may be considered as one of the possible size measures of the conjugated system. Another possible measure would be the number of benzene rings contained in the hydrocarbon. This quantity, however, makes the comparison of catacondensed and pericondensed hydrocarbons difficult.

In the $E-N$ plots mentioned above, individual points corresponding to the given annelation series are connected with straight lines so that the influence of the size of the conjugated system on the quantity E in a series of topologically similar skeletons may be easily followed. A similar method has, in principle, been applied by Clar to the study of dependence of the individual bands in the ultraviolet spectrum of benzenoid hydrocarbons on the structure of the respective molecules.² Such a presentation is a generalization of the graphs in which spectroscopic properties, either in a series of linear polyacenes or in the series of the hydrocarbons with constant number of benzene rings, are plotted.^{13,14}

On the other hand, the $E-N$ graphs enable us to study the influence of the carbon skeleton topology on the quantity E for the fixed size of the molecule.

In the selection of the annelation series of topologically similar carbon skeletons, the following three modes of benzene ring attachment have been considered.

(1) The ring to be annexed has one bond in common with the original system (catacondensation). The most important partial case is the elongation of the existing straight chain of benzene rings following the direction of this chain: in a word, the linear annelation. The transition from naphthalene to anthracene or

from phenanthrene to tetraphene may serve as an example.

(2) The new system arises from the original one through elongation of the linear chain of benzene rings by the addition of one benzene ring; the linear chain in question connects two characteristic and constant groups of benzene rings. This case is illustrated by the transition from the skeleton Ha[0] to Ha[1].

(3) The annexed benzene ring has three neighboring bonds in common with the parent system (pericondensation). The transition from phenanthrene to pyrene serves as an example.

The individual points in the $E-N$ plots belonging to different annelation series in the above-defined sense are connected as mentioned above. These plots are then compared with similar plots in which the experimental value ϵ_{exptl} or the theoretical value of the p-transition excitation energy (ϵ_p), calculated by the method of the limited configuration interaction (LCI), is given as the function of N .

The Hydrocarbons Studied and the Method Used

Besides the plots mentioned in which the quantity E has been plotted against N (Figures 1a-5a), the values of the excitation energy corresponding to the p band found experimentally (ϵ_{exptl}) (Figures 1c-5c) and calculated by means of the LCI (ϵ_p) method (Figures 1b-5b) have also been plotted against the number of atom N . The values E , ϵ_p , and ϵ_{exptl} are given in electron volts. The value of the resonance integral β , both in Hückel and LCI methods, is -2.318 ev. Table II presents the parameters of the linear regression dependence ϵ_{exptl} upon E for different groups of studied molecules for which the experimental data were attainable.

The survey of molecules studied is given in Table I. For the sake of a simple designation of hydrocarbons studied which form the series in the above-mentioned sense, the symbols defined in Table I differ from the conventional chemical nomenclature. To simplify the description of the plots, molecules are numbered as shown in Table I.

The numerical values based on the energy of molecular orbitals in the Hückel approximation have been

(9) K. Ruedenberg, *J. Chem. Phys.*, **34**, 1861, 1884 (1961).

(10) J. R. Platt, "Free Electron Theory of Conjugated Molecules," John Wiley and Sons, Inc., New York, N. Y., 1964.

(11) E. Heilbronner, *Helv. Chim. Acta*, **45**, 1722 (1962).

(12) R. A. Marcus, *J. Chem. Phys.*, **43**, 2643 (1965).

(13) *Cf.* W. Moffit, *ibid.*, **22**, 320 (1954).

(14) *Cf.* N. S. Ham and K. Ruedenberg, *ibid.*, **25**, 13 (1956).

Table I: List of Molecules of Benzenoid Hydrocarbons^a

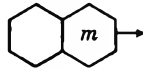
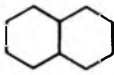
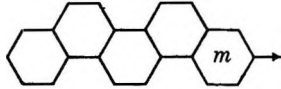

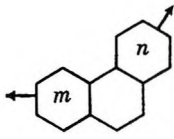
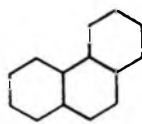
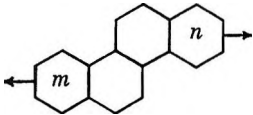
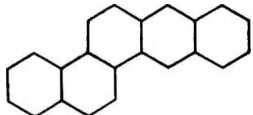
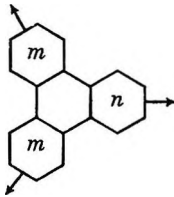

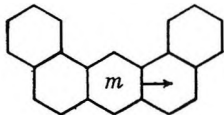
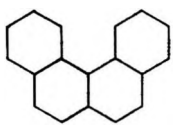
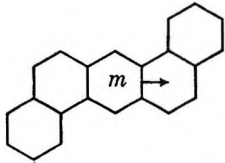
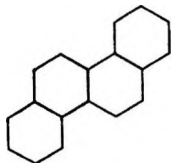
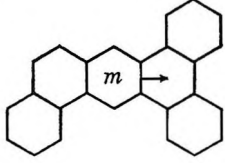
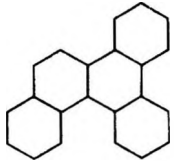
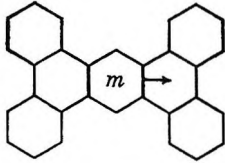
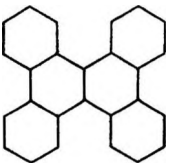
Structural type	Symbol	Individual representatives and their order numbers	Example
	Ac[m]	m : 0, 1, 2, 3, 4, 5 No.: 1, 2, 3, 4, 5, 6	
	Z[m]	m : 0, 1, 2, 3 No.: 7, 8, 9, 10	
	Ph[m,n]	m : 1; n : 1, 2, 3, 4 No.: 11, 12, 13, 14 m : 2; n : 2, 3, 4 No.: 15, 16, 17 m : 3; n : 3, 4 No.: 18, 19 m : 4; n : 4 No.: 20	
	Ch[m,n]	m : 1; n : 2, 3, 4 No.: 21, 22, 23 m : 2; n : 2, 3, 4 No.: 24, 25, 26 m : 3; n : 3, 4 No.: 27, 28 m : 4; n : 4 No.: 29	
	T[m,n]	m : 1; n : 1, 2, 3, 4 No.: 30, 31, 32, 33 m : 2; n : 1, 2, 3 No.: 34, 35, 36 m : 3; n : 1, 2, 3 No.: 37, 38, 39	
	Ha[m]	m : 0, 1, 2, 3 No.: 40, 41, 42, 43	
	Hb[m]	m : 0, 1, 2, 3 No.: 44, 45, 46, 47	
	Hc[m]	m : 0, 1, 2, 3 No.: 48, 49, 50, 51	
	Hd[m]	m : 0, 1, 2, 3 No.: 52, 53, 54, 55	

Table I (continued)

Structural type	Symbol	Individual representatives and their order numbers	Example
	Pa[m,n]	m: 0; n: 0, 1, 2, 3, 4 No.: 56, 57, 58, 59, 60 m: 1; n: 1, 2, 3, 4 No.: 61, 62, 63, 64 m: 2; n: 2, 3, 4 No.: 65, 66, 67 m: 3; n: 3, 4 No.: 68, 69 m: 4; n: 4 No.: 70	
	Pb[m,n]	m: 0; n: 1, 2, 3, 4 No.: 71, 72, 73, 74 m: 1; n: 1, 2, 3 No.: 75, 76, 77 m: 2; n: 2, 3 No.: 78, 79 m: 3; n: 3 No.: 80	
	Pc[m,n]	m: 1; n: 1, 2, 3 No.: 81, 82, 83 m: 2; n: 2, 3 No.: 84, 85 m: 3; n: 3 No.: 86	

* The indices m and n in benzene rings marked with an arrow indicate the number of benzene rings forming a direct chain in the direction of the arrow (in the $Z[m]$ type m is the number of benzene rings forming the continuation of a broken chain of benzene rings). The lines m and n contain the values m and n for the individual molecule types discussed in this work. In the lines marked "No." the order numbers of individual molecules denoting Figures 1-5 are stated.

taken from tables^{15,16} and from results hitherto unpublished.¹⁷ The coefficients of molecular orbitals have been obtained in the usual way. The results of the limited configuration interaction used will be published separately. The parameters used in the LCI calculations as well as the further details of computations may be found elsewhere.¹⁸

Experimental data ϵ_{exptl} have been taken from Clar² and from the papers of his school.¹⁹⁻²³

Numerical calculations have been carried out on a digital computer Ural II in the computing laboratory of the Czechoslovak Academy of Sciences, Prague.

Results and Discussion

The $E-N$, ϵ_p-N , and $\epsilon_{\text{exptl}}-N$ plots of the respective molecules studied are given in Figures 1-5. In these plots the annelations are of the types 1 and 2 defined

above. In Figures 1-4 the hydrocarbons formed by elongation of the longer chain of the molecule (e.g., the series Ph[1,1], Ph[1,2], Ph[1,3], ...) are connected by a full line, while those arising by elongation of the

(15) R. Zahradník and C. Párkányi, *Collection Czech. Chem. Commun.*, **30**, 3536 (1965).

(16) P. Hochmann, J. Dubský, J. Koutecký, and C. Párkányi, *ibid.*, **30**, 3560 (1965).

(17) M. Titz and P. Hochmann, unpublished results.

(18) J. Koutecký, P. Hochmann, and J. Michl, *J. Chem. Phys.*, **40**, 2439 (1964).

(19) B. Boggiano and E. Clar, *J. Chem. Soc.*, 2681 (1957).

(20) E. Clar, A. McCallum, and R. A. Robertson, *Tetrahedron*, **18**, 1471 (1962).

(21) E. Clar and M. Zander, *ibid.*, **19**, 521 (1963).

(22) E. Clar, J. F. Guye-Vuillème, S. McCallum, and I. A. Macpherson, *ibid.*, **19**, 2185 (1963).

(23) E. Clar, J. F. Guye-Vuillème, and J. F. Stephene, *ibid.*, **20**, 2107 (1964).

Table II: Parameters of Regression Dependence ϵ_{exptl} on E for Individual Molecule Groups^a

	N	k	b	r	Δ
1 All hydrocarbons studied	58	1.111	0.456	0.976	0.007
2 Catacondensed hydrocarbons	37	0.859	0.680	0.829	0.025
3 Benzologs of pyrene	21	1.129	0.458	0.971	0.012
4 Ac[m]	5	1.226	0.385	0.998	0.011
5 Z[m]	4	1.015	0.613	0.996	0.005
6 Ac[m], Z[m]	8	1.215	0.393	0.998	0.009
7 Ph[m,n]	7	1.165	0.443	0.991	0.013
8 Ch[m,n]	4	1.246	0.405	0.988	0.016
9 T[m,n]	7	1.122	0.426	0.997	0.009
10 Ac[m], Z[m], Ph[m,n], Ch[m,n], Ha[m], Hb[m]	23	1.192	0.410	0.991	0.008
11 Ha[m], Hb[m], T[1, n]	11	1.166	0.390	0.996	0.003
12 Ha[m], Hb[m], T[1, n], Hc[m], Hd[m]	18	1.136	0.391	0.985	0.011
13 Pa[m,n]	11	1.171	0.404	0.959	0.018
14 Pb[m,n]	8	1.531	0.248	0.998	0.005
15 Pc[m,n]	8	1.508	0.266	0.999	0.003

^a N is the number of molecules in the group, k and b are the parameters of the regression line $\epsilon_{\text{exptl}} = kE + b$, r is the correlation coefficient of the given group of substances, Δ is the median quadratic derivation from the regression line $\Delta = (1/N) \left[\sum_{i=1}^n (\epsilon_{\text{exptl}} - kE^{(i)} - b)^2 \right]^{1/2}$.

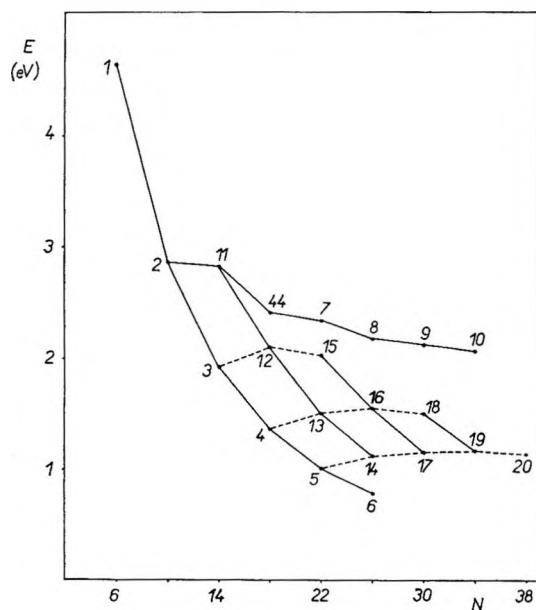


Figure 1a. Dependence of E upon N for molecules of the Ac[m], Ph[m,n], and Z[m] types (molecule Hb[0] is also included).

shorter one (e.g., the series Ac[3], Ph[1,3], Ph[2,3], Ph[3,3]) are connected by dashed lines.

The study of the dependence of E upon N shows that the extension of the conjugated system through annexing of another benzene ring does not always lead to a

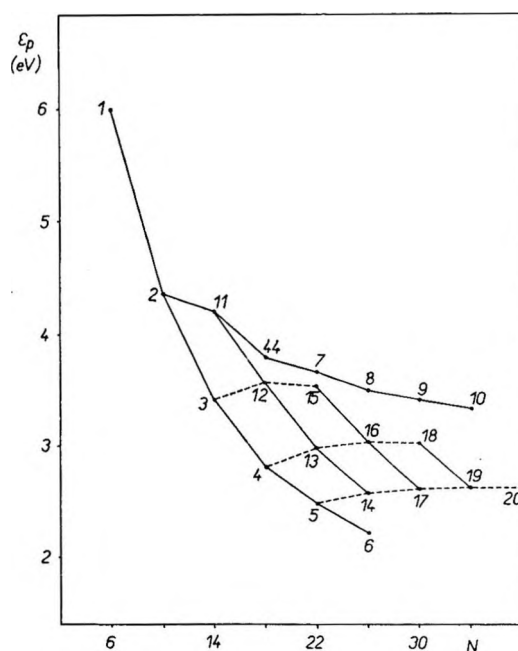


Figure 1b. Dependence of ϵ_p on N for molecules of the Ac[m], Ph[m,n], and Z[m] types (molecule Hb[0] is also included).

decrease of the E value, not even in the case of a linear annelation. This phenomenon has been described for some other classes of hydrocarbons by Pullman.²⁴

(24) B. Pullman and A. Pullman, "Quantum Biochemistry," Interscience Publishers, New York, N. Y., 1963, p 142.

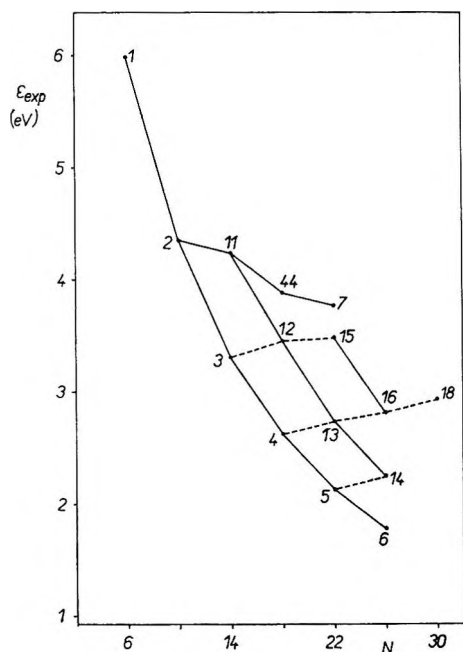


Figure 1c. Dependence of ϵ_{exp} on N for molecules of the $\text{Ac}[m]$, $\text{Ph}[m,n]$, and $\text{Z}[m]$ types (molecule $\text{Hb}[0]$ is also included).

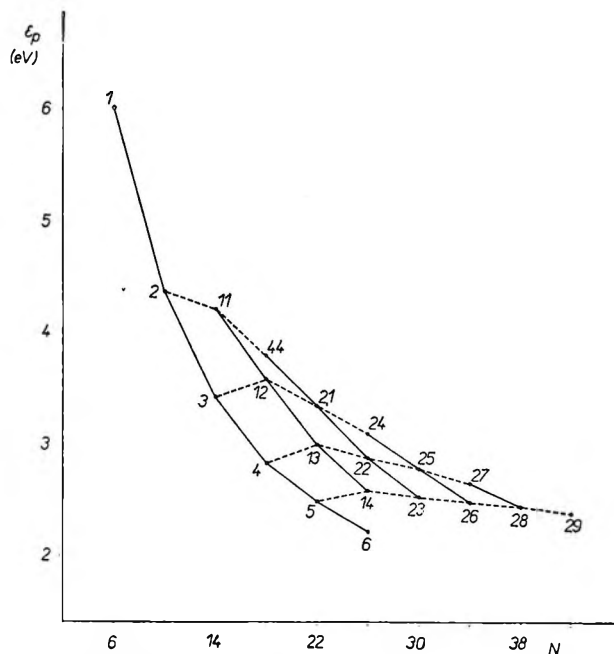


Figure 2b. Dependence of ϵ_p on N for molecules of the $\text{Ac}[m]$, $\text{Ph}[1,n]$, and $\text{Ch}[m,n]$ types.

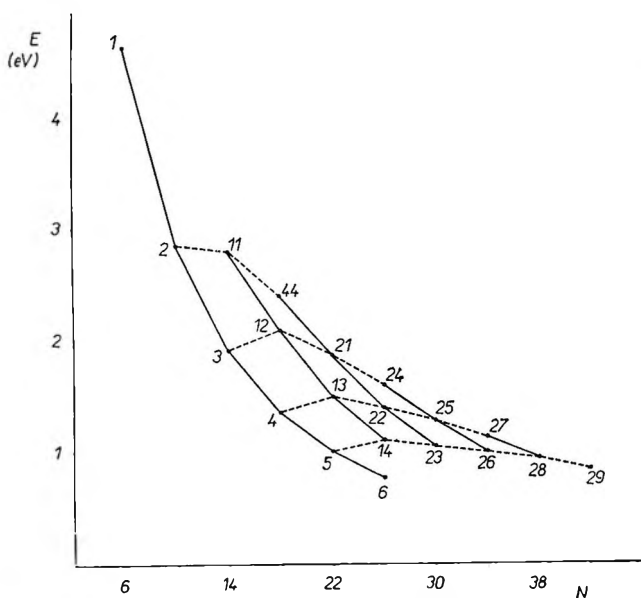


Figure 2a. Dependence of E upon N for molecules of the $\text{Ac}[m]$, $\text{Ph}[1,n]$, and $\text{Ch}[m,n]$ types.

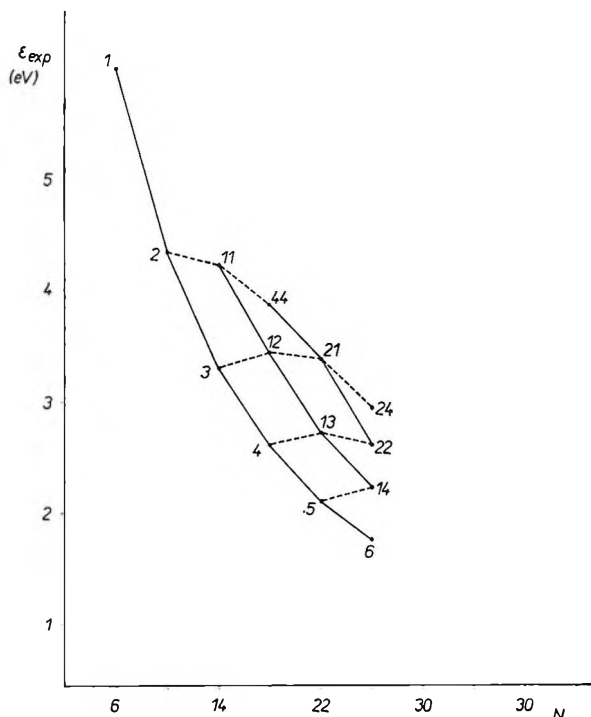


Figure 2c. Dependence of ϵ_{exp} on N for molecules of the $\text{Ac}[m]$, $\text{Ph}[1,n]$, and $\text{Ch}[m,n]$ types.

On the basis of Figures 1–5 the following rules could be observed.

(1) In the molecules of the $\text{Ph}[m,n]$, $\text{Ch}[m,n]$, and $\text{T}[m,n]$, $\text{Pa}[m,n]$, $\text{Pb}[m,n]$ types, a considerable and systematic decrease of the E value occurs only during the linear annelation of the benzene ring into the longer chain of the existing direct chains of benzene

rings, e.g., during the transition from $\text{Ph}[m,n]$ into $\text{Ph}[m, (n + 1)]$ when $n \geq m$. The elongation of the shorter chain leads either to a small decrease of the E value or even to its increase (see Figures 1a–4a).

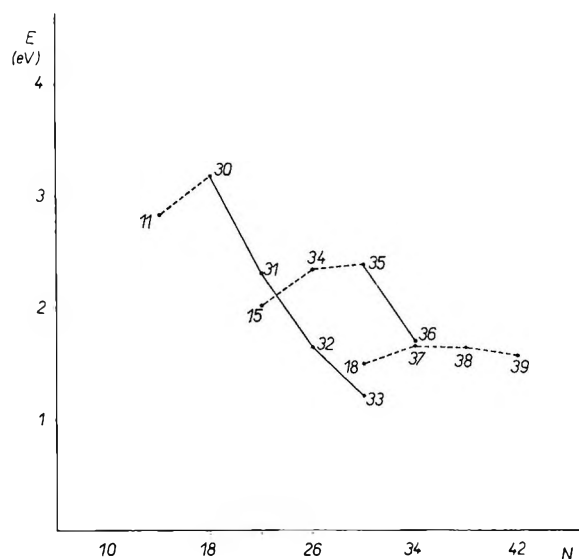


Figure 3a. Dependence of E upon N for molecules of the $\text{Ph}[m,m]$ and $\text{T}[m,n]$ types.

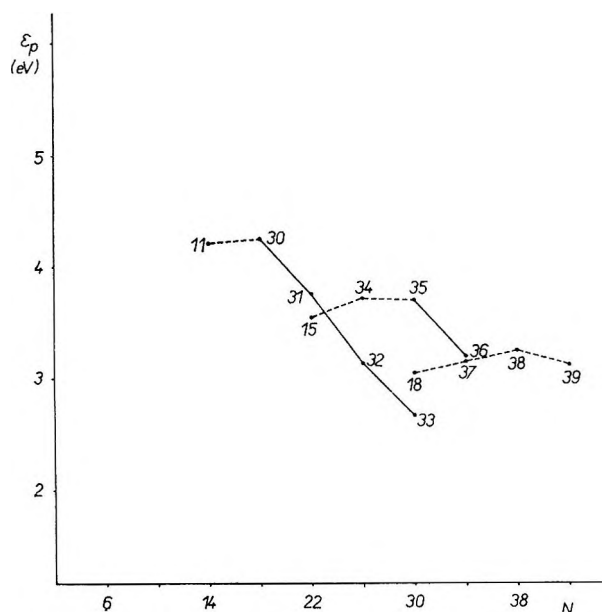


Figure 3b. Dependence of ϵ_p on N for molecules of the $\text{Ph}[m,m]$ and $\text{T}[m,n]$ types.

(2) In the series $\text{Pa}[0,n]$, a heavy decrease of E occurs with regard to the value of this quantity for $\text{Pa}[0,0]$ only for $n \geq 3$. In the series $\text{Pa}[0,0]$, $\text{Pa}[0,1]$, $\text{Pa}[0,2]$, the E value increases. On the other hand, in the series $\text{Pb}[0,n]$ the increase of n results in a strong and systematic decrease of E already for $n > 0$ (see Figure 4a).

(3) In molecules of the $\text{Ha}[m]$, $\text{Hb}[m]$, and especially $\text{Hc}[m]$, $\text{Hd}[m]$ types, the transition $\text{H}[0] \rightarrow \text{H}[1]$

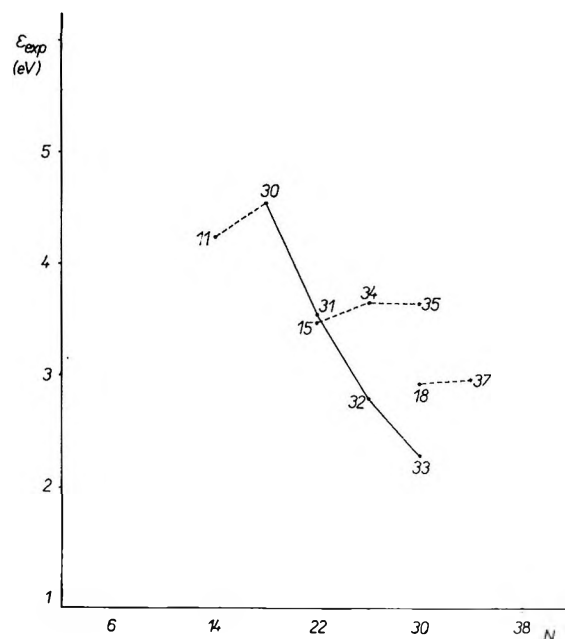


Figure 3c. Dependence of ϵ_{exp} on N for molecules of the $\text{Ph}[m,m]$ and $\text{T}[m,n]$ types.

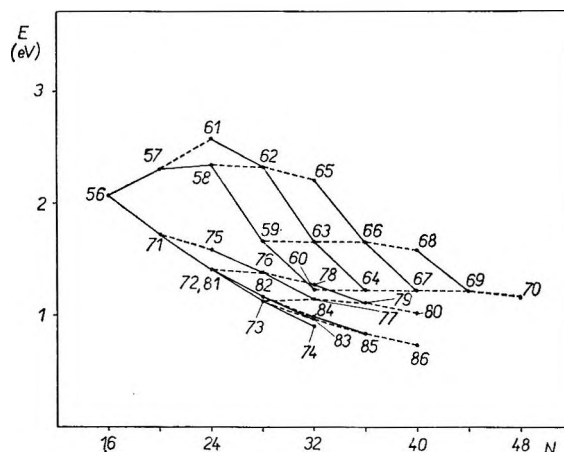


Figure 4a. Dependence of E upon N for molecules of the $\text{Pa}[m,n]$, $\text{Pb}[m,n]$, and $\text{Pc}[m,n]$ types.

is connected with a considerably smaller decrease or possibly increase of the E value. Only a further prolongation of the direct chain of benzene rings leads to a strong and systematic decrease of the E value (see Figure 5a).

(4) The transition in the series $\text{Ac}[n] \rightarrow \text{Ph}[1,n] \rightarrow \text{T}[1,n]$; $\text{Ha}[n-1]$; $\text{Hb}[n-1] \rightarrow \text{Hc}[n-1] \rightarrow \text{Hd}[n-1]$ for $n = 2-4$ appears in the $E-N$ plot as a straight line with a positive slope which becomes smaller with increasing N (see Figure 5a).

(5) The transition from the pyrene benzologs to hydrocarbon from which the benzolog in question

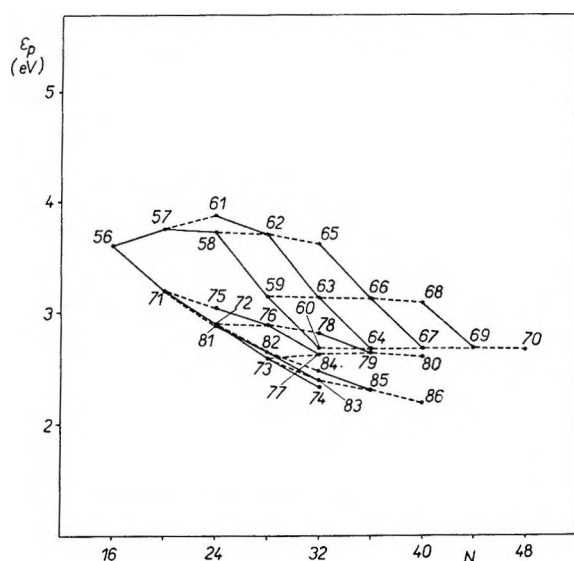


Figure 4b. Dependence of ϵ_p on N for molecules of the $Pa[m,n]$, $Pb[m,n]$, and $Pc[m,n]$ types.

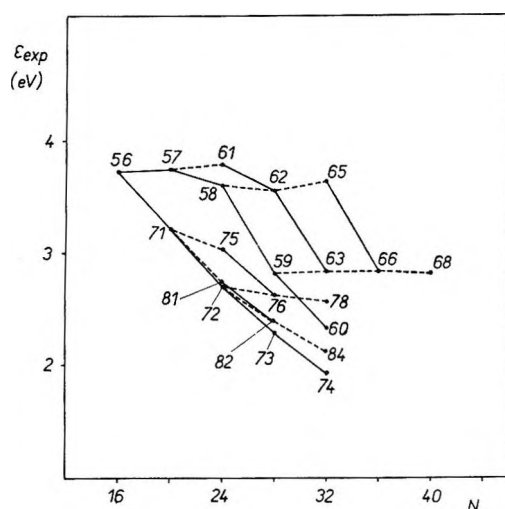


Figure 4c. Dependence of ϵ_{exp} on N for molecules of the $Pa[m,n]$, $Pb[m,n]$, and $Pc[m,n]$ types.

arises by extension of the conjugated system, according to mode 3, leads usually to a decrease of the E value.

(6) In the series of nonbranched chains of benzene rings (types $Ac[m]$, $Z[m]$, $Ph[m,n]$, and $Ch[m,n]$) with a fixed number of benzene rings, the quantity E is the lowest for acenes and increases generally with the number of "foldings" of the chain of benzene rings (compare Figures 1a and 2a).

We are not going to specify further regularities which can be found in $E-N$ plots. Let us only mention that the plots obtained have very characteristic structure.

The rules deduced from the $E-N$ plots are in many

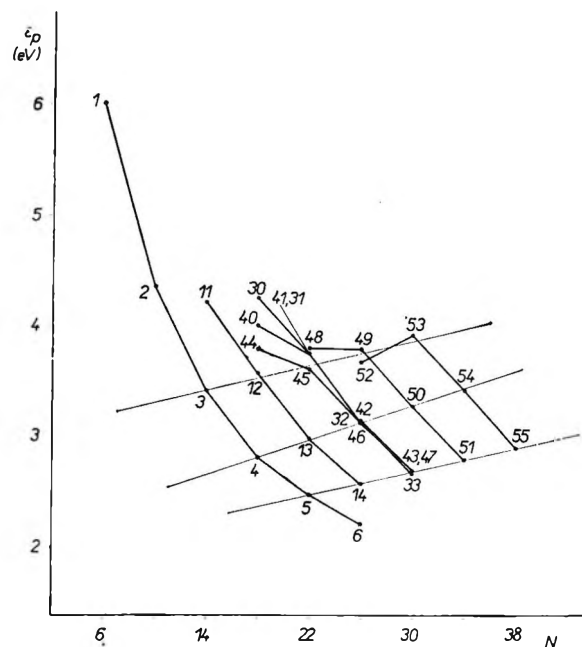


Figure 5a. Dependence of E upon N for molecules of the $Ac[m]$, $Ph[1,n]$, $T[1,n]$, $Ha[m]$, $Hb[m]$, $Hc[m]$, and $Hd[m]$ types. The full thin line connects the points corresponding to the molecules in which the direct chain of benzene rings has the same number of benzene rings.

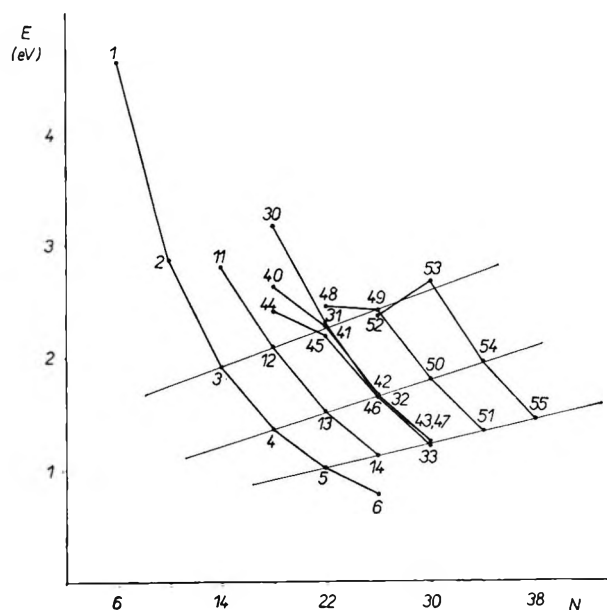


Figure 5b. Dependence of ϵ_p on N for molecules of the $Ac[m]$, $Ph[1,n]$, $T[1,n]$, $Ha[m]$, $Hb[m]$, $Hc[m]$, and $Hd[m]$ types. The full thin line connects the points corresponding to the molecules in which the direct chain of benzene rings has the same number of benzene rings.

cases very similar to those of Clar for the experimentally observed shifts of the p-band positions in the ultra-

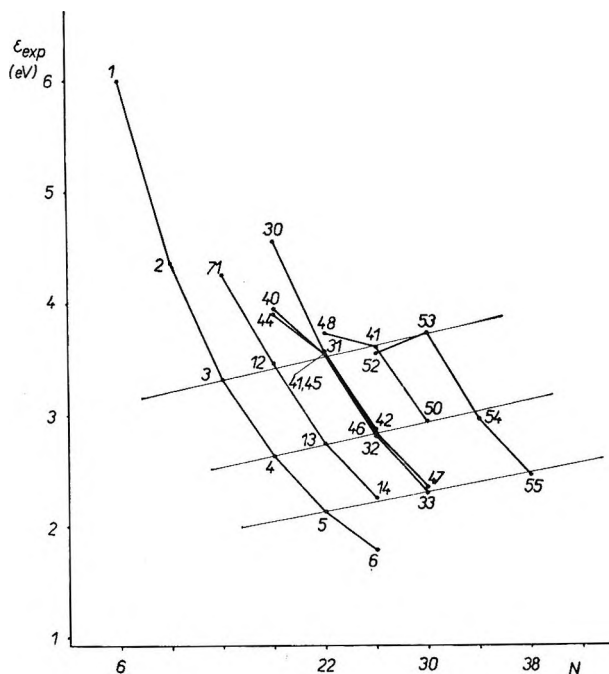


Figure 5c. Dependence of ϵ_{exptl} upon N for the molecules of the Ac[m], Ph[1,n], T[1,n], Ha[m], Hb[m], Hc[m], and Hd[m] types. The full thin line connects the points corresponding to the molecules in which the direct chain of benzene rings has the same number of benzene rings.

violet spectra of benzenoid hydrocarbons. These rules thus represent a quantum-mechanical analog of Clar's rules within the scope of the Hückel method.

The plots obtained by plotting the experimental values of the excitation energy ϵ_{exptl} against the number of atoms N have entirely analogous structures to the $E-N$ plots. In other words, a striking similarity is observed between the plots of the quantity characterizing the topology as a function of the quantity N depending on the size of the molecule, on the one hand, and the plots where the experimental spectroscopic quantity has been plotted against the same quantity N , on the other hand.

The similarity of both types of plots results in the fact that the sequence of the excitation energies ϵ_{exptl} and the quantities E for the fixed chosen N are practically identical. Therefore, the above-stated rules on the influence of annelation of benzene ring upon the quantity E apply to the quantity ϵ_{exptl} as well.

Similarly, the plots of ϵ_p on N show exactly the same character as the $E-N$ plots. A similarity may thus be found between the plots showing the dependence of the theoretical spectroscopic quantity on N and the plots of dependence of the topological characteristic on N .

The addition of another benzene ring to the molecule

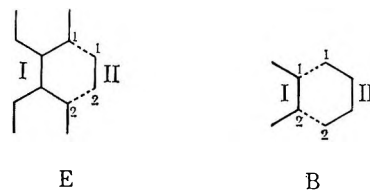


Figure 6. Schematic view showing the joining of an ethylene molecule (E) and a butadiene molecule (B) to a molecule of benzenoid hydrocarbon. The full lines correspond to the bonds in the original systems I and II; the dotted lines are for the new arising bonds.

of hydrocarbon by catacondensation may be considered as a joining of the parent molecule with a molecule of butadiene (see Figure 6B). The addition of another benzene ring by pericondensation may, in a similar way, be considered as a connection of the original molecule with a molecule of ethylene (see Figure 6E). The calculations contained in the Appendix were stimulated by the striking resemblance of the plots for Ph[m,n] and Pb[m,n] or Ch[m,n] and Pc[m,n], respectively. By these calculations it is made possible to obtain a formulation of the sufficient conditions regarding the decrease of the E value during the transition from the original molecule to that molecule which has arisen by joining the molecule of ethylene or butadiene (see Appendix, eq A-12 and A-13). A simplified form of these conditions is

$$\frac{2c_{k1}c_{k2}}{c_{k1}^2 + c_{k2}^2} > -\epsilon_k \quad (1)$$

for joining of ethylene and

$$\frac{2c_{k1}c_{k2}}{c_{k1}^2 + c_{k2}^2} < \epsilon_k(2 - \epsilon_k^2) \quad (2)$$

for joining of butadiene. c_{k1} and c_{k2} are the coefficients in the highest occupied nondegenerated molecular orbital of the parent molecule at the atomic orbitals associated with atoms 1 and 2 on which the joining of the ethylene or butadiene molecule takes place; ϵ_k is the energy of this molecular orbital. These simplified conditions were tested on attainable material, and it has been found that in the majority of cases they predict correctly the change of the quantity E when another benzene ring is being added. It is somewhat surprising, however, that though these conditions have been obtained as sufficient conditions only, an increase of the quantity E occurs in the majority of cases where these conditions have not been fulfilled.

Condition 1 is always fulfilled if the coefficients c_{k1} and c_{k2} have the same sign. In such a case the highest occupied molecular orbital must have an

even number of nodal points²⁵ on the molecule perimeter section connecting atoms 1 and 2. Condition 2 is, in a similar way, always fulfilled if c_{k1} and c_{k2} are of a reverse sign, *i.e.*, if the highest occupied molecular orbital has the nodal point on the bond joining atoms 1 and 2.

The parameters of regression dependence between ϵ_{exptl} and E contained in Table II show that the transition to a structurally more homogeneous group of molecules generally leads to the increase of the correlation coefficient r and to the decrease of the mean quadratic deviation Δ . In comparison with group 1 of all the molecules studied, the qualitative correlation gets worse in the groups of pericondensed and cata-condensed hydrocarbons (groups 2 and 3) which demonstrates the complexity in determining a satisfactory homogenous group. A considerable scattering of slopes and of the regression-line intercepts of individual narrower groups of molecules shows the possibility of serious mistakes in the prediction of ϵ_{exptl} by means of E based on the regression dependence for a heterogeneous group of substances as well as the somewhat problematic significance of the high correlation coefficient and small mean quadratic deviation of this dependence (see group 1).

The LCI method of Pariser and Parr yields very good quantitative predictions of the position of the p band. The LCI method does not predict only a sufficiently large bathochromic effect with prolongation of an already long linear chain of benzene rings present in the hydrocarbon molecule.

Conclusion

The smallest positive eigenvalue of the topological matrix of the molecule in benzenoid hydrocarbon appears to be an important quantity representing the quantitative characteristic of the topology of the respective molecule. For groups of molecules considered, this characteristic gives a satisfactory estimate of the relative value of the excitation energy of the electronic transition corresponding to the p band.

The interpretation of this fact may be such that the topology of the molecule is an important characteristic determining the basic qualitative features of spectral properties of the molecule, at least for the benzenoid hydrocarbons. The topological information transferred by the characteristic values into the semiempirical LCI method is sufficient for obtaining such results in the calculation of the p-band excitation energy which yields approximately the same sequence of excitation energies as the smallest positive eigenvalue of the topological matrix. The qualitative similarity of the p-band position predictions yielded by various versions

of semiempirical^{26,27} as well as more sophisticated "semitheoretical"²⁸ π -electron methods shows how this phenomenon is general (*cf.* the comparison of the methods mentioned in ref 18).

It is possible to formulate the conditions for occurrence of a bathochromic shift of the p band when the benzene ring is annelated. The qualitative character of the approximate formulation of these conditions (the position of the nodal points of the highest occupied orbital) also shows that the shift of the p-band position depends simply on the topological characteristic of the molecule, in this case on the eigenvector corresponding to the smallest positive eigenvalue of the parent molecule.

The general validity of equations for determining the characteristic values of the extended system based on the characteristic values and vectors of the system to be extended shows that similar rules to those found in this work are likely to appear also in other types of hydrocarbons and possibly in heteroanalogs.

Appendix

Let I and II be two mutually noninteracting π -electron systems, their molecular orbitals having the form

$$\psi_i^M = \sum_{\mu \in K_M} c_{i\mu}^M Z_\mu^M$$

where $M = \text{I or II}$. Z_μ^M is the $2p_z$ atomic orbital localized on the μ th atom of the system M , K_M is the set of indices of the atomic orbitals pertaining to the system M . ϵ_i^M is the orbital energy corresponding to the molecular orbital ψ_i^M where $i \in K_M$.

Let us consider the system which arises when systems I and II are connected by means of two bonds between the pairs of atomic orbitals $Z_1^{\text{I}}, Z_1^{\text{II}}$ and $Z_2^{\text{I}}, Z_2^{\text{II}}$. Let the value of the resonance integral of the newly arising bonds be β . The molecular orbitals of the system thus created can be found in the form

$$\psi_W = \sum_{M=\text{I,II}} \sum_{\mu \in K_M} d_\mu^M Z_\mu^M \quad (\text{A-1})$$

W is the orbital energy of the molecular orbital ψ_W . For the coefficients $d_1^{\text{I}}, d_2^{\text{I}}, d_1^{\text{II}}$, and d_2^{II} , the following system of equations holds.²⁹

(25) By "nodal points" we understand in the following the intersection of the nodal line of respective molecular orbital with the bond in the carbon skeleton considered.

(26) (a) R. Pariser, *J. Chem. Phys.*, **24**, 2501 (1956); (b) N. S. Ham and K. Ruedenberg, *ibid.*, **25**, 13 (1956).

(27) J. Koutecký, J. Paldus, and R. Zahradník, *ibid.*, **36**, 3129 (1962).

(28) R. L. Hummel and K. Ruedenberg, *J. Phys. Chem.*, **66**, 2334 (1962).

(29) J. Koutecký, *Advan. Chem. Phys.*, **9**, 85 (1965).

$$\begin{aligned}
 d_1^I &= \beta[L_{11}^I d_1^{II} + L_{12}^I d_2^{II}] \\
 d_2^I &= \beta[L_{21}^I d_1^{II} + L_{22}^I d_2^{II}] \\
 d_1^{II} &= \beta[L_{11}^{II} d_1^I + L_{12}^{II} d_2^I] \\
 d_2^{II} &= \beta[L_{21}^{II} d_1^I + L_{22}^{II} d_2^I]
 \end{aligned}
 \tag{A-2}$$

where

$$L_{\mu\nu}^M = L_{\nu\mu}^M = \sum_{i \in K_M} \frac{c_{i\mu}^M c_{i\nu}^M}{W - \epsilon_i^M} \tag{A-3}$$

The solvability conditions for the system of equations (A-2) may be expressed by the equation

$$\begin{aligned}
 &\beta^4[L_{11}^I L_{22}^I - (L_{12}^I)^2][(L_{11}^{II})^2 - (L_{12}^{II})^2] - \\
 &\beta^2[L_{11}^I + L_{22}^I]L_{11}^{II} - 2\beta^2 L_{12}^I L_{12}^{II} + 1 = 0
 \end{aligned}
 \tag{A-4}$$

The derivation of eq A-4 is based on the assumption $L_{11}^{II} = L_{22}^{II}$, which is fulfilled in the cases under consideration.

When discussing the solution of eq A-4 determining the eigenvalues of the final system, we shall restrict ourselves to those cases in which system I is a benzenoid hydrocarbon and system II is a molecule of ethylene or butadiene and which are joined together as shown schematically in Figure 6. From Figure 6 it may be seen that the atoms 1 and 2 of both systems belong to different classes from the point of view of alternation.

Using the properties of the coefficients and of the energy of molecular orbitals of alternant hydrocarbons, the following expressions are obtained with regard to (A-3).

$$\begin{aligned}
 &[L_{11}^I L_{22}^I - (L_{12}^I)^2] = \\
 &4 \sum_{i,j} \frac{W^2 c_{i1}^I c_{j2}^I - \epsilon_i \epsilon_j c_{i1}^I c_{j2}^I}{(W^2 - \epsilon_i^I)(W^2 - \epsilon_j^I)} \\
 &[L_{11}^I + L_{22}^I] = 2W \sum_i \frac{c_{i1}^I + c_{i2}^I}{W^2 - \epsilon_i^I} \\
 &L_{12}^I = 2 \sum_i \epsilon_i \frac{c_{i1} c_{i2}}{W^2 - \epsilon_i^2}
 \end{aligned}
 \tag{A-5}$$

where the summation extends over the occupied molecular orbitals only. On the right-hand sides of expressions A-5, the upper index has been omitted to simplify the notation. The following symbols have been introduced.

$$\begin{aligned}
 L_{11}^{II} &= P_{II}(W)/R_{II}(W) \\
 L_{12}^{II} &= Q_{II}(W)/R_{II}(W) \\
 (L_{11}^{II})^2 - (L_{12}^{II})^2 &= S_{II}(W)/R_{II}(W)
 \end{aligned}$$

For the ethylene molecule we obtain

$$\begin{aligned}
 P_{II}(W) &= W \\
 Q_{II}(W) &= S_{II}(W) = 1 \\
 R_{II}(W) &= W^2 - 1
 \end{aligned}
 \tag{A-6}$$

In a similar way we obtain for the butadiene molecule

$$\begin{aligned}
 P_{II}(W) &= W(2 - W^2) \\
 Q_{II}(W) &= -1 \\
 S_{II}(W) &= 1 - W^2 \\
 R_{II}(W) &= -(W^4 - 3W^2 + 1)
 \end{aligned}
 \tag{A-7}$$

Equation A-4 may be transformed using eq A-5 and the just defined symbols to the following form

$$\begin{aligned}
 &4\beta^4 W^2 S_{II}(W) \sum_{i,j} \frac{c_{i1}^I c_{j2}^I}{(W^2 - \epsilon_i^I)(W^2 - \epsilon_j^I)} - \\
 &2\beta^2 W P_{II}(W) \sum_i \frac{c_{i1}^I + c_{i2}^I}{W^2 - \epsilon_i^I} - \\
 &4\beta^2 \sum_i \epsilon_i \frac{c_{i1} c_{i2}}{W^2 - \epsilon_i^2} \left[Q_{II}(W) + \beta^2 S_{II}(W) \sum_j \frac{c_{j1} c_{j2}}{W^2 - \epsilon_j^2} \right] = -R_{II}(W)
 \end{aligned}
 \tag{A-8}$$

for $R_{II}(W) \neq 0$. $R_{II}(W)$ equals zero for the following values of argument W

$$W = \pm 1 \text{ (for ethylene)}$$

$$W = \pm 1.618; \pm 0.618 \text{ (for butadiene)}$$

Let $E(W)$ designate the left-hand side of the eq A-8. $E(W)$ and $R(W)$ being odd functions of W , it is sufficient to study the solution of the eq A-8 for positive W values only. Let us formulate the conditions for finding the roots of eq A-8 in the interval $(0, \epsilon_k)$, where ϵ_k is the smallest positive energy of the molecular orbitals of system I.

From eq A-6 and A-7 it follows that

$$E(0) = 4\beta^2 \sum_i \frac{c_{i1} c_{i2}}{\epsilon_i} \left[\pm 1 - \beta^2 \sum_j \frac{c_{j1} c_{j2}}{\epsilon_j} \right] \tag{A-9}$$

where the upper sign holds for ethylene and the lower one for butadiene. From the form of $E(0)$ the following inequality results

$$E(0) \leq 1 \tag{A-10}$$

so that $R_{II}(II)$ is a decreasing function for $W > 0$ and $R_{II}(0) = 1$. For $W \rightarrow \epsilon_i$ we get $|E(W)| \rightarrow \infty$. There-

fore, a sufficient condition for existence of the solution of the eq A-8 in the interval $(0, \epsilon_k)$ is

$$\lim_{W \rightarrow \epsilon_k} E(W) = +\infty \quad (\text{A-11})$$

$$(W < \epsilon_k)$$

Let us find the conditions which must be imposed on c_{i1} , c_{i2} , and ϵ_i in order to satisfy eq A-11. Let ϵ_k be a nondegenerated level. Then condition A-11 is fulfilled for joining the ethylene molecule to system I if the following relation holds.

$$\frac{2c_{k1}c_{k2} \left[1 - 2\beta^2 \left(\frac{c_{k1}c_{k2}}{2\epsilon_k} + \sum_{i \neq k} \frac{\epsilon_i c_{i1}c_{i2}}{\epsilon_i^2 - \epsilon_k^2} \right) \right]}{c_{k1}^2 \left[1 + 2\beta^2 \sum_{i \neq k} \frac{c_{i2}^2}{\epsilon_i^2 - \epsilon_k^2} \right] + c_{k2}^2 \left[1 + 2\beta^2 \sum_{i \neq k} \frac{c_{i1}^2}{\epsilon_i^2 - \epsilon_k^2} \right]} > -\epsilon_k \quad (\text{A-12})$$

In an analogous way we obtain the following condition for joining the butadiene molecule

$$\frac{2c_{k1}c_{k2} \left[1 + 2\beta^2(1 - \epsilon_k^2) \left(\frac{c_{k1}c_{k2}}{2\epsilon_k} + \sum_{i \neq k} \frac{\epsilon_i c_{i1}c_{i2}}{\epsilon_i^2 - \epsilon_k^2} \right) \right]}{c_{k1}^2 \left[(2 - \epsilon_k^2) + 2\beta^2(1 - \epsilon_k^2) \sum_{i \neq k} \frac{c_{i2}^2}{\epsilon_i^2 - \epsilon_k^2} \right] + c_{k2}^2 \left[(2 - \epsilon_k^2) + 2\beta^2(1 - \epsilon_k^2) \sum_{i \neq k} \frac{c_{i1}^2}{\epsilon_i^2 - \epsilon_k^2} \right]} < \epsilon_k \quad (\text{A-13})$$

Assuming that the coefficients at β^2 in eq A-12 and A-13 are small, so that we can neglect them, we obtain the following simplified condition for existence of solution of eq A-8 in the interval $(0, \epsilon_k)$

$$\frac{2c_{k1}c_{k2}}{c_{k1}^2 + c_{k2}^2} > -\epsilon_k \quad (\text{A-12}')$$

for joining the ethylene molecule, and similarly

$$\frac{2c_{k1}c_{k2}}{c_{k1}^2 + c_{k2}^2} < \epsilon_k(2 - \epsilon_k^2) \quad (\text{A-13}')$$

for joining the butadiene molecule. Perturbation theory to the third order gives conditions A-12' and A-13' as well. If ϵ_k is an n -fold degenerated level, i.e., $\epsilon_k^{(1)} = \epsilon_k^{(2)} = \dots = \epsilon_k^{(n)}$, then condition A-11 is fulfilled if the following inequality holds

$$\sum_{p,q} [(c_{k1}^{(p)})^2 (c_{k2}^{(q)})^2 - c_{k1}^{(p)} c_{k2}^{(p)} c_{k1}^{(q)} c_{k2}^{(q)}] > 0 \quad (\text{A-14})$$

where $p = 1, \dots, n$ and $q = 1, \dots, n$.

A Chemical Kinetics Computer Program for Homogeneous and Free-Radical Systems of Reactions

by Richard H. Snow

IIT Research Institute, Technology Center, Chicago, Illinois 60616 (Received January 11, 1966)

A computer program was developed to compute the product distribution in any homogeneous reaction mechanism. The program includes a numerical method to apply the steady-state assumption when a mechanism involves intermediates present in low concentrations. Under this condition standard computation methods fail, but the steady-state assumption is valid. During an induction period the program compares direct integration with the steady-state method, and when they agree it switches to the steady-state method. The program includes a regression procedure to fit rate constants to experimental product distributions. Sample calculations were done for the hydrogen-bromine reaction and for ethane pyrolysis. The results agreed with data from the literature.

I. Introduction

Few, if any, of the gaseous free-radical reactions, once thought simple, are believed to be simple today. The study of complex reactions has been hindered by the difficulty of calculating the product distribution from an assumed mechanism when the rate equations are too complex to be integrated analytically. Snow, Peck, and von Fredersdorff¹ demonstrated a numerical method of solution for one such reaction, a free-radical chain mechanism for the pyrolysis of ethane. With this method they were able to include the reverse reactions of the chain-propagating steps and to obtain quantitative agreement with published data.

It should be possible to calculate numerically the behavior of any reaction system, yet so far as we know such calculations have been reported only for oxidation of hydrogen² in addition to ethane pyrolysis.¹ Since computers are available, the numerical approach should not be neglected, but the need to write a new computer program for each problem has prevented wider adoption of this method. This paper describes a method and a computer program which will compute the product distribution from any given set of elementary reactions without special programming.

The analysis of reaction mechanisms and the determination of rate constants are two problems that cannot be separated. In his monograph, Steacie³ showed how a catalog of rate constants for elementary

reactions can be built up from experiments on a variety of reacting systems. The experiments must either be designed to isolate the effect of a few important reactions in the mechanism, or else the rate constants of all but a few of the reactions must be known. The basic problem is one of regression, to fit values to rate constants in a mechanism such that the calculated and experimentally measured product distributions agree. The results may be expressed in other ways, for example, as ratios of concentrations or as a pressure effect, but these are aspects of the same problem. This paper also presents a general statistical procedure to aid in determining rate constants from complex mechanisms.

II. The Mathematics of Calculation of Product Distributions

The problem can be stated as follows. Given a set of elementary reactions, their rate constants, and a set of initial concentrations, calculate a distribution of products over a period of time.

The problem is to integrate the set of simultaneous

(1) R. H. Snow, R. E. Peck, and C. G. von Fredersdorff, *Am. Inst. Chem. Eng. J.*, **5**, 304 (1959).

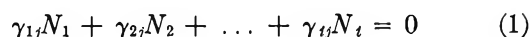
(2) G. B. Skinner, A. D. Snyder, and G. H. Ringrose, "A Research Program for Understanding the Mechanisms of Flame Inhibition," Report APL-TDR-64-40, Contract AF 33(657)-10, Monsanto Research Corp. for Wright-Patterson Air Force Base, Jan 1964.

(3) E. W. R. Steacie, "Atomic and Free Radical Reactions," Vol. I and II, 2nd ed, Reinhold Publishing Corp., New York, N. Y., 1954.

rate equations. As described below, these equations are in a form suitable for application of standard methods, such as Runge-Kutta. However, for free-radical chain mechanisms these methods have been found to fail.⁴ The numerical difficulty is such that it can be avoided by applying the steady-state assumption. The conditions under which this assumption is valid are investigated below and found to be the same conditions for which standard numerical integration methods fail. The method would still not be useful if the steady-state equations had to be programmed for each reaction system studied. The computer program does this by a general Newton numerical procedure, and the user does not have to provide any special programming.

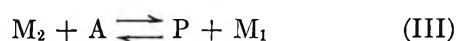
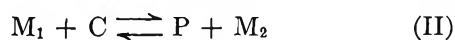
The program is designed for calculation at constant temperature, but it could be generalized to handle the changing temperatures of an adiabatic reactor or a flame.

A. Description of the Computation Procedure. The user of the program specifies a set of reactions by giving a matrix of stoichiometric coefficients of the reactions. A series of chemical reactions can be represented by



where N_i is the name of the i th compound and γ_{ij} is the stoichiometric coefficient of the i th compound in the j th reaction. This coefficient is positive if the compound is a product, negative if the compound is a reactant, and zero if the compound is not involved in the reaction.

For example, for the reactions



where M_1 and M_2 are free-radical intermediates, the stoichiometric matrix is

	A	C	M_1	M_2	P
Reaction I	-1	0	2	0	0
Reaction II	0	-1	-1	1	1
Reaction III	-1	0	1	-1	1

The program deduces the rate laws from the reactions, assuming that they are true elementary reactions of the mechanism. According to the theory of chemical kinetics, the rate of the j th reaction is

$$\text{rate}_j = k_j \prod_i C_i^{|\gamma_{ij}|} + k_j' \prod_i C_i^{|\gamma_{ij}|} \quad (2)$$

where k_j is the forward rate constant for the j th re-

action, k_j' is the reverse rate constant for the j th reaction, C_i is the concentration of the i th component, \prod_i represents the product of compounds for which γ_{ij} is negative, \prod_i^+ represents the product of compounds for which γ_{ij} is positive.

The rate of production of a compound is the sum of its rates of production in each reaction

$$\frac{dC_i}{dt} = \sum_j \gamma_{ij} \text{rate}_j \quad (3)$$

B. Validity of the Steady-State Assumption. The steady-state assumption gives an equation for each radical to which it is applied. If this set of equations can be solved, the radical concentrations are obtained. Then the standard methods of integration can be applied to determine the concentrations of the other substances present. In the following, a method of applying this standard technique to numerical calculation is shown, but first the conditions under which the assumption is valid must be reviewed.

Confusion exists because the steady-state assumption is misnamed, even though it is correctly stated in most texts on kinetics. *The consumption of materials for formation of free radicals is negligible compared with that for formation of molecular products.* For example, the net rate of production of radical M_2 in the above mechanism is

$$\frac{d(M_2)}{dt} = k_2(M_1)(C) - k_3(M_2)(A) = \epsilon \quad (3')$$

The assumption does not mean that $d(M_2)/dt$ is zero, but only that it is small compared to each term on the right side of eq 3'. In general, this is true after some initial period if M_2 remains much smaller than the concentrations of each of the molecular species. Then only a relatively small amount of material can be produced or consumed to change the concentration of M_2 . There is no *a priori* way to prove that M_2 will remain small. Therefore, the steady-state hypothesis can be checked *a posteriori* but in general cannot be proved beforehand.

Equation 3' can be solved for (M_2)

$$(M_2) = \frac{k_2(M_1)(C)}{k_3(A)} - \frac{\epsilon}{k_3(A)} \quad (4)$$

If ϵ is small compared to the terms in eq 3', then the term involving ϵ can also be neglected in eq 4, and the result is the desired expression for (M_2) .

(4) IIT Research Institute, "Analytical Investigation of Combustion Instability in Solid Propellant Rockets," Contract No. AF 49(638)-1094, Final Report, July 1963.

Rice⁵ showed that for a number of important types of reaction mechanisms the assumption is valid when the above condition is met. A general proof of the conditions under which the steady-state hypothesis is valid has never been given. Such a proof is difficult because the mathematical relations depend on the mechanism of the reaction system. To make the demonstration general, mechanisms must be considered which contain several radicals. Then several expressions of the form of eq 3' will exist, and their simultaneous solutions may not be possible in an explicit way. A numerical solution is still possible, and in the process of solution the terms involving ϵ are negligibly small.

Therefore, the hypothesis is valid when the results of the rate integrations show that the radical concentrations remain small compared with molecular quantities. During some induction period ϵ in eq 3' may not be small. For this reason the computer program uses standard integration to explore the induction period and switches to the steady-state method only after it gives acceptable agreement with the direct integration method.

C. Numerical Calculation of Radical Concentrations. According to the steady-state assumption, the right side of eq 3 is set equal to zero for each radical, and the equations are solved for the radical concentrations. In general, this cannot be done explicitly, so Newton's method is used.

Newton's method for solving two simultaneous equations implicit in two variables by iteration is described by Willers.^{6a} The method can be generalized to n variables.

The Newton procedure makes use of derivatives of the rate of production of each material with respect to changes in the concentration of each other material. For a specific mechanism expressions for these derivatives could be written down, but for a general numerical procedure they are determined by recalculating each rate from eq 3 for an arbitrary incremental change in each concentration. Another possible approach would be to let the program derive such expressions from the stoichiometric matrix.

The Newton determination of radical concentrations must be carried out at each step in the integration. In addition to the radical concentrations, eq 3 involves the molecular concentrations. These remain constant during the Newton iteration at each point in time. After values for the radical concentrations have been obtained, eq 3 can be evaluated to give the rate of formation of each compound.

Newton's method did not converge unless it was given starting values near the steady-state radical

concentrations. This difficulty was overcome by adding a weighting factor to the Newton correction. A weighting formula was obtained by generalizing a formula given by Forsythe^{6b} to speed convergence when finding roots of a particular function. That generalized formula is

$$W = 1 - \frac{\Delta x}{|\Delta x| + x} \quad (5)$$

where Δx is the correction computed from Newton's formula. Note that when $0 < x <$ positive root, the weighting function times the computed correction is always less than x , and the procedure cannot diverge. If $x >$ positive root, the weighting function is >1 and the process becomes more unstable although it still converges rapidly when the starting value is close to the root. Fortunately, the induction period calculation always gives starting values for the radicals that are smaller than the steady-state values; therefore, the formula works.

Both the Runge-Kutta and Milne⁷ four-point predictor-corrector integration methods were tried. The rate of calculation with both methods is limited by a tendency toward instability, and the calculation was too slow. A marked improvement in calculation rate was obtained by taking advantage of the tendency of the concentrations to become steady. For the radicals, the predictor equation was replaced by a modified Newton interpolation formula containing the mean of the last two computed derivatives. This technique speeded the calculations about 100-fold, while the predicted and calculated radical concentrations agreed to one part per thousand.

Difficulties were traced also to the use of Milne's three-point formula for interpolating concentrations and derivatives when the interval is halved. This formula was replaced by a Newton backward-difference formula based on the first difference and the mean of the two previous second differences

$$C_0 = [C_1 + C_2 + 1.5\Delta t(\dot{C}_1 + \dot{C}_2)]/2 \quad (6)$$

where C is the concentration, \dot{C} is the time derivative of concentration, t is the time increment, subscript 0 refers to the present time, subscript 1 refers to a preceding instant of time, and subscript 2 refers to an instant of time preceding subscript 1. Formula 6

(5) O. K. Rice, *J. Phys. Chem.*, **64**, 1851 (1960).

(6) (a) F. A. Willers, "Practical Analysis," Dover Publications, New York, N. Y., 1948, pp 223-225; (b) G. E. Forsythe, *Am. Math. Monthly*, **65**, 229 (1958).

(7) W. E. Milne, "Numerical Solution of Differential Equations," John Wiley and Sons, Inc., New York, N. Y., 1953.

strongly damps out oscillations but still follows any persistent trend in the values.

Every 500 Milne steps a Newton steady-state calculation is tried for the last radical in the list of components. If the concentration of this radical agrees within a given factor with the value from the Milne integration, this radical is assumed to have reached a steady state. If more than one radical is present, the test is applied to each until one that is not steady is found. Then the Milne procedure is continued by using the steady method for these steady radicals. At each 500th step the test is repeated to determine whether other radicals have become steady, until all are steady.

D. Regression of Rate Constants. The program can be used to fit values of rate constants to experimental product distributions. If too many of the constants have to be determined by fitting product distributions, there may be too many unknowns for the number of quantitative restrictions imposed by the data. Therefore, the program is of greatest use when all but a few rate constants are already known. The program includes a regression procedure to fit values for rate constants. A general procedure is derived as follows.

Suppose that a product distribution is computed from assumed rate constants, k_n , and that the results are compared with the experimental points in Figure 2. The problem is to find a set of values for the uncertain rate constants such that the calculated product distribution best fits the experimental points.

Let Δ_i represent the deviation of a product from an experimental point i . These points can be numbered in any arbitrary way, and involve all the important products and reactants. In order to calculate the best fitting values of each k_n , it is necessary to determine the change in product distribution that will result from a change in k_n , $\partial\Delta_i/\partial k_n$. This product distribution change can be determined exactly only by repeating the whole product distribution calculation with a changed value of k_n . This repetition must be done for each rate constant to be fitted, but it would be too costly in computer time.

The computer program does calculate the *rate* of production for each product at successive time intervals. Calculation of the change in these rates resulting from a change in each of the rate constants is a simple matter. The change in product distribution then can be estimated by assuming that the deviation is linear. The production of a product, therefore, is that given by the product distribution calculation plus a difference. This is equal to the mean change in production rate at two instants of time, multiplied by the elapsed time, plus the accumulated difference at the first of these

instants of time. The resulting new product distribution curves will give new deviations, Δ_i' , from the available experimental points.

If only one k_n at a time is changed, partial derivatives can be computed from

$$\frac{\partial\Delta_i}{\partial k_n} = \frac{\Delta_i' - \Delta_i}{\Delta k_n} \quad (7)$$

The other rate constants are changed, one by one, to compute the other derivatives.

If n rate constants are changed at once, the deviations are

$$\Delta_i' = \Delta_i + \sum_n \frac{\partial\Delta_i}{\partial k_n} \Delta k_n \quad (8)$$

We wish to determine changes Δk in the rate constants to minimize the sum of the squares of the deviations, Δ_i' . The sum of the deviations is

$$\text{sum} = \sum_i (\Delta_i')^2 = \sum_i \left[\Delta_i + \sum_n \frac{\partial\Delta_i}{\partial k_n} \Delta k_n \right]^2 \quad (9)$$

To find the minimum, we differentiate with respect to each Δk and set the derivatives equal to zero.

$$\frac{\partial(\text{sum})}{\partial \Delta k_e} = \sum_i \left[\left(\Delta_i - \sum_n \frac{\partial\Delta_i}{\partial k_n} \Delta k_n \right) \frac{\partial\Delta_i}{\partial k_e} \right] = 0 \quad (10)$$

$$\sum_i \left[\frac{\partial\Delta_i}{\partial k_e} \Delta_i + \frac{\partial\Delta_i}{\partial k_e} \sum_n \frac{\partial\Delta_i}{\partial k_n} \Delta k_n \right] = 0 \quad (11)$$

Here is a system of equations, one for each Δk , designated by subscript e . Each equation involves all of the other Δk 's, designated by subscript n . This system can be solved by matrix methods to determine the correction, Δk_e , to apply to the rate constants. A new calculation for the product distribution can then be carried out with the corrected rate constants to check the fit with experimental data.

E. Sample Calculations. A trial calculation was made on the simplest type of free-radical reaction mechanism: reactions I, II, and III. This mechanism was discussed by Benson,⁸ who derived equations giving the products and free radical concentrations. These results can be compared with the results computed numerically by the program.

The following rate constants were assumed for a temperature of 1000°K.

Reaction	Rate constants	
	Forward	Reverse
I	1.6×10^{-2}	7×10^{-3}
II	6.52×10^9	0
III	6.52×10^9	0

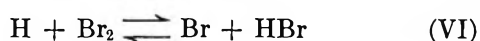
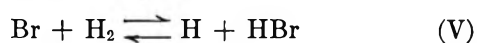
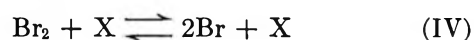
(8) S. W. Benson, "The Foundations of Chemical Kinetics," McGraw-Hill Book Co., Inc., New York, N. Y., 1960, pp 50-54.

Initially, the concentrations of A and C were chosen to be 10^{-5} mole/cc, and P was 0. Benson's equations then show that M_1 and M_2 are 4.8×10^{-11} mole/cc after a steady state is reached. The radical concentrations reached $1/4$ of these steady values when conversion was only 0.01% complete. This occurrence means that the induction period was unimportant. The calculation was carried to 90% conversion. The computed concentrations agreed to 0.2% with results computed from analytic expressions given by Benson after an error of a factor of 2 in Benson's formula was corrected. The precision of the calculation depends on accuracy requirements which may be specified by the user.

III. The Hydrogen-Bromine Reaction

There is one reaction system in which application of the steady-state assumption has been criticized: the hydrogen-bromine reaction. Some writers⁹ have inferred from this reaction that the entire steady-state principle is suspect. For this reason this reaction was chosen to test the validity of the computer method.

The hydrogen-bromine reaction has the same mechanism as that of hypothetical reactions I through III above, except that the rate constant for one of the chain-propagating steps is much smaller than the other, and the rate of the initiating reaction is influenced by any third body, X.



Several other reactions can also participate,¹⁰ but Benson's discussion⁸ shows that they can be omitted under most conditions.

Provision was made in the program to define a third body according to weighted contributions from each of the molecular components present. This provision would make it possible to assign a greater effectiveness, for example, to another bromine molecule than to hydrogen or nitrogen.

Because reaction V is much slower than reaction VI, the concentration of atomic bromine reaches the same magnitude as the concentration of the molecular species. The condition for the validity of the steady-state assumption is then violated. For the hydrogen-bromine system, the bromine atom should be treated mathematically on the same basis as the molecular species. Since the bromine atom concentration is large, its calculation in this way will not force the numerical procedure to use impractically small time increments. The steady-state assumption can still

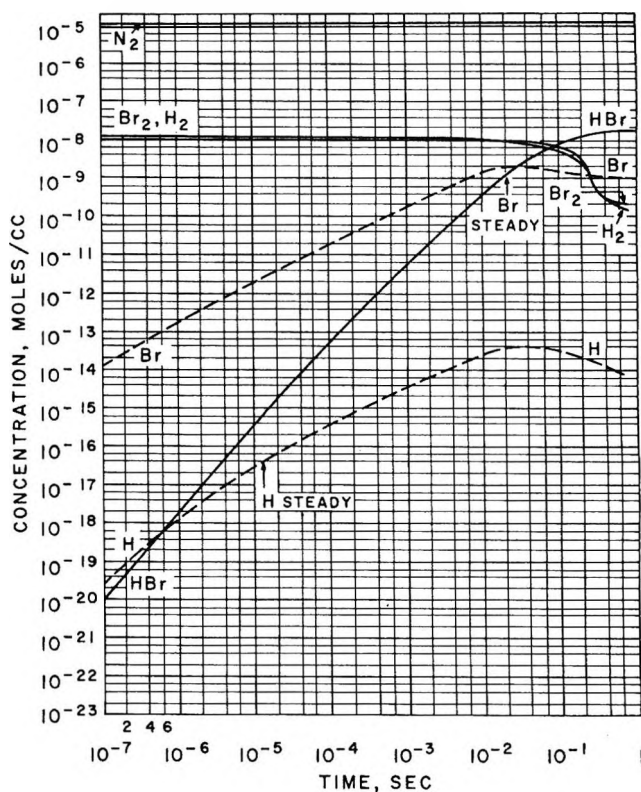


Figure 1. Product distribution calculated for hydrogen-bromine reaction.

be applied to the other radical, atomic hydrogen. These ideas were tested by calculation.

Results of the calculation are compared with Levy's¹¹ flow reaction data at 1003°K in Figure 1. The rate constants in Table I were used. They were taken from Campbell and Fristrom,¹⁰ who reviewed the available data on this subject, except that reduction of the rate constant for reaction V was necessary in order to fit the data. This is valid since Campbell and Fris-

Table I: Rate Constants Used in Hydrogen-Bromine Calculation

Reaction	Rate constants	
	Forward	Reverse
IV	6.26×10^6	1.56×10^{15}
V	2.61×10^9	1.39×10^{13}
VI	1.17×10^{14}	3.31×10^4

(9) E. S. Campbell, "Theoretical Study of the Hydrogen-Bromine Flame," 6th Combustion Symposium, Reinhold Publishing Corp., New York, N. Y., 1957, pp 213-222.

(10) E. S. Campbell and R. M. Fristrom, *Chem. Rev.*, **58**, 173 (1958).

(11) A. Levy, *J. Phys. Chem.*, **62**, 570 (1958).

trom's value was based on a fit of hydrogen-bromine data, but Levy's data were not available to them.

The results in Figure 1 show that the hydrogen atom concentration reaches a steady state very quickly, but the bromine atom concentration does not. In fact, the bromine atom concentration exceeds that of the product, hydrogen bromide, until 1% conversion, when it levels off.

After 3% conversion the program switched to the steady method for bromine atom concentration. At this point the two methods of calculation of radical concentration agreed within 7%. (The user can demand arbitrarily close agreement before the program switches methods.) The complete calculation took 2 min of computer time. The calculation also was done without using the steady-state method for the bromine atom; it took 3 min of computer time. The difference would be larger for other mechanisms.

IV. Ethane Pyrolysis

A calculation was done for the system of reactions previously investigated by Snow, Peck, and von Fredersdorff.¹ These earlier calculations employed the steady-state assumption for the three radicals involved, but the program was specifically written for that system. For the present comparison the conditions of the experiment at 1089°K were chosen. This corresponds to a flow reactor at constant temperature.

The mechanism of Snow, *et al.*, includes two reactions with an empirical set of products having fractional stoichiometric coefficients. The program was modified to include this type of reaction, provided that the corresponding reverse rate constant is zero. Furthermore, the flow reactor is a constant-pressure rather than a constant-volume device, so provision was made in the program to specify constant pressure and to calculate the expansion of products. This situation arises when some reactions produce more moles of products than they consume. The program accomplishes this by normalizing the sum of concentrations at every time step.

With these changes the calculated results agreed with those previously computed by Snow, *et al.*¹ However, the rate constants in Snow's mechanism were based on assumed values of 7×10^{13} for all radical recombination reactions. Recently, Heller¹² and others have measured the rates of these reactions more exactly; their values are given in Table II. Since the rate of the first reaction of the mechanism is known only relative to the rates of the recombination reactions, the former rate had to be decreased proportionately. When these changes were made, the results in Figure

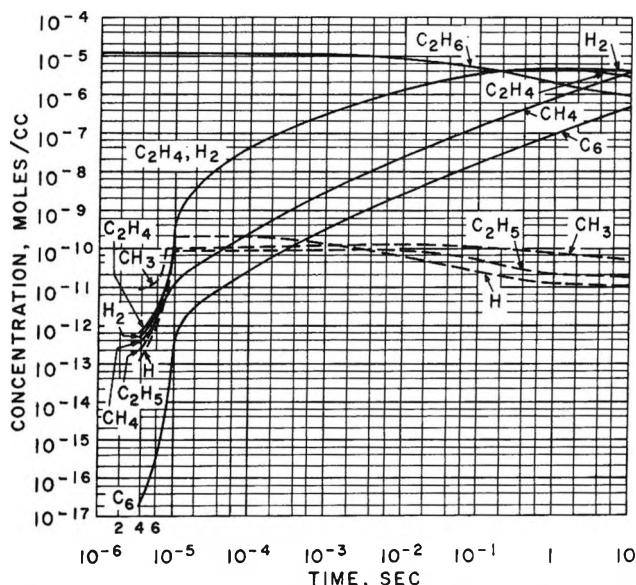


Figure 2. Product distribution calculated for ethane pyrolysis.

Table II: Ethane Pyrolysis Rate Constants as Functions of Temperature, $k_1 = A_1 e^{-E_1/RT}$

Reaction	Rate constants used in calculations	
	Frequency factor, A_1	Activation energy, E_1
$C_2H_6 \rightleftharpoons 2CH_3$	2.0×10^{16}	86,000
	2.2×10^{13}	0
$CH_3 + C_2H_6 \rightleftharpoons CH_4 + C_2H_5$	2.5×10^{11}	10,800
	1.0×10^{11}	13,200
$CH_3 + H_2 \rightleftharpoons CH_4 + H$	1.9×10^{11}	9,500
	1.1×10^9	4,700
$C_2H_5 \rightleftharpoons C_2H_4 + H$	5.3×10^{14}	40,800
	5.4×10^{13}	5,400
$H + C_2H_6 \rightleftharpoons H_2 + C_2H_5$	3.8×10^{12}	7,000
	1.8×10^{12}	11,400
$H + C_2H_5 \rightarrow C_2H_6$	2.0×10^{13}	0
$CH_3 + C_2H_5 \rightarrow C_3H_8$	4.2×10^{13}	0
$2C_2H_5 \rightarrow C_4H_{10}$	2.0×10^{13}	0
$\rightarrow C_2H_4 + C_2H_6$		

2 were obtained. The computation required 6 min of computer time. The product distribution agrees with the one previously calculated and with the experimental data, but the radical concentrations and the relative rates of the recombination reactions are slightly different.

V. Use of the Program

The program in Algol was compiled with the University of Illinois Alcor compiler on the IIT Research

(12) C. A. Heller, *J. Chem. Phys.*, **28**, 1255 (1958).

Institute IBM 7094 computer. A listing of the program and further description are available from the author.

Acknowledgments. The author thanks Jeffrey Lev-

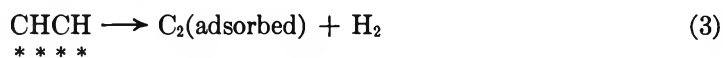
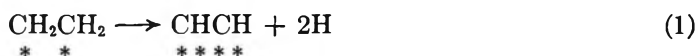
inger for programming assistance and Thomas Church for helpful discussions concerning mathematical techniques. This work was supported by IIT Research Institute.

The Flash Decomposition of Ethylene and Acetylene on Iridium¹

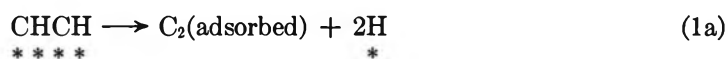
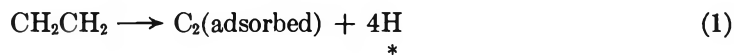
by Robert S. Hansen, John R. Arthur, Jr., V. J. Mimeault, and R. R. Rye

*Institute for Atomic Research and Department of Chemistry, Iowa State University, Ames, Iowa
(Received January 18, 1966)*

The decomposition of ethylene and acetylene adsorbed on iridium at 100 and 300°K was investigated by flash filament desorption spectrometry, with products identified by mass spectrometry. The observed product sequences and dosing temperature dependence could be represented by two distinct reaction sequences occurring on two distinct crystal faces or face classes. The sequences are: on face A



on face B



The hydrogen is equilibrated between faces A and B, but the hydrocarbons are not. The face A sequence is that implied by an earlier field emission microscopy investigation.² The principal desorption product in all cases was hydrogen. Low-temperature bursts of ethylene and acetylene were observed on flashing filaments dosed with these materials at 100°K and are attributed to desorption of physically adsorbed species. Small quantities of methane and ethylene were produced over the temperature range 350–600°K on flashing ethylene-dosed filaments. No ethane production was observed. This is in marked contrast to the findings of Roberts,³ who observed principally ethane production when iridium films were exposed to ethylene at 300°K but at pressures approximately 10⁵ times greater. The hydrogenation of ethylene in Roberts' experiments is ascribed to direct transfer of hydrogen from chemisorbed acetylene or ethylene to ethylene impacting from the gas phase.

Introduction

A field emission electron microscopy study of the adsorption of hydrogen, ethane, ethylene, and acetylene on iridium, previously reported,² indicated that ethylene and acetylene chemisorbed on iridium undergo a sequence of dehydrogenation reactions on increasing the sample temperature. The present work was undertaken to provide additional information concerning these surface reactions.

Opportunities furnished by flash filament desorption techniques have been well summarized by Ehrlich.^{4,5}

(1) Work was performed in the Ames Laboratory of the Atomic Energy Commission. Contribution No. 1851. Based in part on dissertations submitted by J. R. Arthur, Jr. (1961) and V. J. Mimeault (1965) to the Graduate College of Iowa State University in partial fulfillment of the requirements for the degree of Doctor of Philosophy.

(2) J. R. Arthur, Jr., and R. S. Hansen, *J. Chem. Phys.*, **36**, 2062 (1962).

These include the opportunity to establish the formation of gaseous desorption products and the amounts of such products formed, to relate these amounts to metal surface area, and further to study the kinetics of their formation. In the present case, a small bakeable mass spectrometer was used to identify the desorption products.

Experimental Section

The reaction cell was of conventional design (Figure 1), *i.e.*, a 250-ml flask with four outlets, the omegatron, ion gauge, gas supply, and diffusion pump. The cell and vacuum gauges could be isolated from pumps and gas source by a ground-glass valve and a variable leak, respectively. Two ion gauges were used in this work. One was a conventional Bayard-Alpert (BA) gauge⁶ with a tungsten filament; the other was a BA gauge with a lanthanum boride coated tungsten filament.⁷ The partial pressure analyzer was a Leybold omegatron^{8,9} mass spectrometer tube. The ion gauge and the omegatron were connected to the reaction cell through 25-mm tubulation. The ion current from the BA ion gauge was amplified and recorded on a Model 3S Moseley *x-y* recorder, and the ion current from the omegatron was measured with a vibrating-reed electrometer and recorded. The response time of the omegatron-electrometer system is too long to be suitable for kinetic studies with the flash filament technique, although it is quite suitable for the identification of desorption products of mass less than 30 amu. When iridium was dosed with acetylene or ethylene at 100°K and flashed, the rate of desorption of physically adsorbed gas was so great that the omegatron and associated circuitry could not respond sufficiently rapidly to follow it; these experiments were repeated in a similar apparatus in which the omegatron was replaced by a General Electric Model 514 partial pressure analyzer mass spectrometer. The gauge constants for both gauges, 5 mm⁻¹ for the tungsten filament gauge and 3.6 mm⁻¹ for the lanthanum boride coated filament, are in good agreement with Hickmott's⁷ value of 4.4 mm⁻¹. The top part of the reaction cell was a reentrant-type dewar which could be filled with the proper coolant to maintain the filament at a given temperature during adsorption. Liquids used for this purpose were liquid nitrogen (~100°K) and water (300°K).

The temperature of the filament was determined by using the filament as a resistance thermometer. The temperature dependence of resistance of the sample filament was determined by measuring the resistance of the filament when it was immersed in various constant-temperature baths covering the temperature range 77 to 640°K. In a desorption experiment, the filament

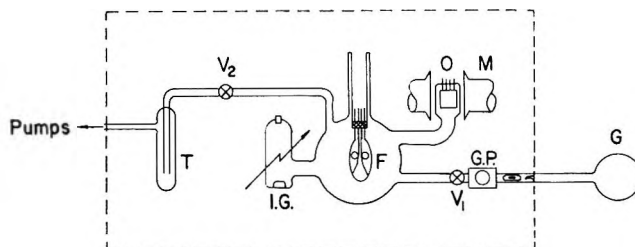


Figure 1. Flash filament desorption spectrometer. Dotted line surrounds bakeable portion. V_1 and V_2 , magnetically controlled ball joint valves; F, 5-mil iridium filament; T, liquid nitrogen trap; I.G., Bayard-Alpert ion gauge; M, magnet, 3250 gauss; O, omegatron; G, gas supply; G.P., Granville-Phillips valve.

was heated by a constant current, and the voltage drop across the filament, for a given current, was a direct measure of the resistance and, hence, the temperature of the filament.

The hydrogen used was Reagent Research grade obtained from the Matheson Co. in 1-l. flasks with break-off tips. Ethylene (Matheson chemically pure, reported by the manufacturer to be 99.8% pure) and acetylene (Matheson) were passed through a Dry Ice-acetone trap, then further purified by repeated freezings and evacuations at 77°K. Gases were then sealed in ampoules equipped with break-off tips, and the ampoules were sealed onto the vacuum system.

When the filament had been annealed and the pressure in the cell had been reduced to 10^{-10} mm, the break-off tip was broken and the gas was admitted to the system through a Granville-Phillips valve until the pressure was about 10^{-8} mm. The filament was again flashed to 2200°K and then held either at 77 or at 300°K for varying periods of time (results presented are for 8-min dose times unless otherwise specified).

Following the adsorption interval, the reaction cell (including the BA ion gauge and the omegatron) was isolated from the pumps by closing the magnetically operated ground-glass valve, the filament was then flashed at the desired heating rate, and the change in the ion current (pressure) was recorded as a function of time. (Constant current flashing resulted in a temperature-time dependence approximately of the form

(3) (a) R. W. Roberts, *J. Phys. Chem.*, **67**, 2035 (1963); (b) *ibid.*, **68**, 2718 (1964).

(4) G. Ehrlich, *J. Appl. Phys.*, **32**, 4 (1961).

(5) G. Ehrlich, *Advan. Catalysis*, **14**, 255 (1963).

(6) R. T. Bayard and D. Alpert, *Rev. Sci. Instr.*, **21**, 571 (1950).

(7) T. W. Hickmott, *J. Chem. Phys.*, **32**, 810 (1960).

(8) H. Sommer, H. A. Thomas, and J. A. Hipple, *Phys. Rev.*, **82**, 697 (1957).

(9) D. Alpert and R. S. Buritz, *J. Appl. Phys.*, **25**, 202 (1954).

$1/T = a + bt$. For a given flash, therefore, dT/dt is not constant. Relatively slow flash rates were used in systems giving multiple peaks to improve their resolution.)

It was found that hydrogen was rapidly pumped during a flash desorption experiment when the pressure increase was monitored with the tungsten filament ion gauge. Separate experiments showed that this pumping rate could not occur through the ground-glass valve. Hydrogen pumping was, therefore, attributed to the hot tungsten filament in the ion gauge; this behavior is to be expected according to the observations of Hickmott.^{7,10}

Mass spectra were obtained with the conventional BA ion gauge operated at 0.4-ma emission current and with this ion gauge off. No appreciable difference was found in the cracking patterns indicating that there is no change in the gas phase composition. Very likely, some cracking occurred on the hot filaments, with the hydrogen produced being rapidly pumped by the filament.

The tungsten filaments in the ion gauge were operated at 2500° for 24 hr in an ambient of 10^{-6} mm of oxygen to remove the carbon in the ion gauge filaments. This treatment was necessary to reduce the formation of CO formed by a complex sequence of reactions¹¹ involving carbon dissolved in the tungsten filament, hydrogen, and oxygen from the glass in the cell walls.

The desorption spectra of hydrogen were analyzed by the method described by Ehrlich,⁴ and the heats of desorption for the various species in the desorption spectra of ethylene and acetylene were obtained by using Redhead's¹² treatment.

Results

When hydrogen dosed on iridium at 100°K was flash desorbed with fast pumping for maximum resolution, two desorption peaks were observed (low-temperature α and high-temperature β) as shown in Figure 2. This indicates that hydrogen adsorbed on iridium at 100°K exists in at least two states. Only a single peak, presumably corresponding to the β state, is observed in the flash desorption spectrum from a filament dosed at 300°K. Detailed kinetic and exchange experiments to be reported elsewhere indicate that hydrogen is adsorbed atomically in both states and that the activation energy for desorption from the β state varies from 24 to 18 kcal mole as coverage varies from 40×10^{12} to 230×10^{12} molecules/cm².

Typical flash desorption curves for iridium dosed with ethylene for 8 min at 5×10^{-8} mm are shown in Figures 3 and 4. Figure 3 shows that a desorption process occurs from iridium dosed with ethylene at

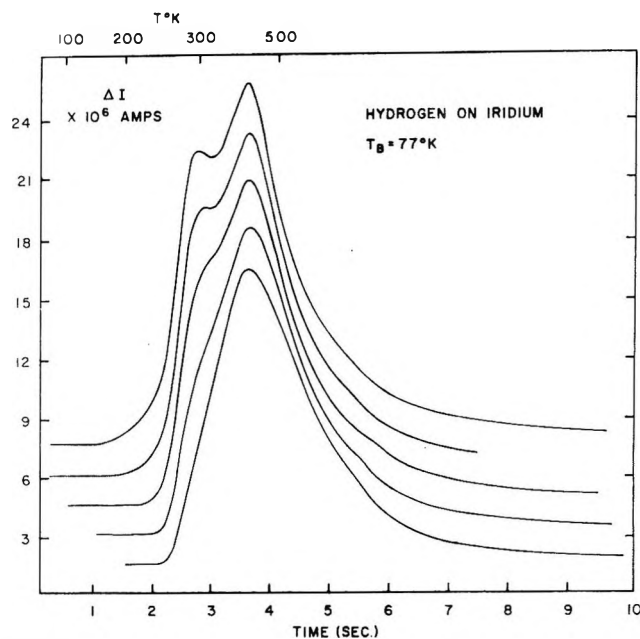


Figure 2. Flash desorption of hydrogen dosed on iridium at 77°K at 5×10^{-8} torr for various dosing times. Curves are translated vertically to avoid overlap. Dosing times, increasing from bottom curve to top curve, are 2, 3, 4, 5, and 6 min.

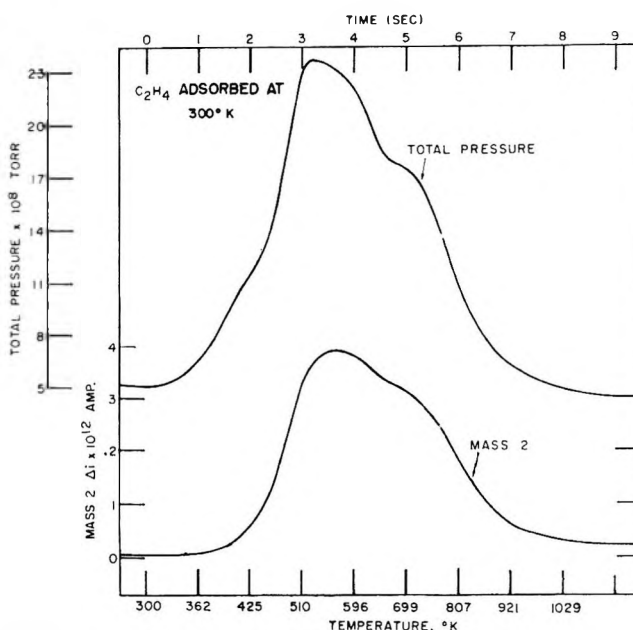


Figure 3. Flash decomposition of C_2H_4 dosed on iridium at 300°K. Total pressure and mass 2 bursts.

(10) T. W. Hickmott, *J. Appl. Phys.*, **31**, 128 (1960).

(11) J. A. Becker, E. J. Becker, and R. G. Brandes, *ibid.*, **32**, 411 (1961).

(12) P. A. Redhead, *Vacuum*, **12**, 203 (1962).

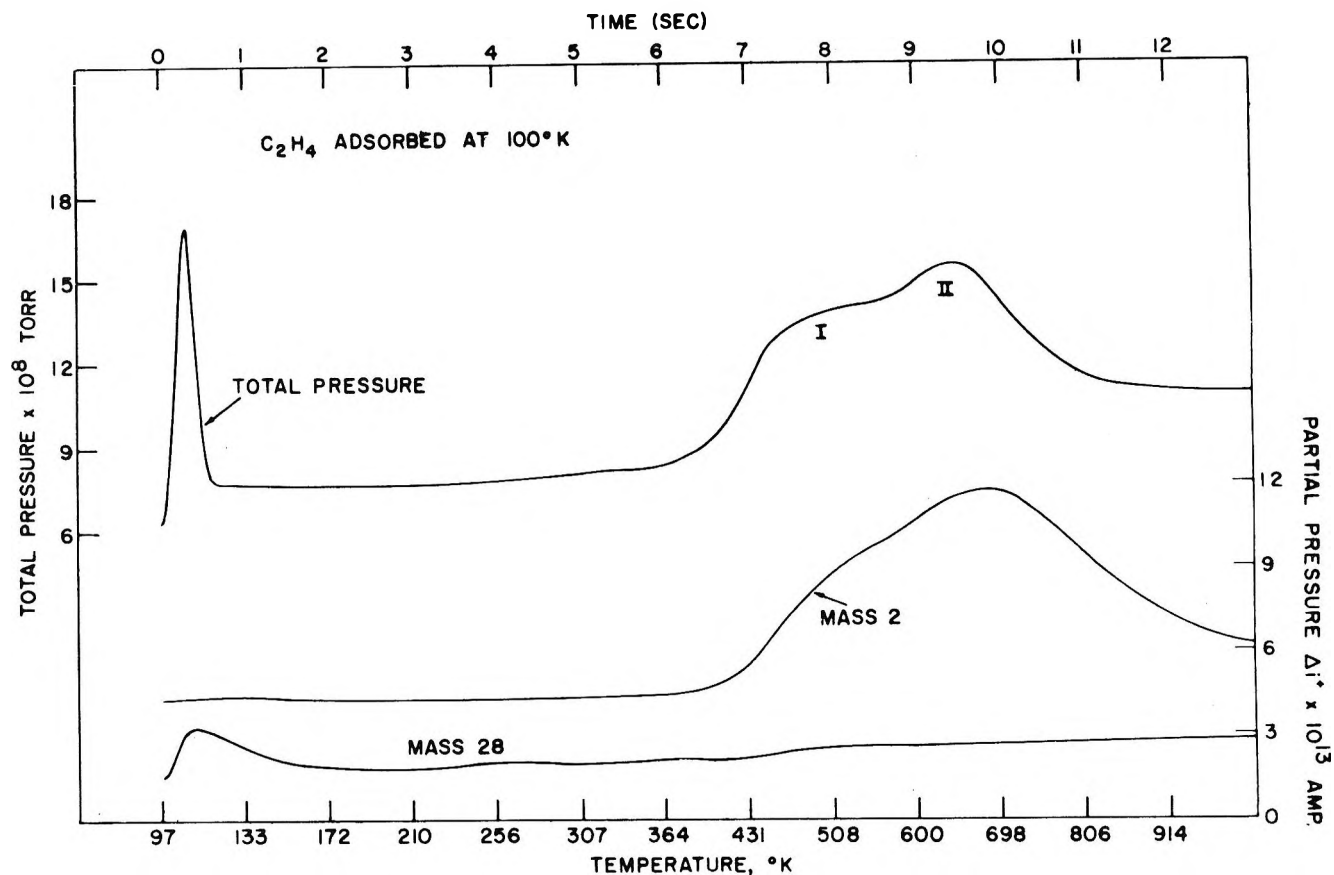


Figure 4. Flash decomposition of C₂H₄ dosed on iridium at 100°K. Total pressure and mass 2 and mass 28 bursts.

300°K and that the desorption range 360–800°K is approximately the range over which a marked increase in work function, attributed to acetylene dehydrogenation, was observed in a separate field emission study.² However, the process cannot be simply hydrogen desorption since in the partial pressure desorption spectrum of hydrogen from iridium, dosed with ethylene at 300°K, two peaks are clearly evident while only a single peak occurs when iridium is dosed with hydrogen at 300°K, and this corresponds to the first peak in the hydrogen desorption spectrum from iridium dosed with ethylene. The two peaks can most simply be attributed to successive dehydrogenations of ethylene, first to acetylene and finally to carbon.

Hydrogen is by far the major flash desorption product from iridium dosed with ethylene at 300°K, but minor products are also observed. These products, with desorption range and peak magnitudes expressed as per cent of maximum hydrogen peak, are ethylene (360–520°K, 3%) and methane (400–600°K, 8%).

The flash desorption spectrum from iridium dosed with ethylene at 100°K is shown in Figure 4. It

differs from that for 300°K dosage principally in the appearance of a low-temperature (110°K) peak due to ethylene (presumably physically adsorbed; Redhead's¹² rule indicates an adsorption energy of 6 kcal/mole) and the reversed orderings of magnitudes of the low-temperature (α') and high-temperature (β') hydrogen peaks, with the former peak greater than the latter on 300°K dosage and smaller at 100°K dosage. The low-temperature peak was identified as physically adsorbed ethylene by monitoring the mass 26, 27, and 28 desorption spectra. The ratios of the peak heights of these partial pressure spectra correspond to the ratios in the cracking pattern of ethylene. The absence of a mass 30 partial pressure spectrum means that there was no detectable ethane formation.

Flash desorption spectra from iridium dosed with acetylene at 100 and 300°K (Figures 5 and 6) are qualitatively very similar to corresponding spectra for ethylene. The low-temperature peak in the case of acetylene (110°K) was identified as acetylene and is attributed to physically adsorbed acetylene. Comparison of the hydrogen peaks shows that at both dos-

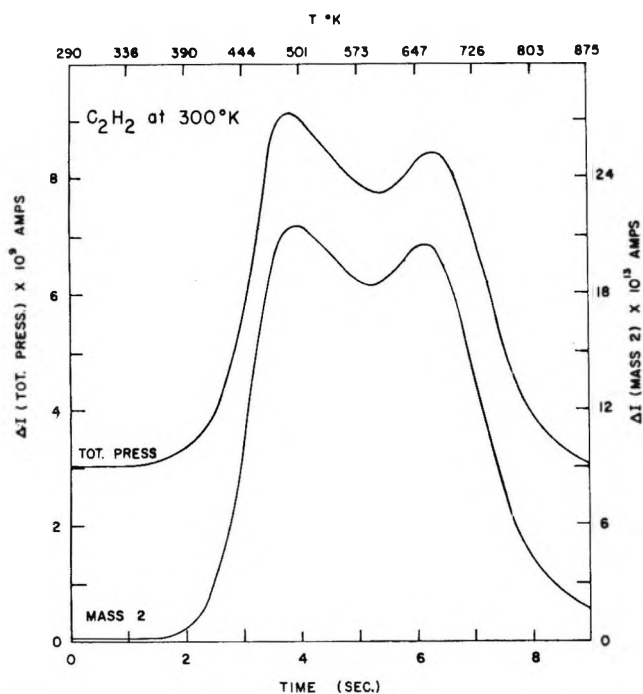
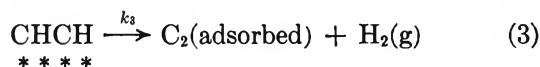
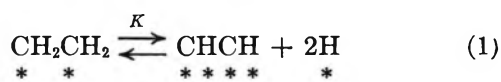


Figure 5. Flash decomposition of C_2H_2 dosed on iridium at $300^\circ K$. Total pressure and mass 2 bursts.

ing temperatures the α' hydrogen peak ($475^\circ K$) is substantially smaller for acetylene decomposition than for ethylene decomposition. The temperatures of the two hydrogen peak maxima correspond closely (475 and $650^\circ K$ for $60^\circ/sec$ flash rates). No hydrocarbons were observed in products formed above $200^\circ K$ in the case of acetylene dosage, while small quantities of methane and ethylene were observed over the range 200 – $600^\circ K$ in the case of ethylene dosage.

Discussion

The mechanism of decomposition of ethylene on iridium inferred by Arthur and Hansen² from their field emission study of these reactions can be summarized by the sequence of reactions



The third reaction was shown to be first order in adsorbed acetylene.¹³ Whether the acetylene lost hydrogen to the gas phase directly or to a chemisorbed hydrogen intermediate which rapidly desorbed could not be resolved. The chemisorbed hydrogen intermediate

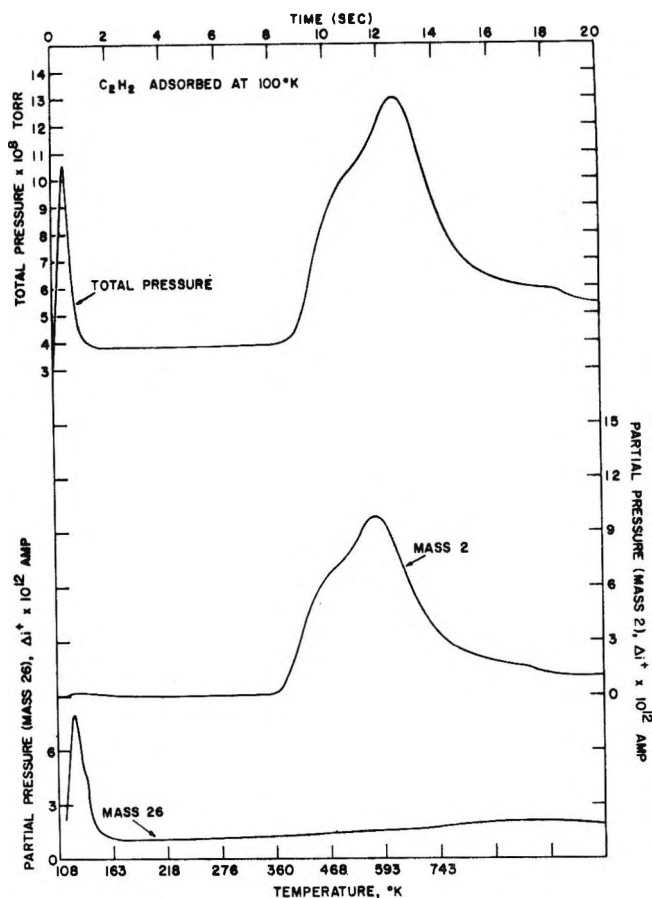


Figure 6. Flash decomposition of C_2H_2 dosed on iridium at $100^\circ K$. Total pressure and mass 2 bursts.

in the first dehydrogenation of ethylene was strongly indicated by the observed work function shifts.

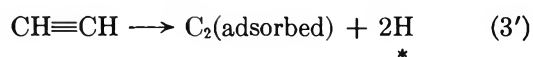
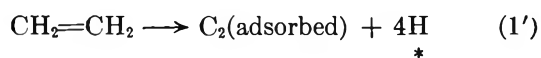
Based on reactions 1–3, the flash decomposition of acetylene on iridium would be expected to produce a single hydrogen peak at about the temperature observed for the β' peak in Figure 5 or 6. Flash decomposition of ethylene dosed on iridium at $100^\circ K$ would be expected to produce two peaks at temperatures corresponding to the α' and β' peaks in Figure 4. For a dosing temperature of $300^\circ K$ it might be expected that some hydrogen would be lost during dosing, so that, while both the α' and β' peaks would be expected in the flash desorption spectrum, it might be expected that the α'/β' ratio would be less for $300^\circ K$ dosing than for $100^\circ K$ dosing.

The mechanism set forth in reactions 1–3 therefore adequately accounts for the β' peaks in acetylene and ethylene decomposition and for the α' peaks in ethylene decomposition. It does not account for the presence

(13) J. R. Arthur and R. S. Hansen, *Ann. N. Y. Acad. Sci.*, **101**, 756 (1963).

of the α' peaks in acetylene decomposition (which are, however, markedly smaller for acetylene than for ethylene), and the observed α'/β' peak height ratio is greater at 300°K than at 100°K, not less as the model implies. The model also fails to account for the appearance of methane in the flash decomposition products from ethylene; since the methane is a minor product, this failure is less serious. The appearance of acetylene and ethylene at low flash temperatures is easily accounted for by desorption of physically adsorbed species, and the appearance of ethylene in flash desorption products from ethylene-dosed filaments over the temperature range 400–600°K may be most simply attributed to desorption of chemisorbed ethylene.

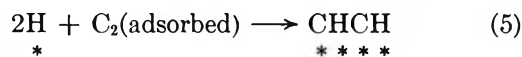
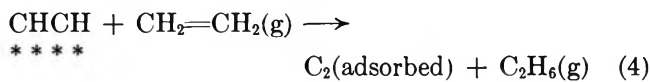
The reaction sequence 1–3 can be readily modified to account semiquantitatively for the discrepancies between its predictions and observations. Suppose that there are two principal faces (*e.g.*, (111) and (100)) on the metal surface and that on one of them, say face A, the reaction proceeds as indicated in reactions 1–3. On the other face, say face B, the reaction sequence is



This reaction sequence is intended to imply that ethylene and acetylene chemisorb with complete dissociation of hydrogen at temperatures substantially below the temperature of rapid hydrogen desorption. It is known² that the chemisorbed hydrocarbons are immobile on iridium at least up to 700°K, so that equilibration of hydrocarbon between faces A and B would not be expected. On the other hand, hydrogen is completely mobile on iridium above 200°K, so that equilibration of hydrogen between faces A and B would be expected and desorption of hydrogen would occur in the α' peak whether dosed on face A or face B. Suppose equal amounts of ethylene were chemisorbed on faces A and B; the α'/β' peak height ratio on flash desorption would be 3. For the case of acetylene, the corresponding ratio would be 1. These ratios are approximately those observed. Further, since the chemisorption reaction on face B is more extensive, it is not un-

reasonable to suppose its rate slower at 100°K than the chemisorption rate on face A. Hence, when the filament is flashed after a given dosing period, desorption of physically adsorbed hydrocarbon would occur principally from face B, and so the α'/β' peak height ratio would be less for 100°K dosing than for 300°K dosing.

Roberts³ has reported the decomposition of ethylene on clean iridium films at 27 and 100°, finding methane and ethane as principal products with only a small amount of hydrogen appearing during the early part of the reaction. These results are radically different from ours, but Roberts' reaction conditions are likewise radically different; for the dosing conditions cited, his ambient pressures must have been in the region of 10^{-3} torr whereas ours were of the order 10^{-8} torr. Under these circumstances, rates of impact of gaseous species with the surface would be greater in his experiments by a factor 10^5 than in ours. The difference in results suggests a mechanism for catalytic hydrogenation which, so far as we are aware, has not previously been proposed. The proposed sequence is



This is intended to imply a direct transfer of hydrogen atoms from chemisorbed acetylene to an ethylene molecule colliding with it from the gas phase. The reaction would be somewhat analogous to diimine hydrogenation of olefins, which has been recently reviewed by Hünig, Müller, and Thier.¹⁴ The $\text{C}_2(\text{adsorbed})$ residue would then react with chemisorbed hydrogen by the reverse of reaction 3 to regenerate chemisorbed acetylene. Obviously, a similar set of reactions could be based on chemisorbed ethylene rather than on chemisorbed acetylene. This mechanism accounts readily for the fact that Roberts observed ethane and little hydrogen, whereas we observed hydrogen but not ethane, in the decomposition of ethylene on iridium. According to the mechanism, the rate of ethane production in Roberts' experiments would be greater than in ours by a factor 10^6 .

(14) S. Hünig, H. R. Müller, and W. Thier, *Angew. Chem.*, **4**, 271 (1965).

On the Importance of the Metastable Liquid State and Glass Transition Phenomenon to Transport and Structure Studies in Ionic Liquids. I.

Transport Properties¹

by C. Austen Angell²

Chemistry Division, Argonne National Laboratory, Argonne, Illinois (Received January 25, 1966)

An attempt is made to show that progress in the understanding of ionic liquid transport properties and structure has been impeded by a lack of information on behavior in the "low-temperature" region of the liquid state, which largely involves the metastable supercooled liquid state. Insight into the nature of this lower region provided by molecular dynamics machine calculations is discussed in relation to the relevance of structural distinctions between crystallizing and noncrystallizing ionic liquids. Associated with the low-temperature region are systematic departures from Arrhenius behavior in the temperature dependence of transport which are not explained by conventional transition state theory. Two theories which lead to the observed form of the temperature dependence are reviewed. The recent Adam-Gibbs theory seems the more promising approach and leads to the recognition of a corresponding temperature scale based on isentropic states (states of equal configurational entropy) which can be used to define the low-temperature region and which may have interesting applications in correlating liquid structural properties. Comparison of this theory with the previous transition state theory approach suggests that the notion that volume and potential energy ("jumping") terms in the temperature dependence can be separated by constant volume measurements may be in error. A tentative explanation of existing constant volume data is offered.

Introduction

In recent investigations,³ we have made use of ionic systems with low liquidus temperatures, and frequently also undercooling tendencies and glass-forming properties, to demonstrate that at these low temperatures striking parallels in transport behavior among different systems become apparent which could not be recognized from the high-temperature behavior of the same systems. For instance, it has been found that the Arrhenius equation

$$D, \phi T, \Lambda T = D_0, \text{ etc.}, \exp\left(-\frac{E}{RT}\right) \equiv D_0, \text{ etc.}, \exp\left(\frac{-k'}{T}\right) \quad (1)$$

D , ϕ , and Λ being diffusivity, fluidity, and equivalent conductance, respectively, which has frequently been

taken as an acceptable means of describing the temperature dependence of transport properties in fused salt systems, is quite inapplicable in the low-temperature region (where "low temperature" is used in a relative sense, explained later). Instead, the temperature dependence is described rather accurately by a modified form of the Arrhenius equation⁴

$$D, \phi T, \Lambda T = D_0, \text{ etc.}, \exp\left(\frac{-k}{T - T_0}\right) \quad (2)$$

(1) Based on work performed under the auspices of the U. S. Atomic Energy Commission.

(2) Department of Chemistry, Purdue University, Lafayette, Ind.

(3) (a) C. A. Angell, *J. Phys. Chem.*, **68**, 218 (1964); (b) C. A. Angell, *ibid.*, **68**, 1917 (1964); (c) C. A. Angell, *ibid.*, **69**, 2137 (1965); (d) C. A. Angell, *J. Electrochem. Soc.*, **112** (12), 1224 (1965).

(4) This equation was first suggested by H. Vogel (*Physik. Z.*, **22**, 645 (1921)). The form of the equation employed in the present investigations allowed for a $T^{1/2}$ term in the preexponential constant.

T_0 being a constant. Not only is the form of this equation apparently correct, but also, for the systems examined, k has the same value within the ability of the experiments to decide.

There are, therefore, some indications of broad relationships for relaxation processes in molten salts similar to those described for polymer systems by the well-known, but also empirical, Williams, Landel, and Ferry (WLF) equation (which, in fact, can be derived from eq 2).⁵ In this paper, we wish to outline some reasons for believing that such relationships should exist and that they may be expected to apply irrespective of whether or not the liquids happen to be metastable with respect to some crystalline phase. The discussion will suggest that the metastable liquid range may be profitably regarded as the "lower half" of the *normal* liquid state which terminates, in a thermodynamic as well as in a practical sense, at the glass transition temperature. If such a viewpoint can be accepted, it will be necessary to conclude that the study of the metastable state is a neglected field in molten salt chemistry, since it would seem that it is in this region that the foundations of understanding of the liquid behavior necessary to interpret the high-temperature properties should be laid.

The reason the metastable ionic liquid state has been paid so little attention outside the interests of the glass industry probably lies in the common tendency to regard the glass-forming liquids as of a distinct class, characterized by great structural complexity. The glass has been thought of merely as a liquid whose viscosity has become excessive due to the inadequacy of the thermal energy content of the liquid in meeting the energy requirement for relative motion of the entangled complex units. Consequently, in this view the behavior of such liquids is not really relevant to the problem of understanding the behavior of "normal" liquids. While such a kinetic interpretation of the *observed* glass transition contains a great deal of truth, the belief that it must be a result of structural complexity due to chemical binding energies is contradicted by the evidence that "fluids" of the very simplest nature, discussed below, can be obtained in the "glassy," *i.e.*, rigid amorphous state.

To anticipate points developed in the later discussion, it is becoming clear, from the work of Gibbs and associates,⁶ Turnbull and Cohen,⁷ and others,^{8,9} that the high viscosity at temperatures approaching the glass transition is fundamentally the result of increasingly severe configurational restrictions to relaxation in the liquid at high packing densities. The experimental glass transition itself is thereby related to the *effective* disappearance, for the time scale of the experi-

ment, of the liquid's configurational entropy. The transition therefore takes the character of a second-order thermodynamic transition, and, in fact, certain second-order transition equations may be successfully applied to glass-forming substances at their T_g .^{8,10} This interpretation thus incorporates the kinetic nature of the observed transition but at the same time shows that it is fundamentally thermodynamic in origin and thus is not necessarily restricted to molecularly complex liquids.

If the glassy state and associated characteristic behavior can in principle occur even for the simplest liquids, then the only possible reason for making class distinctions between glass-forming and crystallizing liquids is the inhibition of the crystallization phenomenon in the former. As our general purpose is to suggest that the study of noncrystallizing liquids in various *mixed* ionic systems can provide valuable correlating information on "*normal*" liquid state behavior, it would seem desirable to establish that failure to crystallize need not imply gross differences in structural character from the more general case of crystallizing liquids. We shall therefore first give some consideration to the crystallization phenomenon.

Supercooling and Structure

In order to put this problem in perspective and also to gain some insight into the metastable liquid and glassy states, it is helpful to consider the place of undercooling in the behavior of the simplest fluids. To this end, Alder and Wainwright's studies in molecular dynamics,¹¹ the computer-based simulation of the dynamic behavior of assemblies of hard spheres by solving simultaneously their equations of motion, are of value. These calculations, which follow the motion of each member of an assembly of up to 500 hard spheres, have shown that, in a certain range of packing densities, the system can exist in two alternative states, one ordered and crystal-like and the other disordered and fluid-like. In the course of a run in this region ($v/v_0 =$

(5) A. A. Miller, *J. Polymer Sci.*, **A1**, 1857 (1963).

(6) (a) J. H. Gibbs and E. A. Dimarzio, *J. Chem. Phys.*, **28**, 373 (1958); (b) J. H. Gibbs, "Modern Aspects of the Vitreous State," Vol. I, J. D. McKenzie, Ed., Butterworth and Co. Ltd., London, 1960, Chapter 7; (c) G. Adam and J. H. Gibbs, *J. Chem. Phys.*, **43**, 139 (1965).

(7) (a) M. H. Cohen and D. Turnbull, *ibid.*, **31**, 1164 (1959); (b) D. Turnbull and M. H. Cohen, *ibid.*, **34**, 120 (1961); (c) D. Turnbull, *Trans. Met. Soc. AIME*, **221**, 422 (1961).

(8) J. M. O'Reilly, *J. Polymer Sci.*, **57**, 429 (1962).

(9) O. G. Lewis, *J. Chem. Phys.*, **43** (8), 2693 (1965).

(10) E. Jenckel, *Z. Anorg. Allgem. Chem.*, **216**, 351 (1934).

(11) (a) B. J. Alder and T. E. Wainwright, *J. Chem. Phys.*, **31**, 459 (1959); (b) B. J. Alder and T. E. Wainwright, *ibid.*, **33**, 1439 (1960); (c) B. J. Alder, *ibid.*, **40**, 2724 (1964).

1.5–1.6, v_0 = ordered close-packed volume), a system may fluctuate several times between the two states. For $v/v_0 > 1.7$, the ordered state always converts to the fluid, but the converse at high densities does not apply. For instance, for $v/v_0 < 1.5$, a 32-particle system initially in the disordered state, could not generate a sufficient fluctuation to revert to the ordered state; *i.e.*, a configurational barrier to crystallization exists. In these conditions an extended fluid-like behavior could be observed with increasing density, reaching a limit at $v/v_0 = 1.15$ when the pressure, at constant energy, $\rightarrow \infty$. The limiting configuration, which may be regarded as the glassy state for hard spheres, was observed to be a somewhat disordered defect-containing version of close packing.^{11b} Results for hard spheres have been confirmed using the Monte Carlo computation method¹² (which gives only equilibrium properties). The ability of the computer techniques to describe real systems has been demonstrated with the latter method by introducing a Lennard-Jones 6–12 interaction potential and showing that the experimental equilibrium properties of gases such as argon can be reproduced with excellent accuracy.¹³

Two points from these valuable studies are of special interest to the present discussion. The first, which is also a matter of practical experience, is that provided the system remains in the “fluid pocket of phase space,”^{11b} *i.e.*, provided no crystals form, no reorganization of the liquid configurations or sudden changes of its thermodynamic properties are to be expected simply because it happens to become metastable with respect to one or other crystalline phase. The second is that there is nothing extraordinary about failure to crystallize: even in the simplest fluids, a density fluctuation to yield a suitable configuration is required, and if this is not produced at some critical stage of the contraction process, the stable state will not be realized. In real systems, where the number of particles is effectively infinite, more than mere geometrical barriers will be required if crystallization is to be suppressed, even at the fastest cooling rates. However, the possibility of noncrystallization with eventual glass formation is always present, and its probability is a function of factors such as cooling rate, sample size and purity, and most importantly, the relation of the height of the nucleation energy barrier to kT .¹⁴ The question of the relevance of studies on metastable liquids to the behavior of crystallizing liquids, therefore, becomes a question of deciding whether or not the additional rigidity, or energetic stability, of the local order in the liquid which is necessary to preclude nucleation of the crystalline phase at practical cooling rates is important

enough to place the noncrystallizing liquids in a separate class.

For the case of fused salts, in which we are mainly interested, the local order is always well defined, particularly when polyvalent cations are present,¹⁵ and energy barriers to nucleation will, therefore, depend largely on the structure of the crystalline phase with respect to which the liquid phase is unstable.¹⁶ Hence, it is not too surprising that, while few pure salts undercool significantly under normal circumstances,¹⁷ instances of molten salt *mixtures* which undercool to the point of glass formation are quite common—more so than is generally realized. A compilation of some systems with glass-forming composition ranges is given in Table I. A great variety of aqueous glass-forming systems, particularly those involving rare earth chlorides and nitrates, are omitted.

It is to be noted that in the majority of systems, neither component of the mixture possesses marked glass-forming tendencies in the pure state. The glass-forming ability of the mixtures, therefore, may not be explained simply in terms of complexity handed down from one of the pure components. On the contrary, complex components in, for example, pure fused $ZnCl_2$ are apparently broken up by addition of a second component.¹⁸ Noting that the liquids in the glass-forming regions of these systems remain thermodynamically stable to unusually low temperatures, we suggest a more thermodynamic explanation of the failure to crystallize. Where the data are available, it would seem that one or other component of the mixtures of Table I has a low heat and a low entropy of fusion. The structural explanation may be quite different in different cases (*e.g.*, lack of nitrate anion rotation in fused $Ca(NO_3)_2$,¹⁹ retention of crystal coordination number, and structural character in fused $ZnCl_2$)¹⁸

(12) W. W. Wood and J. D. Jacobson, *J. Chem. Phys.*, **27**, 1207 (1957).

(13) W. W. Wood and F. R. Parker, *ibid.*, **27**, 720 (1957).

(14) A detailed discussion of the crystallization phenomenon is contained in an article by D. Turnbull.^{7c}

(15) D. M. Gruen and R. L. McBeth, *Pure Appl. Chem.*, **6**, 23 (1963). See also ref 53.

(16) Note, for instance, in the glass-forming univalent nitrate systems (Table I) examined systematically by E. Thilo, C. Wieker, and W. Wieker (*Silikat Techn.*, **15**, 109 (1964)) that the composition region in which glasses may be produced lies in most cases to the divalent nitrate side of the eutectic composition, suggesting that the difficulty of nucleation of these structures is a factor in the occurrence of undercooling and glass formation in these systems.

(17) G. Tammann and E. Elbrachter (*Z. Anorg. Allgem. Chem.*, **267**, 268 (1932)) have shown that various pure salts such as KNO_3 , $NaNO_3$, Tl_2SO_4 , $PbCl_2$ may be obtained in the glassy state by spraying tiny droplets of liquid onto a cold plate.

(18) J. R. Moyer, J. C. Evans, and G. Y.-S. Lo, *J. Electrochem. Soc.*, **113**, 158 (1966). References to earlier work are given therein.

(19) O. J. Kleppa, *J. Phys. Chem. Solids*, **23**, 819 (1962).

Table I: Glass-Forming Molten Salt Systems

Halides	Nitrates	Sulfates	Carbonates	Mixed systems
ZnCl ₂ + KCl ^{*a}	Mg(NO ₃) ₂ + Li, * Na, K,	ZnSO ₄ + K ₂ SO ₄ ⁱ	MgCO ₃ + K ₂ CO ₃ ^{k,l}	CoCl ₂ + K ₂ SO ₄ ^{*i}
ZnCl ₂ + AlCl ₃ ^b	Rb, Cs, NO ₃ ^o	CuSO ₄ + K ₂ SO ₄ ^{*i}	BaCO ₃ + Li ₂ CO ₃ ^{*l}	CuCl ₂ + K ₂ SO ₄ ^{*i}
ZnCl ₂ + Pyr·Cl ^c		K ₂ SO ₄ + H ₂ SO ₄ ⁱ		ZnCl ₂ + Na ₂ SO ₄ ^a
ZnCl ₂ + BiCl ₃ ^c	Ca(NO ₃) ₂ + Na, * K, Rb,			
ZnCl ₂ + BeCl ₂	or CsNO ₃ ^{*o}			PbSO ₄ + Pb ₂ SiO ₄ ^m
ZnCl ₂ + KI ^a				
ZnCl ₂ + NaBr ^{*c}	Sr(NO ₃) ₂ + Rb, * or			CaF ₂ + Ca(OH) ₂ +
	CsNO ₃ ^{*o}			CaCO ₃ + BaSO ₄ ⁱ
BiCl ₃ + KCl ^d	Ba(NO ₃) ₂ + CsNO ₃ ^{*o}			KNO ₂ + Ca(NO ₃) ₂ etc. ^c
BiCl ₃ + NaBr ^{*c}				
	Cd(NO ₃) ₂ + Li, Na, K,			ZnCl ₂ + KNO ₃ ^c
	Rb, Cs, or TlNO ₃ ^o			
BeCl ₂ + AlCl ₃ ^b	La(NO ₃) ₂ + KNO ₃ ^c			
BeF ₂ + KF ^e				
BeF ₂ + NaF ^e				
BeF ₂ + CaF ₂ ^e	Ca(NO ₃) ₂ + H ₂ O ^h			
ZrF ₄ + KF ^c	Mg(NO ₃) ₂ + H ₂ O ^h			
MgF ₂ + HF ^f	La(NO ₃) ₂ + H ₂ O ^c etc.			
CaF ₂ + HF ^f				
PbF ₂ + HF ^f				
BiF ₃ + HF ^f				

^a I. Schulz, *Naturwiss.*, **44**, 536 (1957). All asterisks indicate a weak glass-forming ability. ^b R. F. Belt and H. Scott, *Inorg. Chem.*, **3**, 1785 (1964). ^c C. A. Angell and D. M. Gruen, unpublished work. ^d J. D. Corbett, private communication. ^e G. Heyne, *Angew. Chem.*, **46**, 473 (1933). ^f J. Schröder, *Angew. Chem. Intern. Ed.*, **3**, 376 (1964). ^g See ref 16. ^h See ref 3c. ⁱ See ref 36. ^j T. Forland and W. A. Weyl, *J. Am. Ceram. Soc.*, **33**, 186 (1950). ^k See ref 34. ^l See ref 35. ^m See ref 20.

and BeF₂), but the thermodynamic consequence is the same, *viz.*, a relatively sharp initial depression of the single component freezing point on addition of a second component. This follows from the relation of the freezing point depression constant to the heat of fusion. Unless arrested by the occurrence of stable binary compounds, the resulting steep liquidus curve leads to low binary liquid temperatures. The result is that an otherwise unexceptional regrouping energy barrier may now become sufficient, with respect to kT , to prevent stable phase nucleation. In its emphasis on liquidus temperature and nucleation probability, this view is in accord with the explanation of glass formation embraced by Weyl and Marboe²⁰ in their extensive contributions to the subject. The importance of the liquid's entropy content at the liquidus temperature as distinct from its energy content will be seen in the latter discussion of Figure 2.

Thus, we believe that the ordering factors which inhibit crystallization in the systems of Table I should not be sufficient to warrant any major distinctions between the nature of these liquids and the more general case in which crystallization occurs. However, judgment on this point will have to rest on the extent to which correlations in general fused salt behavior are forthcoming from studies made possible by the extended temperature range available in the supercooling

systems. The type of correlation which may be looked for in this connection will be referred to later; for the moment, we will return to the transport behavior of these liquids, for which it will develop that the issue of structural distinctions can probably be ignored.

Ionic Liquid Transport Theory in the Light of the Low-Temperature Behavior

It seems that a satisfactory general theory of transport in ionic liquids must provide for the validity of eq 2 in the "low-temperature" region. Standard transition state theory approaches would require arbitrary manipulation of the "activation energy" term in order to yield this result and hence are inadequate. Two theoretical approaches leading to eq 2 will be reviewed briefly, and consequences of the Adam-Gibbs theory will then be explored in more detail to indicate how this theory may help to provide a framework for a general correlation of ionic liquid transport properties.

The attempt by Cohen and Turnbull²¹ to justify eq 2 has attracted a great deal of attention.^{3,21} The liquid considered by these authors was composed of simple

(20) W. A. Weyl and E. C. Marboe, "The Constitution of Glasses," Vol. I, Interscience Publishers, Inc., New York, N. Y., 1962, p 238.

(21) (a) A. Bondi, "Rheology," Vol. 4, F. R. Eirich, Ed., Academic Press, New York, N. Y.; (b) N. H. Nachtrieb, E. Fraga, and C. Wahl, *J. Phys. Chem.*, **67**, 2353 (1963).

spherical molecules equivalent to the hard-sphere or δ -12 potential fluids characterized by the fluid branch of the molecular dynamics and Monte Carlo calculations. The diffusion process in this model is assumed to occur by "jumps" of molecular dimensions made possible by the momentary increase in size of the "cage" of neighboring molecules in which the molecules are normally confined. The increase in cage dimensions to the critical size necessary for diffusion to occur arises by the redistribution of "free volume." When the free volume is defined as that volume which can be redistributed among the "cages" without change in over-all energy, it is possible to evaluate the transition (or jump) probability and thereby to arrive at the relation, eq 3, which is nearly equivalent to the empirical Doolittle equation for viscosity

$$D = D_0 \exp\left(-\frac{\gamma v^*}{v_f}\right) \quad (3)$$

where γ is a cage volume overlap factor, v^* is the critical increase in cage volume, and v_f is the total free volume. By making the additional intuitively satisfying assumption that the glass transition arises from the effective disappearance of free volume ($v_f \rightarrow 0$; $\therefore D \rightarrow 0$, $\eta \rightarrow \infty$) which occurs at T_g , and identifying v_f with the total thermal expansion of the liquid above T_0 , eq 2 in the form

$$D = D_0 \exp\left[-\frac{\gamma v^*}{\bar{v}_m \alpha (T - T_{0p})}\right] \quad (4)$$

results. (\bar{v}_m is the mean molecular volume; α is the mean coefficient of expansion over the range $T - T_0$).

The above concept of free volume and free volume disappearance is easy to accept for the hard-sphere fluid where all nonoverlapping configurations have the same energy. Here $v_f = 0$ would correspond to the close-packed volume ($p_{T=\text{const}} \rightarrow \infty$) of the fluid branch. It can also be rationalized for the 6-12 potential liquid^{7b} and, by analogy, for the simple ionic liquid.^{3b} We have previously sought to interpret the validity of eq 2 for the ionic liquid systems we have studied in terms of this model, but have had difficulty in reconciling the experimental value of k (eq 2) with the value expected from eq 4 and the measured expansion coefficient. Also, it is difficult to see why k should be constant when the expansion coefficients vary from system to system, although a possible rationalization has been suggested.^{3d} Measurements of the effect of pressure on relaxation properties have not been in accord with free volume model predictions.^{22,23} The model may be criticized for considering only the contribution to diffusion of molecular diameter sized

jumps; the criticism is strengthened by the most recent molecular dynamics result which shows that at least for hard spheres, there is no characteristic jump distance in fluid diffusion.²⁴ Also, it is difficult to see how the zero energy free volume redistribution concept can apply to molecularly complex systems (e.g., with chain molecules). Such systems are nevertheless those whose conformity to eq 2, or to the equivalent WLF equation, is best documented.

An alternative theory leading to eq 2, which cannot be criticized either on the grounds of restrictive mechanisms or of inapplicability to complex systems, has recently been proposed by Adam and Gibbs.^{6c} In this theory, the intuitive appeal of Cohen and Turnbull's idea connecting glass transition and free volume disappearance at T_0 has not been lost. Rather, it is replaced by the even more appealing proposition that the essential liquid state characteristic which becomes zero at the temperature T_0 is the *configurational entropy* of the liquid. Furthermore, where the free volume disappearance at T_0 was an assumption in Cohen and Turnbull's model, in the Adam-Gibbs theory the vanishing entropy comes as a central result of a successful statistical mechanical theory of chain polymer liquids at high particle densities,^{6a,25} which can presumably be generalized to include nonpolymeric liquids.

In the development of their theory for relaxation properties of glass-forming liquids in the neighborhood of the glass transition temperature, Adam and Gibbs took the view that translational motion of a given molecule (or segment of a molecule) occurs, in a manner which need not be specified, by the cooperative rearrangement of a group of molecules. The temperature dependence of the translational process was then shown to be the result of the effect of temperature on the minimum size of the cooperatively rearranging groups. By making only the assumption that the cooperatively rearranging groups operated independently, *i.e.*, did not interact significantly, it was possible to show that the minimum (critical) size of the cooperatively rearranging group could be expressed in terms of the

(22) A. Gilchrist, J. E. Early, and R. H. Cole, *J. Chem. Phys.*, **26**, 196 (1957).

(23) S. B. Brummer, *ibid.*, **42**, 1636 (1965).

(24) B. J. Alder and T. Einwohner, *ibid.*, **43**, 3399 (1965).

(25) In this theory, the disappearance of the configurational entropy produces a second-order thermodynamic transition, which was shown to have all the characteristics of the glass transition. The fact that particular second-order transition equations are obeyed at the glass transition temperature^{6,10} lends some support to the theory. Its success in predicting the dependence of T_g on molecular properties in polymer systems has been striking.^{6a,9}

macroscopic configurational entropy. On showing that this smallest cooperative region must be that involved in the great majority of transitions, there resulted for the average transition probability, $\bar{w}(T)$, the expression

$$\bar{w}(T) = \bar{A} \exp\left(-\frac{C}{TS_c}\right) \quad (5)$$

where \bar{A} and C are constants, T is the absolute temperature, and S_c is the configurational entropy. This expression should therefore contain the important part of the temperature dependence of any of the familiar mass transport processes.

Introducing the experimental fact that the specific heats of the glass-forming liquids are approximately independent of temperature, and the theoretical result that $S_c = 0$ at T_0 , it could then be shown that, for $[(T - T_0)/T_0]^2 \ll 1$

$$D, \Delta T, \phi T, \text{ etc.} \propto w(T) = A \exp\left(-\frac{C}{\Delta C_p(T - T_0)}\right) \equiv A \exp\left(-\frac{k}{(T - T_0)}\right) \quad (6)$$

with

$$C = \frac{\Delta\mu s_c^*}{R/N} \quad (7)$$

where ΔC_p is the difference in glassy and liquid state specific heats, $\Delta\mu$ is taken as the potential energy hindering the cooperative rearrangement, s_c^* is the configurational entropy of the critical-size cooperative region, and R/N is the Boltzmann constant.

Equation 2 (≡eq 6²⁶) is thus seen to be the necessary consequence of the effect of temperature on the thermodynamic state of the liquid (which may or may not be in a metastable state with respect to some crystalline state) and should therefore apply irrespective of specific liquid structure. Although, in the Cohen-Turnbull model, the $1/(T - T_0)$ temperature dependence arises in essentially the same way through the disappearance at T_0 of a vital liquid-state characteristic, the above conclusion would not follow unless the free volume redistribution energy could be shown to be zero, independent of structure. An important feature of the Adam-Gibbs theory is therefore that it shows that any distinction between crystallizing and noncrystallizing liquids, on the basis of structural complexity, is largely irrelevant as far as the use of the noncrystallizing liquids to obtain information on "low-temperature" transport behavior is concerned. The validity of eq 2 for a variety of ionic³ and complex molecular^{6c} liquids is good evidence for this point.

With this point in mind, it is possible to say that, if Gibbs and co-workers are correct, then molten salt chemists seeking to establish rules governing the transport behavior of ionic liquids in the "normal" temperature range have been working at a serious disadvantage. *If the essential characteristic of the liquid state, viz. its configurational entropy, does not vanish before T_0 , then the temperature range from the melting point down to T_0 is as equally valid a part of the liquid state as the range melting point to boiling point: to date, then, investigators of the post-melting point range have not had the benefit of any understanding of the behavior of this lower part of the ionic liquid range on which to build.* A parallel, which will be explored in more detail in a subsequent publication, may be drawn to the difficulties of understanding the specific heat of solids without information covering the range 0–200°K. An immediate suggestion of this line of thought is that the usual distinction made between the behavior of glass-forming oxide melts and that of common molten salts is largely artificial. At thermodynamically equivalent temperatures (see below), fused salts and oxide melts in fact behave in much the same way, but while the oxide melts have, for practical reasons, been much studied in their "low-temperature regions," fused salt studies have been confined principally to the high-temperature (post-melting point) range.

Let us therefore reproduce in summary what has been learned about transport behavior in the "lower half" of the ionic liquid state by the studies referred to in the opening paragraph, and consider to what extent the Adam-Gibbs theory can be used, through these data, to give perspective to previous observations on high temperature behavior.

In Figure 1 the slope of the ordinary Arrhenius plot for electrical conductance, in the familiar guise of an "activation energy," is plotted as a function of temperature for various systems, some of which are glass-forming. Were the Arrhenius equation to be obeyed, these plots would, of course, be straight lines parallel to the abscissa, as is approximately the case at the high temperatures. In Figure 2, we show how all the curves of Figure 1 coincide when the "activation energies," in this case corrected by an amount of the order of 1 kcal to correspond to the temperature dependence of a diffusion process,^{3b} are plotted against the function T/T_0 , where T_0 is obtained from the best

(26) R. Araujo (*J. Chem. Phys.*, **44**, 1299 (1966)) has now shown that using eq 5, i.e., avoiding the approximations made in the subsequent derivation of eq 6, the viscosity of B_2O_3 (which has abnormal specific heat characteristics) may be described accurately over a much wider temperature range (800°) than is possible using eq 2. This success with B_2O_3 , which had previously seemed an anomalous case, encourages belief in the validity of the Adam-Gibbs approach.

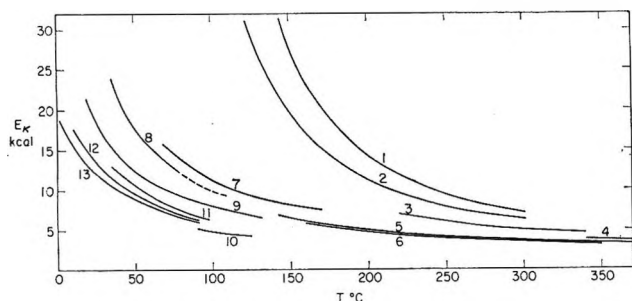


Figure 1. Variation of activation energy for specific conductance with temperature for various molten salts and hydrate melts: 1, $\text{Ca}(\text{NO}_3)_2 + 55\% \text{KNO}_3$; 2, $\text{Ca}(\text{NO}_3)_2 + 62\% \text{KNO}_3$; 3, $\text{Ca}(\text{NO}_3)_2 + 80\% \text{KNO}_3$; 4, pure KNO_3 ; 5, $\text{KNO}_3 + \text{NaNO}_3 + \text{LiNO}_3$ eutectic; 6, $\text{KNO}_3 + \text{NaNO}_3 + \text{NaNO}_2$ eutectic; 7, $\text{H}_2\text{O} + 25.9 \text{ mole } \% \text{Mg}(\text{NO}_3)_2$; 8, $\text{H}_2\text{O} + 24.2\% \text{Mg}(\text{NO}_3)_2$; 9, $\text{H}_2\text{O} + 20.3\% \text{Mg}(\text{NO}_3)_2$; 10, $\text{H}_2\text{O} + 14.7\% \text{Mg}(\text{NO}_3)_2$ ($\sim \text{Mg}(\text{NO}_3)_2 \cdot 6\text{H}_2\text{O}$); 11, $\text{Ca}(\text{NO}_3)_2 \cdot 4\text{H}_2\text{O} + 31\% \text{KNO}_3$; 12, $\text{Ca}(\text{NO}_3)_2 \cdot 4\text{H}_2\text{O} + 10\% \text{KNO}_3$; 13, $\text{Ca}(\text{NO}_3)_2 \cdot 4\text{H}_2\text{O}$.

fit of the data to eq 2.²⁷ These data may be placed on one of Hildebrand's "beautiful straight lines"²⁸ by plotting against the function $[T/(T - T_0)]^2$, as demonstrated for the $\text{Ca}(\text{NO}_3)_2 + \text{KNO}_3$ systems in Figure 2, ref 3a. The slope of this plot gives the value of k (eq 2 and 6) which, within the uncertainty of determination, has the same value for all the systems quoted, 680°K ($\pm 5\%$). Viscosity data at comparable temperatures are only available for $\text{Ca}(\text{NO}_3)_2\text{-KNO}_3$ melts^{29a} and molten $\text{Ca}(\text{NO}_3)_2 \cdot 4\text{H}_2\text{O}$ and $\text{Na}_2\text{S}_2\text{O}_3 \cdot 5.2\text{H}_2\text{O}$.^{29b} The more extensive measurements on the latter two liquids yield the same value of T_0 as for conductance, with k 15–20% higher. For the former system, equal values of T_0 would require $k_7 \approx 1.2k_A$.

It can be observed from the positions of the liquidus temperatures shown by arrows in Figure 2 that the transport behavior is quite independent of whether or not the liquid is in a metastable state with respect to some crystalline phase. In fact, it is rather the probability of crystallization which seems to be influenced by the temperature of crystallization on this corresponding scale; *e.g.*, the only data obtained below the liquidus are for those melts with liquidus temperatures below 1.6 on the T/T_0 scale. That this demonstrates the importance of entropy content to crystallization kinetics will be seen below.

Figure 2 shows that the instantaneous slope of the Arrhenius plot for these systems is a near-universal function of T/T_0 . The usefulness of the "activation energy" concept in the presence of such a great and systematic temperature dependence is questionable,^{3b,30} and it might appear that the Figure 2 correlation of Arrhenius plot slopes is merely a trivial

consequence of the form of eq 2. However, the Adam-Gibbs theory gives the plot considerable significance, since their transition probability expression (eq 5) is also of Arrhenius form and shows that the instantaneous slope of the Arrhenius plot is proportional to the inverse of the liquid configurational entropy (although for variable S_c , the proportionality constant is not simply $-C$). In contrast to the "activation energy" case, it is obvious that the configurational entropy of even the simplest liquids will change with temperature at constant pressure, and its dependence on temperature can be expressed in terms of the specific heat, (which is an independently measurable quantity), according to

$$\frac{dS_c}{dT} = \frac{\Delta C_p}{T} \quad (8)$$

The use of ΔC_p (defined above) rather than C_p serves to separate configurational from solid-like contributions to the total entropy.

Integrating and introducing the theoretical result $S_c = 0$ at $T = T_0$, one obtains

$$S_{c(T)} = \Delta C_p \ln \frac{T}{T_0} \quad (9)$$

the expression which Adam and Gibbs note can be used to obtain eq 7 from eq 6. S_c is thus a function of T/T_0 . The correlation in Figure 2 is therefore a reflection of this relation for the case where k (of eq 2 and 6) has the same value for the different liquids. Allowance for variable k by plotting in the ordinate $(k/k_0) \times [d/d(1/T)] [\ln D, (\Delta T), (\phi T)]$, where k_0 is the value for some reference system, could give a more truly universal plot.

ΔC_p is unlikely to differ greatly among salts in which the cation and anion structural units are simple. This being the case, an important feature of Figure 2 is that it shows how the *low-temperature* transport data may be used to establish a corresponding temperature scale based on *states of equal configurational entropy*, which may be called "isoentropic states." This would seem to be a reasonable basis for a corresponding-states treatment of various liquid properties. It provides

(27) Exceptions are the Li, Na, K, NO_3 , the Na, K, NO_3 , NO_2 , and the Li, K, Cl eutectics, and $\text{ZnCl}_2\text{-KCl}$, for which T_0 was chosen as the value which gave the best fit of the data to the curve established by the other systems. The ability to fit provides a test of compatibility of the transport behavior of these systems with that of the other systems.

(28) J. H. Hildebrand, *Science*, **150**, 441 (1965).

(29) (a) E. Rhodes, W. E. Smith, and A. R. Ubbelohde, *Proc. Roy. Soc. (London)*, **A285**, 263 (1965); (b) C. T. Moynihan, unpublished results privately communicated.

(30) A. Klemm, *Discussions Faraday Soc.*, **32**, 265 (1961).

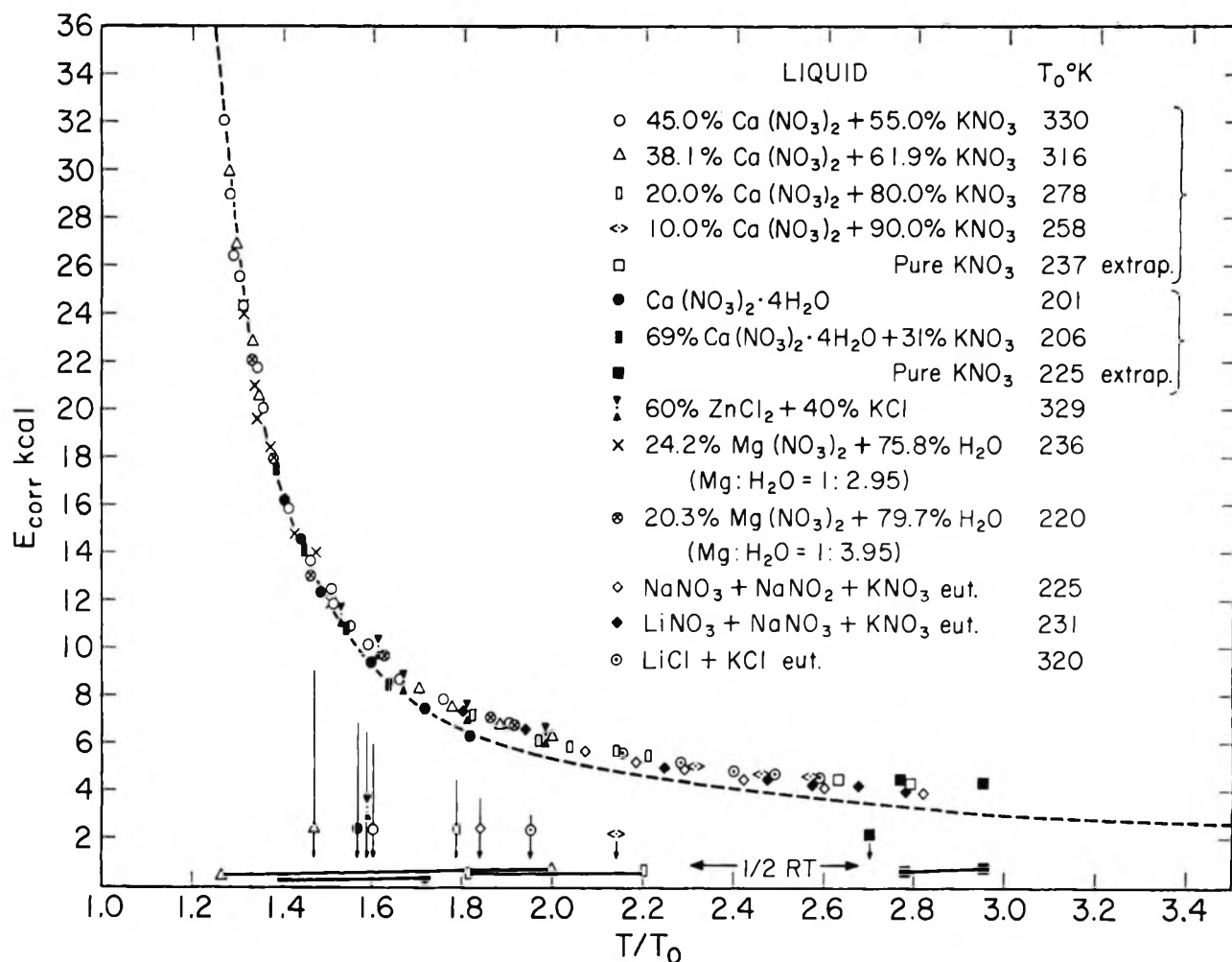


Figure 2. Plot of temperature dependence of electrical conductance, represented by E_{corr} , as a function of T/T_0 for various fused salt systems: dashed line is plot predicted by eq 2 for $k = 680^\circ\text{K}$. For some of the melts T/T_0 values at the liquidus temperature are indicated by arrows. Effect of $T^{1/2}$ term in preexponential on computed E_{corr} shown at base of diagram.

some vindication of the previously empirical use of the T_0 -based corresponding temperature scale in a discussion of diffusion-conductance relations in fused salts.³¹ The general usefulness of such a corresponding temperature scale, however, remains to be demonstrated; the possibilities will be touched on in the concluding remarks.

With the help of Figure 2, we can now explain our use of the term "low temperature" in connection with the region of the liquid state whose importance we are attempting to establish. A liquid can, arbitrarily, be thought of as being in its "low-temperature region" when $T/T_0 \lesssim 2$. Consequently, a given Centigrade temperature may be "low" for one liquid but not for another, depending on the relative T_0 values. In view of the above discussion, "low temperature" in this sense would clearly be better read as "low entropy." Liquidus temperatures below $T/T_0 = 2$ are uncommon

but are presumably a feature of all of the systems of Table I.

It remains to consider how general the ability of the Adam and Gibbs equations to describe transport in ionic liquids may prove. For instance, the plots of Figure 1 can only be expected to superpose as in Figure 2 if the constant k of eq 2 has the same value for the different systems. In the Adam-Gibbs theory, this constant contains the energy term $\Delta\mu$, (eq 7) and Gibbs suggests³² that for ionic liquids $\Delta\mu$ should be a suitable function of the relevant cation-cation and cation-anion pair interaction energies and an effective coordination number. There is therefore some question as to why the coincidence should be as good as it appears to be. To account for the similar consistency

(31) C. A. Angell, *J. Phys. Chem.*, **69**, 399 (1965).

(32) J. H. Gibbs, private communication.

for polymer and alcohol systems implied by the "universal" parameters of the WLF equation, Adam and Gibbs found reasons why changes in ΔC_p should parallel those in $\Delta\mu$. Small differences in k may also be masked by small errors in the choice of T_0 , to which the derived value of k is very sensitive.

In this connection it is probably significant that all the systems of Figures 1 and 2 involve univalent anions. Change in anion charge type may well produce differences in k . The value of $\Delta\mu$, for instance, should double approximately for change of nitrate anion to carbonate anion. It is noteworthy, then, that the (Li, Na, K)₂CO₃ eutectic conductance data,³³ which yield E_a values increasing smoothly from 5.7 to 11 kcal/mole in the temperature range 720–400°, cannot be fitted to the plot in Figure 2. In fact, it seems that k for the carbonate case would need to be roughly double the value applying in Figure 2 for a reasonable fit to be possible. By analogy with the univalent anion systems it would seem that measurements on a supercooling system such as MgCO₃–K₂CO₃^{34,35} may be able to provide a suitable "base" for interpretation of the "normal" carbonate transport behavior, and its relationship to the behavior illustrated in Figure 2. A similar base for molten sulfates may perhaps be obtained from a study of the glass-forming ZnSO₄–K₂SO₄ system.³⁶ The field can no doubt be expanded to include the more complex silicate and borate anion systems, where the temperature range of practical interest is the "low-temperature" region. While further development of this subject is beyond the scope of this paper, it is worth noting that, as long ago as 1925, Fulcher³⁷ showed that viscosity³⁸ data for a sodium silicate melt varying over ten orders of magnitude could be placed on a single straight line by means of eq 2 using $T_0 = 415^\circ$, $k = 5100$.

Concluding Remarks

The evidence obtained from the low-temperature studies on ionic liquids therefore leads to a broad view of the liquid as a state which is continuous through the crystallization temperature and terminates in a glass transition, and whose transport properties are best accounted for by the theory of Adam and Gibbs. It is appropriate now to place this theory in relation to those which have gone before.

The usual treatment of transport in ionic liquids has involved some form of transition state theory, in which the transition probability, $w(T)$ is commonly developed as a two-term exponential expression

$$w(T) = A' \exp\left(-\frac{E_J}{RT}\right) \exp\left(-\frac{E_H}{RT}\right) \quad (10)$$

The first energy term, E_J , is thought of as the potential energy opposing the "jump" from one site to a neighboring vacant site ("hole") and the second term, E_H , is taken as the energy for provision of the hole, *i.e.*, favorable configuration. The Cohen–Turnbull expression may also be regarded as a version of this general equation in which the first term is taken as negligible and the second is calculated from the volume expansion above T_0 . Where this term seemed insufficient, the writer^{3b} and, in more detail, Macedo and Litowitz³⁹ have recovered eq 10 by combining the Cohen and Turnbull version of the second term with a nonzero first term. Bockris and co-workers^{40,41} have used essentially the same approach but have sought to calculate the second term by means of a theory by Fürth.⁴²

In the Adam and Gibbs theory it seems clear from the way eq 6 and 7 of ref 6c are developed that the "rearrangeable subsystems" are in effect sitting on top of the potential energy barrier, $\Delta\mu$, and must therefore be regarded as activated complexes. The theory is thus a new and interesting form of transition-state theory in which the potential energy ($\Delta\mu$) and configuration (S_c) terms occur in a relation (eq 5 of this paper) which does not permit their separation as in eq 10.

This is an important difference since it is on the basis of eq 10 that the belief has arisen that constant volume experiments can yield a "true" activation energy. According to the Adam–Gibbs expression, however, even if S_c were to remain constant at constant volume the configuration term would not be separated; it would only be made temperature independent, so that the Arrhenius plot slope would be constant at $-C/S_{c(v)}$. It can be argued that the pressure dependence of T_0 ^{8,43}

(33) A. T. Ward and G. J. Janz, *Electrochim. Acta*, **10**, 849 (1965).

(34) W. Eitel and W. Skalic, *Z. Anorg. Allgem. Chem.*, **183**, 263 (1929).

(35) R. K. Datta, D. M. Roy, S. P. Faile, and O. F. Tuttle, *J. Am. Ceram. Soc.*, **47**, 153 (1964).

(36) C. A. Angell, *ibid.*, **48**, 540 (1965).

(37) G. S. Fulcher, *ibid.*, **8**, 339 (1925). For recent applications of eq 2 to silicate and borate systems, see E. Eipeltaufer and K. Schaden, *Glastech. Ber.*, **35**, 505 (1962).

(38) While the viscosity and conductance temperature dependences are very similar in the two molten nitrate cases cited above, in silicate and borate melts there are great differences: at the same temperature E_η may be up to four times larger than E_k ; *i.e.*, $k_\eta \rightarrow 4k_k$ if eq 2 may be applied to each process (see, *e.g.*, G. W. Morey, "Properties of Glass," Reinhold Publishing Corp., New York, N. Y., 1938, p 461).

(39) P. B. Macedo and T. A. Litowitz, *J. Chem. Phys.*, **42**, 245 (1965).

(40) J. O'M. Bockris, E. H. Crook, H. Bloom, and N. E. Richards, *Proc. Roy. Soc. (London)*, **A255**, 558 (1960).

(41) J. O'M. Bockris and G. W. Hooper, *Discussions Faraday Soc.*, **32**, 218 (1961).

(42) R. Fürth, *Proc. Cambridge Phil. Soc.*, **37**, 352 (1941).

(43) C. A. Angell, L. J. Pollard, and W. Strauss, *J. Chem. Phys.*, **43**, 2899 (1965).

means S_c cannot be strictly constant at constant volume. However, this should only be important at low T/T_0 , which may be the reason that only Cole, *et al.*,²² working below $2T_0$ have observed non-Arrhenius behavior at constant volume. The more common finding^{23,44,45} is that the constant volume "activation energy," (better, "Arrhenius coefficient"^{5b}) E_v , is temperature independent within experimental error but is a strong and accelerating function of diminishing volume. If, in fact, holding the volume constant holds S_c at some effectively constant value, then the form of eq 5 predicts directly that the quantity defined as E_v should depend inversely on the value of S_c held constant. E_v should therefore show the same sort of curvilinear dependence on diminishing volume that E_p shows on decreasing temperature, as is indeed observed experimentally (*e.g.*, compare Figure 2 of ref 23, and Figure 5 of ref 44a with Figure 1 of this paper. The ability of the Adam-Gibbs theory to accommodate these observations contrasts favorably with that of the Macedo-Litowitz treatment,³⁹ the weakness of which in this respect has been pointed out by Brummer.⁴⁶

Due to the increase of S_c with temperature at constant pressure, E_p at a given volume must, of course, be greater than E_v at that volume, as has always proved the case in practice. While the data referred to above are for organic liquids there seems no reason to believe that similarly detailed measurements on fused salts⁴⁷ will differ in character.

Finally, the Adam-Gibbs equations may be related to the Doolittle-type free volume transport equations⁴⁸ by using the second-order transition Clapeyron equation⁴³ to substitute for ΔC_p in eq 6 above. This leads to the following expression, which is approximate in the same respects as eq 6 (see footnote 26)

$$w(T) = A \exp \frac{-C \frac{d \ln T_0}{dp}}{V \Delta \alpha (T - T_0)} = A \exp \frac{-b}{v_f} \quad (11)$$

V and $\Delta \alpha$ being the molar volume and change of expansion coefficient, respectively, at T_0 . The numerator of the exponential term should be constant at constant pressure, and the denominator may be regarded as an approximation for that part of the thermal expansion above T_0 which gives rise to liquid-like degrees of freedom. Unfortunately, this constitutes yet another definition of free volume (*cf.*, Cohen and Turnbull,^{7a} eq 4, this paper, and discussion in ref 48b): the presence of the $(T - T_0)$ factor in the denominator nevertheless ensures a correct description of the transport temperature dependence. Within the restrictions implied by

eq 11, the usefulness³⁶ of the free volume concept therefore remains intact.

This approach thus has a number of attractive features and, while not free from weaknesses, seems to represent an improvement over previous interpretations of the data. The thermodynamic treatment of short lifetime configurations is, however, no less open to criticism here than in the case of conventional transition state theory; some future development in the spirit of Rice's dynamical approach to crystal lattice diffusion⁴⁹ may be appropriate.

In conclusion, it may be noted that, in view of the intimate connection between transport properties of liquids and their thermodynamic states, transport measurements in general cannot be expected to give any deeper insight into structural details of the liquids than can be derived from other thermodynamic measurements such as entropies of fusion, heats of mixing, and activity coefficients. Exceptions are diffusion and relative mobility measurements which discriminate between entities in the same liquid.

For detailed structural information, one must rely on more direct techniques, principally the study of interactions between electromagnetic radiation quanta and ionic liquids. If the thermodynamic low-temperature limit of the liquid state is a glass in which a close-packed structure is approached, then interesting structural changes must occur in the low-temperature region usually "hidden" by the "crystallization curtain," since X-ray measurements⁵⁰ have shown that, at high temperatures, coordination numbers are well below close-packed values. There is reason to believe, therefore, that studies in the low-temperature region by use of noncrystallizing melts may be rewarding to our general understanding of fused-salt structure. The interesting phenomena of loss of nitrate ion rotational freedom,⁵¹ nonlinear temperature dependence of ultraviolet absorption spectra,²⁸ and temperature-induced

(44) (a) A. Jobling and A. S. C. Lawrence, *Proc. Roy. Soc. (London)*, **A206**, 257 (1951); (b) *J. Chem. Phys.*, **20**, 1296 (1952).

(45) S. B. Brummer and G. J. Hills, *Trans. Faraday Soc.*, **57**, 1823 (1961).

(46) S. B. Brummer, *J. Chem. Phys.*, **42**, 4317 (1965).

(47) M. K. Nagarajan, L. Nanis, and J. O'M. Bockris (*J. Phys. Chem.*, **68**, 2726 (1964)) and J. W. Tomlinson and D. J. Fray (D. J. Fray, Thesis London University, 1965) have initiated such measurements.

(48) (a) A. K. Doolittle, *J. Appl. Phys.*, **22**, 1471 (1951); (b) A. K. Doolittle and D. B. Doolittle, *ibid.*, **28**, 901 (1957).

(49) S. A. Rice, *Phys. Rev.*, **112**, 804 (1958).

(50) (a) H. A. Levy, R. A. Agron, and M. A. Bredig, *Ann. N. Y. Acad. Sci.*, **79**, 762 (1960); (b) J. Zarzicki, *Compt. Rend.*, **224**, 758 (1957); *J. Phys. Radium*, **19**, 13A (1958).

(51) J. K. Wilmshurst and S. Senderoff, *J. Chem. Phys.*, **35**, 1078 (1961).

coordination changes of 3d ions (*e.g.*, Ni(II),^{52,53} Co(II), and Mn(II)),⁵⁴ have all been observed in liquids whose transport behavior places them near or in their respective "low-temperature" [low T/T_0] regions. It may be instructive to study these phenomena in relation to the reduced temperatures on the entropy scale at which they are observed.

Acknowledgments. The author is indebted to Dr. D. M. Gruen and Professors N. H. Nachtrieb and J. H. Gibbs for interesting discussions of this subject.

(52) C. R. Boston and G. P. Smith, *J. Phys. Chem.*, **62**, 409 (1958).

(53) C. A. Angell and D. M. Gruen, *ibid.*, **70**, 1601 (1966).

(54) See ref 20, pp 300-305.

Mass Spectrometric Study of the Rates of the Reactions of

Nitrogen Atoms with Olefins

by John T. Herron

National Bureau of Standards, Washington, D. C. 20234 (Received January 27, 1966)

A mass spectrometric study has been made of the rates of the reactions of nitrogen atoms with a series of olefins. At 340°K the rates are: C₂H₄, $k \sim 1.0 \pm 0.5$; C₃H₆, $k = 1.9 \pm 0.6$; C₄H₈₋₁, $k = 2.0 \pm 0.4$; *t*-C₄H₈₋₂, $k = 1.7 \pm 0.4$; *i*-C₄H₈, $k = 4.2 \pm 1.0$; C₂(CH₃)₄, $k = 2.4 \pm 0.6$; C₄H_{6-1,3}, $k = 3.5 \pm 1.0$ (all $\times 10^{10}$ cm³ mole⁻¹ sec⁻¹). The mechanisms of these reactions are discussed.

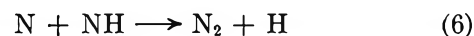
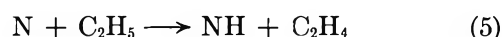
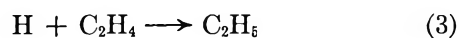
Introduction

Reliable rate data for nitrogen atom reactions are for the most part limited to inorganic reactants. In the case of organic reactants relatively few rate constants have been reported, and these are of doubtful validity in view of the uncertainty in the reaction mechanisms on which they are based.

Recent work on the nitrogen atom-ethylene reaction¹ has shown that it cannot be described adequately by the simple mechanism²



but probably also involves the following additional steps.



The apparent rate constant of reaction 1, which can be defined as

$$k = \ln [(C_2H_4)_0 / (C_2H_4)_t] / \int_0^t (N) dt$$

(where the subscripts refer to time zero and time t), was shown to be a function of $(C_2H_4/N)_0$. It was argued on the basis of the above mechanism that the true rate constant, k_1 , was the value of k at $(C_2H_4/N)_0 = 0$.

These rate measurements have now been extended to a series of olefins, permitting a test of the consistency and generality of the proposed mechanism.

(1) J. T. Herron, *J. Phys. Chem.*, **69**, 2736 (1965).

(2) H. G. V. Evans, G. R. Freeman, and C. A. Winkler, *Can. J. Chem.*, **34**, 1271 (1956).

Experimental Section

The general experimental approach (described in detail elsewhere^{1,3}) was to use a mass spectrometer in conjunction with a fast flow system to measure the partial pressures of reactants and products as functions of the initial partial pressure of the reactants or of time. The reaction time was varied from about 2 to 50 msec by adjusting the distance between the olefin inlet and the sampling orifice of the mass spectrometer. The temperature was 340°K.

Nitrogen atoms were generated by passing nitrogen at a total pressure of about 2 torr through a 2450-MHz electrodeless discharge.

It became apparent during the course of this work that "prepurified" grade nitrogen contained enough minor impurities to lead to gross errors in the measurement of rate constants. Therefore, the nitrogen was further purified by passing it at 1.3 atm over copper turnings heated to 500°, then through a trap filled with silica gel cooled with liquid oxygen, after which it passed through a pressure-reducing valve into the flow system where it flowed through a trap filled with glass beads cooled with liquid nitrogen.

The partial pressures of stable reactants and products were measured using an ionizing energy of 44 ev, while the relative nitrogen atom partial pressure was measured using an ionizing energy of 24 ev. The latter was put on an absolute basis by use of the nitric oxide titration technique.⁴ Although there has been some dispute as to the validity of this technique, the recent absolute pressure change experiments of Elias,⁵ supported by the esr measurements of Westenberg and DeHaas⁶ and of Von Weyssenhoff and Patapoff,⁷ would seem to establish its correctness beyond reasonable doubt.

Determination of the Rate Constants

If olefin A reacts only with nitrogen atoms, then

$$-\frac{d(A)}{dt} = k(N)(A)$$

By separating the variables and integrating between limits, the following expression for the rate constant can be derived

$$k = \ln(A)_0/(A)_t / \int_0^t (N)dt$$

where the subscripts refer to time zero and time t . Both numerator and denominator in this expression are experimentally measurable quantities. The numerator is the ratio of the partial pressure of olefin at time zero to its partial pressure at time t . The integral in the denominator is graphically evaluated from meas-

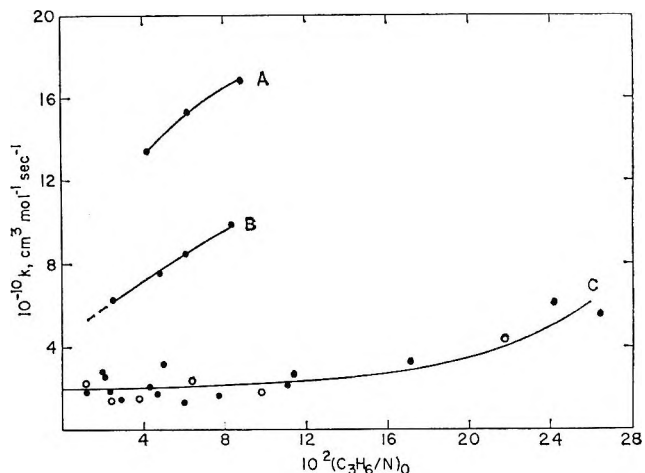


Figure 1. Apparent rate constant as a function of $(C_3H_6/N)_0$: curve C, highly purified nitrogen (open circles are data for C_2D_6); curve B, untreated, "prepurified" grade nitrogen; and curve A, highly purified nitrogen to which about 1% oxygen has been added before the discharge.

urement of the nitrogen atom partial pressure as a function of time.

Rate constants calculated from this expression for the reaction of nitrogen atoms with propene are shown in Figure 1 as a function of $(C_3H_6/N)_0$ for highly purified nitrogen, curve C, and untreated "prepurified" grade nitrogen, curve B. Curve A shows the effect of adding oxygen (before the discharge) to highly purified nitrogen.

The increase in apparent rate constant at high $(C_3H_6/N)_0$ ratios indicates that one (or more) of the reaction products is reacting with propene. The most reasonable assumption is that this reacting product is atomic hydrogen which is almost certainly a product of the reaction and is considerably more reactive toward olefins than is atomic nitrogen. Qualitative support for this view can be had by comparing the shapes of the apparent k vs. $(A/N)_0$ curves for different olefins as in Figure 2. The individual curves in this figure have been shifted to coincide at $(A/N)_0 = 0$. The manner in which the apparent rate constant varies with $(A/N)_0$ is in the same order as the relative rates of reactions with hydrogen atoms (Table I, column 4).

Adding hydrogen to the incoming nitrogen before it goes through the discharge should lead to the production

- (3) F. S. Klein and J. T. Herron, *J. Chem. Phys.*, **41**, 1285 (1964).
- (4) G. B. Kistiakowsky and G. G. Volpi, *ibid.*, **27**, 1141 (1957).
- (5) L. Elias, *ibid.*, **42**, 4311 (1965).
- (6) A. Westenberg and N. DeHaas, *ibid.*, **40**, 3087 (1964).
- (7) H. Von Weyssenhoff and M. Patapoff, *J. Phys. Chem.*, **69**, 1756 (1965).

Table I: Rates of Reaction of Atoms with Olefins at Room Temperature

	$10^{-10}k$, $\text{cm}^3 \text{mole}^{-1} \text{sec}^{-1}$	Relative k					
		N ^a	H ^b	O ^c	S ^d	Se ^e	Br ^f
Ethylene	$\sim 1.0 \pm 0.5$	~ 0.5	0.56	0.17	0.28	0.38	0.57
Propene	1.9 ± 0.6	1.0	1.00	1.00	1.00	1.00	1.00
Butene-1	2.0 ± 0.4	1.1	1.08	1.04	1.0	2.7	1.28
<i>t</i> -Butene-2	1.7 ± 0.4	0.9	0.59	4.90		21.6	5.56
Isobutene	4.2 ± 1.0	2.2	2.47	4.35		17.2	21.7
2,3-Dimethyl- butene-2	2.4 ± 0.6	1.3	0.81	18.2	>20		
1,3-Butadiene	3.5 ± 1.0	1.8	4.85	5.9		37.8	

^a This work (estimated uncertainties). ^b K. R. Jennings and R. J. Cvetanovic, *J. Chem. Phys.*, **35**, 1233 (1961). ^c R. J. Cvetanovic, *ibid.*, **30**, 19 (1959). ^d H. E. Gunning and O. P. Strausz, *Advan. Photochem.*, **1**, 248 (1963). ^e A. B. Callear and W. J. R. Tyerman, *Proc. Chem. Soc.*, 296 (1964). ^f P. I. Abell, *Trans. Faraday Soc.*, **60**, 2214 (1964).

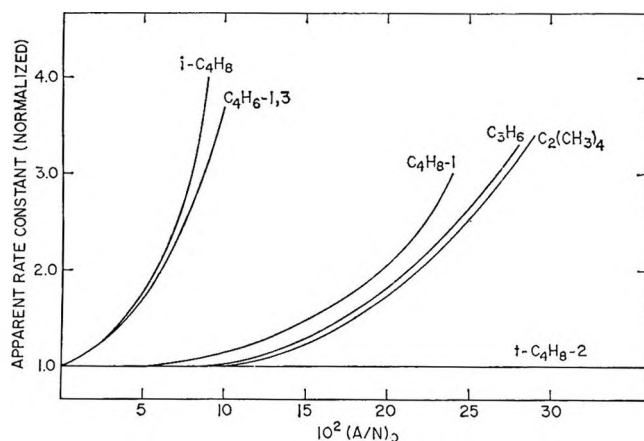
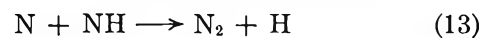
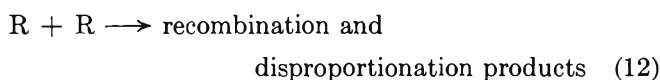
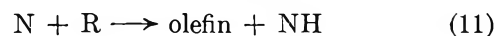
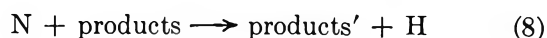
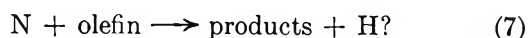


Figure 2. Apparent rate constants for a series of olefins as functions of $(A/N)_0$, normalized to a common origin. (The data for ethylene were too uncertain to be meaningful and have been omitted.)

of hydrogen atoms in addition to nitrogen atoms and hence to an increase in the apparent rate constant. Such an effect is observed as shown in Figure 3 where the apparent rate constant for the propene reaction is given as a function of $(C_3H_6/N)_0$ for differing amounts of added hydrogen. The most interesting feature of these experiments is that even with relatively large amounts of added hydrogen, the limiting value of the rate constant, *i.e.*, k at $(C_3H_6/N)_0 = 0$, is unaffected. By analogy with the mechanism postulated for the ethylene reaction (reactions 1-6), this would imply that propene is regenerated.⁸ The following general mechanism is proposed to account for these observations.⁹



At low conversion where H/N is very small, reaction 11 predominates over (10) and olefin lost in reaction 9 is regenerated. At higher conversions reactions 10 and 12 become more important and olefin is lost, leading to an increase in the apparent rate constant.

On the basis of this mechanism, the true rate constant of the reaction would be the value of k obtained under conditions such that H/N approaches 0, *i.e.*, at $(A/N) = 0$. Rate constants derived by extrapolating the apparent rate constants to $(A/N) = 0$ are given in Table I, column 2, for a series of olefins. The experimental data for the propene reaction are shown in Figure 1, curve C. Curve shapes for the other olefins studied are shown in Figure 3.

This mechanism is, of course, quite speculative. However, it may be noted that for very small values of $(A/N)_0$ the rate expression reduces to the usual approximation for a bimolecular rate constant with one reactant in great excess, *i.e.*

$$k = \ln (A)_0 / (A)_t / (N)t$$

(8) In studying the C_3D_6 reaction in the presence of added hydrogen, the formation of C_3D_5H is observed. It is not certain how much of the C_3D_5H is formed by reactions 9 and 11 and how much by reaction 12 or by simple isotopic exchange.

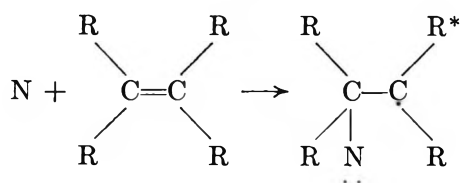
(9) This is a greatly simplified mechanism in which reactions 9 and 10 have been written only in terms of the formation of pressure stabilized products. For olefins other than ethylene this is approximately correct.

where (N) is approximately constant. Since hydrogen and oxygen atom reactions are 10 to 100 times faster than the corresponding nitrogen atom reactions, the presence of even trace amounts of these impurities could affect the measured rate constants.

In the case of hydrogen atoms, it is apparent from Figure 3 that adding hydrogen has no effect on the extrapolated rate constant so that trace impurities are of no consequence. This is certainly not the case for oxygen atom reactions as is shown from curve A of Figure 1. However, if the relative rates of the nitrogen atom reactions are compared with the relative rates of the corresponding oxygen atom reactions, there are seen to be considerable differences. In particular, the 18-fold greater reactivity of tetramethylethylene compared with propene in the case of oxygen atom reactions is not reflected in the comparable rates of the nitrogen atom reactions. Thus it seems safe to conclude that oxygen atom reactions are not making a major contribution to the measured nitrogen atom rate constants.

Discussion

As can be seen from Table I, the relative rates of the nitrogen atom reactions are quite different from those for the electrophilic atomic reactants O, S, Se, and Br. On the other hand, the similarities between atomic nitrogen and hydrogen suggest that the initial step may be the same for both reactants, *i.e.*, addition to the least substituted carbon atom of the double bond to yield an excited radical intermediate



The subsequent rearrangement, cyclization, and decomposition reactions of this intermediate can then give rise to the final products. The details of the mechanism are not known since the nature and the relative abundances of the nitrogen-containing products have yet to be determined for a significant number of reactants. Aside from hydrogen cyanide and methyl cyanide, the only other nitrogen-containing products detected in the present work were compounds of molecular weight corresponding to CN-substituted olefins. Such products have been reported previously in the case of the ethylene and propene reactions and were attributed to CN radical reactions with the reactant olefins.¹⁰ The identification of the same products in the photolysis of ICN in the presence of olefins appears to support this postulate.¹¹ However, the possibility

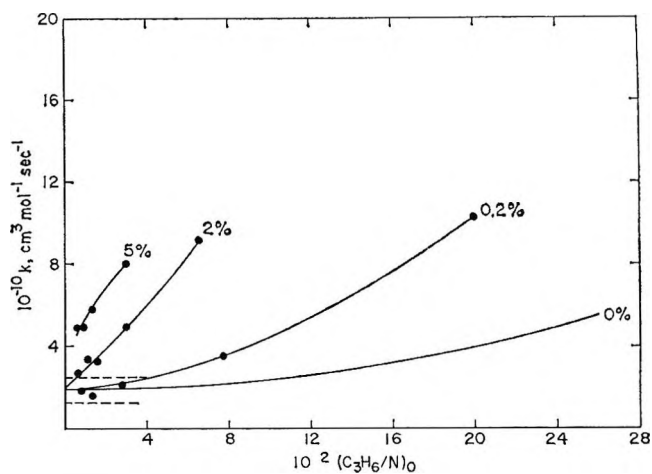
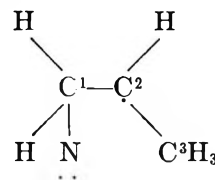


Figure 3. Apparent rate constant as a function of $(C_3H_6/N)_0$ for different amounts of added hydrogen. (Data points for 0% added hydrogen are given in Figure 1, curve C, and are not included here for the sake of clarity.)

that some of these products are degradative or even cyclic in nature cannot be ruled out.

There is some evidence to suggest that cyclization reactions may be of importance. Shinozaki, Shaw, and Lichtin¹² have studied the propene reaction using labeled carbon atoms to trace the origins of the products. The major products are ethylene, hydrogen cyanide, and in lesser yield, methyl cyanide. It was found that both methyl cyanide and ethylene were preferentially formed from the carbon atoms of the original double bond. If, as postulated above, the initially formed intermediate is the triradical



then the formation of $NC^1-C^2H_3$ is readily understood to arise by the splitting off a C^3H_3 group¹³ following rearrangement. However, the formation of $H_2C^1=C^2H_2$,¹⁴ which is almost certainly accompanied by the

(10) J. T. Herron, J. L. Franklin, and P. Bradt, *Can. J. Chem.*, **37**, 579 (1959).

(11) C. A. Goy, D. H. Shaw, and H. G. Pritchard, *J. Phys. Chem.*, **69**, 1504 (1965).

(12) Y. Shinozaki, R. Shaw, and N. N. Lichtin, *J. Am. Chem. Soc.*, **86**, 341 (1964).

(13) By analogy with the propene reaction it might be expected that ethyl cyanide would be a product of the butene-1 reaction. However, this product was not detected, possibly because its mass spectrum could have been masked by the mass spectra of product hydrocarbons.

formation of HC³N, would seem to require the formation of a four-membered cyclic intermediate which may have too short a lifetime to be detectable. For larger olefins, however, there is the possibility of forming five- and six-membered rings which are inherently more stable and which may be detectable. Tsukamoto and Lichtin¹⁵ have reported the formation of pyrrole (cyclic C₄H₅N) as a product of the butadiene reaction. It is difficult to explain the formation of this product

except through the formation of a five-membered cyclic intermediate which yields pyrrole by loss of a hydrogen atom.

(14) Ethylene may be formed directly in the reaction $N + C_2H_6 \rightarrow C_2H_4 + H + HCN$, or by the decomposition of a "hot" ethyl radical formed in the reaction $N + C_2H_6 \rightarrow C_2H_5^* + HCN$. If ethyl radicals are a primary product, they may also be stabilized and yield ethylene via the reaction $N + C_2H_5 \rightarrow C_2H_4 + NH$.

(15) A. Tsukamoto and N. N. Lichtin, *J. Am. Chem. Soc.*, **84**, 1601 (1962).

Nuclear Magnetic Resonance of Oxygen-17 and Chlorine-35 in Aqueous Hydrochloric Acid Solutions of Iron(III)¹

by A. H. Zeltmann and L. O. Morgan²

University of California, Los Alamos Scientific Laboratory, Los Alamos, New Mexico, and Department of Chemistry, The University of Texas, Austin, Texas (Received February 3, 1966)

Nuclear magnetic resonance spectra of O¹⁷ and Cl³⁵ were observed for iron(III) solutions from 0.85 to 13.6 *M* in HCl. Transverse relaxation of each was found to be controlled by the rate of chemical exchange of H₂O or Cl⁻ in the lowest part of that range, by relaxation rate in complex iron(III) species in the upper range, and by both processes in the intermediate range. H₂O was found to exchange principally between the species Fe-(H₂O)₃Cl₃ and the surrounding solvent according to the rate law, $R_{H_2O} = k_{H_2O} [Fe(H_2O)_3Cl_3] a_{\pm}$ mole/l. sec, with $k_{H_2O} = 2.19 \times 10^5$ l./mole sec at $26 \pm 1^\circ$; Cl⁻, between FeCl₄⁻ and solution Cl⁻ according to $R_{Cl^-} = k_{Cl^-} [FeCl_4^-] a_2$ mole/l. sec, with $k_{Cl^-} = 1.17 \times 10^5$ l./mole sec at $26 \pm 1^\circ$. The activities a_{\pm} and a_2 refer to the mean-ion and solute activities of HCl, respectively. Relaxation of ligand nuclei in the complex species is by electron nuclear spin exchange interaction. Coupling constants were found to be $(A/h)_{Cl} = 1.1 \times 10^7$ cps for Cl³⁵ in FeCl₄⁻ and $(A/h)_O = 3 \times 10^7$ cps for O¹⁷ in Fe(H₂O)₃Cl₃.

Introduction

Exchange of water molecules and chloride ions between the coordination spheres of the various iron(III) chloro complexes and bulk solvent has been investigated by Connick and co-workers³⁻⁶ using nuclear magnetic resonance techniques. In the main, those investigations were carried out at low chloride concentrations, where the lower chloro species predominate, and the solutions were principally aqueous sodium chloride.

Blatt⁵ has examined a few concentrated HCl solutions, but not in great detail. Her results are discussed together with those of this work in a later section.

(1) Work performed under the auspices of the U. S. Atomic Energy Commission.

(2) Department of Chemistry, The University of Texas, Austin, Texas 78712.

(3) R. E. Connick and R. E. Poulson, *J. Chem. Phys.*, **30**, 759 (1959).

Iron(III) chloride solutions in concentrated HCl have long been of interest because of the ability of iron(III) and numerous other metal(III) ions to be extracted from such solutions into organic solvents⁷ such as diethyl ether. The species present in iron(III) chloride-hydrochloric acid solutions have been investigated^{8,9} electrometrically and spectrophotometrically as well as by solvent distribution. It is believed that the lower chloro complexes are predominantly octahedral with water molecules occupying the sites not filled by chloride ions, while the tetrachloro species is tetrahedral. Evidence has been presented that the tetrachloro complex is the highest one formed in aqueous HCl solutions.¹⁰⁻¹² Friedman¹² has given the most definitive evidence for four-coordination from ultraviolet and visible spectra of solid tetrachloroferrates, ethylene bromide, diisopropyl and diethyl ether solutions, aqueous HCl solutions, and ether extracts of the latter.

Recently, the spectral evidence for complex configurations¹³ has been interpreted to suggest that the trichloroiron(III) species in HCl solutions is also four-coordinated and tetrahedral. The arguments presented there are somewhat indicative, but hardly conclusive. We must assume that the configuration of the trichloro species is not well established, and consider the possibility that both octahedral and tetrahedral species may be present, depending upon circumstances.

In the interpretation of results of the work reported here, we have relied upon the formation constants of Gamlen and Jordan⁹ for the trichloro and tetrachloro-iron(III) species, and those of Rabinowitch and Stockmayer⁸ for monochloro and dichloro species. Activities of HCl are those listed by Robinson and Stokes,¹⁴ which are sufficiently close to those used¹⁵ by Gamlen and Jordan to ensure that the calculation of species concentrations is not seriously in error. The assumptions made in the calculations were the same as those used in obtaining the constants, the most notable of which is that the ratio of activity coefficients of successive members of the coordination series is a constant.^{16,17} Thus the formation constants are not thermodynamic. However, since our principal interest is in recovering the species concentrations from the constants listed by Gamlen and Jordan, it is only necessary that we follow the same procedures and assumptions they did.

In the following sections we report the results of experimental investigation, by magnetic resonance methods, of iron(III) chloride solutions in 0.85-13.6 M HCl.

Experimental Section

Reagents. Iron(III) perchlorate was prepared by

dissolving chemically pure iron in concentrated perchloric acid. Small amounts of iron(II) ion were oxidized to iron(III) by addition of hydrogen peroxide, the excess of which was destroyed by heating. Crystals of iron(III) perchlorate separated from the solution and were recrystallized from perchloric acid solution. Analysis of the salt corresponded to the formula: $\text{Fe}(\text{ClO}_4)_3 \cdot 10.5\text{H}_2\text{O} \cdot 0.65\text{HClO}_4$. Concentrated HCl, Baker Analyzed, was used in the preparation of all solutions except 13.6 M HCl, which was prepared by supersaturating H_2O^{17} with Matheson tank HCl gas. H_2O^{17} was prepared from NO^{17} by reaction with hot copper to form CuO^{17} , followed by reduction with H_2 to form H_2O^{17} which was redistilled after addition of a small amount of metallic sodium to remove acidic impurities. Analysis for oxygen isotopes 16, 17, and 18 was made mass spectrometrically after complete conversion of samples of water to CO_2 .

Nuclear Measurements. All measurements were made using a Varian wide-line nuclear resonance spectrometer. Both O^{17} and Cl^{35} resonances were observed by phase detection with the spectrometer frequency locked on 8 and 5 Mc/sec, respectively, with either 20- or 40-cps field modulation. The Cl^{35} resonance was broadened by the modulation frequency in the most dilute HCl blanks when phase detection was used even at 20 cps. Therefore, the side-band technique as de-

(4) R. E. Connick and C. P. Coppel, *J. Am. Chem. Soc.*, **81**, 6389 (1959).

(5) E. Blatt, Ph.D. Thesis, University of California, Aug 1964 (UCRL-11584, Lawrence Radiation Laboratory). We were unaware of the part of that research dealing with HCl solutions at high concentrations until this work was completed, and are indebted to Professor R. E. Connick for supplying us with a copy of the thesis.

(6) E. C. Blatt and R. E. Connick, Proceedings of the 8th International Congress on Coordination Chemistry, Vienna, 1964, p 284.

(7) See, for instance, R. M. Diamond, and D. G. Tuck, *Progr. Inorg. Chem.*, **2**, 158 (1960).

(8) E. Rabinowitch and W. H. Stockmayer, *J. Am. Chem. Soc.*, **64**, 335 (1942).

(9) G. A. Gamlen and D. O. Jordan, *J. Chem. Soc.*, 1435 (1953), and references cited therein.

(10) N. H. Nachtrieb and J. G. Conway, *J. Am. Chem. Soc.*, **70**, 3547 (1948).

(11) R. J. Myers, D. E. Metzler, and E. H. Swift, *ibid.*, **72**, 3767 (1950).

(12) H. L. Friedman, *ibid.*, **74**, 5 (1952).

(13) I. I. Antipova-Karataeva, Yu. A. Zolotov, and I. V. Seryakova, *Zh. Neorg. Khim.*, **9**, 1712 (1964) [*Russ. J. Inorg. Chem.*, **9**, 927 (1964)].

(14) R. A. Robinson and R. H. Stokes, "Electrolyte Solutions," 2nd ed, Academic Press, Inc., New York, N. Y., 1959, pp 491, 504.

(15) G. Åkerlöf and J. W. Teare, *J. Am. Chem. Soc.*, **59**, 1855 (1937).

(16) J. Bjerrum, *Kgl. Danske Videnskab. Selskab., Mat.-fys. Medd.*, **22**, No. 18 (1946).

(17) R. Näsänen, *Acta Chem. Scand.*, **4**, 140, 816 (1950).

Table I: Oxygen-17 and Chlorine-35 Line Broadening in Aqueous HCl Solutions at 26 ± 1°

Molarity of HCl	a_{\pm}^a	a_1^b	α_1^c	α_2^c	α_3^c	α_4^c	$pCl^{d} \times 10^3$	$pO^{e} \times 10^3$	$(T_2 pCl')^{-1}, \text{sec}^{-1} \times 10^{-5}$	$(T_2 pO')^{-1}, \text{sec}^{-1} \times 10^{-6}$
0.85	0.72	0.98	0.167	0.540	0.284	0.002	...	6.21	...	0.916
2.28	2.64	0.91	0.028	0.326	0.629	0.018	30.5	1.31	0.120	3.68
2.79	4.09	0.87	0.013	0.239	0.717	0.031	19.2	...	0.376	...
2.80	4.10	0.87	0.013	0.239	0.717	0.031	28.1	1.55	0.396	6.12
3.36	6.03	0.83	0.006	0.175	0.770	0.049	4.65	...	0.823	...
3.68	7.33	0.80	...	0.147	0.787	0.061	23.0	1.68	1.73	13.5
3.92	8.08	0.80	...	0.135	0.797	0.068	71.8	5.50	2.48	14.9
4.15	9.84	0.76	...	0.112	0.803	0.083	23.0	1.91	2.85	15.5
4.29	10.69	0.76	...	0.103	0.806	0.090	17.8	...	2.90	...
4.30	10.72	0.76	...	0.103	0.804	0.091	18.4	1.57	3.16	18.0
5.56	21.5	0.66	...	0.050	0.775	0.175	9.68	1.09	10.94	30.1
7.04	51.3	0.52	...	0.017	0.639	0.344	10.7	1.59	20.17	54.2
9.26	172	0.30	0.356	0.644	7.44	1.53	40.51	43.7
9.68	226	0.30	0.297	0.703	2.22	...	42.68	...
10.57	386	(0.23) ^f	0.198	0.802	7.91	2.00	44.6	12.3
10.96	475	(0.21) ^f	0.167	0.833	0.874	...	42.49	...
11.93	799	(0.15) ^f	0.106	0.894	5.67	1.70	47.4	4.99
13.60	(1208) ^f	(0.12) ^f	(0.073) ^f	(0.927) ^f	5.50	1.78	52.81	3.55

^a See ref 14, pp 491 and 504. ^b J. N. Pearce and A. F. Nelson, *J. Am. Chem. Soc.*, **55**, 3075 (1933). ^c See ref 9. α_n is the mole fraction of Fe(III) species with nCl^- . ^d Mole ratio: total Fe(III)/total Cl^- . ^e Mole ratio: total Fe(III)/total H_2O . ^f Estimated from data at lower HCl concentrations.

scribed by Acrivos¹⁸ was used to measure the line width for the narrowest lines. The modulation frequency thus employed was 398 cps. All measurements, except those of temperature dependence, employed narrow-neck, thin-walled, spherical bulbs containing approximately 2.5 ml. of solutions at ambient temperature, 26 ± 1°. Temperature dependence measurements were made in a vacuum-jacketed cylindrical vessel essentially as described by Swift and Connick.¹⁹ Heated or cooled nitrogen was passed through the nmr cell to maintain the desired temperatures. The field strength of the magnet was monitored at intervals using a Pound-Knight magnetometer with an Li⁷ probe.

Results

Oxygen-17 and chlorine-35 line widths (derivative of absorption, peak-to-peak), measured in the various HCl solutions and corrected for the contribution of corresponding bulk solvent in each case, are listed in Table I. They are given in columns 10 and 11 in terms of T_2^{-1} , normalized by the mole ratio of total iron(III) to total exchanging species, according to the relation

$$(T_2 p_B')^{-1} = \pi(3)^{1/2} \Delta\nu \text{ (moles of B/moles of Fe)} \quad (1)$$

which is valid for an absorption line of Lorentzian shape. In those cases for which the side-band technique was used, T_2 is related to the width of half-maximum amplitude of the side band by

$$(T_2 p_B')^{-1} = \pi \Delta\nu_s \text{ (moles of B/moles of Fe)} \quad (2)$$

The symbols a_1 , a_2 , and a_{\pm} refer to water, hydrogen chloride, and mean ion activities, respectively. Mole fractions of the species $FeCl^{2+}$, $FeCl_2^+$, $FeCl_3$, and $FeCl_4^-$ are listed in the columns headed α_1 , α_2 , α_3 , and α_4 , as calculated from the constants given by Gamlen and Jordan⁹ and by Rabinowitch and Stockmayer⁸ in terms of a_{\pm} .

Representative values of the line widths in HCl solutions, in the absence of iron(III) salts, are listed in Table II, together with the line center positions relative to pure H_2O at 26 ± 1°.

Line widths were obtained as a function of temperature over the entire concentration range. Illustrative data are presented in Figures 1 and 2. Again each value was corrected for contribution of the solvent at the same temperature.

Discussion

Treatment of Data. In the case that the chemical shift is small compared to line broadening in paramagnetic ion solutions, the transverse magnetic relaxation time, T_2 , of nuclei interacting with the paramagnetic ion and undergoing chemical exchange with bulk solvent is given in eq. 3.

(18) J. V. Acrivos, *J. Chem. Phys.*, **36**, 1097 (1962).

(19) T. J. Swift and R. E. Connick, *ibid.*, **37**, 307 (1962).

$$(T_2)^{-1} = (T_{2A})^{-1} + \sum_i [p_B' \alpha_i n_i / (\tau_i + T_{2i})] \quad (3)$$

$$p_{B_i} = p_B' \alpha_i n_i$$

in which T_{2A} is the observed relaxation time in bulk solvent, p_B' is the mole ratio of total paramagnetic ion to exchanging ion or molecule, α_i is the mole fraction of species i , n_i is the coordination number of exchanging ion or molecule in species i , τ_i is its residence time in the species, and T_{2i} is the relaxation time of the nucleus of interest in the species. This equation is a restricted

Table II: Oxygen-17 and Chlorine-35 Relaxation Rates and Chemical Shifts in HCl Solutions at $26 \pm 1^\circ\text{C}$

Solution M HCl	Relaxation rate, T_2^{-1} , sec $^{-1}$		Chemical shift, ^b cps	
	O ¹⁷	Cl ³⁵	O ¹⁷	Cl ³⁵
0	195	...	0	0 ^c
1.0	196	63	4	3
4.0	203	67	44	15
7.0	228	103	97	38
9.0	256	170	145	71
12.0	273	570	262	107

^a O¹⁷ at 8.000 Mc/sec; Cl³⁵ at 5.000 Mc/sec. ^b Downfield. ^c Extrapolated limit.

version of the more complete one given by Swift and Connick¹⁹ (their eq 9), which was derived using the modified Bloch equations of McConnell.²⁰ A similar equation for two components (bulk solvent and coordinated water molecules) was obtained by Pearson, Palmer, Anderson, and Allred.²¹ An essentially different approach was taken independently by Zimmerman and Brittin,²² whose conclusions reduce to the same result when applied to dilute solutions of paramagnetic ions. This representation is generally used in connection with coordination effects and T_{2A} is assumed to include any of those arising from secondary or more distant association. The latter are usually small and are neglected here.

The probability factor $p_B' \alpha_i n_i$ has been specified in terms of its components in order to simplify analysis of the data in terms of individual ionic species and to be able to represent the observed quantities in unambiguous experimental terms.

In the following sections, the normalized relaxation time, $T_2 p_B'$, corrected for bulk solvent contribution, is presented as a function of HCl concentration, and a model representation, in terms of the magnetic interactions and solution composition, is sought.

Oxygen-17 Relaxation. A preliminary examination of the O¹⁷ relaxation data suggested a strong depend-

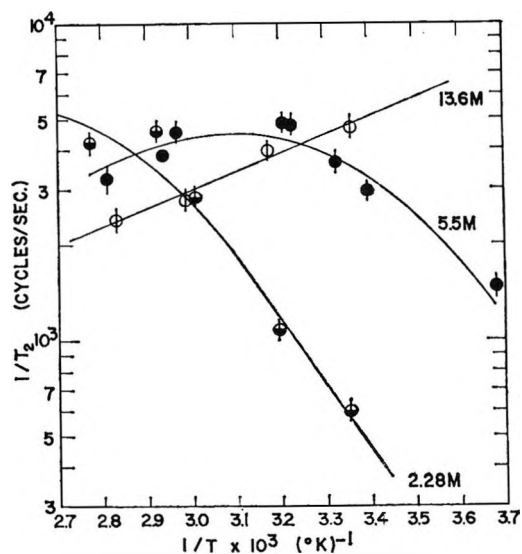


Figure 1. Temperature dependence of O¹⁷ relaxation. At 13.6 M HCl, activation energy equals -2.7 kcal/mole; at 2.28 M HCl, 9.5 kcal/mole.

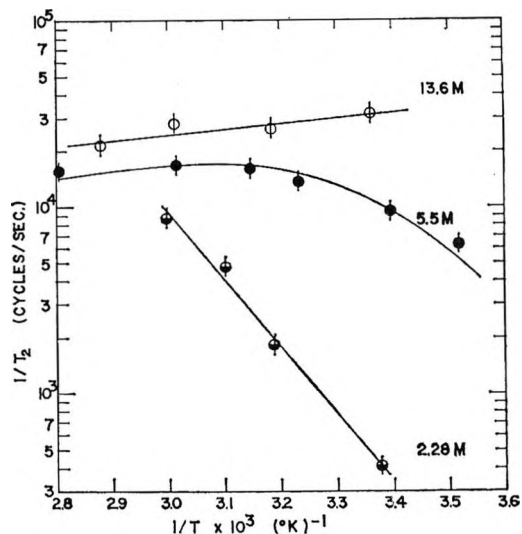


Figure 2. Temperature dependence of Cl³⁵ relaxation. At 13.60 M HCl, activation energy equals -1.4 kcal/mole; at 2.28 M HCl, 16.6 kcal/mole.

ence upon the concentration of FeCl₃, which we assume to be principally Fe(H₂O)₃Cl₃. Neglecting other species, as a first approximation, we have

$$(T_2 p_{O'})^{-1} = 3 \alpha_3 / (\tau_3 + T_{23}) \quad (4)$$

If τ_3 remains constant as HCl concentration is increased

(20) H. M. McConnell, *J. Chem. Phys.*, **28**, 430 (1958).

(21) R. G. Pearson, J. Palmer, M. M. Anderson, and A. L. Allred, *Z. Elektrochem.*, **64**, 110 (1960).

(22) J. R. Zimmerman and W. E. Brittin, *J. Phys. Chem.*, **61**, 1328 (1957).

and if the nature of exchanging species does not change, then $(3T_2p_O'\alpha_3)^{-1}$ should remain constant also. In fact, that quantity is found to increase linearly with a_{\pm} at low HCl concentrations, approach constancy at intermediate concentrations, and then decrease at the highest concentrations ($>8 M$). This suggests that τ_3 decreases with increasing a_{\pm} , becomes less than T_{23} at larger a_{\pm} , and that a change of effective exchanging species occurs at about $8 M$.

Analysis of the data listed in column 11, Table I, for concentrations less than $8 M$ HCl letting $\tau_3 = (k_3a_{\pm})^{-1}$ sec, indicates that best fit is obtained with $k_3 = 7.30 \times 10^4$ l./mole sec and $T_{23} = 9.0 \times 10^{-8}$ sec. Points in Figure 3 are experimental values of $(T_2p_O')^{-1}$ vs. HCl molarity; the solid curve was calculated from the preceding constants. The normalized relaxation rate at $0.85 M$ HCl reveals the contribution of dichloro and/or monochloroiron(III) ions to the over-all relaxation. Experimental points in the concentration range above $8 M$ HCl lie on a curve (dashed line in Figure 3) which is well below the rapid exchange limit expected from analysis of the data at lower concentrations. Although it has not been verified independently, the most plausible explanation is that the rapidly decreasing activity of water in that region causes a change in the actual trichloroiron(III) species, from $Fe(H_2O)_3Cl_3$ to $Fe(H_2O)Cl_3$, perhaps.

There appears to be little need to have recourse to other species to justify the observed O¹⁷ relaxation at HCl concentrations between 2 and $8 M$. It should be noted that observed relaxation rates in iron(III)-HCl solutions are considerably greater than those in sodium chloride solutions at equivalent activities,^{5,6} so that the mechanisms for exchange assumed there are not of primary importance in consideration of relaxation in concentrated HCl solutions.

The dependence of τ_3 on a_{\pm} and of exchange controlled relaxation rate on concentration of $Fe(H_2O)_3Cl_3$ may be conveniently expressed in the form of a rate law for H₂O exchange

$$R_{H_2O} = k_{H_2O}[Fe(H_2O)_3Cl_3]a_{\pm} \text{ mole/l. sec}$$

with $k_{H_2O} = 3k_3$ l./mole sec, and, at the lowest concentrations, $R_{H_2O} = (T_2p_O')^{-1}$ (total Fe(III) molarity) mole/l. sec, which is valid if $\tau_3 \gg T_{23}$.

Temperature dependence data for O¹⁷ relaxation in three HCl solutions are presented in Figure 1. At $2.28 M$ HCl, relaxation is principally chemical exchange rate-controlled, while at $6.0 M$, and above, relaxation in the complex ion predominates. At $5.5 M$ the shift from one mechanism to the other is observed at about 35° . In the low concentration region, the observed dependence is compatible with a chemical

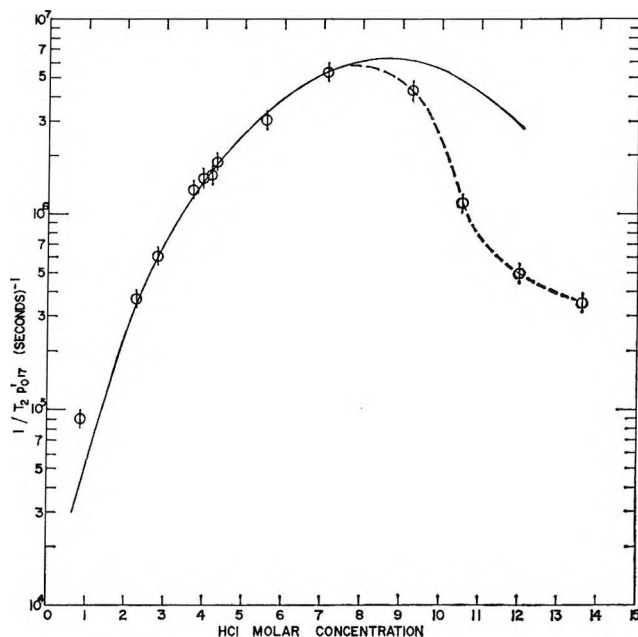


Figure 3. Concentration dependence of O¹⁷ relaxation at 26° . Solid line obtained from $\tau_3 = (k_3a_{\pm})^{-1}$, with $k_3 = 7.30 \times 10^4$ l./mole sec and $T_{23} = 9.0 \times 10^{-8}$ sec. Dashed line represents observed behavior at high concentrations of HCl.

process having an activation energy of 9.5 kcal/mole, while at high concentrations ($7 M$ and above) the temperature dependence is negative with an apparent activation energy of 2.7 kcal/mole.

Without further experimental evidence on this and related systems, it is not possible to assign a mechanism to the exchange process unequivocally. There are several possibilities that appear attractive and bear consideration.

(1) Exchange of H₂O occurs as the result of electrophilic attack by the hydrated proton, $H(H_2O)_z^+$, on the $Fe(H_2O)_3Cl_3$, a water molecule is removed and subsequently replaced from the surrounding solvent. This suggests that the Hammett acidity function would be more proper for correlation of the data than is a_{\pm} . However, that function rises too rapidly with increasing HCl concentration and the best fit to observed relaxation rates is not as good.

(2) Exchange of H₂O occurs as the result of displacement by Cl^- in the first coordination sphere. This is the mechanism that might at first glance seem most likely, but it cannot be supported. If such displacement occurs, it must also serve as a relaxation mechanism for Cl³⁵ in the solution. At the lower HCl concentrations it would lead to a Cl³⁵ relaxation rate that is as much as ten times greater than that observed. Chloride ion could be responsible for the H₂O exchange if it does not enter the first coordination sphere.

(3) Exchange is enhanced by a change in relative activities of $\text{Fe}(\text{H}_2\text{O})_3\text{Cl}_3$ and its possible dehydration products. In effect, this would suggest that the unimolecular dissociation rate of $\text{Fe}(\text{H}_2\text{O})_3\text{Cl}_3$ increases with change in solvent structure as the HCl concentration is increased.

Chlorine-35 Relaxation. The striking increase in Cl^{35} relaxation rate with increasing HCl concentration suggests a correlation with trichloroiron(III) or tetrachloroiron(III) and some function of the HCl activity. Of the correlations attempted, best fit with the experimental data was obtained by consideration of the concentration of FeCl_4^- and a_{\pm}^2 or a_2 . Once again, from eq 3

$$(T_2 p_{\text{Cl}^{35}})^{-1} = 4\alpha_4/(\tau_4 + T_{24}) \quad (5)$$

At the highest HCl concentrations, we obtain $T_{24} = 7.0 \times 10^{-7}$ sec, and from $\tau_4 = (k_4 a_{\pm}^m)^{-1}$ at the lower concentrations, analysis of the data leads to $k_4 = 2.92 \times 10^4$ l./mole² sec and $m = 2$. Calculated values of $(T_2 p_{\text{Cl}^{35}})^{-1}$ using those values are presented as the solid line in Figure 4. For comparison, the best fit with $m = 1$ is found with $k_4' = 1.12 \times 10^6$ l./mole sec, and is represented by the dashed line in Figure 4.

Again, the temperature dependences of Cl^{35} relaxation rate corroborate the occurrence of chemical exchange control at the lower concentrations and relaxation control at the higher. In the chemical exchange region, the apparent activation energy is 16.6 kcal/mole and in the relaxation limiting region, -1.4 kcal/mole (Figure 2). Because $a_{\pm}^2 = a_2$, τ_4 is alternatively given by $\tau_4 = (k_4 a_2)^{-1}$; $k_4 = 2.92 \times 10^4$ l./mole sec. Among the various possible mechanisms leading to such a dependence, it is felt that the most probable is one in which the hydrogen chloride molecule interacts with FeCl_4^- . However, it is possible that the active species is the hydrogen-chloride ion pair, since the dependence on a_2 is the same in either case.

As with H_2O exchange, the rate of Cl^- exchange may be related to the constants and concentrations of reacting species

$$R_{\text{Cl}^-} = k_{\text{Cl}^-}[\text{FeCl}_4^-]a_2 \text{ mole/l. sec}$$

with $k_{\text{Cl}^-} = 4k_4$ l./mole sec, and if $\tau_4 \gg T_{24}$, $R_{\text{Cl}^-} = (T_2 p_{\text{Cl}^{35}})^{-1}$ (total Fe(III) molarity) mole/l. sec.

Nuclear-Electron Spin Exchange. The epr (electron paramagnetic resonance) line width (derivative peak-to-peak width) of hexaquoiron(III) ions in 2 M HNO_3 (ca. 27°) is 1100 gauss²³ while for the complex iron(III) species in 12 M HCl (25°) the observed line width is 615 gauss.⁵ A value of 600 gauss (at 26°) was independently observed in this laboratory. Assuming the latter value to be that for FeCl_4^- , the corresponding

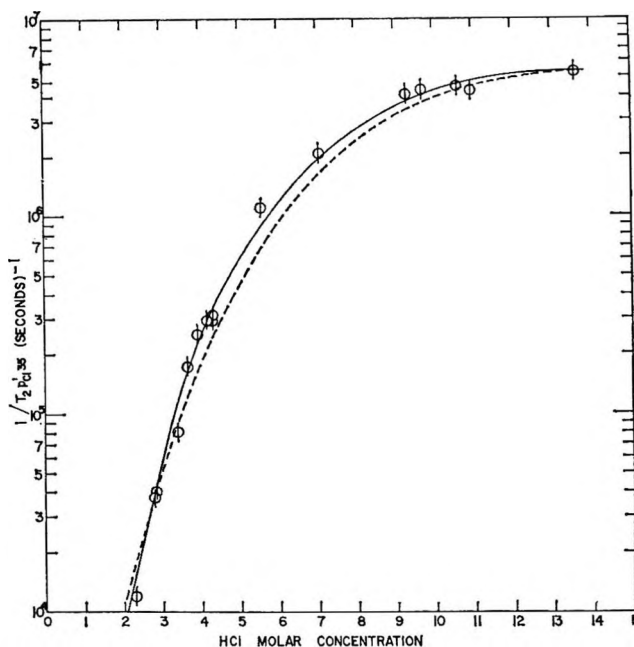


Figure 4. Concentration dependence of Cl^{35} relaxation at 26°. Solid line obtained from $\tau_4 = (k_4 a_2)^{-1}$, with $k_4 = 2.92 \times 10^4$ l./mole sec and $T_{24} = 7.0 \times 10^{-7}$ sec. Dashed line obtained $\tau_4 = (k_4' a_{\pm})^{-1}$, with $k_4' = 1.12 \times 10^6$ l./mole sec, $T_{24}' = 7.0 \times 10^{-7}$ sec, and $m = 1$.

transverse electron relaxation times, T_{2e} , are 6×10^{-11} and 1×10^{-10} sec for $\text{Fe}(\text{H}_2\text{O})_6^{3+}$ and FeCl_4^- , respectively. If T_{1e} , the longitudinal electron relaxation time, is equal to T_{2e} in each case, it is possible to estimate the ligand electron-nuclear exchange constants, (A/\hbar) or (A/h) , with suitable assumptions as to the identities of iron(III) species.

For Cl^{35} , the value of T_{24} , the nuclear transverse relaxation time in the species FeCl_4^- , was found to be 7.0×10^{-7} sec from eq 5. Relaxation is attributable to dipole-dipole, quadrupole, and isotropic contact interactions. Assuming the last ($A \cdot S$) to make the dominant contribution, the value of the constant (A/h) may be estimated from the relation given by Bloembergen²⁴

$$(T_{24})^{-1} = (1/3)S(S+1)(A/h)^2\tau_e \quad (6)$$

in which S is the spin of the ion. The spin-exchange correlation time, τ_e , may be identified with ligand residence time, τ_l , or with T_{1e} , whichever is shorter. In both cases considered here, it is almost certainly true that $\tau_e = T_{1e}$. Then, for Cl^{35} in FeCl_4^-

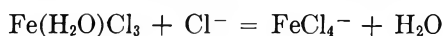
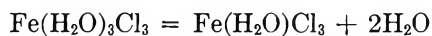
$$\begin{aligned} (A/h)_{\text{Cl}^{35}} &= \left\{ 1 / [(7.0 \times 10^{-7})(1/3)(35/4)(1 \times 10^{-10})] \right\}^{1/2} \\ &= 7.0 \times 10^7 \text{ radians/sec} \end{aligned}$$

(23) B. R. McGarvey, *J. Phys. Chem.*, **61**, 1232 (1957).

(24) N. Bloembergen, *J. Chem. Phys.*, **27**, 572 (1957).

and $(A/h)_{Cl} = 1.1 \times 10^7$ cps. The close correspondence of this value with that calculated from chemical shift data in the following discussion suggests that the contact interaction is indeed the principal contributor to relaxation in this case.

The association of the observed epr line in 12 *M* HCl with FeCl₄⁻ is based largely on the fact that it is expected to be the predominant species in very concentrated HCl solutions. Blatt⁵ has reported that the intensity of the FeCl₄⁻ epr spectral line increases with HCl concentration, although with a steeper slope than that expected from the constants given by Gamlen and Jordan.⁹ That is, the fraction of FeCl₄⁻ at HCl concentrations below 12 *M* is found to be less than is predicted from the listed constants. Those constants were obtained from spectrophotometric data at high HCl concentrations, assuming the only species present were Fe(H₂O)₃Cl₃ and FeCl₄⁻. If in addition, Fe(H₂O)Cl₃ is considered, the constants as given are certainly somewhat in error in the 8–12 *M* HCl range. However, a compatible result is obtained if the visible spectrum attributed to FeCl₄⁻ is in fact due to Fe(H₂O)Cl₃ and FeCl₄⁻, both tetrahedral, and only FeCl₄⁻ is observed in epr. In that case, the Cl³⁵ nmr results should be interpreted in terms of both species, rather than FeCl₄⁻ alone, as was done in the preceding section. In the absence of accurate equilibrium data for the reactions



the previous interpretation has not been corrected for H₂O exchange involving Fe(H₂O)Cl₃.

In 9.68 *M* HCl solution, where the contribution of Fe(H₂O)Cl₃ should be very small, the Cl³⁵ chemical shift was found to be 228 ppm (26°, 5.000 Mc/sec), so that from¹⁹

$$\Delta\omega/\omega = (1/3)S(S+1)p_{Cl}(A/kT)(\gamma_e/\gamma_{Cl}) \quad (7)$$

$$p_{Cl} = p_{Cl}'\alpha_4 \quad (4)$$

one may obtain

$$(A/h)_{Cl} = 1.12 \times 10^7 \text{ cps}$$

in agreement with the value calculated from relaxation data.

Because of uncertainty with respect to species, calculations based on O¹⁷ relaxation and chemical

shift data are not as straightforward as for Cl³⁵. Relying principally on observations at HCl concentrations less than 8 *M*, $T_{23} = 9.0 \times 10^{-8}$ sec from eq 4. Then, using eq 6 with $\tau_e = T_{1e} \cong 6 \times 10^{-11}$ sec, $(A/h)_O = 2.5 \times 10^8$ radians/sec and $(A/h)_O = 4 \times 10^7$ cps.

The largest source of error in the preceding calculation is probably in τ_e . Although Fe(H₂O)₃Cl₃ is presumably octahedral, the electron spin relaxation time is not necessarily the same as that for Fe(H₂O)₆³⁺. McGarvey²³ observed a line width of 330 gauss for FeF₃ in 1.48 *M* KF solution of Fe(NO₃)₃. The line width decrease may not be as great upon formation of FeCl₃, but some decrease is possible which would lead to decrease in the calculated value of (A/h) .

At 10.57 *M* HCl, we assume the exchanging species to be mainly Fe(H₂O)₃Cl₃. The observed chemical shift for O¹⁷ at 26 ± 1° was found to be 56.9 ppm, so that, from eq 7 after correction for exchange rate, $(A/h)_O = 3 \times 10^7$ cps. This is probably the more reliable of the two values.

General Comments. Suggested chemical exchange mechanisms for both H₂O and Cl⁻ in the solutions investigated in this research involve factors which are more or less unique to the aqueous HCl system. In that sense it is understandable that observations made in other types of solution do not obviously lead to the same conclusions. This interpretation is a relatively simple one in which a single, dominant process is adduced in each case. It is entirely possible that more complicated mechanisms are concealed in the parameters employed in the interpretations. We have relied on the spectrophotometric results of Gamlen and Jordan⁹ for evaluation of species concentrations, which may be open to some argument if the species Fe(H₂O)Cl₃ must be accounted for. The concept of an octahedral–tetrahedral transition for trichloroiron(III) appears to be quite reasonable as applied to solutions such as aqueous 8–12 *M* HCl, in which the activity of water decreases sharply as a function of HCl concentration.

Acknowledgments. The authors wish to thank Patricia Stein of this laboratory who made many of the measurements of temperature dependence. They are also indebted to Dr. B. B. McInteer and Mr. R. M. Potter of this laboratory for supplying the enriched NO¹⁷.

The Buoyant Behavior of Bovine Serum Mercaptalbumin in Salt Solutions at Equilibrium in the Ultracentrifuge. II. Net Hydration, Ion Binding, and Solvated Molecular Weight in Various Salt Solutions^{1a,b}

by James B. Ifft and Jerome Vinograd

Contribution No. 3159 from Gates and Crellin Laboratories of Chemistry and the Norman W. Church Laboratory of Chemical Biology, California Institute of Technology, Pasadena, California (Received February 7, 1966)

Bovine serum mercaptalbumin was studied in six salt solutions (CsCl, CsBr, CsI, KBr, RbBr, and Cs₂SO₄) by the method of sedimentation equilibrium in a buoyant density gradient. The band width, the buoyant density, and the effective density gradient were determined in each salt solution at 25°. The binding of anions to the protein in the buoyant solvents was also measured. The bound anions and an equivalent number of cations were assumed to be part of the buoyant complex in a calculation of the molecular weight of the anhydrous protein from ultracentrifuge data. The mean anhydrous molecular weight obtained in these experiments was 69,000 ± 2000. The solvated molecular weights varied from 102,000 to 137,000.

Introduction

In a previous study² of the buoyant behavior³ of bovine serum mercaptalbumin (BMA), it was found that the BMA formed a gaussian concentration distribution in a CsCl density gradient at equilibrium. A comparison of the buoyant density^{1a} with the partial specific volume in CsCl indicated that the BMA was preferentially solvated with 0.20 g of H₂O/g of protein. In this calculation the anhydrous protein was chosen as the macromolecular component. It was recognized, however, that BMA binds anions⁴⁻⁶ in these experiments and, for reasons of electroneutrality, the corresponding number of cations. If the anhydrous protein-salt complex is chosen as the macromolecular component, different and higher values for the preferential solvation by water are required to account for the observed buoyant densities.

This paper deals with three related problems: (1) the determination of the anhydrous molecular weight of a standard protein (BMA) by density gradient centrifugation (such a determination requires an important and somewhat complex correction for preferential solvation and binding of salt), (2) the measurement of the preferential solvation and binding of salt

by BMA in a series of buoyant salt solutions in which both the anion and the cation are varied, and (3) an investigation of the dependence of the net hydration of BMA on the activity of water in the several buoyant salt solutions.

The behavior of BMA was studied in buoyant aqueous solutions of CsCl,⁷ CsBr, CsI, KBr, RbBr, Cs₂SO₄,

(1) (a) Throughout this paper the expression, "buoyant density," refers to the density of the buoyant solution at band center at ambient pressure, rather than at atmospheric pressure. It is the latter buoyant density that is normally reported in the literature. The magnitude of the difference between these two buoyant densities may be seen in Table VI. (b) This investigation was supported in part by Research Grant HE 03394 from the U. S. Public Health Service.

(2) J. B. Ifft and J. Vinograd, *J. Phys. Chem.*, **66**, 1990 (1962).

(3) M. Meselson, F. W. Stahl, and J. Vinograd, *Proc. Natl. Acad. Sci. U. S.*, **43**, 581 (1957).

(4) C. W. Carr, "Electrochemistry in Biology and Medicine," T. Shedlovsky, Ed., John Wiley and Sons, Inc., New York, N. Y., 1955, pp 266-283.

(5) G. Scatchard, W. L. Hughes, F. R. N. Gurd, and R. E. Wilcox, "Chemical Specificity in Biological Systems," F. R. N. Gurd, Ed., Academic Press Inc., New York, N. Y., 1954, pp 193-219.

(6) G. Scatchard, I. H. Scheinberg, and S. H. Armstrong, Jr., *J. Am. Chem. Soc.*, **72**, 535 (1950).

(7) All of the results in CsCl for the density gradient experiments have been abstracted from part I (ref 2) of this series. They are included in the present paper for comparison.

and CsAc. The buoyant density and the band width were measured in each of the foregoing salt solutions. The binding of anions to the isoionic protein in the buoyant salt solutions was evaluated by the method of Scatchard and Black.⁸ From the buoyant density data and the anion binding data the variation of the preferential solvation of the protein-salt complex with water activity was evaluated and used in the determination of α in the expression for the effective density gradient.⁹ This gradient was then used to calculate the molecular weight of the solvated protein-salt complex and of the anhydrous salt-free protein.⁹

In this paper four different density gradients are employed (Table I). The *composition* density gradient results solely from the salt distribution and is a function of $\beta^0 = (d \ln a/d\rho)RT/(1 - \bar{v}\rho^0)M$, where M , a , and \bar{v} are the molecular weight, activity, and partial specific volume of the solute, and ρ^0 is the density of

Table I: Four Density Gradients of Significance in Density Gradient Experiments

Name	Definition
Composition	$(d\rho/dr)_{\text{comp}} = \frac{\omega^2 r}{\beta^0}$ (1)
Physical	$(d\rho/dr)_{\text{phys}} = \left(\frac{1}{\beta^0} + \kappa\rho^0 \right) \omega^2 r$ (2)
Buoyant	$(d\rho/dr)_{\text{buoy}} = \left[\frac{1}{\beta^0} + \frac{(\kappa - \kappa_s)}{(1 - \alpha)\rho^0} \right] \omega^2 r$ (3)
Effective	$(d\rho/dr)_{\text{eff}} = \left[\frac{(1 - \alpha)}{\beta^0} + (\kappa - \kappa_s)\rho^0 \right] \omega^2 r$ (4)

the solution¹⁰ at atmospheric pressure. Numerical values of β^0 , as a function of density, have been evaluated for several salts which include CsCl, RbBr, and KBr.¹⁰ The *physical* density gradient is the sum of the composition gradient and the *compression* gradient. κ is the isothermal compressibility of the solution. The composition and the physical gradients are used to calculate compositions and densities in the solution. The *buoyant* density gradient can be used to calculate the buoyant density from the band position. The quantity κ_s is the apparent compressibility of the solvated polymer.¹¹ The quantity α has been defined⁹ and is a measure of the change in preferential solvation of the polymer with distance in the salt solution. A method for evaluating the buoyant density gradient is given later in this paper. The derivation of the expression for the *effective* density gradient is based on the assumption that the density of the solvated species

in a band is invariant except for the effects of pressure and the activity of the water in the solution.⁹

Experimental Section

Materials. The BMA has been described.² In the anion-binding experiments a mercaptalbumin preparation from Pentex Corp., Lot No. MB-52, was used. This material, however, was found to contain mercury which was removed by column chromatography with an ion-exchange resin bed prepared by the method of Dintzis.¹² The pH of the light yellow 5% solution was 5.18. It was stored at -20° . Sedimentation velocity studies with a 0.75% solution showed the presence of a fast impurity to the extent of 3-4%.

Three of the salts were used as supplied by the manufacturer. The KBr was reagent grade from the Baker Chemical Co. The RbBr was from the De Rewal International Rare Metals Co. with a stated purity of 99.6%. The CsBr was from A. D. Mackay, Inc., with a stated purity of 99.8%. CsI from Penn Rare Metal, Inc., was freed of a soluble dark impurity by centrifugation at 20,000 rpm for 20 min. The Cs_2SO_4 and Cs acetate solutions were kindly supplied by Dr. John Hearst and have been described.¹³ All other chemicals were reagent grade.

Measurement of Density and Refractive Index. The relation between refractive index and density facilitates the preparation of solutions for density gradient experiments. Data for KBr were found in Landolt-Börnstein.¹⁴ Data for the remaining salts were obtained with a Zeiss Abbé refractometer and a calibrated 300- μl micropipet used as a pycnometer. The densities of the RbBr solutions were measured with a Westphal balance with an accuracy of 0.0002 g/ml.

Ultracentrifuge Experiments. The density gradient experiments in KBr and RbBr solutions were carried out in double-sector cells as previously described for CsCl solutions.²

The information required for the evaluation of the results in CsBr, CsI, and Cs_2SO_4 was obtained from dual experiments in which the BMA was banded in

(8) G. Scatchard and E. S. Black, *J. Phys. Colloid Chem.*, **53**, 88 (1949).

(9) J. E. Hearst and J. Vinograd, *Proc. Natl. Acad. Sci. U. S.*, **47**, 999 (1961).

(10) J. B. Ifft, D. E. Voet, and J. Vinograd, *J. Phys. Chem.*, **65**, 1138 (1961).

(11) J. E. Hearst, J. B. Ifft, and J. Vinograd, *Proc. Natl. Acad. Sci. U. S.*, **47**, 1015 (1961).

(12) H. M. Dintzis, Ph.D. Thesis, Harvard University, 1952.

(13) J. E. Hearst and J. Vinograd, *Proc. Natl. Acad. Sci. U. S.*, **47**, 1005 (1961).

(14) W. A. Roth and K. Scheel, "Landolt-Börnstein Physikalisch-Chemische Tabellen," 5th ed, 3rd supplement, part 2, Julius Springer, Berlin, 1935, p 1700.

solutions of two densities which bracketed the buoyant density. An example of such an experiment is given in Figure 1. The approximate buoyant density was established in preliminary runs. The experimental parameters for the final runs are given in Table II. In these experiments it was necessary to use various negative wedges to compensate for the prismatic effect of the refractive index gradient. Column II gives the buoyant density, and column III the difference in initial densities, ρ_e , between the solutions used in the two cells. All experiments were performed at 56,100 rpm at 25°.

Table II: Double-Cell Experiments with BMA

Salt	ρ_0^0	$\rho_{e,2}^0 - \rho_{e,1}^0$	Wedges, deg	BMA concn, g/100 ml
RbBr	1.302	0.053	0, -1	0.10
CsBr	1.306	0.084	-1, -2	0.05
CsI	1.331	0.111	-3, -4	0.03
Cs ₂ SO ₄	1.237	0.111	-1, -2	0.05

Measurement of Anion Binding. The pH values of 1% isoionic BMA in water and in the buoyant salt solutions were measured with a Beckman Model G pH meter equipped with standard glass and calomel electrodes. Each measurement was repeated four times. The salt solutions themselves were checked and found to be essentially neutral. The difference in pH between the isoionic BMA in water and in a salt solution was used to compute the anion binding, $\bar{\nu}$, by the method of Scatchard and Black. The quantity $\bar{\nu}$ is the average increase in negative charge per molecule. Acetate binding could not be investigated by this method because of the buffering action of the acetate ion.

Instrumental response for protein solutions was slow in these measurements. Final readings were made after intermittent stirring and after a minimum of 10–15-min immersion in the protein solution. The protein adsorbed onto the glass electrode after three to four measurements was removed by alternate 1-min immersions in 0.1 *N* HCl and 0.1 *N* NaOH. The final immersion was in acid. The precision of the measurements was ± 0.05 pH unit. One measurement was performed for each salt solution with the BMA preparation used in the density gradient experiment. Confirming measurements were made with the purified preparation of Pentex BMA.

To be sure that the KBr salt solution, which was

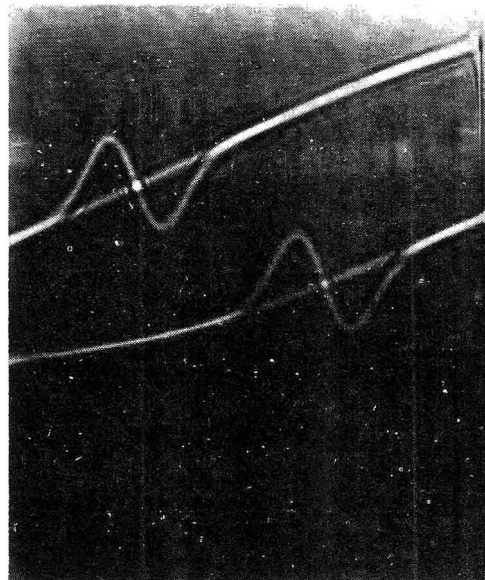


Figure 1. Schlieren photograph of equilibrium distributions of 0.05% BMA in Cs₂SO₄ solutions and of base lines: $\rho_{e,1} = 1.190$ and $\rho_{e,2} = 1.301$, 56,100 rpm, 25.0°, pH 5.5.

slightly alkaline, contained no buffers, it was acidified to pH 4.2 and the pH shift remeasured. The pH shift was the same as was previously found. The effect of protein concentration was measured in RbBr with 1 and 2% BMA. No effect of protein concentration was observed.

Theory and Calculations

Ultracentrifuge Experiments. The concentration distributions were evaluated by numerical integration.² The compressibility coefficient κ for KBr was obtained from the data of Gibson.¹⁵ The compressibility coefficients for CsBr, CsI, and RbBr were evaluated by interpolation from the data of Pohl¹⁶ for CsCl and RbCl and of Gibson for the potassium halides. The value for Cs₂SO₄ was similarly obtained from the data of Gibson for the compression of several salt solutions. The values which are estimated to be accurate to about $\pm 2 \times 10^{-6}$ atm⁻¹ are given in Table III.

The buoyant densities and the physical density gradients in the KBr and RbBr experiments were calculated with the equations and data previously published.¹⁰ Composition density gradients were not available for CsBr, CsI, and Cs₂SO₄ solutions. Experiments with these solutions were evaluated with the buoyant density gradients in twin-cell experiments.

(15) R. E. Gibson, *J. Am. Chem. Soc.*, **56**, 4 (1934); **57**, 284 (1935).

(16) F. Pohl, Dissertation, Rheinische Friedrich-Wilherim Universität, Bonn, Germany, 1906.

The following derivation for the expression for the buoyant density gradient is based on the observations of the effect of hydrostatic pressure on band position.¹¹ In an earlier paper it was shown that the density of the

Table III: Isothermal Compressibilities of Salt Solutions of Buoyant Composition^a

Salt	$\kappa \times 10^6$, atm ⁻¹	Salt	$\kappa \times 10^6$, atm ⁻¹
CsCl	35.1	CsBr	40.5
KBr	33.4	CsI	43.4
RbBr	37.3	Cs ₂ SO ₄	34.0

^a The temperatures at which the compressibility coefficients were determined varied from 13.8 to 25°. Because the isothermal compressibility is an insensitive function of temperature, the values were assumed to be valid at 25°.

buoyant solution at atmospheric pressure ρ_0^0 varies linearly with the pressure, P . For each cell we write the relation

$$\rho_{0,1}^0 = \frac{1}{\bar{v}_{s,0}^0}(1 - \psi_1 P_{0,1}); \quad \rho_{0,2}^0 = \frac{1}{\bar{v}_{s,0}^0}(1 - \psi_2 P_{0,2}) \quad (5)$$

when ψ is $(\kappa - \kappa_s)/(1 - \alpha)$ in eq 3, and $1/\bar{v}_{s,0}^0$ is the value of the buoyant density extrapolated to zero hydrostatic pressure. These equations are combined noting that $\bar{v}_{s,0}^0$ is constant and that ψ_1 and ψ_2 must be substantially the same.

$$(\rho_{0,2}^0 - \rho_{0,1}^0) = -\frac{1}{\bar{v}_{s,0}^0}\psi(P_{0,2} - P_{0,1}) \quad (6)$$

The above pressure differences are closely approximated as

$$P_{0,2} - P_{0,1} = \rho_0^0 \omega^2 (r_{0,2} - r_{0,1}) \bar{r}_0 \quad (7)$$

The quantity \bar{r}_0 is the arithmetic mean of the radial distances and ρ_0^0 is the average of the two closely similar buoyant densities. The latter are composition variables and are calculated with the relation

$$\rho_{0,1}^0 = \rho_{e,1}^0 + \int_{r_{e,1}}^{r_{0,1}} \left(\frac{\omega^2 r}{\beta^0} \right) dr = \rho_{e,1}^0 + \frac{\omega^2 \bar{r}_1}{\beta_1^0} (r_{0,1} - r_{e,1}) \quad (8)$$

where $\bar{r}_1 = (r_{0,1} + r_{e,1})/2$ and r_e is the isoconcentration distance. The quantity β_1^0 is evaluated at the distance \bar{r}_1 . A similar equation can be written for the second cell. The two expressions combined are

$$(\rho_{0,2}^0 - \rho_{0,1}^0) = (\rho_{e,2}^0 - \rho_{e,1}^0) + \omega^2 \left[\frac{\bar{r}_2}{\beta_2^0} (r_{0,2} - r_{e,2}) - \frac{\bar{r}_1}{\beta_1^0} (r_{0,1} - r_{e,1}) \right] \quad (9)$$

Because $r_{e,1} \cong r_{e,2}$, eq 9 can be simplified with negligible error.

$$(\rho_{0,2}^0 - \rho_{0,1}^0) = (\rho_{e,2}^0 - \rho_{e,1}^0) + \omega^2 \left[\frac{\bar{r}_0}{\beta_0^0} (r_{0,2} - r_{0,1}) \right] \quad (10)$$

where $\bar{r}_0 = (r_{0,1} + r_{0,2})/2$, and β_0^0 is evaluated at ρ_0^0 .

Equations 6, 7, and 10 are combined.

$$-\frac{1}{\bar{v}_{s,0}^0} \psi \rho_0^0 \omega^2 (r_{0,2} - r_{0,1}) \bar{r}_0 = (\rho_{e,2}^0 - \rho_{e,1}^0) + \omega^2 \left[\frac{\bar{r}_0}{\beta_0^0} (r_{0,2} - r_{0,1}) \right] \quad (11)$$

Equation 11 is rearranged with the good approximation that $\rho_0^0 = 1/v_{s,0}^0$.

$$\left(\frac{d\rho}{dr} \right)_{\text{buoy},0} = \frac{\rho_{e,2}^0 - \rho_{e,1}^0}{r_{0,1} - r_{0,2}} = \left[\frac{1}{\beta_0^0} + \psi \rho_0^{0,2} \right] \omega^2 \bar{r}_0 \quad (12)$$

The second term in brackets in the buoyant density gradient expresses the fact that the two bands are observed at different hydrostatic pressures.

The buoyant density gradient was used as is shown below in the calculation of the effective density gradient. It was also used to evaluate the quantity ρ_0^0

$$\rho_0^0 = \rho_e^0 + (d\rho/dr)_{\text{buoy},0} \Delta r \quad (13)$$

where Δr is the distance between r_e and r_0 , the band center. The values of r_e were satisfactorily obtained by interpolation of previously published data. It is recognized that $(d\rho/dr)_{\text{comp}}$ should have been used in eq 13. Initial solution densities in the single-cell experiments were always chosen so that bands were formed within 0.5 mm of r_e . The error introduced in ρ_0^0 was therefore less than 0.001 g/ml because the composition and buoyant density gradient are within 10% of each other.

The standard deviations of the top and bottom lobe of each band were measured as previously described.² Because the buoyant density gradient is evaluated at \bar{r}_0 , a position midway between the bands, the average of the four values of σ was used. The error introduced in σ by this procedure is less than 0.2% providing that $r_{0,1}\sigma_1 = r_{0,2}\sigma_2$. With each of the four salts the products agreed within 2%.

Solvation and Anion Binding. The net hydration of salt-free protein is given by the quantity Γ' in the rela-

tion² $\rho_0 = (1 + \Gamma')/(\bar{v}_3 + \Gamma'\bar{v}_1)$ where the subscripts 1 and 3 refer to water and protein, respectively. In molecular terms, the net hydration is the minimum amount of water bound by the protein. In the case of BMA, which binds salt, Γ' does not reveal the water required to provide a buoyant composition for the bound salt.

A quantity designated as Γ_*' , the net hydration of the protein-salt complex, is evaluated with the knowledge of the extent of salt binding with the relation

$$\rho_0 = \frac{1 + z_{XY} + \Gamma_*'}{\bar{v}_3 + z_{XY}\bar{v}_{XY} + \Gamma_*'\bar{v}_1} \quad (14)$$

The quantities z_{XY} and \bar{v}_{XY} are the weight fraction in g of salt/g of protein, and the partial specific volume of the salt, XY (bound to the protein). The value of z_{XY} was calculated with the relation, $z_{XY} = \bar{v}_{XY}M_{XY}/M_a$, where M_{XY} is the molecular weight of the salt and M_a is the molecular weight of the anhydrous protein which we take as 70,500. Measurement of pH shifts provided the value of \bar{v}_{XY} in moles of anions/mole of albumin. The partial specific volume of water was taken to be 1.00. Partial volumes for the bound salts were taken from a recent paper by Mukerjee¹⁷ for ions at infinite dilution.

The anion binding was calculated from pH shifts with the relation of Scatchard and Black

$$\bar{v} = \frac{2.303}{2w} \Delta\text{pH} \quad (15)$$

which has been experimentally confirmed.¹⁸ The value of the electrostatic free-energy term w was computed from the equation

$$w = 0.1190 \left(\frac{1 + 0.581\sqrt{I}}{1 + 8.125\sqrt{I}} \right) \quad (16)$$

where $I = \sum_i m_i z_i^2$, the double ionic strength. Equation 16 was calculated from eq 6 of ref 8 with the protein radius and the distance of closest approach used by these authors.

The derived buoyant density is defined by the relation between the partial specific volumes and net hydration of the protein-salt complex.

$$\rho_{0,*} = \frac{1 + \Gamma_*'}{\bar{v}_3 + \Gamma_*'\bar{v}_1} \quad (17)$$

The derived buoyant density is the density to be expected if no salt were bound and if salt binding did not affect the preferential hydration.

The quantity α in the effective density gradient is⁹

$$\alpha = \left(\frac{\partial \rho_0^0}{\partial a_w^0} \right)_P \left(\frac{da_w^0}{d\rho^0} \right) \quad (18)$$

where a_w^0 is the activity of water. The first factor in eq 18 was evaluated with the relation

$$\left(\frac{\partial \rho_0^0}{\partial a_w^0} \right)_P = \left(\frac{\partial \rho_0^0}{\partial \Gamma_*'} \right)_P \left(\frac{d\Gamma_*'}{da_w^0} \right) = \frac{\rho_0^0(1 - \rho_0^0\bar{v}_1)}{1 + z_{XY} + \Gamma_*'} \left(\frac{d\Gamma_*'}{da_w^0} \right) \quad (19)$$

which was obtained by partial differentiation of eq 14 with respect to Γ_*' . The derivative $d\Gamma_*'/da_w^0$ was obtained by measuring the slopes on Figure 4. The second factor in eq 18 was calculated from the slope of the plots in Figure 2. The activity data were calculated from the molal osmotic coefficients given by Robinson and Stokes.¹⁹ The effective density gradients for the experiments performed with double-cell runs were determined as the product of the buoyancy density gradient and the quantity $(1 - \alpha)$, eq 3 and 4.

In the single-cell experiments performed with CsCl, KBr, and RbBr, the values of β_0^0 , κ , and α in the expression for the effective density gradient were known. The values of κ are listed in Table II, and those for β_0^0 in a previous publication.² An approximate value of κ_s was obtained as follows: Jacobson's²⁰ value of $9.1 \times 10^{-6} \text{ atm}^{-1}$ for the compressibility of horse serum albumin in dilute salt solutions, together with the values of β_0^0 , κ , and α for CsCl, gave a value of 0.127 g/cm^{-4} for the effective density gradient. The

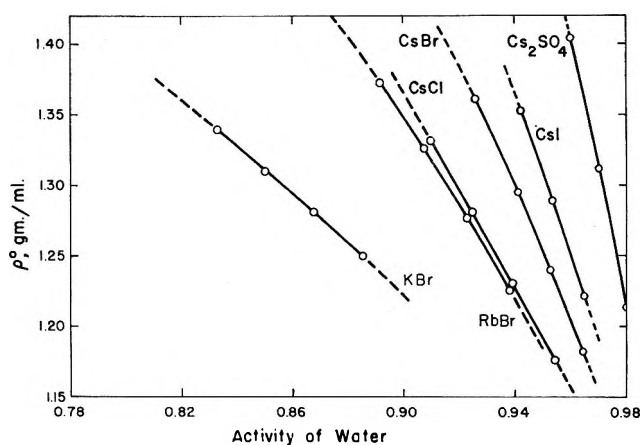


Figure 2. Water activities of various salt solutions.

(17) P. Mukerjee, *J. Phys. Chem.*, **65**, 740 (1961).

(18) G. Scatchard, J. S. Coleman, and A. L. Shen, *J. Am. Chem. Soc.*, **79**, 12 (1957).

(19) R. A. Robinson and R. H. Stokes, "Electrolyte Solutions," Academic Press Inc., New York, N. Y., 1955, pp 469, 470, 473.

(20) B. Jacobson, *Arkiv Kemi*, **2**, 177 (1950).

experimentally determined value¹¹ of $\psi = (\kappa - \kappa_s)/(1 - \alpha)$, for tobacco mosaic virus, together with the same value of β_s^0 , gave a value of 0.125 g/cm⁻⁴ for the effective density gradient.

Because values of ψ were not available in KBr and RbBr solutions for any protein and because the gradients obtained by the two procedures outlined above for CsCl were substantially the same, the effective density gradients for the first three salts listed in Table VIII were computed using the separate terms in eq 4.

The molecular weight of the solvated protein-salt complex was calculated from the relation⁹

$$M_{s,0} = \frac{RT\rho_0}{\sigma^2(d\rho/dr)_{\text{eff}}\omega^2r_0} \quad (20)$$

where ρ_0 is the density at the actual pressure in the experiment of the solution at band center. It is recognized that a term which expresses the variation of z_{XY} with distance in the band should have been included in the formulation of the effective density gradient. The salt binding increases with distance in the band and causes the species to become denser on the dense side and lighter on the light side than at band center. The anticipated effect is thus to lower the effective density gradient. This effect has not been included in the numerical calculations of the molecular weight. The magnitude of the errors incurred are estimated in the discussion. The molecular weight of the anhydrous protein was calculated from the equation

$$M_a = \frac{M_{s,0}}{1 + \Gamma_*' + z_{XY}} \quad (21)$$

Results

Anion Binding. The results of the anion binding experiments are collected in Table IV. The densities of the solutions in which measurements were performed are given in the second column. These correspond to within 0.010 g/ml of the buoyant densities. In concentrated salt solutions the anion binding by bovine albumin is relatively insensitive to salt concentration.²¹

The results for CsBr and RbBr are the least accurate. Two sets of ΔpH 's differing by about 0.2 pH unit were obtained in each case. The value selected for CsBr was that given by three out of five measurements. The value given for RbBr was that which was consistent with the other two bromides. Scatchard and Black⁸ have shown that the nature of the alkali cation has little effect on the extent of anion binding.

Refractive Index-Density Relations. The refractive index-density relations are presented in Table V as coefficients of the linear relation $\rho^{25} = a(n^{25D}) - b$. Equations for KBr and RbBr give densities accurate

to ± 0.001 g/ml. The precision for the other salts is ± 0.002 g/ml.

Table IV: Anion Binding from pH Shifts in Isoionic Protein Solutions

Salt	ρ	\sqrt{I}	w	ΔpH	\bar{v}	No. of anions bound
CsCl	1.278	2.22	0.0153	0.71	53	53
KBr	1.306	2.98	0.0138	0.81	67	67
RbBr	1.315	2.40	0.0149	0.85	66	66
CsBr	1.306	2.04	0.0158	0.96	70	70
CsI	1.331	1.93	0.0162	1.10	78	78
Cs ₂ SO ₄	1.237	2.31	0.0151	0.64	49	25

Table V: Density vs. Refractive Index Relations for Several Aqueous Salt Solutions

Salt	$\rho^{25} = a(n^{25D}) - b$		Density range
	Parameters of equations		
	a	b	
CsCl	10.8601	13.4974	1.25-1.90 ^a
KBr	6.4786	7.6431	1.10-1.35
RbBr	9.1750	11.2410	1.15-1.65
CsBr	9.9667	12.2876	1.25-1.35
CsI	8.8757	10.8381	1.20-1.55
Cs ₂ SO ₄	12.1200	15.1662	1.15-1.40

^a A more accurate relation for $1.10 < \rho < 1.38$, $\rho_4^{25} = 10.2402n^{25D} - 12.6483$, has recently been evaluated for CsCl solutions: R. Bruner and J. Vinograd, *Biochim. Biophys. Acta*, **108**, 18 (1965).

Density Gradient Experiments. The buoyant densities, standard deviations, and the net hydration of salt-free protein for the six salts are given in Table VI.

Table VI: Buoyant Densities, Standard Deviation, and Net Hydrations of BMA in Several Salt Solutions

Salt	ρ_0^0	ρ_0	σ_{av}	Γ'
CsCl	1.278	1.282	0.106	0.200
CsAc	1.291
KBr	1.295	1.302	0.147	0.138
RbBr	1.302	1.310	0.103	0.115
	1.302	1.310	0.106	0.115
CsBr	1.306	1.315	0.084	0.102
CsI	1.331	1.347	0.071	0.025
Cs ₂ SO ₄	1.237	1.241	0.071	0.359

(21) G. Scatchard, Y. V. Wu, and A. L. Shen, *J. Am. Chem. Soc.*, **81**, 6014 (1959).

The buoyant densities in CsCl, KBr, and RbBr are the averages of the results of a number of single-cell experiments. The precision is ± 0.001 g/ml. Only one experiment was conducted in cesium acetate and the buoyant density is accurate to ± 0.005 g/ml. The σ_{av} are the averages of the standard deviations evaluated from the upper and lower half of the distribution. The band widths are values selected from typical experiments, and the precision of each is ± 0.002 cm.

The last four entries of Table VI give the results of the two-cell experiments. The precision in ρ_0 is ± 0.004 cm for RbBr and CsBr, and ± 0.002 cm for CsI and Cs₂SO₄.

The values of Γ' are plotted against water activity in Figure 3. The anion and cation series vary monotonically except for Cs₂SO₄. The precision of the Γ' values is great enough that we can observe a decrease in net hydration with increasing water activity in both series.

Effect of Anion Binding on the Evaluation of Results. The results of including the anion binding in the analysis are shown in Table VII and Figure 4. The uncertainty in z_{XY} produces expected deviations of about 5% in the Γ_{*}' values.

Table VII: Net Hydration of BMA-Salt Complex and Derived Buoyant Densities

Salt	ρ_0	z_{XY}	\bar{v}_{XY}	Γ_{*}'	$\rho_{0,*}$
KBr	1.302	0.113	0.283	0.37	1.24
RbBr	1.310	0.155	0.234	0.46	1.22
CsCl	1.282	0.127	0.233	0.51	1.21
CsBr	1.315	0.211	0.217	0.58	1.20
CsI	1.347	0.288	0.222	0.61	1.20
Cs ₂ SO ₄	1.241	0.128	0.162	0.78	1.17

It is of considerable interest to examine whether or not these values of Γ_{*}' increase monotonically with water activity. Figure 4 demonstrates that an excellent correlation exists.

The derived buoyant densities are given in the last column of Table VII and are plotted in the lower half of Figure 5 against the water activities. Figure 5 indicates the correlation that exists between these values of $\rho_{0,*}$ and water activity as opposed to the lack of correlation in the measured buoyant densities that are plotted in the upper half of the figure.

The parameters required for the evaluation of effective density gradients are given in Table VIII. These density gradients were used in eq 20 to calculate the molecular weight of the solvated BMA-salt complex,

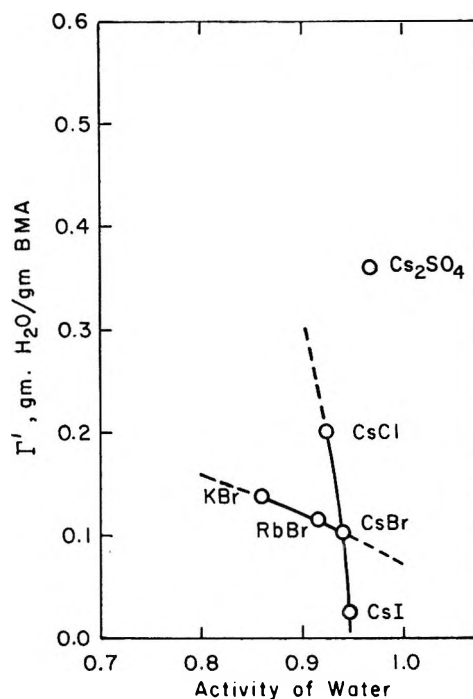


Figure 3. Net hydration of BMA.

$M_{s,0}$. Because both the extent of solvation and ion binding were known, anhydrous molecular weight values could be determined, eq 21. These are tabulated in the last column.

Discussion

The solvated molecular weights range up to values twice as large as that of the anhydrous protein. The anhydrous molecular weights given in Table VIII are in satisfactory agreement with the value of 70,500 obtained from a two-component sedimentation equilibrium experiment. The over-all precision of the method is estimated to be 6-8% in the determination of the molecular weight of a protein which binds ions. The errors are due primarily to uncertainties in the measurement of σ and $(d\rho/dr)_{eff}$. The agreement of the average of these six values indicates that this method of treatment is substantially correct and that no additional important factors have been overlooked.

The two sets of data for M_s in Table VIII differ only in a random manner. This indicates that the two methods of evaluating the effective density gradient are substantially in agreement. A large discrepancy still exists in the RbBr data. The large uncertainties that must be placed on each effective density gradient as well as the value of σ used to calculate the two values of $M_{s,0}$ preclude any conclusion as to the significance of the observed difference.

Table VIII: The Solvated and Anhydrous Molecular Weights of Bovine Serum Mercaptalbumin

Salt	$(\partial \rho_0^0 / \partial a_w^0)_P$	$(d\rho^0/da_w^0)$	α	$(d\rho/dr)_{\text{eff}}^a$	$(d\rho/dr)_{\text{eff}}^b$	$M_{a,0} \times 10^{-3}$	$M_a \times 10^{-3}$
CsCl	-0.72	-3.49	0.21	0.120	...	102	63
KBr	-0.37	-1.70	0.22	0.064	...	103	69
RbBr	-0.71	-3.18	0.22	0.122	...	107	67
RbBr	-0.71	-3.18	0.22	...	0.108	117	73
CsBr	-1.13	-4.57	0.25	...	0.165	112	68
CsI	-1.27	-5.60	0.23	...	0.211	133	70
Cs ₂ SO ₄	-2.08	-10.1	0.21	...	0.195	137	72
						Mean	69 ± 2

^a From composition density gradient. ^b From buoyant density gradient.

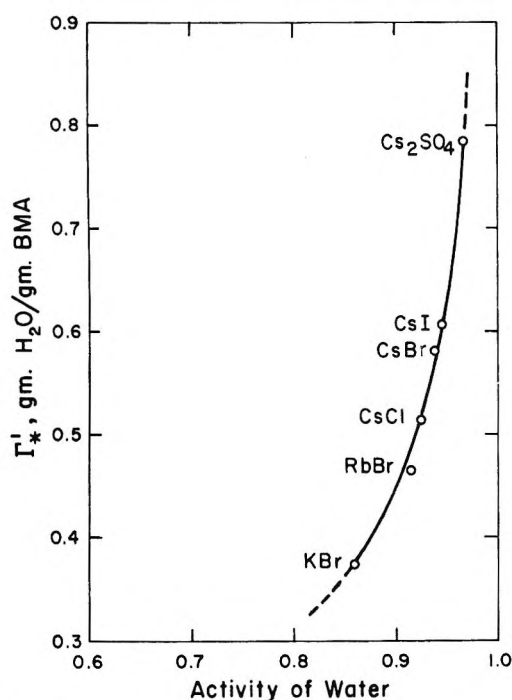


Figure 4. Net hydration of BMA-salt complex.

The calculation of Γ_{*}' and therefore M_a are prejudiced by the assumption of a value for M_a in order to calculate z_{XY} . If the actual value of M_a were 5000 lower than the value used, the Γ_{*}' value would be increased by about 5% and the reported anhydrous molecular weights decreased by 2%. In the case of a protein of unknown molecular weight, if the calculated M_a were significantly different from the assumed value, an iteration procedure could be employed.

Because proteins are polyampholytes, in principle attractive interactions with both of the low molecular weight ions can exist. In our analysis of the results of these experiments, it has been recognized that BMA binds anions and to preserve electroneutrality, a corresponding number of cations in a secondary

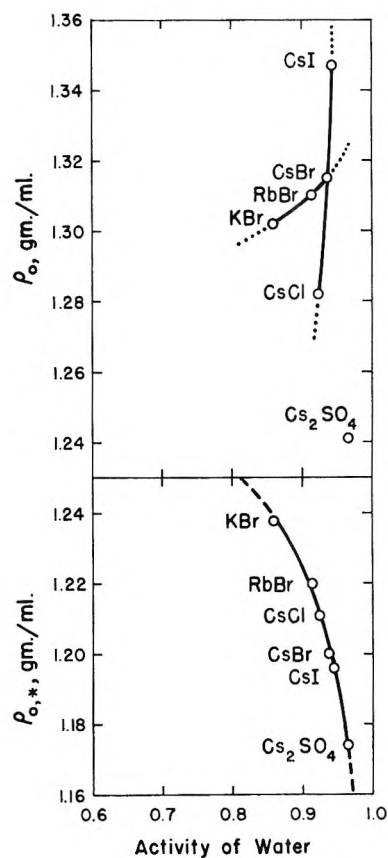


Figure 5. Measured and derived buoyant densities of BMA.

layer. This type of interaction with salt, which has been measured in this work, is accompanied by a further solvation of $(\Gamma_{*}' - \Gamma')$ g of H₂O/g of protein.

Tanford, Swanson, and Shore²² have measured intrinsic dissociation constants for each of the ionizable residues in BSA. Combination of these values with the pH employed in the centrifuge studies reveals that

(22) C. Tanford, S. A. Swanson, and W. S. Shore, *J. Am. Chem. Soc.*, **77**, 6414 (1955).

all 97 of the basic amino acids are protonated, and all but four or five of the 99 carboxyls are ionized. Thus, the protein before binding of anions has only a small net charge, but contains a large number of compensatory negative and positive charges. If we assume that some 50–60 chloride ions are associated with 50–60 positively charged sites on the albumin molecule, there remain some 95 negatively charged sites and 40 positively charged sites.

In dilute solutions (up to 0.1 *M*), Scatchard, *et al.*,⁵ have shown by equilibrium dialysis that few if any Na^+ are bound to human serum albumin in a NaCl solution. Lewis and Saroff²³ studied the binding of K^+ to both human and bovine serum albumin by collodion membranes which are permselective to cations. No K^+ were bound in 0.1 *M* KCl . The absence of cation binding in dialysis equilibrium experiments may alternatively be described as the absence of binding of neutral salt.

No data are available that allow us to assess the occurrence of cation binding in more concentrated salt solutions. In view of the pH results, if such binding occurs, it must be accompanied by primary site anion binding. Should the cation be accompanied by anion binding in secondary layers, the net charge effect would have been reduced in the pH measurements.

A further argument against cation binding is that the binding of neutral salt would increase the molecular weight of the buoyant species and would increase the buoyant density unless accompanied by a new ($\Gamma_{*'} - \Gamma'$) solvation which would render the added salt neutrally buoyant. In the extreme case of 45 additional moles of CsCl bound per mole of albumin, we calculate that the molecular weight would increase by 27,000. Because the buoyant density, radial banding position, and standard deviation are directly measured experimental parameters, the calculated value of $(d\rho/dr)_{\text{eff}}$ would have to decrease by 27,000/102,000 or 26% to obtain the correct molecular weight of the protein. There is no firm way to exclude this effect in part or in total. It seems unlikely, however,

in view of the absence of cation binding in dilute solutions, that large amounts of cation binding will occur in buoyancy experiments.

One result in the work of Cox and Schumaker²⁴ can be compared with the present study. They banded BSA in $(\text{NH}_4)_2\text{SO}_4$. The observed buoyant density, ρ_0^0 , of 1.175 ± 0.005 g/ml corresponds to a value of $\Gamma' = 0.79 \pm 0.05$. The water activity of this solution is 0.88. Because BSA undoubtedly binds large numbers of sulfate ions in this system, as was observed in Cs_2SO_4 , the value of the derived buoyant density and the net hydration of the protein-salt complex would be at least double that predicted by Figure 4. The reason for this discrepancy is not known.

A further set of experiments by Cox and Schumaker is subject to reinterpretation in light of the present findings. They banded BSA in a series of solutions that were 3.6 *M* in $(\text{NH}_4)_2\text{SO}_4$ and which contained increasing amounts of CsCl , from 0 to 0.82 *M*. They found that ρ_0^0 monotonically increased from 1.175 to 1.250 and interpreted this as a decrease in net hydration from 0.79 to 0.35. This result was more probably due to binding of Cl^- to additional sites on the albumin molecule and replacement of Cs^+ for NH_4^+ in the secondary layer. Whether the hydration changes in this series cannot be determined until competitive binding studies are undertaken.

The buoyant behavior of proteins that bind small ions is seen to be considerably more complicated than the behavior of nucleic acids and other polyanions or polycationic electrolytes. In the case of nucleic acids, each phosphate residue binds one cation and, except for solvation by water, the mass of the buoyant species is well defined. A buoyant density of CsDNA can be used to determine directly the extent of solvation. In the case of proteins, it is necessary to know the extent of ion binding, a result which normally must be obtained from other kinds of measurements.

(23) M. S. Lewis and H. A. Saroff, *J. Am. Chem. Soc.*, **79**, 2112 (1957).

(24) D. J. Cox and V. N. Schumaker, *ibid.*, **83**, 2439 (1961).

Energy Transfer in Thermal Methyl Isocyanide Isomerization.

Experimental Survey¹

by F. J. Fletcher, B. S. Rabinovitch, K. W. Watkins, and D. J. Locker

Department of Chemistry, University of Washington, Seattle, Washington 98105 (Received February 9, 1966)

Suitable experimental variables and conditions for the systematic study of energy transfer in thermal unimolecular systems are described in connection with the existing literature. The thermal unimolecular isomerization of methyl isocyanide to acetonitrile has been studied in the low-pressure region at 230.5° in the presence of 19 added gases at up to 200-fold excess of the addend. The falloff of the rate constant for the substrate alone has also been studied down to a value of k/k_∞ of $\sim 3 \times 10^{-4}$. Rate constants have been recalculated on the basis of RRKM theory with new frequency assignments for CH₃NC. Excellent agreement with experiment is observed. The average excess energy of the reacting molecules above the critical energy, E_c , has been calculated; this quantity is central for the operational meaning of collisional energy transfer. Relative deactivation efficiencies of the addends are listed on both a pressure and collision basis. It is obvious that the strong collision assumption does not hold for small molecules; various general conclusions may be drawn with regard to the molecular parameters which may be involved in vibrational energy transfer. No specific efficiency of the triple bonds of cyanides and acetylenes, used as inert addends, appears to exist.

Introduction

The transfer of energy between highly vibrationally excited molecules (say above 20 kcal mole⁻¹; *i.e.*, $\gg RT$) and inert gases is a process which is still imperfectly understood. No complete theory of energy exchange is available, in part because of the paucity of experimental data. In fact, little is known about energy transfer in polyatomic molecules even in the moderate energy region (several RT , say ~ 5 –20 kcal mole⁻¹). Application of the theories of Zener^{2a} and Landau and Teller,^{2b} and extended by Schwartz, Slawsky, and Herzfeld,³ to polyatomic molecules leads to the prediction⁴ that only small amounts of energy (~ 0.01 – 0.1 kcal mole⁻¹) can transfer efficiently, by multiquantum transitions.

In recent years, a significant advance in the theory of unimolecular reactions has been the success of the Marcus–Rice extension⁵ of the Rice–Ramsperger–Kassel (RRK) theory.⁶ One of the main assumptions of these theories is that deactivation of an excited molecule occurs on every collision. Experiment shows that this strong collision assumption *may* be

obeyed by complex molecules,⁷ but apparently not by the rare gases and simple molecules.⁸ Until these matters are clarified by further energy transfer studies there can be no complete theory of unimolecular reactions.

(1) This work was supported in part by the National Science Foundation and in part by the Petroleum Research Fund of the American Chemical Society.

(2) (a) C. Zener, *Phys. Rev.*, **37**, 556 (1931); (b) L. Landau and E. Teller, *Physik Z. Sowjetunion*, **10**, 34 (1936).

(3) R. N. Schwartz, A. I. Slawsky, and K. F. Herzfeld, *J. Chem. Phys.*, **20**, 1591 (1952).

(4) B. H. Mahan, *J. Phys. Chem.*, **62**, 100 (1958).

(5) R. A. Marcus and O. K. Rice, *ibid.*, **55**, 894 (1951); R. A. Marcus, *J. Chem. Phys.*, **20**, 359 (1952); O. K. Rice, *J. Phys. Chem.*, **65**, 1588 (1961).

(6) L. S. Kassel, "Kinetics of Homogeneous Gas Reactions," Chemical Catalog Co., New York, N. Y., 1932.

(7) (a) G. H. Kohlmaier and B. S. Rabinovitch, *J. Chem. Phys.*, **38**, 1692, 1709 (1963); R. E. Harrington, B. S. Rabinovitch, and M. R. Hoare, *ibid.*, **33**, 744 (1960); (b) J. H. Current and B. S. Rabinovitch, *ibid.*, **40**, 2742 (1964).

(8) (a) H. S. Johnston, *J. Am. Chem. Soc.*, **75**, 1567 (1953); D. J. Wilson and H. S. Johnston, *ibid.*, **75**, 5763 (1953); (b) M. Volpe and H. S. Johnston, *ibid.*, **78**, 3903 (1956).

Techniques for the study of energy transfer from vibrationally excited species include sound dispersion,⁹ kinetic spectroscopy,¹⁰ and flash photolysis,¹¹ shock wave studies,¹² fluorescence stabilization,^{13,14} photochemical systems,¹⁵ and chemical activation^{7,16} and low-pressure thermal unimolecular systems.^{8,17} The existing information on the deactivation in binary collisions of complex molecules above the low-energy region may be readily summarized.

Fluorescence studies on aromatic species (at energies up to ~ 25 kcal mole⁻¹) indicate that amounts of energy up to several kcal mole⁻¹ may be transferred to foreign gases.¹³ The amount of energy transferred seems to increase with increasing molecular weight and polarity of the deactivator (paralleling the thermal unimolecular reaction situation—see below). These results contrast with energy transfer studies with highly excited iodine^{14a} which indicate, in part, that lighter molecules may be more effective in producing vibrational transitions (somewhat resembling sound dispersion results at low energies).

At still higher energies, chemically activated ethyl and *sec*-butyl radicals, vibrationally excited to ~ 40 kcal mole⁻¹, were found to lose ~ 2 kcal mole⁻¹ on collision with the rare gases, ~ 2.5 kcal mole⁻¹ on collision with diatomic gases, and ≥ 9 kcal mole⁻¹ on collision with polyatomic molecules.^{7a} The deactivation of chemically activated vibrationally excited cyclopropane and dimethylcyclopropane (≥ 100 kcal mole⁻¹) by ethylene and butene¹⁶ indicates that large amounts of energy may be transferred on collision, ≥ 12 – 15 kcal mole⁻¹.

The most definitive and outstanding thermal study has been that of Johnston and Volpe,^{8b} who analyzed the effect of 16 chaperon gases on the unimolecular decomposition of nitryl chloride. In order to measure relative collisional transition probabilities most simply, they have pointed out that studies should be made in the low-pressure, second-order region of a thermal unimolecular reaction. In this nonequilibrium region, the rate of reaction is the rate of activation by collision. In practice, the behavior of inert molecules has usually been expressed as efficiency relative to the reactant itself. It was remarked by Trotman-Dickenson¹⁸ that the maximum efficiency of energy transfer is reached for complex molecules. Johnston¹⁹ has suggested that efficiency may be correlated with the boiling points of the inert gases and with Lennard-Jones parameters in terms of collision force. The deactivation probability per collision should be below unity (*i.e.*, far from saturation) to show direct proportionality to molecular parameters.

Up to the present time, most thermal studies of this

kind have been relatively unproductive. The results of various workers have usually been obtained at diverse temperatures, total energy level, excess energy level, and energy distribution, and with reactant molecules of widely varying molecular complexity, frequency pattern, and polarity. Widely different systems have often been uncritically compared and no systematic variation of reaction parameters has been investigated for a single system.²⁰ It has been pointed out and illustrated previously^{7b} that the usual definition of inert gas efficiency is a pragmatic operational one; comparisons of efficiencies between various systems which ignore this limitation are not necessarily helpful. For example, scarcely any study in the literature has defined the average energy excess of the reacting molecules^{20b} above the critical threshold; the comparisons in question thus have not been well defined. Usually, no attempt has been made to correlate data with molecular parameters or interaction potentials. Some experimental limitations in many existing studies should also be recognized: work in the higher regions of falloff just below the high-pressure limit may lead to incorrect results because the pressure dependence

(9) (a) T. L. Cottrell and J. C. McCoubrey, "Molecular Energy Transfer in Gases," Butterworth and Co. Ltd., London, 1961; (b) K. F. Herzfeld and T. A. Litovitz, "Absorption and Dispersion of Ultrasonic Waves," Academic Press Inc., New York, N. Y., 1959; (c) J. D. Lambert and R. Salter, *Proc. Roy. Soc. (London)*, **A253**, 277 (1959); J. D. Lambert, D. G. Parks-Smith, and J. L. Stretton, *ibid.*, **A282**, 380 (1964).

(10) J. D. McKinley, Jr., D. Garvin, and M. Boudart, *J. Chem. Phys.*, **23**, 785 (1955); J. C. Polanyi, *ibid.*, **31**, 1338 (1959).

(11) See, for example, the reviews by N. Basco and R. G. W. Norrish, *Can. J. Chem.*, **38**, 1769 (1960); *Discussions Faraday Soc.*, **33**, 99 (1962). For a summary of iodine atom recombination reactions, see G. Porter, *ibid.*, **33**, 198 (1962).

(12) R. C. Millikan and D. R. White, *J. Chem. Phys.*, **39**, 3209 (1963), and references cited; R. C. Millikan, *ibid.*, **40**, 2594 (1964).

(13) (a) B. Stevens, *Can. J. Chem.*, **37**, 831 (1959); *Mol. Phys.*, **3**, 589 (1960); (b) M. Boudart and J. T. Dubois, *J. Chem. Phys.*, **23**, 223 (1955); B. Stevens and M. Boudart, *Ann. N. Y. Acad. Sci.*, **67**, 570 (1957); B. S. Neporent and S. O. Mirumyants, *Opt. Spectry. (USSR)*, **8**, 336, 414 (1960); (c) E. J. Bowen and S. Veljkovic, *Proc. Roy. Soc. (London)*, **A236**, 1 (1956).

(14) (a) R. L. Brown and W. Klemperer, *J. Chem. Phys.*, **41**, 3072 (1964); J. I. Steinfeld and W. Klemperer, *ibid.*, **42**, 3475 (1965); (b) R. C. Millikan, *ibid.*, **38**, 2855 (1963).

(15) G. A. Taylor and G. B. Porter, *ibid.*, **36**, 1353 (1962).

(16) D. W. Setser, J. W. Simons, and B. S. Rabinovitch, *Bull. Soc. Chim. Belges*, **71**, 662 (1962); *J. Chem. Phys.*, **40**, 1751 (1965); **41**, 800 (1965).

(17) D. E. Hoare, J. B. Protheroe, and A. D. Walsh, *Trans. Faraday Soc.*, **55**, 548 (1959); R. R. Baldwin and D. Brattan, 8th Combustion Symposium, Pasadena, Calif., 1960, p 110; W. Forst, *Can. J. Chem.*, **36**, 1308 (1958).

(18) A. F. Trotman-Dickenson, "Gas Kinetics," Butterworth and Co. Ltd., London, 1955.

(19) H. S. Johnston, *Ann. Rev. Phys. Chem.*, **8**, 249 (1957).

(20) (a) For a comparison table of relative collision efficiencies in thermal unimolecular reactions, see ref 9a, p 186; (b) see D. W. Placzek, B. S. Rabinovitch, G. Z. Whitten, and E. Tschuikow-Roux, *J. Chem. Phys.*, **43**, 4071 (1965), for some deactivation of excess energy.

of conventional unimolecular reactions is insensitive to collisional transition probabilities,²¹ and only indirectly related to these,⁸ and because of experimental inaccuracy.²²⁻²⁴

At the low-pressure limit the situation is vastly improved, but still not simple, and must be treated on a stochastic model.^{25a} However, the low-pressure rates can, in principle, be made to yield a connection between the amount of energy transferred on the average per collision and the measured efficiencies of activation.^{25b}

Earlier work from this laboratory²⁶ has shown that the thermal unimolecular isomerization of methyl isocyanide to acetonitrile is a simple, clean, and homogeneous reaction. This reaction offers unique advantages in that a systematic variation of many reaction parameters is possible.²⁶⁻²⁸ Variation of temperature will be attempted over the widest accessible range. More important, the structure of the reactant molecule as well as the nature of the deactivator can be altered, without altering significantly the reaction parameters, to provide an internally consistent reaction series, *e.g.*, CH₃NC, C₂H₅NC, CF₃CH₂NC, and the effects of the frequency pattern change, internal rotation, and low-frequency bending modes, total number of vibration modes, etc., on the collisional transition probabilities can be quantitatively evaluated.

The present paper dealing with the CH₃NC → CH₃CN reaction presents the first in a series which utilizes these systems.

Experimental Section

Materials. Methyl isocyanide was prepared by the general method of dehydration of an N-substituted formamide by an acid halide in the presence of a base.²⁹ N-Methylformamide (Fluka A.G. pure grade) was slowly added to a warm mixture of quinoline (Matheson Coleman and Bell refined grade, vacuum distilled from zinc dust) and *p*-toluenesulfonyl chloride (Eastman White Label). After purification by gas chromatography, no impurities could be detected.

Helium, neon, argon, krypton, xenon, hydrogen, nitrogen, and carbon dioxide were assayed reagent grade gases of the Air Reduction Co. Helium contained 0.017% nitrogen as an impurity. Krypton contained 0.008% xenon, and xenon contained 0.01% krypton. These gases were used without further purification.

Methane (Phillips Petroleum Co., research grade) of stated purity 99.58% was used without purification. Fluoroform (Matheson Co. Inc.) when analyzed by chromatography showed the presence of 6% of non-interfering side product (mainly CH₂F₂). Tetrafluoro-

methane (Matheson Co. Inc.) showed no impurities by chromatography. Methyl fluoride-*d*₃ of 95% isotopic purity was checked by chromatography for interfering side products and was estimated to be of 99% chemical purity. Trifluoroacetonitrile (Columbia Chemicals) contained <1% impurity when analyzed by chromatography. Propionitrile (Eastman White Label, free from isonitrile) and *n*-butyronitrile (Matheson Coleman and Bell) showed no impurities on chromatographic analysis. All of these gases were vacuum distilled and outgassed.

Other inert gases were purified by chromatography prior to use and subjected to the usual vacuum manipulations. All condensible gases were deoxygenated by the freeze-pump-melt method and small amounts of impurity other than oxygen will have a negligible effect on the energy transfer efficiencies.

Apparatus and Procedure. A static method was used for the rate determinations. A 12-l. Pyrex bulb, heated in an air furnace, served as the reactor. Temperature was regulated by a proportional controller and was measured with three calibrated chromel-alumel thermocouples located at different positions in the furnace. During a run the temperature was constant to ±0.1° and was uniform over the bulb to ±0.1°. Over the entire series of runs, temperatures between 279 and 282.5° were used and all rate constants were corrected to a standard temperature of 280.5° with use of the energies of activation at the pressure of the run, as given in I.²⁶

The reactor was initially seasoned with a few millimeters of methyl isocyanide for 12 hr and was re-

(21) F. P. Buff and D. J. Wilson, *J. Chem. Phys.*, **32**, 677 (1960).

(22) Studies of inert gas efficiencies in the isomerization of cyclopropane,^{23a} of methylocyclopropane,^{23b} of 1,1-dimethylcyclopropane,^{24b} and the decomposition of cyclobutane^{23b} suffer from this problem: cyclopropane k/k_{∞} was studied down to ~0.1; for ∇CH_3 , $\nabla(\text{CH}_3)_2$, and \square , k/k_{∞} was studied only down to ~0.5. This grouping is otherwise the only candidate as a consistent set of substrate species.

(23) (a) H. O. Pritchard, R. G. Sowden, and A. F. Trotman-Dickenson, *Proc. Roy. Soc. (London)*, **A217**, 563 (1953); (b) H. O. Pritchard, R. G. Sowden, and A. F. Trotman-Dickenson, *ibid.*, **A218**, 416 (1953).

(24) (a) J. P. Chesick, *J. Am. Chem. Soc.*, **82**, 3277 (1960); (b) M. C. Flowers and H. M. Frey, *J. Chem. Soc.*, 1157 (1962).

(25) (a) E. W. Montroll and K. E. Shuler, *Advan. Chem. Phys.*, **1**, 361 (1958); (b) B. S. Rabinovitch and D. C. Tardy, *Science*, **150**, 382 (1965); *J. Chem. Phys.*, in press.

(26) F. W. Schneider and B. S. Rabinovitch, *J. Am. Chem. Soc.*, **84**, 4215 (1962); called I.

(27) F. W. Schneider and B. S. Rabinovitch, *ibid.*, **85**, 2365 (1963); called II.

(28) B. S. Rabinovitch, P. W. Gilderson, and F. W. Schneider, *ibid.*, **87**, 158 (1965); called III.

(29) The method of I. Ugi and R. Meyr, *Chem. Ber.*, **93**, 239 (1960), as modified by J. Casanova, Jr. We thank Dr. Casanova for helpful advice on synthesis.

seasoned by the same procedure whenever air had been admitted to the heated vessel. A conventional vacuum apparatus served for gas handling, storage, and pressure measurements. Because runs were made at low pressures (pressure of $\text{CH}_3\text{NC} \sim 10^{-2}$ mm), care was taken to exclude mercury vapor and stopcock grease from the reactor. The pressure of a known volume of sample and inert gas was measured with a glass diaphragm click gauge, and the reactor was isolated from the vacuum system by a Springham stopcock with a Viton A diaphragm. (This material absorbs higher boiling polar molecules excessively at pressures above a few millimeters.) Because of the small initial amount of material ($\sim 3.5 \times 10^{-6}$ mole) the whole sample was removed for analysis. Isomerization was carried to between 5 and 35% of reaction.

The efficiency of each foreign gas was measured usually for five or more different concentrations of added gas. The slope of the graph of rate constant *vs.* concentration of added gas was determined by the method of least squares. Temperature constancy was verified by repeating a check run with pure reactant at regular intervals.

Analysis. At the end of a run, the residual methyl isocyanide was quantitatively removed from the acetonitrile by passage of the sample through a short column of silver cyanide. A carrier gas (*n*-butyronitrile) was sometimes added to facilitate handling of the sample which was then analyzed by chromatography on a 1.8-m column of tetraglyme (dimethyl ether of tetraethylene glycol) on Fluoropak 80 (stationary phase). The column was recalibrated periodically with a standard mixture. Analyses were producible to $\pm 1\%$.

In a second procedure, an internal comparison method was employed. About 12% of propionitrile was mixed with the initial methyl isocyanide. The propionitrile was unaffected by the reaction or by passage through the silver cyanide column, and analysis was effected by comparison of product peak height with that for the propionitrile standard. This method avoided the necessity of quantitative measurement of the volume of the sample to be analyzed.

Basis of the Method. Results

Corrections to the Data. Corrections to the data were applied for: (a) temperature variation over the series of runs; all rate constants were standardized to 280.5°; (b) dead space (0.5%); (c) a time correction for removal of the sample at the lowest pressures ($\leq 1\%$).

Low-Pressure Rate Constants for Substrate. The falloff of the rate constant for methyl isocyanide isomerization has been studied down to a new low pres-

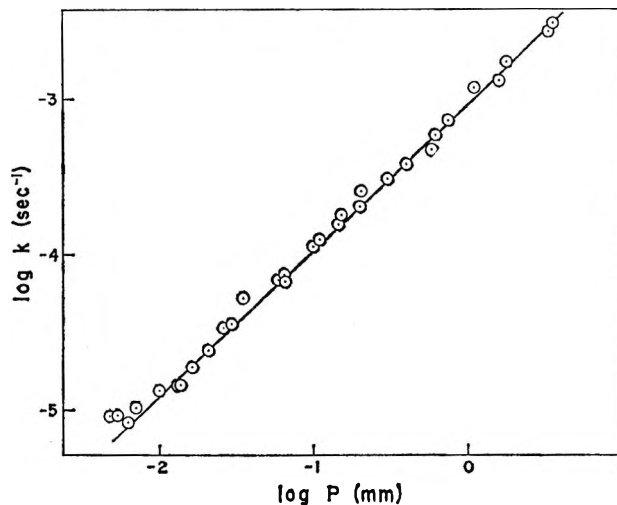


Figure 1. Plot of $\log k$ *vs.* \log (pressure), at low pressures, for methyl isocyanide at 280.5°.

sure of 5×10^{-3} mm ($k/k_\infty = 3 \times 10^{-4}$) at 280.5°. A plot of $\log k$ *vs.* \log (pressure) is shown in Figure 1. An understanding of the behavior of this reference curve is important for the present study. We shall examine some theoretical aspects of this behavior below. In the meantime some more practical aspects may be considered. Of these, two important matters have been emphasized by Johnston;⁸ they are surface effects and true low-pressure collisional efficiencies.

Heterogeneity. The general Lindemann expression for the unimolecular rate constant can be written as³⁰

$$k = \frac{(\text{rate})}{C_A} = \sum_i \frac{k_i^a k_i C_M}{k_i^d C_M + k_i} \quad (1)$$

where k_i^a is the second-order rate constant for activation of the energy state i above the critical energy, E_0 ; k_i^d is a similar quantity for deactivation; and k_i is a specific first-order rate constant for the reaction of excited molecules in the state i ; C_M is the concentration of collisional species.

The low-pressure limit occurs when $k_i^d C_M \ll k_i$ for all i

$$k_0 = \sum_i k_i^a C_M = k^a C_M \quad (2)$$

Equation 2 can afford a test for low-pressure heterogeneity. A first-order heterogeneous reaction would

(30) We use here the discrete-eigenstate general form given in ref 8 and follow Johnston's formulation, in brief (apart from notation). It should be noted that the RRKM semiclassical formulation cannot be handled by such a quantized form. Thus eq 2 of I for k , given as a discrete sum over ϵ^+ , should be written as an integral over ϵ^+ ; we are indebted to Dr. G. Hammes for calling our attention to a dimensional error in that form of the equation for k , with its misleading implication.

add a constant term to eq 2 and the low-pressure limit would become

$$k_0 = k^a C_M + k_{het} \quad (3)$$

Below 6×10^{-3} mm, the isocyanide rate constants very obviously began to deviate positively, indicating that surface effects were significant at that pressure; this was confirmed by packed vessel runs which gave evidence of increased rate at pressures below 10^{-2} mm. (A larger vessel is needed to extend the measurements to even lower pressures, and to this end measurements will be made in a 200-l. vessel.) In order to avoid this doubtful pressure region, a standard reactant pressure of $\sim 1.4 \times 10^{-2}$ mm was used for the present experiments.

A plot of the isocyanide rate data above 10^{-2} mm against pressure gave a zero pressure intercept on the k axis of $\sim 0.1 (\pm 0.1) \times 10^{-5} \text{ sec}^{-1}$. Relative to the value of k at 1.4×10^{-2} mm, which is $1.75 \times 10^{-5} \text{ sec}^{-1}$, this reveals possible heterogeneity of 6% which would be quite negligible at the higher inert gas pressures actually used.

Second-Order Requirement. For the case where M is a gas other than reactant, the first-order rate constant depends on the nature of M as well as on its concentration, and k may be written as⁸

$$k_{uni} = \sum_i \frac{k_i K_i \sum_m k_{mi}^d C_M}{\sum_m k_{mi}^d C_M + k_i} \quad (4)$$

where m denotes the possible dependence of the specific rate constants on the nature of M and, by detailed balance, $k_{mi}^a = k_{mi}^d K_i$, where K_i is the equilibrium fraction of reactant molecules in the excited state i .

It can be seen from eq 4 that, at higher pressures, the ratio of rate constants for different gases does not necessarily have a simple interpretation. It is only at the low-pressure limit that the relative values of rate constants for different foreign gases directly give the relative values of the activating efficiencies of these gases. The simplest condition arises if the relative efficiencies of inert gases are measured in large excess over the reactant concentration, and also if the inert gas pressure approaches zero; both simplifications together are impracticable.

The reaction order becomes second at zero pressure in the Lindemann mechanism but, experimentally, the order is always somewhat less than 2. However, if functional plots of k vs. C_M show little or no curvature, then it may be inferred that eq 2 is substantially obeyed. The plot of the present methyl isocyanide data in Figure 1 is a line of slope 0.96 ± 0.02 , so that the reaction is almost in the second-order region.

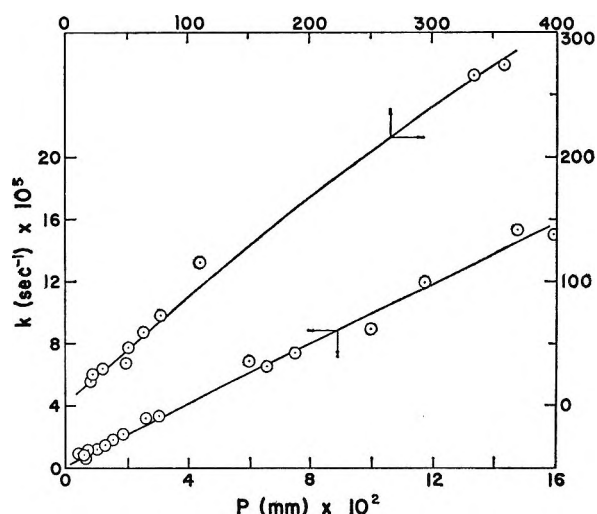


Figure 2. Low-pressure plot of k vs. pressure for methyl isocyanide at 280.5° .

From the more sensitive plot of k vs. p , which shows little curvature, one finds (Figure 2) that the slope scarcely declines over the range 10^{-2} to 0.4 mm, the highest effective pressure used in this study. Thus our data were taken in a region at or near the second-order region.

Further confirmation of this conclusion is given by a plot of the Arrhenius activation energy, E_a , obtained in I, against \log (pressure), as shown in Figure 3. It can be seen that E_a does not begin to increase until a pressure of at least 5 mm. Since the present total effective pressure was always less than 0.4 mm, the energy distribution of the reacting molecules was substantially close to the low-pressure limiting distribution.

RRKM Description of the Isomerization of Methyl Isocyanide. In Figure 4, a plot of falloff, $\log(k/k_\infty)$ vs. \log (pressure), is given for the low-pressure region, including earlier data from I at various temperatures. A recalculation of the falloff of CH_3NC has been carried out on the RRKM basis. The original calculation in I at 230° was based on the frequency assignment of Pillai and Cleveland.³¹ Subsequent results in II²⁷ for CD_3NC were treated on the basis of the frequency assignment for this molecule which had been given in the interim by Mottern and Fletcher.³² The rather heavy calculations in I for CH_3NC were not redone at that time, although the product rule ratio for the heavy and light molecules and activated complexes

(31) M. E. K. Pillai and F. F. Cleveland, *J. Mol. Spectry.*, **5**, 212 (1960).

(32) J. G. Mottern and W. H. Fletcher, *Spectrochim. Acta*, **18**, 995 (1962).

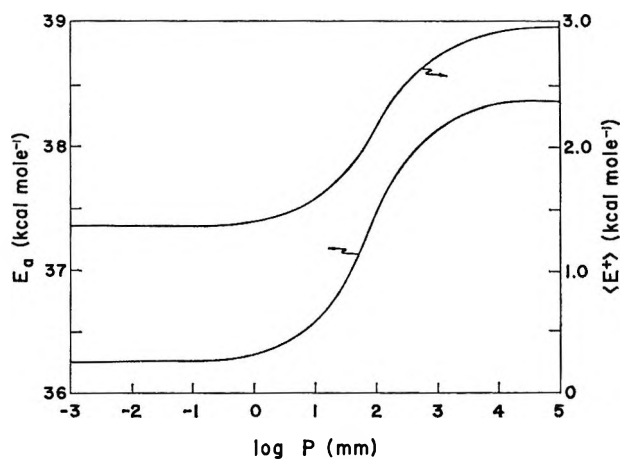


Figure 3. Plots of the experimental Arrhenius activation energy, E_a , and of the RRKM calculated average energy of reacting species above the critical threshold, $\langle E^+ \rangle$, as functions of pressure (log units).

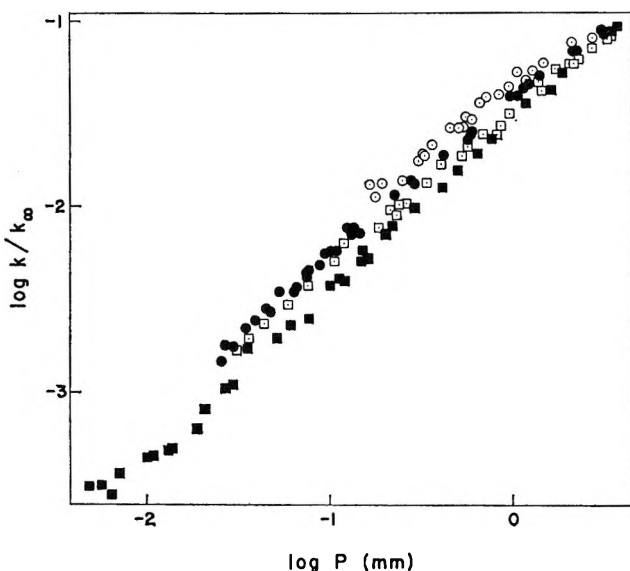


Figure 4. Plot of $\log k/k_\infty$ vs. \log pressure at various temperatures in the low-pressure region of methyl isocyanide isomerization: \circ , 199.4°; \bullet , 230.4°; \square , 259.8°; \blacksquare , 280.5°.

were not in the best agreement (*e.g.*, molecule ratio = 0.775). An improved molecule ratio (0.882) is obtained when the frequency assignment of Williams³³ for CH_3NC is compared with that of Mottern and Fletcher for CD_3NC ; the magnitude of the divergence from unity, due to differential anharmonicity lowerings of the observed frequencies, is of the order of magnitude frequently encountered for three C-H, C-D substitutions, and Williams' assignment is now adopted. It was considered desirable at this time to redo the cal-

culations in order to obtain a better theoretical description of the base curve, especially of the low-pressure rate constant. At the same time, the important quantity, $\langle E^+ \rangle_{p=0}$, the average energies of the CH_3NC molecules in excess of the critical, $E_0 = 37.85$ kcal mole⁻¹, and the energy distribution were reevaluated (see Figure 3).

The ratio 0.882 was taken as standard, and the original frequency assignments of the activated complexes in I and II were modified to yield the same product rule agreement. Specifically, the C-N ring deformation frequencies in the activated complexes were altered. This activated complex frequency represents a median frequency in vibrational assignment. The various frequencies are summarized in Table I.

Table I: Vibration Frequencies (cm^{-1}) for CH_3NC and CD_3NC and "300 Model" ^a Complexes

Species	CH_3NC	$\text{CH}_3\text{NC}^{+b}$	CD_3NC	$\text{CD}_3\text{NC}^{+b}$
C-H str	2966		2251	
	3014 (2)		2263 (2)	
N=C str	2166	1990	2165	1990
CH_3 def.	1429, 1467 (2)		1117, 1058 (2)	
CH_3 rock	1129 (2)		900 (2)	
C-N str	945	650	877	483
C-N-C def	263 (2)	263	249 (2)	249

^a Defined in I.²⁶ ^b Only changes from molecule frequencies shown.

The new assignment brings the calculated values for both k_∞ values, and for their ratio, into much better agreement with experiment; the $(k_{\text{H}}/k_{\text{D}})_\infty$ value is now reduced from the old value, 1.35 to 1.21. Also, $(k_{\text{H}}/k_{\text{D}})_0$ is lowered from 0.35 to 0.315. The old values involved a measured ΔE_a (*i.e.*, $E_{\text{aD}_3} - E_{\text{aH}_3}$) of 0.10 kcal mole⁻¹, which also corresponded to a ΔE_0 (*i.e.*, $E_{0\text{D}_3} - E_{0\text{H}_3}$) of identical magnitude. The new values just quoted are based on the measured $\Delta E_a = 0.10$ kcal; however, with the new frequency assignments, ΔE_0 is now reduced to 0.06 kcal. Considering that the standard deviation of ΔE_a was 0.05 kcal, it is evident that ΔE_0 is best simply taken as zero. On this basis, the calculated values are $(k_{\text{H}}/k_{\text{D}})_\infty = 1.14$ and $(k_{\text{H}}/k_{\text{D}})_0 = 0.294$. The agreement with experiment (Table II) is very good. Figure 5 gives the new plot of $k_{\text{H}}/k_{\text{D}}$ as a function of pressure and the agreement with experiment should be considered very satisfactory. It is evident that most of the variation occurs at pressures above 1 mm, so that the present range of pres-

(33) R. L. Williams, *J. Chem. Phys.*, 25, 656 (1956).

Table II: Calculated Quantities for CH₃NC and CD₃NC (230.4°)

Molecule	Q _v	Q _v ⁺	k _∞ × 10 ⁵ , ^a sec ⁻¹		k ₀ × 10 ⁴ , cc mole ⁻¹ sec ⁻¹ , calcd	⟨E ⁺ ⟩ _{p=0} , kcal mole ⁻¹	(k _H /k _D) _∞		(k _H /k _D) ₀	
			Calcd	Exptl			Calcd	Exptl ²⁷	Calcd	Exptl ²⁸
CH ₃ NC	4.380	2.561	92.6	92.5	1.022 ^b	1.214 ^d	1.14	1.07	0.294	0.28
CD ₃ NC	5.715	3.574	82.2	86.5	0.946 ^c	1.232 ^d				
					3.47 ^b					
					3.23 ^c					

^a Based on E₀ = 37.85 for CH₃NC and for CD₃NC. ^b σ = 4.50 Å. ^c σ = 4.33 Å. ^d Based on the strong collision assumption and, therefore, the maximum possible values;^{25b} calculated as discussed in ref 20b.

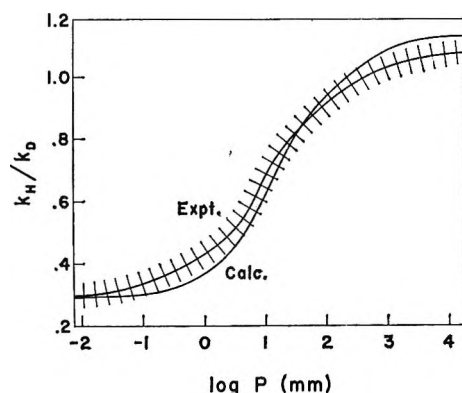


Figure 5. Comparisons of experimental (230.4°) and calculated isotopic rate ratio, k_H/k_D , for CH₃NC and CD₃NC as a function of pressure (log units). The cross-hatching summarizes the scatter of the experimental data described in II.

sures is substantially in the second-order region on this basis also.

An aspect complementary to this, and to the observed variation with pressure of E_a for CH₃NC (Figure 3), is the calculated variation of the average energy of the reacting molecules. At $p = 0, 10^{-2}, 10^{-1}, 4 \times 10^{-1}$ mm (the latter being the highest equivalent pressure used), and ∞ , the respective quantities are for CH₃NC: 1.361, 1.361, 1.364, 1.375, and 2.954 kcal; and for CD₃NC: 1.384, 1.385, 1.399, 1.458, and 3.711 kcal. The increase is slight at 0.4 mm, in agreement with other evidence as to the pressure regime of falloff being utilized here at 280°.

The strong collision low-pressure rate constant is

$$k_0 = \omega \int_{E_0}^{\infty} N(\epsilon) e^{-\epsilon/RT} d\epsilon / Q_v$$

where Q_v is the molecule vibrational partition function. The activated complex properties do not enter the expression for k_0 .

The effect of possible variation of the collision diameter of CH₃NC upon the rate constant (through ω)

can also be seen in Table II, where the calculation was repeated for $\sigma = 4.33$ Å, instead of the uncorrected viscosity value³⁴ of 4.5 Å used in I. The value $\sigma = 4.33$ Å was calculated from the Stockmayer potential for polar molecules;³⁵ k_0 is lowered by 7% when σ is reduced from 4.5 to 4.33 Å. Variations in collision diameters for various types of potential functions will be considered in the Discussion.

Inert Gas Data. Plots of observed rate constant k against pressure of added gas are presented in Figures 6–10. Up to 200-fold excess of added gas was used. Little curvature is evident in these graphs, again indicating that, for practical purposes, these systems are indeed close to the second-order region.

The relative rate constants for activation were found by the method of least squares for the relation $k = b + k_m^a C_M$, where b is an extrapolated intercept constant which tended to be greater than the base rate at around 1.4×10^{-2} mm. Some variations in the initial isocyanide pressure frequently occurred for different gases, or in a series with a given inert gas, but such variation was minor in practice. It can be shown^{25b} that in general k_m^a actually should vary with pressure (parent gas dilution); the present data correspond to the high dilution case and this explains, at least in part, the observed increase in b (extrapolated). These values will be presented and discussed in a later paper.

The relative activation efficiency, β_r , on a pressure-for-pressure basis was obtained from the ratio of the slope of the added gas plot to the slope of the base isocyanide curve. The efficiency was converted to a collision-per-collision basis, β_c , by use of the reduced mass and mean collision diameter for the molecules in question, $\beta_c = \beta_r (\sigma_{AA}/\sigma_{MA})^2$. The collision parameters

(34) P. M. Craven and J. D. Lambert, *Proc. Roy. Soc. (London)*, **A205**, 439 (1951).

(35) J. O. Hirschfelder, C. F. Curtiss, and R. B. Bird, "Molecular Theory of Gases and Liquids," John Wiley and Sons, Inc., New York, N. Y., 1954, p 209.

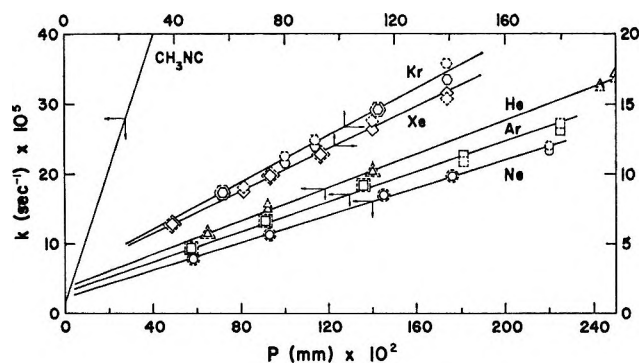


Figure 6. Plots of k vs. pressure for the rare gases. The base line for CH_3NC summarizes the experimental data for the parent gas. The difference in intercepts between Kr and Xe and the other gases is only apparent and due to the difference in scales. Solid and broken symbols refer to different analytical methods.

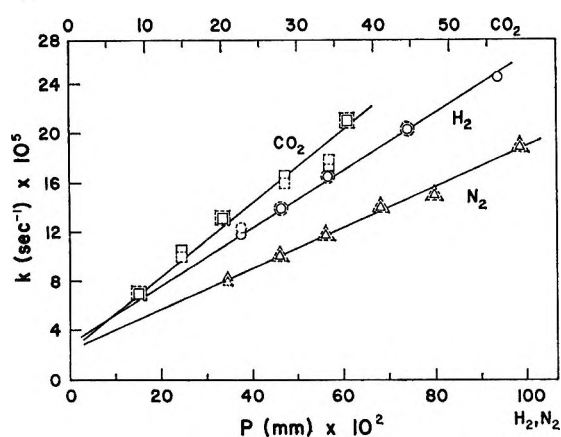


Figure 7. Plot of k vs. pressure for H_2 , N_2 , and CO_2 .

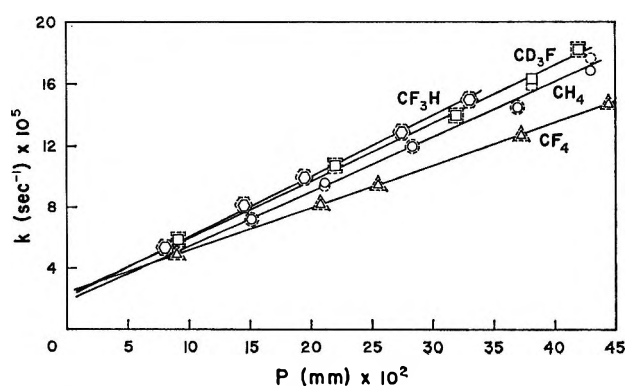


Figure 8. Plots of k vs. pressure for CH_4 , CD_3F , CHF_3 , and CF_4 .

and efficiencies for the inert gases are presented in Tables III and IV, where β_μ is a reduced mass-corrected efficiency, $\beta_\mu = \beta_p (\mu_{\text{MA}}/\mu_{\text{AA}})^{1/2}$; μ_{AA} is the reduced mass of the isocyanide, σ_{AA} is the kinetic collision di-

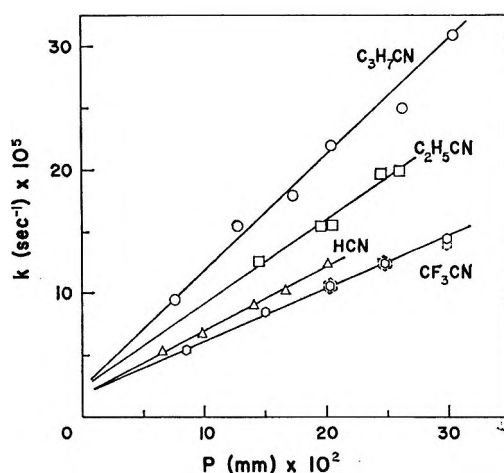


Figure 9. Plots of k vs. pressure for HCN , $\text{C}_2\text{H}_5\text{CN}$, CF_3CN , and $n\text{-C}_3\text{H}_7\text{CN}$. The plot for CH_3NC (Figure 6) virtually coincides with that for $\text{C}_3\text{H}_7\text{CN}$.

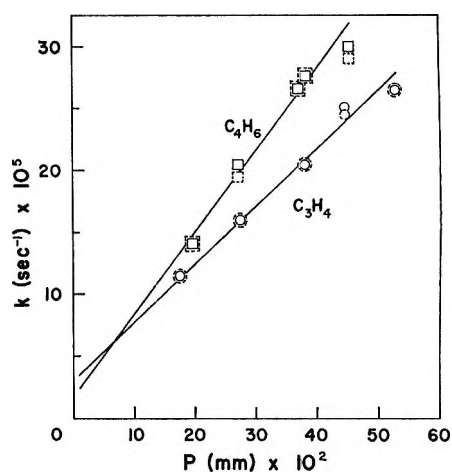


Figure 10. Plots of k vs. pressure for propyne and butyne-1.

ameter of the isocyanide, μ_{MA} and σ_{MA} are the reduced mass of the reactant-inert gas pair and the corresponding mean collision diameter, respectively.

Discussion

Collision Cross Sections. The "standard" cross sections for the nonpolar inert gases used in this study were values obtained from transport properties,³⁵ especially the viscosity. For polar addends, the Stockmayer potential³⁶ was used to calculate, or interpolate, values of the cross section. The assignment of values of the cross sections are of crucial importance in the calculation of β_c . The assignments described just below are made in lieu of any knowledge of appropriate

(36) L. Monchick and E. A. Mason, *J. Chem. Phys.*, **35**, 1676 (1961).

Table III: Collision and Intermolecular Parameters for Various Gases

Molecule	σ , Å ^a	ϵ/k , °K ^a	σ_{AM} , Å	ϵ_{AM}/k , °K	μ' , D. ⁴⁰	$\Omega^{(2,2)*}$, kT/ϵ_{AM}	s_{AM} , Å	s_{AA}^2/s_{AM}^2
CH ₃ NC	4.47 ^b	380 ^b	4.47		3.83	1.330	5.15	1.00
He	2.56	10.2	3.52	62		0.839	3.22	2.56
Ne	2.79	36	3.63	117		0.937	3.51	2.15
Ar	3.42	124	3.95	217		1.087	4.12	1.57
Kr	3.61	190	4.04	268		1.162	4.36	1.40
Xe	4.06	229	4.27	296		1.204	4.69	1.21
H ₂	2.93	37	3.70	117		0.937	3.58	2.07
N ₂	3.68	92	4.08	186		1.042	4.17	1.53
CO ₂	4.00	190	4.24	268		1.162	4.57	1.27
CH ₄	3.80	144	4.14	234		1.113	4.37	1.39
CD ₃ F	4.10 ^c	200 ^c	4.29	276		1.174	4.65	
	3.73 ^d	333 ^d	4.10	356	1.81	1.295	4.67	1.22
CHF ₃	4.38 ^e	254 ^e	4.43	311	1.63	1.226	4.90	1.10
CF ₄	4.70	153	4.59	242		1.124	4.86	1.12
	4.70 ^f	179 ^f	4.59	260		1.151	4.92	1.09
C ₂ H ₆ ^g	4.42	230	4.45	296		1.204	4.88	1.11
HCN ^h	3.93 ^g	320	4.20	348.7	2.95	1.282	4.75	1.17
CF ₃ CN ^h	4.80	300	4.64	337.7	2.1 ⁱ	1.267	5.22	0.973
C ₂ H ₅ CN ^h	5.00	400	4.74	389.8	4.04	1.345	5.50	0.879
C ₃ H ₇ CN ^h	5.50	400	4.98	389.8	4.07	1.345	5.78	0.796
CH ₃ CCH ^j	4.60	250	4.54	308.2	0.75	1.221	5.02	1.06
C ₂ H ₅ CCH ^j	5.20	300	4.84	337.7	0.81	1.267	5.45	0.895

^a All values are from ref 35 unless otherwise specified and are derived from viscosity data where possible. ^b From ref 34; See text for discussion of this quantity. ^c See ref 7a. ^d J. L. Stretton, *Trans. Faraday Soc.*, **61**, 1053 (1965); G. A. Miller and R. B. Bernstein, *J. Phys. Chem.*, **63**, 710 (1959). ^e R. R. Boade and S. Legvold, *J. Chem. Phys.*, **42**, 569 (1965); values derived from a Lennard-Jones 7-28 potential. ^f Data from I—approximate value only. ^g σ (HCN) was calculated from viscosity data,³⁵ assuming a spherical molecule. In view of the similarity of HCN to H₂O where the values of ϵ/k vary widely according to the method of calculation,³⁶ the estimated value of ϵ/k of 320 for HCN must only be regarded as a reasonable estimate; the HCl-alkylhalide series behavior^d is comparable. ^h Values of σ and ϵ/k for the higher nitriles were interpolated from the alkyl chloride and alcohol series listed by Mason.³⁶ ⁱ Calculated value. ^j Parameters for the higher acetylenes were interpolated from the corresponding hydrocarbon values³⁵ and are merely reasonable estimates.

cross sections for the energy transfer process under consideration here.

Nonpolar Gases. The collision cross sections and their temperature dependence were obtained from transport properties with the use of the 6-12 Lennard-Jones potential, $V(r) = 4\epsilon[(\sigma/r)^{12} - (\sigma/r)^6]$. The usual combining rules were employed for the force constants

$$\sigma_{AM} = (\sigma_A + \sigma_M)/2; \epsilon_{AM} = (\epsilon_A \epsilon_M)^{1/2}$$

The temperature-dependent collision diameter, $s_{AM}^2 = \sigma_{AM}^2 \Omega^{(2,2)*}$, was evaluated from the integrals $\Omega^{(2,2)*}(kT/\epsilon_{AM})$ which are tabulated³⁵ as a function of the reduced temperature, $T^* = kT/\epsilon_{AM}$. Collision cross sections at the reaction temperature 280° were used to calculate β_c . The results are tabulated in Table III.

An alternative approach to the temperature variation of cross section has been made by Rowlinson,³⁷ who derived a potential-dependent expression for molecules which approach to a distance, d , or less; d is the maximum internuclear distance which is to be counted as a

collision. For $d = \sigma$, the collision number is just the rate of collisions of hypothetical spheres of this diameter and is proportional to $T^{1/2}$. For $d = r_m$ (where $r_m = 2^{1/6}\sigma$, and $V(r_m) = \epsilon$, the depth of the potential well defined by a Lennard-Jones function) an expression is obtained which is the analog of the Sutherland equation for a hard sphere with an attractive potential. The collision number is increased not only by a factor of $(r_m/\sigma)^2$ over $Z_{\text{hard sphere}}$, but also by a temperature-dependent factor $(1 + \epsilon/kT)$. Depending on the importance of the attractive or repulsive part of the potential for energy exchange, the collision cross section should be defined accordingly. The attractive part is important for the duration of a collision, the repulsive part for the perturbation of the internal states brought about by a collision. The use of s_{AM} considers both features.

Polar Inert Gases. For polar gases, the interaction potential is angular dependent. The most successful

(37) J. S. Rowlinson, *Mol. Phys.*, **4**, 317 (1961).

Table IV: Measured Collision Efficiencies for Various Gases

Molecule	$k_m^a \times 10^6$, mm ⁻¹ sec ⁻¹	β_p	$(\mu_{AM}/\mu_{AA})^{1/2}$	β_μ	β_c
CH ₃ NC	96.0	(1.00)	1.00	(1.00)	(1.00)
He	12.0	0.125	0.422	0.055	0.14
Ne	9.06	0.094	0.813	0.076	0.16
Ar	10.6	0.110	0.993	0.11	0.17
Kr	10.5	0.109	0.158	0.13	0.18
Xe	9.50	0.099	1.234	0.12	0.15
H ₂	23.4	0.244	0.306	0.074	0.15
N ₂	16.4	0.171	0.900	0.15	0.24
CO ₂	44.3	0.462	1.017	0.47	0.60
CH ₄	32.7	0.341	0.749	0.26	0.35
CD ₃ F	37.3	0.389	0.974	0.38	0.46
CHF ₃	40.4	0.421	1.123	0.47	0.52
CF ₄	27.7	0.289	1.168	0.34	0.38
C ₂ H ₆ θ	~0.6
HCN	50.6	0.527	0.861	0.45	0.53
C ₂ H ₅ CN	67.5	0.703	1.07	0.75	0.66
<i>n</i> -C ₃ H ₇ CN	89.9	0.937	1.12	1.05	0.84
CF ₃ CN	42.2	0.440	1.181	0.52	0.51
CH ₃ CCH	46.5	0.484	0.994	0.48	0.51
C ₂ H ₅ CCH	65.0	0.685	1.064	0.73	0.66

^a Data from I.²⁶

potential for polar gases is that of Stockmayer (the 12-6-3 potential)

$$V(r) = 4\epsilon \left[\left(\frac{\sigma}{r} \right)^{12} - \left(\frac{\sigma}{r} \right)^6 \right] - \frac{\mu'_A \mu'_M \zeta}{r^3}$$

where μ'_A and μ'_M are the dipole moments of the two interacting molecules and the angular dependent factor is $\zeta = 2 \cos \theta_A \cos \theta_M - \sin \theta_A \sin \theta_M \cos \phi$. In the limit, as μ'_A or $\mu'_M \rightarrow 0$, the 12-6 potential is recovered.

Hirschfelder, *et al.*,³⁵ and Rowlinson³⁸ have used second virial coefficient data to calculate σ and ϵ/k from the polar potential, but the values obtained sometimes show great inconsistency when examined in homologous or related series of molecules, as compared with values obtained from the 12-6 potential. These discrepancies have been considered by Monchick and Mason,³⁶ who have calculated the potential parameters σ and ϵ/k for a series of molecules from experimental viscosity coefficients with the 12-6-3 potential. The values so obtained proved to be fairly consistent with those derived from the 12-6 potential. Their σ parameters show reasonable trends in homologous series and correspond fairly closely (± 0.1 A) to those obtained from the nonpolar potential. The parameters deduced from second virial coefficients are very sensitive to dipolar forces, indicating that the point dipole model used may be too artificial. These authors conclude that viscosity-derived parameters should be given preference. On this basis, only slight differences arise

between polar and nonpolar molecules of related structure, *e.g.*, CF₃H and CF₄. They have tabulated accurate values of the collision integrals $\Omega^{(2,2)*}$ calculated from the 12-6-3 potential, for a range of values of the angle-dependent function, including zero.

The value of σ for CH₃CN calculated by Rowlinson³⁸ from virial coefficient data, using $\mu' = 3.5$ D., is given as 4.02 A; a recalculation³⁹ using the accepted value⁴⁰ of $\mu' = 3.92$ D. yields a value of $\sigma = 4.42$ A.

Using the same method as Rowlinson with the virial coefficient data of CH₃CN, $\sigma(\text{CH}_3\text{NC})$ is calculated to be 4.33 A with use of $\mu' = 3.83$ D.; also ϵ/k is found to be 310°K.

However, for continuity with earlier work and in line with the above discussion, the value of $\sigma(\text{CH}_3\text{CN}) = 4.47$ A ($\epsilon/k = 380^\circ\text{K}$), as calculated from viscosity measurements and the 12-6 potential by Craven and Lambert,³⁴ was also used for CH₃NC and for the calculation of s_{AM} values at 280° for methyl isocyanide-inert gas pairs.

In cases where viscosity data were not available for polar molecules to allow calculation of the potential parameters by the method of Monchick and Mason,³⁶ and because the parameters derived by the 12-6-3

(38) J. S. Rowlinson, *Trans. Faraday Soc.*, **45**, 972 (1949).

(39) See ref 35, following the method on p 215.

(40) A. L. McClellan, "Experimental Dipole Moments," W. H. Freeman and Co., San Francisco, Calif., 1963.

potential are not very different from those obtained from the 12-6 potential, we have felt justified in calculating values of σ and ϵ/k at 280° using collision integrals $\Omega^{(2,2)*}$ and T^* for the 12-6 potential; the cases concerned are mainly aliphatic acetylenes for which μ' is small (~ 0.8 D.) and its neglect very minor.

General Summary

It can be seen that the efficiencies of inert gases in deactivating highly vibrationally excited levels of polyatomic molecules are quite unlike those for one-vibrational-quantum deactivation of small molecules at low energies.⁹ The entire range of efficiencies β_c is covered here by a factor of 6 (Table IV) and a quasi-statistical collisional relaxation in such cases has been proposed, together with supporting calculations.^{7a}

Some general trends in the results may be noted at this time, although specific consideration of the data and some conclusions regarding the absolute amounts of energy transferred on collision with various inert gases will be delayed to a paper to follow.

For the noble gases, β_c increases monotonically from helium through krypton; the deviation for xenon is suspect. Because molecular size, polarizability, etc., all increase in similar fashion, these data alone cannot determine which individual parameter(s) is most important in determining energy transfer efficiency. The

magnitudes of β_c for the diatomic molecules suggest that rotational degrees of freedom are unimportant here in the transfer of energy.

The series of fluorinated methanes in principle provides an opportunity to assess the importance of change of frequency pattern and dipole moment on energy transfer. The importance of either factor is not clearly apparent from these results in the light of the data on the higher alkyl nitriles and substituted acetylenes. Approximately equal efficiency is obtained with propionitrile and butyne despite the widely differing dipole moments between the two series of addends; [μ' (RCN) ~ 4.0 D.; μ' (RCCH) ~ 0.80 D.].

All of these considerations depend upon the validity of the assignments made for the collision cross section of the inert molecules which have been transferred to the present system from other phenomena which differ greatly in their nature. It is this uncertainty which makes unsuitable any detailed interpretations at this time. It is evident that further and much more extensive data will be required in order to delineate adequately even the qualitative behavior of these thermal systems and to permit deduction of the relevance and magnitude of various molecular and structural parameters in some instances. We are undertaking such studies with the intention, also, of making an assignment of collision cross sections for the energy transfer processes concerned, such not being presently available for any system.

Correlation of Turbidity and Activity Data. III. The System

Tungstosilicic Acid–Sodium Chloride–Water¹

by J. P. Kratochvil, L. E. Oppenheimer,² and M. Kerker

Department of Chemistry and Institute of Colloid and Surface Science, Clarkson College of Technology, Potsdam, New York (Received February 11, 1966)

Light scattering and vapor pressure data for the three-component system 12-tungstosilicic acid (TSA)–sodium chloride–water were obtained over the concentration range up to 1 g/ml for TSA and for NaCl concentrations of 0, 0.02, 0.10, 0.30, 0.50, 1.0, and 3.0 *M*. The effect of the added NaCl is to increase the turbidity very markedly. The corresponding curves of $Hc/\Delta\tau$ vs. c become more linear and exhibit a smaller slope with increasing concentration of NaCl. Each of these curves, when extrapolated to zero concentration, gives the correct molecular weight, indicating the absence of small-ion binding. Attempts to correlate the vapor pressure and turbidity data failed because of the inability to obtain either of these data sufficiently accurately at the highest dilutions.

Introduction

The excess turbidity, $\Delta\tau$, of a binary solution may be expressed by

$$\Delta\tau = -\frac{Hc\bar{V}_1}{d \ln a_1/dc} \quad (1)$$

$$H = \frac{32\pi^3 n^2 \left(\frac{dn}{dc}\right)^2}{3N_A \lambda_0^4} \quad (2)$$

where c is the concentration of the solute in grams per milliliter, \bar{V}_1 and a_1 are the partial molal volume and activity of the solvent, n is the refractive index of the solution, N_A is Avogadro's number, and λ_0 is the wavelength *in vacuo*. This offers the possibility of correlating light scattering results with other experiments which measure activity; indeed, light scattering can be a tool for determining the activity.

In the previous papers of this series,^{3,4} the turbidity and the vapor pressure of 12-tungstophosphoric and 12-tungstosilicic acids were measured up to a concentration of about $c = 1.0$. There was a close correlation between the values of the activity of the water obtained by these two techniques. These experiments are here extended to the ternary system 12-tungstosilicic acid (TSA)–sodium chloride–water. An appropriate equation relating the turbidity and activities in such a three-component system will be given below. The

concentrations of both TSA and NaCl have been varied systematically over a wide range.

The general problem of interpreting light scattering data from multicomponent systems containing ionic species has been extensively reviewed recently.^{5–8} We had hoped that these experiments would enable us to determine the effect of added electrolyte upon the activity of TSA which, in dilute solution, behaves as a 1–4 electrolyte^{9,10} and thus to correlate these activity

(1) Supported in part by the U. S. Atomic Energy Commission, Contract No. AT(30-1)-1801; taken from the M.S. thesis of L. E. Oppenheimer.

(2) Lever Brothers Fellow.

(3) J. B. Goehring, M. Kerker, E. Matijević, and S. Y. Tyree, Jr., *J. Am. Chem. Soc.*, **81**, 5280 (1959).

(4) M. Kerker, J. P. Kratochvil, R. H. Ottewill, and E. Matijević, *J. Phys. Chem.*, **67**, 1097 (1963).

(5) D. Stigter in "Electromagnetic Scattering," M. Kerker, Ed., Pergamon Press Ltd., Oxford, 1963, p 303.

(6) J. Th. G. Overbeek, A. Vrij, and H. F. Huisman in "Electromagnetic Scattering," M. Kerker, Ed., Pergamon Press, Ltd., Oxford, 1963, p 321.

(7) S. N. Timasheff in "Electromagnetic Scattering," M. Kerker, Ed., Pergamon Press Ltd., Oxford, 1963, p 337.

(8) E. F. Casassa and H. Eisenberg, *Advan. Protein Chem.*, **19**, 287 (1964).

(9) E. Matijević and M. Kerker, *J. Am. Chem. Soc.*, **81**, 5560 (1959).

(10) J. R. Keller, E. Matijević, and M. Kerker, *J. Phys. Chem.*, **65**, 56 (1961).

data with the turbidity. However, for reasons which are discussed below, it was not possible to do this.

Experimental Section

Materials. Several commercial samples of TSA were used (Fisher Certified reagent, Baker and Adamson reagent). These were purified by repeated extractions of the acid from aqueous solution with ether and hydrochloric acid, as described elsewhere.⁹ For the Baker and Adamson acid, the purification did not affect the results, whereas Fisher samples, with one exception, had to be purified before reproducible results could be obtained. Most of the experiments were performed with the Fisher sample that was not influenced by the purification. The solutions of the purified samples were colorless and clear even at concentrations approaching saturation (about 2.3 g/ml). Other chemicals were of the highest grade and were used as received. The doubly distilled water was obtained from an all-Pyrex still.

Preparation of Solutions. The procedure described previously⁴ was followed except that the dilutions of the ternary solutions for light scattering measurements were carried out by the addition of clarified NaCl solution directly into the light scattering cell. The initial stock solution also contained the same concentration of sodium chloride so that this quantity remained constant in the course of a series of dilutions. The concentration of the diluted solutions was then determined by weight. This concentration was checked at frequent intervals, usually every third dilution, by refractometry. The concentration of the stock solution was determined in the same way from the known value of the refractive index increment. The diluted solutions prepared in this manner were refiltered whenever necessary. The more dilute ternary solutions were clarified after every addition of NaCl solution. The dilutions were prepared from several stock solutions of different initial concentration of TSA, so that a great deal of overlapping data at close intervals was assured.

Solutions were clarified by repeated filtration directly into the cell through Millipore filters under slight nitrogen pressure. Filters of 220- and 450-m μ porosity were used simultaneously. All solutions were carefully inspected visually in a strong beam of light at low angles. The cell was tightly covered with several layers of Parafilm.

Light Scattering and Refractive Index Measurements. Essentially, technique A of the previous paper⁴ was utilized. This technique, with small modifications, was critically tested recently in the determination of the Rayleigh ratio and depolarization of such weakly scattering liquids as water and CCl₄,¹¹ and the determination of the absolute angular intensities of mono-

disperse Dow polystyrene latexes.¹² The standard 1.2-cm slit system, defining the incident beam of a Brice-Phoenix light scattering photometer, and a Pyrex 2.4-cm square cell or a 4.0-cm semiocagonal cell were used. The instrument was calibrated at frequent intervals using the standard opal diffusors supplied by the manufacturer. The reliability of this calibration procedure for obtaining absolute scattering intensities has been recently discussed in detail.^{13,14} Changes in the calibration constant between determinations were small, usually less than 1%. Polarization measurements were made using Glan-Thompson prisms.

Refractive index measurements were obtained at 25° with a Brice-Phoenix differential refractometer, as described earlier.⁴

Vapor Pressure Measurements. Vapor pressure measurements were obtained with a Mechrolab Model 301A vapor pressure osmometer at 25°. The temperature was controlled by the thermostating unit supplied by the Mechrolab Co. A water-cooled metal jacket surrounded the chamber block of the instrument. It was found that a temperature difference of at least 3° between the working temperature (25°) and the surroundings was needed in order to assure proper thermostating. The instrument was calibrated with aqueous NaCl solutions. A plot of the resistance change, ΔR , against the activity of water for these solutions was made, using the values given by Robinson and Stokes.¹⁵ The calibration curve did not change over a period of 9 months. The calibration curve of activity of water *vs.* ΔR was made from 65 determinations of ΔR on 12 different solutions of NaCl. The data could be represented by the linear equation $a_w = -0.3660 \times 10^{-3} \Delta R + 0.9999$. The standard deviations of the slope and intercept were 1.38×10^{-6} and $\pm 0.95 \times 10^{-4}$, respectively. The standard deviation of the fit was 3.50×10^{-4} .

Since ΔR varies with time, it was necessary to choose an optimum time for taking the readings. The criterion chosen was the time at which the change of ΔR for the NaCl solutions was the slowest. This was found to be 10 min after the solution was placed on the thermistor bead, and all readings were taken at this time. In order to check the consistency of the method, a calibration curve was also prepared for a time of 5 min.

(11) J. P. Kratochvil, M. Kerker, and L. E. Oppenheimer, *J. Chem. Phys.*, **43**, 914 (1965).

(12) J. P. Kratochvil and C. Smart, *J. Colloid Sci.*, **20**, 875 (1965).

(13) J. P. Kratochvil, G. Deželić, M. Kerker, and E. Matijević, *J. Polymer Sci.*, **57**, 59 (1962).

(14) J. P. Kratochvil, *Anal. Chem.*, **36**, 458R (1964).

(15) R. A. Robinson and R. H. Stokes, "Electrolyte Solutions," Butterworth and Co. Ltd., London, 1959.

It was found that the 5-min readings gave values for the activity of water in TSA solutions which were very close to those obtained from the 10-min readings. However, the standard deviations of the measurements were larger when 5-min readings were utilized than those obtained from the 10-min readings.

It was found that in order to obtain reproducible results, the thermistor which held the drop of solution had to be rinsed with 4-6 drops of solution between runs. When the instrument was not in use, distilled water was kept on both thermistors. In most cases, ΔR was found to decrease with time. However, when the water on the bead was replaced by a drop of a solution, or when a more concentrated solution replaced a less concentrated one, the value of ΔR would increase with time, resulting in a large error in the 10-min value of ΔR . This effect could be avoided by allowing a drop of solution to remain on the bead for several minutes and then rinsing with the solution prior to taking the readings.

The instrument could be used to measure activities of water down to 0.96, which corresponds to about 1.2 *m* NaCl. Reproducibility within 1% of ΔR was achieved in consecutive runs, except at the higher concentrations in the usable range for which the reproducibility was within 1.5%. At least two consecutive runs were made with each solution.

Results

Light scattering, refractive index, and vapor pressure data were obtained on solutions of varying concentration containing a constant concentration of NaCl. This varied between zero and 3 *M*. The values of dn/dc for TSA in pure water had been obtained earlier.⁴

A small, but finite, excess depolarization, ρ_u , was observed for these solutions of TSA. The dependence of ρ_u upon TSA concentration is presented in Figure 1 for several NaCl concentrations. The excess depolarization is defined as the ratio of the excess horizontally polarized scattered intensity at 90° to the excess vertically polarized intensity with an unpolarized incident beam. It appears that there is little, if any, effect of the NaCl concentration of ρ_u . The observed $\Delta\tau$ values at various concentrations of TSA were corrected by multiplying by the Cabannes' factor $[(6 - 7\rho_u)/(6 + 3\rho_u)]$. The correction factor varied between 0.97 and 0.93 in the concentration range covered. The solutions were checked for fluorescence and none was found. Dissymmetries of scattering were measured on some solutions and always found to be very close to unity.

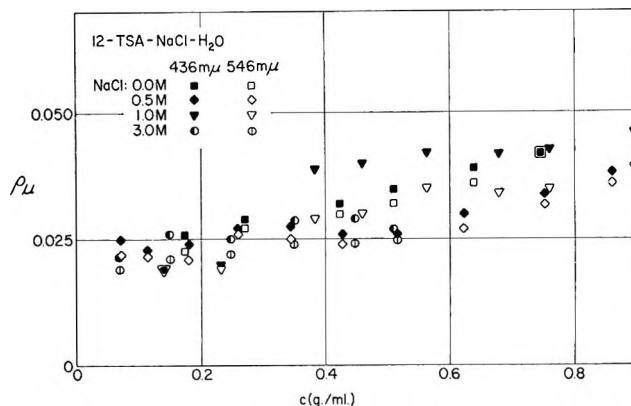


Figure 1. The excess depolarization, ρ_u , vs. concentration, c , of TSA in water and sodium chloride solutions.

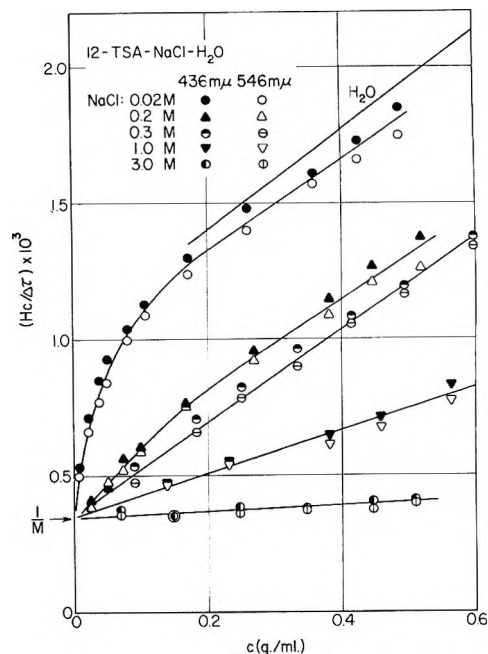


Figure 2. $Hc/\Delta\tau$ vs. c curves for TSA in NaCl solutions. The arrow indicates the value of the ordinate corresponding to the reciprocal of the formula weight of TSA.

The values of $Hc/\Delta\tau$ are plotted in Figure 2 for both wavelengths used (λ_0 436 and 546 $m\mu$) and for several concentrations of NaCl (0.02, 0.2, 0.3, 1.0, and 3.0 *M*). It should be noted that because of the high concentrations of TSA in these experiments, H is not constant, but varies with concentration.⁴

The detailed results are presented in Table I. The second and third columns list the refractive index increments at each of the NaCl concentrations. The $Hc/\Delta\tau$ data are linear over the TSA concentrations given in the fourth column of Table I, and the slopes over these linear ranges as determined by the method

Table I: Light Scattering Results for Solution of TSA in Various Concentrations of NaCl

Concn of NaCl, M	dn/dc , ml/g		Range of cTSA, g/ml	Slope $\times 10^3$	$(Hc/\Delta\tau)_{c=0} \times 10^3$	$\sigma_{fit} \times 10^3$	$M_{TSA} \times 10^3$	$B \times 10^3$, ml mole g^{-2}
	436 $m\mu$	546 $m\mu$						
H ₂ O	0.1066	0.1005	0.174–0.746	1.85		0.053		
0.02	0.1066	0.1005	0.172–0.486	1.68	0.34 ^a	0.036	2.9	10.0 ^b
0.10	0.1066	0.1005	0.163–0.778	1.93	0.34 ^a	0.092	2.9	4.0 ^b
0.20	0.1064	0.1000	0.169–0.518	1.62	0.34 ^a	0.035	2.9	1.2 ^b
0.30	0.1064	0.1000	0.0912–0.811	1.71	0.359	0.024	2.79	0.86
0.50	0.1056	0.0988	0.0726–0.753	1.27	0.356	0.034	2.81	0.64
1.0	0.1046	0.0972	0.140–0.758	0.80	0.351	0.025	2.86	0.40
3.0	0.0968	0.0909	0.0702–0.511	0.12	0.346	0.012	2.89	0.060

^a These intercepts were obtained by graphical extrapolation of the curves of Figure 2. ^b These values were obtained from the limiting slopes at infinite dilution of the curves of Figure 2.

of least squares are given in the fifth column. The next column gives the value of $Hc/\Delta\tau$ at infinite dilution. For NaCl concentrations equal to or greater than 0.3 M NaCl, these limiting values were obtained from the least-squares expressions. At lower salt concentrations, for which the curves bend downward at high TSA dilutions, the limiting values of $Hc/\Delta\tau$ were obtained by graphical extrapolation. The standard deviations between the least-squares-fitted values of $Hc/\Delta\tau$ over the linear range and the experimental values are listed in column seven.

The Debye expression for two-component systems at low concentrations

$$\frac{Hc}{\Delta\tau} = \frac{1}{M} + 2Bc \quad (3)$$

where M is the molecular weight and B is the second virial coefficient, can be used to express these results at sufficiently low concentrations, even though it is not generally valid for three-component systems. The values of M listed in Table I were obtained directly from the tabulated values of $Hc/\Delta\tau$ at infinite dilution. For 0.3 M NaCl and higher concentrations, B was obtained from the least-squares expressions. At lower NaCl concentrations, B was obtained from the limiting tangents to the curve. Obviously, considerable error is involved in this latter procedure. When the $Hc/\Delta\tau$ values for TSA solution in water reported earlier⁴ are corrected for depolarization, as measured in this work, they fall within 3% of the corresponding values in this paper.

The activities of water, as measured by the vapor pressure osmometer, were also subjected to a least-squares analysis. Table II contains the polynomial expressions which best fit the data at each NaCl concentration and the standard deviations. The maximum concentration of TSA that could be attained for

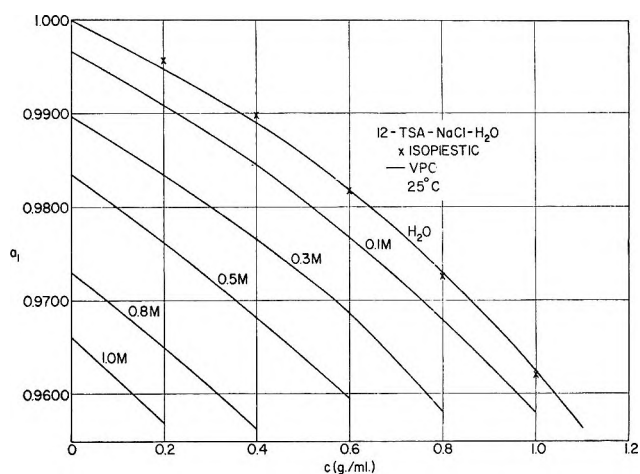


Figure 3. Activity of water, a_1 , vs. c curves in TSA solutions containing NaCl. VPO refers to the vapor pressure osmometer measurements, and isopiestic points are taken from ref 2.

each NaCl concentration is also listed. In Figure 3, these smoothed values of the activity of water are plotted vs. c for each constant concentration of NaCl. In addition to the least-squares criterion, the first term of each equation listed in Table II was chosen to within at least 0.0002 of the known activity of water in aqueous NaCl solutions as given by Robinson and Stokes.¹⁵ As shown in Figure 3, the results in pure water obtained by us with the vapor pressure osmometer agree closely with the isopiestic measurements performed by Professor S. Y. Tyree and reported by us earlier,⁴ except at lower concentration where the latter would be expected to be less accurate.

Discussion

The most striking feature of these results is the large increase in turbidity of the TSA solution, or the large decrease in $Hc/\Delta\tau$, with added NaCl. This parallels

Table II. The Least-Squares Equations of Activity of Water, a_w , as a Function of TSA Concentration, c , the Standard Deviations of the Fit, and the Maximum Concentrations of TSA in the Vapor Pressure Experiments

Concn of NaCl, M		Std dev	Max concn, g/ml
H ₂ O	$a_w = 1.0000 - 0.0224c - 0.0099c^2 - 0.0040c^3 - 0.0008c^4$	5.6×10^{-4}	1.131
0.1	$a_w = 0.9966 - 0.0265c - 0.0087c^2 - 0.0034c^3$	1.5×10^{-4}	1.000
0.3	$a_w = 0.9897 - 0.0317c + 0.0059c^2 - 0.0195c^3$	2.9×10^{-4}	0.785
0.5	$a_w = 0.9834 - 0.0342c - 0.0092c^2$	1.2×10^{-4}	0.584
0.8	$a_w = 0.9731 - 0.0390c - 0.0076c^2$	0.38×10^{-4}	0.364
1.0	$a_w = 0.9660 - 0.0450c$	3.4×10^{-4}	0.200

the result found earlier for both 12-tungstophosphoric and 9-tungstophosphoric acids¹⁶ and is qualitatively similar to effects noted for many charged colloids and macroions.⁵⁻⁸

As can be seen from Figure 2, the values of $Hc/\Delta\tau$ converge to a common intercept whose reciprocal (see Table I) agrees very closely with the monomeric formula weight of 2879 for H₄SiW₁₂O₄₀. This indicates the absence of small-ion binding to the TSA up to concentrations of 3.0 M NaCl and the existence of monomeric tungstosilicate anions in these solutions. The curvature of $Hc/\Delta\tau$ vs. c for the lower range of NaCl concentrations ($<0.3 M$) makes it impossible to determine the molecular weight by the usual linear extrapolation from the region of higher TSA concentration. However, at sufficiently low concentrations of TSA, the Debye expression, eq 3, does represent these data.

The values of the second virial coefficient, B (Table I) obtained from the limiting slopes at high dilution, reflect the strong interactions that exist in TSA solutions even in the presence of a relatively large amount of added electrolyte. Normally, for charged colloids and macroions, the interaction effects are greatly suppressed, or completely eliminated, at an ionic strength of about 0.1 M . In the case of TSA, even in the presence of 1.0 M NaCl, B has a value typical of nonionic polymers in good solvents, and in 3.0 M NaCl, B still has a finite positive value. Our value of B in 0.3 M NaCl is close to that (0.61×10^{-3}) determined by Kronman and Timasheff at this concentration of supporting electrolyte.¹⁷ Their measurements were restricted to the limited range, $c \leq 0.1$ g/ml. (The above value of B has been obtained from Figure 2 in Kronman and Timasheff's paper which we found to have a slope of 1.22×10^{-3} . These authors have erroneously reported this to be 1.22×10^{-2} .)

We have attempted, unsuccessfully, to determine the activity of the TSA in these solutions from the values of the activity of the water. With this information, it would have been possible to correlate the activity

data from the vapor pressure measurements with the turbidity obtained from light scattering. The procedure described by McKay and Perring¹⁸ for the calculation of the activity coefficients of mixed aqueous electrolyte solutions from vapor pressure data appeared promising. This, in turn, required a knowledge of the activity of TSA in pure water which could be obtained, in principle, from the vapor pressure data for the binary solutions in the absence of NaCl.

As is so often the case,¹⁵ particularly for polyvalent electrolytes, the accurate integration of the Gibbs-Duhem equation proved to be a stumbling block. A new technique for graphical integration proposed by Lakhanpahl and Conway¹⁹ at first appeared to offer some promise of success, particularly since we were able to calculate the activity coefficients of sulfuric acid up to concentrations of 0.5 M by this method from the isopiestic water activities.²⁰ The results agreed with those derived from emf measurements²¹ to within 2%. Unfortunately, even this treatment broke down for the TSA data. The distance C in Figure 2 of ref 17 becomes very large. Even an approximate estimate of its value was impossible because the area A in the same figure changes only slightly for large variations in C . It now appears that much more accurate vapor pressure data are needed, and even more importantly, these must be measured at much lower concentrations than appears feasible either by the technique we have used or by the isopiestic technique.²²

(16) E. Matijević and M. Kerker, *J. Am. Chem. Soc.*, **81**, 5280 (1959).

(17) M. J. Kronman and S. N. Timasheff, *J. Phys. Chem.*, **63**, 629 (1959).

(18) H. A. C. McKay and J. K. Perring, *Trans. Faraday Soc.*, **49**, 163 (1953).

(19) M. L. Lakhanpal and B. E. Conway, *Can. J. Chem.*, **38**, 199 (1960).

(20) H. Sheffer, A. A. Janis, and J. B. Ferguson, *Can. J. Res.*, **B17**, 336 (1939).

(21) R. A. Robinson, *Trans. Faraday Soc.*, **35**, 1229 (1939).

(22) We are grateful to Professor R. H. Stokes for useful discussion on this point.

There is still a possibility of utilizing the light scattering data and the vapor pressure data in order to determine the activity of the TSA in the presence of NaCl. The point of departure is the expression for the turbidity of a three-component system in the form given by Stigter²³

$$\frac{\Delta\tau}{H'} = \frac{m_2}{\rho_2} \left[\frac{\left\{ \psi_2 + \psi_3 \left(\frac{\partial m_3}{\partial m_2} \right)_{T,p,\mu_3} \right\}^2}{\left(\frac{\partial \mu_2}{\partial m_2} \right)_{T,p,\mu_3}} + \psi_3^3 \left(\frac{1}{a_3} - \frac{1}{a_{33}^*} \right) \right] \quad (4)$$

where

$$H' = \frac{32\pi^3 n^2 R T}{3N_A \lambda_0^4} \quad (5)$$

We choose component 1 as NaCl, component 2 as TSA, and component 3 as water. This is done because the vapor pressure data enable us to identify the conditions corresponding to constant value of the chemical potential of component 3, μ_3 (constant vapor pressure of water). The other quantities are

m_i = number of molecules of component i per unit volume of NaCl

ρ_i = number of molecules of component i per unit volume of solution

$$\psi_2 = \left(\frac{\partial n}{\partial m_2} \right)_{T,p,m_3} ; \quad \psi_3 = \left(\frac{\partial n}{\partial m_3} \right)_{T,p,m_2}$$

$$a_{33} = \left(\frac{\partial a_3}{\partial m_3} \right)_{T,p,m_2} ; \quad a_{33}^* = \left(\frac{\partial a_3}{\partial m_3} \right)_{T,p,m_2=0}$$

The second term in the square bracket of eq 4 is likely to be sufficiently small so that it may be neglected. Then, it should be possible to evaluate $(\partial \mu_2 / \partial m_2)_{T,p,\mu_3}$ from the turbidity and refractive index data while utilizing the vapor pressure data to determine the condition of constant μ_3 . Integration of this derivative with respect to TSA concentration would then lead to the activity of TSA. This would be with respect to the rather unconventional standard state of an infinitely dilute solution of TSA in NaCl rather than in

water, so that such activities would differ from the conventional one by a constant factor.

However, once again, these attempts to determine the activity of the TSA were frustrated by the lack of sufficient data. It turns out that considerably more accurate measurements than are presently feasible are required, particularly at low concentrations of TSA.

Finally, a word of comment on the observed depolarization of TSA (Figure 1) is offered. Although this is small (0.02–0.04), we are quite confident that it is a real effect rather than an experimental error. The accuracy of our experimental setup for depolarization measurements was recently carefully checked on pure liquids¹¹ and polymer latexes.¹² In addition, we have obtained experimental values as low as 0.005 for the depolarization at high dilution of Ludox SM silica sol. Such a result could not have been obtained if the low-intensity measurements of the cross-component (horizontally polarized component) were spurious.

Since X-ray analysis²⁴ and hydrodynamic studies^{25,26} have demonstrated that TSA is approximately spherical with a diameter of about 11 Å, the observed depolarization indicates an intrinsic structural anisotropy of the ion. In the case of 9-tungstophosphoric acid, the observed depolarizations were much higher (about 0.09 at high dilution and 0.15 at a concentration of 1 g/ml at 436 $m\mu$), in accordance with the suggested dumbbell dimeric structure of 9-tungstophosphoric acid.^{27,28} Similar depolarization values have also been obtained for other electrolytes.^{29,30}

(23) D. Stigter, *J. Phys. Chem.*, **64**, 842 (1960).

(24) H. A. Levy, P. A. Agron, and M. D. Danford, *J. Chem. Phys.*, **30**, 1486 (1959).

(25) M. C. Baker, P. A. Lyons, and S. J. Singer, *J. Am. Chem. Soc.*, **77**, 2011 (1955).

(26) T. Kurucsev, A. M. Sargeson, and B. O. West, *J. Phys. Chem.*, **61**, 1567 (1957).

(27) A. F. Wells, "Structural Inorganic Chemistry," Oxford University Press, New York, N. Y., 1962.

(28) M. Kerker, D. Lee, and A. Chou, *J. Am. Chem. Soc.*, **80**, 1539 (1958).

(29) K. Högbe, *Physik. Z.*, **39**, 23 (1938).

(30) C. Smart and B. A. Pethica, *Trans. Faraday Soc.*, in press.

The Obstruction Effect in the Self-Diffusion Coefficients of Sodium and Cesium in Agar Gels

by A. Laird Slade,¹ Adrien E. Cremers,² and Henry C. Thomas

Department of Chemistry, University of North Carolina, Chapel Hill, North Carolina
(Received February 14, 1966)

Self-diffusion coefficients for sodium and cesium in agar gels, prepared from solutions of the chlorides, have been determined at several salt concentrations up to 0.25 *M* for two temperatures, 10 and 25°, in gels up to 4 wt % agar. The effect of the agar is entirely accounted for by the obstruction effect: the "formation factor" is found to be independent of the nature of the ion, of its concentration, and of the temperature, but to vary linearly with agar content. Diffusion coefficients for pure aqueous solutions are obtained by the corresponding extrapolation. At 0.001 *M* these agree within experimental error with the limiting law for tracer diffusion.

In earlier papers³⁻⁵ descriptions have been given of the method used here to follow the diffusion of isotopically labeled ions in gels carrying a uniform bulk concentration of a salt of that ion. We now report diffusion coefficients for agar gels prepared with solutions of sodium and cesium chlorides. The measurements encompass gels of several agar contents, in equilibrium with solutions of a variety of concentrations, at two temperatures. On the basis of these experiments we try to answer the question: to what extent can the effect of the macromolecules in the gel be described merely as mechanical obstructions in the path of the diffusing ions. We show that this description is adequate for the ions studied over a range of agar content up to 4 wt %, within the experimental uncertainty of about 1% of our diffusion coefficients. The appropriate extrapolation to zero agar content gives the diffusion coefficients for pure aqueous solutions. Confirmatory evidence is supplied by measurements of the conductance of some of the gels and of their equilibrium solutions.

If macromolecules in a gel or suspension act merely to lengthen the path of the diffusion, the effect will be described by a "formation factor," *F*, constant for a given content of macromolecule, that is, independent of solute character, concentration, and temperature. If the path lengthening relative to pure aqueous solution is \sqrt{F} , then, if *D*₀ is the diffusion coefficient for the surrounding solution, we have the relationship

$$D_0 \frac{\partial^2 c}{\partial (x\sqrt{F})^2} = \frac{D_0}{F} \frac{\partial^2 c}{\partial x^2} = \frac{\partial c}{\partial t}$$

We here report cases in which *F* is found to be such a constant.

Experimental Section

The technique of the diffusion experiment has been described in some detail.⁵ In brief, the residue of tracer in a short rod of gel is measured as a function of time, while diffusion from the gel through a thin confining membrane into an "infinite" bath of the equilibrium solution is going on. A single determination of a diffusion coefficient is based upon perhaps a hundred observations over a period of some hours. The course of the drop in activity of the gel is accurately described by a two-parameter solution of the boundary value problem for the experimental arrangement. One of these parameters is the diffusion coefficient we seek, and the other is a measure of the thickness of the con-

(1) The material of this paper is taken in largest part from the dissertation presented by A. L. S. to the Faculty of the Graduate School of the University of North Carolina in partial fulfillment of the requirements for the degree of Doctor of Philosophy, 1964.

(2) Visiting Fellow; Research Fellow of the "Fonds National de la Recherche Scientifique," Belgium, Catholic University of Louvain.

(3) H. C. Thomas, *Proc. Natl. Acad. Sci. U. S.*, **42**, 909 (1956).

(4) T. Fujii and H. C. Thomas, *J. Phys. Chem.*, **62**, 1566 (1958).

(5) G. F. Allen, H. Schurig, L. Slade, and H. C. Thomas, *ibid.*, **67**, 1402 (1963).

fining membrane, which is only of incidental interest here. A considerable number of experiments using different kinds and thicknesses of cellophane membranes has further demonstrated that the value of the diffusion coefficient so found is independent of membrane thickness. Since this point is fundamental to the experiment, the evidence for it is given in Table I, which also shows the precision attainable in D , about 1%.

Confining membranes used are various forms of unwater proofed cellophane, kindly given to us by the Du Pont Co., and here denoted by the manufacturer's symbols. The wet thicknesses (b , mm) of these materials are approximately as follows: experimental,

Table I: Self-Diffusion Coefficients with Various Confining Membranes^a

Membrane	$D \times 10^6$, cm ² /sec	ξ , cm	$10^3\sigma$
Experimental	1.227	0.0084	1.7
	1.221	0.0087	1.5
	1.231	0.0068	1.3
	1.207	0.0081	1.7
	1.222 ± 0.008		
300 PUD	1.222	0.0166	1.4
	1.215	0.0168	1.3
	1.238	0.0161	1.4
	1.242	0.0168	1.4
	1.227	0.0154	...
1.229 ± 0.009			
300 NR	1.206	0.0130	1.4
	1.212	0.0118	1.5
	1.209		
300 GF	1.204	0.0132	1.6
	1.212	0.0131	1.6
	1.208		
Av (13) 1.220 ± 0.010			

^a Conditions: 0.0100 M NaCl; 2% agar; 25°.

0.024; 300-PUD, 0.053; 300-NR, 0.050; 300-GF, 0.125. These numbers are given merely as an indication that the materials were in fact of different thicknesses; the thickness parameter, ξ , significant to our experiment, depends on b through the relation

$$\xi = b \frac{Dc}{D_m c_m}$$

in which D and D_m are the diffusion coefficients in the confined gel and in the confining membrane for the cor-

responding salt concentrations c and c_m . Since the computation treats ξ as an adjustable parameter in a least-squares procedure, we do not need individual values for b , D_m , or c_m .

The fourth column of Table I gives the root-mean-square deviations for the observed values of (count at time t)/(initial count) from those computed for the least-square "best" values of D and ξ , namely, those given in the table. (The details of these computations are described by Allen, *et al.*⁵) Counting statistics at about half-time correspond to $10^3\sigma = 3$.

A total of 79 diffusion runs was made for gels containing 1-4 wt % agar with 0.01 and 0.05 M NaCl using the four types of cellophane. The results given in Table I are typical.

In all of our work the gels were from a single preparation of agar, Purified Agar, Difco Certified, Control No. 437,277.⁶ An appropriate quantity was placed in a 10-ml volumetric flask to which was added exactly 5 ml of a solution of twice the salt concentration desired together with the necessary amount of carrier-free tracer (Na^{22} or Cs^{134}). After dilution to the mark the mixture was slowly warmed and gently stirred. When clear and homogeneous the gel was transferred to ten or twelve small test tubes and tightly stoppered. These portions were used in separate diffusion runs. Most gels were used within 1 week of preparation; none was allowed to stand more than 1 month. The details of filling the cell have been described.⁵ The reproducibility of the preparation of these gels, insofar as self-diffusion in them is concerned, is indicated by the following results for three different preparations on each of which three or four diffusion runs were made. (These gels all contained 1% agar with 0.01 M NaCl.)

	$D \times 10^6$, cm ² /sec				Av
A	1.239	1.245	1.246		1.242
B	1.253	1.249	1.244		1.248
C	1.248	1.240	1.252	1.249	1.247
Av (10) 1.246; max dev 0.007; av dev 0.004					

Results

In Tables II and III are given the averages of the values found for the self-diffusion coefficients of sodium and cesium under the various conditions with the mean deviations between independent runs, the number of these being given in parentheses.

To be able to make a comparison with a somewhat different transport phenomenon, the conductances of two series of agar gels and of the solutions from which they were prepared have been measured. These gels

(6) From Difco Laboratories, Inc., Detroit, Mich.

Table II: Self-Diffusion Coefficients of Sodium in Agar Gels with NaCl Solutions

% agar	$D \times 10^5, \text{cm}^2/\text{sec}$		
	10°		
	0.001 M	0.01 M	0.05 M
1	0.859 ± 0.006 (4)	0.859 ± 0.002 (3)	0.866 ± 0.002 (3)
2	0.837 ± 0.010 (4)	0.840 ± 0.009 (3)	0.848 ± 0.005 (2)
3	0.810 ± 0.006 (3)	0.816 ± 0.003 (3)	0.819 ± 0.004 (3)
4	0.790 ± 0.004 (3)	0.800 ± 0.004 (5)	0.802 ± 0.002 (3)
	25°		
	0.001 M	0.01 M	0.05 M
1	1.282 ± 0.004 (4)	1.247 ± 0.004 (15)	1.247 ± 0.006 (7)
2	1.229 ± 0.013 (5)	1.220 ± 0.010 (13)	1.219 ± 0.004 (9)
3	1.193 ± 0.006 (4)	1.183 ± 0.007 (12)	1.183 ± 0.012 (7)
4	1.143 ± 0.003 (3)	1.158 ± 0.008 (8)	1.150 ± 0.008 (8)
	0.1 M	0.25 M	
1	1.280 ± 0.006 (3)	1.315 ± 0.006 (5)	
2	1.267 ± 0.004 (3)	1.288 ± 0.005 (3)	
3	1.245 ± 0.002 (3)	1.254 ± 0.006 (3)	
4	...	1.234 ± 0.004 (2)	

Table III: Self-Diffusion Coefficients of Cesium in Agar Gels with CsCl

% agar	$D \times 10^5, \text{cm}^2/\text{sec}$	
	10°	
	0.001 M	0.05 M
0.5	...	1.420 ± 0.009 (2)
1	1.379 ± 0.013 (3)	1.398 ± 0.012 (3)
2.5	1.342 ± 0.019 (3)	1.344 ± 0.004 (4)
4	1.293 ± 0.012 (3)	1.297 ± 0.001 (4)
	25°	
0.5	...	1.989 ± 0.011 (2)
1	1.968 ± 0.020 (5)	2.014 ± 0.018 (3)
2.5	1.919 ± 0.024 (5)	1.927 ± 0.003 (4)
4	1.851 ± 0.003 (4)	1.862 ± 0.009 (3)

contained either 3 or 4% agar with no and approximately 0.01, 0.02, 0.03, 0.05, and 0.1 M NaCl. The measurements were made at 1000 cps using a Hewlett-Packard wide-range oscillator, a Leeds and Northrup shielded ratio box, air capacitor, and a Leeds and Northrup No. 4755 AC resistance box in conjunction with a tuned amplifier-detector of 1- μ sensitivity. A Leeds and Northrup dipping conductance cell was slowly immersed in the freshly prepared, molten gel and brought to 25° for measurement. The results are shown in Figure 1 as relations between $K_s - K_g$ and K_s , conductivities of solution and gel, respectively. These are accurately straight lines and correspond to constant formation factors according to the relation

$$K_g = \frac{K_s}{F} + \Delta K$$

which may be taken as a definition of an excess conductance, ΔK , for a heterogeneous system, in terms of a constant F . The constancy of F for a given agar content must be verified to make this definition meaningful. This is done in the plots of Figure 1, which correspond to the relation

$$K_s - K_g = \left(\frac{F - 1}{F} \right) K_s - \Delta K$$

The slopes of the lines measure F and the intercepts give ΔK for the two gels studied.

Over the range of agar content studied, the observed diffusion coefficients vary linearly with the weight fraction of agar. The accuracy of this linearity seems to be well established. For twelve such lines, involving 45 values of D (determined by a total of 189 runs), three values of D deviate from the lines by about 1%, two by about 0.5%, and the remainder by less than 0.5%, with an average deviation of 0.25%. Table IV gives the constants D_0 and a for these lines; $D = D_0 - aw$. Inspection of this table discloses the fact that all of the results, regardless of nature of ion or of the other conditions of the experiment, can be expressed by the relation

$$\frac{D(t,c,w)}{D_0(t,c)} = 1 - 0.023w$$

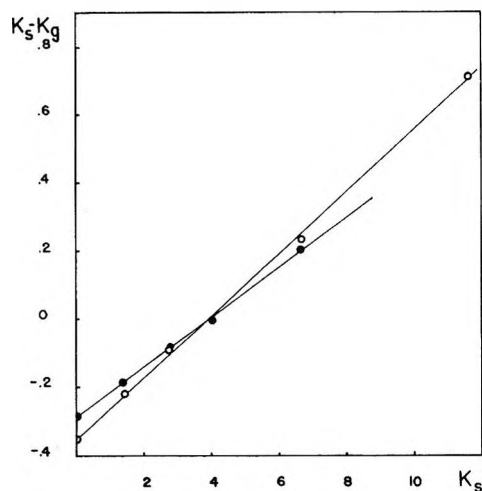


Figure 1. Deviation plot: conductivity of gel as a function of the conductivity of the equilibrium solution (mmhos/cm): ●, 3% agar; ○, 4% agar.

in which w is the weight per cent of agar. The average discrepancy is considerably less than 1%.

Table IV: Dependence of Diffusion Coefficient on Agar Content

$D = D_0(t,c) - aw$		
M	$D_0 \times 10^6$	$100a/D_0 \times 10^6$
NaCl, 10°		
0.001	0.887	2.8
0.01	0.878	2.1
0.05	0.889	2.5
NaCl, 25°		
0.001	1.321	3.4
0.01	1.277	2.3
0.05	1.282	2.6
0.1	1.305	1.6
0.25	1.342	2.1
CsCl, 10°		
0.001	1.410	2.0
0.05	1.434	2.4
CsCl, 25°		
0.001	2.012	2.0
0.05	2.036	2.1

Discussion

As is above experimentally demonstrated, the self-diffusion coefficients of two alkali ions in agar gels, in equilibrium with chloride solutions, are determined, insofar as changes in agar content are concerned, en-

tirely by effects ascribable to the "geometry" of the gel. The obstruction effect of the gel, as measured by the formation factor, is independent of solution concentration, of temperature, and of the nature of the diffusing ion. Our diffusion experiments give

$$F = \frac{1}{1 - 0.023w} \approx 1 + 0.023w$$

The two series of conductance measurements give

$$F = 1 + 0.025w$$

in essentially exact agreement.

The study of transport through heterogeneous materials has a long history, dating back at least to Poisson (1826). For dense suspensions, even of particles of known shapes, sizes, and arrangement, the mathematical treatment and the results thereby obtained are very complex and of uncertain validity. For dilute suspensions of discrete and impervious particles it is seen^{7,8} that the formation factor is given in terms of the porosity, ϕ , the volume fraction of solvent, by

$$F - 1 = k \frac{1 - \phi}{\phi}$$

in which k depends only on the shapes—and not the sizes—of the suspended particles. For an aggregation of spheres, $k = 3/2$; for long needles of circular cross section, randomly oriented, $k = 5/3$. Thus the formation factor is not very sensitive to the geometry of the suspended material for these dilute systems. If we suppose that the density of agar in a gel is about that of sucrose (1.5), and if the gel were a loose mass of needles, we should find $F = 1 + 0.011w$. In a certain sense a real agar gel is about twice as effective in obstructing the motion of ions as this collection of needles.

Insofar as our results can show for the two alkali ions studied, if there is any specific binding between the matrix and the ion, it must be quite small and nearly the same for sodium and cesium.

The nature of F as established by our experiments seems to justify identifying the quantity we have called $D_0(t,c)$, Table IV, with the self-diffusion coefficients for pure aqueous solutions. Although certainly our results are inadequate for a test of the limiting concentration dependence of these quantities, they do give an idea as to the region of concentration in which significant departures from this law occur. In

(7) H. Fricke, *Phys. Rev.*, **24**, 575 (1924).

(8) For an excellent review, especially of recent work, see R. E. Meredith and C. W. Tobias, *Advan. Electrochem. Electrochem. Eng.*, **2**, 15 (1962).

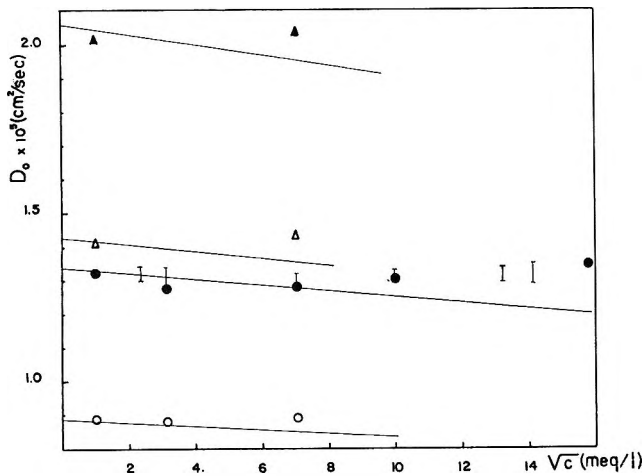


Figure 2. Self-diffusion coefficients of sodium and cesium in solutions of the chlorides: \blacktriangle , Cs at 25°; \triangle , Cs at 10°; \bullet , Na at 25°; \circ , Na at 10°; I, Wang and Miller.¹¹

Figure 2 are given lines for $D(t,c)$ computed from the relation⁹

$$D = D_0 \left\{ 1 - \frac{2.801 \times 10^6}{(\epsilon T)^{3/2}} (1 - \sqrt{d(u)}) \sqrt{c} \right\}$$

where

$$D_0 = \frac{RT}{F^2} \lambda^0$$

$$d(u) = (1 + 2t_{Cl^0})/4$$

and where ϵ is the dielectric constant of the solvent, and t_{Cl^0} the limiting transference number of the chloride ion. We use limiting conductances and transference numbers given by Harned and Owen¹⁰ to compute the values of λ^0 . The agreement with the limiting law is essentially perfect in the four cases at 0.001 M ; deviations of several per cent appear at 0.05 M . For purposes of comparison the data of Wang and Miller¹¹ for sodium at 25° are included. When activation energies are calculated from the $D(t,c,0)$ at $c = 0.001 M$, our values for sodium and cesium lie 120 and 140 cal below those given by the limiting law, an undoubtedly insignificant difference. The results for sodium do show a possibly real decrease in activation energy with increasing concentration, some 350 cal between 0.001 and 0.05 M .

It will be of interest to extend this work to cases in which specific ion binding is to be found, as preliminary experiments indicate to be the case for cobalt and agar.

Acknowledgment. We are grateful to the National Science Foundation for grants which have made this work possible.

(9) R. A. Robinson and R. H. Stokes, "Electrolyte Solutions," Butterworth and Co. Ltd., London, 1959, p 316.

(10) H. S. Harned and B. B. Owen, "The Physical Chemistry of Electrolytic Solutions," 3rd ed, Reinhold Publishing Corp., New York, N. Y., 1958, p 234.

(11) J. H. Wang and S. J. Miller, *J. Am. Chem. Soc.*, **74**, 1611 (1952)

Absorption Spectra of Octahedral Lanthanide Hexahalides

by Jack L. Ryan

Battelle Pacific Northwest Laboratory, Richland, Washington¹

and Chr. Klíxbüll Jørgensen

Cyanamid European Research Institute, Cologne (Geneva), Switzerland (Received February 18, 1966)

Hexahalide 4f group complexes can be prepared in aprotic solvents such as nitriles and in triphenylphosphonium and pyridinium salts. The internal transitions in the partly filled 4f shell correspond to absorption bands much weaker than for the corresponding aqua ions (except the hypersensitive pseudoquadrupolar transitions) and show the vibrational structure characteristic for octahedral complexes with a center of inversion. The nephelauxetic effect is much stronger than for the same central ions in LaCl_3 but not as pronounced as for the oxides. The electron-transfer spectra observed in Ce(IV), Sm(III), Eu(III), Tm(III), and Yb(III) hexahalides are discussed; the apparent optical electronegativities are somewhat higher than for the analogous halide complexes in ethanolic solution. The 4f \rightarrow 5d transitions observed in Ce(III) hexahalides show that the subshell energy difference Δ is larger than 15 kK. The similar transitions in Tb(III) hexahalides seem to involve a spin-forbidden absorption band at relatively low wavenumber and indicate slightly smaller exchange integrals $K(4f, 5d)$ than in the isoelectronic Gd^{+2} .

Introduction

The octahedral symmetry of hexahalides MX_6^{+2-6} allow many group-theoretical arguments to be applied to the energy levels. In particular, the excited levels of the detailed electron-transfer spectra have been classified, using inductive MO theory, in a large number of 4d and 5d group complexes.²⁻⁴ Because of chemical problems, the study of the hexahalides of the other transition groups is far more difficult. Thus, the 5f group hexahalides cannot normally be studied in aqueous solution. However, using anhydrous acetonitrile CH_3CN as solvent, we obtained the absorption spectra of various U(IV), Np(IV), and Pu(IV) hexahalides and identified internal transitions in the partly filled 5f shell, 5f \rightarrow 6d transitions, and electron transfer $\pi \rightarrow 5f$.⁵ Similar techniques allow the study of CeCl_6^{-2} and the much less stable CeBr_6^{-2} . The situation is even more difficult in the case of trivalent lanthanides.

Until recently, many scientists believed that 6 is a common coordination number N for lanthanides. Actually, $N = 8, 9, 10$, or even 12 seems to be far more typical.⁶ For instance, hexanitrate such as $\text{U}(\text{NO}_3)_6^{-2}$ or $\text{Pu}(\text{NO}_3)_6^{-2}$ (ref 7) may not necessarily have $N =$

6 but may contain bidentate nitrate groups. Thus, the crystal structure⁸ of $[\text{Mg}(\text{H}_2\text{O})_6]_2[\text{Ce}(\text{NO}_3)_6]_2 \cdot 6\text{H}_2\text{O}$ confirmed Judd's spectroscopic prediction⁹ of somewhat distorted, icosahedral groups $\text{Ce}(\text{NO}_3)_6^{-3}$ with $N = 12$. X-Ray diffraction studies of aqueous solutions of $\text{Ce}(\text{NO}_3)_6^{-2}$ (ref 10) seem to show $N = 12$. As seen in the Experimental Section, the organic cation $\text{P}(\text{C}_6\text{H}_5)_3\text{H}^+$

(1) The work done at this laboratory was performed under Contract No. AT(45-1)-1830 for the U. S. Atomic Energy Commission.

(2) C. K. Jørgensen, *Mol. Phys.*, **2**, 309 (1959).

(3) C. K. Jørgensen, *Acta Chem. Scand.*, **17**, 1034 (1963).

(4) C. K. Jørgensen and K. Schwochau, *Z. Naturforsch.*, **20a**, 65 (1965).

(5) J. L. Ryan and C. K. Jørgensen, *Mol. Phys.*, **7**, 17 (1963).

(6) C. K. Jørgensen, "Inorganic Complexes," Academic Press Inc., London, 1963.

(7) W. E. Keder, J. L. Ryan, and A. S. Wilson, *J. Inorg. Nucl. Chem.*, **20**, 131 (1961).

(8) A. Zalkin, J. D. Forrester, and D. H. Templeton, *J. Chem. Phys.*, **39**, 2881 (1963).

(9) B. R. Judd, *Proc. Roy. Soc. (London)*, **A241**, 122 (1957).

(10) R. D. Larsen and G. H. Brown, *J. Phys. Chem.*, **68**, 3060 (1964).

(ref 11, 12) has once more shown its suitability for precipitating salts of MCl_6^{-3} and MBr_6^{-3} ,² under nearly anhydrous circumstances. However, the only appropriate solvent we have been able to find in which these salts are sufficiently soluble for spectral studies of the internal 4f transitions is a mixture of acetonitrile and succinonitrile. The reasons why halide complexes are so relatively much more stable in nitriles than, say in alcohols, may be connected with the slightly decreased internuclear distances $M-X$ suggested by the solvent shifts of the electron-transfer spectra of various MX_6^{-2} .^{3,13} From considerations of the ionic radii, one would expect MI_6^{-3} to be stereochemically more favorable. We have not been able to obtain spectra of such species. However, one should not despair; recently, salts of ThI_6^{-2} and UI_6^{-2} have been reported.¹⁴

Experimental Section

Preparation of Compounds. Compounds $[(C_6H_5)_3PH]_3MCl_6$, where M is Ce, Pr, Nd, Sm, Gd, Dy, Ho, Er, Tm, and Yb, were prepared. These compounds were precipitated by mixing the rare earth chloride in HCl saturated or nearly saturated ethanol with a small excess of $(C_6H_5)_3PHCl$ in the same solvent. The compounds tended to supersaturate, and precipitation could be initiated by passing HCl gas through the solution or by seeding with a minute crystal of a salt of another of the lanthanides. The heaviest rare earths were the worst in this regard and precipitated very slowly even after seeding. The lighter rare earth salts tended to precipitate much more readily and usually precipitated as larger crystals. The light rare earth salts precipitated readily from hot solutions, but with the heavy rare earths it appeared necessary to cool the solutions unless the concentration of the reactants was quite high. In order to obtain high yields the water concentration in the ethanol was kept as low as possible. With the light rare earths, the oxides were dissolved directly in absolute ethanol by addition of HCl gas. The heavy rare earth oxides (above Eu) did not dissolve readily in hot HCl-ethanol. In these cases the oxides were dissolved in hot aqueous HCl and taken to dryness on a hot plate. The residue was then dissolved in hot HCl saturated ethanol. This procedure was also used with Pr which was obtained as the higher oxide Pr_6O_{11} . All rare earth oxides were from either American Potash Lindsay Division or Michigan Chemical and were of 99.9% or greater purity. The Tb_4O_7 used contains less than 0.005% lead (hence, the band observed for $TbCl_6^{-3}$ at the same position as a much stronger band of $PbCl_4^{-2}$ cannot have this origin). Triphenylphosphonium chloride solutions were prepared by adding HCl gas to Eastman

triphenylphosphine in absolute ethanol.

The salts were washed with HCl saturated or nearly saturated absolute ethanol. If the salts are washed with pure ethanol, acetone, or similar solvents not containing HCl, decomposition occurs. The light rare earth salts can be readily recrystallized by dissolving them in hot ethanol followed by the addition of HCl gas. With the heavy rare earths (at least above Ho), this resulted in impure products containing less than stoichiometric amounts of triphenylphosphonium chloride. With these an excess of $(C_6H_5)_3PHCl$ in solution is apparently necessary. The purpose of the large concentrations of HCl in all the solutions is to react with water and ethanol to form oxonium ion and ethyloxonium ion and thereby markedly to decrease the coordinating power of the water and ethanol and at the same time to increase chloride activity. The salts were dried with a heat lamp and were stored over anhydrous $Mg(ClO_4)_2$ as they appear to be somewhat deliquescent with decomposition to $MCl_3 \cdot xH_2O$.

Anal. Calcd for $[(C_6H_5)_3PH]_3PrCl_6$: C, 56.7; H, 4.24. Found: C, 55.8; H, 4.74.

Anal. Calcd for $[(C_6H_5)_3PH]_3NdCl_6$: Nd, 12.6; C, 56.5; H, 4.23. Found: Nd, 12.6; C, 55.8; H, 4.25.

Anal. Calcd for $[(C_6H_5)_3PH]_3SmCl_6$: Sm, 13.0. Found: Sm, 13.0.

Anal. Calcd for $[(C_6H_5)_3PH]_3DyCl_6$: C, 55.7; H, 4.16. Found: C, 57.0; H, 4.3.

Anal. Calcd for $[(C_6H_5)_3PH]_3ErCl_6$: Er, 14.3; C, 55.4; H, 4.15. Found: Er, 14.1; C, 55.6; H, 4.35.

Anal. Calcd for $[(C_6H_5)_3PH]_3YbCl_6$: Yb, 14.7. Found: Yb, 14.6.

The compounds $(C_5H_5NH)_3NdCl_6$ and $(C_5H_5NH)_3YbCl_6$ were prepared in the same manner as the triphenylphosphonium salts. The pyridine hydrochloride solution in ethanol was prepared by adding HCl gas to CP pyridine in absolute ethanol. The compounds precipitate readily in good yield. The pyridinium salts, although easily prepared, are very deliquescent and are therefore less useful than the triphenylphosphonium salts. Preparation of other pyridinium rare earth chlorides was not attempted, but they are undoubtedly easily prepared.

Anal. Calcd for $(C_5H_5NH)_3NdCl_6$: Nd, 24.1; Cl, 35.6. Found: Nd, 24.2; Cl, 35.1.

(11) P. Day and L. Venanzi, private communication, and *J. Chem. Soc., Sect. A*, 197 (1966).

(12) C. K. Jørgensen, *Acta Chem. Scand.*, **17**, 251 (1963).

(13) C. K. Jørgensen, *J. Inorg. Nucl. Chem.*, **24**, 1587 (1962).

(14) K. W. Bagnall, D. Brown, P. J. Jones, and J. G. H. Dupreez, *J. Chem. Soc.*, 350 (1965).

Anal. Calcd for $(C_5H_5NH)_3YbCl_6$: Yb, 27.6. Found: Yb, 27.9.

Attempts were made by two methods to prepare compounds of the type $[(C_2H_5)_4N]_3MCl_6$ where M is a trivalent rare earth. The first of these consisted of adding first ethanol and then acetone to a very concentrated aqueous HCl solution of the rare earth (Nd) and $(C_2H_5)_4NCl$ as in the preparation of $[(C_2H_5)_4N]_2UBr_6$.⁶ This results in the precipitation of $MCl_3 \cdot xH_2O$. The second method was that used in preparing the triphenylphosphonium and pyridinium salts. With Nd no precipitation occurred. With Er, using very concentrated reactants, some precipitate formed after initially cooling to -70° and then allowing the reaction mixture to stand at 25° for 18 hr. This material did not correspond to any simple stoichiometry but contained about 25% carbon. It is possible that this was a mixture of $[(C_2H_5)_4N]_3 \cdot ErCl_6$ and $ErCl_3 \cdot xsolvate$. No further attempt was made to resolve this situation.

The compounds $[(C_6H_5)_3PH]_3MBr_6 \cdot (C_6H_5)_3PHBr$ were prepared where M was La, Pr, Nd, Sm, and Eu. The formula of the compound is shown as containing the MBr_6^{-3} complexes rather than MBr_7^{-4} because of the nature of the absorption spectra of the salts as discussed elsewhere in the paper and because the spectrum of the Nd salt is essentially identical with that of $(C_5H_5NH)_3NdBr_6$. These salts were made in the same manner as the corresponding chloro salts. With the bromide systems, somewhat more care is necessary in the preparation than in the case of the chlorides since the solubilities of the reactants, $MBr_3 \cdot xsolvate$ and $(C_6H_5)_3PHBr$, are much less in HBr saturated ethanol than their chloride analogs are in HCl saturated ethanol. Because of this, there is a possibility of contaminating the product with excess of one of the reactants. At first, this was thought to be the reason for the analysis indicating $[(C_6H_5)_3PH]_3MBr_6 \cdot (C_6H_5)_3PHBr$ instead of $[(C_6H_5)_3PH]_3MBr_6$. The Nd compound was recrystallized up to three times by dissolving in hot ethanol and then adding HBr gas. It was also recrystallized from methanol and butanol in the same manner. In all cases the analysis corresponded exactly to $[(C_6H_5)_3PH]_3NdBr_6 \cdot (C_6H_5)_3PHBr$. The erbium salt (and presumably other of the heavy rare earth salts) could not be prepared although the light rare earths were prepared easily in good yield. Several attempts to prepare the Er salt were made. Even though the Er solution was seeded with $[(C_6H_5)_3PH]_3EuBr_6 \cdot (C_6H_5)_3PHBr$, no precipitate could be obtained other than the reactants ($ErBr_3 \cdot xsolvate$, $(C_6H_5)_3PHBr$, or mixtures of these). The salts were somewhat deliquescent (the orange-yellow europium salt changes to white upon exposure to laboratory air

for several hours) and were stored over anhydrous $Mg(ClO_4)_2$.

Anal. Calcd for $[(C_6H_5)_3PH]_3PrBr_6 \cdot (C_6H_5)_3PHBr$: C, 49.3. Found: C, 49.6.

Anal. Calcd for $[(C_6H_5)_3PH]_3NdBr_6 \cdot (C_6H_5)_3PHBr$: Nd, 8.21; C, 49.2; H, 3.64; Br, 31.8. Found: Nd, 8.18; C, 49.1; H, 3.62; Br, 30.7.

Anal. Calcd for $[(C_6H_5)_3PH]_3SmBr_6 \cdot (C_6H_5)_3PHBr$: Sm, 8.53; C, 49.0; H, 3.66. Found: Sm, 8.55; C, 48.1; H, 3.4.

Anal. Calcd for $[(C_6H_5)_3PH]_3EuBr_6 \cdot (C_6H_5)_3PHBr$: Eu, 8.61; C, 49.0; H, 3.66. Found: Eu, 8.92; C, 48.9; H, 3.80.

The salt $(C_5H_5NH)_3NdBr_6$ was prepared in the same manner as the corresponding chloride salt. The same problem of moderately low solubility of the reactants in HBr saturated ethanol was encountered as in the preparation of the triphenylphosphonium lanthanide bromides. Although this salt precipitated readily in good yield, an attempt at preparation of the corresponding Er salt was unsuccessful. $(C_6H_5NH)_3NdBr_6$, like the corresponding chloride salt, was found to be very deliquescent.

Anal. Calcd for $(C_5H_5NH)_3NdBr_6$: Nd, 16.7; Br, 55.5. Found: Nd, 16.8; Br, 56.1.

Attempts at preparation of triphenylphosphonium rare earth iodides by methods similar to those used for the preparation of the chlorides and bromides were unsuccessful. The solubility of the reactants ($MX_3 \cdot solvate$ and $(C_6H_5)_3PHX$) in HX saturated ethanol decrease with increasing size of the halide, X. This becomes a minor problem with the bromides but is a major problem with the iodides. Also HI reacts with the ethanol rather rapidly.

All rare earth analyses were by spectrophotometry. Samples were all dissolved in constant-boiling hydrochloric acid (the organic portion of triphenylphosphonium salts is not appreciably soluble in dilute acid). Standards were prepared by dissolving the dried rare earth oxides in constant-boiling hydrochloric acid. Carbon and hydrogen analyses were performed with an F & M Co. chromatographic carbon, hydrogen, and nitrogen analyzer. Carbon and hydrogen analyses on several of the compounds were also performed by Schwarzkopf Microanalytical Laboratory, Woodside, N. Y. The two sets of carbon and hydrogen numbers were in close agreement. Chloride and bromide analyses were by controlled-potential coulometric titration.¹⁵ The accuracy of halide analyses of the triphenylphosphonium salts is probably not so good as for the pyridinium salts since hydrolysis of triphenyl-

(15) L. R. Duncan, unpublished analytical method.

phosphonium salts (dissolved initially in ethanol) in dilute acid produces insoluble triphenylphosphine.

$[(C_2H_5)_4N]_2CeCl_6$ was prepared in the same manner as was the previously reported tetramethylammonium salt.¹⁶ Freshly prepared $Ce(OH)_4$ was dissolved in cold (below 0°), concentrated HCl, and a solution of $(C_2H_5)_4NCl$ in cold, concentrated HCl was added immediately. The precipitate was washed with cold, concentrated HCl and then acetone and dried. Molar extinction coefficients of $CeCl_6^{-2}$ in acetonitrile were obtained using this salt as a primary standard. Excess Cl^- was not required to maintain the $CeCl_6^{-2}$ complex in this solvent.

The $CeBr_6^{-2}$ complex can be obtained in acetonitrile or nitromethane by two methods. If a solution of $CeBr_6^{-3}$ (containing anhydrous HBr) is allowed to air oxidize or a small amount of Br_2 is added, this Ce(IV) species forms slowly to a very small fraction of the total Ce. Since its charge-transfer band is well above (in wavelength) the absorption region of $CeBr_6^{-3}$ and its molar extinction coefficient is quite large, its spectrum (above about $400\text{ m}\mu$) can be obtained in the presence of a large excess of Ce(III). If a quaternary ammonium bromide and HBr are added to an acetonitrile or nitromethane solution of $CeCl_6^{-2}$, the $CeCl_6^{-2}$ is converted immediately to $CeBr_6^{-2}$ apparently because of the much weaker acidity of HCl than HBr in these solvents. The $CeBr_6^{-2}$ in these solutions decomposes rather rapidly (half-time about 70 sec in nitromethane) at 25° but is much more stable at -30° . The molar extinction coefficient of $CeBr_6^{-2}$ was obtained from a solution prepared by adding a cold nitromethane solution of $[(C_2H_5)_4N]_2CeCl_6$ to a frozen solution of tetrabutylammonium bromide and anhydrous HBr in nitromethane at Dry Ice temperature. The mixture was warmed just enough to melt and was mixed and made up to volume at the freezing point of the solution (about -30°). The $CeBr_6^{-2}$ solution was kept frozen in a Dry Ice bath. An absorbance scan was obtained by barely melting this solution, pouring it into a 1.0-mm cell, and recording the absorbance at $522\text{ m}\mu$ as a function of time. The absorbance was extrapolated back to the time the solution entered the thin cell and thus was warmed to room temperature (about 15 sec before the absorbance trace started in most runs). A correction was made for the expansion of the solution between the temperature at which it was prepared and 25° . Solid $[(C_2H_5)_4N]_2CeCl_6$ can also be converted to $[(C_2H_5)_4N]_2CeBr_6$ by passing a stream of anhydrous HBr over it at 25 to 100° . The time required for the reaction to go to completion has not been measured. The $[(C_2H_5)_4N]_2CeBr_6$ is stable in dry air.

Spectrophotometric Measurements. Spectrophotometric measurements were made with a Cary Model 14 recording spectrophotometer.

Absorption spectra of solids were obtained by preparing a thick paste of the crystalline salts in Kel-F brand chlorofluorocarbon grease and placing this between glass or fused-silica plates. The reference was $CaCO_3$ in Kel-F grease plus in some cases aqueous starch solution. The purpose of the reference mull is to flatten the base line by producing an equivalent wavelength dependence for the scatter. The absolute value of the base line is better controlled by neutral filters (wire screens) in the reference beam. Since the molar extinction coefficients are very low for the MX_6^{-3} internal 4f transitions, very thick mull samples were required. In the visible region, the Cary Model 1471200 high-intensity source was used at full brightness and the spectra were run on the 1.0–2.0 absorbance scale with a reference about 1 absorbance unit less opaque than the sample to minimize slit width and give maximum resolution. Slit widths ran typically 0.04–0.15 mm over the visible region. Spectra of solids at liquid nitrogen temperature were obtained with a liquid helium dewar designed for use with the Cary Model 14. Both dewar compartments were filled with liquid nitrogen. The sample consisted of a typical mull in Kel-F grease as discussed above between thin strips of glass and sealed in 1-cm² fused-silica tubing so that the region around the sample could be evacuated without disruption of the mull. A special beam-condensing system was used in conjunction with the dewar, and slit widths of 0.02–0.15 mm were maintained. Scatter and base line appeared to be better than at 25° on the same sample.

In choosing a solvent for spectrophotometric measurements of the salts of the MX_6^{-3} complexes in solution two criteria are of importance. The solvent must be sufficiently noncomplexing so that the MX_6^{-3} complex can be maintained in the solution and the salt must be sufficiently soluble to obtain useful spectra of the MX_6^{-3} complexes having internal 4f transitions (with the exception of hypersensitive transitions) with molar extinction coefficients generally less than 1. Acetonitrile⁵ and nitromethane¹⁷ have been shown to be satisfactory solvents for the 5f group MX_6^{-2} complexes but do not adequately meet the second criteria mentioned above. Liquid succinonitrile has a dielectric constant of 56.5 at 57.4° , and the solid at 25.7° has a dielectric constant of 65.5.¹⁸

(16) C. K. Jørgensen, *Mol. Phys.*, **5**, 271 (1962).

(17) J. L. Ryan, *J. Phys. Chem.*, **65**, 1856 (1961).

(18) A. H. White and S. O. Morgan, *J. Chem. Phys.*, **5**, 655 (1937).

Also the dielectric constant as a function of temperature shows no discontinuity at the freezing point (54.5°).¹⁸ If it is assumed that the dielectric constants of these very similar solvents are additive, a mixed-nitrile solvent containing 85% succinonitrile and 15% acetonitrile would have a dielectric constant of about 62 at 25° . This is a considerably higher dielectric constant than those for nitromethane or acetonitrile (~ 38). This mixture has been found to be a very effective noncomplexing solvent for salts such as Cs_2UCl_6 , $\text{Cs}_2\text{UO}_2\text{Cl}_4$, and $[(\text{C}_2\text{H}_5)_4\text{N}]_4\text{UO}_2(\text{SO}_4)_3$ which are not appreciably soluble in acetonitrile or nitromethane.¹⁹ The triphenylphosphonium salts used in this work were more soluble in this solvent than in acetonitrile. Acetonitrile was obtained as Spectrograde from Eastman. The succinonitrile (also Eastman), although inherently colorless, was not Spectrograde and was found to be light yellow. The mixed solvent (85 vol. % succinonitrile–15 vol. % acetonitrile) was dried and purified by passing it through a bed of neutral-type activated alumina. This treatment removed the color sufficiently that the mixed-nitrile solvent was usable down to $220\text{ m}\mu$ in 0.1-cm cells and to $260\text{ m}\mu$ in 1.0-cm cells.

The solubilities of the triphenylphosphonium salts in the mixed-nitrile solvent were sufficient to obtain good absorption spectra in the region of the internal 4f transitions ($\epsilon < 1$) using 10-cm cells. The hypersensitive transitions ($\epsilon \sim 10$) could be obtained in the mixed-nitrile solvent with 1.0- or 2.0-cm cells or in acetonitrile with 10-cm cells. It should be noted that these solutions usually supersaturated readily and spectra of solutions could be obtained from which crystals later formed. Both the MCl_6^{-3} and MBr_6^{-3} complexes partially dissociate in acetonitrile or in the mixed-nitrile solvent. This dissociation is easily prevented in the case of the chloride by a small excess of chloride as $(\text{C}_2\text{H}_5)_4\text{NCl}$ or even $(\text{C}_2\text{H}_5)_3\text{NHCl}$. After a small excess of Cl^- has been added, further large additions cause no further change in the spectra, and the spectra become essentially identical with those of the solid triphenylphosphonium salts. With the MBr_6^{-3} complexes, the tendency to dissociate is greater. If the system is kept dry the $[(\text{C}_6\text{H}_5)_3\text{PH}]_3\text{MBr}_6 \cdot (\text{C}_6\text{H}_5)_3\text{PHBr}$ salts can be dissolved in the nitrile solvents containing a large excess of Bu_4NBr without dissociation of the MBr_6^{-3} complexes. The MBr_6^{-3} complexes are very markedly stabilized by addition of HBr gas to the nitrile solutions. This is because it reacts readily with water to form H_3O^+ and with other electron-donor groups in similar manner. This significantly decreases their coordinating power and decreases competition with Br^- . If a large amount

of HBr is added, a solid product is formed because of reaction with the nitrile. Reaction of hydrogen halides with nitriles reportedly produces $\text{R}-\text{CX}=\text{NH}$.²⁰ This reaction of the HBr with the solvent was found not to affect the MBr_6^{-3} spectra. Addition of a large excess of HCl to the MCl_6^{-3} solutions actually destroys rather than stabilizes the MCl_6^{-3} complexes. This is probably due to the greater tendency for Cl^- to hydrogen bond producing HCl_2^- , thus removing Cl^- from MCl_6^{-3} . The weaker bonding of H^+ to Br^- makes HBr a more powerful dehydrating agent than HCl in these solutions.

Since the phenyl and pyridinium groups absorb strongly in the ultraviolet region, the MX_6^{-3} salts cannot be used (with the exception of the EuBr_6^{-3}) to obtain the $\pi \rightarrow 4f$ spectra. The hydrated rare earth chlorides can be dissolved in the nitrile solvents containing a large excess of R_4NCl to produce the MCl_6^{-3} complexes as determined by comparison of the internal 4f spectra of these solutions with those of the solid MCl_6^{-3} salts and the salts in nitrile solutions containing excess Cl^- . With the bromides, a similar situation exists except that HBr gas must be added to dehydrate the solution. Much higher concentrations of MX_6^{-3} in acetonitrile can be obtained in this manner than with the triphenylphosphonium salts. These solutions were used to obtain the electron-transfer spectra of EuCl_6^{-3} , YbCl_6^{-3} , SmCl_6^{-3} , EuBr_6^{-3} , YbBr_6^{-3} , SmBr_6^{-3} , and TmBr_6^{-3} and the $4f \rightarrow 5d$ transitions of TbCl_6^{-3} , TbBr_6^{-3} , CeCl_6^{-3} , and CeBr_6^{-3} .

The procedure for obtaining the MCl_6^{-3} electron-transfer spectra was as follows. A concentrated lanthanide chloride solution in aqueous HCl was diluted about two- to threefold with ethanol, and a large volume of acetone was added rapidly with stirring. The resulting crystals of $\text{MCl}_3 \cdot x\text{H}_2\text{O}$ were acetone washed and dried lightly under a heat lamp. They were then dissolved in a saturated solution of $(\text{C}_2\text{H}_5)_4\text{NCl}$ in acetonitrile, and the absorption spectra were obtained in 0.01- to 0.1-cm cells to minimize absorption by impurities. The reference cells contained the same solutions without rare earth present.

The procedure for obtaining the MBr_6^{-3} electron-transfer spectra was as follows. A concentrated lanthanide solution in aqueous HBr was diluted about twofold with ethanol and saturated with Bu_4NBr , and a large volume of acetone was added. The hydrated bromides precipitated (very slowly after seeding

(19) J. L. Ryan, unpublished results.

(20) M. Silman, "Organic Chemistry, An Advanced Treatise," Vol. II, 2nd ed, John Wiley and Sons, Inc., New York, N. Y., 1943, p 107.

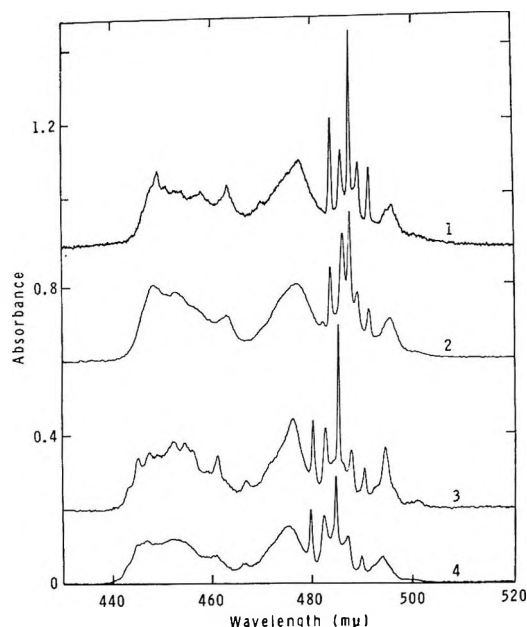


Figure 1. Absorption spectra of praseodymium(III) hexahalides: (1) solid $[(C_6H_5)_3PH]_3PrBr_6 \cdot (C_6H_5)_3PHBr$ (absorbance scale displaced 0.9); (2) 0.039 M $[(C_6H_5)_3PH]_3PrBr_6 \cdot (C_6H_5)_3PHBr$ in 85% succinonitrile-15% acetonitrile containing excess $(C_4H_9)_4NBr$ and HBr in 10.0-cm cell (absorbance scale displaced 0.6); (3) solid $[(C_6H_5)_3PH]_3PrCl_6$ (absorbance scale displaced 0.2%); and (4) 0.032 M $[(C_6H_5)_3PH]_3PrCl_6$ in 85% succinonitrile-15% acetonitrile with excess $(C_2H_5)_4NCl$ in 10.0-cm cell.

in the case of Tm and Yb) and were washed in acetone and dried strongly under a heat lamp. This produced a mixture of rare earth bromides and oxybromides. This was dissolved in Bu_4NBr saturated acetonitrile which had first been sparged with N_2 to remove dissolved oxygen and then had sufficient anhydrous HBr added just to begin to form a solid reaction product with the solvent. Appreciable contact of the solution with air was avoided, and the solution was prepared rapidly in dim light to minimize formation of Br_3^- . Absorption spectra were run immediately in 0.01-cm silica gells.

Molar extinction coefficients of the MX_6^{-3} in the region of the $4f \rightarrow 5d$ and electron-transfer bands were obtained by analysis of the solutions on which spectra were run for total rare earth. Rare earth analyses were made by X-ray fluorescence using an internal standard technique. In the case of $EuBr_6^{-3}$ the molar extinction coefficient for the 409- $m\mu$ band was measured using $[(C_6H_5)_3PH]_3EuBr_6 \cdot (C_6H_5)_3PHBr$ as a primary standard.

Attempts at preparation of MI_6^{-3} complexes using HI in acetonitrile or nitromethane were unsuccessful. Reaction of HI with the solvents to produce I_3^- even

in absence of oxygen was severe. Samarium was allowed to react with HI in an oxygen-free solution of Bu_4NI in chloroform. Hydrogen was evolved but the samarium iodide produced did not go into solution.

Results and Discussion

Internal 4f Transitions. The absorption spectra of the hexahalides containing from two to thirteen 4f electrons are extremely characteristic. We find the same difference as between UCl_6^{-2} , UBr_6^{-2} , and UI_6^{-2} on the one hand^{5,12} and most other U(IV) complexes on the other. Thus, in the octahedral complexes, the electronic transitions are far weaker and are accompanied by vibrational structure (at room temperature stretching below and above the wavenumber of the electronic line). In the case of UX_6^{-2} ,^{21,22} it is possible to identify the three vibrational frequencies corresponding to normal modes of odd parity [99, 114, and 257 $K (=cm^{-1})$ in the chloride and 58, 74, and 184 K for the bromide].

The transition $^3H_4 \rightarrow ^3P_0$ in the praseodymium(III) hexahalides in solution or in the solid salts at 300°K (Figure 1) correspond to five sharp lines, the third of which is supposed to be the vibrationless electronic transition; see values in (1). The crystals con-

	$[P(C_6H_5)_3H]_3PrCl_6$, 80°K				
20, 370	20, 484	20, 590	20, 704	20, 820	
	$[P(C_6H_5)_3H]_3PrCl_6$, 300°K				
20, 384	20, 492	20, 600	20, 708	20, 820	
	$PrCl_6^{-3}$ in CH_3CN , 300°K				
20, 408	20, 520	20, 619	20, 717	20, 833	(10)
	$[P(C_6H_5)_3H]_3PrBr_6 \cdot P(C_6H_5)_3HBr$, 300°K				
20, 350	20, 442	20, 509	20, 584	20, 661	

taining $PrCl_6^{-3}$ show the vibrational wavenumber differences 108 and 225 K , whereas the solution shows 98 and 212 K . As expected, $PrBr_6^{-3}$ has lower wavenumber differences, 70 and 155 K . These values are quite plausible when compared to other hexahalides.^{4,21} The two lowest frequencies corresponding to normal modes of odd parity probably nearly coincide. The ratio between the wavenumbers corresponding to bending and stretching normal modes tends to be relatively large in "compressed" octahedral molecules with strong ligand-ligand interactions, such as SF_6 . $PrCl_6^{-3}$, particularly in the salt, seems to belong to this category.

A closer analysis of the vibrational and J-sublevel structure of the spectra would need very extensive

(21) R. A. Satten, C. L. Schreiber, and E. Y. Wong, *J. Chem. Phys.*, **42**, 162 (1965).

(22) R. Pappalardo and C. K. Jørgensen, *Helv. Phys. Acta*, **37**, 79 (1964).

work and comparison of spectra taken at different temperatures. Hence, we restrict ourselves in this paper to consider the baricenter of each J level. We, as well as Dr. Romano Pappalardo, intend to return to the other much more complicated problems later.

Perhaps an even more striking indication of the octahedral symmetry of our hexahalides is the very low intensity of most of the internal 4f transitions, usually some ten times weaker than the aqua ions (Figure 2). This is the first quantitative evidence from solutions of the strong influence on intensities of the absence of a center of inversion in the aqua ions, though some qualitative observations previously have been made on crystalline samples. Actually, in late years, the general opinion has been that all lanthanide complexes have 4f^q transitions which are about as intense as or slightly more intense than for the aqua ions, with exception of the *hypersensitive pseudoquadrupolar* transitions.²³ In Russell-Saunders coupling, these transitions are characterized by the selection rules $J \rightarrow J - 2$, $S \rightarrow S$, and $L \rightarrow L - 2$, behaving as the strongest electric quadrupole transitions would behave. In our hexahalides, the hypersensitive pseudoquadrupolar transitions are very pronounced; the corresponding absorption bands are at least an order of magnitude stronger than the other bands. The reflection spectra of mixed oxides²⁴ suggest low intensities, and perhaps coexcited vibrations, of 4f^q transitions of lanthanides in sites having a center of inversion such as the eight-coordinated position in pyrochlores of the type ErTiO_{3.5} or the six-coordinated position in perovskites such as high-temperature LaErO₃, when compared to the spectra of disordered fluorites or C oxides. Thus, Kisluk, Krupke, and Gruber²⁵ could not detect any absorption lines from *that* quarter of the erbium(III) ions which are present in C-type Y₂O₃ at sites presenting a center of inversion. However, in these cases, no clear evidence for hypersensitivity is found. It may be remarked that the center of inversion must be present with a large precision before the spectrum is dominated by the weak, coexcited vibrations. The approximate octahedral symmetry of Er(III) in YCl₃ studied by Rakestraw and Dieke²⁶ is not sufficient, and we must admit that the electronic lines still are quite prominent in our spectra, suggesting weak distortions away from cubic symmetry.

Tables I-VII give the baricenters of excited J levels of our hexahalides and, for comparison, also those for the aqua ions, the oxides, and various results for M(III) in LaCl₃ and YCl₃. The nephelauxetic effect can be evaluated from the data by the linear relation²⁴

$$\sigma - \sigma_{\text{aqua}} = d\sigma - (d\beta)\sigma_{\text{aqua}} \quad (2)$$

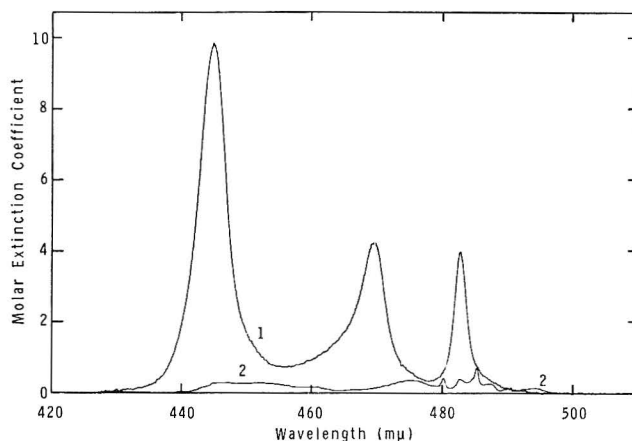


Figure 2. Absorption spectra of praseodymium(III): (1) Pr(III) in 1 M HClO₄ and (2) [(C₆H₅)₃PH]₃PrCl₆ in 85% succinonitrile-15% acetonitrile containing (C₂H₅)₄NCl.

where $d\beta$ is the relative decrease in per cent of the interelectronic repulsion parameters when compared with the aqua ion, σ and σ_{aqua} are the observed wavenumbers of the baricenters, and $d\sigma$ represents the stabilization of the lowest sublevel of the ground J level of the compound considered minus the similar stabilization of the aqua ion. Actually, the linear relation is obeyed fairly well by most, but not all, transitions in a given central atom. Thus, ²H_{11/2} of Nd(III) and Er(III) or ¹I₆ of Pr(III) (*cf.* also ref 27) move less than expected.²⁴

It is seen in Table VIII that $d\beta$ is 2.5 to 4.5 times larger in our hexahalides than in M(III) substituted in LaCl₃, and $d\beta$ is somewhat smaller in hexahalides than in the oxides. Since the oxides are thought²⁴ to have an anomalously large nephelauxetic effect compared with M(III)LaCl₃, our results might perhaps be taken as an argument that it is rather the latter host lattice which produces an anomalously low nephelauxetic effect. The explanation is probably connected with the strong dependence of the overlap integrals between the 4f shell and the ligand orbitals on small variations of the internuclear distances.²⁸ Hence, we cannot establish a unique nephelauxetic series of ligands, which would be a fairly good approximation

(23) C. K. Jørgensen and B. R. Judd, *Mol. Phys.*, **8**, 281 (1964).

(24) C. K. Jørgensen, R. Pappalardo, and E. Rittershaus, *Z. Naturforsch.*, **20a**, 54 (1965).

(25) P. Kisluk, W. F. Krupke, and J. B. Gruber, *J. Chem. Phys.*, **40**, 3606 (1964).

(26) J. W. Rakestraw and G. H. Dieke, *ibid.*, **42**, 873 (1965).

(27) J. Sugar, *Phys. Rev. Letters*, **14**, 731 (1965); *J. Opt. Soc. Am.*, **55**, 1058 (1965).

(28) C. K. Jørgensen, R. Pappalardo, and H. H. Schmidtke, *J. Chem. Phys.*, **39**, 1422 (1963).

Table I: Internal 4f² Transitions in Praseodymium(III) Complexes^a

	PrCl ₆ ⁻²			PrBr ₆ ⁻²			Pr(H ₂ O) ₉ ⁺²		Pr ^{III} - LaCl ₃	Pr ^{III} - GdCl ₃	Pr ^{III} - LaBr ₃
	λ _J	σ _J	ε _{max}	λ _J	σ _J	ε _{max}	σ _J	ε _{max}	σ _J	σ _J	σ _J
¹ D ₂	592	16.89	0.09	595	16.81	0.14	16.78	1.9	16.73	16.69	16.67
³ P ₀	485	20.61	0.94	487.6	20.50	1.0	20.69	4.0	20.47	20.41	20.37
³ P ₁	475	21.05	0.40	477	20.96	0.59	21.29	4.6	21.08	21.01	20.98
³ P ₂	450	22.22	0.34	455.5	21.95	0.45	22.43	10.5	22.23	22.16	22.13

^a λ_J is the wavelength in mμ and σ_J the wavenumber in kK of the baricenter of the band group corresponding to the excited J level indicated. ε_{max} is the molar extinction coefficient of the highest band of each group in the solution absorption spectra; the wavenumber of this band does not necessarily coincide with σ_J.

Table II: Internal 4f³ Transitions in Neodymium(III) Complexes^a

	NdCl ₆ ⁻²			NdBr ₆ ⁻²			Nd(H ₂ O) ₉ ⁺²		Nd ^{III} - LaCl ₃	A-Nd ₂ O ₃
	λ _J	σ _J	ε _{max}	λ _J	σ _J	ε _{max}	σ _J	ε _{max}	σ _J	σ _J
⁴ F _{3/2}	881	11.35	0.31	878	11.39	0.38	11.58	3.6	11.44	11.19
⁴ F _{5/2}	808	12.38	0.65	803	12.45	0.94	12.62	11.8	12.48	12.27
⁴ F _{7/2}	747	13.39	0.56	748	13.37	0.68	13.58	7.2	13.44	13.25
⁴ F _{9/2}	~686	14.58	0.05	685	14.56	0.07	14.84	0.4	14.72	14.47
⁴ G _{5/2}	590	16.95	5.6	587	17.04	10.0	17.40	7.0	17.21	16.72
⁴ G _{7/2}	534	18.73	0.72	533	18.76	1.5	19.18	4.4	19.03	18.60
⁴ G _{9/2}	517	19.34	0.27	520	19.23	0.40	19.63	1.7	19.44	19.17
² P _{1/2}	434	23.04	0.11	434	23.04	0.12	23.40	0.6	23.21	22.84
⁴ D _{3/2}	358	27.93	~1.0	28.28	5.2	27.97	27.20

^a Notation as in Table I.

Table III: Internal 4f⁶ Transitions in Samarium(III) Complexes^a

	[P(C ₆ H ₅) ₃ H] ₃ SmCl ₆			SmCl ₆ ⁻³	Sm(H ₂ O) ₉ ⁺²		Sm ^{III} - LaCl ₃	B-Sm ₂ O ₃
	λ _J	σ _J		ε _{max}	σ _J	ε _{max}	σ _J	σ _J
⁶ F _{3/2}	~1420	7.04	Strong	...	7.15	1.6	7.05	7.34
⁶ F _{7/2}	1255	7.97		...	8.0	2.1	8.00	8.05
⁶ F _{9/2}	1090	9.17		...	9.25	1.8	9.08	9.22
⁴ G _{5/2}	562	17.79	Very weak	0.02	17.9	0.04	17.86	17.57
⁴ F _{3/2}	531	18.83	Very weak	0.01	18.6	0.02	18.86	18.87
...	491	20.37	Weak	0.03	20.02	0.08
...	478	20.92	Weak	0.04	20.88	0.6	20.60	20.75
⁴ I _{13/2}	465	21.51	Weak	0.025	21.55	0.5	21.56	21.41
⁶ P _{5/2}	422	23.70		0.15	24.0	0.5	23.78	23.64
⁶ P	410	24.39		0.67	24.9	3.3	24.54	24.39

^a Notation as in Table I.

in the 3d, 4d, and 5d transition groups.²⁹ Keating and Drickamer³⁰ studied the nephelauxetic effect of high pressures applied to 4f group compounds. A more chemical technique for modifying the internuclear distances was applied by McLaughlin and Conway³¹ studying Pr(III) in LaCl₃, CeCl₃, NdCl₃, SmCl₃, and GdCl₃. The gradually decreasing Pr-Cl distances

produce a strongly increasing nephelauxetic effect, dβ in Table VIII going from 0.8 to 1.2%. On the other

(29) C. K. Jørgensen, "Orbitals in Atoms and Molecules," Academic Press Inc., London, 1962.

(30) K. B. Keating and H. G. Drickamer, *J. Chem. Phys.*, **34**, 143 (1961).

(31) R. D. McLaughlin and J. G. Conway, *ibid.*, **38**, 1037 (1963).

Table IV: Internal $4f^9$ Transitions in Dysprosium(III) Complexes^a

	[P(C ₂ H ₅) ₃ H] ₂ DyCl ₆			Dy(H ₂ O) ₉ ⁺⁺		Dy ^{III} LaCl ₃	C-Dy ₂ O ₃
	λ _J	σ _J		σ _J	ε _{max}	σ _J	σ _J
⁶ H _{9/2} , ⁶ F _{11/2}	1300	7.69	Strong	7.7	1.1	7.67	8.01
⁶ H _{7/2} , ⁶ F _{9/2}	1100	9.09		9.1	1.6	9.02	9.46
⁶ F _{7/2}	910	10.99		11.0	2.5	10.93	11.30
⁶ F _{5/2}	808	12.38		12.35	1.8	12.32	12.58

^a Notation as in Table I.

Table V: Internal $4f^{10}$ Transitions in Holmium(III) Complexes^a

	HoCl ₆ ⁻³			Ho(H ₂ O) ₉ ⁺⁺		Ho ^{III} LaCl ₃	C-Ho ₂ O ₃
	λ _J	σ _J	ε _{max}	σ _J	ε _{max}	σ _J	σ _J
⁶ F ₅	648	15.43	0.17	15.42	3.0	15.48	15.50
⁶ S ₂ , ⁶ F ₄	542	18.45	0.35	18.45	4.5	18.5	18.55
⁶ F ₃	488	20.49	0.12	20.56	1.8	20.62	20.53
³ K ₆	453.8	22.03	9.6	22.25	4.0	22.12	22.22
⁶ G ₅	421	23.75	0.32	24.03	2.5	23.94	23.92
...	397.5	25.16	~0.1	25.4	0.1
⁶ G ₄ , ³ K ₇	383	26.11	~0.06	26.0	0.5	26.14	25.97
⁶ G ₆	362	27.62	3.1	27.74	2.3	27.8	27.47

^a Notation as in Table I.

Table VI: Internal $4f^{11}$ Transitions in Erbium(III) Complexes^a

	ErCl ₆ ⁻³			Er(H ₂ O) ₉ ⁺⁺		Er ^{III} LaCl ₃	Er ^{III} YCl ₃	C-Er ₂ O ₃
	λ _J	σ _J	ε _{max}	σ _J	ε _{max}	σ _J	σ _J	σ _J
⁴ I _{9/2} (⁴ F _{9/2})	656.5	15.23	0.23	15.35	2.1	15.28	15.22	15.29
⁴ S _{3/2}	549	18.21	0.18	18.48	0.8	18.40	18.28	18.21
² H _{11/2}	523.6	19.09	6.0	19.23	3.2	19.15	19.07	19.09
⁴ F _{7/2}	490	20.40	0.20	20.60	2.1	20.51	20.43	20.37
⁴ F _{5/2}	461	21.69	0.37	22.27	0.9	22.18	22.08	22.03
⁴ F _{3/2}	454	22.03	0.09	22.61	0.5	22.52	22.46	22.43
² H _{9/2}	408.5	24.47	0.1	24.63	0.7	24.56	24.49	24.54
⁴ G _{11/2}	379.8	26.32	9.6	26.49	7.2	26.37	26.23	26.28

^a Notation as in Table I.

Table VII: Internal $4f^{12}$ Transitions in Thulium(III) Complexes^a

	[P(C ₂ H ₅) ₃ H] ₂ TmCl ₆		Tm(H ₂ O) ₉ ⁺⁺		C-Tm ₂ O ₃
	λ _J	σ _J	σ _J	ε _{max}	σ _J
³ H ₆	1220	8.20	8.23	0.9	8.37
³ H ₄ (³ F ₄)	800	12.50	12.56	1.1	12.79
³ F ₃	698	14.33	14.48	2.6	14.59
¹ G ₄	474	21.10	21.28	0.5	21.46

^a Notation as in Table I.

Table VIII: Nephelauxetic Parameters Characterizing Lanthanide Complexes^a

	dσ	dβ		dσ	dβ
PrCl ₆ ⁻³	+0.25	1.9	HoCl ₆ ⁻³	+0.15	1.1
PrBr ₆ ⁻³	+0.20	2.3	C-Ho ₂ O ₃	+0.45	2.5
Pr ^{III} LaCl ₃	-0.04	0.8	ErCl ₆ ⁻³	+0.10	1.2
Pr ^{III} GdCl ₃	0	1.2	Er ^{III} LaCl ₃	-0.03	0.3
Pr ^{III} LaBr ₃	-0.05	1.3	Er ^{III} YCl ₃	0	0.9
NdCl ₆ ⁻³	+0.05	2.2	C-Er ₂ O ₃	+0.20	1.6
NdBr ₆ ⁻³	+0.05	2.3	TmCl ₆ ⁻³	+0.10	1.3
Nd ^{III} LaCl ₃	-0.06	0.6	C-Tm ₂ O ₃	+0.30	1.5
A-Nd ₂ O ₃	+0.20	3.6			

^a The relative "ligand-field" stabilization dσ in kK and the nephelauxetic ratio dβ (relative to the aqua ions) in per cent.

hand, Pr(III) has the same absorption spectrum in La(H₂O)₉(C₂H₅SO₄)₃ and Gd(H₂O)₉(C₂H₅SO₄)₃, showing that this lattice has sufficiently many degrees of freedom

to allow the Pr-O distances to achieve the same, most favored, values. A similar effect was found for Er(III)²⁶ having $d\beta$ 3 times larger in the six-coordinated YCl_3 with relatively short Er-Cl distances than in the nine-coordinated LaCl_3 . There is little doubt that our MX_6^{-3} exemplify a similar behavior. In particular, the M-X distances are probably even smaller in organic solvents¹³ such as acetonitrile than they would be in aqueous solution if the complexes did not immediately exchange their halide ligands for water. The molar extinction coefficients of the normal, not hypersensitive, transitions increase from some 0.04 times the intensities of the aqua ion in PrCl_6^{-3} to about one-tenth of ErCl_6^{-3} . This may suggest that the cubic symmetry of ErCl_6^{-3} is perhaps slightly less nearly perfect.

Recently, Sugar²⁷ (who also was so kind as to supply this information at an early stage) found 12 of the 13 levels of the configuration $4f^2$ of gaseous Pr^{+3} . The four levels of Table I are situated at 17.33, 21.39, 22.01, and 23.16 kK. The blue shift of these J levels relative to the aqua ion would indicate that $d\beta$ of Pr^{+3} is some -4.3% , though the relative shifts are smaller than expected in the infrared. As also discussed by Sinha and Schmidtke,³² this effect may be connected with a relatively smaller variation of the Landé parameter ζ_{4f} , say 1.5% , than the variation of the parameters of interelectronic repulsion.

Electron-Transfer Spectra. In the ultraviolet, the hexahalide complexes of the reducible central ions Sm(III), Eu(III), Tm(III), and Yb(III) show broad, moderately strong, absorption bands (Figure 3) which can be ascribed to electron transfer from the highest filled MO, mainly localized on the halide ligands, to the partly filled $4f$ shell.¹⁶ Table IX gives data for those absorption bands and for the only two lanthanide(IV) hexahalides we have been able to study, CeCl_6^{-2} and CeBr_6^{-2} . The bands are much more intense in the latter case, the empty $4f$ orbitals probably being somewhat more delocalized out on the ligands. Surprisingly enough, the intensities of CeCl_6^{-2} and CeBr_6^{-2} are even larger than those of UCl_6^{-2} and the Np(IV) and Pu(IV) hexahalides previously studied.⁵

Since the theory for the variation of the optical electronegativity x_{opt} of $4f$ and $5f$ group elements has been discussed elsewhere,^{5,16,33} we are here restricting ourselves to the much simpler equation

$$\sigma_{\text{obsd}} = [x_{\text{opt}}(\text{X}) - x_{\text{uncor}}(\text{M})] \cdot 30 \text{ kK} \quad (3)$$

where the wavenumber σ_{obsd} of the first electron-transfer band is related to the optical electronegativity of the ligand $x_{\text{opt}}(\text{X})$ and the *uncorrected* value, not taking spin-pairing energy or other forms of interelec-

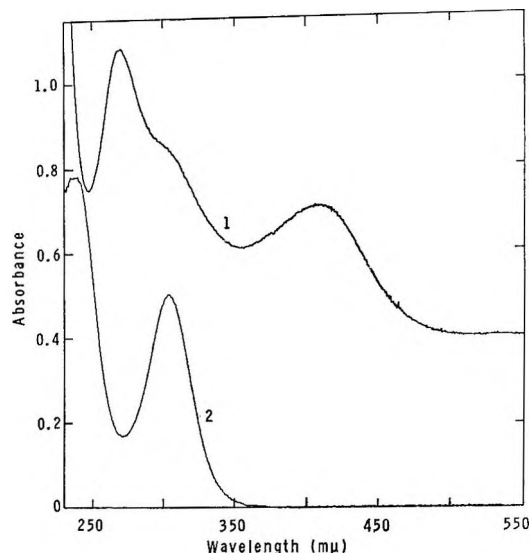


Figure 3. Electron-transfer spectra of europium(III) hexahalides: (1) $0.114 \text{ M EuBr}_6^{-3}$ in acetonitrile containing excess $(\text{C}_2\text{H}_5)_4\text{NBr}$ and HBr in 0.0108-cm cell (absorbance scale displaced 0.4) and (2) $0.0125 \text{ M EuCl}_6^{-3}$ in $(\text{C}_2\text{H}_5)_4\text{NCl}$ -saturated acetonitrile in 0.10-cm cell.

Table IX: Electron-Transfer Spectra of Hexahalides in Nitrile Solution^a

	λ	σ	ϵ	$\delta(-)$
SmCl_6^{-3}	232	43.1	930	2.3
SmBr_6^{-3}	286	35.0	1,050	2.4
EuCl_6^{-3}	301	33.2	400	2.1
	234.5	42.6	640	(3.8)
EuBr_6^{-3}	409	24.5	250	2.0
	(309)	(32.4)	(340)	...
	270	37.0	540	...
TmBr_6^{-3}	~ 260	~ 38.6	~ 300	...
YbCl_6^{-3}	272.5	36.7	160	1.7
YbBr_6^{-3}	342	29.2	105	2.4
	(240)	(41.7)	(450)	...
CeCl_6^{-2}	376	26.6	5,200	2.9
	255	39.2	13,800	3.2
CeBr_6^{-2}	522	19.2	$\sim 5,700$	2.5

^a The wavelengths λ in $\text{m}\mu$, wavenumbers σ in kK , and molar extinction coefficients ϵ are given for maxima (shoulders in parentheses). $\delta(-)$ is the half-width in kK toward smaller wavenumbers.

tronic repulsion effects nor relativistic effects into account, $x_{\text{uncor}}(\text{M})$ for the central atom in a definite oxidation state.

Table X gives the values of $x_{\text{uncor}}(\text{M})$ obtained in a variety of cases. It is seen that the hexabromides

(32) S. P. Sinha and H. H. Schmidtke, *Mol. Phys.*, **10**, 7 (1965).

(33) C. K. Jørgensen, "Lanthanides of $5f$ Elements," Academic Press Inc., London, 1966.

generally indicate values for the central atom some 0.2 unit higher than the bromide complexes in nearly anhydrous ethanol previously studied.¹⁶ The hexachlorides suggest values of $x_{\text{uncor}}(\text{M})$ only about 0.1 unit higher than the chloride complexes in nearly anhydrous ethanol studied by Barnes.³⁴ As pointed out by Barnes, the stoichiometric composition of the latter complexes is not completely certain; they are tentatively described as MCl^{+2} and MBr^{+2} in Table X. A similar argument applies to the Nd(III) chloride complexes formed in strong aqueous hydrochloric acid,³⁵ Malkova, Shutova, and Yatsimirskii³⁶ recently reported such a relation between the HCl activity and the absorption spectrum of the solution that could be exclusively explained by a monochloro complex $\text{NdCl}(\text{H}_2\text{O})_x^{+2}$.

A simple reason for the apparent higher value of $x_{\text{uncor}}(\text{M})$ in MX_6^{-3} compared to MX^{+2} in ethanol may be the smaller M-X distance in the hexahalides already discussed above. Another may be connected with the specific symmetry O_h of the hexahalide. It is normally argued that the highest filled MO in MX_6^{+2-6} just before the partly filled shell is a set of three degenerate $\pi(\text{X})$ orbitals having the symmetry type even γ_4 ($=t_{1g}$). There are two reasons for the high energy of this set: the orbitals are nonbonding

because only g orbitals and higher even l values of the central atom can bond with this set,² and, because of the four angular node-planes, the antibonding X-X interactions are particularly strong.³⁷ Actually, the first electron-transfer band (even γ_4) \rightarrow nd is Laporte-forbidden and relatively weak.^{2,13,38} On the other hand, we find no indication of a weak transition before the first strong electron-transfer band, in agreement with the expectation that (even γ_4) \rightarrow nf is allowed by Laporte's rule.

From group-theoretical reasoning, four Laporte-allowed transitions are predicted for each effective level of the excited configuration $4f^{q+1}$ of the central atom

$$\begin{aligned} (\pi \text{ even } \gamma_4) &\longrightarrow \text{nf} & \text{(I)} \\ (\pi \text{ even } \gamma_6) &\longrightarrow \text{nf} & \text{(II)} \\ (\sigma \text{ even } \gamma_3) &\longrightarrow \text{nf} & \text{(III)} \\ (\sigma \text{ even } \gamma_1) &\longrightarrow \text{nf} & \text{(IV)} \end{aligned} \quad (4)$$

Eu(III) and Yb(III) should be particularly simple because only one low-lying effective level, $^8\text{S}_{7/2}$, exists for the excited configuration $4f^7$. The next levels should not occur before at least 28 kK higher energy. $4f^{14}$ has only one level, $^1\text{S}_0$. The excited states of Ce(IV) involve two effective levels, $^2\text{F}_{5/2}$ and $^2\text{F}_{7/2}$, separated by slightly more than 2 kK.

The energy differences 9.4 kK between the two strong bands of EuCl_6^{-3} and 12.6 kK for CeCl_6^{-2} are most probably caused by the transitions I and III, but the assignments I and II cannot be excluded. In the 4d and 5d group M(III) and M(IV) hexahalides^{2,13,38} the total width of the π orbital energies seems to be 6–8 kK. There is some evidence that this width is somewhat larger in tetrahedral complexes of the 3d group.^{39,40} It is conceivable that either or both of the pairs of transitions I and II or III and IV are nearly degenerate. However, $(\pi \text{ even } \gamma_6) \rightarrow \text{nd}$ has never been identified with certainty in d group hexahalides and might have high wavenumbers, as also $(\sigma \text{ even } \gamma_3) \rightarrow \text{nd}$. Symons⁴¹ suggested that III and IV might have the opposite order of eq 4 arranged according

Table X: Optical Electronegativities Using Eq 3^a

	α_{obsd}	$\alpha_{\text{opt}}(\text{X})$	$\alpha_{\text{uncor}}(\text{M})$
SmBr_6^{-3}	35.0	2.8	1.63
SmBr^{+2} ethanol [16]	40.2	2.8	1.46
SmCl_6^{-3}	43.1	3.0	1.56
SmCl^{+2} ethanol [34]	45.7	3.0	1.48
SmSO_4^+ [34]	48.1	3.2	1.60
EuBr_6^{-3}	24.5	2.8	1.98
EuBr^{+2} ethanol [16]	31.2	2.8	1.76
EuCl_6^{-3}	33.2	3.0	1.89
EuCl^{+2} ethanol [34]	36.2	3.0	1.79
$\text{Eu}^{\text{III}}\text{Y}_2\text{O}_3$ [24, b]	42.5	3.2	1.78
EuSO_4^+ [34]	41.7	3.2	1.81
EuSeO_4^+ [34]	44	3.3	1.83
$\text{Eu}(\text{H}_2\text{O})_9^{+3}$ [c]	53.2	3.6	1.83
TmBr_6^{-3}	38.6	2.8	1.51
TmBr^{+2} ethanol [16]	44.5	2.8	1.32
YbBr_6^{-3}	29.2	2.8	1.83
YbBr^{+2} ethanol [16]	35.5	2.8	1.62
YbCl_6^{-3}	36.7	3.0	1.78
YbCl^{+2} ethanol [34]	41.0	3.0	1.63
YbSO_4^+ [34]	44.5	3.2	1.72
CeBr_6^{-2}	19.2	2.8	2.16
CeCl_6^{-2}	26.6	3.0	2.11

^a References in brackets. ^b N. C. Chang, *J. Appl. Phys.*, **34**, 3500 (1963). ^c C. K. Jørgensen and J. S. Brinen, *Mol. Phys.*, **6**, 629 (1963).

(34) J. C. Barnes, *J. Chem. Soc.*, 3880 (1964).

(35) C. K. Jørgensen, *Kgl. Danske Videnskab. Selskab Mat. Fys. Medd.*, **30**, No. 22 (1956).

(36) T. V. Malkova, G. A. Shutova, and K. B. Yatsimirskii, *Russ. J. Inorg. Chem.*, **9**, 993 (1964).

(37) D. S. McClure, *Solid State Phys.*, **9**, 399 (1959).

(38) C. K. Jørgensen, *Acta Chem. Scand.*, **17**, 1034, 1043 (1963).

(39) A. Carrington and C. K. Jørgensen, *Mol. Phys.*, **4**, 395 (1961).

(40) P. Day and C. K. Jørgensen, *J. Chem. Soc.*, 6226 (1964).

(41) M. C. R. Symons, *ibid.*, 1482 (1964).

to a decreasing number of angular node-planes. An important negative result of our measurements is that no weak electron-transfer bands have been observed before the first strong bands.

Crystalline $[P(C_6H_5)_3H]_3EuBr_6 \cdot [P(C_6H_5)_3H]Br$ shows nearly the same absorption spectrum as the solution of $EuBr_6^{-3}$ with a maximum at 24.6 kK. The half-width $\delta(-) = 2.4$ kK is not directly comparable, because the optical density of solids observed by our technique usually increases less strongly than the actual ϵ . The transition ${}^7F_0 \rightarrow {}^5D_2$ corresponding to a very sharp little hump at 465.2 $m\mu$ is somewhat intensified as in the orange dialkyldithiocarbamates.¹⁶

The measurements in the ultraviolet were made on solutions containing only "aliphatic" constituents and not $P(C_6H_5)_3H^+$. Another experimental problem was constituted by the danger of forming Br_3^- by oxidation of bromide solutions. This species^{42,43} has an extremely intense band ($\epsilon \sim 50,000$) at 37 kK but does not seem to have perturbed our results, largely because of the technique of using very thin cells.

As discussed in the Experimental Section, $CeBr_6^{-2}$ has only a transient existence at room temperature, and the molar extinction coefficient $\epsilon \sim 5700$ of the wine-red solution was obtained by extrapolation toward the time zero.

It may be worthwhile to make the chemical comment that, until recently, octahedral lanthanide complexes in solution were exceedingly rare. There exist some oxides²⁴ and sulfides⁴⁴ with distorted octahedral coordination of 4f group atoms. There appear also to exist a few cases of tetrahedrally coordinated sulfides.⁴⁴

The 4f \rightarrow 5d Transitions in Cerium(III) and Terbium(III) Hexahalides. When $CeCl_6^{-3}$ and $CeBr_6^{-3}$ are prepared according to the same techniques as the other MX_6^{-3} , they show some tendency in acetonitrile solution toward oxidation to $CeCl_6^{-2}$ and $CeBr_6^{-2}$. However, the original spectra can readily be obtained and consist in both cases of a single strong band as seen from Table XI and Figure 4. This band is 2 to 3 times narrower than the electron-transfer bands given in Table IX, and there is every reason to believe that it is the transition from the ground-state ${}^2F_{5/2}$ of $[Xe] 4f$ to the excited configuration $[Xe] (5d\gamma_6)$ containing one electron in the lower subshell of octahedral MX_6 chromophores. The weak red shift from the chloride to the bromide is quite compatible with such an interpretation.^{5,35} It may be mentioned that Feofilov⁴⁵ reported a similar band at 32.7 kK for Ce(III) in the cubic, eight-coordinated position in CaF_2 . However, a much weaker band seems to occur already at 30.3 kK.^{45,46}

The most interesting feature of our spectra is per-

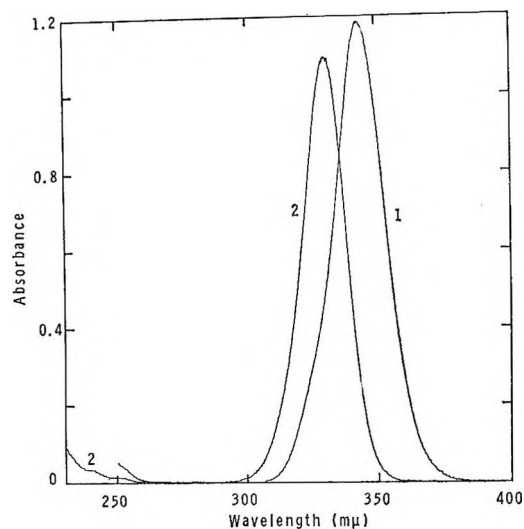


Figure 4. Absorption spectra of cerium(III) hexahalides: (1) 6.8×10^{-2} M $CeBr_6^{-3}$ in acetonitrile containing excess $(C_4H_9)_4NBr$ and HBr in 0.0108-cm cell and (2) 6.4×10^{-2} M $CeCl_6^{-3}$ in acetonitrile containing excess $(C_2H_5)_4NCl$ in 0.0108-cm cell.

Table XI: 4f \rightarrow 5d Transitions in Cerium(III) and Terbium(III) Hexahalides^a

	λ	σ	ϵ	$\delta(-)$	$\delta(+)$
$CeCl_6^{-3}$	330	30.3	1600	0.8	1.05
$CeBr_6^{-3}$	343	29.15	1600	1.05	1.05
$TbCl_6^{-3}$	271.5	36.8	28	1.2	...
	233.8	42.75	1500	0.65	1.1
$TbBr_6^{-3}$	278	36.0	Weak	0.9	...

^a Notation as in Table IX; $\delta(+)$ is the half-width in kK toward higher wavenumbers.

haps the absence of any other absorption bands in the measured range, up to 45 kK in $CeCl_6^{-3}$ and 40 kK in $CeBr_6^{-3}$. This sets a lower limit of some 15 kK for the energy difference Δ between the two 5d subshells γ_6 and γ_3 . This figure may be compared with $\Delta = 20.4$ kK in $RhCl_6^{-3}$ and 25.0 kK in $IrCl_6^{-3}$,²⁹ and suggests a strong σ -antibonding influence on the upper subshell though the Ce-Cl distance must be considerably larger than, say, the Ir-Cl distance.

(42) A. I. Popov and R. F. Swensen, *J. Am. Chem. Soc.*, **77**, 3724 (1955).

(43) J. E. Dubois and H. Herzog, *Bull. Soc. Chim. France*, 57 (1963).

(44) C. K. Jørgensen, R. Pappalardo, and J. Flahaut, *J. Chim. Phys.*, **62**, 444 (1965).

(45) P. P. Feofilov, *Opt. Spectry.* (USSR), **6**, 150 (1959).

(46) P. P. Sorokin, M. J. Stevenson, J. R. Lankard, and G. D. Pettit, *Phys. Rev.*, **127**, 503 (1962).

The absorption band observed for CeCl_6^{-3} is weakly asymmetric, having slightly slower decline toward higher wavenumbers. This may be connected with the energy difference in the LCAO approximation

$${}^3/2\zeta_{\text{eff}} = {}^3/2[a^2\zeta_{5d}(\text{Ce}) + {}^1/2b^2\zeta_{\text{np}}(\text{X})] \quad (5)$$

expected between the levels γ_7 (one Kramers doublet) at higher energy and γ_8 (two Kramers doublets) at lower energy in the case of large Δ . The delocalization coefficient, a , may be rather different from 1, but ζ_{5d} in gaseous Ce^{+3} is 1.00 kK, and the splitting cannot be very prominent. It is surprising that the hexabromide (where $\zeta_{\text{np}} = 2.46$ kK for gaseous Br) does not show a somewhat more pronounced asymmetry.

TbCl_6^{-3} shows a strong, relatively narrow band at 42.75 kK belonging to the excited configuration $4f^75d$ (γ_5). This compares favorably with the band of the terbium(III) aqua ion at 45.9 kK. It had previously

been discussed⁴⁷ whether the aqua ion has a very weak band about 39 kK. This may very well be the case, because our solutions of TbCl_6^{-3} show a band at 36.8 kK. TbBr_6^{-3} shows a similar band at 36.0 kK (and the strong transition is hidden by bromide absorption). The most reasonable assignment is the excited term ${}^9\text{D}$ of $4f^75d$ to which transitions from the ground term ${}^7\text{F}$ of $4f^8$ would be spin-forbidden. Then, the separation 6.0 kK between ${}^9\text{D}$ and ${}^7\text{D}$ would correspond to eight times the effective exchange integral $K_{\text{av}}(4f, 5d)$ which is known to be 1.0 kK in the isoelectronic gaseous species Gd^{+2} .^{33,48} The spin-forbidden transition is 50-fold less intense than the spin-allowed band, agreeing fairly well with the squares of the ${}^7\text{D}$ amplitudes calculated.⁴⁸

(47) Footnote *c* of Table X.

(48) W. R. Callahan, *J. Opt. Soc. Am.*, **53**, 695 (1963).

Studies of Acid-Base Equilibria in Molten Alkali Nitrates

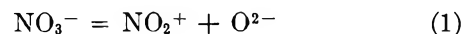
by L. E. Topol, R. A. Osteryoung, and J. H. Christie

North American Aviation Science Center, Thousand Oaks, California 91360 (Received February 23, 1966)

Voltammetric and chronopotentiometric measurements as well as chemical equilibrium studies were made on solutions of acids ($\text{S}_2\text{O}_7^{2-}$, HSO_4^- , NO_2) and bases (NO_2^- , NO , CO_3^{2-} , O^{2-} , OH^- , O_2^{2-}) in molten NaNO_3 - KNO_3 (50:50 mole %) at 275-350°. The existence of the species NO_2^+ , postulated to exist in acidic nitrate melts, could not be confirmed. Instead, the addition of a strong acid resulted in the formation of a species similar chemically and electrochemically to dissolved NO_2 . This species could be reduced in a one-electron process to NO_2^- but could not be oxidized.

Introduction

Although many thermodynamic and transport properties of fused salts have been measured,¹ far less is known of the basic chemistry and electrochemistry in these systems. In molten nitrates, for example, some acid-base titrations² and reactions^{3,4} have been studied, but only one direct measurement⁵ has been reported on the acid species NO_2^+ , postulated to occur in the self-dissociation^{4f} of NO_3^- shown in eq. 1.



Although the existence of the nitronium ion⁶ NO_2^+ , as well as the nitrosonium ion^{6b,7} NO^+ , has been substantiated in highly acidic aqueous media, neither has

(1) See (a) "Molten Salt Chemistry," M. Blander, Ed., Interscience Publishers, Inc., New York, N. Y., 1964; or (b) "Fused Salts," B. R. Sundheim, Ed., McGraw-Hill Book Co., Inc., New York, N. Y., 1964.

been directly observed in nitrate melts. In spite of this, NO_2^+ has been assumed as an intermediate to explain some kinetic investigations⁴ as well as electrode reactions⁸ in molten nitrates. To study the occurrence and behavior of NO_2^+ and NO^+ , chronopotentiometry and linear-sweep voltammetry have been applied to the molten $\text{NaNO}_3\text{-KNO}_3$ (50:50 mole %) system at 275–350°.

Experimental Section

All the salts used were standard reagents and were dried by heating in a vacuum oven at 150°. Matheson NO_2 (99.5% pure) and NO (99% pure) were used without further treatment.

The linear-sweep voltammetric measurements were made with an apparatus similar to that described elsewhere.⁹ Potential span velocities of 0.1–1.0 v/sec were used. A conventional set-up with a John Fluke Model 351A dc constant-current source was employed for chronopotentiometry. A Moseley Model 2D X-Y recorder or a Tektronix Type 564 storage oscilloscope was used to record data. Chronopotentiometric transition times were measured by the method of Voorhies and Furman.¹⁰

The Pyrex cell assembly¹¹ consisted of a capped vessel with ground-glass joints to accommodate a thermocouple well or gas bubbling tube and three half-cells, the reference, the counter, and the indicator. The reference half-cell was $\text{Ag}|\text{AgNO}_3$ (0.06 M), $\text{NaNO}_3\text{-KNO}_3$ while a Pt helix and a 0.0254-cm diameter Pt wire, sealed in glass, served as the counter and indicator electrodes, respectively. Weighed quantities of pre-dried $\text{NaNO}_3\text{-KNO}_3$ were added to the half-cells and container to yield a common level of melt throughout. The indicator compartment contained gas bubbling and exit tubes so that the melt here as well as in the container could be purged with NO_2 and/or Ar before measurements were begun. An argon atmosphere was maintained in the container during the experiment *via* gas entry and exit lines at the upper sides of the container. Holes connecting the counter and reference electrode compartments above the level of the melt prevented a pressure differential. Electrolytic contact between the half-cells and the bulk melt was achieved with fritted disks of medium porosity at the bottom of each compartment.

For the equilibration experiments a Pyrex flask containing addition tubes and a gas sampling tube was employed.³ The apparatus had provisions for evacuation and filling with gas. The cell or flask was heated in a Marshall or pot furnace, respectively, controlled by a chromel–alumel thermocouple and West controller.

Results

NaNO₃-KNO₃ Melt. A typical linear-sweep voltammetric curve for a $\text{NaNO}_3\text{-KNO}_3$ (50:50 mole %) melt at 285° with no added solute is shown in Figure 1 (solid line). The cathodic and anodic potential limits were –1.6 and +1.2 v *vs.* $\text{Ag}|\text{AgNO}_3$ (0.06 M) and are in agreement with those found by Swofford and Laitinen,¹² who employed a similar reference electrode. Other features of the current–voltage curves are reduction waves at +0.4 and –1.0 v (the latter also found by Swofford and Laitinen) and oxidation waves at –0.3 and +0.5 v. The waves at –1.0 v (due to water¹²) and at +0.4–0.5 v (due to nitrite, see below) were found in all the alkali melts after bubbling with dry argon, but both waves could be eliminated by purging the melt with NO_2 .

NaNO₂ Solution. Current–voltage curves obtained on cycling for a nitrate melt containing NaNO_2 are identical with those found in the nitrate solvent above except for the increase in the waves occurring at +0.4–0.5 v. This is shown in Figure 1 by the dashed line for the voltage sweep cycled between 0 and +0.6 v. The average peak separation between the anodic and cathodic waves is 0.10 v in good agreement with the theoretical value of 0.108 v for a reversible one-electron process^{13a} at 300°. Upon oxidation of the solution at +0.5

(2) A. M. Shams El Din, *Electrochim. Acta*, **7**, 285 (1962); A. M. Shams El Din and A. A. A. Gerges, *J. Electroanal. Chem.*, **4**, 309 (1962); *Electrochim. Acta*, **9**, 123, 613 (1964); A. M. Shams El Din, A. A. El Hosary, and A. A. A. Gerges, *J. Electroanal. Chem.*, **6**, 131 (1963); **8**, 312 (1964).

(3) J. D. Van Norman and R. A. Osteryoung, *Anal. Chem.*, **32**, 398 (1960).

(4) (a) F. R. Duke and M. L. Iverson, *J. Am. Chem. Soc.*, **80**, 5061 (1958); (b) *Anal. Chem.*, **31**, 1233 (1959); (c) F. R. Duke and S. Yamamoto, *J. Am. Chem. Soc.*, **81**, 6378 (1959); (d) F. R. Duke and W. W. Lawrence, *ibid.*, **83**, 1269 (1961); (e) F. R. Duke and E. A. Shute, *J. Phys. Chem.*, **66**, 2114 (1962); (f) F. R. Duke, *J. Chem. Educ.*, **39**, 57 (1962); (g) reference 1b, p 409.

(5) G. Delarue, 13th Meeting of International Committee of Electrochemical Kinetics and Thermodynamics, Rome, Italy, Sept 1962, Abstract No. 8.2.

(6) (a) C. K. Ingold, D. J. Millen, and H. G. Poole, *J. Chem. Soc.*, 2576 (1950); (b) D. J. Millen, *ibid.*, 2600 (1950).

(7) W. R. Angus and A. H. Leckie, *Nature*, **134**, 572 (1934); *Proc. Roy. Soc. (London)*, **A149**, 327 (1935); *Trans. Faraday Soc.*, **31**, 958 (1935).

(8) N. Gupta and B. R. Sundheim, *J. Electrochem. Soc.*, **112**, 836 (1965).

(9) G. Lauer, H. Schlein, and R. A. Osteryoung, *Anal. Chem.*, **35**, 1789 (1963).

(10) J. D. Voorhies and N. H. Furman, *ibid.*, **30**, 1656 (1958).

(11) D. L. Hill, J. Perano, and R. A. Osteryoung, *J. Electrochem. Soc.*, **107**, 698 (1960).

(12) H. S. Swofford, Jr., and H. A. Laitinen, *ibid.*, **110**, 814 (1963).

(13) P. Delahay, "New Instrumental Methods in Electrochemistry," Interscience Publishers, Inc., New York, N. Y., 1954: (a) pp 120, 137; (b) p 184; (c) p 182.

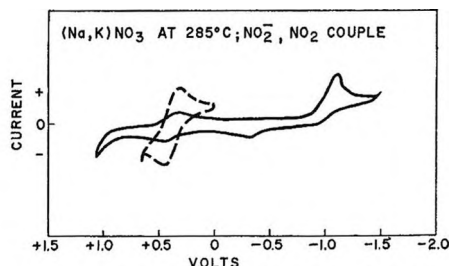


Figure 1. Current-potential curve for $\text{NaNO}_3\text{-KNO}_3$ melt at 285° (solid line); same melt with NaNO_2 added and cycled between 0 and $+0.6$ v (dashed line). The cathodic current is +, anodic -.

v for a length of time, bubbles of gas (NO_2 , see below) were evolved from the electrode. Anodic chronopotentiograms on a 0.0145 M NaNO_2 solution (Figure 2) yielded constant $i\tau^{1/2}$ values over a range of τ 's of $0.061\text{-}2.60$ sec (Table I). For longer transition times

Table I: $i\tau^{1/2}$ Values on Pt Electrode for NaNO_2 (0.0145 M) in $\text{NaNO}_3\text{-KNO}_3$ at 298°

i , ma	τ , sec	$i\tau^{1/2}$, ma sec ^{1/2}
5.00	0.0615	1.24
4.50	0.075	1.22
4.00	0.095	1.22
3.50	0.126	1.24
3.00	0.172	1.24
2.50	0.238	1.22
2.00	0.375	1.23
1.50	0.71	1.26
1.25	0.97	1.23
1.00	1.64	1.28
0.80	2.60	1.29
0.60	4.85	(1.32)

$$\bar{A}v = 1.24 \pm 0.02$$

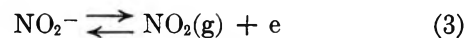
$$D = 5.2 \times 10^{-5} \text{ cm}^2/\text{sec}$$

the results were erratic, presumably owing to bubbles of NO_2 produced on the Pt electrode. The diffusion coefficient D of NO_2^- was calculated to be 5.2×10^{-5} cm^2/sec at 298° from the relation^{13b}

$$D = \frac{4i^2\tau}{\pi n^2 F^2 C^2 A^2} \quad (2)$$

where i is the current, τ the transition time, n the number of equivalents per mole of reactant, F the Faraday constant, and C the concentration. The area A of the Pt wire electrode (0.15 cm^2) was calculated from its dimensions. From $\log [(\tau/t)^{1/2} - 1]$ vs. E plots^{13c} of these anodic chronopotentiograms (similar to that shown in Figure 4 below for the reverse reaction),

straight lines of theoretical slope for a reversible one-electron reaction and an $E_{1/4} = 0.47$ v were obtained. The oxidation is consistent with the reaction



These results are in agreement with those found voltammetrically by Swofford and McCormick.¹⁴ Reverse current chronopotentiograms, with reversal before the transition time (Figure 2), resulted in ratios of forward to reverse transition times that were always greater than the theoretical value of 3 to 1. This is taken to indicate that some of the product of the forward step (NO_2) is lost by processes other than simple diffusion, *e.g.*, volatilization and/or reaction. Acidifying a nitrite solution resulted in a decrease or removal in the nitrite wave without the appearance of a new wave that could be attributed to NO^+ .

Addition of Strong Acids and NO_2 . The addition of strong acids (substances that accept oxide ion) such as $\text{K}_2\text{S}_2\text{O}_7$, KHSO_4 , $\text{Cr}(\text{NO}_3)_3$, and $\text{Al}(\text{NO}_3)_3$ resulted in the formation of a yellowish solution and evolution of a brownish gas. An anodic shift of the equilibrium potential and the appearance of a cathodic wave (at $+0.40\text{-}0.50$ v) that decreased with time were also observed. Current-voltage curves of these melts resembled those shown in Figure 1. Similar current-voltage curves and chronopotentiograms (Figure 3) were obtained with solutions containing NO_2 . Thus the cathodic wave resulting from the addition of acids appears to be due to NO_2 , the other half of the NO_2^- couple. Plots of E vs. $\log [(\tau/t)^{1/2} - 1]$ from cathodic chronopotentiograms were linear and yielded $E_{1/4}$'s of about 0.50 v and slopes corresponding to a reversible one-electron process (Figure 4). This result is in contrast to that of Swofford and McCormick,¹⁴ who reported no electrochemical activity for dissolved NO_2 . A tabulation of the average $E_{1/4}$ values for both forward and reverse chronopotentiometric waves for melts containing $\text{K}_2\text{S}_2\text{O}_7$, KHSO_4 , and NO_2 , as well as NaNO_2 , is given in Table II. The potentials for the different melts can be considered to be identical within experimental error.

Addition of Bases. A base in these systems is a compound that yields oxide ions. Solution of Na_2O_2 , Na_2CO_3 , or NaOH in the molten alkali nitrates resulted in a cathodic shift of the equilibrium potential. Anodic waves were obtained with all these solutions. The Na_2O_2 on oxidation yielded two approximately equal waves, the first occurring at about -0.2 v and presumably involving the O_2^{2-} and the second at $+0.3$ v involving

(14) H. S. Swofford, Jr., and P. G. McCormick, *Anal. Chem.*, **37** 970 (1965).

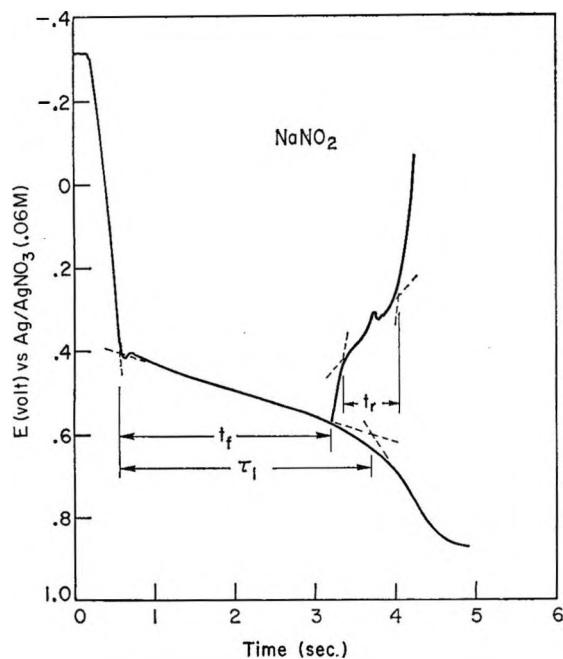


Figure 2. Chronopotentiograms for NaNO_2 solution in NaNO_3 - KNO_3 at 290° : τ_1 , anodic transition time; t_f , time of forward (anodic) current; t_r , transition time for reverse (cathodic) process.

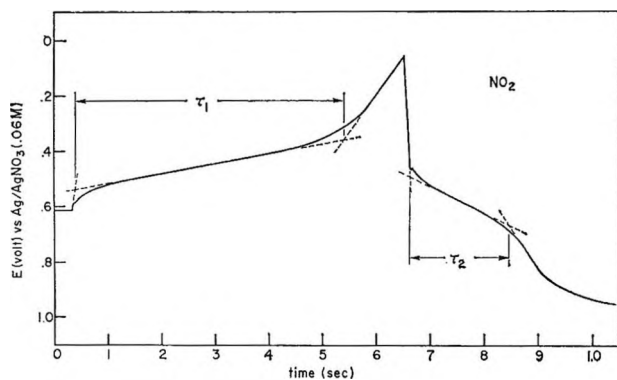


Figure 3. Chronopotentiograms for dissolved NO_2 in NaNO_3 - KNO_3 melt: τ_1 , cathodic transition time; τ_2 , transition time for reverse (anodic) process due to oxidation of products formed during τ_1 .

Table II: Average $E_{1/4}$ Values at Pt Electrode (vs. $\text{Ag}|\text{AgNO}_3$ (0.06 M) Reference) in NaNO_3 - KNO_3 at 300°

Solute	$E_{1/4}$, v ^a	
	Cathodic	Anodic
NaNO_2	0.44 (r)	0.47 (f)
NO_2	0.42 (f)	0.45 (r)
$\text{K}_2\text{S}_2\text{O}_7$	0.42 (f)	0.47 (r)
KHSO_4	0.41 (f)	0.45 (r)

^a f = forward wave, r = reverse wave.

the O^{2-} . Swofford and McCormick apparently found a single wave, but it is not clear from their presentation if a second wave may have existed. The Na_2CO_3 and NaOH solutions each produced one wave at about +0.4 and -0.3 v, respectively. On reversal of current after these waves, single reduction waves at -0.6 to -0.9 v were found in all these melts. (When the electrode potential was cycled between +0.1 and -0.6 v, anodic waves due to a solid on the electrode were frequently found at about 0.0 v.) Solutions containing $\text{NaNO}_2 + \text{Na}_2\text{CO}_3$ or $\text{NaNO}_2 + \text{Na}_2\text{O}_2$ (Figure 5) were titrated with $\text{K}_2\text{S}_2\text{O}_7$. It was observed that both the carbonate and peroxide, being stronger bases than nitrite, were neutralized before the nitrite. However, the expected stoichiometry did not seem to be obeyed. Figure 6 shows the neutralization of a Na_2O_2 melt by purging with NO_2 .

Addition of NO and Oxygen. When nitric oxide was bubbled through the nitrate melt, the only electrochemical reaction observed was an oxidation; linear voltammetric and chronopotentiometric measurements were the same as for solutions to which NO_2^- had been added. These results indicated that a reaction took place between NO and the nitrate melt (see below).

Attempts to reduce gaseous oxygen in these melts were unsuccessful. This result differs from that of Kust and Duke¹⁵ but is in agreement with the findings of Swofford and McCormick.¹⁴

Discussion

For the NaNO_3 - KNO_3 melt the limiting reactions at -1.6 (cathodic) and +1.2 v (anodic) have been attributed to the reduction of NO_3^- to NO_2^- and O^{2-} and the oxidation of NO_3^- to NO_2 and O_2 , respectively.¹² The anodic wave at -0.3 v can be ascribed to oxidation of the Pt electrode and/or of oxide ion formed during the reduction of NO_3^- . Nitrate solutions containing various bases show anodic waves which may involve the same over-all oxidation process, *i.e.*, depolarization of the platinum electrode by oxide. The difference in potentials at which these processes occur in the various solutions may be indicative of the different basic characteristics of the oxide donors.

The electrochemical studies demonstrate that the species NO_2^+ , assumed to exist in measurable concentration¹⁶ in acidic nitrate melts, cannot be detected by the techniques employed above. The same electrochemical techniques have been utilized successfully in a recent study¹⁶ of NO^+ and NO_2^+ in concentrated

(15) R. N. Kust and F. R. Duke, *J. Am. Chem. Soc.*, **85**, 3338 (1963).

(16) L. E. Topol, R. A. Osteryoung, and J. H. Christie, *J. Electrochem. Soc.*, **112**, 861 (1965).

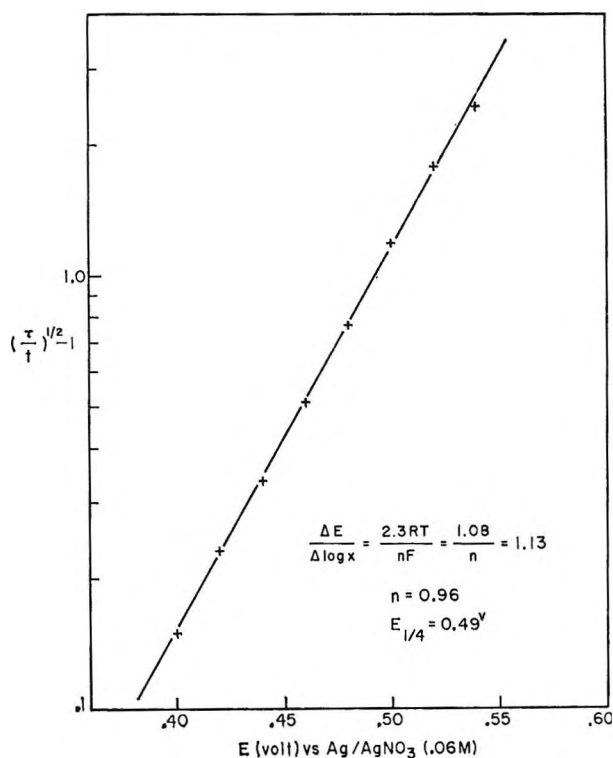


Figure 4. $\text{Log} [(\tau/t)^{1/2} - 1]$ vs. E for the electrode reaction $\text{NO}_2 + e \rightarrow \text{NO}_2^-$.

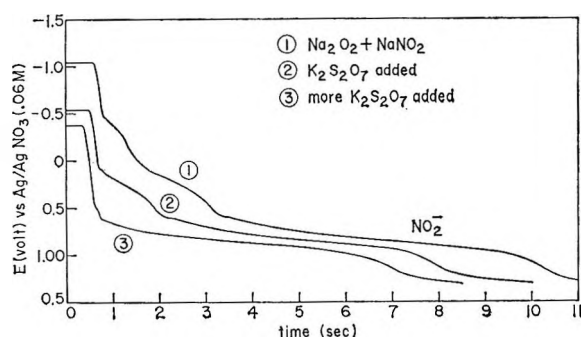
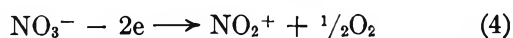


Figure 5. Reaction of $\text{Na}_2\text{O}_2 + \text{NaNO}_2$ with $\text{K}_2\text{S}_2\text{O}_7$ in $\text{NaNO}_3\text{-KNO}_3$ at 300° .

sulfuric acid. Attempts to oxidize NO_2 and NO at Pt electrodes in the molten nitrates were also unsuccessful. Furthermore, recent thin-film infrared-emission measurements¹⁷ of acidic nitrate melts yielded no evidence of the existence of NO_2^+ . These results are in disagreement with Delarue,⁵ who reported the coulometric production of NO_2^+ by the reaction



and claimed to have identified the electrode reaction



Our results regarding the electrochemical behavior of

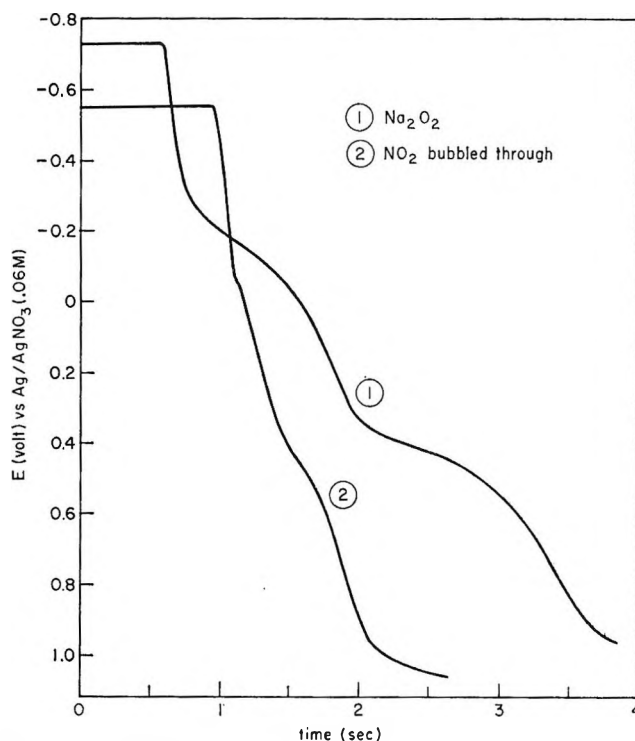
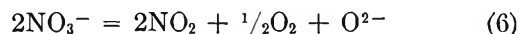


Figure 6. Reaction of Na_2O_2 with NO_2 in $\text{NaNO}_3\text{-KNO}_3$ at 300° .

NO_2 are in opposition to those of Swofford and McCormick, who state that NO_2 "exhibits no significant electrochemical activity." We are in agreement regarding the existence of a reversible one-electron oxidation of NO_2^- to NO_2 . The voltammetry and reverse-current chronopotentiometry on nitrite as well as NO_2 support the reversibility of reaction 3. Certainly, Swofford and McCormick's conclusion regarding a reversible couple requires that NO_2 be reducible to NO_2^- , and we are unable to suggest a cause for their finding NO_2 electrochemically inert.

Kust and Duke,¹⁵ using an oxygen electrode in acid nitrate melts, claim to have measured the dissociation constant for reaction 1. However, their dissociation constant increased with time and it may be that here, as well as in previous kinetic studies,⁴ the reaction observed was



or in the presence of acids, e.g., $\text{S}_2\text{O}_7^{2-}$

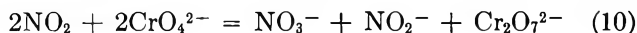
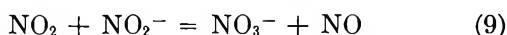
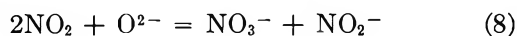


The present electrochemical studies have shown that

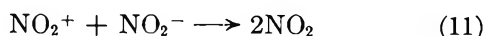
(17) J. R. Moyer, Dow Chemical Co., private communication.

the $\text{NO}_2\text{-NO}_2^-$ couple is reversible on Pt and that the only detectable electroactive species in solution upon the addition of strong acids to nitrates is NO_2 . The diffusion coefficient of NO_2 dissolved in these melts could not be determined from eq 2 since the gas concentration or solubility is not known. If one assumes that the diffusion coefficients of NO_2 and NO_2^- are approximately equal, the solubility of NO_2 in $\text{NaNO}_3\text{-KNO}_3$ is calculated to be about $(5 \pm 3) \times 10^{-3}$ mole/l. at 300° .

It was further demonstrated that NO_2 itself behaves as an acid, reacting with strong bases and nitrite and converting chromate to dichromate, possibly *via* the following reactions.



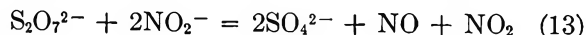
In an equilibrium study, reaction 9 was found to proceed far to the right as written. However, the reverse reaction can also be observed by bubbling NO through a nitrate melt as was demonstrated by the electrochemical results. This also appears to disagree with the findings of Swofford and McCormick, although their experimental conditions may preclude comparison with our data. It was also found that equilibrating nitrite with an acid such as $\text{K}_2\text{S}_2\text{O}_7$ or $\text{K}_2\text{Cr}_2\text{O}_7$ in a nitrate melt always resulted in the formation of a gaseous mixture of NO and NO_2 . The relative amounts of the two gases varied with the acid used, the percentage of NO decreasing from over 90% with $\text{K}_2\text{Cr}_2\text{O}_7$ to about 50% with $\text{K}_2\text{S}_2\text{O}_7$ at 275° . If NO_2^+ were the acid species, then one would expect to find NO_2 primarily, according to the reactions



and

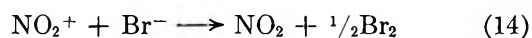


However, the reaction occurring appears complicated but may be



or may also involve reactions 7 and 9. With dichromate the reaction would be similar to (13) except that chromate would be formed instead of sulfate, and reaction 10 must also be considered. These reactions with the appropriate equilibrium constants could account for the low NO_2 concentration at equilibrium in the dichromate system. In any event it is difficult to reconcile these results with the assumption of NO_2^+ as the acid species.

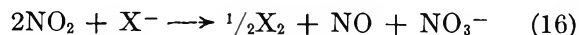
Finally, NO_2^+ has been postulated as the intermediate in the acid oxidation of bromide ion,^{4b} *i.e.*



and also, oxidation of iodide³ has been found in metaphosphate-containing melts, the reaction suggested as



It was decided to check these reactions and to see if NO_2 could oxidize these halide ions. Solutions of KI and $\text{K}_2\text{Cr}_2\text{O}_7$ in $\text{NaNO}_3\text{-KNO}_3$ were equilibrated overnight *in vacuo* and the reaction was found to be complex in that it required about four parts of dichromate to one of iodide for complete iodide oxidation. The gas phase was analyzed by mass spectrometry and consisted entirely of NO in every case in contrast to NO_2 reported and postulated earlier.^{3,4b} To test the effect of nitrogen dioxide, some experiments were run in which NO_2 was bubbled through nitrate melts containing Br^- or I^- . Both halogen and NO were found indicating the over-all reaction to be



Thus, here again the observed behavior of NO_2 is equivalent to that attributed to NO_2^+ in acidified melts, and although the chemical evidence above does not preclude the existence of NO_2^+ , it certainly favors NO_2 as an acid intermediate, if one is required, rather than NO_2^+ .

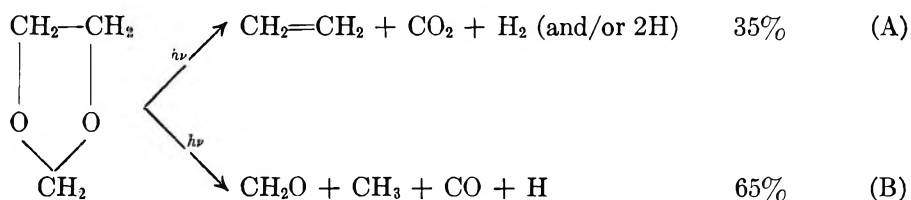
Acknowledgments. This work was supported in part by the U. S. Atomic Energy Commission and was presented at the molten salt session of the Electrochemical Society Meeting, San Francisco, Calif., May 9-13, 1965.

The Photochemistry of 1,3-Dioxolane¹

by B. C. Roquette

Radiation Research Laboratories, Mellon Institute, Pittsburgh, Pennsylvania (Received February 25, 1966)

The gas phase photodecomposition of 1,3-dioxolane with the full light of a medium-pressure mercury arc has been investigated in the pressure range 11–82 mm and at temperatures 27–110°. The reaction products found were H₂, CO, CO₂, CH₄, C₂H₆, C₂H₄, C₄H₁₀, and CH₂O. Experiments were carried out with various additives (O₂, C₂D₄, *n*-C₄H₁₀, and *i*-C₄H₁₀). Two primary processes are important in the decomposition



The azomethane-sensitized decomposition of 1,3-dioxolane has also been studied briefly.

Introduction

As part of a general study of the photochemistry of cyclic molecules containing one or two oxygen atoms in the ring, the present study of the photochemical decomposition of 1,3-dioxolane was undertaken. It was of particular interest to ascertain whether the photochemical modes of decomposition are analogous to the thermal decomposition² of 1,3-dioxolane. Therefore attention was focused on the direct unimolecular decomposition processes in this molecule, although its radical-sensitized decomposition was briefly studied. This paper describes the first study of the photochemical decomposition of 1,3-dioxolane.

Experimental Section

Materials. Eastman Kodak White Label 1,3-dioxolane was distilled under vacuum and a middle fraction was retained for most of the experiments reported here. Analysis by gas chromatography using a 2-m Carbowax column and a 2-m dinonyl phthalate column showed that the distilled sample contained only one component.

Oxygen from the Matheson Co. was used directly from the cylinder.

The ethylene-*d*₄ was obtained from Volk Radio-Chemical Co. It was degassed and distilled from –160 to –196°. Both 2,3-dimethylbutane and *n*-

butane (research grade) from Phillips Petroleum Co. were outgassed and distilled under vacuum in the usual way.

Apparatus and Procedure. A Hanovia U-type medium-pressure mercury arc was used as a light source in all of the experiments. The light was partially collimated onto a quartz cell of 189-cc volume mounted in an electrically heated furnace. The temperature of the cell could be controlled within ±3° during a run. In most of the runs no filter was used since it was noted that, when using a Corning filter 7910, which transmits light of wavelength longer than 2100 Å, the photochemical decomposition was negligible. In the azomethane-sensitized decomposition a Corning filter 5860 was used to isolate 3660-Å light. The high-vacuum system was of standard type provided with two LeRoy traps, a solid nitrogen trap, and a Toepler pump-gas buret for gas analysis. Before photolysis a sample was expanded in the cell and then condensed at liquid nitrogen temperature and degassed. In experiments with added gas the reactant and added gas were thoroughly mixed by means of an all-glass circulating pump before being exposed to the radiation.

(1) Supported, in part, by the U. S. Atomic Energy Commission.

(2) W. B. Guenther and W. D. Walters, *J. Am. Chem. Soc.*, **73**, 2127 (1951).

Table I: Photolysis of 1,3-Dioxolane

Prod- ucts	Press., mm													
	11.0	20.0	20.0	20.0	46.5	50.0	50.0	50.0	50.0	50.0	61.0	73.0	81.0	82.0
	Temp, °C													
	27	27	81	110	110	27	27	27	27	27	80	27	110	80
μmoles	Exposure time, min													
	120	120	120	121.5	120.0	19.0	30.0	58.0	120.7	183.8	122.2	50.0	120.0	120.0
H ₂	2.90	3.82	4.72	5.62	7.58	0.64	1.08	2.21	4.63	7.01	6.85	3.36	9.60	7.64
CO	2.60	3.45	3.12	3.49	4.63	0.41	0.72	1.53	3.64	5.86	4.79	2.77	5.81	5.29
CH ₄	0.39	0.48	0.61	0.89	1.34	0.09	0.12	0.27	0.62	1.02	1.12	0.36	1.80	1.31
C ₂ H ₆	0.26	0.29	0.27	0.37	0.53	Trace	0.03	0.08	0.20	0.37	0.43	n	0.70	0.35
CO ₂	1.89	2.51	3.20	4.48	5.37	0.47	0.59	1.11	2.38	3.49	4.82	n	7.34	4.48
C ₃ H ₈	2.10	2.89	3.13	4.21	5.44	0.64	0.80	1.52	3.22	4.80	5.40	n	7.14	5.21
C ₄ H ₁₀	n ^a		0.31	0.29	0.31	n	n	0.09	0.17	0.33	0.39	n	0.28	n
CH ₂ O	n	2.51	2.47	2.64	n	0.74	n	1.73	2.99	3.96	3.70	2.55	4.05	n

^a n = not analyzed.

After each run the products were condensed at -196° and then distilled through two LeRoy traps at -196° and a solid nitrogen trap (-210°). In experiments in which oxygen was added to the reactant, the non-condensable gases were pumped off, while in runs which were performed without oxygen, the noncondensable gases were measured in a Toepler pump-gas buret. The noncondensable fraction which contained H₂, CH₄, and CO was analyzed by a mass spectrometer. The condensable fraction was transferred quantitatively into an ampoule and then introduced into the inlet system of a dual-column, dual-detector gas chromatograph. The two columns and the detectors were connected in series, and the electrical signals from the detectors were fed into a double-pen recorder. One of the columns was 2 m long, packed with 25 wt % Carbowax 600 on Chromosorb, while the other was 1.5 m long and packed with silica gel. Ethane, carbon dioxide, ethylene, and butane were all resolved very well in the silica gel column. The Carbowax column could resolve acetaldehyde, ethylene oxide, and 1,3-dioxolane. The columns were calibrated using known quantities of authentic samples. Since it was not possible to analyze formaldehyde by gas chromatography, it was estimated quantitatively by the color reaction.³ In order to analyze all of the products, two runs were carried out under identical conditions, of which one was used for analysis of formaldehyde while the other one was used for analysis of all other products.

Results

Within the decomposition range 0.5–2.5%, the principal products of the reaction were hydrogen, carbon monoxide, carbon dioxide, methane, ethane, ethylene, *n*-butane, and formaldehyde (Table I).

Acetaldehyde was not detected as a product, and, if it were present at all, it could not be more than a few per cent of the total products.

The product yields at different exposure times are shown in Figures 1 and 2, which demonstrate the leveling off of formaldehyde at longer exposure while the other products were linearly proportional with time except carbon monoxide, the rate of which increased with time.

The scavenging effect of ethylene-*d*₄ (Table II) on the hydrogen yield is prominent in Figure 3. The purpose of added ethylene-*d*₄ was dual. First, it acted as a scavenger of the hydrogen atom. Second, it acted as a detector of shorter wavelengths since

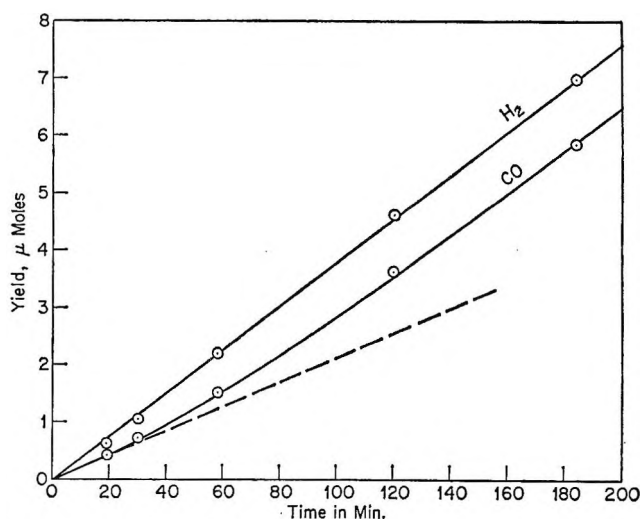


Figure 1. Yield of CO and H₂ vs. time.

(3) D. Matsukawa, *J. Biochem.* (Tokyo), **30**, 386 (1939).

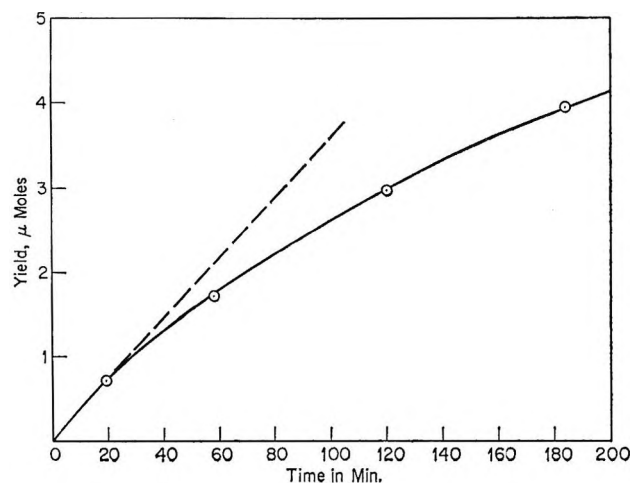
Table II: Effect of Addends in the Photolysis of 1,3-Dioxolane^a

Addends	Press., mm							
	20.0	3.0	10.0	1.5	4.0	9.0	284.0	101.0
O ₂	...	3.0	10.0
C ₂ D ₄	1.5	4.0	9.0
<i>n</i> -C ₄ H ₁₀	284.0	...
<i>i</i> -C ₄ H ₁₀	101.0
Products	μmoles							
	20.0	3.0	10.0	1.5	4.0	9.0	284.0	101.0
H ₂	3.82	n	n	1.71	1.47	1.25	3.28	3.71
CO	3.46	n	n	3.34	3.33	3.17	2.72	3.00
CH ₄	0.48	n	n	0.41	0.35	0.36	0.48	0.69
C ₂ H ₆	0.29	a ^c	a	n	n	n	n	0.26
CO ₂	2.51	1.81	1.79	n	n	n	n	2.50
C ₂ H ₄	2.89	1.90	1.99	n	n	n	n	2.60
C ₄ H ₁₀	n ^b	a	a	n	n	n	n	n
CH ₂ O	2.51	2.50	n	n	n	n	n	2.40

^a Pressure of 1,3-dioxolane 20.0 mm; exposure time 120.0 min; temperature 27°. ^b n = not analyzed. ^c a = absent.

ethylene starts absorbing light at a wavelength of 1900 Å. A trace amount of D₂ (~0.1%) was detected as a product of runs with added ethylene-*d*₄; therefore, it was concluded that wavelengths shorter than 1900 Å were not playing an important role in the decomposition of 1,3-dioxolane.

Product yields were determined with added oxygen as well. In these runs the reactant pressure (20 mm) and exposure time (120 min) were kept constant. These results are given in Table II. The effect of temperature on the products of the photolysis with 20 mm of 1,3-dioxolane is shown in Figure 4. All of the products increased with increasing temperature except carbon monoxide; hydrogen increased the most and formaldehyde the least.

Figure 2. Yield of CH₂O vs. time.

The mole ratios H:C, H:O, and C:O for the total observed products are given in Table III. It appears that, within experimental errors, the material balance was reasonably good.

In Table IV the product yields of the azomethane-sensitized decomposition of 1,3-dioxolane are summarized.

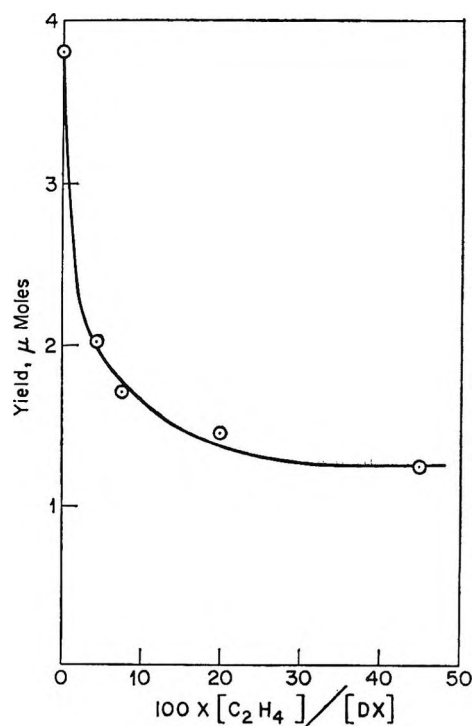


Figure 3. Yield of hydrogen vs. per cent of added ethylene.

Table III: Mass Balance of the Products of Photolysis of 1,3-Dioxolane

Press., mm	Temp, °C	Exposure time, min	H:C	H:O	C:O
20.0	27	120.0	1.90	2.99	1.57
20.0	110	121.5	1.93	2.78	1.44
50.0	27	58.0	2.0	3.00	1.50
50.0	27	120.7	1.95	2.94	1.50
61.0	80	122.2	1.93	2.96	1.53
Theoret	2	3	1.5

Table IV: Methyl Radical Sensitized Decomposition of 1,3-Dioxolane^a

Products	DX press., mm			
	20.0	52.5	53.5	99.0
	Azomethane press., mm			
	2.0	3.5	1.5	2.0
	Exposure time, min			
	964.8	968.4	957.6	906.3
H ₂	0.12	0.33	0.44	0.41
N ₂		12.48	6.76	5.86
CO	0.05	0.25	0.06	0.13
CH ₄	0.27	4.96	3.06	4.25
C ₂ H ₆	n ^b	7.43	3.68	4.20
CO ₂	n	5.51	3.13	9.88
C ₂ H ₄	n	0.99	0.71	0.87
C ₄ H ₁₀	n	n	n	n
CH ₂ O	0.09	0.60	n	0.85

^a Wavelength 3600 Å; temperature 27°. ^b n = not analyzed.

Photochemically Effective Wavelength. It appears that the ultraviolet absorption spectrum of 1,3-dioxolane has not been determined previously. Owing to the limitation of the Cary 14 spectrophotometer, it was not possible for us to take the complete spectrum down to 1900 Å. Nevertheless, it appears certain that 1,3-dioxolane starts absorbing around 2000 Å. In the absence of a complete absorption spectrum, the following experiments were performed to determine the photochemically effective wavelength. The decomposition of 1,3-dioxolane was carried out using the same light source in combination (1) with a Vycor filter, (2) with an interference filter (band width 100 Å with maximum at 2100 Å), and (3) without filter. The results are given in Table V where the total amounts of noncondensable products are listed. In a medium-pressure mercury arc the effective light is largely continuous with a few superimposed lines in the region 2000–1849 Å. Owing to the presence of a long air path through which the light has to travel before entering the reaction cell, most of the 1849-Å

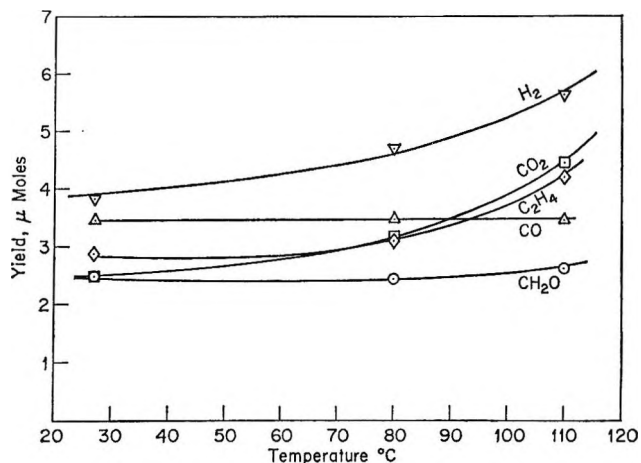


Figure 4. Effect of temperatures on the product yields.

wavelength is absorbed by the air. Therefore, the wavelengths which are most effective lie in the region 2000–1900 Å.

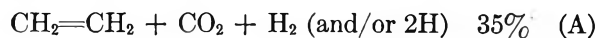
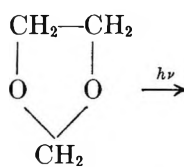
Table V^a

Filter	Product, μmoles	Rel amt of decompn
Vycor	0.081	1
Interference	0.311	3.8
None	7.49	92.5

^a Exposure time 120 min.

Discussion

The experimental evidence suggests that at least two primary processes which take place are

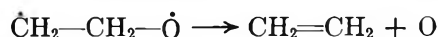


The quenching effect of addends *n*-butane and isobutane on the product yields (Table II) does not appear to be significant. This perhaps suggests that excited molecules do not play an important part in the decomposition of 1,3-dioxolane.

In the present system, the formation of hydrogen atoms and molecules seems unquestionable. The decrease in the yields of hydrogen with increasing amounts

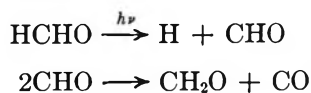
of ethylene was due to the addition of the hydrogen atom to the ethylene double bond. As is evident from Figure 3, the hydrogen yield was reduced to about 55% by the addition of 7.5% of ethylene. Extrapolation of the linear part of the curve in Figure 3 to infinite concentration of ethylene showed that about 33% of hydrogen from 1,3-dioxolane decomposition was produced as molecular hydrogen and therefore was unscavengable by ethylene.

Both ethylene and carbon dioxide were produced in abundant quantities in the presence of oxygen (Table II). This indicated that a major portion of ethylene and carbon dioxide was formed in a direct molecular process. The persistent production of formaldehyde in large amounts, even in the presence of oxygen and ethylene, indicated that perhaps it was formed by a direct molecular process and may, in fact, be the same process which yielded CH₃, CO, and part of the hydrogen atom. The presence of methyl radical in the photolysis was obvious. The formation of methane and ethane in the pure 1,3-dioxolane and removal of C₂H₆ by the addition of oxygen can only be explained by the reactions of methyl radical. Since no acetaldehyde was detected as a product, the diradical $\dot{\text{C}}\text{H}_2\text{-CH}_2\text{-}\dot{\text{O}}$, a possible intermediate formed after the elimination of formaldehyde, could decompose after the migration of a hydrogen atom into CH₃, CO, and H. On the other hand, the diradical could split to give CH₂=CH₂ and the O atom. In the flash photolysis of ethylene oxide we have observed such a process.⁴ In addition, the data of Table I show that, at a pressure of 50 mm of dioxolane and at 27°, the ethylene yield is greater than CO₂. This may indicate that excess ethylene might have come from such a process as



Then the number of oxygen atoms is given by [C₂H₄] - [CO₂]; at higher conversion this difference is a large number. Thus, all of these oxygen atoms could react with the substrate by some radical mechanism to produce the observed products.

The decrease in the formaldehyde rate with reaction time (Figure 1) indicates consumption of the product formaldehyde in secondary reactions. Since the carbon monoxide rate increased with time, it is certain that a portion of CO has been formed by the secondary decomposition of formaldehyde



An approximate estimate indicates that at least 35% of the decomposition proceeds *via* process A and the

rest *via* process B, provided, of course, no other primary processes are involved.

The decrease in the yield of CO₂ and C₂H₄ by the addition of 3 mm of oxygen in 20 mm of 1,3-dioxolane suggests that perhaps the triplet state was the precursor of about 28% of the CO₂ and C₂H₄ formed in the system. Further addition of oxygen (10 mm) did not quench the products CO₂ and C₂H₄ anymore within experimental errors. This is in contrast to the decomposition of acetone⁵ where very small amounts of oxygen were very effective in removing the triplet state. It is possible that the major part of CO₂ and C₂H₄ originated *via* singlet state and that is why they are not quenched completely. However, it has been indicated that the diagnostic test of triplet by the use of oxygen is not effective in every case.⁶

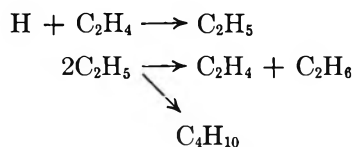
The existence of diradicals in the present system cannot be ignored and requires some comment. It is possible that the initial act of a photon in this system might lead to the formation of diradicals such as $\dot{\text{C}}\text{H}_2\text{-CH}_2\text{-O-CH}_2\text{-}\dot{\text{O}}$ (I) and/or $\dot{\text{O}}\text{-CH}_2\text{-CH}_2\text{-O-}\dot{\text{C}}\text{H}_2$ (II) and these could decompose to yield observed products or re-form the starting compound. Since the C-O bond in 1,3-dioxolane is of the order of 75-80 kcal/mole⁷ and since the radiation absorbed corresponds to 144 kcal/mole or greater, the diradical formed will be highly energetic and might decompose to give the observed products. The temperature dependence of the product yield (Figure 4) indicates that the decomposition of diradical I into C₂H₄, CO₂, and H₂ (and/or 2H) was favored by higher temperatures whereas the breakdown of diradical II into CH₂O, CO, CH₃, and H atom was almost independent of temperature in spite of the fact that in both cases the rupture of C-O bond(s) was essential. Owing to the polychromatic nature of the light source, photons with varying amounts of energies are absorbed in the system. Thus, it is possible that the diradicals I and II, formed by primary process, have different lifetimes and consequently behave differently with increasing temperature. Since quantum yields are not measured, it was virtually impossible to ascertain as to what extent these diradicals re-formed 1,3-dioxolane. Finally the formation of *n*-butane in this system could be explained as the result of the reaction of ethyl radicals which were formed by addition of H atom to ethylene

(4) B. C. Roquette, *J. Phys. Chem.*, **70**, 2699 (1966).

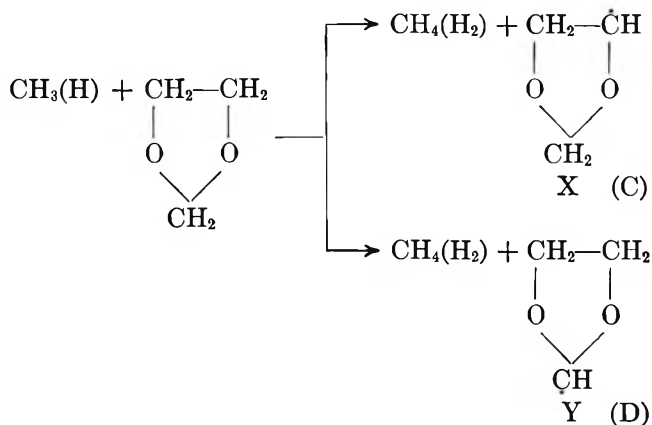
(5) G. W. Luckey and W. A. Noyes, Jr., *J. Chem. Phys.*, **19**, 227 (1951); J. Heicklen, *J. Am. Chem. Soc.*, **81**, 3863 (1959).

(6) D. W. Setser, D. W. Placzek, *et al.*, *Can. J. Chem.*, **40**, 2179 (1962).

(7) P. Gray and A. Williams, *Chem. Rev.*, **59**, 239 (1959).



Methyl Radical Sensitized Decomposition. Magram and Taylor⁸ have pointed out that an oxygen atom will affect the ease of removal of the hydrogen atom on an adjacent carbon atom. It may be expected from this that the hydrogen atoms on the methylene group flanked by two oxygen atoms will be more reactive than those of the other two methylene groups in 1,3-dioxolane. Since methyl radicals and hydrogen atoms are formed in the primary process(es), it is quite likely that they will react with the labile hydrogen atoms



In order to decide the fate of the radicals X and Y, the methyl radical sensitized decomposition of 1,3-dioxolane was undertaken. It is postulated that these radicals decomposed to give the observed products (Table IV). It should be noted that the ratio $\text{CO}_2:\text{CH}_2\text{O}$ is much higher than that in the direct photolysis of 1,3-dioxolane. This may be interpreted to mean that, because the hydrogen atoms in CH_2 flanked by oxygen atoms are more reactive, radical Y was produced at a higher frequency than the X radicals, and the former decomposed to give CO_2 and ethylene and H atom. It may be pointed out that yield of C_2H_4 in the methyl radical sensitized decomposition was much too small compared to the yield of CO_2 and this probably was due to removal of ethylene by some secondary reactions.

In conclusion, the present study provides evidence that in the photolysis of 1,3-dioxolane two primary processes account for most of the products. It is interesting to note that, whatever the detailed mechanism may be, the end products in both the thermal and photochemical decompositions are surprisingly similar.

Acknowledgment. The author is grateful to Dr. K. O. Kutschke for his comments on this work.

(8) S. J. Magram and H. A. Taylor, *J. Chem. Phys.*, **9**, 755 (1941).

Dissociation Constant of Morpholinium Ion and Related Thermodynamic Quantities from 0 to 50°

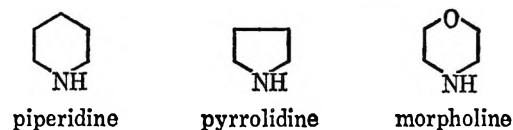
by Hannah B. Hetzer, Roger G. Bates, and R. A. Robinson

National Bureau of Standards, Washington, D. C. (Received February 28, 1966)

The thermodynamic dissociation constant of morpholinium ion (MH^+) at 11 temperatures from 0 to 50° has been determined from emf measurements of hydrogen-silver chloride cells without liquid junction. The dissociation constant (K_a) for the process $MH^+ + H_2O \rightleftharpoons M + H_3O^+$ is given as a function of T (°K) by the equation $-\log K_a = 1663.29/T + 4.1724 - 0.0042239T$. At 25°, $-\log K_a$ is 8.492, ΔH° is 39,030 joules mole⁻¹, ΔS° is -31.7 joules deg⁻¹ mole⁻¹, and ΔC_p° is 48 joules deg⁻¹ mole⁻¹.

Introduction

The measurement of the dissociation constant of piperidine over a range of temperature has been described¹ in an earlier communication. More recently, similar measurements for pyrrolidine have been reported.² Pyrrolidine differs structurally from piperidine in that it has a five-membered ring with one CH_2 group less than piperidine. Morpholine (tetrahydro-1,4-oxazine) has a six-membered ring in which one CH_2 group of piperidine is replaced by an oxygen atom. The three related bases have the following structures



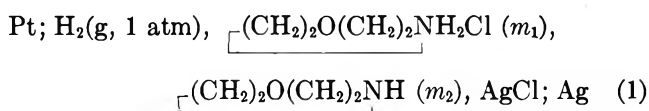
The pK_a value of piperidinium ion at 25° is 11.123 and that of pyrrolidinium ion is 11.305; hence the values of ΔG° for the dissociation process differ by 1040 joules mole⁻¹. The values of ΔH° at 25° differ by 1080 joules mole⁻¹, whereas those of ΔS° differ by less than 0.2 joule deg⁻¹ mole⁻¹.

The thermodynamic quantities associated with the dissociation of piperidinium and pyrrolidinium ions are therefore quite similar in magnitude. On the contrary, literature values³⁻⁶ for the pK_a of morpholinium ion range from 8.3 to 8.5, corresponding to a value for ΔG° of about 48.5 kjoules mole⁻¹ for the dissociation process. This value is to be compared with 64.5 kjoules mole⁻¹ for pyrrolidinium ion. It is of interest

therefore to make pK measurements for morpholinium ion over a range of temperature, in order to ascertain if the ΔH° and ΔS° values are also markedly different. We have now determined thermodynamic quantities for the dissociation process $MH^+ + H_2O \rightarrow M + H_3O^+$ from 0 to 50° and have calculated pH values for a buffer mixture over this temperature range.

Method

The method used followed closely that for pyrrolidine,² except that the silver-silver chloride electrode was used instead of the silver-silver bromide electrode. The cell can be represented as



where m is molality.

Three corrections sometimes needed in emf measurements of solutions of bases proved unnecessary in this case. One is the consideration of the partial pressure of the amine in correcting the pressure of hydrogen to 1 atm. The allowance in the case of pyrrolidine solu-

(1) R. G. Bates and V. E. Bower, *J. Res. Natl. Bur. Std.*, **57**, 153 (1956).

(2) H. B. Hetzer, R. G. Bates, and R. A. Robinson, *J. Phys. Chem.*, **67**, 1124 (1963).

(3) H. K. Hall, *ibid.*, **60**, 63 (1956).

(4) H. K. Hall, *J. Am. Chem. Soc.*, **79**, 5439 (1957).

(5) A. R. Ingram and W. F. Luder, *ibid.*, **64**, 3043 (1942).

(6) A. Marxer, *Helv. Chim. Acta*, **37**, 166 (1954).

tions was negligible² even at 50°. Since morpholine (bp 128° (760 mm)) is even less volatile than pyrrolidine (bp 86.5° (760 mm)), the correction can be omitted with certainty. This conclusion was confirmed by measurements of the emf of two cells of type 1 containing a solution of composition $m_1 = \sim 0.1$, $m_2 = \sim 0.05$ at 25, 40, 45, 50° and then again at 25°. One cell contained a single hydrogen saturator, and the other was provided with an extra triple saturator. Since the values for the two cells agreed within 0.05 mv at all temperatures, the cells with one saturator were deemed to be adequate for the determination of the dissociation constant.

Secondly, the increase in the chloride ion concentration resulting from the solubility of silver chloride in the cell solution has to be considered. The logarithm of the stability constant of the morpholine-silver complex ion has been reported⁷ to be 4.98 at 25° and was found in the present work to be 4.2 at 50°. The increase in chloride ion concentration calculated in the usual way for the morpholine buffer solutions used here was negligible even at 50°, and the correction was consequently omitted.

Thirdly, in calculating pK from emf data, the ratio $(m_1 - m_H + m_{OH})/(m_2 + m_H - m_{OH})$ is required. In this instance, this ratio could be taken equal to m_1/m_2 because neither neutral morpholine nor its protonated cation is appreciably hydrolyzed in the buffer mixtures studied.

Materials

Examination of a "purified" commercial grade of morpholine by mass spectrometry⁸ indicated about 99% purity, with about 0.1% of heavier materials and a small amount of water present. This material was distilled under reduced pressure through a Podbielniak column with platinum Heligrad packing, rated at about 100 theoretical plates. Three intermediate fractions, interspersed with small samples for test, were removed and sealed under vacuum. Mass spectra of the distilled material were consistent with the structure of morpholine. There was some evidence of traces of water, but no trace of substances heavier than morpholine was detected. Gas-liquid partition chromatograms of the distilled morpholine, using four different substrates, revealed only single peaks.

The buffer solutions were prepared, under nitrogen, by first adding morpholine to hydrochloric acid of known composition and then diluting this stock solution. Three sets of solutions were prepared using morpholine from vials opened immediately before use, and a fourth set was made from one kept stoppered for

6 weeks after opening. No evidence of decomposition of morpholine was observed in this last set of solutions.

The ratio of salt to free base (m_1/m_2) in three sets of solutions was approximately 2 and in a fourth set approximately 1.2. The molality of free base was determined by weight titration with standard hydrochloric acid to the calculated equivalence point (pH 4.8 for an approximately 0.07 *M* solution of the salt), detected with a glass electrode.

Results

The emf values of cell 1 for 19 solutions are recorded in Table I. The emf of the cell is related to the pK_a value of morpholinium ion by the equation

$$pK_a = (E - E^\circ)/k + \log (m_1^2/m_2) + \log (\gamma_{MH} + \gamma_{Cl^-} / \gamma_M)$$

where k denotes $(RT \ln 10)/F$ and M stands for morpholine. Introducing the Debye-Hückel equation with zero ion-size parameter, we obtain

$$pK_a' = (E - E^\circ)/k + \log (m_1^2/m_2) - 2Am_1^{1/2} \quad (2)$$

where A is the Debye-Hückel parameter on the molal scale. With the E° values of Bates and Bower,⁹ good straight-line extrapolations of pK_a' against m_1 gave limiting values of pK_a at $m_1 = 0$, using a zero ion-size parameter. The standard deviation of the intercept was 0.001 at all temperatures. These pK_a values are given in Table II along with those calculated from the equation¹⁰

$$pK_a = A_1/T - A_2 + A_3T \quad (3)$$

with $A_1 = 1663.29$, $A_2 = -4.1724$, and $A_3 = -0.0042239$ ($0^\circ\text{C} = 273.15^\circ\text{K}$).

Discussion

Equation 3 leads, by standard thermodynamic equations, to values of the enthalpy, entropy, and heat capacity changes for the dissociation process. Values at 25° for morpholinium ion and for the two closely related substances are as shown in Table III.

These values for piperidinium ion and pyrrolidinium ion are remarkably similar except, perhaps, for the heat capacity change. However, for morpholinium ion

(7) R. J. Bruehlmann and F. H. Verhoek, *J. Am. Chem. Soc.*, **70**, 1401 (1948).

(8) The authors are indebted to Mr. E. E. Hughes for the mass spectrometric analyses, to Dr. R. T. Leslie for the distillation, and to both Dr. Leslie and Mr. Hughes for the gas-liquid partition chromatographic analyses of morpholine.

(9) R. G. Bates and V. E. Bower, *J. Res. Natl. Bur. Std.*, **53**, 283 (1954).

(10) H. S. Harned and R. A. Robinson, *Trans. Faraday Soc.*, **36**, 973 (1940).

Table I: Electromotive Force of the Cell: Pt; H₂ (g, 1 atm), (CH₂)₂O(CH₂)₂NH₂Cl (*m*₁), (CH₂)₂O(CH₂)₂NH (*m*₂), AgCl; Ag from 0 to 50° (in v)

<i>m</i> ₁	<i>m</i> ₂	0°	5°	10°	15°	20°	25°	30°	35°	40°	45°	50°
0.10082	0.04334	0.77859	0.77881	0.77878	0.77859	0.77818	0.77752	0.77686	0.77588	0.77482	0.77360	0.77218
0.09024	0.07330	0.79542	0.79593	0.79621	0.79635	0.79627	0.79599	0.79555	0.79497	0.79420	0.79332	0.79224
0.08599	0.04446	0.78541	...	0.78403	0.78308	0.78200	0.78062
0.07955	0.03420	0.78279	0.78309	0.78318	0.78303	0.78271	0.78218	0.78156	0.78068	0.77974	0.77857	0.77727
0.07858	0.03860	0.78622	0.78657	0.78669	0.78663	0.78637	0.78590	0.78533	0.78442	0.78353	0.78240	0.78114
0.07271	0.03760	0.78876	...	0.78750	0.78661	0.78555	0.78432
0.06962	0.05655	0.80000	0.80068	0.80105	0.80127	0.80130	0.80102	0.80081
0.06542	0.03213	0.78943	0.78990	0.79007	0.79011	0.78995	0.78956	0.78904	0.78825	0.78736	0.78635	0.78508
0.05966	0.02565	0.78800	0.78842	0.78852	0.78855	0.78829	0.78787	0.78736	0.78654	0.78554	0.78444	0.78319
0.05513	0.02851	0.79441	...	0.79323	0.79251	0.79145	0.79035
0.05066	0.02488	0.79424	0.79479	0.79509	0.79523	0.79515	0.79484	0.79437	0.79368	0.79290	0.79178	0.79057
0.04989	0.04053	0.80628	0.80715	0.80772	0.80806	0.80821	0.80814	0.80798	0.80757	0.80704	0.80632	0.80544
0.03965	0.017047	0.79581	0.79637	0.79674	0.79687	0.79683	0.79656	0.79623	0.79562	0.79489	0.79397	0.79290
0.03475	0.017968	0.80409	...	0.80341	0.80284	0.80204	0.80111
0.02905	0.014267	0.80511	0.80585	0.80626	0.80655	0.80667	0.80658	0.80639	0.80585	0.80529	0.80450	0.80359
0.02068	0.008890	0.80875	0.80954	0.81014	0.81052	0.81069	0.81070	0.81047	0.81012	0.80958	0.80887	0.80808
0.017231	0.008910	0.81940	...	0.81911	0.81873	0.81822	0.81752
0.014732	0.007236	0.81861	0.81962	0.82031	0.82091	0.82129	0.82141	0.82147	0.82114	0.82077	0.82026	0.81961
0.009693	0.007873	0.83949	0.84087	0.84202	0.84295	0.84369	0.84418	0.84460	0.84475	0.84477	0.84459	0.84426

Table II: Values of p*K*_a from 0 to 50°

<i>t</i> , °C	p <i>K</i> _a (exptl)	p <i>K</i> _a (calcd) ^a
0	9.108	9.108
5	8.978	8.977
10	8.850	8.851
15	8.727	8.728
20	8.608	8.608
25	8.492	8.492
30	8.380	8.379
35	8.268	8.269
40	8.161	8.161
45	8.056	8.057
50	7.955	7.955

$$^a \text{p}K_a = 1663.29/T + 4.1724 - 0.0042239T.$$

Table III

	p <i>K</i> _a	Δ <i>H</i> ^o , joules mole ⁻¹	Δ <i>S</i> ^o , joules deg ⁻¹ mole ⁻¹	Δ <i>C</i> _p ^o , joules deg ⁻¹ mole ⁻¹
Morpholinium	8.492	39,030	-31.7	48
Piperidinium	11.123	53,390	-33.9	88
Pyrrolidinium	11.305	54,470	-33.7	68

there are marked differences both in p*K*_a and in the enthalpy change. Thus, not only is there a large difference (2.813) in p*K*_a between morpholinium ion and

pyrrolidinium ion at 25° but the difference changes with temperature in a manner consistent with the differences in the other thermodynamic quantities. The p*K*_a values of morpholinium ion decrease with increased temperature less rapidly than do those of pyrrolidinium ion. Thus the difference in p*K*_a is only 2.601 at 50°.

While mixtures of morpholine and morpholinium hydrochloride are not proposed as pH standards, they may have some uses in biochemical work when a medium of controlled pH is needed. We have, therefore, interpolated in Table I to obtain values of p(*a*_Hγ_{Cl}) (≡ -log *a*_H+γ_{Cl}-) and have derived the corre-

Table IV: Values of p(*a*_Hγ_{Cl}) and p*a*_H for a Buffer Solution Composed of Morpholine Hydrochloride (0.1 *m*) and Morpholine (0.05 *m*) from 0 to 50°

<i>t</i> , °C	p(<i>a</i> _H γ _{Cl})	p <i>a</i> _H
0	9.068	8.963
5	8.934	8.828
10	8.809	8.702
15	8.687	8.579
20	8.567	8.458
25	8.453	8.343
30	8.341	8.231
35	8.231	8.120
40	8.125	8.013
45	8.021	7.908
50	7.921	7.806

sponding values of p_{a_H} ($\equiv -\log a_{H^+}$) by application of the Bates-Guggenheim¹¹ convention

$$-\log \gamma_{Cl} = Am^{1/2}/(1 + 1.5m^{1/2})$$

The values obtained for the p_{a_H} of one buffer mixture from 0 to 50° are given in Table IV.

(11) R. G. Bates and E. A. Guggenheim, *Pure Appl. Chem.*, **1**, 163 (1960).

The γ Radiolysis of Liquid 2-Propanol. II.^{1a} The Reaction of Solvated Electrons with Mono- and Disubstituted Benzenes

by Warren V. Sherman^{1b}

Soreq Nuclear Research Centre, Yavne, Israel (Received March 1, 1966)

The effect of a number of mono- and disubstituted benzenes on the gaseous products of the radiolysis of solutions of nitrous oxide in 2-propanol has been studied. The substituted benzenes decrease the nitrogen yield, and this is interpreted as being due to competition with nitrous oxide for solvated electrons. From the measurements of $G(N_2)$ the relative reactivities of the substituted benzenes have been calculated. The site of attack of the solvated electron appears to be the aromatic ring since the substituent effects correlate well with those found generally in aromatic bimolecular nucleophilic substitution. In addition, satisfactory correlation is observed between reactivity and the Hammett σ_{para} functions. The ρ value for the monosubstituted benzenes is 3.1. The ρ value remains approximately constant for a given series of disubstituted benzenes in which one substituent is kept unchanged. However, the σ values for disubstituted benzenes are not additive.

Introduction

Solvated electrons are produced in the radiolysis of aliphatic alcohols.² A knowledge of the subsequent reactions of this species is necessary for the complete understanding of the radiation chemistry of alcohols and alcoholic solutions. It has been shown^{1a} that the molecular nitrogen produced in the radiolysis of dilute solutions of nitrous oxide in 2-propanol is a convenient measure of the solvated electrons which are amenable to solute scavenging. Utilizing this technique, the measurement of the relative rate constants of a number of mono- and disubstituted benzenes are reported.

Experimental Section

Materials. 2-Propanol was purified as described previously.^{1a} The mono- and disubstituted benzenes

were of reagent grade and used without further purification.

Procedure. The preparation and irradiation of the samples, and the analysis of gaseous products were as described previously.^{1a} The mean dose rate during the course of the present series of experiments was 3.7×10^{17} ev ml⁻¹ min⁻¹. All solutions were irradiated for 15 min.

(1) (a) Part I: W. V. Sherman, *J. Phys. Chem.*, **70**, 667 (1966). A preliminary communication of some of the results reported here appears in W. V. Sherman, *J. Am. Chem. Soc.*, **88**, 1567 (1966). (b) The Radiation Laboratory, University of Notre Dame, Notre Dame, Ind.

(2) M. C. Sauer, S. Arai, and L. M. Dorfman, *J. Chem. Phys.*, **42**, 708 (1965), and references therein.

Table I: γ Radiolysis of 2-Propanol Solutions of Nitrous Oxide and a Substituted Benzene

	Substituted benzene, mM	Nitrous oxide, mM	$G(H_2)$	$G(CH_4)$	$G(N_2)$	k_{N_2O}	
	None	5.0	3.37 ^a	1.36 ^a	1.70 ^a	...	
	None	10	3.25 ^a	1.36 ^a	2.06 ^a	...	
	None	50	3.18 ^a	1.36 ^a	2.70 ^a	...	
1	Phenol	50C	5.0	3.52	1.10	0.83	0.010
2	Toluene	50C	5.0	2.11	1.06	0.70	0.014
3	Benzene	0.021 ^e
4	Fluorobenzene	10C	10	2.86	1.05	1.37	0.050
5	Chlorobenzene	5C	50	2.78	1.30	1.76	0.54
6	Bromobenzene	5C	50	2.46	1.16	1.32	1.0
7	Iodobenzene	5C	50	2.12	1.38	1.09	1.5
8	Benzaldehyde	5C	50	2.78	1.37	1.09	1.5
9	Benzoic acid	5C	50	2.68	1.29	1.37	0.97
10	Benzophenone	50	50	2.12	1.47	1.17	1.3
11	Acetophenone	5C	50	2.63	1.41	1.00	1.7
12	Benzonitrile	5C	50	2.48	1.27	0.93	1.9
13	Nitrobenzene	2.3 ^a
14	<i>p</i> -Chlorophenol	5C	50	2.78	1.38	1.98	0.36
15	<i>p</i> -Bromophenol	5C	50	3.03	0.61	1.41	0.92
16	<i>p</i> -Hydroxybenzoic acid	5C	50	3.05	0.64	1.66	0.63
17	<i>p</i> -Hydroxyacetophenone	50	50	2.81	0.90	1.56	0.73
18	<i>p</i> -Hydroxybenzotrile	50	50	2.80	0.66	1.14	1.4
19	<i>p</i> -Hydroxynitrobenzene	5C	50	2.82	0.43	0.93	1.9
20	<i>p</i> -Chlorotoluene	5C	50	2.42	1.50	1.82	0.48
21	<i>p</i> -Dichlorobenzene	5C	50	2.50	1.21	1.15	1.3
22	<i>p</i> -Bromochlorobenzene	50	50	2.43	1.29	1.02	1.6
23	<i>p</i> -Chloriodobenzene	50	50	2.58	1.49	0.77	2.5
24	<i>p</i> -Chlorobenzoic acid	50	50	2.25	1.25	1.13	1.4
25	<i>p</i> -Chlorobenzotrile	50	50	2.62	1.39	0.92	1.9
26	<i>p</i> -Chloronitrobenzene	50	50	2.56	1.23	0.79	2.4
27	<i>m</i> -Dinitrobenzene	50	50	2.43	1.09	0.68	3.0

^a Taken from ref 1a.

Results and Discussion

The yields of gaseous products from the radiolysis of solutions of 2-propanol containing nitrous oxide and a substituted benzene are listed in Table I. In all cases hydrogen, nitrogen, and methane were the sole products volatile at liquid-air temperature. Qualitatively, all the aromatic compounds studied decreased the hydrogen and nitrogen yields below those observed from 2-propanol solutions containing nitrous oxide alone. The yield of methane appears to be relatively insensitive to the addition of the aromatic compounds except those containing the hydroxy group where a distinct decrease in $G(CH_4)$ may be observed.

The decrease in $G(N_2)$ observed in the presence of the substituted benzenes may be taken to indicate competition with nitrous oxide for the solvated electron.^{1a} The reactivities of the substituted benzenes relative to nitrous oxide, k_{N_2O} , may be calculated from expression A^{1a} and are listed in the last column of Table I.

$$k_{N_2O} = \frac{\Delta G(N_2)}{G(N_2)} \frac{(N_2O)}{(ArX)} \quad (A)$$

The solvated electron is a strongly nucleophilic species. Its reactions with aromatic compounds may be expected to conform to the general pattern of bimolecular nucleophilic substitution, S_N2 , if the insertion of the solvated electron into the aromatic ring is the rate-determining step of the electron-capture process I.



The modified Hammett equation, $\log k_{C_6H_6} = \rho^- \sigma^-$, where $k_{C_6H_6}$ is the rate of the substituted benzene relative to benzene, has been used to correlate the substituent effect in the reactions of a number of nucleophilic species (e.g., CH_3O^- , N_3^- , SCN^-) with substituted benzenes.^{3,4} In Figure 1 the logarithm of the

(3) P. R. Wells, *Chem. Rev.*, **63**, 191 (1963).(4) J. Miller, A. J. Parker, and B. A. Bolto, *J. Am. Chem. Soc.*, **79**, 93 (1957).

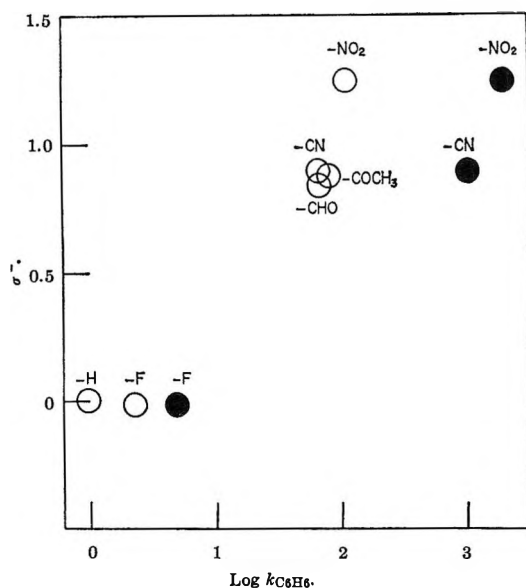


Figure 1. Plot of σ^- functions^{3,4} for nucleophilic substitution vs. $\log k_{\text{C}_6\text{H}_6}$ values for the electron in 2-propanol (O) and water⁵ (●).

rate constants relative to that of benzene for several monosubstituted benzenes is plotted against the substituent constants, σ^- , for $\text{S}_\text{N}2$ reactions on the ring. A "best straight line" does not pass through the point for benzene, and this may indicate that there is a contribution to the observed reactivity from the direct interaction between the solvated electron and the substituent. The ρ^- value (ca. 2) corresponding to the slope of "best straight line" is somewhat lower than those observed with other nucleophiles (3.1 to 9.2).⁴ This low sensitivity to substituent effects probably reflects the high intrinsic reactivity of the solvated electron toward aromatic substrates. In their study of the reactivity of substituted benzenes toward hydrated electrons, Anbar and Hart⁵ noted that the correlation between reaction rates and σ^- values was less than satisfactory in three cases where the reactivity of the aromatic compound toward nucleophilic substitution is known. The data on the hydrated electron are included in Figure 1 for comparison with the present data.

In Figure 2 the values of $\log k_{\text{C}_6\text{H}_6}$ for the monosubstituted benzenes are plotted against the corresponding rate constants for the reaction of the hydrated electron with monosubstituted benzenes.⁵ A good linear correlation may be noted. The slope differs from unity, and it may be concluded that the reactions of the solvated electron in 2-propanol are less sensitive to substituent effects than the equivalent reactions of the solvated electron in water.

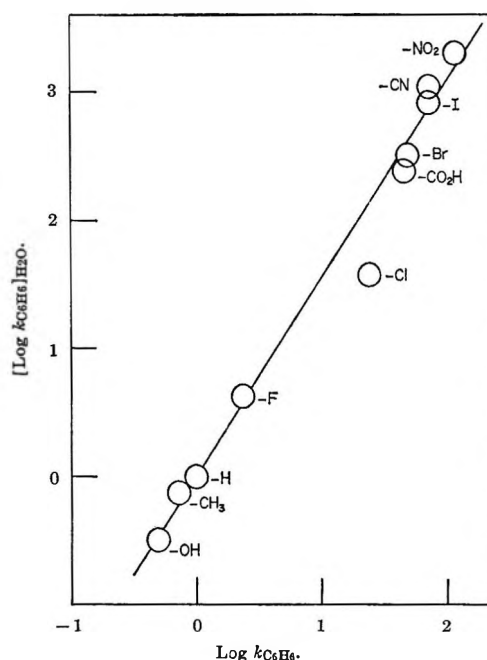


Figure 2. Plot of $\log k_{\text{C}_6\text{H}_6}$ values for the electron in 2-propanol vs. corresponding results of Anbar and Hart⁵ for the hydrated electron.

In a plot of $\log k_{\text{C}_6\text{H}_6}$ values for the monosubstituted benzenes against mean Hammett σ_{para} values (Figure 3), there is considerable scatter about a best straight line. This scatter may also be noted in the study of the hydrated electron.⁵ However, if the spread of all calculated σ values⁶ is taken into account, the $\log k_{\text{C}_6\text{H}_6}$ values, with the exception of chloro-, bromo- and iodobenzene, conform to a straight-line plot. The ρ value is 3.1 and may be compared with $\rho = 4.8$ obtained by Anbar and Hart for the reactions of the hydrated electron.⁵ The relatively large deviation of bromobenzene and iodobenzene from the best straight line was also noted in the study of the hydrated electron. An explanation put forward in this case was that there may be a direct interaction between the hydrated electron and the substituent which would contribute toward an increased reaction rate. Another rationalization may be suggested. The gas phase electron affinity of the chlorine, bromine, and iodine atoms⁷ exceeds the dissociation energy of the corresponding carbon-halide bond.⁸ If (1) is in fact an equilibrium,

(5) M. Anbar and E. J. Hart, *J. Am. Chem. Soc.*, **86**, 5633 (1964).

(6) σ_{para} values are taken from the review of H. Van Bekkum, P. E. Verkade, and B. M. Wepster, *Rec. Trav. Chim.*, **78**, 815 (1959).

(7) F. H. Field and J. L. Franklin, "Electron Impact Phenomena," Academic Press Inc., New York, N. Y., 1957, p 149.

(8) T. L. Cottrell, "The Strengths of Chemical Bonds," Butterworth and Co. Ltd., London, 1954, pp 211, 213, 277.

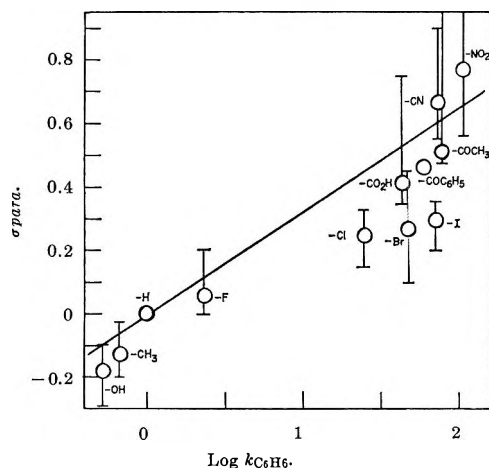


Figure 3. Plot of Hammett σ_{para} functions vs. $\log k_{C_6H_6}$ values for the electron in 2-propanol. The mean values for the σ_{para} functions are taken from the review of Van Bekkum, *et al.*,⁶ The vertical lines encompass the spread of values for these functions.

then dissociation of the carbon-halide bond may occur before the back reaction and enhance the observed rate of the electron-capture process.

A similarly satisfactory correlation between reactivity and σ values may be observed in the case of the disubstituted benzenes. The ρ values for the chlorobenzene and phenol series are 0.86 and 3.6, respectively (see Figure 4). However, as was the case in the monosubstituted benzene series, the chloro and bromo derivatives are somewhat anomalous and show a reactivity which is greater than would be expected of aromatic compounds containing substituents with these σ values. In the application of the Hammett equation to aromatic substitution, the effect of a second substituent is generally additive as long as there is no additional resonance interaction between the second substituent and the reactive center.³ In the reactions of the solvated electron in 2-propanol, this additivity rule does not hold. It appears that a series containing

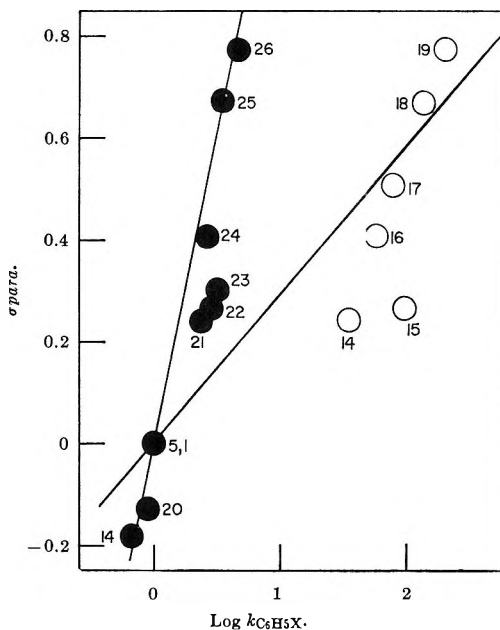


Figure 4. Plot of Hammett σ_{para} functions⁶ vs. $\log k_{C_6H_5X}$ values for monosubstituted chlorobenzenes (●) and phenols (○). $k_{C_6H_5X}$ is the reactivity relative to the parent chlorobenzene or phenol.

a substituent which activates the ring toward the solvated electron (*e.g.*, the chlorobenzenes) has a lower ρ value than the monosubstituted series. In the case of the nitrobenzenes, where the nitro group strongly activates the ring, the rate constant is almost insensitive to the second substituent. In a series where the substituent deactivates the ring, (*e.g.*, the phenols) the rate constant is more sensitive to the second substituent and an enhanced ρ is observed. These observations parallel those made by Anbar and Hart on the reactivity of the hydrated electron.⁵

Acknowledgments. This work was carried out during the tenure of an Israel Atomic Energy Commission Fellowship. The author wishes to thank Dr. Arie Rajbenbach for many helpful discussions.

Temperature Dependence of Electrolytic Conductance: Tetrabutylammonium Fluoroborate in Phenylacetonitrile^{1,2}

by Ernesto J. del Rosario³ and John E. Lind, Jr.

Department of Chemistry, Cornell University, Ithaca, New York (Received March 4, 1966)

The electrolytic conductance of dilute solutions of tetrabutylammonium fluoroborate in phenylacetonitrile has been measured between 25 and 175°, and the theory of Fuoss and Onsager has been used to correlate the data. The variations of the physical constants, characterizing the solutions for the sphere-in-continuum model, largely compensate for one another so that the data present more of a test of the model than of the theoretical approximation of the model. The model appears adequate, although the association constant goes through a slight maximum rather than rising continuously with the inverse of the product of dielectric constant and temperature.

Recently, Fuoss and Onsager⁴ reexamined their theory for ionic conductance in dilute solutions and have obtained a more exact solution for the model of spheres in a continuum. They have shown the adequacy of the theory primarily by applying it to systems where the electrical properties and the viscosity of the solvent were varied by using mixed solvents at 25°. Data are presented here to show the adequacy of the theory and the model when the electrical properties and viscosity are changed by changing the temperature of a pure solvent. The measurements were made on tetrabutylammonium fluoroborate in phenylacetonitrile over the range 25–175°.

This system is especially useful for showing whether there are inadequacies in the model rather than in the mathematical approximation of the model. The fractional change of the equivalent conductance with concentration is predicted by the model to be about the same at all temperatures for this system if Walden's rule applies. This means that all discrepancies caused by mathematical approximations should contribute proportionally the same at all temperatures and not cause changes in the values of the arbitrary parameters needed to fit the equation to the data.

The reasons for these statements are as follows. Since the thermal motion is always attempting to destroy the effects of the electrical forces, the electrostatic energy always appears divided by the thermal energy, and thus the dielectric constant is always

multiplied by the temperature raised to the same power. Because the dielectric constant decreases with increasing temperature, their product for phenylacetonitrile is decreased by only 8% while the temperature changes 50%. So far as the electrostatic theory for the sphere-in-continuum model is concerned, little change is noticed in the association of the ions during this large change of the temperature. The relaxation-type terms in the equation for the equivalent conductance depend only upon the reciprocal of this product of temperature and dielectric constant and upon the limiting equivalent conductance at infinite dilution. Thus these terms are just scaled by the limiting conductance or by the inverse of the viscosity if the Walden product is constant. The electrophoretic-type terms not only depend on the inverse of the product of dielectric constant and temperature but also upon the reciprocal of the viscosity. The result is that the whole equation is just scaled by either the limiting conductance or the reciprocal of the viscosity. Now if there are effects such as significant van der

(1) This study was aided by a grant from the Office of Saline Water, U. S. Department of the Interior.

(2) This paper is based on a thesis presented by E. J. del Rosario to the Graduate School of Cornell University in partial fulfillment of the requirements for the M.S. degree, Jan 1966.

(3) Ford Foundation Scholarship, University of the Philippines-Cornell University Graduate Education Program.

(4) R. M. Fuoss, L. Onsager, and J. F. Skinner, *J. Phys. Chem.*, **69**, 2581 (1965).

Waals forces between ions or between ions and solvent molecules, these should cause marked changes in the parameters of the equation since these forces are not directly related to the dielectric constant and the viscosity.

Experimental Section

Tetra-*n*-butylammonium fluoroborate was prepared by titrating a methanolic solution of tetrabutylammonium hydroxide with an aqueous solution of fluoroboric acid. The salt was recrystallized three times from 1:1 methanol-water mixtures and dried at 70° under vacuum to constant weight. The melting point was 161°. Fluorine analyses yielded 22.99 and 22.86% compared to the theoretical 23.08%.

The phenylacetonitrile was dried over molecular sieves and carefully fractionated. The specific conductance was less than 0.3×10^{-7} mho/cm and the refractive index was n_D^{25} 1.5208. The dielectric constants of the solvent were measured on a General Radio 716-C Schering bridge equipped with a 716-P4 guard circuit. To reduce the effects of the higher solvent conductances at high temperature, measurements were made at 263 kHz and checked at 100 kHz. The capacitance cell consisted of an inner high potential electrode $1\frac{1}{8}$ in. in diameter and $5\frac{9}{16}$ in. long which was suspended in a deep cup leaving an annulus of $\frac{3}{16}$ in. The cup was the grounded electrode and the top inch of it was a guard ring. All metal parts were of stainless steel and the insulation was Supramica. The capacitance cell was calibrated at 25° with nitrobenzene and ethylene dichloride whose dielectric constants are 34.82 and 10.36, respectively.⁵ The nitrobenzene was purified by the method⁶ used previously, yielding a specific conductance of less than 7×10^{-9} mho/cm. The Eastman Spectrograde ethylene dichloride was redistilled and had a specific conductance of much less than 2×10^{-9} mho/cm. The cell constant was 0.04213 which was independent of temperature within the precision of the measurements. The results in Table I agree with the approximate value of Grimm and Patrick^{5,7} and are about 1–2% above those of Walden.⁸

The viscosities were measured under argon in Ubbelohde viscometers. The densities were measured in a Sprengle-type pycnometer on which the two arms were interconnected and the whole pycnometer was completely submerged in the thermostat. The small vapor space required a maximum correction for the vapor volume of 0.03% at 200°.

The conductance bridge, the method of calibration, and the technique for the conductance measurements were similar to those used by one of the authors pre-

Table I: Dielectric Constant of Solvent

Temp. °C	Dielectric constant
24.9	18.77
58.9	16.57
78.6	15.46
99.0	14.45
117.7	13.53
138.9	12.69
162.8	11.86
185.4	11.14
201.4	10.72

viously.⁶ The cells used were two erlenmeyer cells whose cell constants were 0.15591 ± 0.00002 and 2.0714 ± 0.0003 cm⁻¹. Both cells were calibrated directly with KCl. A small cell with a volume of about 20 ml was also used for the high-temperature runs and the cell constant was 2.8278 ± 0.0003 . The temperatures were measured by a platinum resistance thermometer and the variation was no greater than $\pm 0.03^\circ$ at the highest temperature. All runs were performed with the solutions under an atmosphere of argon. The runs at 25 and 100° were performed by diluting the solutions in the erlenmeyer cell. The run at 75° was made in the same cell by diluting the solution successively in a flask at room temperature and then transferring a portion of the solution by a syringe to the cell. This could be done easily because the vapor pressure of the solvent at room temperature was so low that there was no significant amount of solvent lost through evaporation. This technique had to be used for the runs at 150 and 175° since decomposition was noticeable and thus a single sample could not be diluted for measurement at five different compositions. The small cell was used for these two high-temperature runs and the vapor space at equilibrium was only about 1 ml, so that no correction for the amount of solvent in the vapor space was needed. The decomposition at 150° caused a resistance change of 0.1% in 30 min and at 175° the change was 1% in the same period. For these two runs the resistance was measured only at 10 kHz since the runs at lower temperature indicated that the value extrapolated to infinite frequency differed by only about 0.01%.

(5) A. A. Maryott and E. R. Smith, "Tables of Dielectric Constants of Pure Liquids," National Bureau of Standards Circular 514, U. S. Government Printing Office, Washington, D. C., 1951.

(6) J. E. Lind, Jr., and R. M. Fuoss, *J. Phys. Chem.*, **65**, 999 (1961).

(7) F. V. Grimm and W. A. Patrick, *J. Am. Chem. Soc.*, **45**, 2794 (1923).

(8) P. Walden, *Z. Physik. Chem.*, **70**, 569 (1910).

The resistance at 10 kHz was then extrapolated back to zero time, ignoring the initial period when the temperature had not reached equilibrium. A run was made at 200° but discarded because resistances changed of the order of 10% in 0.5 hr.

The physical constants are summarized in Table II and the conductance measurements in Table III. The values of the dielectric constant in Table II are interpolated from Table I.

Table II: Solvent Properties

Temp, °C	Dielectric constant	Density, g/ml	Viscosity, poise	Specific conductance, 10 ⁷ mho/cm
25.00	18.77	1.0125	0.01971	0.13
75.00	15.66	0.9719	0.00949	0.60
100.00	14.38	0.9506	0.00716	0.51
150.00	12.31	0.9079	0.00473	0.84
175.00	11.45	0.8866	0.00396	0.75
200.00	10.67	0.8637	0.00334	2.0

Table III: Conductance of Tetrabutylammonium Fluoroborate in Phenylacetonitrile

10°C	Λ	ΔΛ	10°C	Λ	ΔΛ
<i>t</i> = 25.00°			<i>t</i> = 75.00°		
31.004	21.882	-0.008	18.664	48.137	-0.006
24.720	22.664	0.011	14.873	49.697	0.008
18.432	23.635	0.002	11.072	51.628	0.002
12.450	24.858	-0.012	7.401	54.045	-0.010
6.290	26.711	0.004	3.976	57.197	0.004
<i>t</i> = 100.00°			<i>t</i> = 150.00°		
28.929	57.284	0.001	17.726	90.06	0.00
23.194	59.427	-0.011	13.886	93.74	-0.04
17.393	62.218	0.027	10.304	98.03	0.05
11.695	65.772	-0.021	6.898	103.00	-0.04
5.876	71.120	0.006	4.502	107.59	0.01
<i>t</i> = 175.00°					
16.037	105.84	-0.00			
9.642	114.46	0.02			
6.479	120.19	-0.02			
4.095	125.78	0.01			

Discussion

Fuoss and Onsager obtain eq 1 when they retained the Boltzmann factor in the exponential form during the integration of the equation of continuity

$$\Lambda = \Lambda_0 - Sc^{1/2} + E'c \ln \tau^2 + Lc - A\Lambda_0cf^2 \quad (1)$$

All terms depend upon the adjustable parameter Λ_0 and the last two also depend upon the ion-size

parameter, which represents the distance of closest approach of cation and anion. The A term has the form of the Bjerrum approximation to the association constant. Fuoss, Onsager, and Skinner have shown that this equation is applicable where "association" is very low. For systems where association is high and especially for association arising in part from forces not accounted in the model such as van der Waals forces, the law of mass action can be introduced by replacing the last term by the analogous expression given by the law of mass action. The conductance equation becomes

$$\Lambda = \Lambda_0 - S(c\gamma)^{1/2} + E'(c\gamma) \ln \tau^2\gamma + Lc\gamma - K_A\Lambda c\gamma f^2 \quad (2)$$

where the association constant, K_A , becomes the third independent parameter.

To either equation an additional term was proposed to account for termination of power series arising out of lower order effects. This B term is $[\tau^3(2b - 3)\Lambda_0/b^2]$ and is subtracted from the right-hand side of the equation. It is of the three-halves power of the concentration and depends upon only the same arbitrary parameters, Λ_0 and a , upon which the L term depends. In Table IV are tabulated the parameters and the terms required to fit the data with eq 2 both with and without the B term. The precision of three of the five sets of data is increased appreciably by the addition of the B term, while the other two are not affected. At the same time, the association constants K_A increase 60% but do not change significantly their dependence upon temperature and dielectric constant of the solvent. The values of the ion-size parameter, a_L , arise from the L term and the B term, and they become larger and more reasonable when the B term is used. The values a_L both with and without the additional term decrease at high temperature. It is important to remember that the L term and the B term vary the most rapidly of any terms with concentration. Thus they are small terms which are most sensitive to the final fit and will gather into the parameter a_L all the inadequacies of the theory and the model. Because the Walden product is nearly constant, the coefficients of the conductance equation with the B terms are scaled by the limiting conductance and are given in Table V. As predicted, the scaled values vary slowly with temperature. The one exception is the L term at high temperature which drops to half its low-temperature value. This result is reflected in the slight decrease of K_A at high temperatures. To account for this variation, consider the electrostatic model modified with a "solvation" energy⁹ (shown in eq. 3)

Table IV: Constants in the Conductance Equation

$t, ^\circ\text{C}$	σ	Λ_0	L	K_A	a_L	a_K
Without B Term						
25.00 ± 0.01	0.01	31.16 ± 0.05	202 ± 34	94 ± 7	4.1 ± 0.1	5.5 ± 0.2
75.00 ± 0.02	0.01	65.20 ± 0.04	711 ± 63	145 ± 4	4.56 ± 0.09	5.00 ± 0.05
100.00 ± 0.02	0.03	83.8 ± 0.1	283 ± 68	117 ± 5	3.95 ± 0.07	5.6 ± 0.1
150.00 ± 0.03	0.05	125.0 ± 0.3	-645 ± 327	119 ± 13	3.4 ± 0.2	5.9 ± 0.3
175.00 ± 0.03	0.02	145.3 ± 0.1	-985 ± 171	114 ± 6	3.40 ± 0.08	6.2 ± 0.1
With B Term						
25.00 ± 0.01	0.002	31.444 ± 0.007	1256 ± 6	175.7 ± 0.9	7.75 ± 0.02	4.486 ± 0.007
75.00 ± 0.02	0.002	65.44 ± 0.01	2758 ± 17	207 ± 1	7.86 ± 0.03	4.510 ± 0.006
100.00 ± 0.02	0.04	84.7 ± 0.2	3463 ± 157	214 ± 11	7.6 ± 0.2	4.60 ± 0.06
150.00 ± 0.03	0.06	125.5 ± 0.3	2912 ± 413	178 ± 15	5.7 ± 0.3	5.1 ± 0.1
175.00 ± 0.03	0.007	145.72 ± 0.04	3017 ± 57	167 ± 2	5.48 ± 0.03	5.38 ± 0.02

$$K_A = \frac{4\pi N a_K^3}{3000} \exp(e^2/aDkT - E_s/kT) \quad (3)$$

where the first term in the exponential is the coulomb energy and E_s is the remainder of the energy difference between the free ions and the ion pair. As can be seen in Figure 1, where the two lines represent eq 3 with E_s of zero and a_K of 5.5 and 7.5 Å, no single value of a_K will fit the equation to the data. The several values needed to fit the data are given in Table IV. A single value of E_s other than zero does not represent the data. In fact, for these two values of a_K , E_s has values favoring ion pair formation which go through a maximum of 400-800 cal/mole, respectively, and decrease to a few hundred at higher temperatures. Such an effect could be caused by van der Waals forces. These forces might decrease with temperature because the motion of the chains of the cation increases with temperature resulting in fewer of the atoms of the chains interacting with the anion. The accuracy of the data and the questions arising in the definition of an ion pair, which primarily affect the preexponential term in eq 3, do not warrant a more careful analysis of the association constants.

Table V: Scaled Constants for the Conductance Eq 2 with the B Term

$t, ^\circ\text{C}$	S/Λ_0	E'/Λ_0	L_1/Λ_0^2	L/Λ_0	Λ_{07}
25	3.736	14.51	49.43	39.95	0.620
75	3.836	15.81	53.76	42.2	0.621
100	3.943	16.56	56.33	40.8	0.607
150	4.107	18.12	61.62	23.2	0.594
175	4.227	18.93	64.42	20.7	0.577

^a L_1 is the part of L which is independent of the parameter a .

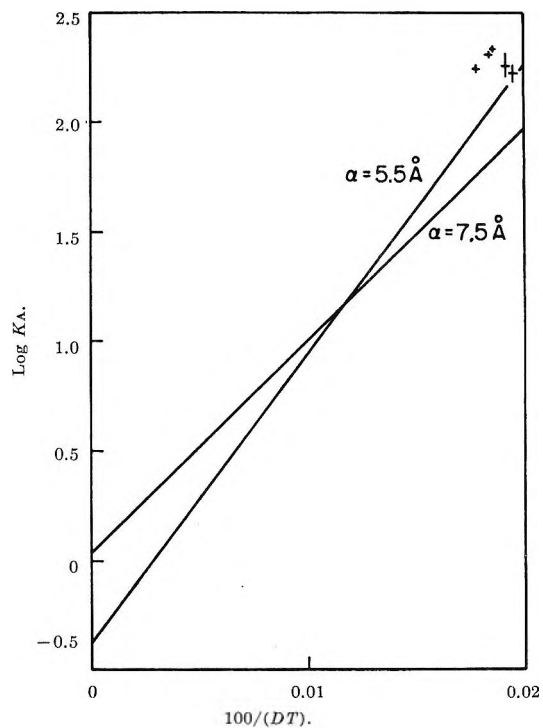


Figure 1. Comparison of the experimental values of the association constant with eq 3 for $E_s = 0$.

In conclusion, the model of spheres in a continuum of dielectric fluid seems to account well for the electrolytic conductance. However, further investigation should pursue the finer detail of the small deviations of the association constants in such systems where any limitations of the theory are minimized and the inadequacies of the model are more readily seen.

(9) H. Sadek, E. Hirsch, and R. M. Fuoss, "Electrolytes," Pergamon Press Ltd., Oxford, 1962, p 134.

Multipulse Potentiodynamic Studies of the Competitive Adsorption of Neutral Organic Molecules and Anions on Platinum Electrodes. I. Competitive Adsorption of Carbon Monoxide and Chloride Ions¹

by S. Gilman

General Electric Research & Development Center, Schenectady, New York (Received March 7, 1966)

In the absence of Cl^- and in the potential range -0.1 to 0.6 v, the structure of the adlayer, the maximum coverage, and the experimental rate of adsorption (initially diffusion controlled) remain constant for the adsorption of CO from 1 *N* HClO_4 solution. In the presence of any extent of initial surface coverage with Cl^- in this potential range, the characteristics of the CO adsorption remain unchanged. Therefore, the system tends toward full coverage with CO and very small residual coverage with Cl^- . For any transient coverage with CO, there is an equilibrium coverage with Cl^- which is rapidly (probably transport limited) established by either desorption or adsorption of the ions. There is a simple linear relationship between equilibrium coverage with Cl^- and transient coverage with CO. It is possible to explain the inhibitive effect of dissolved chloride ions on the "polarization curve" on the basis of the findings of the competitive adsorption studies.

Introduction

It has long been recognized that the adsorption of anions can have profound effects on the adsorption and reaction of neutral molecules.²⁻⁴ Quantitative determinations of mixed surface coverages would seem a necessary prerequisite toward the understanding of such effects. Such determinations appear to be lacking, although there have been considerable studies of individual adsorbates.²

Since (on platinum) adsorbed organic and anionic species have distinctly different voltammetric properties, it is possible to devise a multipulse potentiodynamic (MPP) sequence which permits quantitative study of competitive adsorption. For the first study, CO and Cl^- were chosen because of availability of considerable previous information for these adsorbates.⁵⁻¹¹

Experimental Section

The glassware, electronic equipment, etc. have been described previously.⁶ The electrolyte was 1 *N* perchloric acid, prepared from the AR grade acid and quartz-distilled water. The hydrochloric acid was AR grade. Gas mixtures of CO and argon were pre-

pared, bottled, and analyzed by the Matheson Co., using CP grade CO and "prepurified" grade argon. The working electrode was a length of CP grade platinum wire which was annealed in a hydrogen flame and sealed in a soft-glass tube so that a geometric area of 0.071 cm^2 was exposed to the electrolyte. The "saturation hydrogen coverage," sQ_H , measured using a linear cathodic sweep⁵ was 0.29 mcoulomb/

(1) This paper was presented at the spring meeting of the Electrochemical Society, Cleveland, Ohio, May 1-6, 1966.

(2) (a) A. N. Frumkin in "Modern Aspects of Electrochemistry," Vol. 3, J. O'M. Bockris and B. E. Conway, Ed., Butterworth Inc., Washington, D. C., 1964, Chapter 3; (b) P. Delahay, "Double Layer and Electrode Kinetics," Interscience Publishers, Inc., New York, N. Y., 1965.

(3) M. W. Breiter, *Electrochim. Acta*, **9**, 827 (1964).

(4) B. I. Podlovchenko and Z. A. Iofa, *Zh. Fiz. Khim.*, **38**, 211 (1964).

(5) S. Gilman, *J. Phys. Chem.*, **66**, 2657 (1962).

(6) S. Gilman, *ibid.*, **67**, 78 (1963).

(7) S. Gilman, *ibid.*, **68**, 2098 (1964).

(8) S. Gilman, *ibid.*, **68**, 2112 (1964).

(9) T. B. Warner and S. Schuldiner, *J. Electrochem. Soc.*, **111**, 992 (1964).

(10) R. A. Munson, *J. Electroanal. Chem.*, **5**, 292 (1963).

(11) S. B. Brummer and J. I. Ford, *J. Phys. Chem.*, **69**, 1355 (1965).

cm². This implies a surface roughness factor (RF) of 1.4 based on RF = 1 for $sQ_H = 0.21$ mcoulomb/cm². All experimental quantities are reported on the basis of the *geometric area* unless otherwise noted. Measurements were made at $30 \pm 0.1^\circ$. All potentials are reported against a reversible hydrogen electrode immersed in the adsorbate-free solution.

Procedures and Results

I. CO Adsorption in the Absence of Chloride Ions. The adsorption on smooth platinum of CO has been studied recently by several investigators.^{5,6,9-11} Generally, the adsorption studies have been confined to a rather narrow range of potentials. For the purpose of this study, it was necessary to gather additional information on the effect of potential and partial pressure on the rate of adsorption and on the final surface coverage.

Procedure. The sequence of Figure 1 was used in making these measurements. The electrode was normally held at a potential of 0.4 v. Step A was introduced to eliminate possible adsorbed anionic impurities. During step B adsorbed CO is oxidized to CO₂ and desorbed. At the same time, a passive oxygen film is deposited on the surface, preventing readsorption of CO. In step C, the passive film is retained, allowing (in the absence of significant reaction at the surface) equilibration of the solution adjacent to the electrode with the bulk of the solution. For $U > 0.6$ v, step D was introduced ($T_D = 10$ msec) for pre-reduction of the surface. After reduction of the surface either during step D or (for $U < 0.6$ v) during the first few milliseconds of step E, the adsorption was allowed to proceed for time duration, T_E . For $U < 0.2$ v, step F ($T_F = 10$ msec) was introduced to decrease the hydrogen-oxidation current during subsequent sweep G. The total duration of steps D, F, and G was always sufficiently brief so that appreciable adsorption occurs only during step E. Traces corresponding to particular values of U and T_E appear in Figure 1. Values of Q_{CO} (charge corresponding to quantitative oxidation of CO to CO₂) may be obtained from such traces by subtracting the area under the trace for the clean surface from that of the CO-covered surface.⁵

Results. For 0.1 atm partial pressure of CO, values of Q_{CO} were obtained for several values of adsorption time and potential. The results appear in Table I. For each adsorption time, the braces indicate a range of potentials over which Q_{CO} is constant with the indicated per cent average deviation. Measurement ($U = 0.4$ v and $T_E = 100$ sec) at 0.01–1.0 atm partial pressure of CO, gave the constant value of 0.38 mcoulomb/cm² for Q_{CO} .

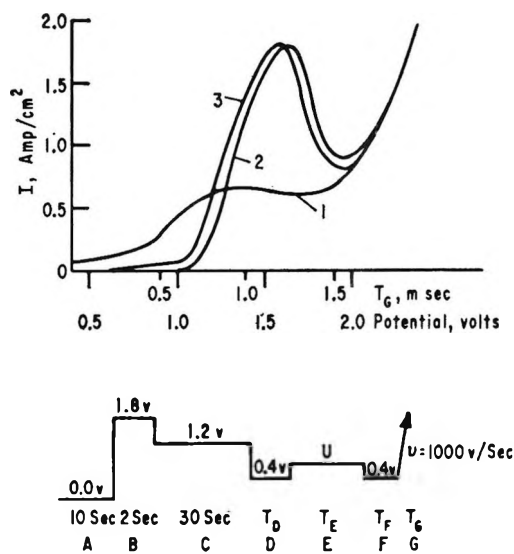


Figure 1. Linear anodic sweep traces corresponding to the adsorption of CO in the absence of Cl⁻. The solution was 1 N HClO₄ saturated with a gas mixture of 10% CO and 90% argon (30°) and was paddle stirred (360 rpm). Step E is the adsorption step. Steps D and F are surface reduction and hydrogen removal steps, respectively. Trace 1 (clean surface): $U = 0.4$ v; $T_E = 10$ msec; $T_D = T_F = 0$. Trace 2: $U = -0.1$ to 0.7 v; $T_E = 10$ sec; $T_D = 0$ for $U \leq 0.6$ v; $T_D = 10$ msec for $U = 0.7$ v; $T_F = 0$ for $U > 0.3$ v; $T_F = 10$ msec for $U \leq 0.2$ v. Trace 3: $U = -0.2$ v; $T_E = 10$ sec; $T_D = 0$; $T_F = 10$ msec.

For 0.1 atm partial pressure and $T_E = 10$ sec, traces corresponding to values of U from -0.1 to 0.7 v may be superimposed (trace 2 of Figure 1), while the trace corresponding to -0.2 v is shifted to less anodic potentials (trace 3, Figure 1). For 0.1 atm partial pressure and $T_E = 100$ sec, the traces from $U = 0.4$ –0.8 v are identical; however, for potentials lower than 0.0 v, the trace for the CO-covered surface does not merge with that of the clean surface but is otherwise identical with the traces obtained at higher potentials.

II. Mixed Adsorption of CO and Cl⁻ Starting with Initial CO Coverage of Zero. Procedure. A solution of 1 N perchloric acid, containing 10⁻⁴ M HCl and with a partial pressure of 0.01 atm of CO, was employed. The pulse sequence used appears in Figure 2. The electrode was normally held at 0.4 v. Step A causes desorption of Cl⁻ but not of CO, which adsorbs at even lower potentials (Table I). In step B, only 2% of a monolayer of Cl⁻ is adsorbed,⁷ all previously adsorbed CO is oxidized to CO₂ and desorbed, and a passive oxygen film forms, preventing further adsorption of Cl⁻ or of CO. In step C, the passive film is retained while the solution adjacent to the surface is equilibrated with the bulk (including elimination of the products CO₂, Cl₂, and O₂, from step B). In step D, the passive

Table I: CO Adsorption in the Absence of Cl⁻

$T_E = 1 \text{ sec}$		$T_E = 10 \text{ sec}$		$T_E = 100 \text{ sec}$	
$U, \text{ v}$	$Q_{\text{CO}}, \text{ mcoulomb/cm}^2$	$U, \text{ v}$	$Q_{\text{CO}}, \text{ mcoulomb/cm}^2$	$U, \text{ v}$	$Q_{\text{CO}}, \text{ mcoulomb/cm}^2$
-0.20	0.234	-0.20	0.354	0.4	0.378
-0.1	0.286	-0.10	0.331	0.7	0.378
0.0	0.301	0.00	0.375	0.8	0.369
0.4	0.284	0.40	0.340	} 1% av	
0.6	0.268	0.70	0.338	} dev	
0.7	0.179	0.80	0.182		
0.8	0.111				

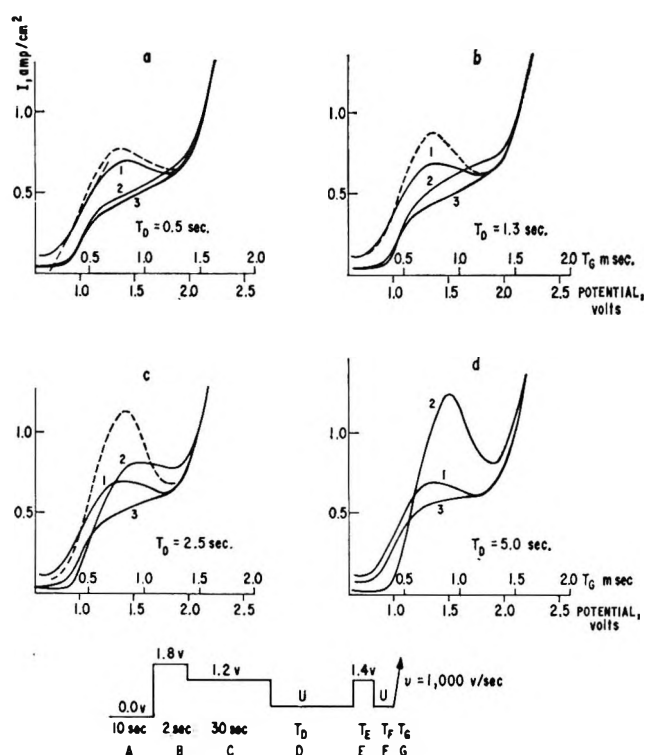


Figure 2. Linear anodic sweep traces corresponding to mixed adsorption of CO and Cl⁻ at $U = 0.6 \text{ v}$. The solution was 1 N HClO_4 containing 10^{-4} M HCl and saturated with a gas mixture of 1% CO and 99% argon (30°, paddle stirred at 360 rpm). Step D is the adsorption step. Steps E and F are used to eliminate adsorbed CO for separate determination of Cl⁻ coverage. Trace 1 (clean surface, measured in absence of CO and Cl⁻): $T_E = T_F = 0$. Trace 2 (surface covered with both CO and Cl⁻ from step D): $T_E = T_F = 0$. Trace 3 (surface covered with only Cl⁻ from step D): $T_E = 2 \text{ msec}$; $T_F = 8 \text{ msec}$; the dashed traces correspond to CO adsorbed in the absence of Cl⁻ under conditions approximating those for trace 2.

film is largely reduced within the first few milliseconds, allowing adsorption to commence. In the absence of the adsorbates, when $T_E = T_F = 0$, the trace obtained upon applying sweep G (traces 1 of Figure 2) is that

for the clean surface. In the presence of the adsorbates the adlayer contains both CO and Cl⁻ after adsorption for time interval, T_D . Hence, when $T_E = T_F = 0$, the application of sweep G results in traces (those marked 2 in Figure 2) which are characteristic of the mixed adsorption. If step E is introduced ($T_E = 2 \text{ msec}$), the CO portion of the mixed adlayer is desorbed, the Cl⁻ is retained,⁸ and (after reduction of the surface for $T_F = 8 \text{ msec}$) the trace obtained (traces 3 of Figure 2) after application of sweep G is characteristic of the Cl⁻ portion of the mixed adlayer obtained after adsorption time, T_D . It should be noted that the total duration of steps E, F, and G is sufficiently brief so that adsorption during these steps is negligible. The dashed traces correspond to CO adsorbed in the absence of Cl⁻ and were included for comparison with traces 2.

Results. The extent of surface coverage with CO and Cl⁻ may be derived from traces such as those of Figure 2 as follows. Using Figure 2a as an example, all charge lying to the left of the dashed tangent to trace 1 is disregarded (assumed largely capacitive). The charge ΔQ_{1-3} is obtained by subtracting the area under trace 3 from the area under trace 1. The charges ΔQ_{2-1} and ΔQ_{2-3} are obtained in similar fashion. The charge ΔQ_{1-3} is equivalent to ΔQ_0 , which in turn is the charge equivalent of "oxygen adsorption" blocked by Cl⁻ adsorption⁷

$$\Delta Q_{1-3} = \Delta Q_0 \quad (1)$$

Since 1 equiv of Cl⁻ blocks 2 equiv of oxygen

$$\Delta Q_0 = 2F\Gamma_{\text{Cl}^-} \quad (2)$$

where Γ_{Cl^-} is the absolute surface coverage with Cl⁻ in moles per square centimeter. The charge ΔQ_{2-1} comprises ΔQ_0 and also Q_{CO} (charge equivalent of quantitative oxidation of adsorbed CO to CO₂, ref 5). Hence

$$\Delta Q_{2-1} = Q_{\text{CO}} - \Delta Q_0 \quad (3)$$

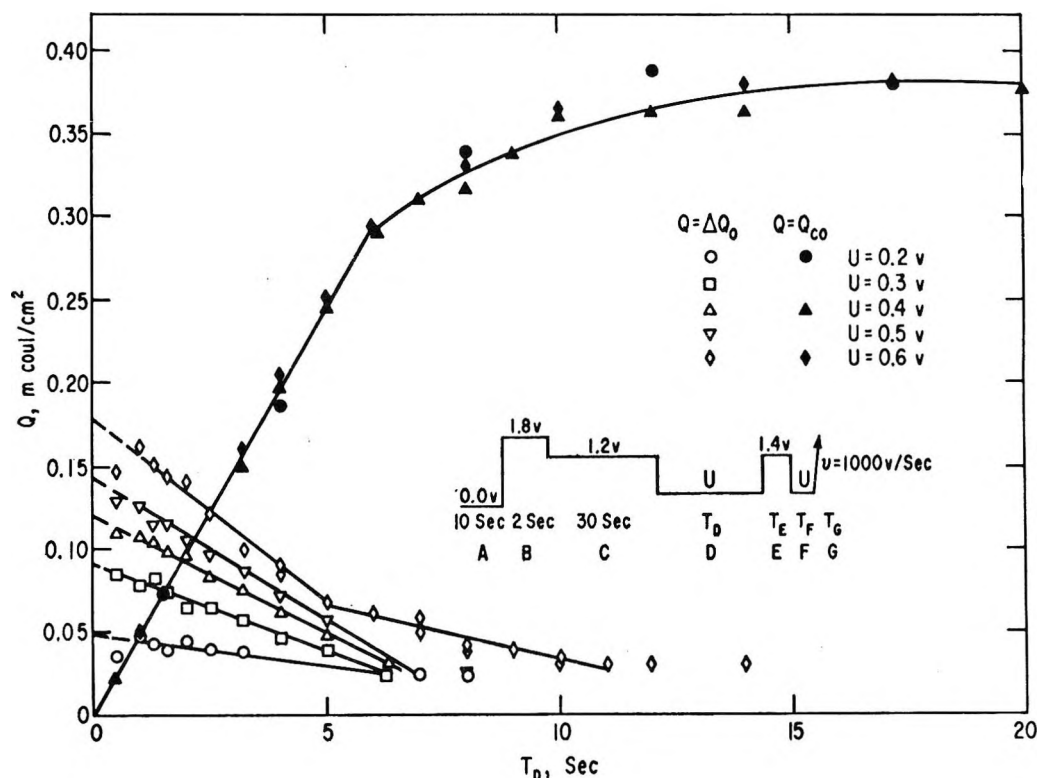


Figure 3. Mixed adsorption of CO and Cl⁻. T_D is the adsorption time for both CO and Cl⁻ from 1 N HClO₄ containing 10⁻⁴ M HCl and saturated with a gas mixture of 1% CO and 99% argon (30°, paddle stirred at 360 rpm). ΔQ_O is related to absolute and relative coverages with Cl⁻ by eq 2 and 7, respectively. Q_{CO} is related to absolute and relative coverages with CO by eq 4 and 6, respectively. ΔQ_O and Q_{CO} were evaluated from traces similar to those of Figure 2.

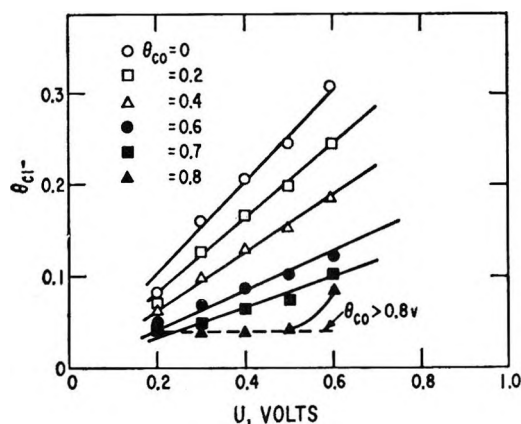


Figure 4. The dependence of Cl⁻ surface coverage on potential for different constant CO surface coverages (derived from data of Figure 3).

also

$$Q_{CO} = 2F\Gamma_{CO} \tag{4}$$

where Γ_{CO} is the absolute surface coverage with CO. Combining eq 1 and 3

$$\Delta Q_{2-3} = Q_{CO} \tag{5}$$

Hence absolute surface coverages may be derived from the charges ΔQ₁₋₃ and ΔQ₂₋₃ using eq 1, 2, 4, and 5.

Results. Values of Q_{CO} and ΔQ_O were obtained for values of U from 0.2 to 0.6 v and as a function of adsorption time, T_D. These values are plotted in Figure 3. A second representation of the data appears in Figure 4, in terms of fractional surface coverages. These are defined as

$$\theta_{CO} = \frac{Q_{CO}}{(Q_{CO})_{max}} \tag{6}$$

where (Q_{CO})_{max} = 0.38 mcoulomb/cm² and

$$\theta_{Cl-} = \frac{\Delta Q_O}{2sQ_H} \tag{7}$$

where sQ_H = 0.29 mcoulomb/cm². These definitions of fractional surface coverage are somewhat arbitrary but may be converted to absolute coverage by means of eq 2 and 4. In particular, θ_{Cl-} is based on the assumption that one adsorbed chloride ion formally occupies one hydrogen adsorption site.

III. Mixed Adsorption of CO and Cl⁻ Starting with Initial CO Coverage Greater Than Zero. In section II,

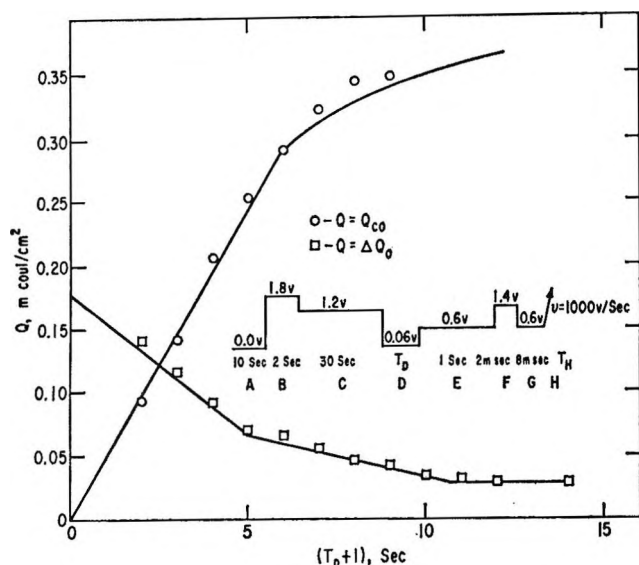


Figure 5. Sequential mixed adsorption of CO and Cl^- . The 1 N HClO_4 contained 10^{-4} M HCl , was saturated with a gas mixture of 1% CO and 99% argon (30°) and was paddle stirred (360 rpm). Adsorption of CO occurs during both steps D and E for $T_D + 1$ sec. Adsorption of Cl^- occurs only during step E (for 1 sec). Q_{CO} is related to absolute and relative coverages with CO by eq 4 and 6, respectively. ΔQ_O is related to absolute and relative coverages with Cl^- by eq 2 and 7, respectively. ΔQ_O and Q_{CO} were evaluated from traces similar to those of Figure 2.

above, adsorption was conducted at potential U so that CO and Cl^- could adsorb *simultaneously*. In the experiments described below, CO was first adsorbed at a potential (0.06 v) at which only CO could adsorb. After achieving a desired CO coverage, the potential was then raised to 0.6 v, at which potential both CO and Cl^- could adsorb.

Procedure. The pulse sequence used appears in Figure 5. Steps A-C of the sequence are identical with those employed in section II above. In step D, CO only was adsorbed for time interval T_D . In step E, further adsorption of CO could occur at 0.6 v, along with adsorption of Cl^- . The rest of the sequence served to obtain ΔQ_O and Q_{CO} , as described in the previous section.

Results. Values of charge are plotted against the total time ($T_D + 1$) allowed for CO adsorption in Figure 5. The solid curves passing through the data points are identical with those measured in the previous section, for adsorption at 0.6 v.

IV. The "Polarization Curve" for CO. The linear anodic sweep (1st) traces of Figures 1 and 2 correspond to CO adsorbed *before* the application of the rapid sweep. There is thus no appreciable "turnover" (additional adsorption and reaction) during the sweep. For exami-

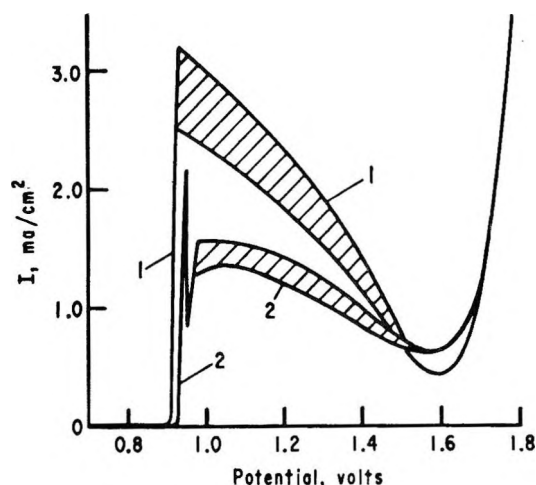


Figure 6. Anodic "polarization curves" for CO. The traces were recorded during the positive-going portion of a periodic triangular sweep (sweep speed, $v = 0.04\text{ v/sec}$) operating between 0.4 and 1.8 v. Trace 1 was obtained in the absence and trace 2 in the presence of 10^{-4} M HCl . The 1 N HClO_4 electrolyte was saturated with pure CO (30°) and was paddle stirred (360 rpm). The hatched areas correspond to regions of oscillation of the current.

nation of the qualitative effects of Cl^- adsorption on steady-state anode performance, a slow periodic triangular sweep was applied alternatively in the presence and absence of dissolved Cl^- . The results appear in Figure 6.

Discussion

I. Adsorption of CO in the Absence of Cl^- . Structure of the Adsorbed Layer. Previous studies of the CO adlayer at 0.4 v⁶ suggested that the adsorbed layer retained the *composition* of the adsorbate in the gas phase. The results were also consistent with the conclusion that the adlayer comprised CO bonded to the surface in both bridged and linear configurations. The last traces measured for $-0.1\text{ v} \leq U \leq 0.7\text{ v}$ after 10-sec adsorption time (trace 2, Figure 1) are identical. This suggests that the adlayer formed over this range is constant in composition and structure. On the other hand, the trace obtained at -0.2 v is noticeably shifted to the left on the potential axis (trace 3, Figure 1). At medium potentials (*e.g.*, 0.4 v, ref 6), such shifts sometimes correspond to decreasing coverage for an adsorbed phase of constant composition.¹² However, since the oxidative charge corresponding to trace 3 is almost identical with that for trace 2, the observed potential shift is not simply a surface coverage effect but must likely represent a change in composition or

(12) S. Gilman, *J. Phys. Chem.*, **67**, 1898 (1963); **68**, 70 (1964).

structure of the adlayer (*e.g.*, partial reduction at highly cathodic potentials).

It is the opposing rate of oxidation of CO (to CO₂) which prevents buildup of CO surface coverage at potentials much above 0.7 v. If, for the conditions of Figure 1, the adsorption time is increased to 100 sec, it is possible to compare the last traces for as high as 0.8 v. It is then found that the traces for potentials between 0.1 and 0.8 v are identical. The traces for lower potentials are similar, but the traces for the clean surface (trace 1 of Figure 1) and that for the CO-covered surface no longer merge in the high-potential region. This effect may again be due to the final buildup of some small quantity of refractory reduction product or may be due to the accumulation of a small amount of an (cationic) impurity.

The over-all results suggest that the structure of the adlayer remains constant over a range of potentials extending from -0.1 to 0.8 v.

Rate of Adsorption of CO. It has already been shown⁶ that, at 0.4 v, the adsorption of CO from a quiescent or paddle-stirred solution is transport controlled until almost full coverage is achieved. The constancy of Q_{CO} after 1.0 sec of adsorption over a range of -0.1-0.6 v (Table I) suggests that the adsorption is transport controlled over this entire range.

At 0.0 and -0.1 v, the solution adjacent to the electrode is saturated with H₂ (perhaps supersaturated at the lower potential). Hence, the observation of transport-controlled CO adsorption at these potentials implies a relatively slow rate of displacement of dissolved CO by dissolved H₂ (in a region extending from the surface through the diffusion layer and into the bulk of the solution). The lower rate of CO adsorption at -0.2 v might, on the other hand, be due to an appreciable rate of displacement of CO in the solution phase, by very vigorously evolved H₂, rather than to slow adsorption kinetics.

The lower values of Q_{CO} for $U = 0.7$ and 0.8 v are likely due to the oxidation of some CO to CO₂. For the 10- and 100-sec points of Table I, it may be seen that even $U = 0.7$ and 0.8 v fall within the region of constancy. This is because the adsorption is no longer transport controlled in the higher range of coverage⁵ and there is sufficient transport of CO to the surface to allow both further adsorption and oxidation of CO.

Maximum Surface Coverage with CO. After the region of transport-controlled adsorption (approximately 85% of full coverage for a quiescent solution with 1 atm partial pressure of CO, ref 5; approximately 75% of full coverage for a stirred solution with 0.01 atm partial pressure of CO, Figure 3), the adsorption

becomes activation controlled and changes gradually with time. After 100 sec, approximately the same maximum charge was obtained for 0.01 and 0.1 atm partial pressure of CO. This charge, $(Q_{CO})_{max}$, has the value 0.38 mcoulomb/cm² (geometric area). We may obtain the charge per unit of "hydrogen area" by dividing by the "roughness factor." Hence, $(Q_{CO})_{max}/RF = 0.28$ mcoulomb/cm² ("hydrogen area"). As previously pointed out⁶ "full coverage" is not meant to imply that all (hydrogen) sites are occupied. In fact, hydrogen-codeposition experiments suggest that 10-20% of the hydrogen sites are still vacant. (Hydrogen-codeposition experiments are not sensitive at very high coverages with CO. Determinations suggest 20% of the hydrogen sites remain vacant, but a value of only 10% would be in better agreement with the apparent ratio of bridged to linear CO.⁶) It is also possible even higher coverages would very slowly result if the adsorption were continued over much longer periods of time. Without considerable improvements in the level of solution purity such measurements would be suspect.⁶

Validity of CO-Coverage Determinations. There are some working assumptions implicit in MPP determinations of surface coverage^{5,6} as is generally the case with quantitative voltammetric measurements of other types. The validity of the final results for this particular system, however, is best supported by the good quantitative agreement between adsorption rates and diffusion theory which applies until full coverage is almost complete.⁶ Although this paper relies mainly on the low-coverage data, it seems justifiable to make comparison with the full-coverage values of others, in view of current interest.

Munson¹⁰ measured medium- to low-current galvanostatic transients (after adsorption at 0.40) for 0.1 *N* perchloric acid saturated with CO at 25°. After graphically eliminating mass-transport contributions to the measured transition times, Munson obtained a coverage with CO approximately 30% higher than corresponding adsorption of hydrogen. This is equivalent to $(Q_{CO})_{max}/RF = 0.27$, which is in good agreement with the value 0.28 mcoulomb/cm² ("hydrogen area") offered here. Warner and Schuldiner⁹ report values (sulfuric acid), which are over 50% higher than those reported here. Brummer and Ford¹¹ have already suggested that these values are in error owing to faulty evaluation of the transition time. Brummer and Ford¹¹ have offered (1 *N* HClO₄, 40°, 0.3 v) the value of 0.365 mcoulomb/cm² (32% higher than reported here) for Q_{CO}/RF and have suggested that the value offered in a previous paper⁵ and here is in error owing to improper correction for "oxygen

adsorption." Although several rather arbitrary corrections were made by Brummer and Ford in arriving at their final value, the main issue is whether they have made a proper correction for "oxygen adsorption" using their particular cathodic reduction scheme. Vetter and Berndt,¹³ Laitinen and Enke,¹⁴ and Feldberg, Enke, and Bricker¹⁵ have all concluded that balance could not be attained between the charges passed in oxidizing and reducing the surface. Gilman¹⁶ showed that charge balance (within 10%) could be attained by reducing the surface at 0.4 v. However, the reduction followed an exponential decay law so that from 200 msec (for small oxygen coverage) to 10 sec (for large coverage) was required to achieve charge balance. Brummer and Ford's¹¹ typical reduction was made in only *ca.* 3 msec, making it likely that the surface was only partially reduced. This would have led to undercorrection for "oxygen" and values of Q_{CO} which are too high.

II. *Proof of the Thermodynamic Dependence of Chloride Ion Surface Coverage on the Instantaneous Coverage of the Surface with Carbon Monoxide.* The data of Figure 3 correspond to the following experimental situation. (1) Adsorption (step D) occurs when passive film is reduced. (2) The concentration of dissolved chloride ion is approximately 10 times higher than that of dissolved CO and the rate of transport of the two species to the surface is in approximately the same ratio. (3) The initial value of θ_{CO} is zero. (4) The initial value of chloride coverage is very low ($\theta_{Cl^-} = 0.04$).

The experimental results appearing in Figure 3 may be summarized as follows. (1) The adsorption of CO follows the same law over the entire range of potentials studied (activation controlled at high coverage; transport controlled at lower coverage) in the presence of adsorbed chloride ion. This law is identical with that observed in the absence of Cl^- . (2) Within 1 sec (the approximate time required for transport control), the adsorption of Cl^- reaches a maximum value close to the equilibrium value measured in the absence of CO.⁸ The Cl^- coverage then decreases linearly as CO coverage increases. Extrapolation of the linear θ_{Cl^-} -time plots back to zero adsorption time yields intercepts which agree (within a few per cent) with the equilibrium values measured on this electrode in the absence of CO. Agreement with equilibrium values previously determined on another electrode⁸ is within 8%.

The results suggest that the *experimental* rate of CO adsorption is unaffected by the presence of adsorbed Cl^- . Since this rate is transport controlled (through most of the range of coverage), this does not preclude

the possibility that the large *kinetic* rate is affected. The adsorption of CO goes to the usual state of completion, causing the gradual desorption of chloride ions. There are two possible explanations for the observed *experimental* rate of desorption of Cl^- . (1) The desorption may be an activated process, and the rate of Cl^- desorption may reflect *kinetics* of desorption. (2) There may be an *equilibrium* value of Cl^- surface coverage (with kinetics of adsorption and desorption both rapid, compared with mass transport) corresponding to each value of CO surface coverage. The apparent rate of desorption of Cl^- may reflect only an *indirect* dependence on the rate of CO adsorption. The experimental results presented in Figure 5 establish that possibility 2 is the correct interpretation.

The data of Figure 5 correspond to the following experimental conditions. (1) Adsorption of CO is allowed to proceed for time T_D at 0.06 v. Because of the low potential, θ_{Cl^-} remains zero.⁷ (2) The potential is then raised to 0.6 v for 1.0 sec. During this time both CO and Cl^- may adsorb. In Figure 5, values of ΔQ_0 and Q_{CO} are plotted against CO adsorption time ($T_D + 1$). For each point, the total adsorption time for Cl^- is, however, only 1.0 sec. The results are in good agreement with those obtained when the adsorption is conducted entirely at 0.6 v (Figure 3). When we recall that all of the values of ΔQ_0 for Figure 5 are arrived at by *adsorption* of Cl^- in just 1.0 sec and that all of the corresponding values in Figure 3 are obtained by gradual *desorption* of Cl^- , this constitutes proof that the measured Cl^- coverages bear a *thermodynamic* relationship to the CO coverages.

III. *Quantitative Dependence of Cl^- Coverage on CO Coverage, Electrode Potential, and Concentration of Dissolved Cl^- .* In the last section, we established that Cl^- adsorption-desorption is a reversible process with the equilibrium Cl^- coverage dependent on the instantaneous CO surface coverage. Previous results⁸ show that Cl^- adsorption is also reversibly dependent on the potential. The thermodynamic data are presented in a convenient form in Figure 4. We see that for any value of $\theta_{CO} \leq 0.6$, the Cl^- coverage decreases linearly with decrease in potential. For $\theta_{CO} = 0.7$, the Cl^- coverage decreases linearly with decreasing potential at first but does not drop below $\theta_{Cl^-} = 0.04$, which seems to be the minimum attainable (by displacement with CO) Cl^- coverage. Hence, for

(13) K. J. Vetter and D. Berndt, *Z. Elektrochem.*, **62**, 378 (1958).

(14) H. A. Laitinen and C. G. Enke, *J. Electrochem. Soc.*, **107**, 773 (1960).

(15) S. W. Feldberg, C. G. Enke, and C. E. Bricker, *ibid.*, **110**, 826 (1963).

(16) S. Gilman, *Electrochim. Acta*, **9**, 1025 (1964).

$\theta_{\text{Cl}^-} > 0.04$ and $\theta_{\text{CO}} < 0.8$, the θ_{Cl^-} vs. θ_{CO} plots are linear and extrapolate back to the origin. In this linear range the results may be represented by

$$\theta_{\text{Cl}^-}/U = S \quad (8)$$

where S is constant for any fixed value of θ_{CO} and has the value 0.50 for $\theta_{\text{CO}} = 0$. A plot of S vs. θ_{CO} yields a straight line with the slope 0.49. Hence at $[\text{Cl}^-] = 10^{-4} M$

$$\theta_{\text{Cl}^-}/U = 0.50 - 0.49\theta_{\text{CO}} \quad (9)$$

In the absence of CO, the dependence of Cl^- surface coverage on concentration of dissolved Cl^- may be expressed as⁸

$$\theta_{\text{Cl}^-}/U = 0.77 + 0.069 \ln [\text{Cl}^-]_0 \quad (10)$$

where $[\text{Cl}^-]_0$ is the concentration of dissolved Cl^- near the surface. Assuming that the same concentration dependence holds in the presence of CO, we may combine eq 9 and 10

$$\theta_{\text{Cl}^-}/U = 0.77 + 0.069 \ln [\text{Cl}^-]_0 - 0.049\theta_{\text{CO}} \quad (11)$$

for $\theta_{\text{Cl}^-} > 0.04$, $\theta_{\text{CO}} < 0.8$. Equation 11 describes the empirical behavior of the system over most of the range of conditions encountered.

Referring to eq 11, we may now summarize the behavior of the system. In the presence of excess CO, θ_{CO} will eventually become 1.0, with the adsorption transport controlled until high coverage is achieved. As CO adsorbs, Cl^- will rapidly adsorb or desorb to yield the equilibrium values of θ_{Cl^-} predicted by eq 11. Equation 11 will fail to hold once θ_{Cl^-} approaches 0.04 or θ_{CO} exceeds 0.8.

In the absence of CO (eq 10) the results resemble those previously found for other systems. A linear dependence of coverage (in the higher range of coverages) on potential was found for the adsorption on mercury of a number of anions, including Cl^- (calculations made by Parsons on the experimental work of Grahame,¹⁷) and for the adsorption of I^- on platinum.¹⁸ Dependence of surface coverage on the logarithm of activity of the ion in solution has been found for I^- adsorption on mercury.¹⁹

We may now consider the origin of the dependence of Cl^- surface coverage upon CO surface coverage, as given by eq 11. It is clear that CO does not simply "crowd out" Cl^- since the combined coverage with both adsorbates is always less than a monolayer. The coverage with specifically adsorbed anions may be expected to depend on the heat of adsorption of the ion (in the absence of a field)¹⁷ and on the charge stored in the ionic double layer.²⁰ We might expect variations in the heat of adsorption of the anion (in the presence

of CO) to affect the y intercept, rather than the slope of the θ_{Cl^-} vs. potential plot. Since the slope is affected, an explanation based on the charge is preferred. The adsorption of a neutral molecule drives down the double-layer capacity^{2b} and hence the charge stored in the double-layer at fixed potential. Thus the linear dependence of θ_{Cl^-} upon θ_{CO} (at fixed potential) may reflect a linear dependence of charge upon CO coverage and a linear dependence of Cl^- coverage upon the charge.

IV. *The Effect of Chloride Ion Adsorption on the Electrochemical Oxidation of CO.* A proper quantitative treatment of the effect of adsorbed chloride ions on CO oxidation kinetics would require considerable information of the type previously¹² presented for the Cl^- -free system. Such a treatment will be postponed to some future date. However, the information presently at hand makes possible a qualitative discussion of the topic and, particularly, of the CO "polarization curve."

The dashed traces of Figure 2 correspond to the oxidation of adsorbed CO and of the platinum surface, in the absence of adsorbed chloride ions. The characteristics (shape, position) of the trace are determined by a variety of factors (sweep speed, coverage, etc.). However, the general tendency of the initial rise in current to shift to more anodic potentials with increase in surface coverage (or adsorption time) is probably a manifestation of the second-order kinetics law followed for the oxidation of adsorbed CO.¹² The traces marked 2 in Figure 2 correspond to oxidation of CO and of the surface, in the presence of adsorbed chloride ions. For any fixed coverage with CO (or fixed adsorption time), the adsorbed Cl^- results in increased overvoltage for the oxidation of the adsorbed CO, corresponding to the shift from the dashed trace to trace 2. This corresponds approximately to the shift for the surface oxidation trace measured in the absence of Cl^- (trace 1) to more anodic potentials when Cl^- is adsorbed (trace 3). Under these particular experimental conditions, a plot of the potential shift vs. θ_{Cl^-} was found to be linear with a slope of 0.75. The potential shift represents an additional overvoltage due to ion adsorption; hence, the current corresponding to the oxidation of adsorbed CO may be represented by

$$I = I_i \exp(-m\theta_{\text{Cl}^-})$$

where I and I_i are the currents measured for CO oxidation in the presence and absence, respectively, of

(17) N. F. Mott and R. J. Watts-Tobin, *Electrochim. Acta*, **4**, 79 (1961).

(18) K. Schwabe and W. Schwenke, *ibid.*, **9**, 1003 (1964).

(19) D. C. Grahame, *J. Am. Chem. Soc.*, **80**, 4201 (1958).

(20) R. Parsons, *Trans. Faraday Soc.*, **51**, 1518 (1955).

adsorbed chloride, but under otherwise identical conditions. The term $m\theta_{\text{Cl}^-}$ represents the increased overvoltage due to the ion adsorption and m may vary with the conditions of the experiment (but was found to have the value 0.75 for the experiments of Figure 2, as mentioned above). The ion may exert the type of effect given by eq 12 through a "double-layer" effect.²

Current-voltage curves obtained at low sweep speed for stirred, CO-saturated solutions appear in Figure 6. The general characteristics of the "polarization curve" for the Cl^- -free system (trace 1, Figure 6) have been discussed previously.^{5,12} During the anodic portion of trace 1, the current remains negligibly small until the potential rises above 0.9 v. At 0.92 v, there is an abrupt increase in current to a value corresponding to the CO-transport limit and then a gradual decrease in anodic current until the onset of appreciable oxygen evolution (1.6 v). The decreasing current accompanies buildup of surface "oxygen." The effect of addition of Cl^- (trace 2, Figure 6) is to shift the initial vertical rise in current to 0.95 v (30-mv shift) and then to decrease the current (up to 40%) over the range extending from 0.95 to 1.6 v. From section III, above, we know that the surface is covered with CO to the same extent (approximately a monolayer) below 0.9 v, both in the presence and absence of Cl^- . In the presence of dissolved Cl^- , there is additionally 4% of a chloride ion monolayer on the surface. This small Cl^- coverage decreases the reactivity of the *previously adsorbed* CO (according to eq 12) and causes the small (30-mv) shift in potential. It is to be emphasized that the shift is small because of the tendency for CO to drive the

anion off the surface. Conversely, the more pronounced effect of the specifically adsorbed ion on the kinetics of oxidation of methanol³ and of ethanol and acetaldehyde⁴ may correspond to a decreased tendency for the anion to be desorbed by the organic adsorbate.

After the initial surge in current, $\theta_{\text{CO}} = 0$ for both traces of Figure 6. Hence, the decreasing current of trace 1 does not reflect a decrease in reactivity of the adlayer but possibly the rate of some "surface activation" step (essentially the rate of adsorption at $\theta_{\text{CO}} = 0$, ref 12). For trace 2, once the coverage with CO drops to zero (at 0.95 v), the coverage with Cl^- may rise close to its maximum value of $\theta_{\text{Cl}^-} = 0.5$.³ The first sharp drop in current corresponds to approximately the time required for Cl^- transport from solution. This relatively high coverage with Cl^- simply produces an effect similar to that produced by increased coverage with "oxygen." Toward 1.6 v, where the combined coverage with Cl^- and "oxygen" probably approaches a monolayer for both systems, traces 1 and 2 of Figure 6 tend to merge.

Acknowledgment. The author wishes to acknowledge helpful discussions with M. W. Breiter and F. Will. This work is a part of the program under Contracts DA-44-039-AMC-479(T) and DA-44-009-ENG-4909, ARPA Order No. 247, with the U. S. Army Engineer Research & Development Laboratories, Ft. Belvoir, Va., to develop a technology which will facilitate the design and fabrication of practical military fuel cell power plants for operation on ambient air and hydrocarbon fuels.

The Interaction of Acridine Orange and Proflavine with Polyadenylic Acid¹

by Gordon G. Hammes and Colin D. Hubbard

Department of Chemistry, Cornell University, Ithaca, New York 14850 (Received March 7, 1966)

A kinetic study of the reactions between acridine orange and polyadenylic acid and between proflavine and polyadenylic acid has been made with the temperature-jump method at pH 7.5 where the polynucleotide is single stranded. In both systems a discrete relaxation time, which is independent of both reactant concentrations, can be discerned from the observed relaxation spectrum. This single relaxation process which is characteristic of an intramolecular process subsequent to polymer-dye complex formation, is probably a consequence of "stacking" of dye molecules along the polymer chain. Base-dye interactions appear to retard the rate of the "stacking" process markedly and conformational changes may be rate determining in the "stacking" interaction.

Introduction

The relaxation effect which occurs in temperature-jump experiments with poly- α -L-glutamic acid (PGA) and acridine orange, 2,8-dimethyldiaminoacridine (AO), solutions at pH 4.7 and at pH 7.5 can be quantitatively described by two relaxation times, τ_1 and τ_2 .² A study of the dependence of τ_1 and τ_2 on polyglutamic acid and acridine orange concentrations yielded data which could not be quantitatively reconciled with any of several possible mechanisms of interaction between the dye and the polymer. However, the processes occurring are intramolecular and can be identified either with the aggregation or "stacking" of the dye upon the polymer chain or to solvent and counterion substitution by the dye subsequent to a very rapid initial interaction. Unfortunately, the data did not permit a sharp distinction between these possibilities to be made. The forward and reverse rate constants for the AO monomer-dimer reaction were also measured, and if "stacking" is directly involved in the rate-controlling steps of the AO-PGA interaction, this phenomenon occurs considerably more slowly than in free solution.

In the present study, the interaction of acridine orange and its diamine analog proflavine (2,8-diaminoacridine, PR) with the synthetic polynucleotide polyadenylic acid (poly A) has been investigated by the temperature-jump method and by absorption spectroscopy at pH 7.5 where the poly A is single stranded and both dyes are protonated. For both dyes the observed relaxation effect is a complex spectrum of

relaxation processes which virtually encompasses the whole time range of the temperature-jump apparatus used (approximately 2×10^{-5} to 1.0 sec). A discrete relaxation effect in the millisecond range can be distinguished for both dyes. The relaxation time for this effect can be estimated, and because it is independent of the concentrations of poly A and the dye, this part of the relaxation spectrum can be identified with an intramolecular process. Correlation of equilibrium spectral measurements with the kinetic results suggests that the observed discrete relaxation effect is characteristic of the "stacking" of the dye molecules into dimers along the poly A chain, or of conformational changes necessary to facilitate "stacking." A knowledge of the time constants characteristic of dye "stacking" may be useful in understanding the "stacking" of nucleic acids.

Some preliminary data obtained with the temperature-jump method for the acridine orange-calf thymus DNA system are also reported.

Experimental Section

Acridine orange from the National Aniline Division was recrystallized twice from methanol. Proflavine sulfate from Mann Research Laboratories was recrystallized from water; the crystals were washed with di-

(1) This work was supported by a grant from the National Institutes of Health (GM13292).

(2) G. G. Hammes and C. D. Hubbard, *J. Phys. Chem.*, **70**, 1615 (1966).

ethyl ether and dried under vacuum over phosphorus pentoxide. Polyadenylic acid was supplied from Miles Chemical Co. as the potassium salt with a given weight-average molecular weight of 100,000 to 2,000,000 and a number-average of 40,000 to 70,000. Calf thymus DNA was purchased from Worthington Biochemical Corp. Chloroquine diphosphate (chloroquine, CQ, is 7-chloro-4-(4-diethylamino-1-methylbutylamino)quinoline) was generously donated by Dr. R. O. Clinton of the Sterling Winthrop Research Institute, Rensselaer, N. Y. All other materials were standard reagent grade chemicals. Doubly distilled water was used for the preparation of all solutions.

Solutions of poly A were made by gently stirring a suspension of the material in a NaCl-Tris-HCl medium of pH 7.5 at 4°; the concentrations were estimated spectrophotometrically by measuring the absorption at 257 m μ .³ DNA solutions were made by a carefully controlled, very slow stirring of a suspension of DNA into a similar medium of pH 7.0 at 4°. Each DNA solution made was subjected to a hyperchromicity test.^{4,5} This showed that the sample was at least 95% native. The concentration of DNA was estimated simultaneously. Solutions of the two acridine dyes and chloroquine were made by weighing out suitable amounts for stock solutions and diluting aliquots of these as required.

The absorption spectra of all solutions were measured with a Beckman Model DU spectrophotometer fitted with a thermostated cell housing. Polymer dye solutions were made by combining appropriate amounts of the stock solutions of each component and making up to a standard volume with addition of suitable quantities of NaCl and/or Tris-HCl buffer to the desired ionic strength. The ionic strength of the solutions was 0.1 M (usually 0.01 M in Tris-HCl buffer and 0.09 M in NaCl), although some solutions were used in which the ionic strength was considerably lower. The pH of the solutions was 7.5 for the poly A-AO, poly A-PR, and poly A-CQ systems, 7.0 for the DNA-AO system, 5.9 for the DNA-AO system, and 5.9 for the DNA-CQ system as measured with a Radiometer pH meter.

The temperature-jump apparatus has previously been described in detail.⁶⁻⁸ Temperature-jump experiments on the poly A-AO and poly A-PR systems were performed over a range of poly A concentration from about 4×10^{-3} to 3×10^{-5} M (the molarity is expressed as the monomer concentration) and at AO and PR concentrations of 5.0×10^{-5} and 2.5×10^{-5} M. Kinetic runs were performed at 25.0° and the ionic strength indicated in Table I. The wavelengths used for observation of the chemical relaxation were 486 m μ for the poly A-AO system and either 420, 440, or 470

m μ for the poly A-PR system. Kinetic runs on all systems were preceded by the testing of the component parts of each solution in the temperature-jump cell to ensure that the observed relaxation effects are due entirely to the polymer-dye interaction. The precaution of excluding light from solutions containing acridine dyes was carried out in the manner described previously.² The construction and performance of the flow apparatus used is described elsewhere.⁹

Results

The spectral changes occurring in solutions of poly A and AO are qualitatively similar to those observed for the PGA-AO system and are consistent with spectra reported for basic poly A-AO solutions:¹⁰ at large values of the ratio [poly A]/[AO], the predominant absorption peak is near 500 m μ and is accompanied by a less intense band with a maximum at 464 m μ ; at

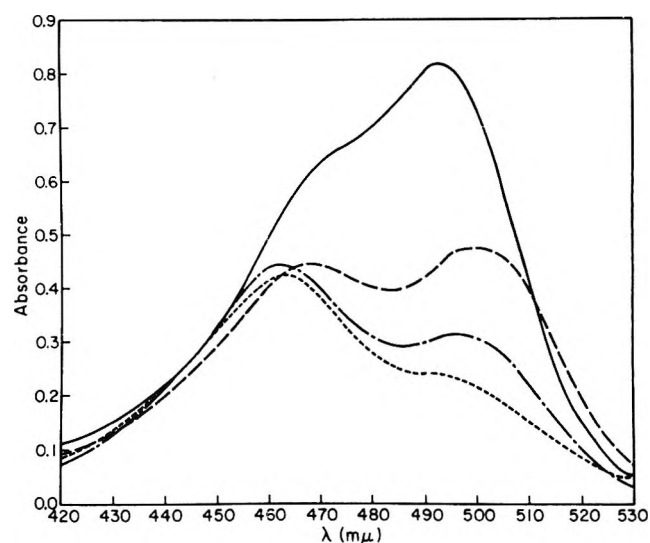


Figure 1. Spectra of poly A-AO solutions at pH 7.5, 25.0°, ionic strength = 0.1 M, [AO] = 2.5×10^{-5} M: —, [poly A] = 0 M; - - -, [poly A] = 4.24×10^{-3} M; - · - ·, [poly A] = 2.12×10^{-3} M; · · · ·, [poly A] = 3.39×10^{-5} M.

(3) G. Felsenfeld and A. Rich, *Biochim. Biophys. Acta*, **26**, 457 (1957).

(4) E. Chargaff, "The Nucleic Acids," Vol. I, E. Chargaff and J. N. Davidson, Ed., Academic Press Inc., New York, N. Y., 1955, p 307.

(5) R. D. Hotchkiss, *Methods Enzymol.*, **3**, 708 (1957).

(6) G. G. Hammes and J. I. Steinfeld, *J. Am. Chem. Soc.*, **84**, 4639 (1962).

(7) G. G. Hammes and P. Fasella, *ibid.*, **84**, 4644 (1962).

(8) R. E. Cathou and G. G. Hammes, *ibid.*, **86**, 3240 (1964).

(9) J. E. Erman and G. G. Hammes, *Rev. Sci. Instr.*, **37**, 746 (1966).

(10) D. F. Bradley and M. K. Wolf, *Proc. Natl. Acad. Sci. U. S.*, **45**, 944 (1959).

Table I: Relaxation Data for Poly A-Acridine Dye Systems at 25°

System	[Poly A], <i>M</i>	[Dye], <i>M</i>	[Poly A]/ [dye]	$10^{-3}\tau^{-1}$, sec ⁻¹	λ , m μ	<i>I</i> , <i>M</i> ^a
Poly A-AO	4.24×10^{-3}	2.5×10^{-5}	170	0.168	486	0.1
	2.12×10^{-3}	2.5×10^{-5}	85	0.169	486	0.1
	1.06×10^{-3}	2.5×10^{-5}	42.4	0.172	486	0.1
	4.24×10^{-4}	2.5×10^{-5}	17	0.178	486	0.1
	1.69×10^{-4}	2.5×10^{-5}	6.76	0.228	486	0.1
	3.39×10^{-5}	2.5×10^{-5}	1.36	0.107	486	0.1
	4.08×10^{-3}	2.5×10^{-5}	163	0.173	486	0.05
	2.04×10^{-3}	2.5×10^{-5}	81.5	0.164	486	0.026
	1.02×10^{-3}	2.5×10^{-5}	40.8	0.166	486	0.026
	4.08×10^{-4}	2.5×10^{-5}	16.3	0.215	486	0.026
	1.63×10^{-4}	2.5×10^{-5}	6.52	0.192	486	0.026
	3.27×10^{-5}	2.5×10^{-5}	1.31	0.194	486	0.026
	4.05×10^{-3}	5.0×10^{-5}	81	0.148	494	0.05
	2.03×10^{-3}	5.0×10^{-5}	40.5	0.159	494	0.026
	1.02×10^{-3}	5.0×10^{-5}	20.3	0.175	494	0.026
	4.05×10^{-4}	5.0×10^{-5}	8.1	0.237	494	0.026
	1.62×10^{-4}	5.0×10^{-5}	3.24	0.264	494	0.026
3.24×10^{-5}	5.0×10^{-5}	0.65	0.211	494	0.026	
Poly A-PR	1.82×10^{-3}	2.5×10^{-5}	72.8	No relaxa- tion	440	0.1
	7.28×10^{-4}	2.5×10^{-5}	29.1	0.96	470	0.1
	3.64×10^{-4}	2.5×10^{-5}	14.6	1.20	440	0.1
	1.82×10^{-4}	2.5×10^{-5}	7.28	1.60	440	0.1
	9.1×10^{-5}	2.5×10^{-5}	3.64	1.17	440	0.1
	4.55×10^{-5}	2.5×10^{-5}	1.82	1.01	440	0.1
	2.28×10^{-5}	2.5×10^{-5}	0.91	0.90	440	0.1
	9.1×10^{-4}	5.0×10^{-5}	18.2	1.29	470	0.1
	5.46×10^{-4}	5.0×10^{-5}	10.9	0.94	470	0.1
1.82×10^{-4}	5.0×10^{-5}	3.64	1.43	470	0.1	

^a *I* = ionic strength.

smaller values of the ratio [poly A]/[AO] the shorter wavelength peak becomes slightly more intense while the peak at 500 m μ diminishes. This type of behavior is accentuated when the ionic strength of similar solutions is lowered. A typical set of spectra is illustrated in Figure 1.

Solutions of proflavine of concentration less than 5×10^{-5} *M* exhibit a broad absorption band in the visible region with a maximum at 444 m μ . The peak is shifted to longer wavelengths in the presence of high concentrations of poly A, but remains at the same position or shifts to a slightly shorter wavelength when the poly A concentration is lowered. This behavior is similar to that observed with AO, but the changes in wavelength are much smaller, and with all values of the ratio [poly A]/[PR] investigated the band was not separated into two peaks. At intermediate values of [poly A]/[PR] the band is broadened and has a less well-defined maximum which lies at wavelengths between the long and short wavelength limits of approximately 455 and 440 m μ , respectively. In the spectra

of the poly A-AO system the peaks are separated by about 40 m μ . Typical poly A-PR spectra are shown in Figure 2.

A much less detailed study was made of the spectra of the DNA-AO, DNA-CQ, and poly A-CQ systems. However, the observed characteristics of the first two systems were essentially identical with those previously reported.^{11,12}

The results obtained with the poly A-AO system will be considered first. A typical relaxation effect is initially curved, but subsequently the amplitude of the effect decreases virtually linearly with time. If a straight line is drawn through the latter sloping part of the trace and extrapolated to the zero-time ordinate, then the distance between this extrapolated line and the actual trace, at any time *t*, is the amplitude of the first relaxation effect since the straight line is the limit-

(11) A. R. Peacocke and J. N. H. Skerrett, *Trans. Faraday Soc.*, **52**, 261 (1956).(12) S. N. Cohen and K. L. Yielding, *J. Biol. Chem.*, **240**, 3123 (1965).

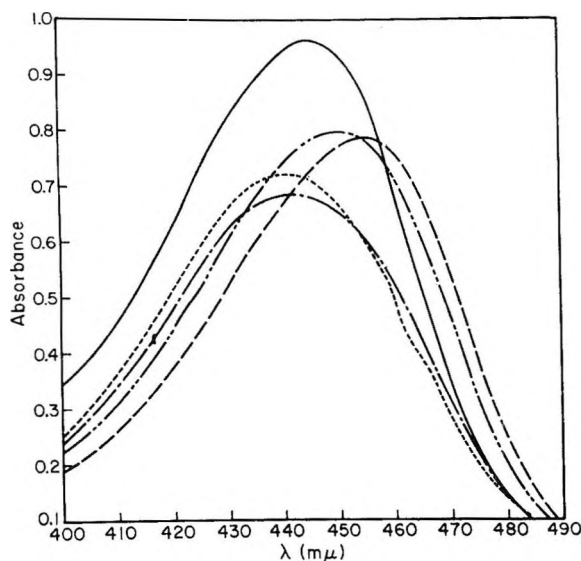


Figure 2. Spectra of poly A-PR solutions at pH 7.5, 25.0°, ionic strength = 0.1 M, [PR] = 2.5×10^{-6} M: —, [poly A] = 0 M; ---, [poly A] = 1.82×10^{-3} M; - · - ·, [poly A] = 7.28×10^{-4} M; · · · ·, [poly A] = 1.82×10^{-4} M; - - - -, [poly A] = 2.28×10^{-5} M.

ing value of this relaxation process at infinite time. A plot of the logarithm of the amplitude against t is linear. Figure 3 shows a typical oscilloscope trace and the semilogarithmic plot extracted from it by the above procedure. The relaxation time obtained in this manner is to a good approximation independent of the concentrations of poly A and AO (in the limited concentration range of the latter employed) and appears to be independent of the ionic strength of the solution. However, when the value of [poly A]/[AO] is reduced to less than about 6, a faster relaxation process can be distinguished. The method given above was applied to evaluation of the relaxation times of both processes, the faster of which is of the order of 0.7 msec, while the magnitude of the slower relaxation is of the same order of magnitude as its counterpart at high poly A concentrations. The precision with which the relaxation times can be measured is very poor when both processes are observed; this is due to the fact that the amplitude of the faster process is very small and that both processes have relaxation times of the same order of magnitude. In view of the small concentration range in which the faster process can be distinguished, and the polydisperse nature of the poly A, a detailed interpretation will not be attempted. The faster relaxation process is probably always part of the over-all relaxation spectrum but only becomes discernible at very low concentrations of poly A. The complexity of the relaxation spectrum prevents a more exact evaluation of the relaxation parameters.

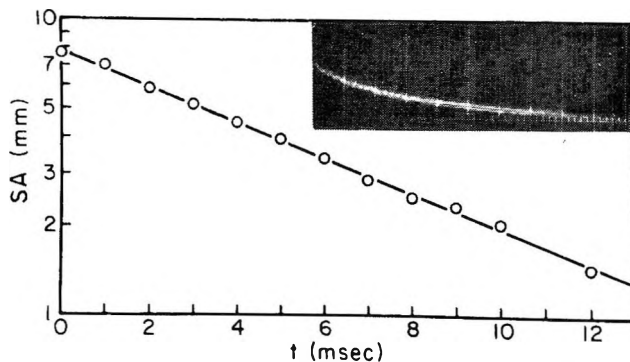


Figure 3. A typical relaxation effect and plot of logarithm of amplitude of light intensity change, SA, vs. time. [Poly A] = 4.24×10^{-3} M, [AO] = 2.5×10^{-8} M, pH 7.5, $\tau = 6.05$ msec. The time scale on the photograph is one large division of the horizontal axis = 2 msec. Details of the method for obtaining the plot are described in the text.

Measurement of the relaxation time characterizing the slowest part of the over-all relaxation effect was attempted by use of both the Guggenheim¹³ and the Swinborne methods,¹⁴ but the difficulty of distinguishing between chemical relaxation effects and absorption changes of the solution due to convection within the temperature-jump cell after 200 msec has elapsed after the temperature jump makes any estimate extremely dubious. Attempts to characterize quantitatively the slowest part of the relaxation spectrum by a concentration-jump method and by direct mixing of polymer and dye in a flow apparatus were not successful because of the very small amplitude of the relaxation effect in the former experiments and because of the lack of reproducibility in measurement of the slow reactions in the latter method. However, the results indicate a relaxation process with a relaxation time of approximately 0.5 to 2.0 sec is occurring. The fact that only an order of magnitude can be placed upon the relaxation time of the slowest part of the relaxation effect prevents evaluation of its dependence on the reactant concentrations and the molecularity of the process involved. Therefore, attention is confined to the faster relaxation process.

Qualitatively, the observed relaxation effect for the poly A-PR system is similar to that for the poly A-AO system in that it is a spectrum which extends over the time range measurable by the temperature-jump technique, and has a step in the first part of the spectrum which yields a linear semilogarithmic plot obtained in the manner already described. Nevertheless, significant differences from the poly A-AO system

(13) E. A. Guggenheim, *Phil. Mag.*, 2, 538 (1926).

(14) E. S. Swinborne, *J. Chem. Soc.*, 2371 (1960).

exist: the relaxation effect is not observed at values of $[\text{poly A}]/[\text{PR}]$ greater than about 30 in an electrolyte medium of ionic strength 0.1 and increases in amplitude as the concentration of poly A is reduced. When the concentration of poly A is decreased further so that $[\text{poly A}]$ is approximately equal to $[\text{PR}]$, the amplitude again diminishes.

The relaxation spectrum arising from the interaction of DNA with AO, observed at $486 \text{ m}\mu$, is similar to that described for the PGA-AO system,² but is not quantitatively described by two relaxation times as was found for the latter system. However, rough estimates of the maximum and minimum relaxation times of the spectrum can be made by use of the initial and final slopes of the usual plots of the logarithm of the signal amplitude *vs.* time. The minimum relaxation time is in the range of 70–400 μsec and estimates for the maximum relaxation time are from 0.5 to 7.0 msec. The variations in both times are random within the concentration range of DNA employed ($0.108\text{--}6.35 \times 10^{-4} M$; the molarity refers to the concentration of phosphorus). In contrast to the poly A-AO system, a very slow relaxation process was not observed. Large absorbance differences between a solution of chloroquine and a solution of chloroquine in the presence of poly A or DNA occur between 325 and 345 $\text{m}\mu$, but no relaxation effects were observed.

Discussion

Two features of the poly A-AO spectra are in contrast to the PGA-AO spectra; a blue shift of the shorter wavelength band does not occur when the value of the ratio $[\text{poly A}]/[\text{AO}]$ is reduced to unity, and the band which at large values of $[\text{PGA}]/[\text{AO}]$ remains at the same wavelength as that of the monomer band in free solution shows a small red shift in the poly A-AO system. Such differences have previously been observed in analogous systems,¹⁰ and are not prejudicial to the general interpretation of the spectra, namely, that the band in the poly A-AO spectra at approximately $500 \text{ m}\mu$ is characteristic of an unstacked dye-poly A complex while the peak at $464 \text{ m}\mu$ arises from a dimer dye-poly A complex. The solutions used in the temperature-jump experiments on the poly A-AO system most probably contain a mixture of monomer dye complex and dimer dye complex.

Proflavine does not aggregate in free solution at concentrations less than $5 \times 10^{-5} M$, but is thought to interact with adjacent molecules of proflavine when these are bound to DNA. The existence of two types of binding sites in DNA for proflavine has been demonstrated by equilibrium studies;¹¹ these have been identified as a binding which is electrostatic, that is, the

attraction between the negatively charged phosphate residues and the cationic dye molecules, and an interaction between aromatic rings of the dye and the bases of the DNA. Mutual interaction between bound proflavine molecules has also been proposed.

An analogous interpretation to that for the poly A-AO spectra has been used for the poly A-PR spectral measurements. The shift of the proflavine peak to longer wavelengths at large values of the ratio $[\text{poly A}]/[\text{PR}]$ means that proflavine is bound in an unstacked manner to the polymer, and the short wavelength peak represents a complex containing proflavine dimer stacks or possibly higher aggregates along the polymer chain. The lack of resolution into two bands indicates that when there is a mixture of species in solution, the absorption peaks of each complex species superpose resulting in a single broad band. An acceptance of this explanation of the changes in the absorption spectra allows a qualitative understanding of the relaxation data.

The data obtained restrict us to a qualitative discussion of the mechanism of interaction between bound acridine dyes. The independence of the relaxation time of the poly A-AO and poly A-PR systems upon either the concentration of poly A or the concentration of dye, except at very low poly A concentrations, almost certainly implicates an intramolecular process which takes place subsequently to initial binding on the polynucleotide chain. The relaxation effect of the poly A-PR system is observed only when the relative concentrations of the reactants are those which yield dimer dye-poly A complexes, as judged by the absorption spectrum. In the case of AO-poly A complexes, dimeric stacks are present over the entire concentration probed. The presence in the equilibrium mixture of a species having aggregated dye groups along the polymer chain is a requirement for the observed relaxation effect to occur. This is consistent with the fact that no relaxation effect is observed in the DNA-CQ and poly A-CQ systems where the cation is thought not to interact with itself in solution or when bound to DNA.¹² However, the kinetic studies themselves do not distinguish dimer stacks from any other type of "interacting dye" structure, so these results cannot be considered as proof of the interpretation given to the spectra. The fact that a relaxation time characteristic of intermolecular complex formation cannot be measured enables a lower limit to be placed upon the bimolecular rate constant for binding. This lower limit is about $2 \times 10^8 M^{-1} \text{ sec.}^{-1}$, which means that complex formation occurs at a rate controlled essentially by diffusion together of the reactants. However, the dependence upon reactant concentration of the fastest re-

Table II: Characteristic Time Constants of "Stacking" Interactions at 25°

System	Conformation of macromolecule	pH	"Stacking" relaxation time, sec	Interacting groups
AO-AO ^a	...	4.7	<10 ⁻¹⁰	AO-AO
PGA-AO ^a	Coil	7.5	2 × 10 ⁻⁶ or 2 × 10 ⁻⁴	AO-AO
PGA-AO ^a	Helix	4.7	5 × 10 ⁻⁴ or 3 × 10 ⁻³	AO-AO
Poly A-AO ^b	Single strand	7.5	5 × 10 ⁻³	AO-AO Adenine-AO Adenine-adenine PR-PR Adenine-PR
Poly A-PR ^b	Single strand	7.5	1 × 10 ⁻³	Adenine-adenine Base-base
Poly A-poly U ^c	Single strands	7.0	<10 ⁻²	AO-AO Base-AO Base-base
DNA-AO ^b	Double helix	7.0	1 × 10 ⁻⁴ to 2 × 10 ⁻³	Base-base
DNA-DNA ^d	Single strands		<6 × 10 ⁻⁴	Base-base

^a See ref 2. ^b This work. ^c See ref 23. ^d See ref 24.

laxation process observed only at low poly A concentrations in the poly A-AO system could not be evaluated, and it is possible that this relates to complex formation. If this is the case, the bimolecular rate constant for complex formation would be approximately $3 \times 10^7 M^{-1} \text{sec}^{-1}$.

The relaxation time is a rough measure of the lifetime of a dimer stack (*i.e.*, the "interacting dye" structure) and/or the migration time of the dye on the polymer. These constants are assembled in Table II for the DNA, PGA, and poly A-dye systems and the dimerization of acridine orange. Both of the measured relaxation times are included for the PGA-AO system although the longer time is probably related to the dimer stacking process. Although these time constants cannot be interpreted quantitatively, several regularities are clear: the shortest relaxation time is for free acridine orange followed in order by "stacking" along the flexible PGA random coil, "stacking" on PGA helix, and finally "stacking" on poly A. The slowness of this process on poly A is probably a reflection of the interaction between dye and bases and/or of the difficulty in achieving the correct degree of orientation for "stacking." A minimum overlap of aromatic systems is necessary for significant interaction.¹¹ Apparently, the mobility of the dye structure is even restricted on PGA, possibly because of the strong electrostatic interactions between dye and polymer. The time constants of the DNA-dye system do not fit into this logical pattern because of the spectrum observed. The relaxation time for PR is shorter than for AO, which is consistent with the fact that the PR-PR interaction is weaker than that for AO-AO. Unfortunately, the data obtained do not enable us to make any distinction

between the models proposed for the structures of nucleic acid-dye complexes.¹⁵⁻¹⁷

The nature of the interaction between bases in nucleic acids should be closely related to that between dyes. In the former case hydrogen bonding between pairs of bases which are not involved in stacking with each other may be of importance, but hydrogen bond formation and breakage is much more rapid than the times associated with dye stacking.¹⁸⁻²⁰ The relaxation times associated with the helix-coil transition in PGA, which is probably a hydrogen-bonding process, are about 10⁻⁷ sec.^{21,22} Very few direct measurements of the rate of base stacking in nucleic acids are available. The kinetics of formation of the double-strand poly (A + U) complex from the single strands is initially second order, but becomes first order as the reaction proceeds.²³ If orientation of base pairs for "stacking" is rate limiting for the first-order growth process, the associated time constant for dimeric interaction must be greater than 10² sec⁻¹, or the relaxation time must be less than 10⁻² sec. The replication rate

(15) L. S. Lerman, *J. Mol. Biol.*, **3**, 18 (1961); *Proc. Natl. Acad. Sci. U. S.*, **49**, 94 (1963).

(16) G. Weill and M. Calvin, *Biopolymers*, **1**, 401 (1963).

(17) S. F. Mason and A. J. McCaffery, *Nature*, **204**, 468 (1964).

(18) W. Maier, *Z. Elektrochem.*, **64**, 132 (1960).

(19) K. Bergmann, M. Eigen, and L. de Maeyer, *Ber. Bunsenges. Physik. Chem.*, **68**, 819 (1963).

(20) G. G. Hammes and H. O. Spivey, *J. Am. Chem. Soc.*, **88**, 1621 (1966).

(21) R. Lumry, R. Legare, and W. G. Miller, *Biopolymers*, **2**, 489 (1964).

(22) J. J. Burke, G. G. Hammes, and T. B. Lewis, *J. Chem. Phys.*, **42**, 3520 (1965).

(23) P. D. Ross and J. M. Sturtevant, *J. Am. Chem. Soc.*, **84**, 4503 (1962).

of T2 DNA at 37° is about 2 min/molecule or 6×10^{-4} sec/base pair.²⁴ The similarity of this time to the other time constants in Table II suggests that orientational effects involved in "stacking" may be rate limiting rather than hydrodynamic resistance to unwinding of the strands as suggested by Crothers,²⁴ unless hydrodynamic effects are also responsible for the rate of the dye interactions, which seems unlikely. However, at present the relationship between dye interactions and DNA base interactions is quite speculative. For the sake of comparison, the characteristic time constants of these nucleic acid interactions are included in Table II. The nature of the forces involved in base and dye interactions is still not certain; presumably, hydrophobic, dipolar, and π - π interactions are all involved.

The interaction of acridine dyes with polymer molecules is still not clearly understood. Obviously, the nature of the binding sites and the conformation of the macromolecule are important among the many factors which influence the "stacking" interactions. Intermolecular complex formation occurs at rates approaching those characteristic of diffusion-controlled processes. The results presented in Table II indicate that the phenomenon of "stacking" occurs relatively slowly and may be controlled by the rate of orientation of dye and polymer into a favorable interaction position. Similar interactions may be of importance in DNA replication.

(24) D. M. Crothers, *J. Mol. Biol.*, **9**, 712 (1964).

Henry's Law Studies of Solutions of Water in Organic Solvents¹

by W. L. Masterton and M. C. Gendrano

Department of Chemistry, University of Connecticut, Storrs, Connecticut (Received March 7, 1966)

A study of the relationship between activity and concentration of water in benzene, chloroform, and 1,2-dichloroethane gives evidence for association of water molecules in the latter two solvents. The data in these solvents can be explained adequately in terms of an equilibrium between water monomer and dimer.

Introduction

A survey of recent literature shows some disagreement concerning the association of solute water molecules in nonhydrogen-bonded organic solvents. Gordon, *et al.*,² found that the apparent molal volume of water dissolved in benzene and toluene at 60–70° decreases with increasing concentration. Attributing this effect to association, Gordon calculated that at 90% of saturation at 67°, the molecular weight of water dissolved in benzene is approximately 45. On the other hand, Christian, *et al.*,³ report that solutions of water in benzene at 25° obey Henry's law, a behavior which seems to preclude extensive association. The same sort of evidence is cited⁴ to indicate the absence of association of water in carbon tetrachloride solu-

tion. However, these authors note, in solutions of water in 1,2-dichloroethane, a pronounced curvature in the plot of concentration of water *vs.* activity. This is attributed to association of water molecules. In particular, it is stated that the data are most readily interpreted in terms of an equilibrium between mono-

(1) Abstracted in part from the M.S. Thesis of M. C. Gendrano, University of Connecticut, Oct 1965.

(2) M. Gordon, C. Hope, L. Loan, and R. Roe, *Proc. Roy. Soc. (London)*, **A258**, 215 (1960).

(3) S. Christian, H. Affsprung, and J. Johnson, *J. Chem. Soc.*, 1896 (1963).

(4) J. Johnson, S. Christian, and H. Affsprung, *ibid.*, 1 (1965).

mer and trimer or monomer and tetramer.^{5,6}

Recently, we have undertaken a thermodynamic study designed to give information concerning molecular interactions in solutions of water in organic solvents. As a part of that study, we have conducted isopiestic measurements similar to those of Christian, *et al.*, on solutions of water in benzene, chloroform, and 1,2-dichloroethane. We find, as did these authors, that solutions of water in benzene obey Henry's law, while solutions of water in 1,2-dichloroethane deviate from Henry's law in a manner which is most readily interpreted in terms of association of water molecules. The same sort of evidence indicates that water in chloroform solution is associated to approximately the same extent as in 1,2-dichloroethane.

Experimental Procedure

The 1,2-dichloroethane used as a solvent was distilled through a 3-ft silver-coated column at a reflux ratio of 13. The refractive index of the distillate agreed with the literature value (n_D^{20} 1.444) within ± 0.001 ; moreover, a vapor phase chromatogram showed only one peak. Reagent grade chloroform, containing a small amount of ethyl alcohol, was purified by washing repeatedly with distilled water until the alcohol peak virtually disappeared from a vapor phase chromatogram. The purified chloroform was used immediately to avoid photochemical decomposition. Thiophene-free benzene was used without further purification.

The organic solvents were equilibrated with pure water and with a series of aqueous solutions of calcium chloride ranging in concentration from 1 to 6 *m*. The apparatus used was similar in all respects to that described by Christian, *et al.*^{3,7} Equilibration was allowed to take place for at least 2 days with the entire apparatus immersed in a water bath held at constant temperature to within $\pm 0.05^\circ$. After equilibration, the calcium chloride solutions were analyzed by titrating weighed samples with silver nitrate. Preliminary experiments indicated that the concentration of calcium chloride changed by less than 1% during equilibration.

The equilibrated organic phases were analyzed for water by the Karl Fischer method (dead-stop end point). The Fischer reagent was standardized before each determination by titrating a sample of distilled water introduced from a calibrated micrometer buret. Weighed samples of the organic phases, chosen so as to contain 10–40 mg of water (equivalent to 2–7 ml of Fischer reagent), were introduced from a syringe into the titration assembly. The microburet used for the titrations was read to ± 0.01 ml. Each of the openings to the apparatus was protected from atmospheric moisture by phosphorus pentoxide drying tubes. All

titrations were carried out in an atmosphere of dry nitrogen.

Results

Data for the systems studied are presented in Table I, where the concentration of water in moles per liter (C_w) is given as a function of the molality of calcium chloride and the activity of water (a_w) derived therefrom. Each result represents the mean of at least two determinations. Water analyses on duplicate samples showed an average deviation from the mean of slightly less than ± 0.0002 . Values for the solubility of water in benzene and 1,2-dichloroethane at 25° ($a_w = 1$) are in good agreement with the results of Christian, *et al.* ($C_w = 0.0349$ in benzene, 0.1252 in 1,2-dichloroethane).^{3,5}

Table I: Solubility of Water in Organic Solvents as a Function of Activity

C_w	CaCl ₂ , <i>m</i>	a_w	C_w	CaCl ₂ , <i>m</i>	a_w
Benzene at 25°			Chloroform at 25°		
0.0347	...	1.000	0.0738	...	1.000
0.0327	0.951	0.948	0.0693	0.979	0.947
0.0299	1.898	0.871	0.0632	1.978	0.864
0.0266	2.858	0.767	0.0544	2.965	0.754
0.0227	3.701	0.662	0.0455	3.940	0.631
0.0180	4.839	0.518	0.0368	4.901	0.511
0.0139	5.838	0.407	0.0275	6.006	0.391
1,2-Dichloroethane at 25°			1,2-Dichloroethane at 5°		
0.1264	...	1.000	0.0696	...	1.000
0.1202	0.976	0.947	0.0637	1.073	0.940
0.1084	1.926	0.869	0.0581	2.025	0.857
0.0945	2.880	0.765	0.0500	3.004	0.745
0.0791	3.800	0.649	0.0411	3.959	0.619
0.0645	4.698	0.535	0.0323	4.945	0.488
0.0488	5.802	0.411	0.0286	5.494	0.422

Water activities in calcium chloride solutions at 25° were calculated from a semiempirical equation given by Lietzke and Stoughton⁸ which reproduces the measured values reported by Stokes⁹ with an average deviation of less than ± 0.001 .

The calculation of water activities at 5° is complicated by a lack of reliable isopiestic data for calcium

(5) T. Lin, S. Christian, and H. Affsprung, *J. Phys. Chem.*, **69**, 2980 (1965).

(6) J. Johnson, S. Christian, and H. Affsprung, *J. Chem. Soc.*, 77 (1966).

(7) S. Christian, H. Affsprung, J. Johnson, and J. Worley, *J. Chem. Educ.*, **40**, 419 (1963).

(8) M. Lietzke and R. Stoughton, *J. Phys. Chem.*, **66**, 508 (1962).

(9) R. Stokes, *Trans. Faraday Soc.*, **41**, 637 (1945).

chloride solutions at this temperature. The equation

$$\frac{d \ln a_w}{dT} = \frac{-\bar{L}}{RT^2} \quad (1)$$

where \bar{L} is the differential heat of dilution, was used to estimate water activities at 5° from accurately known values at 25°. The results at rounded molalities of calcium chloride are given in Table II.

Table II: Water Activities in CaCl₂ Solutions at 25 and 5°

CaCl ₂ , <i>m</i>	<i>L</i> , cal/mole	<i>a_w</i> at 25°	<i>a_w</i> at 5°
1	...	0.945	0.945
2	-20	0.861	0.859
3	-50	0.750	0.745
4	-120	0.623	0.614
5	-300	0.499	0.481
6	-500	0.391	0.368

Values of \bar{L} were interpolated from literature data.^{10,11} Unfortunately, the heat of dilution of calcium chloride is strongly dependent upon both concentration and temperature; as a result, the \bar{L} values in Table II may be in error by as much as 20%. Although variations in \bar{L} have little effect upon water activities in dilute solution, an error of 20% in 6 *m* calcium chloride would change the activity of water in this solution at 5° by 0.005.

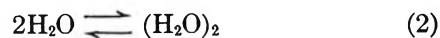
In calculating water activities, the small amount of organic solvent transferred to the aqueous phase during equilibration was neglected. This is entirely justifiable when the equilibrating medium is pure water. For example, the mole fraction of water in a solution saturated with chloroform is known to be 0.999. If Raoult's law is obeyed, the activity of water in this solution would be 0.999, 0.1% less than that given in Table I. This error is negligible compared to the uncertainty in the measured value of the concentration of water.

It is more difficult to estimate the effect of dissolved organic solvent on the activity of water in calcium chloride solutions. However, the solubility of the organic liquid can be expected to decrease with increasing salt concentration. This was confirmed qualitatively from vapor phase chromatograms of the aqueous phases; the peak associated with the organic solvent was considerably reduced in the more concentrated calcium chloride solutions.

Interpretation of Data

To investigate the effect of association upon the relationship between the concentration of water, C_w ,

and its activity, a_w , consider a simple equilibrium between monomer and dimer.



The equilibrium constant for dimerization, K , may be written as

$$K = C_2/C_1^2 \quad (3)$$

where C_1 and C_2 represent the concentrations of monomer and dimer, respectively. The total concentration of water, C_w , is

$$C_w = C_1 + 2C_2 \quad (4)$$

or, from (3)

$$C_w = C_1 + 2KC_1^2 \quad (5)$$

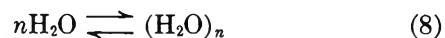
Noting that water vapor is monomeric and assuming that the monomer in solution obeys Henry's law

$$C_1 = ka_w \quad (6)$$

where k is the Henry's law constant. Substituting (6) in (5) gives

$$C_w = ka_w + 2Kk^2a_w^2 \quad (7)$$

In the more general case, where the monomer is in equilibrium with a polymeric species containing n molecules of water



it is readily shown that

$$C_w = ka_w + nKk^n a_w^n \quad (9)$$

From eq 7 or 9, it is clear that if only monomer is present ($K = 0$), the concentration of water will be a linear function of its activity. If, on the other hand, significant association occurs, the data will be better fit by a polynomial in a_w . In such a case, the equilibrium constant for association can be calculated from the coefficients of the equation relating C_w to a_w .

The data for the benzene solutions can be fitted by a least-squares technique to the linear equation

$$C_w = 0.0345a_w \quad (10)$$

The average deviation of an experimentally determined concentration from the value predicted by this equation is ± 0.0002 , the estimated experimental error in C_w . If one attempts to fit the data with a second-degree polynomial of the form

$$C_w = Aa_w + Ba_w^2 \quad (11)$$

(10) J. Hepburn, *J. Chem. Soc.*, 562 (1932).

(11) W. Tucker, *Phil. Trans. Roy. Soc.*, A215, 338 (1915).

the coefficient of the quadratic term is extremely small (0.0003), and the average deviation remains ± 0.0002 . Increasing the degree of the polynomial to 3 or 4 (*i.e.*, $n = 3$ or 4 in eq 9) does not improve the fit. Thus, our data show no evidence for association of water molecules in benzene solution.

The situation in chloroform solutions of water is quite different. Fitting the data to an equation of the same form as (10) gives

$$C_w = 0.0729a_w \quad (12)$$

The average deviation here is ± 0.0006 , three times the estimated error in C_w . Moreover, the deviations at low water activities (< 0.8) are all negative, while those at higher values of a_w are positive. This suggests that a second-degree polynomial of the form of (11) would give a better fit. Least-squares treatment gives

$$C_w = 0.0691a_w + 0.0045a_w^2 \quad (13)$$

The average deviation is now reduced to ± 0.0002 ; positive and negative deviations occur randomly. Statistical analysis¹² reveals that the coefficient of the quadratic term is significant at the 99.5% confidence limit. We conclude that significant association of water molecules occurs in chloroform solution.

On the basis of our data, it is not necessary to postulate the presence of polymeric water species higher than dimers in chloroform solution. Fitting the data to an equation of the form of (9) with $n = 3$ gives

$$C_w = 0.0707a_w + 0.0030a_w^3 \quad (14)$$

The average deviation in this case is ± 0.0002 , precisely that obtained with eq 13.

The conclusions reached with chloroform solutions are equally valid for solutions of water in 1,2-dichloroethane. The relations between concentration and activity of water are best expressed by the second-degree polynomials

$$(25^\circ) \quad C_w = 0.1131a_w + 0.0138a_w^2 \\ \text{(av dev } \pm 0.0002) \quad (15)$$

$$(5^\circ) \quad C_w = 0.0639a_w + 0.0049a_w^2 \\ \text{(av dev } \pm 0.0004) \quad (16)$$

The increased scatter of the data at 5° may reflect errors in estimating the activity of water in calcium chloride solutions at this temperature. Statistical analysis shows that the coefficients of the quadratic terms in (15) and (16) are significant at the 99.5 and 98% confidence limits, respectively. Third-degree equations similar to (14) do not improve the fit; the

average deviations between experimental and calculated values of C_w remain ± 0.0002 at 25° and ± 0.0004 at 5°.

Equilibrium constants for dimer formation can be calculated from the coefficients of the linear and quadratic terms of eq 13, 15, and 16. Comparison of eq 7 and 11 shows that

$$K = \frac{B}{2A^2} \quad (17)$$

It is evident from Table III that, at a given temperature and concentration, water is associated to approximately the same extent in chloroform as in 1,2-dichloroethane. The relatively small change with temperature of the equilibrium constant for association of water in 1,2-dichloroethane is rather surprising. It is difficult, however, to attribute too much significance to this because of the uncertainties in the values of a_w at 5°. One can calculate that a change of 20% in the value of the heat of dilution could increase K at 5° to about 0.7 l. mole⁻¹.

Table III: Equilibrium Constants for $2\text{H}_2\text{O} \rightleftharpoons (\text{H}_2\text{O})_2$

Solvent	Temp, °C	K , l. mole ⁻¹
Chloroform	25	0.47
1,2-Dichloroethane	25	0.54
1,2-Dichloroethane	5	0.6

It should be emphasized that the equilibrium constants reported in Table III correspond to relatively small amounts of association. One can calculate, for example, that in a saturated solution of water in chloroform at 25°, only about 6% of the water molecules would be associated.

Christian, *et al.*,⁶ found somewhat larger deviations from Henry's law in solutions of water in 1,2-dichloroethane than those reported here. Likewise, they observed a larger temperature dependence of the association constant for this system.

Acknowledgment. This work was supported, in part, by a grant from the Research Foundation of the University of Connecticut. We are indebted to Mr. Peter Skribanowitz for constructing the apparatus used to determine dissolved water and to Miss Lillian Acayan for assisting in the statistical analysis.

(12) F. Graybill, "An Introduction to Linear Statistical Models," Vol. I, McGraw-Hill Book Co., Inc., New York, N. Y., 1961, p 166.

Nuclear Magnetic Resonance Studies of Complexes Involving β -Diketones and Some Neutral Organophosphorus Esters

by George Pukanic,^{1a} Norman C. Li,^{1b} Wallace S. Brey, Jr.,^{1c} and George B. Savitsky^{1d}

Department of Chemistry, Duquesne University, Pittsburgh, Pennsylvania, and Department of Chemistry, University of Florida, Gainesville, Florida (Received March 7, 1966)

Nuclear magnetic resonance studies of hydrogen bonding between the hydrogen donors—thenoyltrifluoroacetone, hexafluoroacetylacetone, and trifluoroacetylacetone—and the electron donors—tributyl phosphate, diethyl ethyl phosphonate, and tri-*n*-octylphosphine oxide—have been carried out. Of the three β -diketones studied, hexafluoroacetylacetone gives the most stable complex with a given phosphorus ester, as is expected. With a given β -diketone, the equilibrium constant of hydrogen bond formation with the phosphorus esters increases in the order tributyl phosphate, diethyl ethyl phosphonate, and tri-*n*-octylphosphine oxide and is in line with the relative basicity of the phosphorus ester. Evidence for the preferred enol form of thenoyltrifluoroacetone is presented and indicates that the preferred form is the one where the carbonyl group is adjacent to the perfluoromethyl group. Frequency assignments for the thiophene ring protons in thenoyltrifluoroacetone have also been made and are based on hydrogen-bonding studies. The modes of interaction of hexafluoroacetylacetone with methanol have been studied by nuclear magnetic resonance methods.

Introduction

Three previous papers from the laboratory of Duquesne University²⁻⁴ have described solvent-extraction studies of ternary metal complexes of β -diketones and neutral organophosphorus esters. This paper presents nuclear magnetic resonance studies of complexes involving the β -diketones—thenoyltrifluoroacetone (HTTA), trifluoroacetylacetone (HTFA), hexafluoroacetylacetone (HHFA)—and the neutral organophosphorus esters—tri-*n*-octylphosphine oxide (TOPO), (C₈H₁₇)₃PO, diethyl ethyl phosphonate (DEEP), (C₂H₅O)₂(C₂H₅)PO, and tri-*n*-butyl phosphate (TBP), (C₄H₉O)₃PO. These were chosen because mixtures of the β -diketones and organophosphorus esters have been found to enhance the extraction of metal ions from aqueous to organic phase, the so-called “synergistic effect,”²⁻⁶ and the synergistic extraction of metal ions depends upon the nature of the β -diketone and of the phosphorus ester.

It is well known that β -diketones exhibit keto-enol tautomerism. Burdett and Rogers⁷ have determined the percentages of enol tautomers for acetylacetone,

HTFA, HHFA, and HTTA in CS₂ to be 81, 97, 100, and 100, respectively. Substitution of electron-withdrawing groups, as the perfluoromethyl group and the aromatic ring in HTTA, for the methyl group in acetylacetone results in an increase in enolization. Rogers and Burdett⁸ have shown that in “inert” solvents, the β -diketones are principally in the enol form, since the internally hydrogen-bonded molecule is less polar than the keto molecule. In CCl₄ as solvent, two possible enol structures (I and II) can be postulated for HTTA.

(1) (a) Research assistant on a U. S. Atomic Energy Commission contract, No. AT(30-1)-1922, with Duquesne University; (b) Duquesne University; (c) University of Florida; (d) Clemson University.

(2) R. L. Scruggs, T. Kim, and N. C. Li, *J. Phys. Chem.*, **67**, 2194 (1963).

(3) W. R. Walker and N. C. Li, *J. Inorg. Nucl. Chem.*, **27**, 411 (1965).

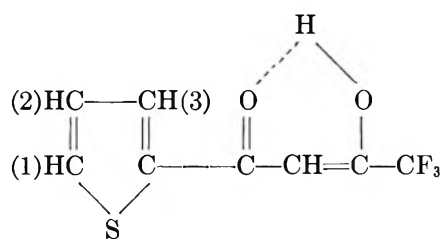
(4) N. C. Li, S. M. Wang, and W. R. Walker, *ibid.*, **27**, 2263 (1965).

(5) T. V. Healy, *ibid.*, **19**, 338 (1961).

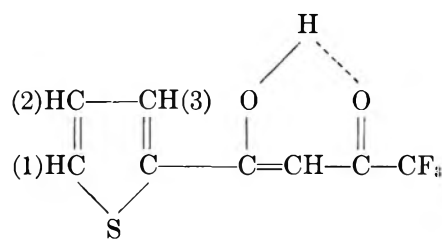
(6) L. Newman, *ibid.*, **25**, 304 (1963).

(7) J. L. Burdett and M. T. Rogers, *J. Am. Chem. Soc.*, **86**, 2105 (1964).

(8) M. T. Rogers and J. L. Burdett, *Can. J. Chem.*, **43**, 1516 (1965).



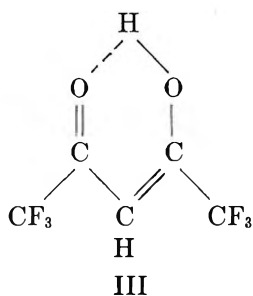
I



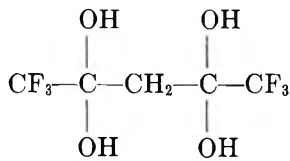
II

Intermolecular hydrogen bonding between HTTA molecules is negligible because HTTA remains monomeric and the proton magnetic resonance frequencies remain constant over a wide range of HTTA concentrations in CCl_4 at constant temperature and in the absence of a second solute. The participation of fluorine in intramolecular hydrogen bonding may be ruled out because such a bond would involve a strained five-membered ring. Because of the importance of HTTA as an extractant in solvent extraction, we have carried out nuclear magnetic resonance measurements for the purpose of determining whether I or II is the preferred enol form. As a by-product of such measurements, we were able to make frequency assignments of the thiophene ring protons in HTTA: CH(1), (2), and (3). The results are presented in this paper.

In experiments using HHFA in CCl_4 , great care has to be taken to exclude moisture from the air, since the presence of water changes HHFA from the enol form (III) to the keto hydrate form (IV).⁹ The keto hydrate, $\text{HHFA} \cdot 2\text{H}_2\text{O}$, itself is insoluble in organic



III



IV

solvents. When TOPO is present, however, it dissolves owing to hydrogen bonding. We considered it of interest therefore to obtain the nuclear magnetic

resonance spectra of HHFA in the presence of water, TOPO, and methanol. The results with methanol are included in this paper.

Experimental Section

Materials. TBP, a Fisher reagent, was washed with 1 *M* HCl, then with 1 *M* NaOH, and finally with distilled water until the organic layer was clear and the washings were neutral. The washed product was distilled under reduced pressure. DEEP, an Eastman Organic chemical, was distilled under reduced pressure. TOPO, also an Eastman Organic chemical, was used without further purification. The β -diketones were purchased from Peninsular Chem Research, Inc. HTTA was recrystallized from benzene, while HTFA and HHFA were redistilled just before use.

Nuclear Magnetic Resonance Measurements. The preparation of samples and method of proton magnetic resonance measurements, using an A-60 nmr spectrometer, were identical with those described by Takahashi and Li.^{10,11} Chemical shifts of the signals were measured with respect to tetramethylsilane used as an internal standard and are quoted as cps. The signals are all downfield from tetramethylsilane. In experiments in which the vinyl proton in the β -diketones was measured, a side band of the tetramethylsilane was placed before and after the vinyl proton resonance peak at a separation of 10–15 cps. The side-band frequencies were measured by means of audiooscillators and a frequency counter. The molarity of the solutions, at temperatures other than room temperature, was calculated from the change in density with temperature of carbon tetrachloride.

Fluorine magnetic resonance spectra were obtained with a Varian DP-60 spectrometer system with the use of a 56.4-Mc radiofrequency unit. The F^{19} chemical shifts are relative to anhydrous trifluoroacetic acid used as an external standard.

Calculation of Equilibrium Constants

By keeping the concentration of HTTA in CCl_4 constant and varying the concentration of TBP, keeping the latter in large excess over the complexed HTTA, Scruggs, Kim, and Li² calculated the equilibrium constant for hydrogen bond formation of a 1:1 complex using the equation

$$\frac{1}{\nu - \nu_f} = \frac{1}{K \Delta_c} \frac{1}{d} + \frac{1}{\Delta_c} \quad (1)$$

(9) B. G. Schultz and E. M. Larsen, *J. Am. Chem. Soc.*, **73**, 1806 (1949).

(10) F. Takahashi and N. C. Li, *J. Phys. Chem.*, **68**, 2136 (1964).

(11) F. Takahashi and N. C. Li, *ibid.*, **69**, 2950 (1965).

Table I: Proton Magnetic Resonance Frequency of Vinyl Proton in HTTA, HHFA, and HTFA (0.300 *M* in CCl_4) as a Function of Concentration of DEEP

-37°		-21°		10°		2°	
CDEEP	Cps	CDEEP	Cps	CDEEP	Cps	CDEEP	Cps
(a) HTTA							
0	382.3	0	382.9	0	383.4	0	383.8
0.615	391.5	0.627	393.0	0.635	394.6	0.644	396.4
1.193	398.2	1.217	400.5	1.233	402.6	1.250	404.8
1.716	402.6	1.749	405.4	1.772	408.0	1.798	409.7
2.364	407.6	2.411	410.6	2.443	413.3	2.478	415.6
2.976	411.9	3.034	415.6	3.074	417.8	3.118	420.7
(b) HHFA							
0	381.6	0	382.2	0	382.8		
0.594	372.4	0.605	372.0	0.613	371.5		
0.885	370.5	0.903	370.2	0.915	369.8		
1.192	369.5	1.215	369.2	1.231	369.0		
1.494	368.9	1.523	368.7	1.543	368.4		
(c) HTFA							
0	352.1	0	352.6	0	353.2	0	353.8
0.599	356.6	0.610	357.4	0.619	357.9	0.627	358.8
0.908	359.3	0.925	360.6	0.938	361.4	0.951	362.3
1.200	361.1	1.224	362.5	1.240	363.5	1.258	364.6
1.531	362.9	1.561	364.2	1.582	365.1	1.605	366.3
1.790	364.2	1.825	365.3	1.849	366.6	1.875	367.9

where Δ_c , the hydrogen bond shift, is the difference between the vinyl proton frequencies of the free and complexed HTTA as hydrogen donor, and d is the total concentration of TBP, which acts as electron donor. Equation 1 was first derived by Mathur, Becker, Bradley, and Li,¹² and applied to hydrogen-bonding equilibria with the following assumptions: (a) the equilibria involve very rapid reactions, so that the observed frequency, ν , is the weighted average of the characteristic frequencies of the free and complexed hydrogen donor (respectively, ν_f and ν_c), and (b) the concentration of the electron donor is in large excess over the complexed hydrogen donor, so that the concentration of the free electron donor is equal to the total concentration, d . From eq 1, a plot of $1/(\nu - \nu_f)$ vs. $1/d$ yields a straight line, from which the values of Δ_c and K can be determined separately.

In the present investigation, the concentrations of the hydrogen donors HTTA, HTFA, and HHFA in CCl_4 were kept constant at 0.300 *M*, while the concentrations of the electron donors, DEEP and TBP, were varied and kept in large excess. The vinyl proton frequency in the β -diketone was measured, and eq 1 was used in obtaining Δ_c and K .

The equilibrium constant of the reaction $\text{HTTA} + \text{TOPO} = \text{HTTA} \cdot \text{TOPO}$ was obtained from a plot of eq 1 using F^{19} resonance frequencies, rather than the vinyl proton frequencies. This is because, with the

latter, the intercept, $1/\Delta_c$, was too small (of the order of 0.005) for an accurate value of K to be obtained. Mixtures of TOPO and HTFA and of TOPO and HHFA were prepared; however, the F^{19} nmr spectra indicated that side reactions in addition to simple complex formation occurred in these systems.

Results and Discussion

Thermodynamic Data on Hydrogen Bonding. Table I lists the proton magnetic resonance results for HTTA, HTFA, and HHFA bonding to DEEP, while Table II gives the F^{19} results for HTTA bonding to TOPO. An example of plots of eq 1 at different temperatures is given in Figure 1 for the system HTTA-DEEP. Values of Δ_c and K are tabulated in Table III.

Figure 2 contains plots of $\log K$ vs. $1/T$ for the various systems investigated. The values of ΔH were calculated from the slopes and are included in Table III.

From Table I it is seen that in the absence of DEEP, the vinyl proton frequency in HTFA lies at higher field than HHFA or HTTA. This is reasonable since there is only one electron-withdrawing group in HTFA, whereas two electron-withdrawing groups are present in HHFA and HTTA. The vinyl proton in HTFA,

(12) R. Mathur, E. D. Becker, R. B. Bradley, and N. C. Li, *J. Phys. Chem.*, **67**, 2190 (1963).

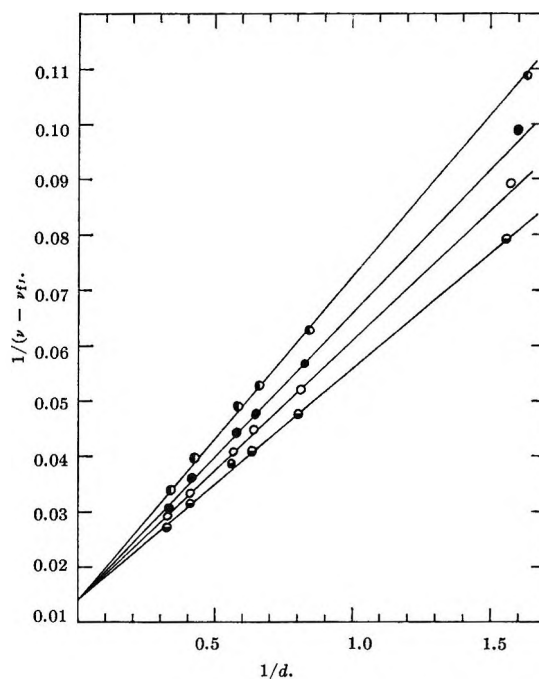
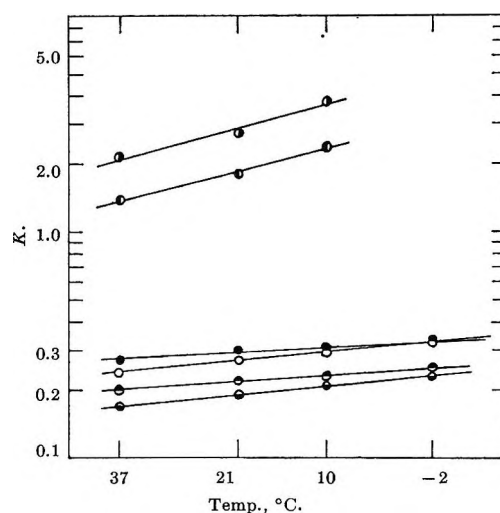
Table II: Fluorine Magnetic Resonance Frequency of HTTA (0.350 *M* in CCl₄) as Function of Concentration of TOPO, 34°

TOPO, <i>M</i>	Cps, downfield from CF ₃ COOH
0	155.5
0.622	169.3
0.808	173.4
0.991	174.9
1.183	176.3
1.306	177.7

Table III: Summary of Results of HTTA, HTFA, and HHFA Hydrogen Bonding

System	Temp, °C	<i>K</i>	-Δ <i>H</i> , kcal/mole	Δ <i>c</i> , cps
HTFA-TBP	37	0.20	0.9	48
	21	0.22		
	10	0.23		
	-2	0.25		
HTFA-DEEP	37	0.27	0.7	37
	21	0.30		
	10	0.31		
	-2	0.32		
HTTA-TBP	37	0.17	1.3	91
	21	0.19		
	10	0.21		
	-2	0.23		
HTTA-DEEP	37	0.24	1.3	72
	21	0.27		
	10	0.29		
	-2	0.33		
HTTA-TOPO	34	0.34		
HHFA-TBP	37	1.39	3.4	12
	21	1.81		
	10	2.38		
HHFA-DEEP	37	2.16	3.7	17
	21	2.73		
	10	3.79		

therefore is less deshielded than in HHFA and HTTA. The value of ν_t , the vinyl proton frequency in the absence of DEEP for the three β -diketones, is slightly temperature dependent, with an average $d\nu_t/dT = 0.04$ cps/deg over the range -2 to 37° . This small variation indicates that the β -diketones are predominantly monomeric, thus justifying our initial implicit assumption that ν_t is the frequency of the monomer. The small temperature effect on ν_t has been taken into account by using for the determination of K at each

**Figure 1.** HTTA-DEEP system. Plots of $1/(\nu - \nu_t)$ vs. $1/[\text{DEEP}]$ at the following temperatures: ●, 37°; ●, 21°; ○, 10°; ○, -2°.**Figure 2.** Plot of $\log K$ vs. $1/T$ for the following systems: ○, HTFA-TBP; ●, HTFA-DEEP; ○, HTTA-TBP; ○, HTTA-DEEP; ●, HHFA-TBP; ○, HHFA-DEEP.

temperature the value of ν_t found at that temperature. This treatment has been described by Mathur, *et al.*,¹² for benzenethiol.

Table III shows that with TBP and DEEP as hydrogen acceptors the equilibrium constant and enthalpy change of hydrogen bond formation are greater for HHFA than for HTTA and HTFA. The greater

hydrogen-donor strength of HHFA is in line with its greater acid strength (pK_a of HHFA, HTTA, and HTFA = 4.35, 5.70, and 6.40, respectively¹³) and with the smaller stability of its binary metal complex ($\log k_1$ values for $\text{Cu}(\text{HFA})^+$, $\text{Cu}(\text{TTA})^+$, and $\text{Cu}(\text{TFA})^+$ are 2.70, 6.55, and 6.59, respectively¹³). When one considers the presence of two electron-withdrawing CF_3 groups in HHFA, *vs.* the presence of one CF_3 and one CH_3 group in HTFA, the greater hydrogen-donor strength and greater acid strength of HHFA become completely reasonable.

Wang, Walker, and Li¹⁴ report the equilibrium constant at 26° of the reaction $\text{Zn}^{2+} + 2\text{HTTA} + \text{TOPO} = \text{Zn}(\text{TTA})_2 \cdot \text{TOPO} + 2\text{H}^+$ to be 0.1 and of the reaction $\text{Zn}^{2+} + 2\text{HHFA} + \text{TOPO} = \text{Zn}(\text{HFA})_2 \cdot \text{TOPO} + 2\text{H}^+$ to be 12. Since HHFA gives a more stable ternary complex, $\text{ZnA}_2 \cdot \text{TOPO}$, than HTTA, one would expect that HHFA is more effective in enhancing extraction (synergism) than HTTA, and this is experimentally observed.^{4,14,15} Because of the two electron-withdrawing CF_3 groups in HHFA, the electron density around the central Zn^{2+} ions in the ZnA_2 complex is decreased, thus enhancing the ability to form an adduct with TOPO. From the above discussion it is seen that the hydrogen-donor strength, acid strength, and solvent-extraction characteristics of HHFA are all inter-related.

TBP has one more alkoxy oxygen than DEEP, so that the phosphoryl oxygen in TBP would have a lower electron-donating tendency than in DEEP. One may expect therefore that the TBP hydrogen-bonded complex would be less stable than the corresponding DEEP hydrogen-bonded complex. The equilibrium constants listed in Table III bear this out, although the values of ΔH for TBP and DEEP as hydrogen acceptors for a given β -diketone seem to be about the same.

Studies on the Preferred Enol Form of HTTA and the Frequency Assignment of the Thiophene Ring Protons in HTTA. Table IV gives the F^{19} magnetic resonance frequency of enolic HTTA and HHFA in CCl_4 , in the absence and presence of various concentrations of TBP. It is seen that the presence of TBP does not affect the F^{19} frequency of HTTA, whereas the effect on HHFA is considerable. The data show that the preferred enol form of HTTA is II, rather than I. This is because TBP is an electron donor and would bond with HTTA through the enolic $-\text{COH}$. If the preferred enol form of HTTA were I, then the presence of TBP should have affected the F^{19} chemical shift, as it does with HHFA. Since no effect was observed with HTTA, the conclusion is that the preferred enol form is II, where the fluorine atoms are farther away from the hydrogen-bonding site.

Table IV: F^{19} Magnetic Resonance Frequency (cps Downfield from CF_3COOH) of Enolic HTTA and HHFA in the Absence and Presence of TBP at 32°

-0.322 M HTTA in CCl_4 -		-0.350 M HHFA in CCl_4 -	
C_{TBP}	Cps	C_{TBP}	Cps
0	155.7	0	105.7
0.624	155.8	0.728	95.1
0.832	156.3	1.092	91.6
1.04	155.7	1.820	84.5
		2.184	80.6

Hydrogen-bonding studies have been found to be useful in making frequency assignments of the thiophene ring protons in HTTA. In the absence of an electron donor, the proton magnetic resonance spectrum of a 0.300 M solution of HTTA in CCl_4 is shown in Figure 3a, with the OH signal omitted. The singlet is ascribed to the vinyl proton. Chemical shifts of the thiophene ring protons are given in Table V. The multiplet at 7.16 ppm is ascribed to CH(2) (for the proton number, see I) and arises from coupling to CH(1) and CH(3). The protons CH(1) and CH(3) are contained in the lowest field multiplet, and the question is which of the first-order doublets in this lowest field multiplet represents which proton.

Table V: Chemical Shifts (ppm) of Thiophene Protons in 0.300 M HTTA in CCl_4 as a Function of Concentrations of TBP, DEEP, and TOPO

C_{TBP}	CH(2)	CH(1)	CH(3)
0	7.16	7.70	7.80
0.712	7.19	7.84	7.96
1.072	7.20	7.89	8.03
2.477	7.22	8.06	8.24
C_{DEEP}			
0.615	7.18	7.83	7.96
1.193	7.19	7.90	8.07
1.513	7.20	7.96	8.12
1.716	7.21	7.98	8.15
2.976	7.24	8.10	8.29
C_{TOPO}			
0.691	7.17	7.92	8.12
0.985	7.18	7.99	8.23
1.190	7.18	8.03	8.32

(13) L. G. Van Uitert, Thesis, Penn State College, Jan 1951; cited by A. E. Martell and M. Calvin, "Chemistry of the Metal Chelate Compounds," Prentice-Hall Inc., New York, N. Y., 1952.

(14) S. M. Wang, W. R. Walker, and N. C. Li, *J. Inorg. Nucl. Chem.*, **28**, 875 (1966).

(15) W. R. Walker and N. C. Li, *ibid.*, **27**, 2255 (1965).

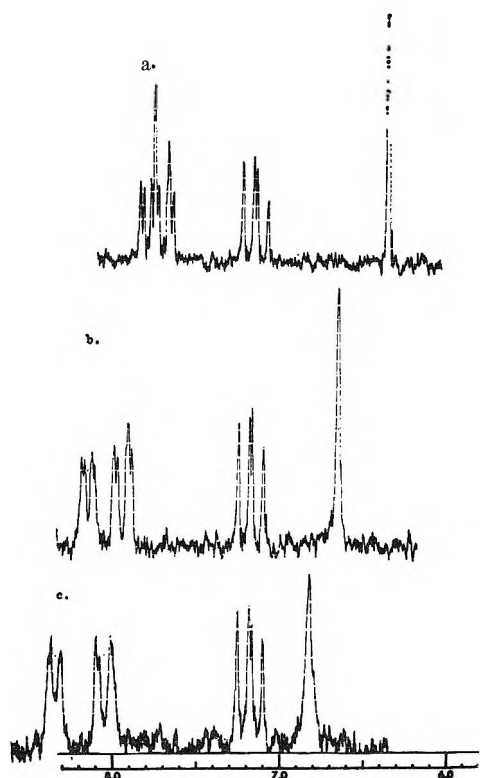


Figure 3. Proton magnetic resonance spectra of thiophene ring protons of 0.300 *M* HTTA in CCl_4 : (a) in the absence of electron donor; (b) in the presence of 0.691 *M* TOPO; (c) 1.190 *M* TOPO.

Upon the addition of an electron donor to HTTA in CCl_4 , the lowest field multiplet in Figure 3a is now resolved into two first-order doublets, and the lower field doublet is shifted further downfield than the higher field doublet on increasing the concentration of electron donor (see Figure 3b, Figure 3c, and Table V). Since the electron donor is bonded to the enolic OH, H(3) is closer to the coordination site than H(1), and one would expect, therefore, that the signal of H(3) would be shifted further downfield. Our reasoning is in line with that of Li, Scruggs, and Becker¹⁶ and Mathur and Li,¹⁷ who account for the order of chemical shifts of metal complexes of amino acids on the basis of the proximity of protons to the binding sites. We therefore conclude that the lowest field multiplet in Figure 3a is due to a superposition of the H(1) and H(3) signals, and that H(3) has the lower frequency of the two.

In the absence of an electron donor, there is intramolecular hydrogen bonding involving OH. Since H(3) is closer to the coordination site also, its signal lies further downfield than H(1). Our frequency assignment is in agreement with the order given by Varian Associates¹⁸ in which H(1) and H(3) are listed as 7.73 and 7.82 ppm, respectively, in CDCl_3 . In ref 18, however,

no reason is given for this assignment. We have shown here a quick method of making frequency assignments by observing the downfield shifts caused by the presence of an electron donor in hydrogen bond formation.

From Table V it is seen that TOPO causes a greater downfield shift of H(1) and H(3) than TBP or DEEP. This is as expected, since TOPO is the strongest electron donor of the three phosphorus esters. With a given β -diketone, therefore, TOPO would form the strongest hydrogen bond.

Effects of Adding Methanol to Solutions of HHFA in CCl_4 . On adding methanol to a 0.704 *M* HHFA solution in CCl_4 , it was found that in addition to the vinyl proton (enol) signal at 382 cps, there is an additional proton signal at 135 cps, ascribed to the methylene protons in the keto form. After an interval of about 24 hr, equilibrium ratios ($K = (\text{keto})/(\text{enol})$) were obtained by integration of the two resonance peaks. At least four integrations were performed. In the F^{19} spectrum of this system there appear also two peaks; that associated with the enol form of the HHFA is 5.1 ppm downfield from that associated with the keto form. Table VI contains data from both types of spectra. As is expected, an increase in methanol concentration results in an increase in K . By analogy with keto hydrate of hexafluoroacetylacetone,^{9,14} the intermolecular hydrogen-bonded species may be a keto methanolate.

The value of K as determined from an F nmr spectrum was found to change with time over a period of an

Table VI: Keto/Enol Ratio (K) for 0.70 *M* HHFA in CCl_4 Containing Various Concentrations of Methanol

CH_3OH concn, <i>M</i>	K from proton resonance (37°)	K from F resonance (34°)
0.49	0.40	...
0.53	...	0.30
0.68	...	0.80
0.71	0.80	...
0.88	1.65	...
0.96	...	2.2
1.11	...	2.5
1.25	...	3.1

(16) N. C. Li, R. L. Scruggs, and E. D. Becker, *J. Am. Chem. Soc.*, **84**, 4650 (1962).

(17) R. Mathur and N. C. Li, *ibid.*, **86**, 1289 (1964).

(18) "High Resolution NMR Spectra Catalog," Varian Associates, Palo Alto, Calif., 1962, Spectrum No. 185.

hour or two after the solution had been prepared. The peak corresponding to the enol form decreased in intensity while that corresponding to the keto form increased in intensity. Preliminary kinetic study of the enol-keto conversion in carbon tetrachloride showed it to be approximately first order in the concentration of

enol, with a half-time at 34° of about 10 min for a solution containing 1.54 *M* concentration of methanol.

Acknowledgments. This work was done under Contract No. AT-(30-1)-1922 with the U. S. Atomic Energy Commission, and under an NSF Summer Faculty Participation Program.

Hydrogen-Deuterium Equilibration over Palladium Hydride

by R. J. Rennard, Jr., and R. J. Kokes

Department of Chemistry, The Johns Hopkins University, Baltimore, Maryland 21218
(Received March 7, 1966)

Equilibration of a 50:50 mixture of hydrogen and deuterium over palladium hydride has been studied as a function of composition at -195 and -183° . Sorption of hydrogen and deuterium occurs at these temperatures, but exchange of gas phase deuterium with palladium hydride (or *vice versa*) does not. The rate of equilibration decreases with increasing hydrogen content of the catalyst. It is concluded that once hydrogen adsorption occurs, exchange or incorporation follows and that the relative rates of these two processes are independent of hydride concentration in the palladium.

Introduction

Palladium hydride¹ is a general term applied to a nonstoichiometric series of compounds ranging in gross composition from roughly $H/Pd = 0.0$ to $H/Pd = 0.8$.¹ Above 310° , palladium hydride forms a single phase; below 310° , it forms two phases. At room temperature, the pure α phase exists in the approximate range, $0 < H/Pd < 0.06$; in the range $0.06 < H/Pd < 0.55$, a mixture of α and β phases is found; only the pure β phase is found for $H/Pd > 0.55$. (These boundaries depend somewhat on preparative conditions.) Despite the complexity of this system, the magnetic susceptibility² is a linear function of concentration that approaches zero at $H/Pd = 0.66$; similarly, the electrical resistivity³ is a linear function of concentration up to $H/Pd = 0.80$. These linear relations hold through the two-phase region. Thus, hydrogen behaves approximately like an alloying metal that fills up the holes in the d band at the composition $PdH_{0.66}$. Several researchers⁴⁻⁷ have observed that hydride

formation affects the activity of the catalysts both for the *ortho-para* conversion and ethylene hydrogenation. Of these reactions, the former is by far the simpler, but it can proceed primarily by the magnetic conversion and, hence, shed relatively little light on the chemistry of the hydrogen activation process.⁸ Accordingly, we have selected the hydrogen-deuterium equilibration for study as a function of the hydrogen content of palladium hydride.

(1) D. P. Smith, "Hydrogen in Metals," University of Chicago Press, Chicago, Ill., 1948.

(2) C. Kittel, "Solid State Physics," John Wiley and Sons, Inc., New York, N. Y., 1956, p 334.

(3) R. E. Norberg, *Phys. Rev.*, **86**, 745 (1952).

(4) A. Farkas, *Trans. Faraday Soc.*, **32**, 1667 (1936).

(5) A. Couper and D. D. Eley, *Discussions Faraday Soc.*, **8**, 172 (1950).

(6) M. Kowaka, *J. Japan Inst. Metals*, **23**, 625 (1959).

(7) R. J. Rennard, Jr., and R. J. Kokes, *J. Phys. Chem.*, **70**, 2543 (1966).

(8) G. C. Bond, "Catalysis by Metals," Academic Press Inc., New York, N. Y., 1962.

Experimental Section

Palladium was prepared by a modification⁷ of the procedure used by Gillespie and Hall.⁹ This yielded a palladium sponge with a surface area of 0.48 m²/g. Prior to each kinetic run, the palladium was heated for 16 hr in 200 mm of hydrogen at 400° and degassed at 450° for 30 min. Then the sample was cooled in helium to -78° and evacuated. The hydride was prepared by sorption of a measured amount of gaseous hydrogen; at -78° sorption was rapid, irreversible, and complete for compositions up to PdH_{0.5}. After the hydride was formed, the sample was cooled in helium to -195° (or -183°), evacuated, and a 50:50 mixture of hydrogen-deuterium was admitted to the reaction flask. From time to time, a small sample of the reactant gas was withdrawn and analyzed mass spectrographically. From the analysis and mass balance it was possible to compute not only the amount of HD produced but also the amount of sorption of hydrogen and deuterium that accompanied the equilibration reaction. All equilibration runs were carried out in a 30-cc conical reaction flask with the catalyst at the bottom. The catalyst sample (40-60 mesh) consisted of 320 mg of palladium admixed with 1.5 g of crushed Vycor (40-60 mesh).

In studies of adsorption alone, a 5-g sample of palladium in a tightly packed tube was used. These results agreed reasonably well with results obtained during kinetic experiments.

Results

Exchange Experiments. At -195°, no exchange occurred in 3 hr between palladium deuteride and gaseous hydrogen or gaseous deuterium and palladium hydride. At -183°, no exchange between gaseous deuterium and palladium hydride was detected.

Adsorption Experiments. Figure 1 shows a plot of the hydrogen uptake at 200 mm by pure palladium and PdH_{0.23} at -195°. It is clear that bulk reaction occurs even at -195° for the amount of sorbed hydrogen greatly exceeds a monolayer; after 300 min, the uptake of hydrogen for both samples is of the order of 30 monolayers. (Results of Knor, Ponec, and Cerney¹⁰ can be interpreted in terms of bulk sorption at -195°.)

Initially, the rate of sorption for the pure palladium is lower than that for PdH_{0.23}, but in time, the rate for pure palladium becomes nearly linear and greater than that found for PdH_{0.23}. In what follows we shall term the initial nonlinear portion of this curve the induction period.

Deuterium sorption by palladium at -195° is at least an order of magnitude slower than that for hy-

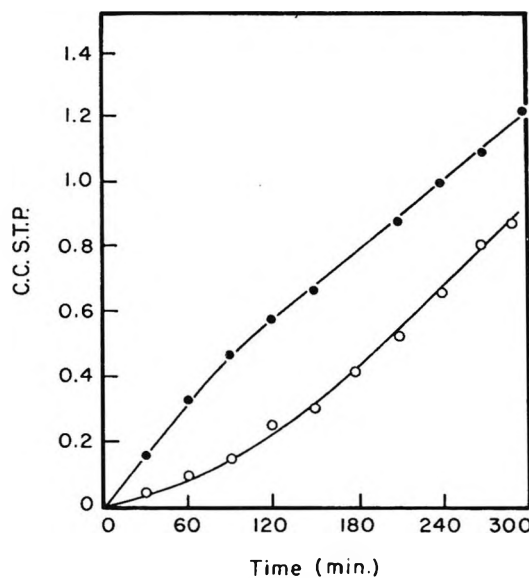


Figure 1. Sorption of hydrogen at -195°: open circles, pure palladium; solid circles, PdH_{0.23}.

drogen. The induction period is correspondingly longer.

Figure 2 shows a plot of the hydrogen uptake at 200 mm by pure palladium and PdH_{0.23} at -183°. The rate is an order of magnitude greater than at -195° and the induction period is much shorter. From these data it is much clearer that the sorption rate for pure palladium eventually becomes greater than that of PdH_{0.23}. At -183°, the rate of deuterium adsorption is about 30% of that for hydrogen.

Comparison of rates at -195 and -183° shows that the activation energy for sorption is of the order of 2-3 kcal. Extrapolation of these data shows that the rate should be about 10⁶ times faster at -78°. This is in agreement with the experimental observation that the half-time for sorption with an initial pressure of 200 mm of hydrogen is of the order of 5 sec at -78° compared to an estimated 10⁴ min at -195°.

Equilibration. At -195°, the rate of HD formation from a 50:50 H₂-D₂ mixture is quite low; for example, after 300 min exposure to the most active catalyst, about 1% of the gas phase is HD. As with sorption, there is a prolonged induction period for pure palladium, but none is evident for the hydrides. Equilibration rates were estimated from the straight-line portion of the curves of HD formation *vs.* time; these rates, relative to that for pure palladium, are plotted in Figure 3.

(9) L. J. Gillespie and F. P. Hall, *J. Am. Chem. Soc.*, **48**, 1207 (1926).

(10) Z. Knor, V. Ponec, and S. Cerney, *Kinetics Catalysis (USSR)*, **4**, 437 (1963).

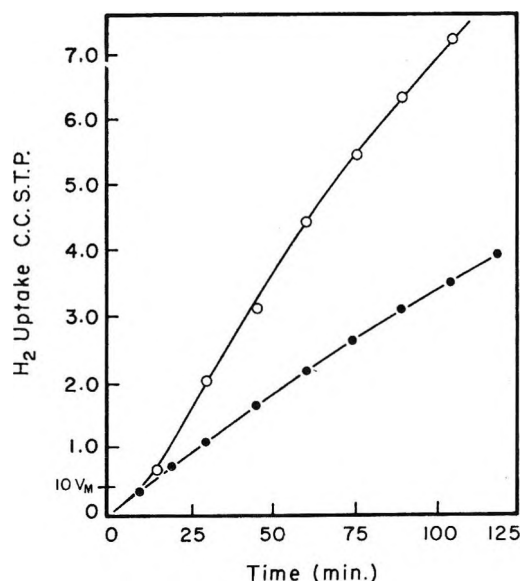


Figure 2. Sorption of hydrogen at -183° : open circles, pure palladium; solid circles, $\text{PdH}_{0.23}$.

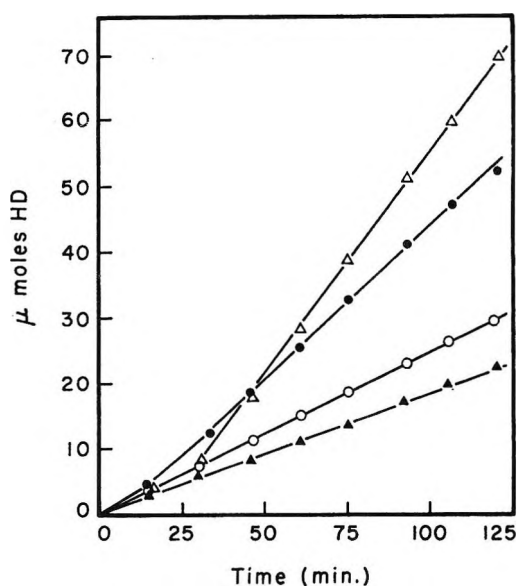


Figure 4. HD formation at -183° : open triangles, pure palladium; solid circles, $\text{PdH}_{0.066}$; open circles, $\text{PdH}_{0.233}$; solid triangles, $\text{PdH}_{0.408}$.

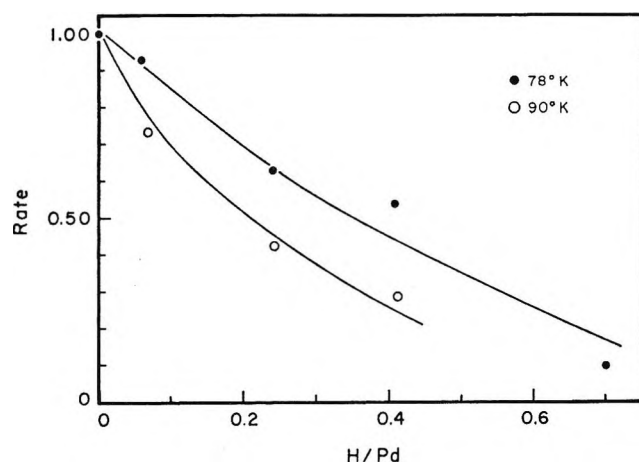


Figure 3. Relative equilibration rate vs. composition: solid circles, -183° ; open circles, -195° .

Figure 4 shows a plot of the amount of gaseous HD formed at -183° as a function of time when a catalyst with the indicated composition is exposed to a 50:50 $\text{H}_2\text{-D}_2$ reactant. In these runs, after 300 min, as much as 10% of the gas phase was HD. Comparison of the rates over pure palladium at -183 and -196° suggests that the activation energy for the equilibration is of the order of 2-3 kcal, a value comparable to that for sorption.

At -183° , the rate of sorption of hydrogen and deuterium from the reactant mixture could be obtained from the analysis and mass balance. The accuracy of these data was not as good as that shown in Figures

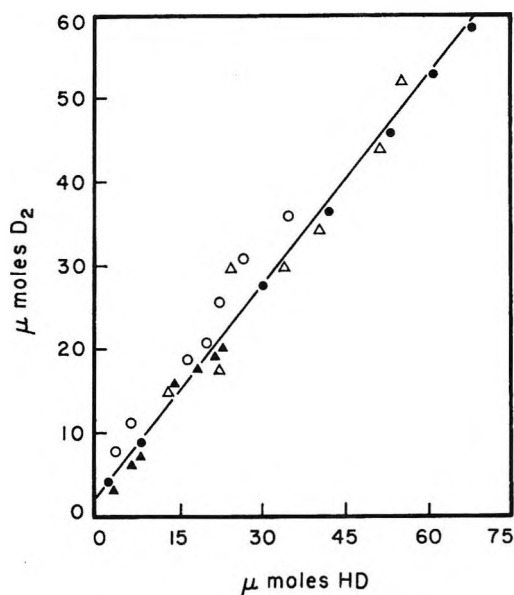


Figure 5. Deuterium uptake vs. HD formation at -183° : solid circles, pure palladium; open triangles, $\text{PdH}_{0.066}$; open circles, $\text{PdH}_{0.233}$; solid triangles, $\text{PdH}_{0.408}$.

1 and 2, but separate check experiments showed the rate data were reliable to about 10%. The hydrogen uptake curves were similar to those shown in Figure 2; the deuterium uptake curves were also qualitatively similar except for the curve for pure palladium which showed a more pronounced induction period than that in Figure 2. Quantitatively, the curves for deuterium

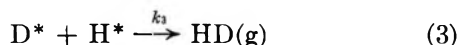
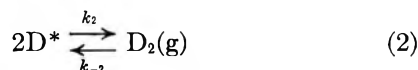
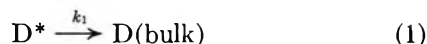
differed from those for hydrogen; the rate of deuterium uptake was only 25 to 30% that found for hydrogen.

Rates of deuterium sorption for the various catalysts at -183° were clearly similar to the rates of equilibration. This similarity is illustrated by Figure 5, which plots for each catalyst the amount of deuterium sorbed (as HD or D_2) vs. the amount of HD formed for each of the catalysts studied. In spite of the fact that the curves for equilibration (Figure 4) differ greatly in magnitude and shape, the plot in Figure 5 is represented by a single straight line through the origin within the experimental error.

For runs at -183° , the hydride composition changed significantly during the course of the reaction because of sorption. In Figure 3 we plot the relative rate of HD formation (from the straight line portion of Figure 4) vs. the initial H/Pd ratio. At the end of these experiments the ratio (H + D/Pd) was 0.02 to 0.04 higher than at the beginning of the experiment.

Discussion

Presumably, hydrogen adsorbed on palladium is in atomic form, and we can express the fate of an adsorbed deuterium atom, D^* , by the equations



The lack of exchange with palladium deuteride shows reaction 1 is irreversible; the reverse of reaction 3 is unlikely to be important when the amount of HD formed is low. With the steady-state approximation we obtain

$$-\frac{dD^*}{dt} = k_1(D^*) + \frac{1}{2}k_2(D^*)^2 - \frac{1}{2}k_{-2}D_2 + k_3(D^*)(H^*) = 0$$

wherein the rate constant, k_{-2} , probably depends on the surface coverage. The results show that we may write $k_1D^* = \beta k_3(D^*)(H^*)$, where β is the slope of the

line in Figure 5. When this is substituted in the above equation, we find

$$\frac{dHD}{dt} = k_3(H^*)(D^*) = \frac{k_{-2}(D_2) - k_2(D^*)^2}{2(\beta + 1)}$$

Figure 3 gives plots of the rates of HD formation relative to that for pure palladium as a function of hydride composition at -183 and -195° . If, *and only if*, β is a constant at all compositions, this plot also represents the net relative rate of formation of adsorbed deuterium atoms, *i.e.*, the rate of deuterium activation. At -183° , β is very nearly a constant (Figure 5); even at -195° , the less accurate adsorption data suggest β is a constant. Accordingly, Figure 3 suggests that the rate of deuterium activation approaches zero near H/Pd = 0.6.

The susceptibility also decreases linearly² with H/Pd and becomes zero at H/Pd = 0.66. Thus, it is clear that the change in catalytic activity parallels the change in magnetic susceptibility. In this concentration range ($0 < \text{H/Pd} < 0.66$) phase changes occur, the lattice parameter changes, and the holes in the d band are filled. No doubt all these factors influence the susceptibility and catalytic activity. It seems clear, however, that the simplest correlation is with the holes in the d band; as the d bands are filled, both the susceptibility and the activity decrease.

The constancy of β ($= k_1/k_3H^*$) implies that H^* is sensibly constant in the concentration range studied. This could be achieved if, due to the relative isotope effects for adsorption and bulk diffusion, the surface is sparsely covered with D^* and nearly covered with H^* . If this be so, the rate-determining process would be the reverse of reaction 2. (The forward reaction would be insignificant.) In this event, the similarity of the observed activation energies for sorption and exchange is to be expected.

Acknowledgment. Acknowledgment is made to the donors of the Petroleum Research Fund, administered by the American Chemical Society, for support of this research.

Micellar Properties and Critical Opalescence of Dimethylalkylphosphine Oxide Solutions

by K. W. Herrmann, J. G. Brushmiller, and W. L. Courchene

Miami Valley Laboratories, The Procter & Gamble Company, Cincinnati, Ohio 45239
(Received March 8, 1966)

Phase diagrams and light-scattering measurements of a homologous series of dimethylalkylphosphine oxides are used to determine the micellar molecular weights and their relation to consolute phase boundaries in these systems. The temperature dependence of micellar molecular weights is discussed with regard to both light-scattering and solution theory, and it is concluded that, in systems which show consolute boundaries, the light-scattering behavior can be qualitatively explained on the basis of existing theory without invoking any large temperature or concentration dependence of micellar molecular weight. The observed light-scattering behavior can easily be accounted for by the nonideality of a micellar solution and the temperature dependence of micellar-water interactions. Light-scattering measurements at the critical concentration for phase separation of the dimethyldodecylphosphine oxide-water system have also been made and show that critical opalescence is observed in this system. These results are discussed in the light of existing theoretical treatments of this phenomenon, and the experimental results are shown to agree qualitatively with the theory.

Introduction

In recent years there has been considerable work reported in the literature dealing with the micellar properties of nonionic surfactants,¹⁻⁸ particularly the alkylethylene oxide surfactants, $\text{CH}_3(\text{CH}_2)_m(\text{OCH}_2\text{CH}_2)_n\text{OH}$ ($m = 8-16$, $n = 6-9$).^{3,4,9-16} Aqueous solutions of these surfactants show "cloud points"; *i.e.*, relatively dilute solutions of these surfactants become very turbid at a well-defined temperature when the solution is heated.¹⁷ At temperatures above this "cloud point" the light-scattering turbidities of these surfactant solutions are large and very temperature dependent; however, the solutions have dissymmetries which are close to unity.^{11,12} The increase in solution turbidity with increasing temperature as the "cloud point" is approached has been interpreted as meaning that the micelle molecular weight increases exponentially with increasing temperature in these systems.^{1,8,11,12,15} We believe there may be another explanation.

This paper reports on the phase behavior and solution properties of the C_8 , C_{10} , and C_{12} homologs of di-

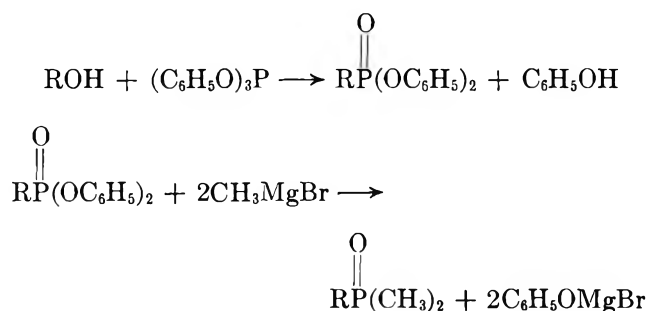
methylalkylphosphine oxide [$\text{C}_n\text{H}_{2n+1}\text{P}(\text{CH}_3)_2\text{O}$]. The three homologs will be abbreviated as DC_8PO , DC_{10}PO , and DC_{12}PO .

- (1) K. Shinoda, T. Nakagawa, B. Tamamushi, and T. Isemura, "Colloidal Surfactants. Some Physicochemical Properties," Academic Press Inc., New York, N. Y., 1963, Chapter 2.
- (2) L. M. Kushner, W. D. Hubbard, and A. S. Doan, *J. Phys. Chem.*, **61**, 371 (1957).
- (3) L. M. Kushner and W. D. Hubbard, *ibid.*, **58**, 1163 (1954).
- (4) M. J. Schick, S. M. Atlas, and F. R. Eirich, *ibid.*, **66**, 1326 (1962).
- (5) K. W. Herrmann, *ibid.*, **66**, 295 (1962).
- (6) W. L. Courchene, *ibid.*, **68**, 1870 (1964).
- (7) L. Benjamin, *ibid.*, **68**, 3575 (1964).
- (8) K. Kuriyama, *Kolloid-Z.*, **180**, 55 (1962).
- (9) T. Nakagawa and K. Tori, *ibid.*, **168**, 132 (1960).
- (10) J. M. Corkill, J. F. Goodman, and R. E. Ottewill, *Trans. Faraday Soc.*, **57**, 1627 (1961).
- (11) R. R. Balmbra, J. S. Clunie, J. M. Corkill, and J. F. Goodman, *ibid.*, **60**, 979 (1964).
- (12) R. R. Balmbra, J. S. Clunie, J. M. Corkill, and J. F. Goodman, *ibid.*, **58**, 1661 (1962).
- (13) J. M. Corkill, J. F. Goodman, and S. P. Harrold, *ibid.*, **60**, 202 (1964).
- (14) P. H. Elworthy and C. B. Macfarlane, *J. Chem. Soc.*, 537 (1962); 907 (1963).

The critical micelle concentrations (cmc) and micelle molecular weights (mmw) of these surfactants are presented and the effect of temperature on the scattering of light by dilute and concentrated DC₁₂PO solutions is reported and discussed. "Cloud point" phenomena are discussed in terms of consolute solution theory, and light-scattering data obtained at the critical concentration of DC₁₂PO are examined using Debye's critical opalescence theory. The solution properties of these surfactants are correlated with the phase boundaries shown by their respective systems, DC_nPO-H₂O.

Experimental Section

Materials. The C₈, C₁₀, and C₁₂ homologs of dimethylalkylphosphine oxide were prepared by a two-step synthesis.



All surfactants were greater than 99.5% pure as indicated by gas phase chromatography. Elemental analyses were as follows. *Anal.* Found for DC₈PO: C, 63.2; H, 12.0; P, 15.9. Found for DC₁₀PO: C, 65.6; H, 12.2; P, 13.5.

Light Scattering. A Phoenix Precision Instrument Co. light-scattering photometer (Model 1000) provided with narrow slits was used for all investigations except that dealing with the critical opalescence shown by DC₁₂PO which will be discussed separately. Measurements were made at 30° using a cylindrical cell (Catalog No. C-101) and using the blue line of mercury (λ 4358 Å). Calibration of the Phoenix instrument, temperature control, and the method of solution clarification were identical with those described previously.⁵ Scattered intensities observed at an angle of 90° are expressed as turbidities for dilute solutions near the cmc; the intensities for the more concentrated solutions are given simply as *I*₉₀. Dissymmetry values (*Z*₄₅) were calculated from

$$Z_{45} = \frac{I_{45}(\text{solution}) - I_{45}(\text{solvent})}{I_{135}(\text{solution}) - I_{135}(\text{solvent})}$$

Where the critical opalescence of DC₁₂PO solutions was examined, a Sofica light-scattering photometer

(Model 701-42000) was employed with the standard measuring cell (25-mm i.d.), λ 4358 Å, and the special temperature-controlled vat was equipped with a variable-speed magnetic stirrer. Calibration of this instrument was similar to that described earlier for the Phoenix instrument.⁵ For the critical opalescence study, the scattered intensity was measured as a function of angle at several temperatures. The intensities reported were obtained by multiplying the measured galvanometer readings by an instrument constant and the appropriate (sin θ)/(1 + cos² θ) correction factor. The temperatures of the solutions being examined were maintained constant within 0.05°.

Refractive Index Increments. A Brice-Phoenix differential refractometer was used to determine the refractive index increment (dn/dc) required for the calculation of micelle molecular weights. The instrument was calibrated with sucrose solutions using light of λ 4358 Å. Average dn/dc values from three or four solutions whose concentrations were above, but near, the cmc are reported.

Phase Studies. Fixed compositions of DC_nPO-H₂O were sealed in small (4-ml) glass test tubes and were equilibrated in a controlled-temperature bath. Continuous agitation was supplied by a mechanical rocking device. The temperatures at which phase separations occurred were determined on both heating and cooling over the range -5 to 200°, the system being under considerable pressure at the higher temperatures. Separation of a second isotropic phase was indicated by a great increase in turbidity; marked birefringence, shown by the samples being equilibrated between crossed nicols, was observed when a mesomorphic phase formed. Surfactant crystals could be detected with the eye. At least two heating and cooling cycles were made to obtain the results reported. Identification of the mesomorphic phases was made using a polarizing-light microscope and the characteristic "textures" reported by Rosevear.¹⁸

Results and Discussion

Phase Behavior of DC_nPO Surfactants. The phase diagrams for DC₈PO, DC₁₀PO, and DC₁₂PO in water are shown in Figures 1, 2, and 3, respectively. The middle and neat phases exhibited by these surfactants are typical mesomorphic (liquid crystal) phases¹⁸⁻²⁰

(15) P. H. Elworthy and C. McDonald, *Kolloid-Z.*, **195**, 16 (1964).

(16) C. W. Diggins, Jr., and R. J. Bolen, *J. Phys. Chem.*, **65**, 1787 (1961).

(17) W. N. Maclay, *J. Colloid Sci.*, **11**, 272 (1956).

(18) F. B. Rosevear, *J. Am. Oil Chemists' Soc.*, **31**, 628 (1954).

(19) A. J. Mabis, *Acta Cryst.*, **15**, 1152 (1962).

(20) V. Luzzati, H. Mustacchi, and A. Skoulios, *Nature*, **180**, 600 (1957); *Discussions Faraday Soc.*, **25**, 43 (1958).

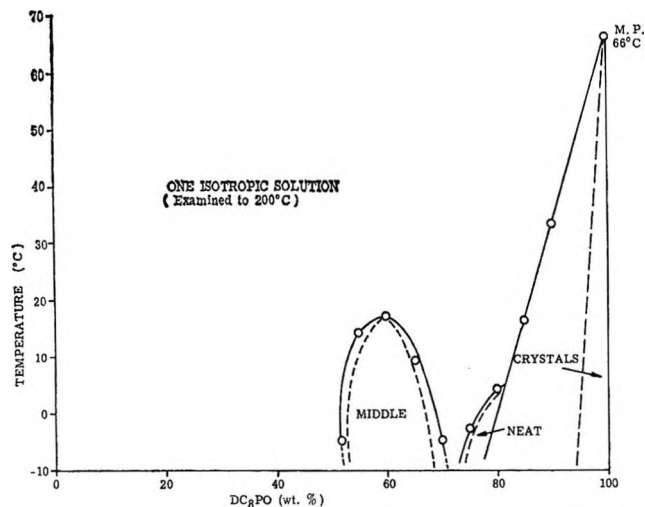


Figure 1. Phase diagram for dimethyloctylphosphine oxide-water.

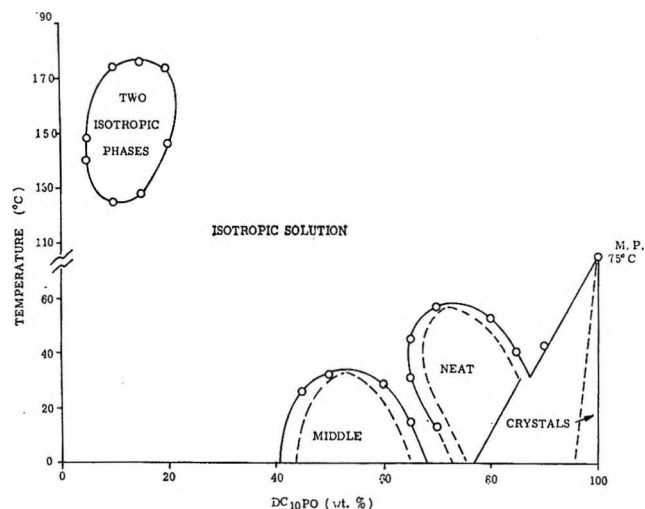


Figure 2. Phase diagram for dimethyldodecylphosphine oxide-water.

and will not be considered any further in this paper. The part of the phase diagram of particular interest here is the region where two immiscible isotropic solutions coexist (Figures 2 and 3). In binary solution terminology,²¹ the two immiscible isotropic solutions are referred to as conjugate solutions. The temperature at which phase separation occurs is called an upper consolute temperature when a maximum occurs in the phase boundary. The surfactant concentration at which the maximum or minimum occurs is called the critical concentration. The temperature at which the maximum occurs in the consolute boundary is called an upper critical solution temperature, and the temperature at which the minimum occurs in the

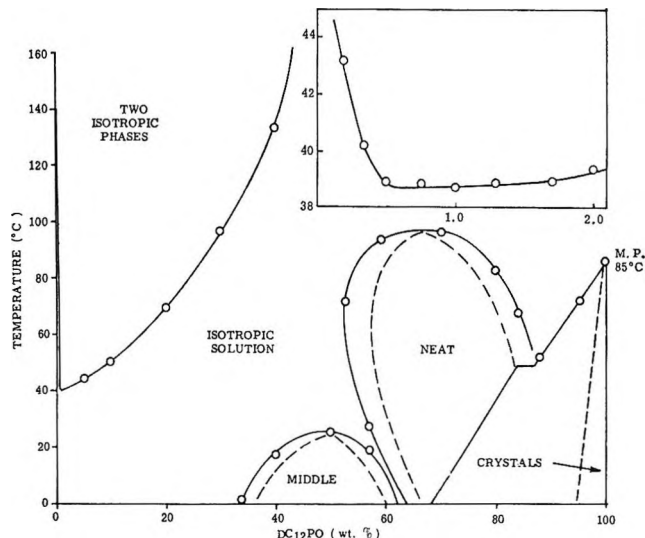


Figure 3. Phase diagram for dimethyldodecylphosphine oxide-water. Insert shows consolute boundary at low concentrations.

consolute temperature is called a lower critical solution temperature. Thus, while DC₈PO does not form immiscible isotropic solutions at the temperature examined, both the DC₁₀PO and DC₁₂PO binary systems do exhibit critical solution behavior. If one examines phase data for ethylene oxide surfactant-water systems published in the literature,^{11,12} it can be seen that the term "cloud point," as used by the authors, is really the lower consolute temperature of the system. Hence, we equate the term "cloud point" and lower consolute temperature.

The temperature and composition ranges over which conjugate solutions exist in the dimethylalkylphosphine oxide-water systems decrease with decreased alkyl chain length in the surfactant (see Figures 1, 2, and 3). Only DC₁₂PO exhibits a lower consolute boundary which extends over a wide range of temperatures and compositions; the critical solution temperature and concentration were visually estimated to be approximately 38.8° and about 0.7% DC₁₂PO, respectively. The DC₁₀PO system exhibits both an upper and lower consolute boundary with critical temperatures of about 177 and 124°, respectively, and critical concentrations between 10 and 15% DC₁₀PO. Considerable pressure must have developed in the sealed phase tubes at the temperatures where the conjugate solutions of DC₁₀PO were observed; the effect of pressure on this type of phase separation is unknown. The DC₈PO system does not form conjugate solutions below 200°.

General Light-Scattering Properties and Theory.

(21) S. Glasstone, "Textbook of Physical Chemistry," 2nd ed, D. Van Nostrand Co., Inc., New York, N. Y., 1946, Chapter X.

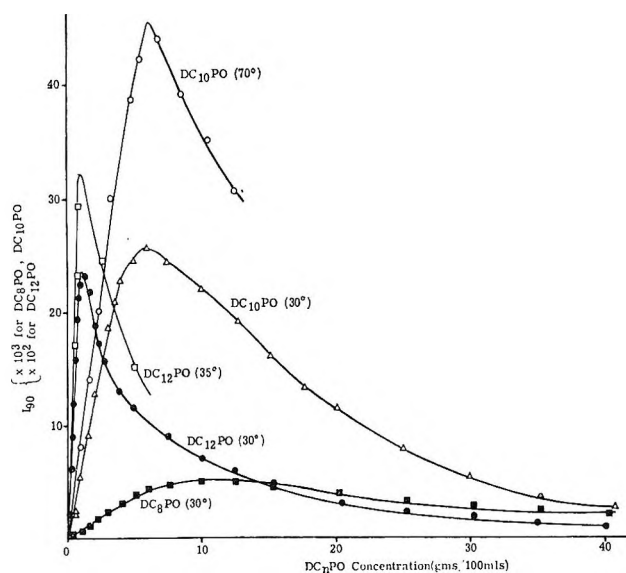


Figure 4. Scattered light intensity of DC_nPO solutions.

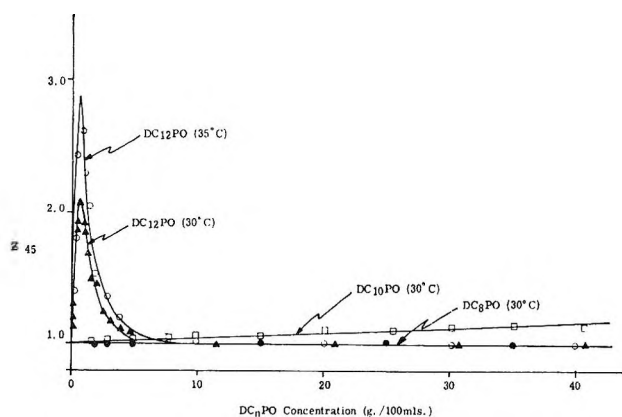


Figure 5. Dissymmetry of DC_nPO solutions.

Figures 4 and 5 show the concentration dependence of scattered light intensity (I_{90}) and dissymmetry (Z_{45}) for solutions of DC_8PO , $DC_{10}PO$, and $DC_{12}PO$ at 30° up to surfactant concentrations of 40 g/100 ml. All three surfactant systems exhibit a turbidity maximum in their respective turbidity vs. concentration curves. This behavior is similar to that observed for other nonionic surfactants such as the alkylethylene oxides^{11,12} and dimethylalkylamine oxide,²² but is slightly different from that observed for anionic surfactant systems.²³ Only $DC_{12}PO$ shows a dissymmetry maximum.

To explain properly the light-scattering data obtained for both dilute and concentrated surfactant solutions in systems exhibiting a lower consolute boundary, it is necessary to review briefly the theoretical basis for light scattering by solutions. According to Einstein

and Debye,²⁴ the excess turbidity (τ) of a solution is given by

$$\tau = HcRT/(d\Pi/dc) \quad (1)$$

where H is an optical constant equal to $32\pi^3n_0^2(dn/dc)^2/3N\lambda^4$. Here n_0 is the refractive index of the solvent, N is Avogadro's number, λ is the wavelength of the incident radiation *in vacuo*, dn/dc is the specific refractive index increment of the solute, Π is the osmotic pressure of the solution, R and T are the gas constant and absolute temperature, respectively, and c is the concentration of solute. Equation 1 holds as long as the scattering entities are small compared with the wavelength of the light and can be rearranged to

$$\frac{d\Pi}{dc} \frac{1}{RT} = \frac{Hc}{\tau} \quad (2)$$

Thus, as pointed out by Debye,²⁴ Hc/τ is intimately connected with the behavior of the osmotic pressure of the solution and is directly proportional to the slope of the Π vs. c plot. If the light-scattering experiment is carried out on very dilute solutions, the van't Hoff expression ($\Pi = RTc/M$) may adequately describe the concentration dependence of Π . For higher concentrations a modified expression is often used [$\Pi = RTc(1/M + Bc)$]. Figure 6 shows the expected behavior of the osmotic pressure in such solutions and also illustrates the concentration dependence of $d\Pi/dc$, which is equivalent in form to that expected for Hc/τ . When we are dealing with a binary solution exhibiting a critical concentration and a critical consolute temperature, osmotic pressure, $d\Pi/dc$, and Hc/τ will behave as shown in Figure 7²⁵ in the region of the critical point. Near the critical concentration $d\Pi/dc$ and Hc/τ are markedly dependent on concentration and decrease as the solution temperature approaches the critical temperature; these values become zero at the critical concentration and at the critical temperature. In our surfactant systems, and perhaps in others showing lower consolute boundaries, this means that turbidity data must be obtained as close to the critical micelle concentration (cmc) as possible if valid micelle molecular weights are to be obtained by the usual practice of extrapolating Hc/τ curves to the cmc. This point will be discussed in greater detail in the next section.

(22) J. M. Corkill and K. W. Herrmann, *J. Phys. Chem.*, **67**, 934 (1963).

(23) J. N. Phillips and K. J. Mysels, *ibid.*, **59**, 325 (1955).

(24) A. Einstein, *Ann. Physik*, **33**, 1275 (1910); P. Debye, *J. Appl. Phys.*, **15**, 338 (1944); *J. Phys. Colloid Chem.*, **51**, 18 (1947).

(25) O. K. Rice, *ibid.*, **54**, 1293 (1950).

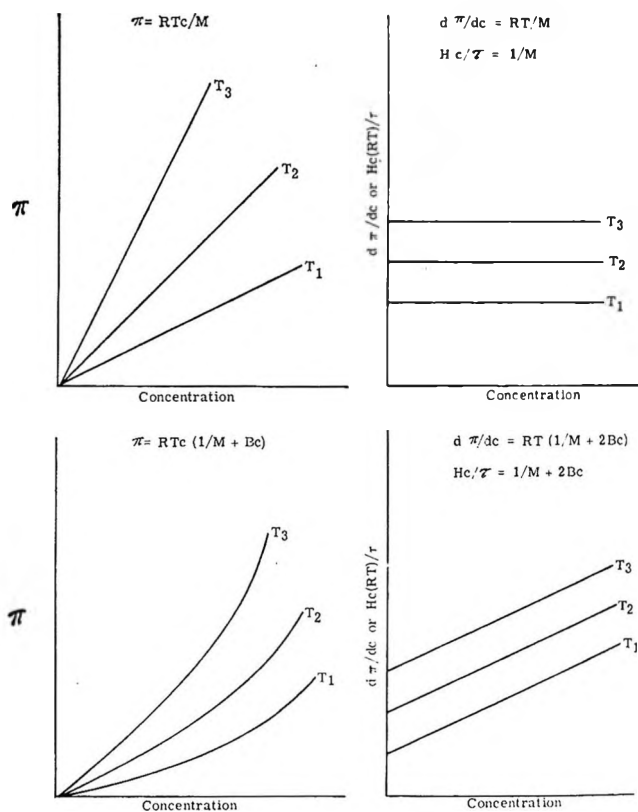


Figure 6. Hypothetical osmotic-pressure and light-scattering curves in the absence of a consolute boundary.

It is obvious from Figure 7 that the presence of a lower consolute boundary indicates solution non-ideality which complicates the interpretation of light-scattering data at surfactant concentrations well above the cmc, for, now, observed variations of Hc/τ with concentration may be due not only to changes in molecular weight but also to the extreme nonideality. This point also will be treated further in a subsequent section.

Micellar Properties of Dimethylalkylphosphine Oxide Surfactants near the Cmc. The cmc's and weight-average micelle molecular weights (mmw) of the DC₈PO, DC₁₀PO, and DC₁₂PO surfactants in water at 30° were determined by the usual light-scattering techniques. Since the DC₁₂PO surfactant system possesses a lower consolute boundary having a critical concentration at 0.5 g/100 ml, as indicated by dissymmetry results (Figure 5), and a critical temperature of about 38.8°, light-scattering data were obtained at surfactant concentrations just above the cmc. Figures 8–10 show both the total solution turbidity *vs.* concentration plots and the $H(c - c_0)/(\tau - \tau_0)$ *vs.* $c - c_0$ plots for DC₈PO, DC₁₀PO, and DC₁₂PO, respectively. In the above expression, H is the previously defined optical constant, c is the total surfactant concentration

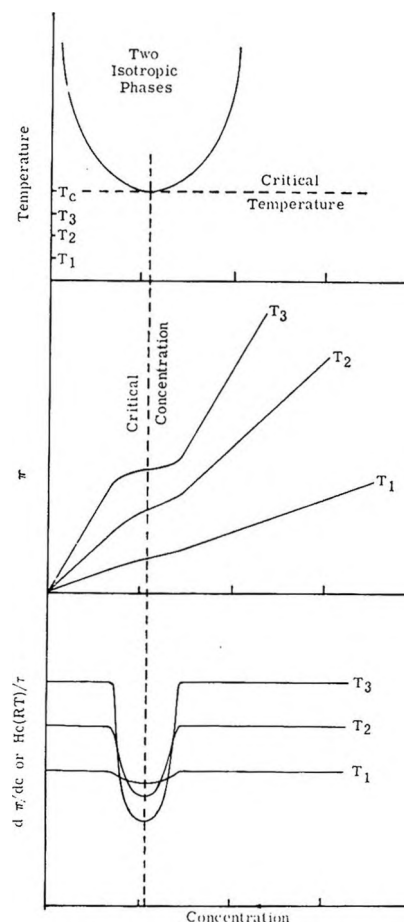
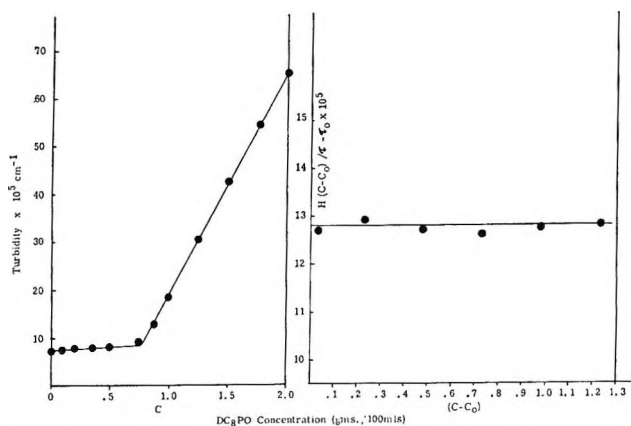
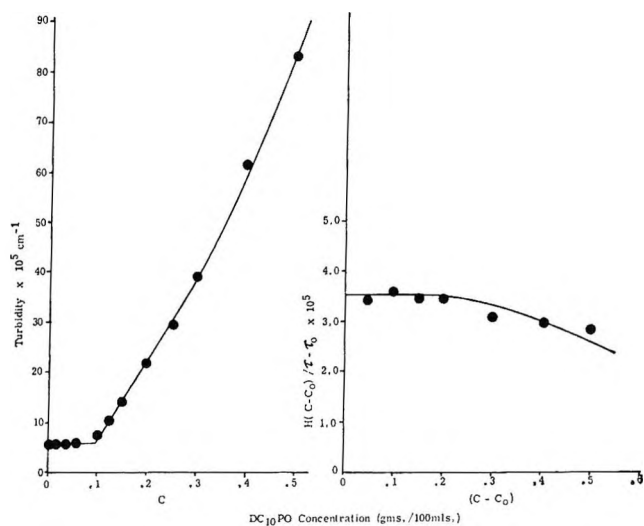
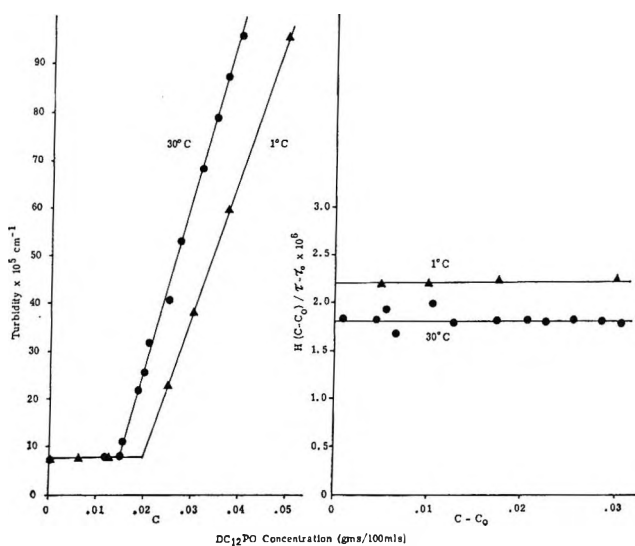


Figure 7. Hypothetical osmotic-pressure and light-scattering curves for system showing consolute boundary.

in g/100 ml, c_0 is the critical micelle concentration, τ is the total turbidity of the solution, and τ_0 is the turbidity at the cmc. Table I summarizes the results of the light-scattering studies and in addition gives some cmc values determined from surface tension data. It can be seen from the data in Table I that the cmc's determined from surface tension measurements are lower than those determined from light-scattering data. Several other investigators have also observed this difference;^{10,12} the specific reason for it is unknown at present. In making the Hc/τ plots, the light-scattering cmc's were used; using a cmc obtained from surface tension measurements would yield a curve that increases nonlinearly as zero concentration ($c - c_0$) is approached.

Light-scattering experiments were also carried out on dilute solutions of DC₁₂PO at 1° to determine the micelle molecular weight at a temperature some distance removed from the lower consolute boundary (Figure 10). The cmc is 0.020 g/100 ml and the mmw is 460,000. This corresponds to about a 20% decrease in

Figure 8. Light-scattering results for DC₃PO.Figure 9. Light-scattering results for DC₁₀PO.Figure 10. Light-scattering results for DC₁₂PO.**Table I:** Micellar Properties of Some Dimethylalkylphosphine Oxide Surfactants

Surfactant	Temp, °C	Cmc, g/100 ml			Mmw
		Light scattering	Surface tension	dn/dc, ml/g	
DC ₃ PO	30	0.77	0.79	0.148	7,800
DC ₁₀ PO	30	0.10	0.082	0.144	28,600
DC ₁₂ PO	30	0.014	0.008	0.155	555,000
DC ₁₂ PO	1	0.020	458,000

mmw for a 29° reduction in temperature, a small temperature effect compared to those reported in the literature for other nonionic surfactants having a lower consolute boundary.^{8,11,12,15} Unless there is a threshold temperature above which the micelle molecular weight increases exponentially,¹⁵ and the existence of such a point above 30° cannot be ruled out on the basis of these experiments, the reported exponential increase in micelle molecular weight with temperature^{8,11,12,15} may indeed only be reflecting the variation of $d\Pi/dc$ with temperature as the critical temperature is approached and not a true variation in molecular weight. Micelle molecular weights have sometimes been determined from the minimum in the Hc/τ plots¹¹ which presumably occur at or near the concentration where the minimum in the lower consolute boundary occurs. Based on the previous discussion and Figure 7, we would predict that $d\Pi/dc$ or Hc/τ at the critical concentration should decrease as the critical temperature is approached. This could make it appear that the temperature dependence of molecular weight is very large. If the molecular weights were compared at or near the cmc, as we have done, such a marked temperature dependence might not have been observed. We have concluded that the higher order concentration terms in the osmotic pressure equations are highly temperature dependent for systems having lower consolute boundaries and that it is, therefore, improper to interpret quantitatively light-scattering data for these systems in terms of micellar molecular weights at any concentration other than infinite dilution of the micelles, *i.e.*, at or very near the cmc.

It can be seen from the data in Table I that increasing the alkyl chain length attached to the hydrophilic head group decreases the cmc and increases the mmw. A decrease in free energy of micellization of $1.06kT$ is calculated from the light-scattering cmc data for an increase of one CH₂ group. This agrees well with values of this parameter obtained previously for other surfactants.¹ The very high micelle molecular weight found for the DC₁₂PO surfactant as compared to the

DC₈PO and DC₁₀PO surfactants is unusual and suggests that the DC₁₂PO surfactant possesses a much different micellar structure than its C₈ and C₁₀ homologs. The shape of the DC₁₂PO micelles is likely to be that of a cylinder or prolate ellipsoid of high axial ratio and a radius comparable to the extended length of a single surfactant molecule, while the DC₈PO and DC₁₀PO micelles are most likely spheres of radii comparable to their respective surfactant molecular lengths.

Concentrated Solutions. Figure 4 shows that solutions of all three DC_nPO surfactants exhibit a turbidity maximum in their turbidity-concentration curves. This is similar to the behavior observed for dimethylalkylamine oxides.²² Debye and Bueche²⁶ have suggested that such maxima might be used to estimate the molecular weight of polymers. In their analysis a Flory-Hildebrand type of expression for the osmotic pressure is substituted into eq 1 and an expression similar to (3) is obtained for the excess turbidity of the solution

$$\tau = HcMV_1 \left[V_1 + M\bar{v}^2c \left(\frac{1}{1 - c\bar{v}} - 2\chi \right) \right] \quad (3)$$

where H and c have the same meaning as in eq 1, and \bar{v} , M , V_1 , and χ are the partial specific volume, the molecular weight of the solute, the molar volume of solvent, and the dimensionless parameter characterizing solute-solvent interactions, respectively. Differentiation of (3) with respect to concentration leads to the fact that a turbidity maximum will occur at a concentration given by

$$c_{\max}\bar{v} = \frac{1}{1 + (M\bar{v}/V_1)^{1/2}} \quad (4)$$

Since M is large, the molecular weight corresponding to the concentration at which the maximum occurs may be calculated from

$$M = \frac{V_1}{\bar{v}^2 c_{\max}^2} \quad (5)$$

Equation 5 was applied to the dimethylalkylphosphine oxides with the results shown in Table II. It is apparent that molecular weights determined in this way (M at c_{\max}) are low when compared to those determined by the usual extrapolation of a light-scattering Hc/τ vs. concentration curve (M_{cmc}). However, they are qualitatively in the correct order and differ from the correct molecular weight by a relatively constant factor. The deficiencies of a Flory-Hildebrand type of free energy of mixing expression are well known, and quantitative agreement of experimental data with expressions derived from this theory would not be

Table II: Molecular Weight by Debye-Bueche Method

Surfactant	\bar{v} , ml/g ^a	c_{\max} , g/100 ml	M at c_{\max}	M_{cmc}/M at c_{\max}
DC ₈ PO	1.09	9.89	1,420	5.5
DC ₁₀ PO	1.11	5.59	4,210	6.7
DC ₁₂ PO	1.11	1.13	102,000	5.5

^a L. Benjamin, private communication.

expected for surfactant-water systems. Qualitative predictions of the theory would be expected to apply since it was derived for solutions of big solute molecules in a solution containing much smaller solvent molecules.

It is instructive to consider some of the predictions of this theory with regard to surfactant-water systems. For example, the theory predicts separation of the solution into two homogeneous isotropic solutions whenever χ reaches a critical value given (approximately) by the expression²⁷

$$\chi_c = 0.5 + (V_1/M\bar{v})^{1/2} \quad (6)$$

As originally derived this could lead only to an upper critical temperature, but if the temperature dependence of χ is more than just linear (quadratic in $1/T$), then a lower critical temperature can also occur.²⁸ Based on mmw's determined at infinite dilution of micelles, χ_c for DC₁₀PO and DC₁₂PO are 0.523 and 0.505, respectively.

Furthermore, if χ is such a function of temperature and increases as the lower critical temperature is approached, the turbidity-concentration curves for the surfactant-water system should behave as shown in Figure 11, where we have plotted τ vs. concentration for a hypothetical micellar solution using eq 3 and several values of χ . The dependence of the initial slope of the τ - c curve on the value of χ means this slope will be a function of temperature, generally increasing with increasing temperature. Such behavior is observed by us, as shown in Figure 4, and has been observed by other workers who examined other surfactant-water systems.^{8,11,12} Note, however, that there is little, if any, change in the position of the turbidity maximum with increasing temperature suggesting that large molecular weight changes are not occurring as temperature is increased (*cf.* previous discussion regarding τ_{\max} and mmw results at 1 and 30° for DC₁₂PO quoted earlier). It should be pointed out that theory predicts that the turbidity maximum,

(26) P. Debye and A. M. Bueche, *J. Chem. Phys.*, **18**, 1423 (1950).

(27) P. J. Flory, "Principles of Polymer Chemistry," Cornell University Press, Ithaca, N. Y., 1953.

(28) P. Debye, private communication.

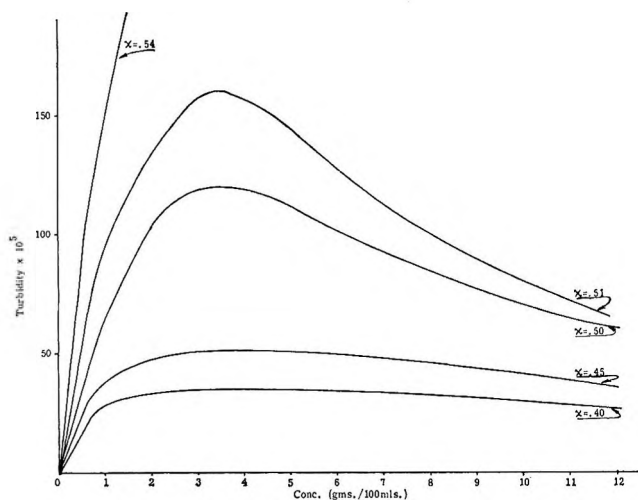


Figure 11. Theoretical curves calculated from eq 3; $V_1 = 18$, $M = 10,000$, $\bar{v} = 1.125$, $H = 6.9 \times 10^{-6}$.

dissymmetry maximum, and the critical temperature for separation of the system into two isotropic solutions will occur at the same concentration. Figures 2–5 show that these conditions are approximately met for DC₁₀PO and DC₁₂PO. The magnitude of this turbidity maximum is strongly dependent upon temperature (the value of χ), and this does not necessarily mean that molecular weight is increasing rapidly with temperature.

To carry the application of this theory one step further, Figure 12 shows an Hc/τ vs. concentration curve for DC₁₂PO and a theoretical curve calculated from eq 3 using the molecular weight found by extrapolation of the dilute solution light-scattering results and the other parameters shown in Figure 12. It is obvious that there is quite good qualitative agreement of the two curves. It therefore seems unnecessary, as has sometimes been done, to invoke an increase in micelle molecular weight with increasing concentration to account for the negative slope of an Hc/τ vs. concentration curve slightly above the cmc. It does not appear to be possible using light-scattering data alone to decide whether negative slopes in Hc/τ vs. concentration curves for surfactant–water systems are due to increasing molecular weight of the micelle or to contributions to nonideality of the solution at quite low concentrations due to solvent–solute, solute–solute, and solvent–solvent interactions.

It would appear that a Flory–Hildebrand type of mixing theory qualitatively predicts the behavior observed in surfactant–water systems, but quantitative agreement of experiment with theory must await the development of a more refined free energy of mixing expression for surfactant–water systems.

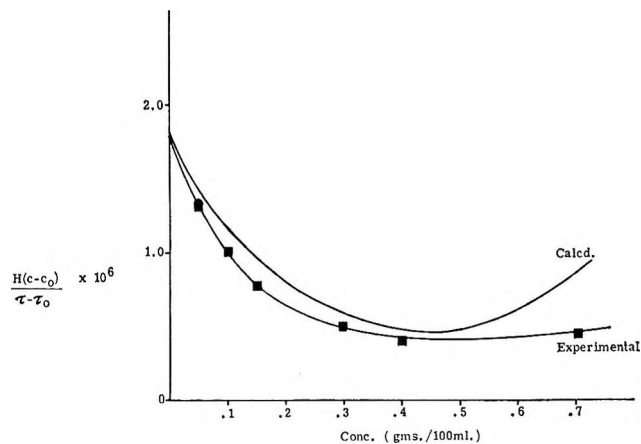


Figure 12. Comparison of theory and experiment for DC₁₂PO solutions. Calculated curve from eq 3; $\bar{v} = 1.1$, $\chi = 0.5046$, $M = 555,000$.

Critical Opalescence in DC₁₂PO–H₂O Solution. Figure 5 shows that the dissymmetry (Z_{45}) exhibited by solutions of DC₁₂PO at 30° has a maximum at a concentration of 0.5 g/100 ml, very close to the concentration at which a minimum occurs in the lower consolute boundary. This is believed to be due to critical opalescence, similar to that observed in high polymer solutions^{29–34} and several other binary systems.^{35–38} This phenomenon has received much experimental and theoretical attention in recent years. Debye³⁹ has generalized the light-scattering fluctuation theory of Smoluchowski–Einstein to present an explanation for the strong dissymmetry near the critical point and has extended the theory to binary critical mixtures.³¹ Several other authors^{40–42} have presented theoretical treatments which give results nearly equivalent to those of Debye. The Debye theory depends upon the fact that the

(29) P. Debye, H. Coll, and D. Woermann, *J. Chem. Phys.*, **33**, 1746 (1960).

(30) P. Debye, B. Chu, and D. Woermann, *ibid.*, **36**, 1803 (1962).

(31) P. Debye, *ibid.*, **31**, 680 (1959).

(32) D. McIntyre, A. Wims, and M. S. Greer, *ibid.*, **37**, 3019 (1962).

(33) R. Fürth and C. L. Williams, *Proc. Roy. Soc. (London)*, **A224**, 104 (1954).

(34) P. Debye, D. Woermann, and B. Chu, *J. Polymer Sci.*, **A1**, 255 (1963).

(35) B. Zimm, *J. Phys. Colloid Chem.*, **54**, 1306 (1950).

(36) B. Chu, *J. Chem. Phys.*, **41**, 226 (1964).

(37) B. Chu, *J. Am. Chem. Soc.*, **86**, 3557 (1964).

(38) B. Chu and W. P. Kao, *Can. J. Chem.*, **43**, 1803 (1965).

(39) P. Debye in "Scattering of Radiation by Noncrystalline Media in Noncrystalline Solids," V. D. Fechet, Ed., John Wiley and Sons, Inc., New York, N. Y., 1960, pp 1–25.

(40) M. Fixman, *J. Chem. Phys.*, **33**, 1357 (1960).

(41) A. Münster, *J. Chim. Phys.*, **57**, 492 (1960).

(42) E. W. Hart, *J. Chem. Phys.*, **34**, 1471 (1961).

scattered light intensity depends not only on the average square of the amplitude of the fluctuations, but also on the average square of the gradient of the fluctuations. It is near the critical point that this additional term becomes important.

According to the Debye theory, the relative scattered intensity should be given by eq 7 if the composition of the binary mixture corresponds to the critical concentration^{36,43}

$$\frac{1}{I} = F(T)(T_c/T) \left[\frac{\Delta T}{T_c} + \frac{8\pi^2 l^2}{3\lambda^2} \sin^2 \frac{\theta}{2} \right] = A + B \sin^2 (\theta/2) \quad (7)$$

I is the relative scattered intensity, T is the temperature in degrees Kelvin, T_c is the critical temperature for phase separation, $\Delta T = T - T_c$, λ is the wavelength of the light in the medium, l is the molecular interaction range, and θ is the scattering angle. The nature of the correction factor $F(T)$ has been discussed,³⁶ but its exact form is unimportant as long as it has no angular dependence. Equation 7 predicts that measurement of light-scattering intensity at several angles for small temperature distances from T_c should give plots of $1/I$ vs. $\sin^2 (\theta/2)$ which are linear with slope B and intercept A . The treatment of the data has been described elsewhere.^{36,43} Figure 13 is such a plot for DC₁₂PO at several different temperatures and a concentration of 0.5 g/100 ml. Straight lines are indeed obtained indicating that the phenomenon of critical opalescence is being observed and that the approximate Debye theory is being obeyed. It is a further consequence of the theory that the zero-angle intensity should be proportional to $(T - T_c)^{-1}$ if the scattered intensity of the critical mixture is high. This is also the case for DC₁₂PO since Figure 14 shows the reciprocal of the zero-angle intensity plotted against temperature.

From eq 7

$$\frac{A}{B} = \frac{3\lambda^2}{8\pi^2 l^2 T_c} (T - T_c) \quad (8)$$

and therefore a plot of A/B vs. temperature can be used to obtain both T_c and l . Figure 15 is such a plot for the DC₁₂PO system from which is found $T_c = 40.2^\circ$, in reasonably good agreement with the visually observed value of 38.8° . The molecular interaction range (l) is found to be 140 Å. This value is considerably larger than any of the previously reported values for other systems, all of which have been reviewed by Chu.³⁷ This may result from the fact that the Debye theory for binary mixtures includes the use of a Flory-Hildebrand type of free energy of

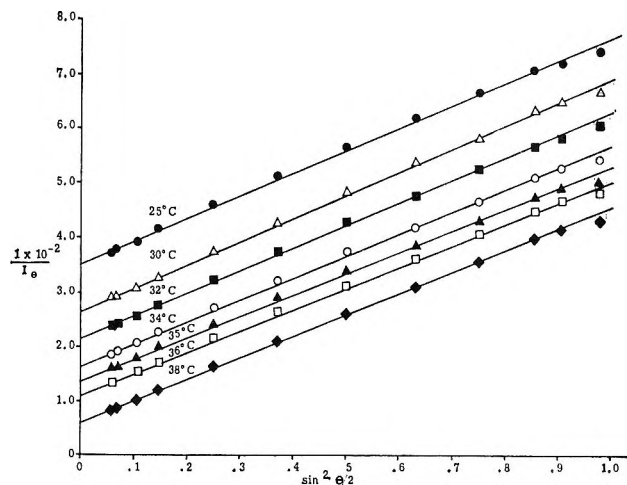


Figure 13. Reciprocal relative scattered intensity vs. $\sin^2 (\theta/2)$ for a solution of 0.5 g of DC₁₂PO/100 ml.

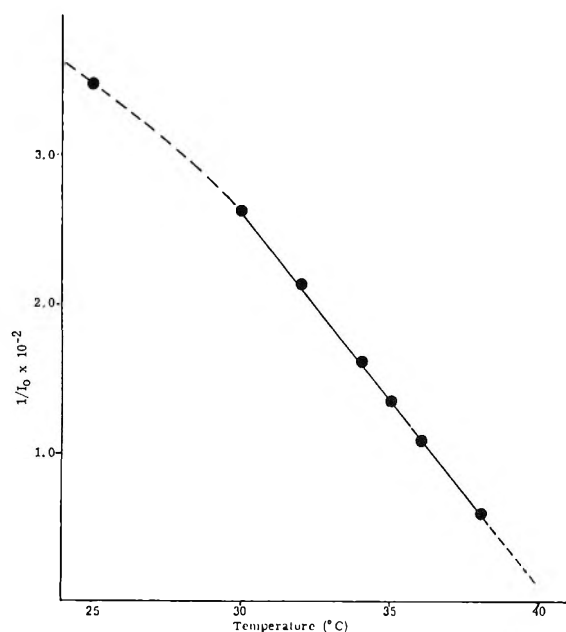
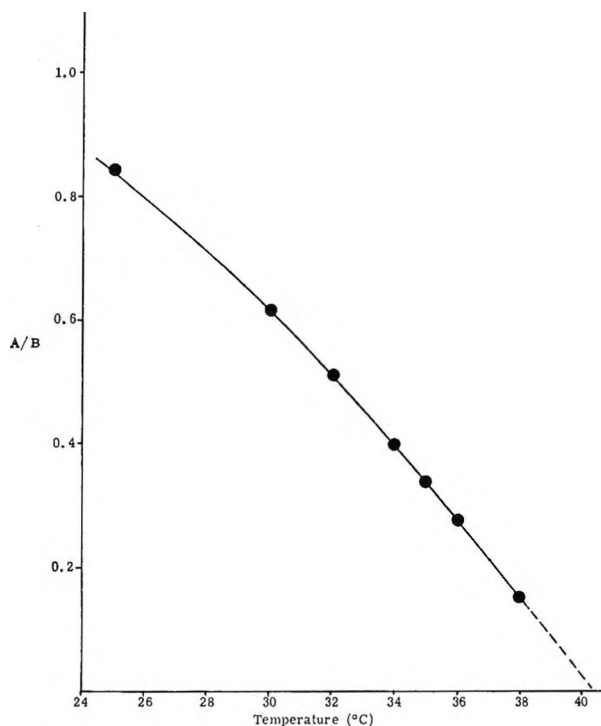


Figure 14. Reciprocal zero-angle intensity (I_0) vs. temperature.

mixing expression. Such an expression has only qualitative significance in surfactant-water systems as was pointed out previously in this discussion. There is one other point to be made about the l value obtained for the DC₁₂PO-H₂O system. This involves the fact that the curve of Figure 15 is not a straight line but has curvature when the temperature is more than 8–10° away from the critical temperature. Debye³⁰ has discussed the problem of whether l is temperature dependent for the case of polystyrene-cyclohexane and

(43) P. Debye, B. Chu, and H. Kaufmann, *J. Chem. Phys.*, **36**, 3378 (1962).

Figure 15. A/B vs. temperature.

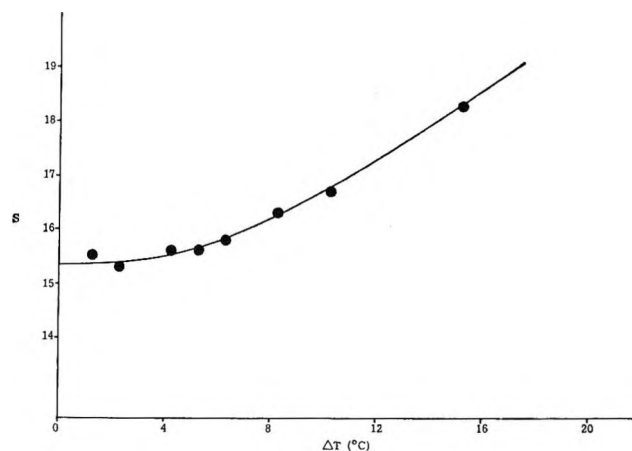
concluded that it was not. In order to show this, a quantity S is defined, given in the simple theory described above by

$$S = (B/A)\Delta T = \frac{8\pi^2 l^2}{3\lambda^2} T_c \quad (9)$$

Figure 16 is a plot of S vs. ΔT for the $\text{DC}_{12}\text{PO-H}_2\text{O}$ system. If l were temperature independent, this would be parallel to the abscissa. However, the fact that curvature is observed does not necessarily mean that l is temperature dependent, especially since the curve is parallel to the abscissa at small temperature distances from T_c . In the case of polystyrene-cyclohexane, where the polystyrene is of large enough molecular weight to contribute to the dissymmetry because of the extension of the polymer coil, Debye³⁰ showed that the quantity S , defined in eq 9, should really be written as

$$S = (B/A)\Delta T = \frac{8\pi^2 l^2}{3\lambda^2} T_c + \frac{16\pi^2 r^2}{3\lambda^2} \Delta T \quad (10)$$

Since the radius of gyration (r) is temperature de-

Figure 16. S vs. ΔT .

pendent for the polystyrene-cyclohexane case, the S - T curve for that system shows curvature of the kind shown in Figure 16 for our system. At large temperature distances from the critical point (1°), dissymmetry (Z_{45}) is still observed in a 0.5 g/100 ml solution of DC_{12}PO indicating that some theoretical equation similar to eq 10 should apply to our case rather than the simple theory represented by eq 9. Also, since the molecular weight of the micelle changes with temperature (Table I), the S - T curve should not be a straight line but should be curved owing to this temperature dependence. How this theory should be formulated to obtain both the range of molecular forces and the size of the micelles for a surfactant-water system is a difficult question, especially since the micellar aggregation number is probably both temperature and concentration dependent. In any case, the system qualitatively obeys the Debye critical opalescence theory. Results similar to those shown in Figures 13-16 were also obtained at a concentration of 1 g of $\text{DC}_{12}\text{PO}/100$ ml, which is well removed from the concentration at which the dissymmetry maximum occurs.

Acknowledgments. We gratefully acknowledge the assistance of Dr. R. G. Laughlin, who prepared the DC_nPO surfactants, and that of Dr. R. C. Mast, who determined the surface tension cmc values. We are especially indebted to Professor P. Debye for his encouragement and for many helpful discussions regarding the applicability of light-scattering and consolute-solution theory to the surfactant solutions studied.

The Reaction of Isopropylbenzene on γ -Irradiated Silica Gels

by Enrique A. Rojo and Robert R. Hentz

Department of Chemistry and the Radiation Laboratory,¹ University of Notre Dame, Notre Dame, Indiana 46556
(Received March 9, 1966)

Dealkylation of isopropylbenzene was studied on three γ -irradiated silica gels. Little or no visible coloration occurs in these solids on irradiation at 37° to doses of 4×10^{21} ev g⁻¹. The yield of benzene initially increases linearly with dose to the solid but approaches a limiting value at large doses; for one of the solids, limiting yields were 2.6 and 15.5 in units of 10^{17} molecules (g of solid)⁻¹ at 37 and -196°, respectively. Initial slopes correspond to $G_0(\text{C}_6\text{H}_6) = 0.067$ at 37° and $G_0(\text{C}_6\text{H}_6) = 4$ at -196°; the latter value suggests a trapping efficiency for free charge carriers of near 100%. Room-temperature annealing of solid irradiated to saturation at -196° gives a limiting yield identical with that attained in a 37° irradiation. Therefore, the 37° limiting yield must correspond to essentially complete population of certain solid defects. Room-temperature irradiation of solid irradiated to saturation at -196° reduces the benzene yield at a considerably greater rate (than simple annealing) to the 37° limit; $G(\text{loss in benzene yield}) \approx 4$. Thus, the -196° limiting yield appears to correspond to a steady-state population of certain defects that are not populated appreciably at 37°. A remarkably good correlation exists between the behavior of benzene yields on irradiated silica gel and the reported behavior of certain trapped-electron color centers associated with specific vacancies in a silica matrix. The over-all results suggest that limiting yields, particularly at -196°, are not governed by aluminum content. Irradiation of isopropylbenzene adsorbed on silica gel also was studied. Results are similar to those obtained previously with a silica-alumina. The results suggest that dealkylation of adsorbed isopropylbenzene occurs under irradiation, $G(\text{C}_6\text{H}_6) \approx 2$, by direct capture of free charge carriers produced in the solid with an efficiency approximating that for their capture by silica matrix defects at -196°.

Introduction

Studies of the dealkylation of isopropylbenzene on γ -irradiated silica-alumina gels have been reported in a series of papers.² These studies suggest that at least a portion of the long-lived dealkylation excitations³ in irradiated silica-alumina may be associated with visible color centers of the irradiated solid; the latter have been associated rather conclusively with the presence of aluminum as a substitutional impurity in the silica matrix.⁴⁻⁸ The formation of acid sites on irradiation of silica gel at -196° has been reported by Barter and Wagner.⁹ Since inherent acid sites are implicated in the catalytic dealkylation of isopropylbenzene on unirradiated silica-aluminas,¹⁰ a question arises as to the role of such radiation-induced acid sites in the dealkylation reaction on irradiated silica-aluminas. The dealkylation excitations produced on room-

temperature irradiation of silica-alumina are stable at room temperature;² on the other hand, the acid sites formed by irradiation of silica gel at -196° decay at

(1) The Radiation Laboratory of the University of Notre Dame is operated under contract with the U. S. Atomic Energy Commission. This is A.E.C. Document No. COO-38-454.

(2) Cf. R. R. Hentz, L. M. Perkey, and R. H. Williams, *J. Phys. Chem.*, **70**, 731 (1966), which includes references to earlier papers in this series.

(3) The general expression "excitations" is used in the absence of definitive evidence for the mechanism of energy storage in the solid. It is considered probable that these long-lived excitations are trapped electrons and/or concomitant positive holes.

(4) For a review of the evidence on irradiated quartz, cf. the following papers: A. Halperin and J. E. Ralph, *J. Chem. Phys.*, **39**, 63 (1963); J. H. Mackey, Jr., *ibid.*, **39**, 74 (1963).

(5) E. Lell, *Phys. Chem. Glasses*, **3**, 84 (1962).

(6) H. W. Kohn and E. H. Taylor, *Proc. Intern. Congr. Catalyse*, **2e**, Paris, 1960, **2**, 1461 (1961).

(7) S. Lee and P. J. Bray, *Phys. Chem. Glasses*, **3**, 37 (1962).

room temperature with a half-time of 2–3 hr.⁹ In order to elucidate further the nature of the radiation-induced excitations effective in isopropylbenzene dealkylation, particularly with regard to the role of aluminum and other impurities, the study of this phenomenon has been extended to high-purity silica gels irradiated at room temperature and at -196° .

Experimental Section

A. Chemicals. Eastman Kodak 1481 isopropylbenzene was used; purification procedures have been described.² Three silica gels were used. Most of the work was performed with solid A which had a surface area (measured by nitrogen adsorption) of 384 m²/g and contained 30 ppm of aluminum (30 μ g of aluminum/g of solid). This solid was prepared from an acidic alcoholic solution of tetraethyl orthosilicate that was gelled with an alcoholic ammonium hydroxide solution. The hydrogel was washed with water, dried 20 hr at 110° , and then calcined in air for 10 hr at 540° . Solids B and C were obtained from Dr. H. W. Kohn of the Oak Ridge National Laboratory. Their properties and methods of preparation have been described.¹¹ Solid B is the silica gel specified to contain 5 ppm of aluminum, and solid C is the ultrapure gel stated to contain no impurities detectable by the spark spectrograph. For both solids B and C a surface area of 600 m²/g is given.

B. Procedures. The general procedures have been described;² a review will be presented of the most pertinent features with emphasis on modifications introduced.

The solids were crushed with a Diamonite mortar and pestle to particle sizes of less than 5 mm in longest dimension. After a pretreatment of several days at 500° in air, samples were weighed into 13-mm o.d. Pyrex tubes and evacuated at 10^{-6} torr and 460° for 18–20 hr. In all experiments, the isopropylbenzene was degassed by the conventional freeze–pump–thaw technique and dried over a fresh sodium surface just prior to introduction to the solid. Traces of moisture were found to cause erratic results.

The Reaction of Isopropylbenzene on Irradiated Silica Gel. In these experiments, 0.25 g of isopropylbenzene was transferred to 1.0 g of the irradiated solid by means of liquid nitrogen on the reaction cell. This amount of liquid relative to solid gave sufficiently rapid diffusion to preclude a competitive consumption of the product benzene,² and to minimize loss by thermal decay of the less stable excitations formed in -196° irradiations of the solid, yet gave sufficiently high benzene concentrations for convenient and accurate analysis. After warming to room temperature, the liquid

and solid were allowed to remain in contact for a period of 90 min (much longer than really necessary) prior to recovery of the liquid and products. The recovery procedure employed boiling water on the reaction cell and liquid nitrogen on an adjacent trap with collection and measurement of noncondensable gas in the calibrated volume of a modified Saunders–Taylor apparatus; recovery was quantitative in 1 hr.

In those experiments in which the solid was irradiated at -196° , the solid was kept in liquid nitrogen until introduction of the isopropylbenzene and then was allowed to come to room temperature. In annealing experiments, after irradiation at -196° , the solid was maintained at room temperature for the desired length of time prior to introduction of isopropylbenzene by the standard procedure.

Irradiation of Isopropylbenzene Adsorbed on Silica Gel. The procedures used were identical with the foregoing with a few exceptions. The desired weight of isopropylbenzene was transferred to a given weight of solid, and the reaction cell was sealed; at least 2 hr elapsed with the reaction cell at room temperature prior to irradiation. The entire range of composition was studied with special emphasis on low isopropylbenzene concentrations. At the lowest concentrations of isopropylbenzene in the system, product recovery times were extended to 2 hr. As in the earlier studies with silica-alumina,² the ratio of dose absorbed by the system to weight of isopropylbenzene present was maintained constant but at the much lower value of 1.4×10^{18} ev/mg of isopropylbenzene.

Irradiations. All samples were irradiated in a 10-kc ⁶⁰Co source under conditions giving a dose rate of 1.75×10^{18} ev g⁻¹ min⁻¹ to a Fricke dosimeter solution using $G(\text{Fe}^{3+}) = 15.6$. Dose to a particular system was determined by correction for the electron density relative to that of the dosimeter and for decay of the ⁶⁰Co. Samples initially at room temperature attained a temperature of 37° during irradiation; these will be referred to as room-temperature irradiations. The -196° irradiations were performed with the reaction cell immersed in a dewar of liquid nitrogen. The small change in dose rate under these conditions was shown to be without effect.

Analyses. The liquids were analyzed by vapor phase chromatography on an F and M Model 609 with a

(8) G. K. Borekov, V. B. Kazanskii, Yu. A. Mishchenko, and G. B. Pariiskii, *Dokl. Akad. Nauk SSSR*, **157**, 384 (1964).

(9) C. Barter and C. D. Wagner, *J. Phys. Chem.*, **68**, 2381 (1964).

(10) Cf., e.g., A. E. Hirschler, *J. Catalysis*, **2**, 428 (1963), and D. Barthomeuf, *Compt. Rend.*, **259**, 3520 (1964).

(11) H. W. Kohn, *J. Catalysis*, **2**, 208 (1963).

flame-ionization detector. A 2-m column of Apiezon-L on Chromosorb-P was used at 200°.

Results

The Reaction of Isopropylbenzene on Irradiated Silica Gel. On solid A at both irradiation temperatures, 37 and -196° , the yield of benzene initially increases linearly with increased dose to the solid but approaches a limiting value at large doses (*cf.* Figure 1). Only the limiting yields were determined on solids B and C; comparison of the saturation yields is presented in Table I. The initial rates of increase in yield with dose to solid A differ greatly at the two irradiation temperatures; at -196° the initial rate corresponds to $G_0(\text{C}_6\text{H}_6) = 4$, and at 37° to $G_0(\text{C}_6\text{H}_6) = 0.067$. (G_0 is the number of molecules formed per 100 ev absorbed by the solid at low dose.) Further, the approximate dose required for attainment of a yield essentially equal to the saturation value is about 16 times greater at 37° . On solid A, the saturation yields of gas (noncondensable at -196°) were 0.22×10^{17} and 0.03×10^{17} molecules/g of solid at irradiation temperatures of -196 and 37° , respectively. No products could be detected in blank experiments on the unirradiated solids.

Table I: Comparison of Benzene Yields^a in Reaction of Isopropylbenzene on γ -Irradiated Silica Gels

Al content ^b	Solid		
	A	B	C
	6.7	1.1	<0.11
Benzene yield ^b			
Temp ^c = 37°	2.6	0.10	0.11
Temp ^c = -196°	15.5	0.28	0.31

^a Yields are saturation values obtained by averaging yields on the plateau reached at large values of dose per gram of solid.

^b Aluminum content and benzene yield are expressed in units of 10^{17} atoms or molecules, respectively, per gram of solid.

^c Irradiation temperature.

A sample of solid A that was irradiated to a saturation dose at 37° was allowed to stand 20 days at room temperature prior to introduction of isopropylbenzene; no decrease in benzene yield was observed. Similarly, a sample of solid A irradiated at -196° showed no decay of activity after 24 hr at -196° . However, when the solid is irradiated at -196° and then allowed to warm up and stand at room temperature for some period prior to introduction of isopropylbenzene, the results are quite interesting (anneal time is measured as the interval between the removal of liquid nitrogen after irradiation

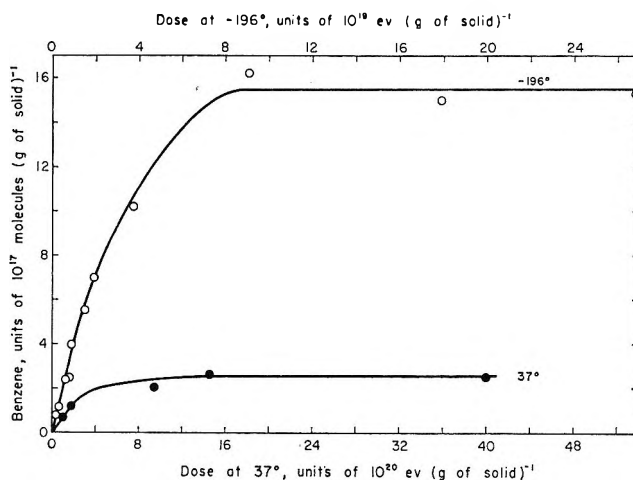


Figure 1. Benzene yields in reaction of isopropylbenzene on γ -irradiated silica gel A.

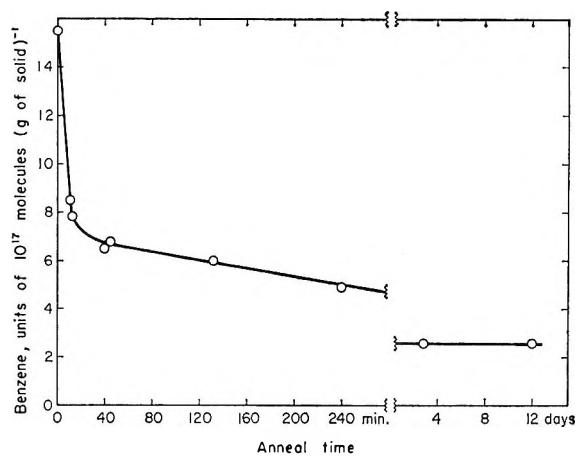


Figure 2. Benzene yields after annealing at room temperature of silica gel A irradiated to saturation at -196° .

tion of the solid at -196° and the replacement of liquid nitrogen for introduction of isopropylbenzene).

On irradiation of solid A to a saturation dose at -196° , the yield of benzene is halved after an anneal time of only 13 min (*cf.* Figure 2).¹² This relatively rapid decay of the activity, of a sample irradiated to saturation at -196° , is followed by a much slower decay; after an anneal time of 68 hr, the benzene yield has fallen to a value equal to the saturation yield obtained in a 37° irradiation. No further decrease was observed in a sample irradiated at -196° and stored 12 days at room temperature. Thus, the limiting yield attained

(12) When isopropylbenzene is introduced to solid irradiated at -196° without prior warm-up (zero anneal time), it seems probable that some decay of activity would occur before complete diffusion and reaction of the isopropylbenzene as the system is allowed to warm up. Thus, all zero anneal time yields are lower limits; such yields are quite reproducible.

by room-temperature annealing of solid irradiated at -196° is identical with the limiting yield attained in a room-temperature irradiation. Such annealing behavior was observed for all samples of solid A irradiated at -196° to a dose sufficient to give a benzene yield in excess of 2.6×10^{17} molecules/g of solid, the saturation yield in 37° irradiations. In -196° irradiations of solid A to doses corresponding to benzene yields less than 2.6×10^{17} molecules/g of solid, no decay was observed for anneal times up to 20 days.

In a series of experiments, the results of which are presented in Table II, solid A first was irradiated to a saturation dose at -196° . About 3 min after removal from liquid nitrogen, the solid again was irradiated (at near room temperature) for the time specified in Table II; it then was allowed to stand at room temperature to give the total anneal time, inclusive of the room-temperature irradiation time, between removal from liquid nitrogen after the first irradiation and immersion in liquid nitrogen for introduction of isopropylbenzene. Obviously, rigorous control of all experimental conditions is not possible in such experiments. Nevertheless, the results clearly establish that irradiation at room temperature accelerates the decay of excitations produced by irradiation at -196° . Furthermore, the limiting value of the benzene yield obtained is again the same as that obtained in a 37° irradiation, 2.6×10^{17} molecules/g of solid. Finally, the decrease in benzene yield of $\sim 3 \times 10^{17}$ molecules/g of solid for a dose of 7.6×10^{18} ev g^{-1} (cf. Table II) corresponds to $G \approx 4$ for the destruction of excitations, which may be compared to $G_0(\text{C}_6\text{H}_6) = 4$ in irradiation at -196° . Considering the experimental uncertainties and over-all complexity of the situation in such an irradiated solid, such an exact correspondence of the two G values is probably fortuitous; however, even an approximate correspondence would be very suggestive.

On irradiation of solid A at 37° , no color was observed at doses up to 4×10^{21} ev g^{-1} ; a very slight, non-uniform coloration was observed in solids B and C. Beginning a few seconds after removal from liquid nitrogen of solid A irradiated at -196° , a strong green glow was observed that decayed almost completely by the time room temperature was reached; no quantitative observations of the thermoluminescence have been made.

Irradiation of Isopropylbenzene Adsorbed on Silica Gel. The results obtained in irradiation of isopropylbenzene adsorbed on solid A are shown in Figure 3. (G is the number of molecules formed per 100 ev absorbed by the whole system; F is the electron fraction of isopropylbenzene in the system.) The results for both $G(\text{C}_6\text{H}_6)$ and $G(\text{gas})$ are very similar to those obtained

Table II: The Effect of Irradiation During Room Temperature Annealing of Solids Initially Irradiated^a at -196°

Anneal ^b time, min	Irradiation ^c time, min	Benzene ^d yield
11	...	8.5
11	5	5.4
13	...	7.8
13	7	4.0
40	...	6.5
40	18	2.6

^a Initial irradiations at -196° were to a sufficiently large dose to ensure attainment of saturation. ^b Total time between removal of liquid nitrogen after the initial irradiation and its replacement prior to introduction of isopropylbenzene (includes room-temperature irradiation time). ^c Room-temperature irradiation time at a dose rate to the solid of 1.51×10^{18} ev g^{-1} min^{-1} . ^d Units of 10^{17} molecules per gram of solid.

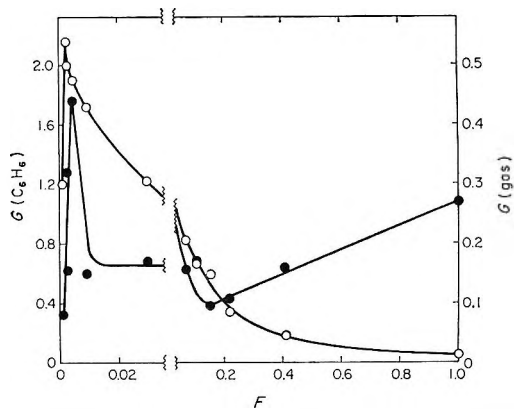


Figure 3. Yields in irradiation of isopropylbenzene adsorbed on silica gel A: O, C_6H_6 ; ●, gas volatile at -196° . F is the electron fraction of isopropylbenzene in the system.

earlier with a silica-alumina (10% by weight of alumina);¹³ e.g., in the earlier work, $G(\text{C}_6\text{H}_6)$ reached a maximum of 1.45 at $F = 0.0018$, and $G(\text{H}_2)$ reached a maximum of 0.21 at $F = 0.007$ and then passed through a minimum at $F \approx 0.15$, in the neighborhood of complete surface coverage. The passage of $G(\text{H}_2)$ through a minimum at $F \approx 0.15$ was more evident in results obtained on another silica-alumina, for which the maximum $G(\text{H}_2) = 0.28$ occurred at $F = 0.0046$.¹⁴ The lower values of $G(\text{C}_6\text{H}_6)$ obtained in the earlier work are attributable to the use of a dose about 20 times larger in that work than in the present study; irradiation of isopropylbenzene adsorbed on solid A to the same large dose at $F = 0.007$ gave $G(\text{C}_6\text{H}_6) = 1.01$

(13) R. R. Hentz, *J. Phys. Chem.*, **66**, 1625 (1962).

(14) R. R. Hentz, *ibid.*, **68**, 2889 (1964).

which may be compared with $G(\text{C}_6\text{H}_6) = 1.05$ obtained at $F = 0.007$ for the silica-alumina.¹³ At the lower doses used in this work, decomposition of isopropylbenzene was of the order of 1%.

Discussion

A. The Reaction of Isopropylbenzene on Irradiated Silica Gel. In quartzes and silica-base glasses and gels, the mechanism of formation and the nature and interrelationships of the many color centers formed by high-energy radiation are not thoroughly understood.^{4,5,15-18} Consequently, it would be premature to attempt the development of a unique and integrated interpretation of the chemical effects occurrent on interaction of isopropylbenzene and other substances with irradiated silica and silica-alumina gels. Nevertheless, certain color centers in silica-base solids have been rather thoroughly studied, and their behavior and nature have been established with reasonable certainty. By comparison of the behavior of such color centers with that of the isopropylbenzene dealkylation reaction on irradiated silica and silica-alumina gels, a strong correlation is established between these color centers and the excitations effective in dealkylation.

The Role of Impurities. The results in Table I are to be compared with benzene yields of $13\text{--}233 \times 10^{17}$ molecules/g of solid obtained on silica-aluminas irradiated at room temperature to a saturation dose;^{2,14} these silica-aluminas contained $\sim 1.2 \times 10^{21}$ atoms of Al/g of solid. For the room temperature irradiations, a qualitative correlation is observed between the yield of benzene and the aluminum or total impurity content.¹⁹ Similar qualitative correlations have been reported between the aluminum content of irradiated silica gels and their visible color, $\text{H}_2\text{--D}_2$ exchange activity, and irreversible H_2 adsorption.^{8,11} Nevertheless, the relationship between benzene yield and impurity content is quite evidently not a proportional one; certainly the aluminum content does not govern the limiting yield. Similarly, poor quantitative correlations have been obtained between aluminum content and the visible color of irradiated quartz and silica; this has been accounted for as owing to presence of part of the aluminum in interstitial sites,²⁰ rather than in substitutional sites where aluminum acts as a positive-hole trap and gives rise to the visible color²¹ and a characteristic esr signal.²² Such an explanation cannot account for the low benzene yields relative to aluminum content on the silica-aluminas for which a major fraction of the benzene yield has been associated with the visible color centers;² in such solids, the aluminum appears to be largely substitutional.²³ The benzene yield on silica-alumina may be limited by the availability of stable electron traps or of

specific charge-compensation ions essential to stabilization of positive holes on substitutional aluminum.^{4,5}

Although the aluminum content of the three silica gels is sufficient to account for the yields of benzene in room-temperature irradiation, the absence of significant visible coloration in the irradiated solids suggests that the traces of aluminum are not substitutional in these solids. On solids A and C irradiated at -196° , benzene yields actually exceed the aluminum content. One might argue that benzene yields on the irradiated silica gels are related to total impurity content, which may exceed the benzene yield even in the case of solid A irradiated at -196° . In the ensuing discussion, remarkably good correlations are established between the behavior of benzene yields on irradiated solid A and that of certain color centers, namely the E' centers (trapped electrons) absorbing at $\sim 0.22 \mu$, associated with specific vacancies in the silica matrix. It is our opinion that limiting benzene yields on the three silica gels are governed by the availability of defects inherent in the silica matrix and not by cationic impurities. The difference between the benzene yield on solid A and those on solids B and C may be attributable to the effect of the very different methods of preparation on the concentration of silica matrix defects produced; *e.g.*, it has been observed that anion impurities, particularly OH^- , may occupy oxygen vacancies and preclude formation of E' centers on irradiation.¹⁸ Solids B and C were prepared with SiCl_4 , while the solid A preparation used ethyl silicate. Although the large difference in surface area of solid A as compared to solids B and C reflects an effect of preparation method on structure, it is evident that benzene yields are not directly related to surface area. It should be noted that an appreciable fraction of the benzene yield on irradiated silica-alumina was shown not to be associated with visible color centers;² it is probable that this yield of benzene arises from the same centers that are effective in the silica gels.

(15) Cf. the ten papers from the Mellon Institute Symposium on Defect Structure of Quartz and Glassy Silica, *J. Phys. Chem. Solids*, **13**, 271 (1960).

(16) W. D. Compton and G. W. Arnold, Jr., *Discussions Faraday Soc.*, **31**, 130 (1961).

(17) C. M. Nelson and R. A. Weeks, *J. Appl. Phys.*, **32**, 883 (1961).

(18) R. A. Weeks and E. Lell, *ibid.*, **35**, 1932 (1964).

(19) Other impurities—such as iron, magnesium, copper, calcium, and sodium—were present in silica gels A and B at about the same level as the aluminum.

(20) A. J. Cohen, *J. Phys. Chem. Solids*, **13**, 321 (1960).

(21) R. W. Ditchburn, E. W. J. Mitchell, E. G. S. Paige, J. F. Custers, H. B. Dyer, and C. D. Clark, Bristol Conference on Defects in Crystalline Solids, The Physical Society, London, 1955, p 92.

(22) M. C. M. O'Brien and M. H. L. Pryce, ref 21, p 88.

(23) A. Leonard, S. Suzuki, J. J. Fripiat, and C. DeKimpe, *J. Phys. Chem.*, **68**, 2608 (1964).

Correlations with the E' Centers. In fused silicas of high purity, in which no visible color is produced by irradiation, certain radiation-induced ultraviolet absorption bands are enhanced by irradiation at -196° .^{16, 24, 25} Arnold and Compton²⁵ report that on irradiation and measurement at 77°K , the intensity of the $0.215\text{-}\mu$ band (an E' center) was ~ 10 times greater than the intensity observed after an irradiation at $\sim 300^\circ\text{K}$ and measurement at 77°K . In addition, these authors observed that when the sample irradiated at 77°K is warmed to room temperature and then immediately remeasured at 77°K , the $0.215\text{-}\mu$ absorption is reduced to about half its original value. Further loss in the $0.215\text{-}\mu$ absorption was observed to occur slowly at room temperature and to approach the value obtained when the irradiation was made at room temperature. The parallel between these results and the benzene yield results is striking (*cf.* Figures 1 and 2).

The same limiting yield of benzene is attained in room-temperature irradiation as in the decay at room temperature of centers produced by a saturation dose at -196° ; therefore, this limiting yield of benzene at room temperature must correspond to essentially complete population of certain silica matrix defects, rather than to attainment of a radiation-induced steady-state population of such defects. Furthermore, the annealing behavior suggests a quantitative conversion of centers formed on irradiation at -196° into available room-temperature centers on warming. Again, a similar interconversion of electron-type centers has been observed in optical bleaching experiments on irradiated fused silicas;²⁶⁻²⁹ *e.g.*, Nelson and Weeks observe that interconversion of E₁' and E₂' centers occurs with only a small loss of total intensity and conclude that it is easier to transfer electrons between electron-type centers than to cause electron-hole recombination at a hole center.

The results of Table II show that centers produced on irradiation at -196° are converted into the room-temperature centers by irradiation at room temperature;³⁰ the loss in benzene yield due to the room-temperature irradiation corresponds to a $G(-\text{C}_6\text{H}_6) \approx 4$, which equals $G_0(\text{C}_6\text{H}_6)$ at -196° . Such a result suggests that the limiting yield of benzene in irradiation at -196° corresponds to a steady-state population of the unstable (at room temperature) centers; these centers must have a negligible cross section for formation at room temperature. The $G_0(\text{C}_6\text{H}_6) \approx 4$ at -196° corresponds to 25 ev per center, which is about what might be expected for the formation of free charge carriers in silica. Thus, at -196° a high capture efficiency for the free charge carriers is indicated; that for forma-

tion of the room-temperature centers is ~ 60 -fold smaller.

Correlation with Other Chemical Effects on Irradiated Silica Gels. The dealkylation of isopropylbenzene appears to occur on a variety of color centers produced by irradiation of silica and silica-alumina gels. The centers effective in dealkylation that are produced by irradiation of silica gel at -196° seem to correspond to the acid centers of Barter and Wagner.⁹ These authors observed no coloration of their irradiated silica gel and observed decay of the radiation-induced acid centers at room temperature. We suggest that such centers are associated with some kind of color center characteristic of the silica matrix. In addition, there are radiation-induced dealkylation centers in silica gel and in silica-alumina that are stable at room temperature and also do not absorb in the visible and, hence, are not associated with positive holes trapped on substitutional aluminum impurity. Such are the centers formed at room temperature in solid A and those which remain after a hydrogen or thermal bleach of visible color centers in silica-alumina.² These centers, to which -196° centers convert on warming of a -196° irradiated silica, also appear to be related to defects inherent in the silica matrix. Finally, in silica-alumina² dealkylation of isopropylbenzene has been shown to occur also on the visible color centers (stable at room temperature) identified as positive holes trapped on substitutional aluminum. Boreskov, *et al.*,⁸ have demonstrated that in a silica gel that is colored by irradiation, such aluminum centers are responsible for the color, for the irreversible adsorption of hydrogen concomitant with bleaching of the color, and for a major part of the H₂-D₂ exchange activity measured at -196° . It has been noted previously² that dealkylation of isopropylbenzene does not occur on the radiation-induced H₂-D₂ exchange sites studied by Kohn and Taylor;⁶ these sites do not absorb in the visible (they remain after hydrogen bleaching) and are poisoned by oxygen.

B. Irradiation of Isopropylbenzene Adsorbed on Silica

(24) P. W. Levy, *J. Phys. Chem. Solids*, **13**, 287 (1960).

(25) G. W. Arnold and W. D. Compton, *Phys. Rev.*, **116**, 802 (1959).

(26) F. S. Dainton and J. Rowbottom, *Trans. Faraday Soc.*, **50**, 480 (1954).

(27) C. M. Nelson and R. A. Weeks, *J. Am. Ceram. Soc.*, **43**, 396 (1960).

(28) C. M. Nelson and J. H. Crawford, Jr., *J. Phys. Chem. Solids*, **13**, 296 (1960).

(29) The existence of such interconversions in the alkali halides has been known for some time; *cf.* K. Przibram, "Irradiation Colours and Luminescence," Pergamon Press Ltd., London, 1956, p 72.

(30) A similar effect has been observed in KCl by H. U. Harten, *Z. Physik*, **126**, 619 (1949).

Gel. The results obtained in irradiation of isopropylbenzene adsorbed on silica gel are similar to those obtained earlier on silica-alumina.¹³ Such similarity casts doubt on the earlier identification of the occurrence of a maximum in $G(\text{C}_6\text{H}_6)$ with saturation by added isopropylbenzene of inherent catalytic sites in the solid. Rather, the effects must now be considered as independent of aluminum content and related to some characteristic inherent in the microporous silica-base solids.

A maximum $G(\text{C}_6\text{H}_6) \approx 2^{31}$ occurs at low doses per gram of solid corresponding to those for which $G_0(\text{C}_6\text{H}_6) \approx 4$ in the -196° irradiations of solid without isopropylbenzene. This suggests the possibility that the dealkylation reaction in irradiation of adsorbed isopropylbenzene at room temperature may occur *via* the unstable -196° centers; this would require that the rate of reaction be rapid relative to the rate of radiation-induced destruction of these centers. Such a possibility would also require the rate of formation of unstable -196° centers to be about the same at room

temperature as at -196° ; however, such a requirement cannot be reconciled with the essentially zero steady-state yield of the unstable centers in irradiation of the solid without isopropylbenzene at room temperature. Consequently, we conclude that dealkylation of adsorbed isopropylbenzene occurs under irradiation by direct capture of free charge carriers with an efficiency almost equal to that for their capture by silica matrix defects at -196° .

Acknowledgment. The authors are grateful to Socony Mobil Oil Company, Inc., for synthesis and characterization of the silica gel designated as solid A and to Dr. H. W. Kohn of the Oak Ridge National Laboratory for the silica gels designated as solids B and C.

(31) Although the dose per milligram of isopropylbenzene was maintained approximately constant in most of these experiments, the point for $G = 2.0$ in Figure 3 corresponds to a sixfold greater dose. Thus, the four points in Figure 3 in the range $G = 1.72$ - 2.16 , inclusive, cover a range of doses per gram of solid under very similar conditions and give an average $G(\text{C}_6\text{H}_6) \approx 2$.

Pure Quadrupole Resonance of Halogens in Some Hexahalorhenates(IV)

by Ryuichi Ikeda, Akinobu Sasane, Daiyu Nakamura, and Masaji Kubo

Department of Chemistry, Nagoya University, Chikusa, Nagoya, Japan (Received March 10, 1966)

The nuclear quadrupole resonance of halogens in various hexahalorhenates(IV) $R_2[ReX_6]$ ($R = NH_4, Rb, Cs$; $X = Cl, Br, I$) was observed at various temperatures. The change in the number of observed resonance lines reveals the existence of a phase transition of ammonium hexaiodorhenate(IV) at 44–46°. From the dependence of resonance frequencies on the kind of cations R , it is concluded that, in addition to the direct electrostatic effect of external charges, an indirect effect, due to neighboring ions, is significant on the field gradient at the resonant halogen nucleus. Sternheimer's antishielding accounts for the large field gradient amplification at least with regard to the sign and the order of magnitude of the indirect effect relative to the direct effect. All these complexes show a positive temperature coefficient of quadrupole resonance frequencies with the single exception of ammonium hexachlororhenate(IV). It is suggested that hydrogen bonding or some electrostatic interaction between hydrogen and chlorine atoms in crystals is responsible for the exceptional behavior of this complex.

Introduction

In a preceding paper,¹ we have reported that positive temperature coefficients of quadrupole resonance frequencies were found for potassium hexachlororhenate(IV), hexabromorhenate(IV), and hexachlorotungstate(IV). The temperature range was that in which these complexes show a single resonance line, *i.e.*, the range in which they form cubic crystals having the potassium hexachloroplatinate(IV) structure. A theoretical explanation was made in terms of the $d\pi-p\pi$ bond character of metal-ligand bonds in paramagnetic complexes having one or more vacancies in their $d\epsilon$ orbitals. However, the field gradient at the resonant nucleus leading to the positive temperature coefficient does not originate solely from the electron distribution within the complex ion containing the nucleus: charges on other ions should make an appreciable contribution as well. Therefore, we have undertaken a systematic study of the temperature coefficient of quadrupole resonance frequencies of hexachloro-, hexabromo-, and hexaiodorhenates(IV) having ammonium, rubidium, and cesium ions as cations. Potassium hexaiodorhenate(IV) has been already examined,¹ but it does not crystallize in a cubic structure at any accessible temperature. No reports have ever been published on the possible formation of lithium and sodium hexahalorhenates(IV).

Experimental Section

Apparatus. A Dean-type, self-quenching, superregenerative spectrometer, already described,² was used for the observation of quadrupole resonance frequencies of chlorine isotopes. For detecting the resonance absorptions of bromine and iodine isotopes, a self-quenching, superregenerative spectrometer² equipped with Lecher lines was employed. Resonance frequencies were determined at room, Dry Ice, and liquid nitrogen temperatures. For ammonium hexaiodorhenate(IV), frequency determination was extended up to about 100° in order to locate a possible phase transition to a cubic structure. For all of the complexes studied, the temperature coefficient of the resonance frequencies was determined between Dry Ice and room temperatures.

Materials. When ammonia solution was added to an aqueous solution of rhenium(VII) heptoxide, Re_2O_7 , ammonium perrhenate(VII), $(NH_4)ReO_4$, separated as a white precipitate. It was dissolved in concentrated hydrochloric acid and reduced with hypophosphorous acid to prepare ammonium hexachlororhenate-

(1) R. Ikeda, D. Nakamura, and M. Kubo, *J. Phys. Chem.*, **69**, 2101 (1965).

(2) D. Nakamura, Y. Kurita, K. Ito, and M. Kubo, *J. Am. Chem. Soc.*, **82**, 5783 (1960).

(IV).³ Rubidium and cesium hexachlororhenates(IV) and ammonium, rubidium, and cesium hexabromorhenates(IV) were synthesized in a similar manner from appropriate starting materials (rubidium carbonate and cesium carbonate) using hydrobromic acid in place of hydrochloric acid for obtaining the hexabromo complexes. In order to identify the samples, each complex was decomposed with a sodium or potassium hydroxide solution and the halogens were determined by Volhard's method. *Anal.* Calcd for $(\text{NH}_4)_2\text{ReCl}_6$: Cl, 48.9. Found: Cl, 47.3. Calcd for Rb_2ReCl_6 : Cl, 37.3. Found: Cl, 37.3. Calcd for Cs_2ReCl_6 : Cl, 32.0. Found: Cl, 31.7. Calcd for $(\text{NH}_4)_2\text{ReBr}_6$: Br, 68.5. Found: Br, 67.2. Calcd for Rb_2ReBr_6 : Br, 57.3. Found: Br, 55.9. Calcd for Cs_2ReBr_6 : Br, 51.5. Found: Br, 50.7.

Ammonium, rubidium, and cesium hexaiodorhenates(IV) were synthesized from the corresponding perrhenates(VII) in accordance to a method employed by Briscoe, *et al.*,⁴ for the preparation of potassium hexaiodorhenate(IV) and identified by the analysis of iodine by Volhard's method. *Anal.* Calcd for $(\text{NH}_4)_2\text{ReI}_6$: I, 77.4. Found: I, 76.2. Calcd for Rb_2ReI_6 : I, 68.1. Found: I, 66.3. Calcd for Cs_2ReI_6 : I, 62.7. Found: I, 61.0.

For the rubidium and cesium complexes thus prepared, the resonance signals were barely detectable or undetectable. Therefore, each sample was sealed in a glass tube, heated at 80–100° for 3–5 hr, and annealed. The signal-to-noise ratio (S/N) increased to 2–3 for chlorine and 2–5 for bromine and iodine.

Results

All of the hexachloro complexes yielded a single absorption of weak intensity in the whole temperature range studied. The observed resonance frequencies are unequivocally attributable to ^{35}Cl for the following reasons. First, if it is assumed that they were due to ^{37}Cl , those of the more abundant isotope should be observed in a frequency region of high sensitivity of the spectrometer used. This result would have been in contradiction with our observations. Second, the observed frequencies are close to the resonance frequency, 13.9 Mc, of ^{35}Cl in potassium hexachlororhenate(IV),¹ for which the frequencies of both isotopes have been observed. It is quite reasonable to suppose that, in the present study, the resonance frequencies of ^{37}Cl escaped detection because they fell in a frequency region in which the sensitivity of the spectrometer used was relatively low. Another reasonable supposition is that the natural abundance of the ^{37}Cl isotope is smaller (about one-third) than that of ^{35}Cl , which showed only a weak signal anyway ($S/N = 2-3$).

Each of the three hexabromo complexes showed two weak absorptions ($S/N = 3-5$). The frequency ratio, 1.197, of the two lines agreed excellently with the known isotopic frequency ratio of bromine.

Rubidium and cesium hexaiodorhenates(IV) gave rise to two absorptions of frequency ratio equal to 1:2 at room and Dry Ice temperatures as expected for ν_1 and ν_2 of ^{127}I . At liquid nitrogen temperature, single lines were observed for both ν_1 and ν_2 of the cesium salt, whereas the rubidium salt showed two closely spaced ν_1 lines of a very weak intensity ($S/N < 1.5$). It is very likely that the corresponding ν_2 also is a doublet. However, owing to the low sensitivity of the spectrometer in this frequency range, only a single line was located accurately. Surely, a phase transition takes place at some temperature between Dry Ice and liquid nitrogen temperatures.

The temperature dependence of the resonance frequency of ammonium hexaiodorhenate(IV) is fairly complicated, as shown in Figure 1. At room temperature, two pairs of lines were observed, with a frequency ratio of about 1:2. These lines are attributable to ν_1 and ν_2 , respectively, indicating the existence of two kinds of crystallographically nonequivalent iodine atoms in crystals. The high-frequency doublet component was about twice as intense as the low-frequency component. The frequencies of the doublet lines decreased with increasing temperature. The lines disappeared at about 46° while a new single line of a stronger intensity and a lower frequency appeared at 44.5° for each of ν_1 and ν_2 . Above the transition point, the resonance frequency showed a positive temperature coefficient. Below room temperature, the doublet structure of ν_1 and ν_2 persisted down to about -100°. The low-frequency line of each doublet showed a positive temperature coefficient below about -50°. At the temperature of liquid nitrogen, triplet lines were observed for both ν_1 and ν_2 , indicating the existence of three kinds of nonequivalent iodine atoms in the rhenate crystals. Therefore, it is concluded that a phase transition takes place between Dry Ice and liquid nitrogen temperatures.

The resonance frequencies of ^{35}Cl , ^{79}Br , and ^{127}I , observed at various temperatures, are listed in Table I. The frequencies of a less abundant isotope, ^{81}Br , are omitted, because they give the correct isotope frequency ratio.

The foregoing results indicate that all halogen atoms are equivalent to one another in a crystal of

(3) C. L. Rulfs and R. J. Meyer, *J. Am. Chem. Soc.*, **77**, 4505 (1955).

(4) H. V. A. Briscoe, P. L. Robinson, and A. J. Rudge, *J. Chem. Soc.*, 3218 (1931).

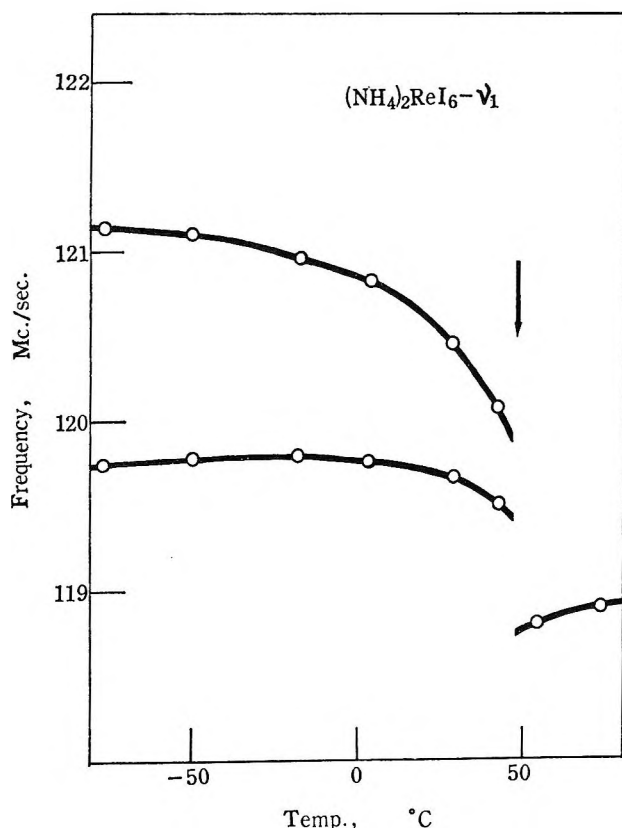


Figure 1. Temperature dependence of pure quadrupole ν_1 resonance frequencies of ^{127}I in ammonium hexaiodorrhenate (IV).

these hexahalo complexes at room temperature, except for ammonium hexaiodorrhenate(IV). This is in agreement with the results of X-ray analysis which show that some of these complexes form cubic crystals of the potassium hexachloroplatinate(IV) type (Fm3m) at room temperature.⁵⁻⁷ For complexes with no X-ray crystallographic data as yet, Norelco X-ray powder patterns were taken and analyzed to determine the lattice constants. The results are shown in Table II.

The X-ray powder patterns of ammonium hexaiodorrhenate(IV) taken at room temperature could not be interpreted as due to a cubic or tetragonal structure. However, those taken at about 80° indicated that the crystal had the potassium hexachloroplatinate(IV) structure. Accordingly, it is concluded that this compound undergoes a phase transition at 45° from a structure of a lower than tetragonal symmetry to the cubic structure.

From the observed frequencies, ν_1 and ν_2 , of ^{127}I in the hexaiodo complexes, the quadrupole coupling constants and the asymmetry parameters were evaluated using Livingston and Zeldes' table⁸ as shown in Table III. When a multiplet structure appeared as in ammonium hexaiodorrhenate(IV), the theoretical

Table I: Pure Quadrupole Resonance Frequencies of ^{35}Cl , ^{79}Br , and ^{127}I in Some Hexahalorhenates(IV)

Compd	Temp, °C	Freq, Mc/sec	
		ν_1	ν_2
$(\text{NH}_4)_2\text{ReCl}_6$	26	14.086 ± 0.001	
	-72	14.106 ± 0.001	
Rb_2ReCl_6	Liquid N ₂	14.125 ± 0.001	
	20	14.277 ± 0.001	
Cs_2ReCl_6	-66	14.264 ± 0.001	
	Liquid N ₂	14.248 ± 0.001	
$(\text{NH}_4)_2\text{ReBr}_6$	18	14.611 ± 0.001	
	-66	14.608 ± 0.001	
$(\text{NH}_4)_2\text{ReBr}_6$	Liquid N ₂	14.604 ± 0.001	
	27	114.02 ± 0.05	
Rb_2ReBr_6	-71	113.98 ± 0.05	
	Liquid N ₂	113.95 ± 0.05	
Rb_2ReBr_6	27	116.09 ± 0.05	
	-75	115.95 ± 0.05	
Cs_2ReBr_6	Liquid N ₂	115.73 ± 0.05	
	26	118.87 ± 0.05	
Cs_2ReBr_6	-73	118.76 ± 0.05	
	Liquid N ₂	118.41 ± 0.05	
Compd	Temp, °C	Freq, Mc/sec	
$(\text{NH}_4)_2\text{ReI}_6$	105	118.96 ± 0.08	237.7 ± 0.2
	56	118.80 ± 0.08	237.3 ± 0.3
	18	120.62 ± 0.05	240.68 ± 0.10
			239.54 ± 0.10
	-67	121.20 ± 0.05	241.22 ± 0.10
			239.44 ± 0.10
	Liquid N ₂	122.62 ± 0.05	242.03 ± 0.10
			241.03 ± 0.10
			239.42 ± 0.10
	Rb_2ReI_6	28	122.08 ± 0.05
-73		121.96 ± 0.05	243.7 ± 0.2
Liquid N ₂	122.8 ± 0.1	244.8 ± 0.2	
		122.4 ± 0.1	
Cs_2ReI_6	18	124.91 ± 0.05	249.83 ± 0.10
	-74	124.73 ± 0.05	249.49 ± 0.10
Liquid N ₂		124.49 ± 0.05	249.01 ± 0.10

requirement, $2\nu_1 \geq \nu_2$, makes the correspondence between ν_1 and ν_2 unambiguous, except for the two high-frequency multiplet components of this compound at liquid nitrogen temperature. Here, it was assumed that the ν_1 and ν_2 multiplet components of the highest frequency correspond to each other. The asymmetry parameter is practically zero for complexes of cubic symmetry.

(5) B. Aminoff, *Z. Krist.*, **A94**, 246 (1936).

(6) D. H. Templeton and C. H. Dauben, *J. Am. Chem. Soc.*, **73**, 4492 (1951).

(7) K. Schwochau, *Z. Naturforsch.*, **19a**, 1237 (1964).

(8) R. Livingston and H. Zeldes, "Table of Eigenvalues for Pure Quadrupole Spectra, Spin 5/2," ONRL Report 1913, Oak Ridge National Laboratory, Oak Ridge, Tenn., 1955.

Table II: Lattice Constants a of R_2ReX_6 -Type Crystals at Room Temperature

Compd	a , Å	Ref
K_2ReCl_6	9.861 ± 0.003	5
	9.843 ± 0.002	7
$(NH_4)_2ReCl_6$	9.922 ± 0.003	
Rb_2ReCl_6	9.977 ± 0.002	7
	9.950 ± 0.007	
Cs_2ReCl_6	10.243 ± 0.007	
K_2ReBr_6	10.445 ± 0.005	6
	10.387 ± 0.002	7
	10.381 ± 0.003	
$(NH_4)_2ReBr_6$	10.441 ± 0.003	
Rb_2ReBr_6	10.490 ± 0.002	7
Cs_2ReBr_6	10.700 ± 0.005	
$(NH_4)_2ReI_6$	11.27 ± 0.01 (at $\sim 80^\circ$)	
Rb_2ReI_6	11.320 ± 0.002	7
Cs_2ReI_6	11.409 ± 0.005	

Table III: Quadrupole Coupling Constants and Asymmetry Parameters of ^{127}I in Hexaiodorhenates(IV)

Compd	Temp, °C	eQq , Mc/sec	η
$(NH_4)_2ReI_6$	105	792.0 ± 1.0	0.0
	56	791.0 ± 1.0	0.0
	18	802.5 ± 0.3	0.043 ± 0.007
		797.9 ± 0.4	0.0
	-67	804.6 ± 0.2	0.062 ± 0.004
		798.2 ± 0.3	0.012 ± 0.012
Liquid N ₂	811.0 ± 2.0	0.101 ± 0.003	
	804.0 ± 1.0	0.101 ± 0.003	
	796.9 ± 0.8	0.012 ± 0.012	
Rb_2ReI_6	28	813.4 ± 0.5	0.0
	-73	812.4 ± 0.6	0.0
	Liquid N ₂	810.0 ± 6.0^a	0.036 ± 0.040
Cs_2ReI_6	18	832.7 ± 0.5	0.0
	-74	831.6 ± 0.5	0.0
	Liquid N ₂	829.4 ± 0.5	0.0

^a Calculated from the mean value of two ν_i frequencies.

Discussion

Effect of Cations on Nqr Frequencies. The resonance frequencies of hexachloro- and hexabromorhenates(IV) increase with increasing ionic radius of cations in the order of potassium, ammonium, rubidium, and cesium (see Table IV). This was already found for hexachloro- and hexabromoplatinates(IV).⁹

From the observed resonance frequency ν , one can calculate the field gradient q at the resonant halogen nucleus (^{35}Cl or ^{79}Br) by

$$h\nu = \frac{1}{2} |eQq| \quad (1)$$

Table IV: Nqr Frequencies of Hexahalorhenates(IV) and Hexahaloplatinates(IV) at 20°

Compd	ν_i , Mc/sec	Compd	ν_i , Mc/sec
K_2ReCl_6	13.887	K_2ReBr_6	112.70
$(NH_4)_2ReCl_6$	14.087	$(NH_4)_2ReBr_6$	114.02
Rb_2ReCl_6	14.277	Rb_2ReBr_6	116.08
Cs_2ReCl_6	14.611	Cs_2ReBr_6	118.86
K_2PtCl_6	25.816	K_2PtBr_6	200.21
$(NH_4)_2PtCl_6$	26.071	$(NH_4)_2PtBr_6$	202.54
Rb_2PtCl_6	26.29	Rb_2PtBr_6	204.38
Cs_2PtCl_6	26.60	Cs_2PtBr_6	207.20

where eQ is the quadrupole moment of a halogen nucleus ($Q_{^{35}Cl} = -0.07894 \times 10^{-24}$ cm², $Q_{^{79}Br} = 0.33 \times 10^{-24}$ cm²).^{10,11} Now, the field gradient is given by

$$q = q_{fi} + q_{ext} \quad (2)$$

where q_{fi} is the field gradient in an isolated or free complex ion and q_{ext} includes all effects due to external ions in a crystal. Since the sign of eQq cannot be determined by nqr spectroscopy, the observed values of q are absolute values. The field gradient q_{fi} originating from charges within a free complex ion, except for the resonant halogen nucleus, is positive. This is because the halogen atom has partial vacancy in the p_z orbital whereas both p_x and p_y orbitals are filled. It is expected theoretically that the absolute value of q_{ext} due to external ions decreases with increasing lattice constant. The aforementioned fact that the observed resonance frequencies increase with increasing lattice constant leads to a conclusion that q_{ext} is negative and its absolute value is smaller than q_{fi} .

In principle, one would be able to calculate q_{fi} theoretically if the wave function were known for an isolated complex ion. Since it is hopeless at the present stage to perform such a calculation, let the difference Δq be taken between complexes having the same kind of complex anions. Then, one has

$$\Delta q = \Delta q_{ext} \quad (3)$$

where Δq is a quantity capable of being determined experimentally. One may presume further that q_{ext} is the sum of two terms.

$$q_{ext} = q_{dir} + q_{ind} \quad (4)$$

Here, q_{dir} stands for the field gradient due to the direct

(9) D. Nakamura and M. Kubo, *J. Phys. Chem.*, **68**, 2986 (1964).

(10) V. Jaccarino and J. G. King, *Phys. Rev.*, **83**, 471 (1951).

(11) J. G. King and V. Jaccarino, *ibid.*, **94**, 1610 (1954).

electrostatic effect of external ions, while q_{ind} takes into account the indirect effect, *i.e.*, the distortion or polarization of the complex anion in question caused by external ions. The first term q_{dir} is calculated below for various hexahalorhenates(IV) having alkali metals as cations in order to compare Δq_{dir} with the observed Δq . (We have used q_{ci} and q_{ni} given by $q_{\text{ci}} = q_{\text{fi}} + q_{\text{ind}}$ and $q_{\text{ni}} = q_{\text{dir}}$ in preceding papers.^{1,9})

The z axis was chosen along a Re–X bond involving the resonant halogen atom X. For a potassium hexachloroplatinate(IV)-type crystal, the principal axes of the field gradient tensor \mathbf{q}_{dir} coincide with those of the field gradient originating from charges within the complex anion in question, except for the resonant halogen nucleus. The asymmetry parameter is zero as was confirmed experimentally. Each of the central metal atoms and halogen atoms in complex anions MX_6^{2-} , as well as cations R^+ , was assumed to bear a point charge ρ . The net charges calculated from the extent of ionic character¹ of the metal–halogen bonds in these complex anions were used for ρ_{M} and ρ_{X} , whereas ρ_{R} is equal to $+e$. With this point-charge model, q_{dir} can be calculated as

$$q_{\text{dir}} = \sum_i \rho_i \frac{3z_i^2 - r_i^2}{r_i^5} \quad (5)$$

where z_i and r_i are, respectively, the z coordinate and the distance of the i th point charge ρ_i from the origin at the given nucleus with respect to the given z axis, and the sum is over all external ions in the lattice.

The lattice constants are tabulated in Table II. The Re–Cl and Re–Br bond distances have been determined by X-ray analysis as 2.37 and 2.50 Å in potassium hexachlororhenate(IV)⁵ and potassium hexabromorhenate(IV),⁶ respectively. It was assumed that these distances are independent of the kind of cations. The calculations of q_{dir} were performed by means of an NEAC digital computer. The summation was extended over all external ions contained in a sphere having its center at the resonant nucleus, the radius being 36, 37, and 38 Å for potassium, rubidium, and cesium hexachlororhenates(IV) and 38, 39, and 40 Å for potassium, rubidium, and cesium hexabromorhenates(IV), respectively. Similar calculations have also been made for hexachloroplatinates(IV). The results are shown in Table V. Unfortunately, exact X-ray crystal data are not available for the Pt–Br distance of a hexabromoplatinate(IV) ion.

From the observed frequencies shown in Table IV, Δq was calculated by use of eq 1, while Δq_{dir} was obtained from the values of q_{dir} shown in Table V. From these, Δq_{ind} can be evaluated using eq 3 and 4. The results are shown in Table VI. It is evident that

Δq_{dir} is one or two orders of magnitude smaller than Δq . In other words, the direct electrostatic effect

Table V: Field Gradient q_{dir} Calculated for Some Hexahalorhenates(IV) and Hexahaloplatinates(IV)

Compd	$10^2 q_{\text{dir}}$, e A ⁻³	Compd	$10^2 q_{\text{dir}}$, e A ⁻³	Compd	$10^2 q_{\text{dir}}$, e A ⁻³
K ₂ ReCl ₆	-7.79	K ₂ ReBr ₆	-6.46	K ₂ PtCl ₆	-7.95
Rb ₂ ReCl ₆	-7.50	Rb ₂ ReBr ₆	-6.18	Rb ₂ PtCl ₆	-7.45
Cs ₂ ReCl ₆	-6.64	Cs ₂ ReBr ₆	-5.69	Cs ₂ PtCl ₆	-6.66

of external charges is too small to account for the observed field gradient difference. One is led to conclude that the charge distribution within the complex anion is altered to a certain extent by external ions and that the indirect effect is significant on the field gradient at a resonant halogen nucleus.

Table VI: Contributions of Various Effects to the Field Gradient Difference

Anion	Cation	Field gradient differences $\times 10^2$, e A ⁻³			
		Δq_{ext}	Δq_{dir}	Δq_{ind}	$\Delta q_{\text{ext calcd}}$
ReCl ₆	Rb–K	28.4	0.29	28.1	16.7
	Cs–K	52.7	1.15	51.5	66.2
PtCl ₆	Rb–K	35	0.50	34.5	28.8
	Cs–K	57	1.29	55.7	74.3
ReBr ₆	Rb–K	58.8	0.28	58.5	28.0
	Cs–K	107.2	0.77	106.4	77.0

Sternheimer and others^{12–14} have shown that, when a spherically symmetric ion is placed in an inhomogeneous electric field, the charge distribution is altered by the field in such a way that an additional field gradient, due to the polarization, acts on the nucleus. The effect is approximated quantitatively by introducing Sternheimer's antishielding constant γ .

$$q_{\text{ext}} = (1 - \gamma)q_{\text{dir}} \quad (6)$$

The value of the antishielding constant γ is -56.6 for a chlorine ion and -99.0 for a bromine ion as evaluated by Sternheimer and Foley¹⁵ and by Wikner and Das,¹⁶ respectively. In other words, the direct electrostatic effect is amplified by an electronic cloud

(12) R. Sternheimer, *Phys. Rev.*, **80**, 102 (1950).

(13) G. Burns and E. G. Wikner, *ibid.*, **121**, 155 (1961).

(14) R. Bersohn, *J. Chem. Phys.*, **29**, 326 (1958).

(15) R. Sternheimer and H. M. Foley, *Phys. Rev.*, **102**, 731 (1956).

(16) E. G. Wikner and T. P. Das, *ibid.*, **109**, 360 (1958).

surrounding the resonant nucleus. Although a halogen nucleus in a hexahalo complex anion has an electronic environment different from that of a simple ion, the amplification of the field gradient must surely be present in complex ions also. Therefore, in order to estimate roughly the extent of field gradient amplification as a check, Δq_{ext} was calculated from Δq_{dir} by use of eq 6 with γ values for simple ions. The results are shown in the last column of Table VI. Comparison of the calculated Δq_{ext} with the observed Δq_{ext} indicates that Sternheimer's antishielding effect accounts for the large indirect effect, at least with regard to the sign and the order of magnitude of q_{ind} relative to q_{dir} .

Temperature Coefficients of Nqr Frequencies. The temperature dependence of the resonance frequencies of hexachlororhenates(IV) is linear in the temperature range in which the complexes form cubic crystals. The observed temperature coefficients are shown in Table VII. As was anticipated, they are positive regardless of the kind of cations except for ammonium hexachlororhenate(IV). This compound shows a negative temperature coefficient, the absolute value being small compared with those of diamagnetic complexes having a similar structure. We have already explained¹ the positive temperature coefficients of quadrupole resonance frequencies of hexahalorhenates(IV) and

hexahalotungstates(IV) in terms of the partial $d\pi$ - $p\pi$ bond character of the metal-ligand bonds. In view of this theoretical conclusion, it is rather strange that a negative temperature coefficient was found for the

Table VII: Temperature Coefficient $(1/\nu)d\nu/dT$ of Quadrupole Resonance Frequencies of Halogens in $R_2[ReX_6]$ Crystals at Room Temperature

Compd	$(1/\nu)d\nu/dT$ $\times 10^6$
K_2ReCl_6	9.4
$(NH_4)_2ReCl_6$	-13
Rb_2ReCl_6	10
Cs_2ReCl_6	3.8
K_2ReBr_6	22
$(NH_4)_2ReBr_6$	4.7
Rb_2ReBr_6	7.0
Cs_2ReBr_6	5.2
$(NH_4)_2ReI_6$	22 (50-140°)
Rb_2ReI_6	11
Cs_2ReI_6	15

single exception. Possibly, hydrogen bonding or an electrostatic interaction of some sort between hydrogen in ammonium ions and chlorine in the complex anions is responsible for the exceptional behavior of ammonium hexachlororhenate(IV).

The Melting Point and Decomposition Pressure of Neptunium Mononitride

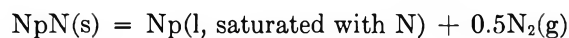
by W. M. Olson and R. N. R. Mulford

University of California, Los Alamos Scientific Laboratory, Los Alamos, New Mexico (Received March 11, 1966)

Decomposition pressures for the reaction $\text{NpN(s)} = \text{Np(l)} + 0.5\text{N}_2(\text{g})$ in the temperature range 2210–2830° are presented. NpN melts congruently at $2830 \pm 30^\circ$ under a nitrogen pressure of about 10 atm. An equation, $\log p \text{ (atm)} = 8.193 - [(29.54 \times 10^3)/T] + 7.87 \times 10^{-18}T^5$, was found to describe the decomposition pressure–temperature relation for NpN. A lattice parameter of $a = 4.8987 \pm 0.0005 \text{ \AA}$ was measured for the cubic nitride.

Introduction

At ambient nitrogen pressures below the pressure where NpN melts congruently the following reaction occurs.



At sufficiently high temperatures the solid will liquefy as soon as the decomposition pressure exceeds the ambient nitrogen pressure. Therefore the decomposition pressure–temperature relation can be determined by observing the apparent melting point as a function of nitrogen pressure. If the ambient nitrogen pressure is high enough to suppress decomposition, the congruent melting point may be observed.

Experimental Section

Apparatus. The apparatus and procedure have been fully described previously.¹ Briefly, about 5 mg of NpN powder was placed in a 30° vee formed in a tungsten strip which was heated resistively. The sample was observed and its temperature determined by means of a calibrated Pyro micro optical pyrometer sighted through a quartz window and prism located at the top of the stainless steel vacuum-pressure can.

Temperatures were corrected for the absorption of the prism and window, and also for the emissivity of the tungsten vee. It is estimated that the accuracy of the temperatures reported is $\pm 30^\circ$.

Preparation of NpN. Most of the NpN was made in the following manner. Neptunium metal, which contained 230 ppm of carbon as the principal impurity, was cleaned in an inert atmosphere by removing the surface with a file. The cleaned metal was reduced to filings which were placed in a tungsten vee and heated resistively under vacuum for approximately 5 min at

about 500° to remove absorbed gases. The filings were then cooled to room temperature, and 1 atm of spectroscopic grade nitrogen, to which had been added about 0.5% hydrogen (Linde Ultra Pure) to serve as a catalyst, was introduced into the system.

The reaction between the neptunium filings and the gas was started by heating the filings to 600°. After the reaction appeared to be complete, the temperature was increased to 1500° and the gas was pumped off. This procedure decomposed any neptunium hydride which had not been converted to nitride during the heating at 600° and volatilized any unreacted neptunium metal. An X-ray diffraction pattern showed only NpN to be present. The resulting NpN powder was stored under vacuum, and small portions were used for the melting point determinations.

Procedure. In determining the melting point, or decomposition temperature, about 5 mg of NpN powder was placed in a tungsten vee, the apparatus was evacuated, and the sample heated to about 1000°. Spectroscopically pure nitrogen was then introduced into the system until the desired pressure was attained. Then the temperature was raised until the sample started to melt. Temperature and pressure readings were taken just before and just after melting had occurred, and the true values were assumed to be the averages. The before and after temperature readings were usually about 10° apart.

Results

The decomposition pressures obtained for NpN are plotted in Figure 1 as $\log p \text{ (atm)}$ vs. $10,000/T$

(1) W. M. Olson and R. N. R. Mulford, *J. Phys. Chem.*, **67**, 952 (1963).

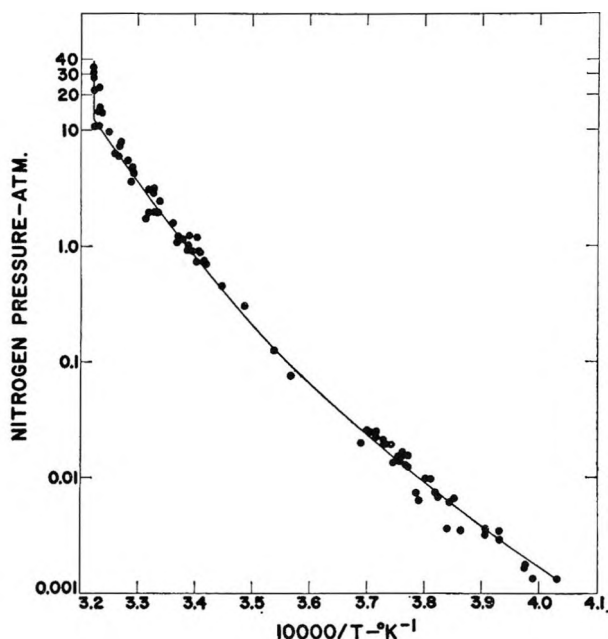


Figure 1. Decomposition pressure of NpN.

(°K). The data points are considerably scattered, but it is apparent that they fall along a gentle curve which intersects the vertical line representing congruent melting at a pressure of about 10 atm. The congruent melting point, as established by this vertical line on the plot, is $2830 \pm 30^\circ$.

In previous work, oxygen impurity had been found to have considerable influence on the decomposition of ThN.² In the present work with NpN no clear influence of oxygen was detected. Some of the points in Figure 1 were obtained with nitride made from sawdust which definitely contained oxide as a result of the sparking and burning that accompanied the sawing process. The other points were obtained from nitride prepared from bulk metal by the method previously described. There was no apparent difference between the pressure-temperature results from the two nitride sources. No oxide was detected in X-ray patterns from the nitride made from the bulk metal.

Neptunium, like plutonium, forms only a mononitride. The lattice parameter of this cubic, sodium chloride type nitride was found to be $a = 4.8987 \pm 0.0005$ Å which agrees well with the value reported by Zachariasen,³ $a = 4.897 \pm 0.002$ Å.

Discussion

Since the liquid neptunium in equilibrium with the nitride is saturated with nitrogen, and therefore its activity is some unknown value less than unity, the present data cannot be used to provide an accurate value for the standard heat of formation of NpN.

The solubility of nitrogen in liquid neptunium presumably varies with temperature, the solubility increasing, and, consequently, the neptunium activity decreasing as the temperature increases. This temperature dependence of the solubility is reflected in the curvature shown by the data in Figure 1. A limit for ΔH°_{298} may be obtained from the lowest experimental point, where the activity of the neptunium was nearest to unity, by combining the experimental value with entropy and heat capacity estimates. If, for the formation of 1 mole of NpN from pure neptunium and nitrogen gas, we assume $\Delta S^\circ_{298} = -20$ cal/deg mole and $\Delta C_p^\circ = 1.5$ cal/deg mole as an average between 298 and 2500°K, the heat of formation at 298°K is found to be more negative than -61 kcal/mole. The entropy of formation is taken to be the same as that of UN, as calculated from the measured absolute entropy of UN.⁴

In previous similar work with UN,¹ PuN,⁵ and ThN,² it was found that an equation of the form $\log p = A + (B/T) + CT^6$ fitted the experimental points well. This equation, which was derived empirically has the property of approaching a straight line as the temperature becomes lower. This behavior is plausible for the nitrogen pressure over a univariant mixture of liquid metal and nitride; that is, the deviation from linearity is caused by the lowering of the activity of the metal in the liquid phase. As the temperature decreases, less and less nitrogen remains in solution and the metal activity approaches unity. For the decomposition pressure of NpN, the data in Figure 1 are fitted by (T is in °K)

$$\log p \text{ (atm)} = 8.193 - [(29.54 \times 10^3)/T] + 7.87 \times 10^{-18}T^6$$

It is of some interest to compare the stability of NpN with the stabilities of the other actinide nitrides.^{1,2,5} For accurate comparisons, the standard free energies of formation of the nitrides are needed, but these cannot be obtained because the activities of the metals in their liquid phases are unknown. One is thus forced to compare decomposition pressures. Small differences among the decomposition pressures may reflect only the variation of nitrogen solubility in the liquid metals, but it is likely that a large difference

(2) W. M. Olson and R. N. R. Mulford, *J. Phys. Chem.*, **69**, 1223 (1965).

(3) W. H. Zachariasen, *Acta Cryst.*, **2**, 388 (1949).

(4) E. F. Westrum, Jr., "International Symposium on Compounds of Interest in Nuclear Reactor Technology," University of Colorado, Boulder, Colo., Aug 3-5, 1964.

(5) W. M. Olson and R. N. R. Mulford, *J. Phys. Chem.*, **68**, 1048 (1964).

between the decomposition pressures of two nitrides is a true indication of different stabilities or bond strengths. Comparison of the known decomposition pressures of the actinide shows an increase in decomposition pressure at constant temperature as atomic number increases. At 2500°K, the lowest temperature for which measured pressures are available, comparison of the logarithms of the decomposition pressures calculated from the equations shows that, while UN, NpN, and PuN are not too dissimilar in stability, ThN is possibly significantly more stable than the other three. However, small differences in entropy or heat capacity or solubility of nitrogen in the liquid

metal phase could easily account for the differences among observed pressures. Similarly, differences in stoichiometry of the nitride phases could affect the observed pressures. Benz and Bowman⁶ have found a departure from stoichiometry at high temperatures for UN.

Acknowledgment. We are grateful to F. H. Ellinger for making the X-ray measurements on NpN. This work was performed under the auspices of the U. S. Atomic Energy Commission.

(6) R. Benz and M. G. Bowman, *J. Am. Chem. Soc.*, **88**, 264 (1966)

The Americium-Hydrogen System¹

by W. M. Olson and R. N. R. Mulford

University of California, Los Alamos Scientific Laboratory, Los Alamos, New Mexico (Received April 18, 1966)

Pressure-temperature-composition measurements and X-ray data are presented for the americium-hydrogen system. Two hydride phases were found: one, face-centered cubic of composition AmH_{2+x} ; the other, hexagonal of composition AmH_3 . Both phases are isostructural with the corresponding plutonium and neptunium hydrides. The plateau pressures for the Am-AmH₂ univariant composition range are represented by $\log p(\text{atm}) = 7.190 - 8812/T(^{\circ}\text{K})$. The derived heat of formation of AmH_2 is $\Delta H_f = -40.3$ kcal/mole.

Introduction

The uranium-hydrogen,² neptunium-hydrogen,³ and plutonium-hydrogen^{4,5} systems have been studied previously. Now, with sufficient americium metal available, it seemed appropriate to extend our knowledge of the hydrides to this seventh member of the actinide series. Such a study should be especially interesting because no very regular behavior, as is seen for the rare earth hydrides, has yet been found for the actinide hydrides.

Experimental Section

The apparatus and method have been described in detail previously.³ Briefly, a sample of americium

metal was contained in an yttria crucible which was placed in a silica tube attached to a standard Sievert's apparatus. The sample was out-gassed at 800°. Then, measured amounts of hydrogen were added to the sample, the pressure in the system being determined by means of a combination mercury manometer

(1) Work done under the auspices of the U. S. Atomic Energy Commission.

(2) F. H. Spedding, *et al.*, *Nucleonics*, **4**, 4 (1949).

(3) R. N. R. Mulford and T. A. Wiewandt, *J. Phys. Chem.*, **69**, 1641 (1965).

(4) R. N. R. Mulford and G. E. Sturdy, *J. Am. Chem. Soc.*, **77**, 3449 (1955).

(5) R. N. R. Mulford, *ibid.*, **78**, 3897 (1956).

(pressures above 2 torr) or a McLeod gauge (pressures below 2 torr). The accuracy of measurement of the hydrogen pressure was such that the H/Am atom ratio is believed to be known to ± 0.02 . The silica sample tube was enclosed within a silver block to smooth temperature variations in the sample, and an automatically controlled tube furnace able to maintain the sample temperature within $\pm 0.1^\circ$ was used. The sample temperature was determined with a calibrated Pt-Pt-10% Rh thermocouple having its measuring junction in a reentrant well in the sample bulb.

The Am^{241} isotope was used and contained 0.15% by weight of Ca and 0.20% La as the principal metallic impurities. A trace of AmO_2 was also detected in the X-ray diffraction pattern of the metal. The computed H/Am ratios were not corrected to take account of the impurities in the americium. Matheson Co. ultra-pure grade hydrogen, claimed by the manufacturer to contain less than 10 ppm total impurities, was used directly from the cylinder.

The procedure consisted of adding small increments of hydrogen to the system, measuring the pressure and temperature after each increment until the highest H/Am ratio had been obtained, then removing the hydrogen in successive decrements and again measuring the pressure and temperature after each decrement. Since it was not possible to attain a predetermined temperature exactly, the isotherm points were obtained by short interpolations. The pressure-temperature curve for each amount of hydrogen in the system was obtained for both ascending and descending temperature. Hysteresis was observed, as described below, only for compositions close to AmH_3 .

Results

The P - T - C data are plotted in Figures 1 and 2. The isotherm plots in Figure 1 show some solubility of hydrogen in americium at the higher temperatures, about 16 atom % being soluble at 800° . Figure 1 also reveals that the dihydride phase has a lower composition limit that is almost temperature independent over the range studied. The inference, if any, is that the phase becomes slightly hydrogen deficient as the temperature increases.

When the ratio of hydrogen to metal exceeded 2, hydrogen dissolved in the AmH_2 phase until a composition of about $\text{AmH}_{2.7}$ was reached. When more hydrogen was added, a hexagonal AmH_3 phase was found. However, this conversion is sluggish, and single-phase AmH_3 was not obtained. Up to $\text{AmH}_{2.7}$, good reproducibility in the pressure-temperature data was obtained, but some hysteresis was observed at higher hydrogen contents, as can be seen in Figure 2.

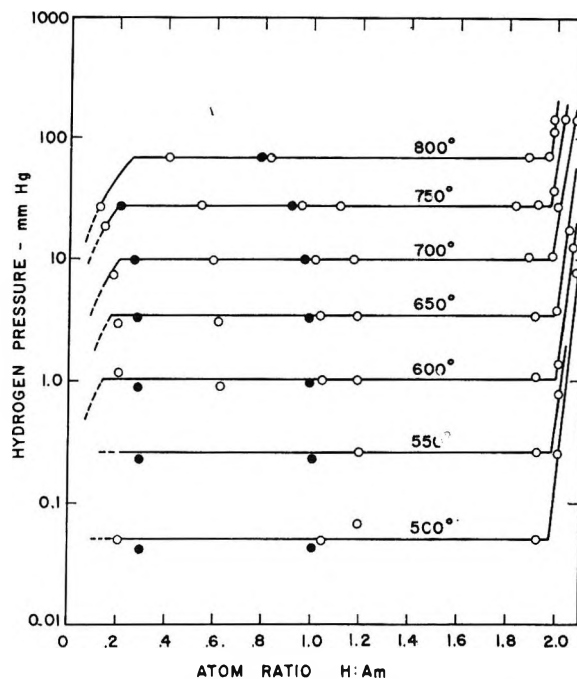


Figure 1. Pressure isotherms vs. sample composition for the range Am to AmH_2 . Open circles are for addition of hydrogen, solid circles are for removal of hydrogen.

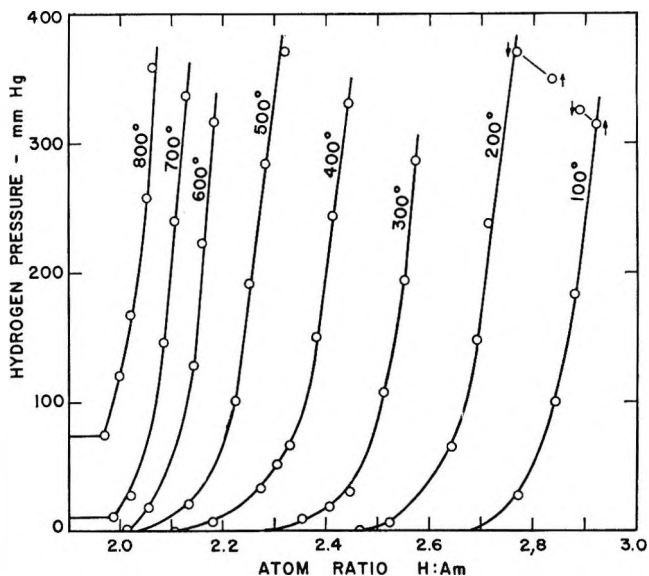


Figure 2. Pressure isotherms for the composition AmH_2 to AmH_3 . Arrows show direction of temperature approach to the point.

Because of the extreme sluggishness of the reaction forming AmH_3 , no well-defined hysteresis loops were observed.

In Table I, X-ray data for several compositions are presented. It was very difficult to obtain samples

which could provide X-ray patterns sufficiently sharp to permit determination of the AmH_3 lattice parameters. A satisfactory pattern was finally obtained from a sample that had been annealed under 530 torr of hydrogen pressure for 40 hr at 100° .

Table I: X-Ray Data

Sam- ple	H/Am ratio	Phases present	Lattice parameter, A
1	0.46	Cubic only	$a_0 = 5.347 \pm 0.001$
2	1.76	Cubic only	$a_0 = 5.349 \pm 0.001$
3	2.67	Cubic only	$a_0 = 5.338 \pm 0.004$
4	2.92	Cubic + hex	Cubic: $a_0 = 5.340 \pm 0.005$ Hex: Poor pattern
5	2.96	Cubic + hex	Hex: $a_0 = 3.77 \pm 0.01$ $c_0 = 6.75 \pm 0.01$

The AmH_{2+x} ($0 \leq x \leq 0.7$) phase is face-centered cubic, presumably of the fluorite type, and is isostructural with PuH_{2+x} ⁶ and NpH_{2+x} ³ as well as with most of the rare earth dihydrides. The lattice parameters observed for the cubic phase are given in Table I; the calculated density of $\text{AmH}_{2.0}$ is 10.6 g/cm^3 .

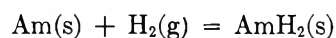
The AmH_3 phase is hexagonal and is isostructural with PuH_3 ,⁶ NpH_3 ,³ and the trihydrides of the heavy rare earths.⁷ The calculated density of $\text{AmH}_{3.0}$ is 9.76 g/cm^3 . As the hydrogen positions have not been determined for any of these compounds except CeH_2 , the assumption that they are isostructural rests on their having similar metallic lattices.

It is seen from Table I that the lattice parameter shrinks as the hydrogen content of the cubic AmH_{2+x} phase increases. Similar behavior is exhibited by PuH_{2+x} and the rare earth hydrides of comparable structure. However, the lattice parameter of NpH_{2+x} expands with increasing hydrogen content.

When the logarithms of the plateau pressures of Figure 1 are plotted *vs.* the reciprocal of the temperature, a straight line is obtained whose slope gives the heat per mole of hydrogen gas for the formation of AmH_2 from americium and hydrogen. The americium and AmH_2 phases for which this heat is appropriate have compositions as defined by the ends of the plateau, but in view of the small solubility of hydrogen in americium and the small departure from stoichiometry of the AmH_2 on the hydrogen-poor side, the heat may be assumed to be close to that for the reaction involving the pure phases. The equation for the line is

$$\log p(\text{atm}) = 7.190 - 8812/T(^{\circ}\text{K})$$

The slope, for the process



gives an enthalpy change

$$\Delta H = -40.3 \text{ kcal/mole (773-1073}^{\circ}\text{K)}$$

which should be nearly correct for the standard heat of formation of AmH_2 in the temperature range given.

A brief comparison of the actinide hydrides is of interest. Pertinent data are listed in Table II. Different crystal structures and compositions are found for the lower hydrides in the respective systems. Thus ThH_2 is tetragonal, PaH_3 and $\beta\text{-UH}_3$ are cubic, and NpH_2 , PuH_2 , and AmH_2 , although also of cubic symmetry, are structurally different from PaH_3 and $\beta\text{-UH}_3$. If, however, the metal-hydrogen bond lengths are computed for each hydride, assuming that NpH_2 , PuH_2 , and AmH_2 have the fluorite structure from analogy to CeH_2 , it is seen that for all except ThH_2 the distances are close to 2.32 Å.

Table II

Com- pound	Structure	Lattice parameter, A	M-H distance, A	$-\Delta H_f$, kcal/ mole of H_2
ThH_2	Tetragonal	$a = 4.10,$ $c = 5.03$	2.41(?)	34
PaH_3	Cubic	6.648	2.33	..
$\beta\text{-UH}_3$	Cubic	6.631	2.32	20
NpH_2	Fcc	5.343	2.314	28
PuH_2	Fcc	5.359	2.320	37
AmH_2	Fcc	5.348	2.316	40

The heats of formation per mole of hydrogen gas show a fairly large increase with atomic number; ThH_2 is again an exception. Thus the actinide hydrides above thorium become more stable as atomic number increases, at least as far as americium. In the comparable fluorite-structure dihydrides formed by the rare earth series, no trend is evident in the heats of formation; all the known heats are close to -50 kcal/mole of H_2 . In the rare earth hydrides the lanthanide contraction is clearly evident; that is, the metal-hydrogen distance decreases uniformly with atomic number.⁷ The actinide hydrides, however, do not exhibit any effect that can be attributed to actinide contraction, although such contraction is clearly evidenced in other series of more ionic actinide compounds, the dioxides

(6) F. H. Ellinger in "The Metal Plutonium," A. S. Coffinberry and W. N. Miner, Ed., University of Chicago Press, Chicago, Ill., 1961, p 291.

(7) A. Pebler and W. E. Wallace, *J. Phys. Chem.*, **66**, 148 (1962).

and the halides, for example. Unfortunately, not enough data are available to permit comparison of the actinide hydride bond lengths with those of other actinide compounds, such as the monosulfides, in which the cation can be called divalent.

Further comparison is possible for the hexagonal trihydrides of neptunium, plutonium, and americium. The heats of formation of these compounds cannot easily be derived accurately from existing pressure

measurements, but the unit cell dimensions are available. In the heavy rare earth trihydride series, an unequivocal contraction is evident,⁷ but again, no such effect is seen for the three comparable actinide trihydrides.

Acknowledgment. We gratefully acknowledge the determination of the lattice parameters by Finley H. Ellinger.

Infrared Study of OH and NH₂ Groups on the Surface of a Dry Silica Aerogel

by J. B. Peri

Research and Development Department, American Oil Company, Whiting, Indiana (Received March 14, 1966)

Infrared and gravimetric study of transparent plates of pure silica aerogel yielded further evidence on the characteristics of the OH groups retained after strong drying, the replacement of OH groups by NH₂ groups, and the formation of NH₂ groups by chemisorption of NH₃. Reactions of D₂, D₂O, HCl, Cl₂, SiCl₄, and CCl₄ with surface OH groups were investigated briefly to obtain additional information on the surface structure and the reactivity of surface groups. Spectra and the retention of OH groups were generally as reported for other silicas, but evidence was also found for some rotation or torsional oscillation. The Si-OH bond angle appears to be about 113°. Spectra of hot silica showed that OH groups persist on the surface at 800°. Exchange of OH groups with D₂ was slow on dry silica even at 700°, but D₂O exchanged rapidly at 100° or lower. All OH groups left after drying at 600° were on the surface. Chemisorption of NH₃ occurred slowly on samples predried at 800°, producing bands (3526 and 3446 cm⁻¹) assigned to NH₂ groups. Maximum chemisorption was 1.3 to 1.4 molecules/100 Å². No HCl was chemisorbed, and it exchanged H only very slowly with surface OD groups. Both Cl₂ and CCl₄ replaced surface OH with Cl, which could in turn be readily replaced with NH₂ groups. The NH₂ groups could again be replaced by Cl by treatment with HCl. Reaction with SiCl₄ and subsequent hydrolysis provided evidence that surface OH groups are relatively immobile on "dry" silica, even at 800°, and are often paired. Steric factors are probably often important in reactions involving such groups.

Introduction

Because their surface properties are both practically and theoretically important, silica gels and other high-area silicas have been intensively studied in many laboratories.^{1,2} Silica surfaces are usually covered

with a layer of OH groups and adsorbed H₂O. Heating at elevated temperatures removes most of this layer,

(1) R. K. Iler, "The Colloid Chemistry of Silica and Silicates," Cornell University Press, Ithaca, N. Y., 1955.

(2) J. A. Hockey, *Chem. Ind.* (London), 57 (1965).

but some OH groups are retained very tenaciously.³ Substitution of other groups for the OH groups is often sought to modify adsorptive and other properties of silicas.

Much of our present knowledge of their surface structure has come from infrared studies of high-area silicas.⁴⁻¹⁸ Because typical silica gels scatter much radiation, special forms of high-area silica such as Aerosil (Cabosil) and microporous glass have been used in most studies to date. Neither of these materials represents typical silica gel. Microporous glass is, moreover, very impure (96% silica), containing boria, alumina, and other impurities. Only a few studies of more typical silica gels prepared by "wet" methods have been reported.^{5,11,14} To minimize scattering losses, these silica gels have been studied as self-supporting pressed disks. The high pressures used in disk formation can apparently significantly alter the behavior of the silica, however.^{5,16}

Considering the variety of materials studied, the major characteristics of their infrared spectra are remarkably similar. A sharp band at 3750 cm^{-1} is universally assigned to "isolated" (*i.e.*, not H-bonded) OH groups. A tail, or close-lying band, in the $3600\text{--}3750\text{-cm}^{-1}$ region appears to be caused by weakly H-bonded OH groups. Absorption centered in the $3400\text{--}3500\text{-cm}^{-1}$ region is attributed to strongly H-bonded OH groups and/or adsorbed H_2O . Because the bands in this region are generally associated with a band near 1630 cm^{-1} (presumably caused by H_2O deformation), assignment to H_2O is usually favored. Attribution of a band at 3500 cm^{-1} to geminal OH groups (*i.e.*, two groups attached to the same silicon atom) has been suggested, however.^{2,11}

A band found at 4540 cm^{-1} on microporous glass has been assigned to the combination of isolated OH stretching with Si-O stretching vibrations,¹³ while a similar band on silica gel has been assigned to the combination of OH stretching with Si-OH bending.¹⁴ A band near 870 cm^{-1} has been assigned to deformation of surface OH groups.⁹

Bands at 1635 , 1870 , and 2000 cm^{-1} (shoulder) in the spectrum of dry silicas appear to arise from combinations and/or overtones of lattice vibrations,^{9,10} as do weaker bands in the region from 2200 to 2950 cm^{-1} in the spectrum of microporous glass.^{10,13,17}

Spectra in the H_2O deformation region indicate that little or no adsorbed H_2O remains after the silica has been dried above 250° ^{4,10} and that most H_2O can be eliminated at considerably lower temperatures. Evidence from reaction of silica gels with AlCl_3 and BCl_3 has, however, been interpreted to mean that molecular

H_2O can be strongly held even after the silica has been dried under vacuum at 350° or higher.¹⁹

Prevailing opinion holds that most of the OH groups in silica gel are on the surface. Characteristically, however, a significant fraction of the OH content, even on silicas predried at 600° , is not removed by reaction with reagents such as diborane,^{3,20} CH_3MgI , and CH_3Li ,⁴ suggesting that the groups are held internally rather than on the surface. Absence of reaction could, however, reflect steric factors, possibly arising from the presence of geminal OH groups.²

Little is presently known about the mobility, attachment, or arrangement of OH groups on the surface. It has even been suggested⁵ that the OH groups left after the silica has been dried at very high temperatures may not actually exist on the hot surface but may reform only at lower temperatures as traces of H_2O are again chemisorbed.

Replacement of OH groups on microporous glass by NH_2 groups¹⁵ and by fluoride¹⁸ have been studied, but little infrared study of reactions of OH groups on pure silica has been reported to date. Some NH_3 is slowly chemisorbed on silica, but chemisorption never exceeds 1.5 molecules/100 A^2 of surface.²¹ No infrared study of such adsorption has been reported, but physical adsorption of NH_3 has been investigated.⁶⁻⁸

- (3) C. Naccache and B. Imelik, *Bull. Soc. Chim. France*, 553 (1961); C. Naccache, J. F. Rosetti, and B. Imelik, *ibid.*, 404 (1959).
- (4) J. J. Fripiat and J. Uytterhoeven, *J. Phys. Chem.*, 66, 800 (1962); J. J. Fripiat, M. C. Gastuche, and R. Brichard, *ibid.*, 66, 805 (1962).
- (5) R. S. McDonald, *ibid.*, 62, 1168 (1958).
- (6) A. N. Sidorov, *Dokl. Akad. Nauk SSSR*, 95, 1235 (1954).
- (7) N. W. Cant and L. H. Little, *Can. J. Chem.*, 42, 803 (1964).
- (8) M. Folman and D. J. C. Yates, *Proc. Roy. Soc. (London)*, A246, 32 (1958); *J. Phys. Chem.*, 63, 179 (1959).
- (9) H. A. Benesi and A. C. Jones, *ibid.*, 63, 179 (1959).
- (10) L. H. Little and M. V. Mathieu, *Actes Intern. Congr. Catalyse*, 2^e, Paris, 1, 771 (1961).
- (11) J. A. Hockey and B. A. Pethica, *Trans. Faraday Soc.*, 57, 2247 (1961).
- (12) G. J. Young, *J. Colloid Sci.*, 13, 67 (1958).
- (13) V. A. Nikitin, A. N. Sidorov, and A. V. Karyakin, *Zh. Fiz. Khim.*, 30, 117 (1956).
- (14) J. H. Anderson and K. A. Wickersheim, *Surface Sci.*, 2, 252 (1964).
- (15) M. Folman, *Trans. Faraday Soc.*, 57, 2000 (1961).
- (16) F. H. Hambleton, J. A. Hockey, and J. A. G. Taylor, *Nature*, 208, 138 (1965).
- (17) N. Sheppard and D. J. C. Yates, *Proc. Roy. Soc. (London)*, A238, 69 (1956).
- (18) T. H. Elmer, I. D. Chapman, and M. E. Nordberg, *J. Phys. Chem.*, 67, 2219 (1963).
- (19) H. P. Boehm, M. Schneider, and F. Arendt, *Z. Anorg. Allgem. Chem.*, 320, 43 (1963).
- (20) I. Shapiro and H. G. Weiss, *J. Phys. Chem.*, 57, 219 (1953); H. G. Weiss, J. A. Knight, and I. Shapiro, *J. Am. Chem. Soc.*, 81, 1823 (1959).
- (21) V. W. Stober, *Kolloid-Z.*, 145, 17 (1956).

Prospects were seen for obtaining better spectral data (and avoiding possible pressure effects) through preparation and study of pure silica aerogel in the form of transparent plates. Such data are also needed to permit close comparison of the silica surface with those of silica-alumina and other catalysts made from it. Gravimetry and isotopic exchange of surface OH groups with D₂ or D₂O were used to supplement infrared study. Adsorption of NH₃, ether, and HCl, and reactions of surface OH groups with Cl₂, CCl₄, and SiCl₄ were investigated to obtain additional information on the surface structure and on the reactivity of surface groups.

Experimental Section

Most of the equipment, techniques, and procedures have been described.^{22,23} Various combinations of cells and spectrometers permitted infrared study from 1400 to 5000 cm⁻¹ on samples at room temperature and from 2000 to 5000 cm⁻¹ on hot samples at temperatures up to 900°. Ethyl iodide and 1,2,4-trichlorobenzene²⁴ were used for calibration (LiF prism) from 3900 to 4700 cm⁻¹. Calcination in O₂, evacuation, and other treatments of the samples were normally carried out while the cells were in place in the spectrometers. In one type of cell the sample was suspended from a quartz helix so that weight changes could be followed concurrently with spectral changes and surface area could be measured by N₂ adsorption while the sample was in the cell. Such a cell (cell D) containing a silica aerogel plate is shown in Figure 1.

Because preparation of strong, clear aerogel plates is an art, the method is given in detail. Typically, 50 ml of stock solution containing 40 vol % ethyl orthosilicate (Fisher Purified) in methanol (Baker and Adamson reagent) was mixed with 30 ml of concentrated HCl (Baker Analyzed reagent), filtered, and poured onto mercury in a crystallization dish 7.25 in. in diameter. The dish was then covered. Within 3 hr, a glass-clear sheet of gel was formed. After an additional 16 hr, the gel was broken into smaller pieces and transferred to a 400-ml bath of 50% aqueous methanol. The following day the bath was changed to 25% aqueous methanol, and later in the day to distilled H₂O. During the following week, the H₂O was changed four times. The gel plates were then aged for 4 hr in H₂O at 100° in a closed autoclave. They were then transferred to 50% aqueous methanol, and after a few hours, to absolute methanol.

After five successive changes of methanol (400 ml each) during the next 3 weeks, the plates were transferred to a 250-ml glass autoclave liner. Methanol was added to fill the liner completely, and the plates

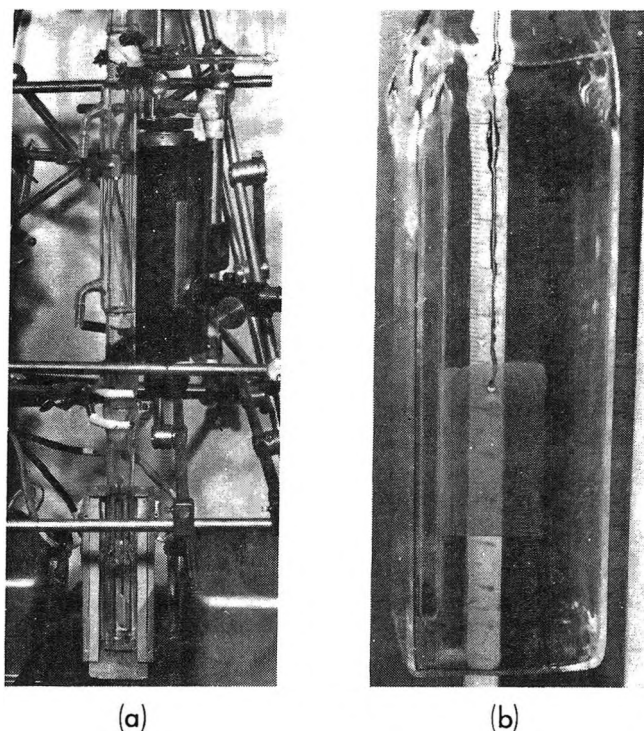


Figure 1. Cell D: (a) cell positioned in spectrometer (one side of furnace removed); (b) lower cell showing aerogel plate.

were autoclaved at 250–300° while methanol was vented slowly to maintain pressure between 1200 and 1500 psi until most of the methanol had been vented. After the pressure had dropped to 1 atm, the autoclave was evacuated for 2 hr while cooling. The autoclaving took roughly 7 hr.

The final plates were relatively flat, transparent, and free from cracks. Their dimensions ranged up to 1 × 3 in. Thicknesses averaged between 1/16 and 1/8 in. Surface areas, after calcination in O₂ and evacuation at 600° for 2 hr, were 750–850 m²/g as measured by N₂ adsorption. The plates did not lose transparency or develop cracks on heating under vacuum at temperatures up to 900° and lost surface area only slowly at 800° (~3%/hr). Silica gel, made by the same procedure, except dried normally from the hydrogel (after aging at 100°) gave a surface area of 807 m²/g, showing that autoclave drying of the alcogel had little effect on surface area. Density was about 0.18 g/cc and calculated average pore diameter was 250 Å. Analysis showed less than 0.020% impurities, including,

(22) J. B. Peri and R. B. Hannan, *J. Phys. Chem.*, **64**, 1526 (1960).

(23) J. B. Peri, *Actes, Intern. Congr. Catalyse*, **2^e**, Paris, **1**, 1333 (1961).

(24) N. Acquista and E. K. Plyler, *J. Res. Natl. Bur. Std.*, **49**, 13 (1952).

as oxides, Mg (0.0074%), Al (0.0060%), Cu (0.0043%), and Fe (0.0017%).

The SiCl_4 (Matheson, 99.8% minimum) was purified and freed from HCl by vacuum distillation immediately before use. The CCl_4 (Mallinckrodt AR) was dried with P_2O_5 and degassed by repeated freezing and evacuation. The Cl_2 (Matheson) was dried with P_2O_5 .

Methanol and ethyl ether (Baker Analyzed AR) were degassed by vacuum distillation, freezing, and evacuation. Sources and purification of HCl, NH_3 , D_2 , and D_2O have been described.²²

Plates used in infrared studies typically weighed 0.15 to 0.30 g, giving about 35 mg/cm² in the infrared beam. In typical experiments, a "virgin" aerogel plate was mounted in the cell and calcined in O_2 (200 torr) at 600° for 1–2 hr or at 800° for 1 hr. Final pressure after evacuation was always below 10^{-4} torr. Some spectra were recorded while the silica was hot, but usually the sample was first cooled to room temperature. In experiments involving treatment with SiCl_4 , the usual cells and procedures were used. Evolved HCl and excess SiCl_4 were frozen out in a trap cooled with liquid N_2 , and HCl was then determined by the pressure change on warming to -78.5° .

Results

Calcination and Drying. As removed from the autoclave, the silica aerogel was partially covered with methoxy groups in addition to OH groups and H_2O . Calcination in O_2 at 600° followed by brief evacuation removed all spectral evidence of the methoxy groups, leaving the bands characteristically reported for silica gel.

When the silica was dried under vacuum at high temperatures, there was a rapid initial loss of OH groups after which OH groups were lost only very slowly. When the temperature was increased, additional rapid initial loss was again observed. Similar behavior has been reported for microporous glass²⁵ and for γ -alumina aerogel.²⁶ The rate of loss of OH groups at 800° in the "plateau" region appeared comparable to the rate of loss of surface area. Because of this behavior, prolonged evacuation seemed neither necessary nor desirable in predrying the plates. By reaction with SiCl_4 , typical plates were found to hold 3.1 and 1.4 OH/100 A^2 after evacuation for 2 hr at 600° and 1 hr at 800°, respectively.

Figure 2 shows spectra (LiF prism, Perkin-Elmer 12C spectrometer) of an aerogel plate, first calcined in O_2 at 600°, and then dried by evacuation at 600, 700, and 800°. To provide additional information, the silica was partly exchanged with D_2O before drying

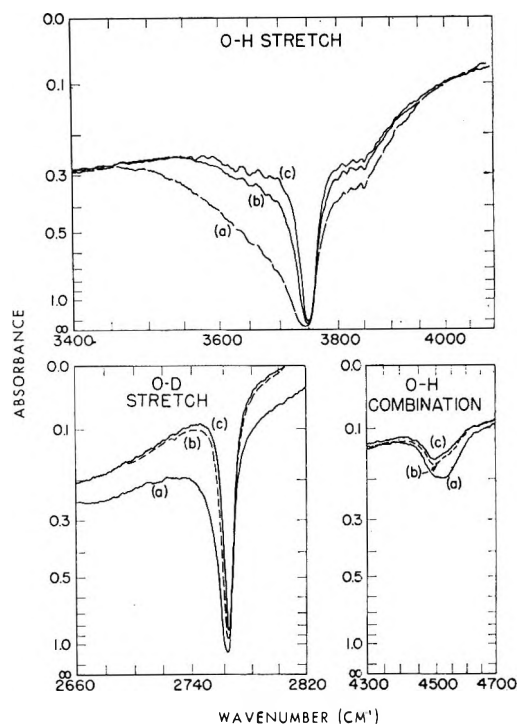


Figure 2. Spectral changes on dehydration. Sample dried at (a) 600°, (b) 700°, and (c) 800°.

at 600° to produce a small OD band. In the regions shown, the bands left after drying at 600° were reduced to under half their integrated intensities by drying at 800°. Bands at 1635, 1870, and 2000 cm^{-1} were not significantly affected by drying between 600 and 800° or by removal of all OH groups through reaction with SiCl_4 . No bands were evident in the 2500–3000- cm^{-1} range.

Exchange of D_2 or D_2O with OH Groups. The OH groups and adsorbed H_2O on silica aerogel exchanged H (or OH) with D_2O rapidly and apparently completely at $\leq 100^\circ$. The OH bands were replaced with corresponding OD bands at lower frequencies (~ 2760 cm^{-1} for isolated OD groups).

The OH groups exchanged H far less readily with D_2 gas than with D_2O . On aerogel predried at 700°, only very slow exchange occurred at 300°. The rate of exchange increased moderately with increasing temperature, but complete exchange required several hours even at 700°.

Spectra recorded after almost complete conversion of OH groups to OD groups through exchange with D_2 at 700° on an aerogel plate predried at 800° are illustrated in Figure 3 for the OH and OD stretching

(25) M. J. Rand, *J. Electrochem. Soc.*, **109**, 402 (1962).

(26) J. B. Peri, *J. Phys. Chem.*, **69**, 211 (1965).

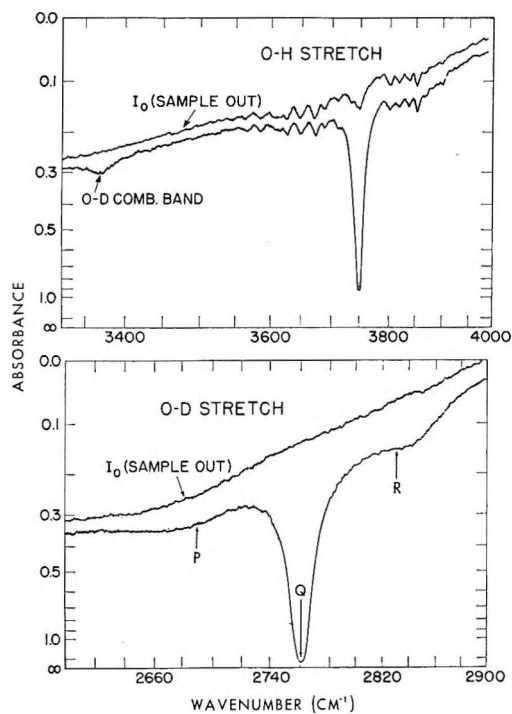


Figure 3. Spectra after exchange with D₂ (silica predried at 800°).

regions (LiF prism, Perkin-Elmer 12C spectrometer). The characteristics of the OD bands correspond closely to those of the OH bands shown in Figure 2. Weak P and R branches²⁷ appear to accompany both the isolated OH and OD stretching bands, but (as indicated in Figure 3) they are evident only when the bands are intense. The band at 3363 cm⁻¹ (Figure 3), appearing only on deuterated silica, clearly has an origin similar to that of the band at 4520 cm⁻¹ (which disappeared on D₂ exchange).

Changes in the Isolated OH Bands at High Temperature. Typical spectra obtained at 400, 600, and 800° after the silica had been predried at 800° are shown in Figure 4. The "hot" spectra are distinguished principally by shifting of the isolated OH band to lower frequencies, broadening of this band, and appearance of a small "hot band" near 3580 cm⁻¹ at temperatures above 600°.

Between ~30 and 800°, the total shift was about 18 cm⁻¹ for the OH band and 12–13 cm⁻¹ for the OD band, being comparable to shifts observed for the OH bands on hot alumina.²⁶ The integrated intensity of the OD band did not change significantly as the band broadened at high temperatures. The number of OH groups remained constant, and all the changes were reversible.

Adsorption of Ether and NH₃ on Silica Aerogel. Exchange of OH groups with D₂ or D₂O does not prove

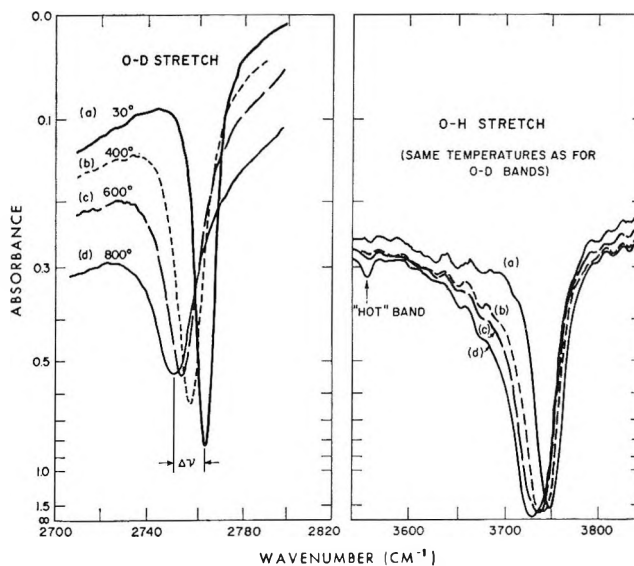


Figure 4. Spectra of OH and OD bands for silica at various temperatures.

that the groups are surface groups, since D₂ or D₂O might penetrate the silica lattice or internal OH groups might migrate to the surface. If, however, OH groups are affected at low temperatures by adsorbed molecules that cannot penetrate the silica lattice, the OH groups must be on the surface.⁵

Physical adsorption of NH₃ or ethyl ether at room temperature and at pressures below 1 atm completely eliminated bands caused by the isolated and weakly H-bonded OH groups left after the silica had been dried at 600°. A broad H-bonded OH band was produced at lower frequencies in both cases.

Chemisorption of NH₃. Chemisorption of NH₃ did not occur readily on silica, and after brief contact nearly all adsorbed NH₃ was usually removed by very brief evacuation at room temperature. Immersion of dry aerogel in liquid NH₃ did not yield any permanent addition or exchange of NH₂ for OH groups after subsequent evacuation. Heating silica in gaseous NH₃ up to 800° also failed to replace OH groups with NH₂ groups.

On aerogel completely exchanged with D₂ and predried at 800°, however, NH₃ was slowly chemisorbed at room temperature on a limited number of sites. Typical spectra are shown in Figure 5. Adsorption initially produced a band at 3419 cm⁻¹, apparently caused by the ν₃ stretching vibration which appears at 3417 cm⁻¹ for NH₃ in CCl₄ solution.²⁸ This band

(27) G. Herzberg, "Molecular Spectra and Molecular Structure," Vol. II, D. Van Nostrand Co., New York, N. Y., 1945.

(28) C. G. Cannon, *Spectrochim. Acta*, 10, 341, 425 (1958).

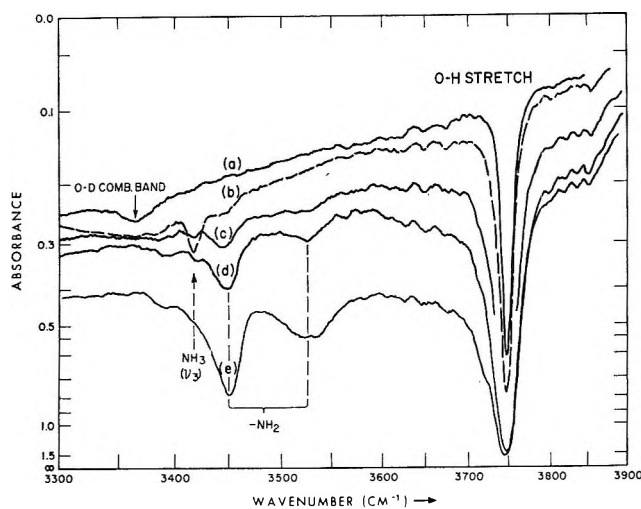
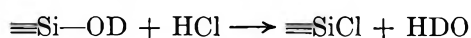


Figure 5. Spectra of NH_3 adsorbed on dry silica: (a) silica predried at 800° after deuteration; (b) after adsorption of 1 molecule of $\text{NH}_3/1000 \text{ \AA}^2$; (c) after exposure to 3 torr of NH_3 for 0.5 hr plus brief evacuation; (d) after exposure to 5 torr of NH_3 for 0.5 hr; (e) after redrying at 800° and exposure to 10 torr of NH_3 for 8 days.

changed slowly with time to give two bands at 3526 and 3446 cm^{-1} . The isolated OH band became more intense. The bands at 3526 and 3446 cm^{-1} are evidently caused by NH_2 groups.¹⁵ (As was found later, the NH_2 deformation band occurs near 1555 cm^{-1} .) After the aerogel had been exposed to NH_3 at higher pressures and for a longer time, these bands were more intense, but the maximum chemisorption of NH_3 after 8 days at 100 torr was only 1.3 to 1.4 molecules/ 100 \AA^2 . Chemisorbed NH_3 was not readily desorbed at 200° but was mostly removed by heating to 600° . Traces remained, however, even after evacuation at 800° for 30 min. These experiments resulted in almost complete exchange of the OD groups initially present. Such exchange precluded clearly establishing that one new OH group is formed for each NH_3 molecule chemisorbed, although this is probably the case.

Reactions with $\text{HCl}(g)$, Cl_2 , and CCl_4 . Pure, dry HCl was not detectably chemisorbed on dry deuterated silica ($\ll 1$ molecule/ 1000 \AA). Exchange between HCl and the OD groups was very slow at room temperature, and was not rapid even at 700° . Few, if any, new OH groups were formed at 700° . On the other hand, heating the silica at 700° in flowing dry HCl failed to remove OH groups. The reaction



apparently does not occur to an appreciable extent. However, all OH groups were removed by reaction with Cl_2 at $700\text{--}950^\circ$ or with CCl_4 at $350\text{--}600^\circ$. The

weight changes indicated that they were replaced by Cl. The principal gaseous products of the reaction with CCl_4 were COCl_2 and HCl .

Replacement of Surface Cl by NH_2 Groups. When silica from which OH groups had been removed by reaction with Cl_2 or CCl_4 was exposed to NH_3 , strong bands indicating NH_4Cl formation were produced. When the silica was subsequently heated at $400\text{--}600^\circ$, the NH_4Cl sublimed out of the plate, leaving a surface covered with NH_2 groups. Weight changes were consistent with replacement of Cl by NH_2 . Spectra obtained during replacement of OH with Cl and subsequent replacement of Cl with NH_2 groups are shown in Figure 6. Replacement of Cl by NH_2 groups also produced a band near 1555 cm^{-1} , evidently caused by NH_2 deformation. The NH_2 groups were as difficult to remove by evacuation at high temperatures as the OH groups which they replaced. They were, however, rapidly removed (<2 min) when HCl was admitted to the cell at low pressures at 600° and then (after evacuation) were rapidly restored (<2 min) when NH_3 was admitted at 600° ; NH_4Cl was also produced.

Exposure of a chlorided surface to water vapor rapidly replaced Cl with OH groups, restoring the spectrum of the silica to its original appearance. The NH_2 groups were moderately resistant to hydrolysis, however, although prolonged heating in H_2O vapor gradually replaced NH_2 with OH. Calcination in O_2 at 600° readily removed NH_2 groups and restored the OH groups.

Reaction with SiCl_4 . Reaction of SiCl_4 with the aerogel removed protons rather than OH groups, HCl being evolved. All OH bands could be removed

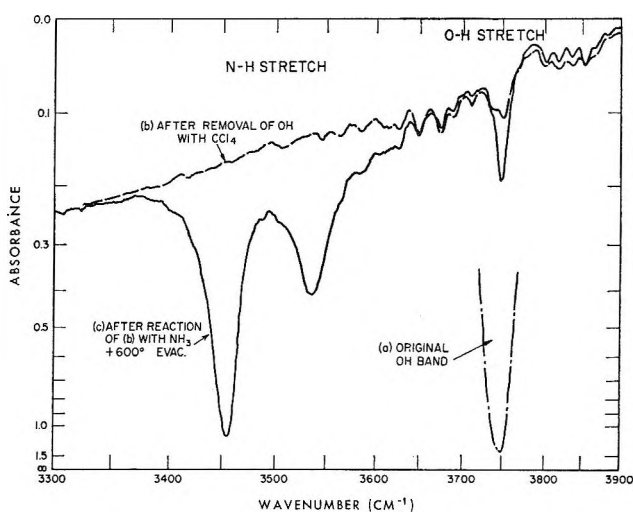


Figure 6. Spectral changes resulting from replacement of OH groups on silica by Cl and by NH_2 groups.

from spectra by such reaction below 600°. The number of OH groups with which each attached SiCl₄ molecule had reacted was calculated from the amount of HCl liberated and the net gain in the weight of the plate (or from the HCl produced on subsequent hydrolysis). Most of the SiCl₄ molecules reacted with two rather than with one OH group on fresh aerogel calcined and predried at 600°. Even after the silica was predried at 800°, over 40% of the SiCl₄ molecules reacted with two OH groups. When, however, the virgin silica was first heated under vacuum at 800° (all methoxy groups were removed without discoloration of the silica), calcined in O₂ at 600°, and finally redried at 800°, a different result was obtained. In this case reaction occurred mainly in the ratio of one OH group per SiCl₄ molecule. Similar 1:1 reaction was later noted on silica aerogel that had been exposed to air for over 1 year. Supporting data will be presented in a subsequent paper.

There were no significant differences in the characteristics of the isolated OH stretching bands, either with respect to frequency or the relative intensities of the P, Q, and R branches (prior to SiCl₄ reaction) between samples on which 1:1 reaction occurred and those which gave 1:2 reaction. No spectroscopic evidence for adsorbed H₂O was found in either case.

Figure 7 shows spectra obtained (cell A—CaF prism, Perkin-Elmer Model 112) when silica, predried at 800°, was treated with SiCl₄ to remove all OH groups, hydrolyzed at 400°, and redried at 400 and 800°. About 63% of the original OH groups were paired (*i.e.*, reacted in the ratio of two OH groups per Si atom attached). The arrangement and number of the surface OH groups might conceivably be markedly changed by such reactions. Isolated, widely separated, OH groups might react with SiCl₄ and subsequently hydrolyze to produce -Si(OH)₃ groups which could not readily condense either internally or with other groups to eliminate H₂O. Initial reaction of two OH groups with one SiCl₄ molecule followed by hydrolysis might lead to =Si(OH)₂ groups (geminal OH). The spectra, however, failed to show any difference between the original (800° predried) spectrum and that obtained after the silica was finally redried at 800°. Weight readings in similar experiments showed that all the Si added initially was retained after hydrolysis and redrying.

Discussion

The major spectral features of silica aerogel are quite similar to those of other similarly dry silicas. Drying above 700° appears to leave only isolated OH groups.

The behavior of the bands at 4520 and 3363 cm⁻¹ on

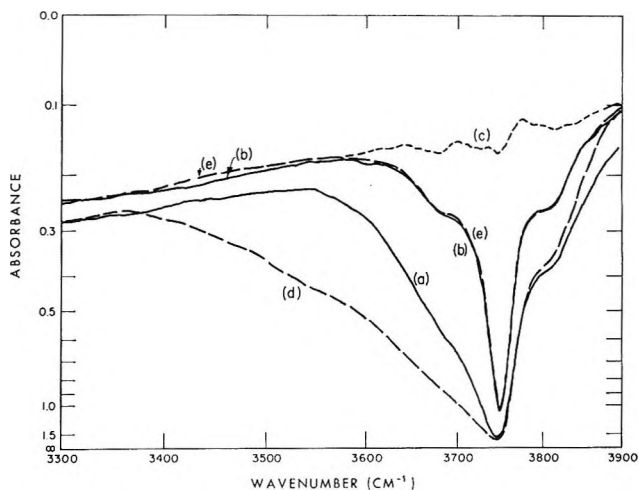


Figure 7. Spectral changes resulting from reaction of OH groups on dry silica with SiCl₄ and from subsequent hydrolysis and redrying: (a) silica aerogel after drying at 600°; (b) after subsequent drying at 800° for 1 hr; (c) after reaction of (b) with SiCl₄ at <600°; (d) after hydrolysis of (c) followed by drying at 400°; (e) after final drying at 800° for 1 hr.

dehydration or exchange shows that they are combination bands involving the isolated OH and OD bands, respectively. The 4520-cm⁻¹ band is 770 cm⁻¹ higher in frequency than the isolated OH band (3750 cm⁻¹). The 3363-cm⁻¹ band is 603 cm⁻¹ higher than the isolated OD band. The difference between the separations observed with OH and OD groups suggests that the bands represent combinations of the stretching and out-of-plane deformation modes for the OH groups and OD groups rather than combinations involving Si-OH bending¹⁴ or Si-O stretching.¹³ The out-of-plane deformation frequencies (770 and 603 cm⁻¹) for Si-OH and Si-OD would thus be similar to those of free OH and OD groups in alcohols.²⁸ The apparent existence of out-of-plane deformation argues that at least some of the OH groups cannot freely rotate.

The existence of weak P and R branches above and below the isolated OH and OD stretching bands indicates that some quantized rotation or torsional oscillation of surface OH and OD groups must occur. Although individual satellite bands are not resolved, a rough value can be calculated for the rotational constants (assuming free rotation) from the separation of the P and R branch maxima.²⁷

To obtain the separations of the branch maxima more accurately, background spectra in the OH and OD regions (sample out) were obtained immediately following spectra of the silica. After subtraction of background absorbance, the spectra were plotted on a linear absorbance scale, and the OH and OD bands were separated into branches by assuming an approximate

Lorentz shape for the central band. The separations in the P and R branch maxima were approximately 200 cm^{-1} for the OH band and 140 cm^{-1} for the OD band.

The separation $\Delta\nu$ (cm^{-1}) is given by

$$\Delta\nu = \sqrt{8kTB/hc} = 2.358\sqrt{TB}$$

where T is the absolute temperature, and B , the rotational constant, is equal to $h/8\pi^2cI_B$. For linear molecules, I_B is the moment of inertia about an axis perpendicular to the internuclear axis and going through the center of mass. For diatomic molecules, $I_B = \mu r^2$ where μ is the reduced mass and r is the distance between atom centers. The surface silicon atom to which an OH group is attached is also bound to three O atoms; it can probably be regarded as an essentially infinite mass. Only a single axis of rotation exists, passing through the Si atom and very close to the O atom. Assuming a bond angle $>90^\circ$, the OH group was approximated as a diatomic molecule with the atomic masses of O and H rotating about the axis of rotation and separated from each other by $r_{\text{eff}} = r \cos(\phi - 90^\circ)$, where ϕ is the angle between the axis of rotation and the O-H axis.

$$I_B = \mu r^2 \cos^2(\phi - 90^\circ)$$

where $\mu = m_1m_2/(m_1 + m_2)$. Assuming an equilibrium O-H distance r (as in H_2O) = 0.958×10^{-8} cm, values were calculated for expected separations between P and R branch maxima as a function of the angle ϕ . For values of ϕ ranging from 90 to 125° , the separations ranged from 180 to 220 cm^{-1} . The observed separation (~ 200 cm^{-1}) falls in midrange—corresponding to roughly 115° ; ϕ is slightly larger than θ , the true Si-OH bond angle. Calculations indicate that at $\phi = 115^\circ$, $\theta = 113^\circ$. The difference is less than the error involved in the approximations and in measuring the separations of the P and R branch maxima.

Similar calculations were made for OD groups, and the observed separation in P and R maxima (~ 140 cm^{-1}) again corresponded to a bond angle of $\sim 113^\circ$.

The calculated bond angle seems reasonable, but torsional oscillation (or possibly other causes) could give similar bands. Since I is the same for torsional oscillation as for free rotation, the branch maxima separations should be the same. The P and R branches are very weak compared to the strong central (Q branch) band. Perhaps rotation is strongly hindered.¹⁷ Perhaps only some of the OH groups, situated differently from the rest, rotate freely while the others do not. If so, differences in the rate of exchange with D_2O , or in other chemical behavior, might alter the ratio of the intensities of the central and side branches. Although present data cannot exclude minor alterations in the

relative intensity of the branches, no major differences were observed following D_2O exchange or during any of the other reactions described.

The bands reported between 2700 and 3000 cm^{-1} in the spectrum of microporous glass^{10,13} may reflect impurities not present in silica, or possibly adsorbed hydrocarbons.⁵ No such bands were found for silica aerogel.

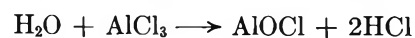
As silica is dried at progressively higher temperatures, the "tail" below the 3750- cm^{-1} disappears more rapidly than does the 3750- cm^{-1} band itself. The H-bonded OH groups are thus eliminated more easily than those that are not H bonded. This indicates that these OH groups are bonded to other OH groups, because H bonding to an oxide ion should not, *per se*, promote elimination of the OH group (as H_2O).

The spectral changes observed for hot silica probably reflect changing interactions with the local environment as well as direct effects of temperature on the O-H bond vibrations. However, the OH and OD groups clearly remain on much the same type of sites at high temperature as those on which they are found after cooling. They are not desorbed as H_2O at high temperatures and reformed when H_2O readsorbs on cooling.

The evidence obtained from adsorption of ethyl ether or NH_3 on silica aerogel predried at 600° or above shows that all the OH groups remaining are surface groups.

Evidence from reaction with SiCl_4 suggests that steric factors are probably usually responsible for the incomplete reaction of OH groups. Even on silica holding <2 OH/100 A, a surprising number of the surface OH groups are sufficiently close together to permit two of them to react with one SiCl_4 molecule. Such close proximity of OH groups would probably make quantitative removal by reaction with diborane, CH_3MgI , or CH_3Li at low temperatures extremely difficult.

Boehm, *et al.*,¹⁹ conclude that production of two molecules of HCl for each molecule of AlCl_3 which reacts with the silica surface results from the reaction



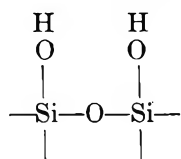
A similar explanation does not appear possible for the results obtained with SiCl_4 in the present work, because SiOCl_2 is unknown,²⁹ and no spectroscopic evidence was found for H_2O (as such) on silica aerogel dried at 600° or above. Clearly, however, close proximity of two OH groups on the surface provides an alternative explanation in both cases.

Present evidence suggests that OH groups are vir-

(29) A. F. Wells, "Structural Inorganic Chemistry," Oxford University Press, Oxford, 1962, pp 776-778.

tually immobile on the surface of dry silica below 800°. Even at 900°, the groups remaining after the first hour of evacuation are eliminated only extremely slowly. Ready migration of OH groups or protons would presumably cause rapid formation and elimination of H₂O. Migration of OH as such requires that Si-O bonds be broken to form Si⁺ sites or unsaturated valencies, and it would probably not occur much more readily than bulk rearrangement of the silica structure. Migration of protons might occur more easily, but if migration occurs very readily, it is hard to understand why NH₂ groups on silica are not more rapidly replaced by OH groups when exposed to H₂O vapor at elevated temperatures (and *vice versa*). If OH groups are very mobile, it is also difficult to see how those left on the surface after predrying at 800° could be paired in some cases and single in other cases as indicated by reaction with SiCl₄. The OH groups on silica appear less mobile than those on alumina.²⁶

If surface OH groups are indeed relatively immobile, their arrangement must be very important in possible reactions with one another or with other molecules. Despite much speculation, there is no evidence to date concerning such arrangement. Isolated OH groups are not necessarily widely separated. The results of reaction of SiCl₄ indicate that, on the contrary, they are often close together. Vicinal OH groups, *i.e.*



are not necessarily H bonded and may be difficult to remove because removal requires edge linking of SiO₄ tetrahedra. Geminal OH groups (=Si(OH)₂) are probably not H bonded to their partners because a five- or six-member ring is normally needed for "intramolecular" H bonding.³⁰ Triplet OH groups (-Si(OH)₃) should be equally free of internal H bonding. Elimination of H₂O by internal condensation of geminal pairs or triplet OH groups would require formation of =Si=O groups. Silicon is not believed to form such groups;²⁹ so, unless geminal or triplet OH groups adjoin OH groups on adjacent Si atoms, their removal through

H₂O formation would probably be very difficult. Probably, particularly on fresh silica gels, geminal and triplet OH groups do exist, but this has not been proved. Interesting questions are raised by the fact that reaction with SiCl₄ plus hydrolysis and redrying fails to alter significantly either the number of surface OH groups or the appearance of the OH bands. The best apparent interpretation is as follows. During hydrolysis, =Si(OH)₂ or -Si(OH)₃ groups, which as initially produced protrude above the surface, are further hydrolyzed and migrate as Si(OH)₄ to other locations where they add to the existing structure in a more stable fashion, simply extending the original surface slightly without changing its character. It has not been established, nor is it evident, that geminal or triplet OH groups which are not H bonded can be readily distinguished spectroscopically from widely separated single OH groups.

The slow chemisorption of a limited amount of NH₃ or very dry silica implies the existence of a small number of highly strained¹² or ionic siloxane linkages on the surface which react with NH₃ to produce -NH₂ + -OH. As found here, the maximum number of such sites is about 1.4/100 A². Chemisorption of NH₃ on silica, as an alumina, appears to be analogous to chemisorption of H₂O. The failure of HCl to chemisorb similarly on dry silica is somewhat surprising.

Conclusion

Although infrared spectroscopic studies have provided considerable information about the surface of silica, many questions concerning the details of surface structure remain unanswered. Answers to most of these questions probably cannot be obtained without supporting studies with other techniques. Additional evidence seems particularly needed on the relative abundance of single, paired, and triplet hydroxyl groups. Evidence on this subject will be presented in a subsequent paper.

Acknowledgments. Discussions with A. L. Hensley, Jr., and Professor R. L. Burwell, Jr., were very helpful in this work. The assistance of J. Kekich in the experimental work is also gratefully acknowledged.

(30) G. C. Pimentel and A. L. McClellan, "The Hydrogen Bond," Reinhold Publishing Corp., New York, N. Y., 1960.

Sedimentation Equilibrium of Ovalbumin in Concentrated Cesium Chloride¹

by Julie Hill and David J. Cox

Clayton Foundation Biochemical Institute and the Department of Chemistry,
The University of Texas, Austin, Texas 78712 (Received March 16, 1965)

Ovalbumin has been examined in the ultracentrifuge at sedimentation equilibrium in concentrated cesium chloride. From the position of the band of protein in the density gradient generated by the redistribution of the salt in the centrifugal field, the buoyant density of ovalbumin was found to be 1.296 ± 0.003 g/cm³. This value agrees quite well with the apparent hydrodynamic density of ovalbumin obtained by plotting the viscosity-corrected sedimentation coefficients observed at several cesium chloride concentrations against the density of the salt solutions, and extrapolating the resulting linear relation to $S = 0$. Sedimentation equilibrium experiments at different rotor speeds and with solution columns of different lengths indicate that the variation of the buoyant density of ovalbumin with hydrostatic pressure is small.

Introduction

A previous report has described measurements of the sedimentation velocity of ovalbumin in concentrated aqueous solutions of five different salts.² When the sedimentation coefficients, measured at several concentrations of a given salt, were corrected to a reference viscosity and plotted against the densities of the solvents, each set of points defined a straight line which, on extrapolation, crossed the density axis well below the reciprocal of the partial specific volume of the protein ($1/\bar{v}_p$). The discrepancy between the density intercept and $1/\bar{v}_p$ could be accounted for by variation of the frictional ratio of ovalbumin with salt concentration, by the binding of water in preference to salt of the protein, or by certain combinations of the two effects. For reasons cited previously, it seems improbable that either the molecular weight or the partial specific volume of ovalbumin varies in these solvents.

Cesium chloride was one of the salts in which the sedimentation velocity of ovalbumin was measured. In cesium chloride, a direct determination of the density of the sedimenting unit can be done—at one salt concentration—by means of the banding method developed by Meselson, Stahl, and Vinograd.^{3,4} Comparison of the buoyant density of the protein measured by the banding method with the density intercept obtained from the sedimentation velocity measurements allows the elimination of several of the possible ways

of accounting for the way in which the sedimentation coefficient of ovalbumin varies with the concentration of cesium chloride. For example, if variation of the frictional ratio alone were responsible for the observed dependence of the sedimentation coefficient on the density of the solvent, then the two densities could not agree. If the two values agree and the frictional ratio does change significantly with the composition of the solvent, then the protein must bind one component of the solvent in preference to the other and the degree of preferential solvation must also vary with salt concentration. The simplest explanation of the velocity experiments, that the protein binds water in preference to salt, and that neither the degree of preferential hydration nor the frictional ratio varies with salt concentration, would require agreement between the density intercept of the velocity data and the buoyant density measured by the banding method.

(1) This work was supported by Grant GM-11749 from the U. S. Public Health Service. Some of the work was reported at the Southwest-Southeast Regional Meeting of the American Chemical Society, Memphis, Tenn., Dec 8-10, 1965.

(2) J. Hill and D. J. Cox, *J. Phys. Chem.*, **69**, 3032 (1965).

(3) M. Meselson, F. W. Stahl, and J. Vinograd, *Proc. Natl. Acad. Sci. U. S.*, **43**, 581 (1957).

(4) J. Vinograd and J. E. Hearst, *Progr. Chem. Org. Natl. Prod.*, **20**, 372 (1962).

Experimental Section

Materials. The ovalbumin was twice-crystallized material purchased from Worthington Biochemical Corp. The protein was taken from the same lot used in previous work.² Cesium chloride was obtained from the Gallard-Schlesinger Chemical Manufacturing Corp. Salt solutions for the ultracentrifuge experiments were prepared by dissolving the appropriate amounts of cesium chloride in potassium phosphate buffer at pH 6.8. The buffer was 0.01 *M* with respect to phosphate and was prepared using glass-distilled water. Solvent densities were measured using 1-ml vented-cap pycnometers, and the results were reproducible within ± 0.001 g/cm³. A sample of the dense and insoluble fluorocarbon FC-43, produced by Minnesota Mining and Manufacturing Corp., was obtained from the Spinco Division of Beckman Instruments, Inc.

Ultracentrifugation. Solutions of ovalbumin in concentrated cesium chloride were brought to sedimentation equilibrium at 20° in a Spinco Model E analytical ultracentrifuge, and the experiments were observed using schlieren optics. The cesium chloride concentrations used were so selected that the position of the band of protein at equilibrium lay near the middle of the solution column. Ovalbumin, with a molecular weight of 45,000, formed relatively wide bands at sedimentation equilibrium and, in order to obtain bands that were sharp enough to be located accurately, it was necessary to operate the centrifuge at relatively high rotor speeds. Double-sector cells could not be used with dense solutions at high velocities, since these generally leaked across the partition between the sectors. The protein solutions and the solvents were, therefore, run separately in single sector cells equipped with 1° negative wedge windows.

In order to calculate the density gradient obtained at sedimentation equilibrium in any particular experiment, the schlieren photograph of water at the same rotor speed was required. In principle, the appropriate base line for the density gradient calculation would be derived from a photograph of the schlieren pattern of the salt solution taken as the rotor reaches the operating speed, but before the salt gradient has developed.^{4,5} In practice, it was found that the gradient began to develop rapidly from the ends of the solution column during acceleration and, by the time the rotor reached top speed, no more than the central third of the schlieren pattern remained unperturbed by the redistribution of the salt.

Experiments were done in which the developing schlieren pattern of a cesium chloride solution was photographed at several angular velocities as the rotor was accelerated to 59,780 rpm. In separate experi-

ments, the cell was filled to the same level with water, and its schlieren pattern was photographed at each of the rotor speeds at which the cesium chloride solution had been observed. The water and cesium chloride base lines both rose appreciably as the centrifugal field was increased. However, at a given angular velocity, the water pattern coincided quite closely with whatever portion of the cesium chloride base line was still unaffected by the development of the salt gradient. It was concluded that the schlieren pattern of water at the appropriate rotor speed could be used as the base line for the density gradient calculation in these particular measurements. This procedure might not be correct for other solvents, and its use would have to be justified experimentally in each case.

All three of the runs required for a given buoyant density measurement—protein and salt, salt alone, and water—were done in the same cell, using the same windows. The rotor speed, the schlieren bar angle, and the length of the solution column were carefully matched among the three runs. It was found that the column lengths could be reproduced most precisely by weighing the amounts of solutions or solvents introduced into the cell.

The relation between the density gradient at sedimentation equilibrium and the area under the schlieren pattern was determined in separate experiments using a valve-type synthetic boundary cell. A cesium chloride solution of known density (ρ_1) was introduced into the centerpiece of the cell, and a solution of lower density (ρ_2) was placed in the cup. The schlieren bar was set at the same position as was used for the equilibrium runs. The rotor was accelerated until the cup emptied, and the boundary was allowed to diffuse until the entire schlieren pattern was visible. The pattern was photographed, the area under the boundary ($A_{1,2}$) was measured, and the quantity $K = (\rho_1 - \rho_2)/A_{1,2}$ was calculated. The measurements were most conveniently done using pairs of solutions that differed in density by about 0.05 g/cm³, and seven pairs were chosen which covered the range of densities encountered in the cell at sedimentation equilibrium. The precision (± 2 –3%) of the individual measurements of K was not sufficient to allow the detection of a significant trend in the values with density; a mean value was used in subsequent calculations. In a few cases, after the schlieren pattern had been photographed at a relatively low rotor speed, the rotor was accelerated to 59,780 rpm and the pattern was photo-

(5) J. E. Hearst, J. B. Ifft, and J. Vinograd, *Proc. Natl. Acad. Sci. U. S.*, **47**, 1015 (1961).

graphed again. The areas under the boundary at the two speeds were compared and were found to be the same.

In each of the centrifuge runs to be described, 0.02 ml of FC-43 was introduced into the cell, along with the solution to be examined, in order to ensure that the entire length of the solution column could be observed.⁵ It was determined that neither water nor cesium chloride was soluble in FC-43 to any measurable extent, and no water-extractable impurities could be detected in the fluorocarbon.

In a few of the experiments, the ovalbumin sample used contained a small amount of insoluble material, presumably denatured protein. During centrifugation to sedimentation equilibrium, this material formed a sharp band which migrated rapidly to a point somewhat below the position eventually occupied by the center of the band of soluble protein. The amount of insoluble protein did not increase visibly during experiments prolonged for several days. Sedimentation velocity experiments carried out with similar, very slightly turbid solutions indicated that the protein remaining in solution was entirely homogeneous. The presence of the precipitated material did not interfere with the measurement of the buoyant density of the soluble protein.

When the ultracentrifuge cell was completely filled, giving a solution column about 1.2 cm long, and the centrifuge was operated at top speed (59,780 rpm), the salt reached its equilibrium distribution in about 8 hr and the ovalbumin was at equilibrium within 20 hr. A few experiments were continued for an additional 12 to 24 hr, but no further change in the solute distribution could be detected. In cases where the effect of rotor speed on the apparent buoyant density of ovalbumin was to be examined, a solution of the protein in concentrated cesium chloride was run to sedimentation equilibrium at 59,780 rpm. The rotor speed was then decreased and the experiment was continued for another 20 hr at a lower speed. The rotor speed was again decreased and the experiment was continued in the same manner. The complete series of measurements was thus done over the course of several days without emptying and refilling the cell.

Calculations. Conservation of mass requires that

$$\int_{r_m}^{r_b} \rho_r d(r^2) = \rho_0 \int_{r_m}^{r_b} d(r^2) \quad (1)$$

where r is the distance from the axis of rotation, ρ_0 is the density everywhere in the cell at the beginning of the run, ρ_r is the density at sedimentation equilibrium at position r , and the integration is carried out between the upper and lower boundaries of the solution column.

Subtracting, from both sides of eq 1, the quantity $\rho_m \int_{r_m}^{r_b} d(r^2)$, where ρ_m is the density at the meniscus sedimentation equilibrium

$$\int_{r_m}^{r_b} (\rho_r - \rho_m) d(r^2) = (\rho_0 - \rho_m)(r_b^2 - r_m^2) \quad (1a)$$

Twenty to thirty areas between the meniscus and various positions r and between the equilibrium schlieren pattern for the cesium chloride and the water base line were measured. The areas were multiplied by the factor K , whose measurement is described above, to obtain a series of values of $(\rho_r - \rho_m)$. The integral on the left side of eq 1a was evaluated numerically or graphically, and the equation was solved for ρ_m . With the density at the meniscus known, ρ_r was calculated for each r .

The position in the gradient at which the diphasic schlieren pattern corresponding to the band of ovalbumin crossed the salt base line was taken as the buoyant density of the protein. Since no correction was made for the compressibility of the salt solutions, the values obtained were, more properly, apparent buoyant densities.⁵ The purpose of the experiments was to compare the buoyant density with the apparent hydrodynamic density derived from sedimentation velocity measurements. Since the latter values were not corrected for the compressibility of the solvent, the uncorrected buoyant densities were the appropriate ones to use for comparison. As will be seen, the pressure corrections are probably small in any case.

Results

The apparent buoyant density of ovalbumin in cesium chloride was measured by the banding method at four different protein concentrations. The centrifuge cell was filled with about 0.7 ml of the protein-cesium chloride solution in each case, and the length of the solution column was about 1.2 cm. The initial density of each solvent was about 1.30, and each measurement was carried out at a rotor speed of 59,780 rpm. The results are shown in Table I. The table records the ovalbumin concentration at the beginning of the run; at sedimentation equilibrium, when the protein had collected in a band near the middle of the solution column, the concentration at the center of the band was between four and five times the initial value. The data in Table I show that, in a given solvent and at a given rotor speed, the apparent buoyant density of ovalbumin is essentially independent of protein concentration. All subsequent experiments were done using an initial protein concentration of 3 mg/ml.

Table I: Apparent Buoyant Density of Ovalbumin as a Function of Protein Concentration

Ovalbumin concn, mg/ml	Buoyant density, g/cm ³
4	1.297
3	1.296
2	1.296
1	1.300

The measurement, by the banding method, of the buoyant density of a protein of relatively low molecular weight is subject to considerably larger errors than those commonly encountered when the method is applied to proteins of very high molecular weight or to nucleic acids.^{4,6} When the cell is completely filled with a cesium chloride solution whose density is 1.30 and sedimentation equilibrium is established at 59,780 rpm, the density increases by about 0.21 g/cm³ between the meniscus and the bottom of the cell. Even in the steepest gradients obtainable in the ultracentrifuge, the protein band is rather wide, and the location of the point at which it crosses the base line is subject to small errors. In addition, there is a slight uncertainty in the calculation of the gradient itself, primarily in the reproducible leveling of the schlieren photographs of the salt and water base lines. The relative importance of these difficulties varies somewhat from one run to the next, depending on the rotor speed and on the length of the solution column. Taking these sources of error into account, along with the possible uncertainty of the measurement of ρ_0 , errors as large as ± 0.003 g/cm³ could be encountered in the measured values of the buoyant density of ovalbumin. Duplicate experiments gave results that were reproducible within ± 0.002 g/cm³.

A series of experiments was undertaken in an attempt to find conditions under which the precision of the buoyant density measurement could be improved. The two experimental variables tested were the rotor speed and the length of the solution column. Decreasing the rotor speed, for example, reduced the steepness of the density gradient, so that a given absolute error in the location of the band of protein produced a smaller error in the buoyant density. On the other hand, the band itself was less sharp at the lower rotor speed, and the precision with which its center could be located was correspondingly decreased. With shorter solution columns, errors in the calculation of the density gradient were reduced, but the correct matching of the protein and salt patterns was more difficult. No great improvement in the precision of the results could

be obtained by varying either the rotor speed or the length of the solution column. There seemed to be some slight advantage in the use of short columns and high rotor speeds.

The experiments in which the angular velocity or the length of the solution column was varied also provided an opportunity to observe any substantial effect of hydrostatic pressure on the apparent buoyant density of ovalbumin in cesium chloride. Measurements were done with solution columns of three different lengths, each at four or five rotor speeds. The results are collected in Table II. The initial densities of the cesium chloride solutions were so selected that the protein bands formed near the middle of the solution columns at each rotor speed. The variation of the angular velocity from 42,040 to 59,780 rpm therefore represents, at a given column length, a two-fold change in the pressure at the protein band, since the pressure is roughly proportional to the square of the rotor speed. The length of the solution column was varied over a threefold range. At any given column length, there was no significant variation of the apparent buoyant density with rotor speed. When the results using different column lengths are compared, however, a trend is observed. The buoyant density appears to be slightly higher with longer columns and thus at higher pressures. The apparent variation of the buoyant density with column length is, however, of doubtful significance, since the precision of the individual data cannot be assumed to be better than ± 0.003 g/cm³. It can be concluded that, if the buoyant density does vary with hydrostatic pressure, the variation is small.

Table II: Apparent Buoyant Density (g/cm³) of Ovalbumin in Cesium Chloride as a Function of Column Length and Rotor Speed

Rotor speed, rpm	Column length		
	1.21 cm	0.80 cm	0.39 cm
59,780	1.297	1.295	1.293
56,100	1.299
52,600	1.297	1.295	1.293
47,660	1.300	1.295	1.293
42,040	1.300	1.296	1.293

Hearst, *et al.*,⁵ have measured the buoyant density of bacteriophage T-4 DNA and of tobacco mosaic virus as a function of hydrostatic pressure. They

(6) D. J. Cox and V. N. Schumaker, *J. Am. Chem. Soc.*, **83**, 2439 (1961).

report that the apparent buoyant densities of these materials decrease slightly as the pressure is increased. An equally moderate trend of the buoyant density of ovalbumin with pressure would not be outside the experimental uncertainty of the present data.

Discussion

All of the values of the buoyant density of ovalbumin in cesium chloride measured by the banding method fall between 1.293 and 1.300 g/cm³. These values agree very well with the apparent buoyant density calculated by plotting the viscosity-corrected sedimentation coefficients of ovalbumin in cesium chloride solutions of various concentrations against the solvent densities and extrapolating the plot to $S = 0$. Three separate determinations, by the plotting method, of the apparent buoyant density of ovalbumin in cesium chloride gave values of 1.293, 1.298, and 1.302 g/cm³. Bruner and Vinograd⁷ have reported experiments with bacteriophage T-4 DNA in cesium chloride which allow a similar comparison to be made. As is the case with ovalbumin, the viscosity-corrected sedimentation coefficient of T-4 DNA varies linearly with solvent density, and the S vs. ρ plot crosses the density axis at the buoyant density measured by the banding method.

If the protein did not bind water in preference to salt and if the frictional ratio did not vary with salt concentration, a plot of the viscosity-corrected sedimentation coefficient against the density of the solvent would be linear and would cross the density axis at the reciprocal of the partial specific volume,^{8,9} which is 1.335 for ovalbumin.¹⁰ It is necessary to account for the fact that the experimental plots are linear but cross the density axis significantly below $1/\bar{v}$.

The results are consistent with a situation in which the frictional ratio of the protein is independent of cesium chloride concentration and in which the protein binds water in preference to the salt to a degree which is also independent of salt concentration. There are, however, other possible models, consistent with the information available, which involve the possible variation with salt concentration of the frictional ratio or the degree of preferential solvation.

The agreement between the buoyant densities derived from the plotting and banding methods serves to eliminate one possible explanation of the behavior of ovalbumin in sedimentation velocity experiments in cesium chloride. If the frictional ratio varied and the protein did not bind water in preference to salt, then either the sedimentation coefficient vs. density plots would be nonlinear or they would cross the density

axis at a point different from the buoyant density measured by the banding method. If the frictional ratio does vary with salt concentration, then the protein must bind water in preference to salt and, moreover, the degree of preferential hydration and the frictional coefficient must vary together in a rather special way in order to produce a linear relation between the sedimentation coefficient and the density of the solvent which, on extrapolation, crosses the density axis at the equilibrium buoyant density of the protein.

Even if the frictional ratio does not vary with salt concentration, a linear relation between the sedimentation coefficient and the density of the solvent which yields the "correct" buoyant density on extrapolation need not imply that the preferential solvation of the macromolecule is independent of salt concentration. It has recently been shown⁷ that results of the kind described here for ovalbumin will be obtained if the variation of the preferential hydration with density satisfies the equation (Bruner and Vinograd's eq 5)

$$\left(\frac{\partial\Gamma'/\partial\rho}{\partial^2\Gamma/\partial\rho^2}\right) = \frac{1 - \bar{v}_w\rho}{2\bar{v}_w} \quad (2)$$

In eq 2, Γ' is the preferential hydration in grams of preferentially bound water per gram of protein and \bar{v}_w is the partial specific volume of water.

There are, therefore, three possible ways to explain the linear relation between the sedimentation coefficient of ovalbumin in cesium chloride and the density of the solvent. The preferential solvation and the frictional ratio may vary together with salt concentration, the preferential solvation may vary alone, in the way implied by eq 2, or both the frictional ratio and the preferential solvation may be independent of salt concentration. The range of possibilities would be further narrowed if it could be determined whether or not the degree of preferential hydration varies with salt concentration. Hearst and Vinograd¹¹ have measured the buoyant density of bacteriophage T-4 DNA in a series of cesium salts and have found that the preferential hydration of the nucleic acid varies from one salt to another. The activity of water in the salt solutions at the respective buoyant densities of the nucleic acid

(7) R. Bruner and J. Vinograd, *Biochim. Biophys. Acta*, **108**, 18 (1965).

(8) H. K. Schachman and M. A. Lauffer, *J. Am. Chem. Soc.*, **71**, 536 (1949).

(9) S. Katz and H. K. Schachman, *Biochim. Biophys. Acta*, **18**, 28 (1955).

(10) M. O. Dayhoff, G. E. Perlmann, and D. A. MacInnes, *J. Am. Chem. Soc.*, **74**, 2515 (1952).

(11) J. E. Hearst and J. Vinograd, *Proc. Natl. Acad. Sci. U. S.*, **47**, 1005 (1961).

also varies from salt to salt, and there is a smooth correlation between water activity and preferential hydration. On the basis of these data, each obtained in a different salt, Bruner and Vinograd⁷ suggest that the preferential hydration of a macromolecule in a given salt should vary with salt concentration since the activity of water does so. Their interpretation would argue against the possibility that the sedimentation behavior of ovalbumin may be accounted for by the constancy with salt concentration of preferential

hydration and the frictional ratio. It should be possible to approach the problem more directly by measuring the buoyant density of ovalbumin in cesium chloride and deuterium oxide. The salt concentration and thus the water activity at the protein band should be different in water and in deuterium oxide, and it should be possible, in this way, to determine whether or not the preferential solvation of the protein is the same at two different concentrations of the same salt.

The Radiolysis of Ethyl Mercaptan¹

by J. J. J. Myron and R. H. Johnsen

Department of Chemistry and the Institute of Molecular Biophysics, Florida State University, Tallahassee, Florida (Received March 21, 1966)

A study of the radiolysis of liquid ethyl mercaptan has been undertaken. The data strongly suggest that the radiolytic behavior of the mercaptan differs significantly from that of the corresponding alcohol. A comparison of the two radiolyses in the light of the present results is presented.

Introduction

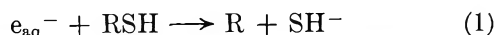
In the past, radiolytic studies of compounds containing sulfhydryl groups have generally been carried out on dilute aqueous solutions of polyfunctional thiols. Except for data on the esr spectra of irradiated methyl and ethyl mercaptan² taken at 77°K, no studies on the radiolytic behavior of these compounds appear to have been made. Investigation of simple mercaptans in the "pure" state should be of interest as a comparison to that of the corresponding aliphatic alcohols which have been extensively studied by various workers.³⁻⁶

The possible importance of thiol radiolysis studies is evidenced by the number of publications dealing with biological systems in which mercaptans were present as additives. Compounds such as cysteine,⁷⁻⁹ cysteamine,¹⁰ and glutathione^{11,12} have been widely used as "protectors" of biologically significant systems against radiation damage. Oxidation of the thiol group by radiation-produced radicals from the other compo-

nents of the system is probably an important mode of "protection" or "inhibition" afforded by the sulfur compound. The corresponding disulfide and small amounts of hydrogen sulfide are the usual products of oxidation.

- (1) Research supported in part by A.E.C. Contract AT-(40-1)-2001 and in part by A.E.C. Contract AT-(40-1)-2690.
- (2) C. L. Luck and W. Gordy, *J. Am. Chem. Soc.*, **78**, 3240 (1956).
- (3) (a) W. McDonnell and A. S. Newton, *ibid.*, **76**, 4651 (1954); (b) I. A. Taub and L. M. Dorfman, *ibid.*, **84**, 4053 (1962).
- (4) (a) J. G. Burr, *J. Phys. Chem.*, **61**, 1477 (1957); (b) G. E. Adams, J. H. Baxendale, and R. D. Sedgwick, *ibid.*, **63**, 854 (1959).
- (5) E. M. Hayon and J. Weiss, *J. Chem. Soc.*, 3962 (1961).
- (6) R. H. Johnsen, *J. Phys. Chem.*, **65**, 2144 (1961).
- (7) S. L. Whitcher, M. Rotheram, and N. Todd, *Nucleonics*, **11**, 30 (1953).
- (8) P. Riesz and B. E. Burr, *Radiation Res.*, **16**, 661 (1962).
- (9) C. N. Trumbore, *et al.*, *J. Am. Chem. Soc.*, **86**, 3177 (1964).
- (10) B. Shaprio and L. Eldjar, *Radiation Res.*, **3**, 225 (1955).
- (11) G. E. Woodward, *Biochem. J.*, **27**, 1411 (1933).
- (12) E. S. G. Barron and V. Flood, *J. Gen. Physiol.*, **33**, 229 (1950).

Much less work has been published concerning the radiolytic behavior of aqueous solutions containing simple aliphatic mercaptans such as methanethiol or ethanethiol. However, Armstrong and Wilkening¹³ have recently demonstrated marked yield dependences on pH for both hydrogen and methane production from aqueous methanethiol. Their results indicate that mercaptans may function as solvated electron scavengers as well as radical traps by means of the reaction



The following is a report of some experiments that have been made on the radiolysis of ethyl mercaptan in the gaseous, liquid, and solid phases.

Experimental Section

Eastman White Label ethyl mercaptan was used for all irradiations. Gas chromatographic analysis revealed the presence of five impurity peaks which amounted to approximately 0.5 mole % of the substrate.

Because of the extremely noxious character of ethanethiol, it was decided not to attempt any rigorous purifying procedures on the substrate. However, some purification was effected by using only the middle third portion of distillate from a distillation into a reservoir on a vacuum line (impurity content 0.2 to 0.3%). Whenever possible, the mercaptan was handled in a Pyrex vacuum system or in a glove box that was vented to an exhaust system. Various other containment procedures employing fume hoods, vacuum desiccators, etc., were also necessarily employed during sampling for product analysis.

Liquid samples consisted of approximately 1 ml of liquid contained in 15-mm o.d. tubes of about 4-ml capacity. All samples were prepared on the Pyrex vacuum system and were thoroughly degassed before the sample cell was sealed prior to irradiation. Blank unirradiated samples were prepared and analyzed at intervals to check on the composition of the substrate and to check preparative and analytical technique. The amount of substrate was determined by volume measurements at 0° in a calibrated graduated tube in the vacuum system.

A few gas phase samples were run at room temperature (at pressures of about 270 torr). These were irradiated in a Pyrex cylinder of 400-ml capacity which was fitted with a stopcock and small "freeze down" side arm for sample preparation. An esr spectrum of the radicals formed and trapped at 77°K was obtained using a quartz cell and a Varian esr spectrometer.

All irradiations were carried out by X-rays generated by allowing 3-Mev electrons from a Van de Graaff

accelerator to impinge upon a tungsten target. The temperature during irradiation for both liquid and gaseous samples was $25 \pm 2^\circ$. For liquid samples, dosimetry measurements were made during each irradiation employing the Fricke dosimeter. To obtain dose rates for mercaptan samples, the assumption was made that the rate was proportional to the ratio of the electron densities. The dose rate for mercaptan was approximately 1.1×10^{20} ev/g hr. Total doses ranged from 0.25 to 10×10^{20} ev/g of mercaptan. Gas phase dosimetry was carried out by measuring the hydrogen yield from propylene radiolysis using the ratio of electron densities and a $G(H_2)$ from propylene = 1.1.¹⁴

Gases that were noncondensable at 77°K (hydrogen and methane) were measured together by breaking the ampoule (or for a gas sample, opening the stopcock to the cell) and toeplering the gas mixture into a calibrated gas buret. An aliquot of this mixture was then analyzed in a Perkin-Elmer 154-B gas chromatograph using a 6-ft charcoal column.

Chromatograms of liquid products were obtained from a Perkin-Elmer 800 (flame ionization detector) gas chromatograph using a di-*n*-decyl phthalate on Chromosorb W column and a silicone 200 oil on Chromosorb W column.

Results

Figure 1 shows a plot of $G(H_2)$ vs. total dose from 0.25 to 10×10^{20} ev/g of liquid mercaptan. Although there is considerable scatter in the points, particularly at the low dose end of the scale, there is no apparent dose dependence of hydrogen yield over this dose range. Consequently, the initial G value for hydrogen production was taken as the average of all determinations, $G_i(H_2) = 7.1$.

A plot of the yield of methane vs. dose over the same dose range in the liquid phase is given in Figure 2. The scatter is greater than that of the hydrogen plot due to the fact that the methane amounted to only 1–2% of the gas mixture, and accuracy in its measurement, especially at low conversions, is difficult to attain. The average of all measurements gave $G(CH_4) = 0.10$, so that in the liquid phase, $G(H_2)/G(CH_4) \approx 70$.

After subtraction of impurity peaks from "blank" samples were made, gas chromatography showed a total of twelve product peaks at the highest dose employed ($\approx 1 \times 10^{21}$ ev/g). However, the three largest peaks accounted for 97% of the total liquid products that could be detected. These products were diethyl

(13) D. A. Armstrong and V. G. Wilkening, *Can. J. Chem.*, **42**, 2631 (1964).

(14) K. Yang and P. L. Grant, *J. Phys. Chem.*, **65**, 1861 (1961).

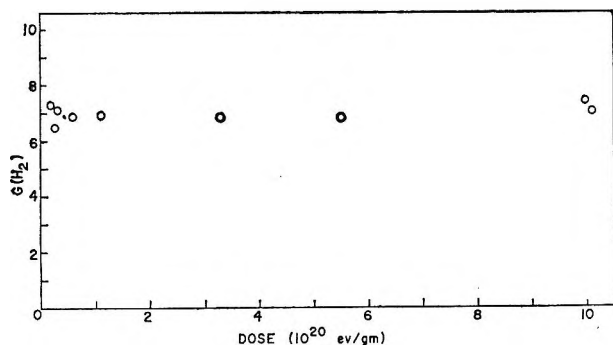


Figure 1. Hydrogen yields from liquid ethyl mercaptan as a function of dose.

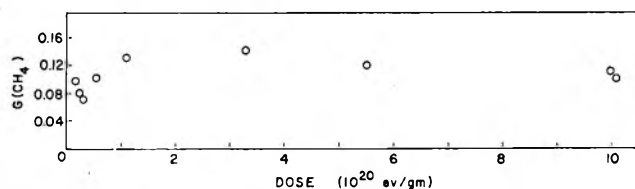


Figure 2. Methane yields from liquid ethyl mercaptan as a function of dose.

disulfide, diethyl sulfide, and probably 1,4-butanedithiol, and these constituted 80, 15, and 2%, respectively, of the liquid products. There was no evidence for the presence of 2,3-butanedithiol. The sulfide and disulfide could be measured from 0.25 to 10×10^{20} ev/g, and no definite dose dependence was evident. If it is assumed that relative retention times of sulfur compounds on silicone oil are an indication of molecular weight, it appears that six of the remaining nine peaks that constitute the other 3% also have a molecular weight greater than the substrate. As these products are minor ones and authentic samples of possible product compounds were not available, no attempt was made at identification.

A solution of thioacetaldehyde in methanol was chromatographed to obtain its retention time and special attention was paid to determine if it was present as a product of the radiolysis. If thioacetaldehyde was present, it was in very small amounts even at the highest doses.

Gas yields from irradiation in the gas phase at room temperature at a dose of 7×10^{19} ev/g were $G(\text{H}_2) = 17 \pm 2$ and $G(\text{CH}_4) = 3.1 \pm 0.4$. Therefore, the ratio $G(\text{H}_2)/G(\text{CH}_4)$ is reduced from 70 to 5.5 in going from the liquid to the gaseous state at room temperature.

The esr spectrum obtained at 77°K (Figure 3) was a broad asymmetric peak with indications of some possible hyperfine structure. After irradiation, the solid mercaptan exhibited a deep orange color which

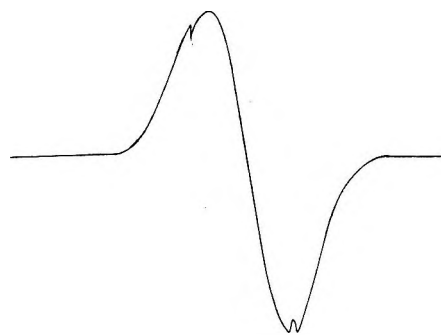


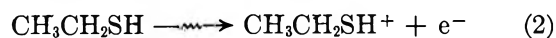
Figure 3. The esr spectrum of X-irradiated ethyl mercaptan at 77°K.

faded upon warming. The photolytic behavior of the solid is now under investigation.

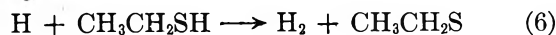
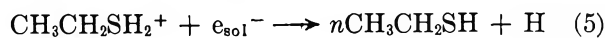
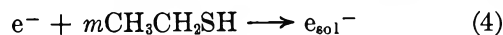
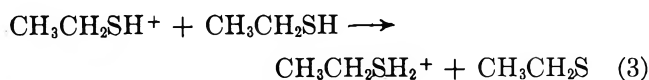
Discussion

Due to the structural similarity of the ethyl mercaptan and the ethyl alcohol molecules and the fact that the radiolysis of ethanol has been widely investigated,³⁻⁶ the discussion of the results will involve, to a large extent, a comparison of the radiolysis of the two compounds.

As is usual with aliphatic compounds, hydrogen is a major product [$G(\text{H}_2) = 7.1$]. The initial hydrogen yield from the oxygen analog (ethyl alcohol) is $G_1(\text{H}_2) \approx 5$.^{5,15,16} The substantially higher yield from the mercaptan might be due to the lower ionization potential of the mercaptan (I.P. = 9.2 ev)¹⁷ compared to that of the alcohol (I.P. = 10.5 ev).¹⁸ This could result in a greater amount of the initial reaction



as compared to the analogous alcohol reaction. The ionization would presumably be followed by



Reactions similar to (3) to (5) have been postulated in a mechanism for the radiolysis of ethanol.¹⁶

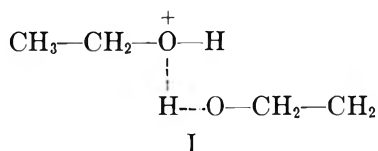
(15) G. E. Adams and R. D. Sedgwick, *Trans. Faraday Soc.*, **60**, 865 (1964).

(16) J. J. Myron and G. R. Freeman, *Can. J. Chem.*, **43**, 381 (1965).

(17) I. Omura, K. Higasi, and H. Baba, *Bull. Chem. Soc. Japan*, **29**, 504 (1956).

(18) K. Watanabe, T. Nakayama, and J. Mottl, *J. Quant. Spectry. Radiative Transfer*, **2**, 369 (1962).

However, in the ethanol system there is evidence that the reaction similar to (3) occurs to a significant extent in the liquid but not in the gas phase.¹⁹ This appears to be due to the fact that the hydrogen bonding present in the liquid phase could not aid the formation of the transition complex I in the gas phase.¹⁹



Hydrogen bonding in ethyl mercaptan occurs to a much lesser extent than in ethyl alcohol due to the significantly smaller electronegativity of the sulfur atom as compared to the oxygen atom. Therefore, the formation of the transition complex necessary for reaction 3 is not as likely in liquid mercaptan as it is in liquid ethanol and, therefore, this mechanism for H₂ is relatively less important.

The various bond strengths (in kilocalories) that have been reported (or estimated) for the ethyl mercaptan and alcohol molecules are listed in Table I.^{20,21} The

Table I

Type of bond	Bond strength, kcal
Ethanol	
O-H	99 ^a
C-O	90 ^a
C-C	83 ^b
C-H(methylene)	90 ^b
C-H(methyl)	96 ^b
Ethanethiol	
S-H	87 ^c
C-S	73 ^c

^a See ref 20. ^b Estimated bond strength, see text. ^c See ref 21.

bond strengths that were estimated for the ethanol molecule were arrived at as follows. The C-H value for the methyl group was assumed to be that quoted for ethane by Cottrell,²² who also cited a 6-kcal difference in dissociation energy for the primary and secondary C-H bonds in propane. Hence, the approximate value of 90 kcal for the C-H bond in the methylene position for ethanol is given. The C-C bond strength is that quoted for ethane.²² The corresponding bond strengths for the mercaptan molecule will, in all likelihood, be somewhat greater due to

the sulfur atoms' smaller electronegativity. These figures, while approximate, should give a reasonable estimate of the relative bond strengths for the molecules.

It thus appears that the O-H bond in the alcohol is the strongest and methylene C-H bond is the weakest among the bonds to hydrogen atoms. This supposition is supported by the esr spectra of ethyl alcohol^{23,24} at 77°K and the nature of the major liquid products from the radiolysis.^{3,16}

Both these types of data indicate that at some stage in the radiolysis CH₃CHOH is present in appreciable quantities. On the other hand, the S-H bond in the mercaptan appears to be the most labile of all bonds to hydrogen in both molecules. It is possible that the greater hydrogen yield is due to the relatively great ease of abstraction by hydrogen atoms (produced by reaction 5 and/or other reactions) from the S-H group.

The lability of the bond to the sulfhydryl hydrogen atom should result in products that attest to the presence of CH₃CH₂S radicals in the system. Diethyl disulfide and diethyl sulfide constitute 95% of the condensation products while the 1,2-dithiol was not observed. As the formation of these products is most easily explained by the combination of two ethylthiyl radicals and the combination of an ethylthiyl and an ethyl radical, respectively, the presence of thiyl radicals can be inferred.

Further evidence for the presence of thiyl radicals at some stage in the radiolysis can be obtained from data on mercaptan samples that were irradiated and subjected to esr analysis before and after photolysis with selected wavelengths at 77°K. These experiments show that the species giving rise to the original esr signal is converted by light to another paramagnetic intermediate which has been identified as CH₃CH₂S.²⁵ This interpretation is consistent with Truby's^{26,27} work on disulfides in which he postulates that the esr spectrum of irradiated disulfides consists of contributions from ionic species (predominantly) and RS

(19) J. J. Myron and G. R. Freeman, *Can. J. Chem.*, **43**, 1484 (1965).

(20) P. Gray, *Trans. Faraday Soc.*, **52**, 344 (1956).

(21) J. L. Franklin and H. E. Lumpkin, *J. Am. Chem. Soc.*, **74**, 1023 (1952).

(22) T. L. Cottrell, "The Strengths of Chemical Bonds," Butterworth and Co. Ltd., London, 1958.

(23) H. Zeldes and R. Livingstone, *J. Chem. Phys.*, **30**, 40 (1959).

(24) B. Smaller and M. S. Matheson, *ibid.*, **28**, 1169 (1958).

(25) S. B. Milliken, K. Morgan, and R. H. Johnsen, to be published.

(26) F. K. Truby, *J. Chem. Phys.*, **40**, 2768 (1964).

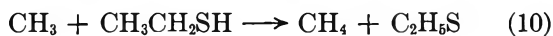
(27) F. K. Truby, D. C. Wallace, and J. E. Hess, *ibid.*, **42**, 2845 (1965).

(thiyl) radicals and alkyl radicals. It appears that the initial (prebleached) spectrum of ethyl mercaptan is largely due to the presence of entities such as $\text{CH}_3\text{-CH}_2\text{SH}^+$ and $\text{CH}_3\text{CH}_2\text{SH}^-$. Upon photolysis the following reactions are feasible.



These reactions can reasonably account for the observed (postbleached) thiyl radical production.

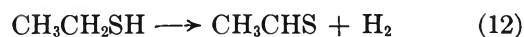
The fact that diethyl sulfide constitutes 15% of the liquid products seems to indicate that there is appreciable rupture of the C-S bond (as would be expected from its low bond strength). However, the Franck-Rabinowitch cage effect would obscure the true extent of the C-S bond scission. Evidence for the operation of a cage effect can be gotten from the $G(\text{H}_2)/G(\text{CH}_4)$ ratio in the liquid and gas phase. The ratio decreases from 70 to 5.5 on going from the liquid to the gas phase. If it is assumed that the methane yield is due to C-C bond scission followed by abstraction from the substrate by the methyl group, the G ratio reflects the greatly decreased cage effect in the gas phase.



Kerr and Trotman-Dickenson²⁸ have demonstrated that ethanethiol is an efficient methyl radical scavenger due to the efficiency of reaction 10.

The enhanced over-all decomposition of the mercaptan in the gaseous phase as compared with the liquid phase is probably due to two effects. The first is the lack of a cage effect in the gas phase. The second factor is the much larger probability that ion pairs escape immediate recombination and are thus capable of undergoing reactions that result in stable radiolytic products.

It is interesting to note that the sulfur analogs of the two major liquid products from ethanol radiolysis (2,3-butanedithiol and thioacetaldehyde) were present, if at all, only in negligible quantities. This appears to minimize reactions such as



in the radiolysis.

The data obtained to date indicate that the radiolytic decomposition mechanism for ethyl mercaptan is dictated largely by the two bonds to the sulfur atom. Mercaptan radiolysis products, therefore, differ in nature from those of the corresponding alcohol in which the methylene hydrogen atoms largely govern the decomposition.

Acknowledgment. The authors wish to thank Mr. D. Pritchett for technical assistance and Mr. S. Milliken for helpful discussions concerning the work, and for providing the esr spectrum.

(28) J. A. Kerr and A. F. Trotman-Dickenson, *J. Chem. Soc.*, 3322 (1957).

Multiple Knudsen Cell Effusion. Enthalpies of Vaporization of Indium and Gallium¹

by G. J. Macur, R. K. Edwards, and P. G. Wahlbeck

Department of Chemistry, Illinois Institute of Technology, Chicago, Illinois 60616 (Received March 28, 1966)

In order to determine several vapor pressures at one well-defined temperature, several Knudsen cells were heated simultaneously in a massive molybdenum block which served to provide a uniform temperature environment. With this multiple-cell technique, it was hoped that the precision in a set of vapor pressure measurements determined in a single isothermal experiment would be better than that achieved in individual pressure measurements. The vapor pressures of liquid indium and gallium were determined. The precision of pressure measurements was better than what is usually achieved with the Knudsen method. The standard enthalpies of vaporization of indium and gallium at 298°K were found to be 56.58 ± 0.10 and 64.62 ± 0.22 kcal/g-atom, respectively; these values agree well with the literature values.

I. Introduction

The Knudsen effusion method has been used extensively for the determination of vapor pressures of materials at high temperatures. In many experiments it would be desirable to determine a set of vapor pressures at one fixed temperature. Examples are (1) the evaluation of activities, through vapor pressure measurements at a given temperature, of components of an alloy as a function of composition, *e.g.*, activities for the Cu–Au system by Edwards and Brodsky;² (2) the evaluation of nonideality effects of effusion orifices, *e.g.*, the study by Freeman;³ and (3) the evaluation of effects due to variation of orifice areas, *e.g.*, the nonunit vaporization coefficient. At elevated temperatures there is a considerable error in temperature measurement, and it is very difficult to reproduce temperatures. Therefore, it is most difficult to achieve highly precise agreement in a set of isothermal vapor pressure values which are taken from individual measurements. A higher precision should be achieved when several cells are used simultaneously in an isothermal enclosure. In order to have many Knudsen cell measurements at a well-defined temperature, 14 Knudsen cells were placed in a large molybdenum block. Thus, it was possible to obtain 14 vapor pressure measurements simultaneously at one temperature.

The measurements of vapor pressures of pure liquid

gallium and indium reported here were performed in preparation for measurements of the activities of gallium and indium in Ga–In liquid solutions.¹ Standard enthalpies of vaporization of liquid gallium and indium have been calculated from these vapor pressures.

II. Experimental Section

Apparatus. The apparatus as used in this experiment is shown in Figure 1. It consisted of a high-speed vacuum pumping system, an inert gas inlet system, pressure gauges, an electrical furnace with a temperature controller, a temperature-measuring device, and a set of Knudsen cells in a thermostating molybdenum block.

The vacuum pumping system consisted of an oil diffusion pump with forevacuum produced by a mechanical pump. Argon could be admitted through the stopcock at the top of the apparatus. The Philips gauge was used to measure pressures below 1 torr, and

(1) Based on a thesis by G. J. Macur, submitted to the Illinois Institute of Technology in partial fulfillment of the requirements for the Ph.D. degree, June 1965.

(2) R. K. Edwards and M. B. Brodsky, *J. Am. Chem. Soc.*, **78**, 2983 (1956).

(3) R. D. Freeman, Technical Document No. ASD-TDR-63-754, 1963. He has attempted to establish isothermal conditions for effusion by heating eight Knudsen cells simultaneously in a thermostated block.

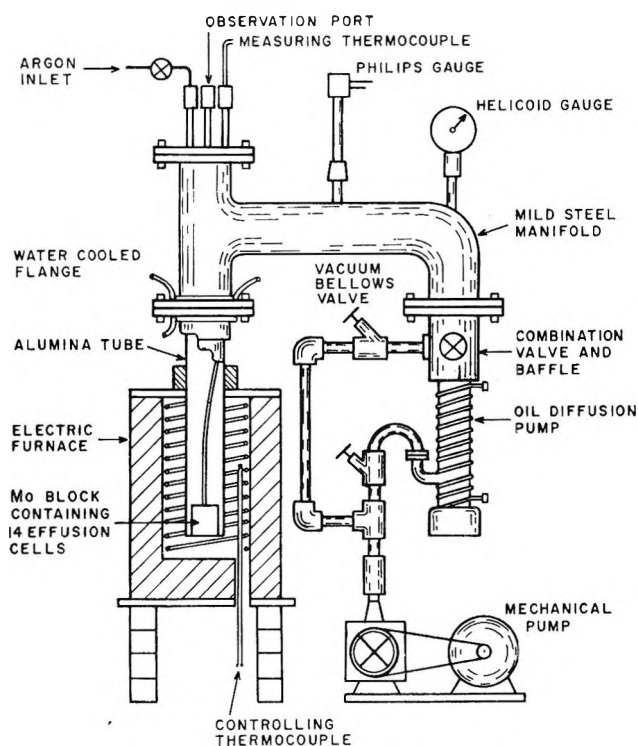


Figure 1. Multiple Knudsen cell effusion apparatus.

the Helicoid gauge was used to measure higher pressures.

The electric furnace was a Hevi-Duty HDT-812 furnace capable of achieving 1260° . Its power was controlled by a West JSB-2, 5 KVA saturable-core reactor controller regulated by a sensing thermocouple; the temperature was controlled to within $\pm 1^{\circ}$. The temperature of the experiment was determined from the emf of a platinum-platinum-10% rhodium thermocouple calibrated at the freezing points of antimony, silver, and copper. Calibration before and after the experiments showed no appreciable change.

The effusion cells were fabricated of alumina, AP35 (99% Al_2O_3), by the McDanel Refractory Porcelain Co. A cap and cylinder design was used; the caps were cemented and fired to the cylinders. The effusion cells were 60 mm long and 14 mm in o.d. with a wall thickness of *ca.* 1 mm. The nominal orifice diameters ranged from 0.5 to 1.8 mm in 0.1-mm intervals. Effective orifice areas were determined by measuring the rate of effusion of pure mercury from the cells; a separate vacuum apparatus was used for these effective orifice area measurements. The vapor pressure of mercury was calculated from the equation suggested by Carlson, *et al.*,⁴ based on the data of Busey and Giauque.⁵ Two calibration runs were made for each orifice; agreement of the results to *ca.* 1% was obtained.

For the high-temperature runs, the coefficient of thermal expansion of $7.8 \times 10^{-6} \text{ deg}^{-1}$ for alumina⁶ was utilized to correct for the expansion of the orifice. The effusion cells were inserted into larger alumina cups which effectively lined the wells in the molybdenum block and also aided insertion and removal of the cells. The thermostating cylindrical block was 5 in. long and 5.75 in. in diameter; 14 wells for the effusion cells and a central well for the thermocouple were drilled in the block. A molybdenum handle was attached to the block.

Procedure. Samples were placed in the alumina effusion cells through the orifices with special care not to damage the orifices (which had been calibrated previously). The cells were placed in alumina cups which were then positioned in the molybdenum block in a systematic order. The molybdenum block was lowered into the large alumina tube shown in Figure 1. The calibrated thermocouple was then positioned in its well in the molybdenum block. The large alumina tube with the Knudsen cell assembly was then brought near the water-cooled flange, the mechanical vacuum pump was started, and the alumina tube was pressed against a rubber gasket on the water-cooled flange until the vacuum was sufficient so that atmospheric pressure would hold the alumina tube in place. All electrical connections were then made.

With the diffusion pump, a pressure as low as 10^{-5} torr was achieved. The temperature of the furnace was brought up to 200° and left overnight for outgassing purposes. The temperature was raised then to 600° over a period of 4 hr. Isolation of the manifold from the pumps was achieved, and argon was added to the system so that the pressure was brought to 0.7 atm. The inert gas at this pressure was used to block effusion until the starting time of the run. The temperature was adjusted then to the desired value; a constant temperature was achieved in about 2 hr.

The run was started by evacuation of the manifold, and a timer was started when the pressure reached 10^{-4} torr. This pumpdown required *ca.* 2 min. During the course of the run, temperature and pressure were monitored.

After an appropriate period of time, the run was stopped by adding argon to 0.7 atm after isolating the manifold from the vacuum pumps. The temperature

(4) K. D. Carlson, P. W. Gilles, and R. J. Thorn, *J. Chem. Phys.*, **38**, 2725 (1963).

(5) R. H. Busey and W. F. Giauque, *J. Am. Chem. Soc.*, **75**, 806 (1953).

(6) Bulletin No. D 763, "Physical Properties," McDanel Refractory Porcelain Co., Beaver Falls, Pa.

Table I: Data for the Vaporization of Indium

Temp, °K	Cell ^a	Mass loss, mg	Time, min	p , atm \times 10^{-6}	ΔH°_{298} , kcal/g- atom	Av p , atm \times 10^{-6}	% av dev	Av ΔH°_{298} , kcal/g- atom
1198.0	B·	9.41	720.2	1.488	57.10	1.504	1.2	57.08
	B*	8.80		1.528	57.04			
	C	13.22		1.507	57.07			
	D	17.21		1.469	57.14			
	E	18.51		1.538	57.02			
	F	35.50		1.493	57.09			
	G	44.94		1.505	57.07			
1273.6	B·	48.54	760.4	7.486	56.51	7.602	3.4	56.47
	B*	41.95		7.107	56.64			
	C	69.72		7.751	56.42			
	D	97.48		8.115	56.30			
	E	95.48		7.738	56.42			
	F	178.23		7.313	56.57			
	G	235.93		7.708	56.43			
1373.4 ^b	B·	182.68	600.4	37.00	56.44
	B*	209.19		46.54	55.81			
	C	273.24		39.89	56.23			
	D	199.28		21.78	57.88			
	E	360.13		38.32	56.34			
	F	203.54		10.97	59.75			
	G	329.05		14.12	59.06			
1472.7	B·	561.66	474.3	148.89	56.30	151.5	2.3	56.25
	B*	487.53		141.97	56.44			
	C	798.72		152.63	56.23			
	D	1063.28		152.15	56.24			
	E	1100.96		153.36	56.21			
	F	2156.59		152.10	56.24			
	G	2846.25		159.83	56.09			
1196.5	B·	11.36	720.4	1.795	56.58	1.767	2.3	56.62
	B** ^c			
	C	16.14		1.838	56.53			
	D	19.60		1.670	56.76			
	E	28.32		1.792	56.59			
	F	32.95		1.751	56.64			
	G	57.38		1.755	56.64			
1220.3	B·	14.02	640.4	2.515	56.86	2.545	1.2	56.83
	C	19.38		2.506	56.87			
	D	26.90		2.605	56.77			
	E	35.06		2.520	56.85			
	F	42.50		2.566	56.81			
	G	43.70		2.561	56.81			
1273.8	B·	25.28	466.9	6.585	56.84	6.814	1.5	56.75
	C	37.10		6.966	56.70			
	D	49.02		6.893	56.72			
	E	66.34		6.826	56.75			
	F	77.53		6.802	56.76			
	G ^d	185.57		9.343	55.95			
1320.7	B·	37.32	192.2	16.96	56.39	18.00	5.8	56.24
	C	39.22		17.55	56.30			
	D	51.85		17.38	56.32			
	E	69.71		20.63	55.87			
	F	83.62		17.50	56.30			
	G ^d	181.57		21.87	55.72			

Table I (Continued)

Temp, °K	Cell ^a	Mass loss, mg	Time, min	<i>p</i> , atm × 10 ⁻⁵	ΔH°_{298} , kcal/g- atom	Av <i>p</i> , atm × 10 ⁻⁵	% av dev	Av ΔH°_{298} , kcal/g- atom
1289.2	B	21.58	273.6	9.306	56.62	9.450	1.0	56.58
	C	31.03		9.645	56.53			
	D	40.89		9.517	56.56			
	E	54.25		9.384	56.60			
	F	64.71		9.400	56.59			
	G ^d	138.93		11.615	56.05			
1248.9	B	24.85	510.2	5.658	56.24	5.477	2.7	56.24
	C	34.52		5.666	56.14			
	D	43.99		5.407	56.25			
	E	58.02		5.296	56.30			
	F	69.91		5.359	56.27			
	G ^d	106.10		4.681	56.62			

^a The orifice areas in square centimeters for the cells at 50° were: B, 0.0009568; B*, 0.001051; C, 0.001458; D, 0.001947; E, 0.002000; F, 0.003950; G, 0.004962. Expansion-of-orifice corrections were made using the coefficient of thermal expansion of $7.8 \times 10^{-6} \text{ deg}^{-1}$.⁶ ^b These data are not reliable because an air leak developed during the run and are shown for comparison only. These data are not included in the over-all averages. ^c Data for cell B* are not shown for this and later runs because it contained an alloy. ^d Data for cell G are not considered reliable because a crack developed in the cell wall. Data are shown only for completeness and are not included in the averages.

of the furnace was lowered in a systematic manner to prevent cracking of alumina.

After the furnace cooled, the apparatus was dismantled, the mass loss of the effusion cells was determined, and vapor pressures were calculated.

Materials. Indium wire was purchased from A. D. Mackay, Inc., with a stated purity of 99.999%. The wire was washed with pure benzene prior to insertion into the effusion cells. The indium wire was easily inserted into the cells.

Gallium metal was purchased from A. D. Mackay, Inc., with a stated purity of 99.999%. Since gallium reacts slowly with moist air, the amount of exposure to the laboratory atmosphere of the gallium was minimized. Gallium was introduced into the effusion cell by hypodermic syringe.

Argon used as the inert atmosphere was purchased from the Matheson Co., with a stated minimum purity of 99.998%.

III. Results and Discussion

Vaporization of Indium. In Table I are found the experimental data, *i.e.*, temperature, cell designation, effective orifice area, mass loss, duration of run, and the calculated vapor pressure. The indium vapor has been assumed to be monatomic. In a mass spectroscopic study of indium-rich indium-antimony solutions vaporizing from molybdenum Knudsen cells, DeMaria, *et al.*,⁷ found the ratio of diatomic to mon-

atomic indium to be of the order of $(1-3) \times 10^{-5}$. The "third law" standard enthalpies of vaporization were calculated by using free energy functions, $(G^\circ - H^\circ_{298})/T$, for gaseous and liquid indium tabulated by Hultgren, *et al.*⁸ Also tabulated in Table I are the average pressure observed for the set of cells in each run, the average per cent absolute deviation from the mean pressure, and the average third-law standard enthalpy of vaporization at 298°K.

One usually expects an irreproducibility of about 10%⁹ in vapor pressure measurements with single Knudsen cells, although this may be reduced to about 5%¹⁰ under favorable conditions. The uncertainty in pressure measurements at a given temperature is less than 3% in the work being reported. There was no correlation between location of the cell in the molybdenum block and the value of the observed pressure. Thus, the large molybdenum block distributed the heat uniformly and reduced the temperature variation which appears to have decreased the irreproducibility.

(7) G. DeMaria, J. Drowart, and M. G. Inghram, *J. Chem. Phys.*, **31**, 1076 (1959).

(8) R. Hultgren, R. L. Orr, P. D. Anderson, and K. K. Kelley, "Selected Values of Thermodynamic Properties of Metal Alloys," John Wiley and Sons, Inc., New York, N. Y., 1963.

(9) J. L. Margrave, "Physicochemical Measurements at High Temperatures," J. O'M. Bockris, J. L. White, and C. D. MacKenzie, Ed., Butterworth and Co. (Publishers) Ltd., London, 1959, Chapter 10.

(10) R. J. Ackermann and R. J. Thorn, *Progr. Ceram. Sci.*, **1**, 39 (1961).

Table II: Third-Law Evaluation of Selected Indium Data^a

Investigator	No. of observations	ΔH°_{298} , kcal/g-atom	Method	Container material
This work	53	56.58 ± 0.10^b	Multiple effusion	Alumina
Alcock, <i>et al.</i> ¹¹	7	57.24	Effusion	Beryllia
Alcock, <i>et al.</i> ¹¹	3	57.08	Transportation	Beryllia
Anderson ¹²	8	58.23	Effusion	Quartz
Herrick ¹³	88	58.09 ± 0.15	Torsion-effusion	Graphite
Kohlmeyer and Spandau ¹⁶	1	56.33	Boiling point (1 atm)	(?)
McGonigal, <i>et al.</i> ¹⁷	1	56.54 ± 0.83	Boiling point (1 atm)	Graphite
Priselkov, <i>et al.</i> ¹⁴ (recalcd)	9	56.79	Effusion	Porcelain
Lyubimov and Lyubitov ¹⁶ (recalcd)	10	57.95 ± 0.4	Mass spectrometer	Quartz

^a Calculated with the use of $(G^\circ - H^\circ_{298})/T$ functions by Hultgren, *et al.*⁸ ^b Average deviation.

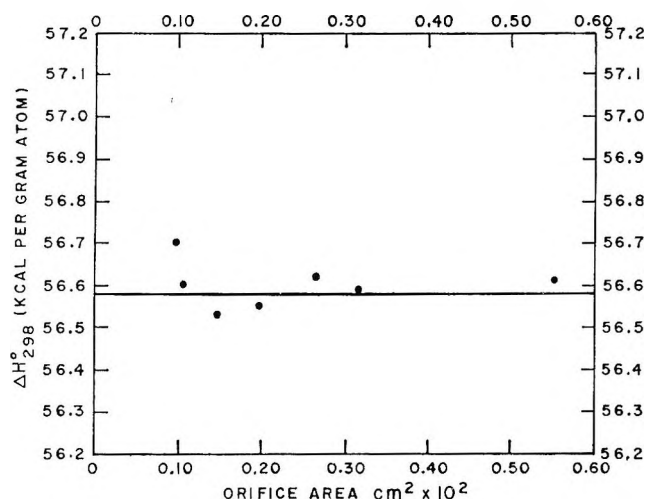


Figure 2. Variation of ΔH°_{298} of vaporization for indium with orifice area.

The variation of ΔH°_{298} is seen in Figure 2 to be small and independent of orifice area, and, thus, there is no indication of a nonunit evaporation coefficient.

The vapor pressure data are compared in Figure 3 with data by Alcock, *et al.*,¹¹ Anderson,¹² Herrick,¹³ and Priselkov, *et al.*¹⁴ Third-law standard enthalpies of vaporization at 298°K are tabulated in Table II with values by Alcock, *et al.*,¹¹ Anderson,¹² Herrick,¹³ Kohlmeyer and Spandau,¹⁵ Lyubimov and Lyubitov,¹⁶ McGonigal, *et al.*,¹⁷ and Priselkov, *et al.*¹⁴

The vapor pressure data obtained in this work agree well with the results of Alcock and Cornish¹¹ and Prisel-

kov, *et al.*¹⁴ Agreement is less good with Herrick¹³ and the early work of Anderson.¹² The ΔH°_{298} value of this study is in agreement with those of Alcock and Cornish,¹¹ Kohlmeyer and Spandau,¹⁵ McGonigal, *et al.*,¹⁷ and Priselkov, *et al.*,¹⁴ and in less good agreement with those of Anderson,¹² Herrick,¹³ and Lyubimov and Lyubitov.¹⁵

Evaluation of the several studies leading to ΔH°_{298} values does not lead to an objective basis for discriminating in favor of the results of any particular investigation. Therefore, it is probably best to choose 57.51 kcal/mole, the average weighted according to the number of observations, and to allow the uncertainty of 1.25 kcal/mole so as to include all data.

Vaporization of Gallium. In Table III are found the experimental data, the calculated vapor pressures, and the calculated third-law enthalpies of vaporization. The gallium vapor has been assumed to be monatomic. In a mass spectrometric study by Martynovich,¹⁸

(11) C. B. Alcock, J. B. Cornish, and P. Grievsen, IAEA Symposium on Thermodynamics with Emphasis on Nuclear Materials and Atomic Transport in Solids, Vienna, 1965, No. SM-66/34.

(12) J. S. Anderson, *J. Chem. Soc.*, 141 (1943).

(13) C. C. Herrick, *Trans. AIME*, **230**, 1439 (1964).

(14) Y. A. Priselkov, Y. A. Sapozhnikov, A. Y. Tsepelyeva, and V. V. Karelin, *Izv. Vysshikh Uchebn. Zavedenii, Khim. i Khim. Tekhnol.*, **3**, 447 (1960).

(15) E. J. Kohlmeyer and H. Spandau, *Z. Anorg. Chem.*, **253**, 37 (1945).

(16) A. P. Lyubimov and Y. N. Lyubitov, *Obrabotka Stali i Splavov, Moskov, Inst. Stali im I. V. Stalina, Sbornik*, **36**, 191 (1957).

(17) P. J. McGonigal, J. A. Cahill, and A. D. Kirshenbaum, *J. Inorg. Nucl. Chem.*, **24**, 1012 (1962).

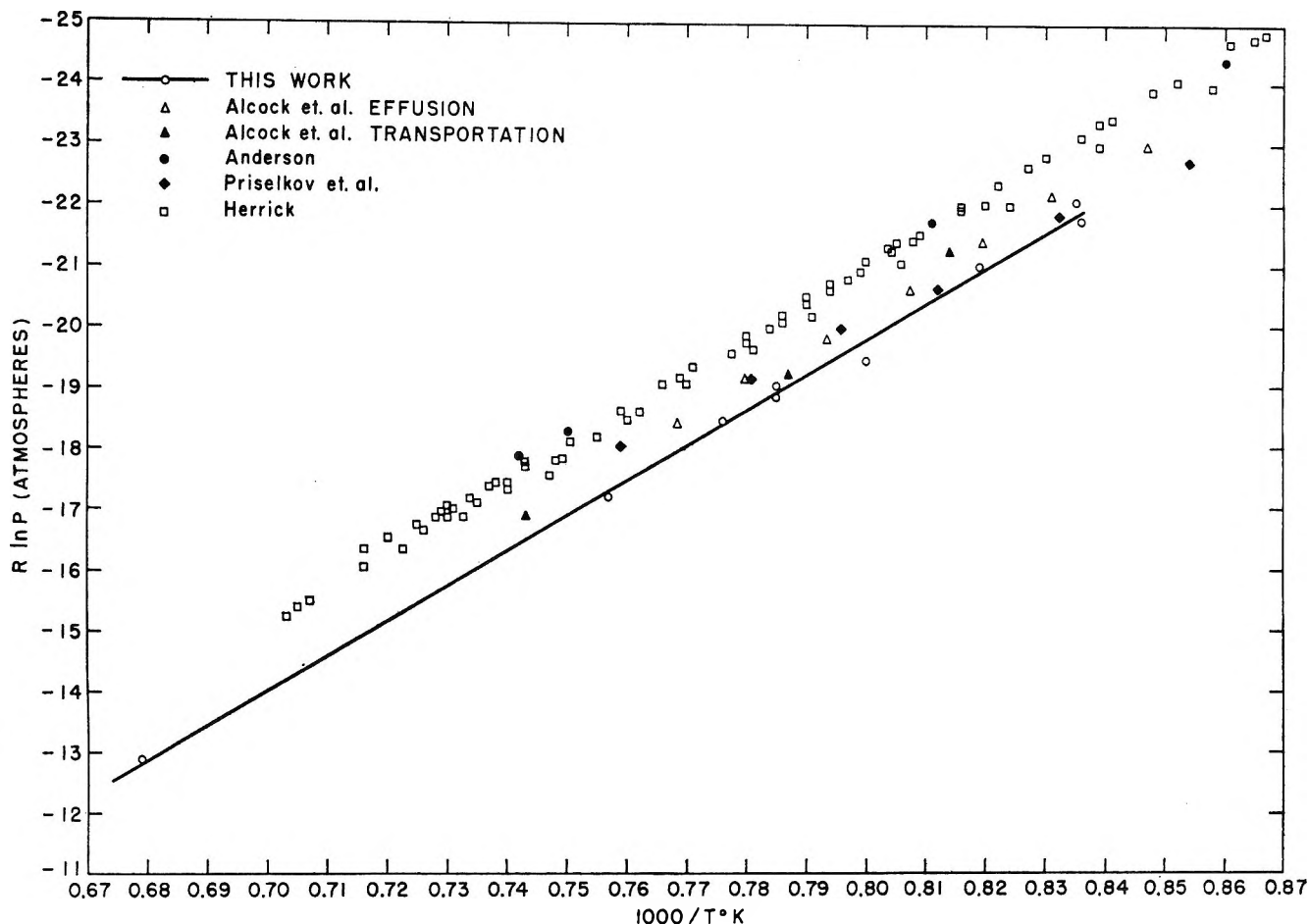


Figure 3. Comparison of vapor pressure data for indium.

the ratio of diatomic to monatomic gallium was found to be of the order of $(2-4) \times 10^{-5}$. Also Drowart and Honig¹⁹ studied the vaporization of gallium from graphite using a mass spectrometer; they concluded that monatomic gallium was the major species.

The irreproducibility found in these multiple-effusion measurements for gallium vapor pressures was 4.6%. This is somewhat larger than that for the indium measurements but does not seem to be attributable to temperature variation within the molybdenum block; it is to be noted that sets of results for both elements were obtained simultaneously at each block temperature. Sources of error which appear peculiar to the results for gallium were observed. A partial plugging of the orifice (by a gray material) of the cells containing gallium was detected occasionally in post-experimental observations. It seems plausible to suspect that molybdenum oxide particles (originating in a previous apparatus failure), subjected to vibration, fell from upper portions of the apparatus and into the effusion orifices (larger for the case of gallium than

for indium); then, some reduction reaction within the cell led to volatilization and reaction-deposition of the observed dark gray material. Another possible source of error was cracking of some cells due to expansion on freezing of gallium; thus, some cracks in some cells were observed, and hence the inference seems reasonable that some cracks may have escaped detection. Also "bumping" of gallium during initial pumpdown seems a possibility (in some cases small droplets were found on the top of the effusion cell after an experiment).

The variation in third-law ΔH°_{298} of vaporization of gallium is seen in Figure 4 to be small and independent of orifice area. Thus, there is no indication of nonunit evaporation coefficient.

The vapor pressure data are compared in Figure 5 with data by Alcock, *et al.*,¹¹ Munir and Searcy,²⁰

(18) G. M. Martynovich, *Vestn. Mosk. Univ., Ser. Mat., Mekhan., Astron., Fiz. i Khim.*, No. 2, 151 (1958); No. 5, 67 (1958).

(19) J. Drowart and R. E. Honig, *Bull. Soc. Chim. Belges*, **66**, 411 (1957).

Table III: Data for the Vaporization of Gallium

Temp, °K	Cell ^a	Mass loss, mg	Time, min	p , atm \times 10^{-6}	ΔH°_{298} , kcal/g- atom	Av p , atm \times 10^{-6}	% av dev	Av ΔH°_{298} , kcal/g- atom
1198.0	H	3.63	720.2	1.551	64.27	1.405	5.2	64.51
	I ^b			
	J ^b			
	K	6.43		1.282	64.72			
	L	6.87		1.442	64.44			
	M	7.86		1.381	64.54			
	N	8.60	1.370	64.56				
1273.6	H	17.73	760.4	7.390	64.25	6.847	5.7	64.75
	I	17.13		6.158	65.85			
	J	25.13		6.173	64.70			
	K	36.77		7.152	64.33			
	L	34.11		6.983	64.39			
	M	41.54		7.119	64.34			
	N	46.98	6.953	64.40				
1373.4 ^c	H	87.34	600.4	47.80	64.02
	I	51.70		2.44	65.85			
	J	12.59		4.06	...			
	K	7.80		1.99	...			
	L	73.85		19.85	...			
	M ^{*d}	179.43		37.65	64.67			
	N	272.67	52.99	63.74				
1472.7	H	243.90	472.3	174.7	64.09	168.0	8.9	64.74
	I	288.69		178.4	64.63			
	J ^{e,k}	177.00				
	K	403.45		134.9	65.45			
	L	508.49		178.9	64.72			
	M [*]	568.28		156.4	65.01			
	N	729.27	185.5	64.52				
1196.5	H ^f	...	720.4	1.380	7.9	64.54
	I	4.08		1.502	64.28			
	J ^{*g}	3.31		1.069	65.07			
	K ^{*h,k}	4.28		0.964	65.32			
	L	6.65		1.394	64.44			
	M ^{*i}	7.66		1.408	64.42			
	N	9.08	1.376	64.47				
1220.3	H	4.99	640.4	2.419	64.35	2.13	6.1	64.66
	I	5.28		2.207	64.58			
	J ^{*j,k}	3.52		1.291	65.87			
	K [*]	7.22		1.848	65.00			
	L	9.12		2.172	64.61			
	M [*]	10.20		2.130	64.66			
	N	11.73	2.028	64.77				
1273.8	H	9.20	466.9	6.477	64.59	6.29	3.3	64.66
	I	10.84		6.582	64.55			
	J [*]	11.81		6.295	64.66			
	K [*]	15.37		5.717	64.90			
	L	18.16		6.279	64.67			
	M [*]	21.46		6.511	64.57			
	N	24.58	6.144	64.72				
1320.7	H	10.46	192.2	17.54	64.27	17.70	1.5	64.24
	I	12.50		18.09	64.22			
	J [*]	13.54		17.21	64.32			

Table III (Continued)

Temp, °K	Cell ^a	Mass loss, mg	Time, min	p , atm \times 10^{-6}	ΔH°_{298} , kcal/g- atom	Av p , atm \times 10^{-6}	% av dev	Av ΔH°_{298} , kcal/g- atom
1320.7	K*	20.01	192.2	17.75	64.16	17.70	1.5	64.24
	L	21.69		17.87	64.22			
	M*	24.92		18.03	64.20			
	N	29.37		17.50	64.28			
1289.2	H	8.40	273.6	9.789	64.29	9.60	4.7	64.35
	I	10.27		10.32	64.16			
	J*	11.42		10.08	64.22			
	K*	14.30		8.807	64.56			
	L	16.30		9.330	64.42			
	M* ^{j,k}	8.22		4.129	...			
	N	22.33		9.240	64.44			
1248.9	H	7.25	510.2	4.460	64.29	4.51	1.1	64.26
	I	8.60		4.564	64.23			
	J* ^{e,k}	4.25		2.940	65.33			
	K* ^{e,k}	8.10		2.633	65.60			
	L ^{e,k}	8.41		2.542	...			
	M* ^{e,k}	7.25		1.922	...			
	N ^{e,k}	13.03		2.847	65.40			

^a The orifice areas in square centimeters for the cells at 50° were: H, 0.004955; I, 0.005750; J, 0.008434; K, 0.010604; L, 0.010310; M, 0.012156; N, 0.014022. Expansion-of-orifice corrections were made using the coefficient of thermal expansion of $7.8 \times 10^{-6} \text{ deg}^{-1}$.

^b Some gallium was lost in handling before weighing. ^c Data from this run are shown only for completeness because an air leak developed during the run. These data are not included in the over-all averages. ^d Cell M was broken and was replaced by a similar new cell designated as M*. ^e Low mass loss due to partial plugging of orifice by foreign material. ^f Error made in weighing before run so mass loss could not be calculated. ^g Cell J was broken and was replaced by a similar new cell designated as J*. ^h Cell K was broken and was replaced by a similar new cell designated as K*. ⁱ Cell M* was broken and was replaced by a similar new cell designated as M*. ^j There is no apparent reason for this low result, but it was rejected because it was considered to be statistically improbable. ^k These data are not included in the averages.

 Table IV: Third-Law Evaluation of Selected Gallium Data^a

Investigator	No. of observa- tions	ΔH°_{298} , kcal/g-atom	Method	Container material
This work	56	64.62 ± 0.22^b	Multiple effusion	Alumina
Alcock, <i>et al.</i> ¹¹	9	64.83	Effusion	Beryllia
	3	65.04	Transporta- tion	Beryllia
Cochran and Foster ²²	6	68.96 ± 0.19	Recording effusion	Alumina
Harteck ²³	20	66.30 ± 1.10	Effusion	Quartz
Munir and Searcy ²⁰	53	65.44 ± 0.23	Torsion- effusion	Graphite
Speiser and Johnston ²¹	19	64.86 ± 1.10	Effusion	Quartz

^a Calculated with the use of $(G^{\circ} - H^{\circ}_{298})/T$ functions by Hultgren, *et al.*⁸ ^b Average deviation.

Speiser and Johnston;²¹ the agreement is good. Third-law ΔH°_{298} values for vaporization are tabulated in Table IV with values by Alcock, *et al.*,¹¹ Cochran and Foster,²² Harteck,²³ Munir and Searcy,²⁰ and Speiser and Johnston.²⁰ The value obtained from this study

(20) Z. A. Munir and A. W. Searcy, *J. Electrochem. Soc.*, **111**, 1170 (1964).

(21) R. Speiser and H. L. Johnston, *J. Am. Chem. Soc.*, **75**, 1469 (1953).

(22) C. N. Cochran and L. M. Foster, *J. Electrochem. Soc.*, **109**, 144 (1962).

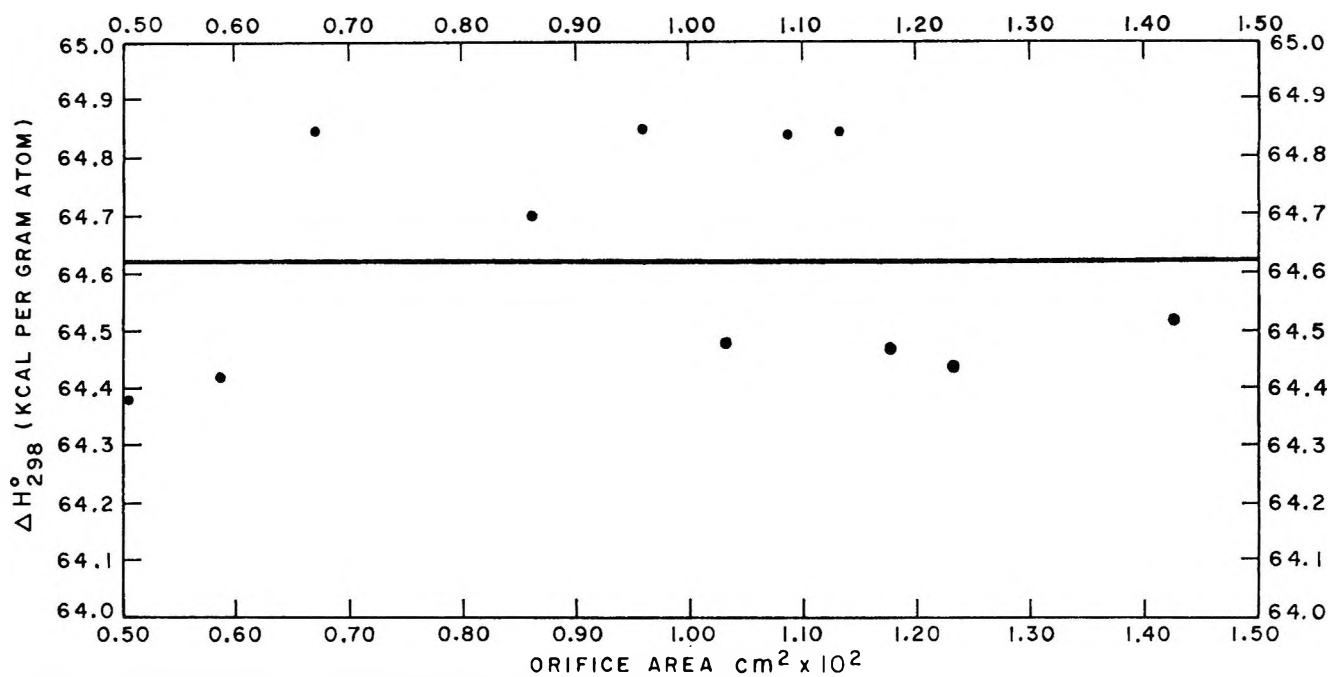


Figure 4. Variation of ΔH°_{298} of vaporization for gallium with orifice area.

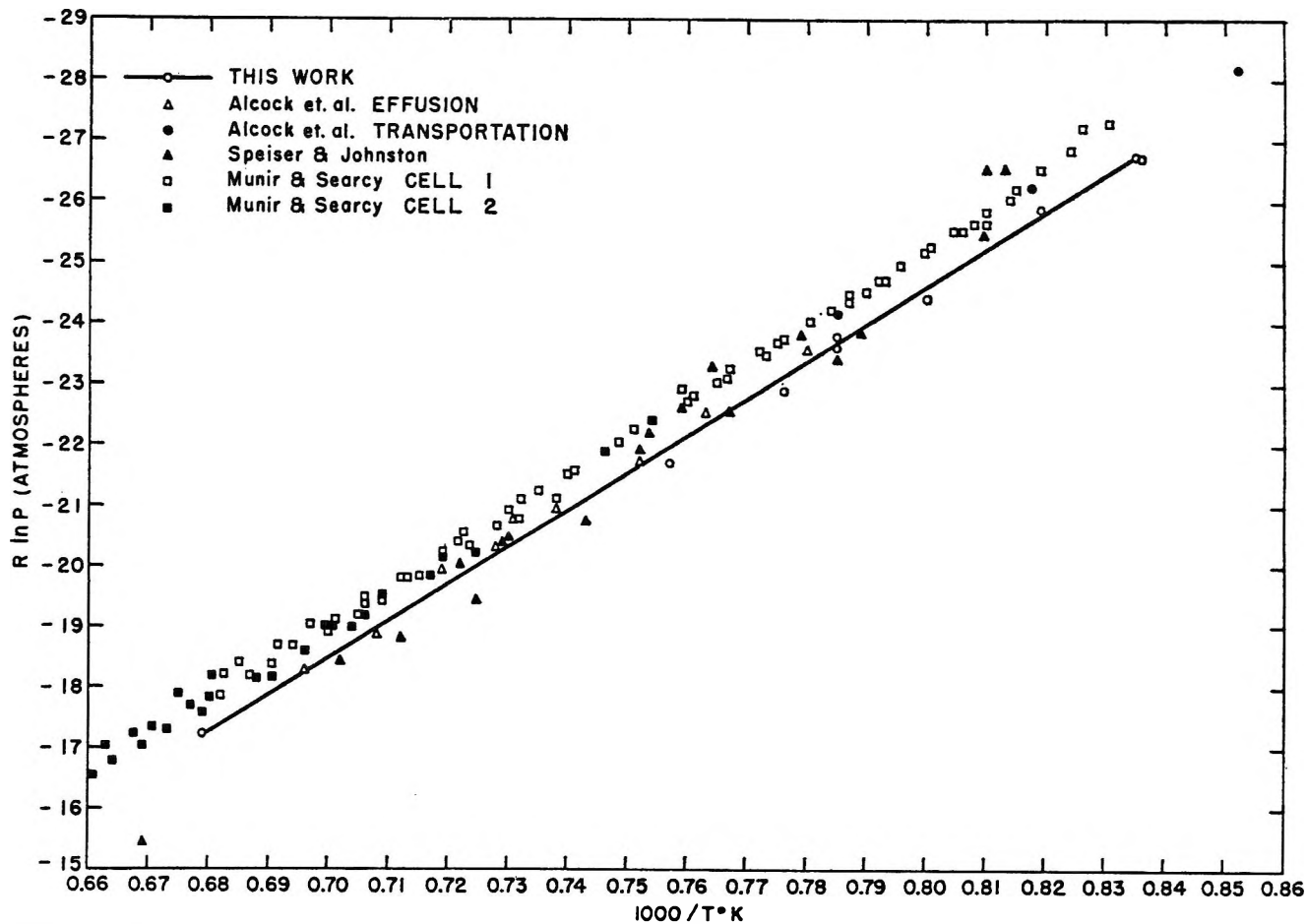


Figure 5. Comparison of vapor pressure data for gallium.

agrees with the other values cited with the exception of the values by Cochran and Foster²² and Harteck.²³ Munir and Sercy²⁰ have discussed the discrepancy with the value of Cochran and Foster,²² and Speiser and Johnston²¹ have discussed the discrepancy with the value of Harteck.²³ A value of 65.00 ± 0.5 kcal/mole has been chosen based on the average of all values weighted according to the number of observations exclusive of those by Cochran and Foster²² and those by Harteck.²³

Conclusions. A multiple-effusion cell apparatus has been constructed, tested, and found capable of giving several vapor pressure measurements at one well-defined temperature with better precision than is general for many separate measurements in a single cell.

The standard enthalpies of vaporization at 298°K for indium and gallium, from observations during the course of this work, are 56.58 ± 0.10 and 64.62 ± 0.22

kcal/g-atom, respectively. Evaluation of this work with other literature values leads to 57.51 ± 1.25 and 65.00 ± 0.5 kcal/mole, respectively.

Acknowledgments. The authors gratefully acknowledge the support of this research by the Air Force Office of Scientific Research through Contract No. AF 49(638)-346 and the Atomic Energy Commission through Contract No. AT(11-1)-1029. G. J. M. wishes to thank the Illinois Institute of Technology for a fellowship for the 1958-1959 academic year. G. J. M. and R. K. E. acknowledge the support of the Chemical Engineering Division of Argonne National Laboratory during the preparation of the manuscript. P. G. W. wishes to acknowledge support received from the Graduate School of the Illinois Institute of Technology through a Faculty Research Fellowship during the fall of 1965.

(23) P. Harteck, *Z. Physik. Chem.*, **134**, 1 (1928).

Solubilization of a Water-Insoluble Dye as a Method for Determining Micellar Molecular Weights

by Hans Schott

Research Center, Lever Brothers Company, Edgewater, New Jersey 07020 (Received March 28, 1966)

Micellar molecular weights (mmw) and critical micelle concentrations (cmc) of detergents can be determined by means of solubilization of the water-insoluble dye Orange OT, based on the following two observations: little or no dye was solubilized below the cmc; and in solutions saturated with dye at higher detergent concentrations, only one dye molecule was solubilized per micelle. The experimental procedure consists of saturating aqueous detergent solutions of known concentration with dye, filtering off the excess dye, and measuring absorbancies. From these, plus a knowledge of the molar extinction coefficient of the dye and the cmc of the detergent, mmw values are readily calculated. The mmw of two nonionic detergents determined by solubilization and by light scattering agree very well. The mmw of two anionic detergents determined by solubilization were nearly the same in the presence and absence of supporting electrolyte, while literature values for the mmw of one of those, sodium dodecyl sulfate, determined by light scattering are increased considerably by supporting electrolyte. The mmw determined by solubilization is inside the range of the widely scattered published mmw values of sodium dodecyl sulfate determined by ultracentrifugation and light scattering in the presence of supporting electrolyte. The published mmw of the two anionic detergents in water alone determined by light scattering are considerably lower than those determined by dye solubilization. The mmw of the four detergents obtained by solubilization were not affected by the presence of small amounts of impurities of the kind which occurs in incompletely purified detergents.

Introduction

In the course of other work,¹ it was found that the limit of solubilization of the water-insoluble dye Orange OT in aqueous solutions of the nonionic detergent 1-dodecanol-28 ethylene oxide (EO) units, C₁₂(EO)₂₈, was one dye molecule per micelle. If this solubilization limit were general, the micellar molecular weight (mmw) of detergents could be determined from the amount of dye solubilized in detergent solutions saturated with the dye. Such a method would be experimentally and theoretically less complicated than light scattering and ultracentrifugation; no added electrolyte is needed. At the same time, dye solubilization can be used to determine the critical micelle concentration (cmc),^{2,3} the value of which is needed to calculate the mmw. The amount of carefully purified dye solubilized below the cmc is very slight or zero.¹⁻⁴

Combining published data on solubilization of Orange OT and of dimethylaminoazobenzene with available mmw and cmc values⁵ generally yields solubilization ratios (number of micelles per solubilized dye molecule at saturation) considerably greater than 1. For instance, the values range from 7 to 20 for commercial grade Aerosol OT (sodium dioctyl sulfosuccinate) and from 12 to 40 for Aerosol MA (sodium

(1) H. Schott, *J. Phys. Chem.*, **68**, 3612 (1964).

(2) I. M. Kolthoff and W. Stricks, *J. Phys. Colloid Chem.*, **52**, 915 (1948).

(3) R. J. Williams, J. N. Phillips, and K. J. Mysels, *Trans. Faraday Soc.*, **51**, 729 (1955).

(4) M. W. Rigg and F. W. J. Liu, *J. Am. Oil Chemists' Soc.*, **30**, 14 (1953).

(5) K. Shinoda, T. Nakagawa, B. Tamamushi, and T. Isemura, "Colloidal Surfactants," Academic Press Inc., New York, N. Y., 1963.

dihexyl sulfosuccinate),⁶ being lowest and fairly constant at the highest detergent concentrations. For potassium laurate, the ratio is between 4 and 6,^{2,4,7} but, for dodecylamine hydrochloride, it is between 1.0 and 2.2.^{2,4}

If these measurements were made and interpreted correctly, solubilization ratios greater than unity could be due either to wrong mmw values or to the presence of impurities. Considering that one molecule of Orange OT can saturate a micelle, it should cause little surprise that suitable impurities contained in a technical grade detergent, though present only in relatively small amounts, could preempt a large fraction of the solubilizing capacity of the detergent for Orange OT.

In addition to studying the effect of known amounts of added impurities on the solubilizing capacity of pure detergents for Orange OT, it is necessary to establish that the solubilized dye does not change the micellar size.

Experimental Section

Materials. Purifications of Orange OT (1-*o*-tolyl-azo-2-naphthol) and of the nonionic detergent C₁₂-(EO)₂₈ have been described.¹ Another nonionic detergent was prepared in the laboratories of General Aniline & Film Corp. by adding an average of 14 EO to 1-dodecanol and stripping out unreacted alcohol plus the lowest adducts, containing up to 5 EO, in a molecular still. The remaining material was freed from any glycols and salts it might have contained by ultrafiltration. The final product, designated C₁₂-(EO)₁₆, contained 16.1 EO according to the infrared method of determining the EO chain length.¹ Sodium decane sulfonate was prepared from decyl bromide (Humphrey-Wilkinson Inc., taking the middle cut during a fractional distillation) and sodium sulfite. The product was recrystallized three times from water and four times from ethanol; it was twice dissolved in methanol, precipitated with petroleum ether (bp 40–60°), and finally extracted with ethyl ether. A sample which was merely recrystallized and which exhibited a minimum in the surface tension–log concentration curve was used in one experiment. Sodium dodecyl sulfate was prepared by sulfating lauryl alcohol (Givaudan-Delawanna Inc.) with chlorosulfonic acid, neutralizing, precipitating the inorganic salts in hot ethanol, concentrating the filtrate, and cooling and filtering off the crystallized detergent. This was followed by three recrystallizations from a mixture of 50% 2-propanol and 50% ethanol and by washing with acetone. Since this sample had a minimum in the surface tension–log concentration curve, addi-

tional solubilization experiments were made with another sample which was further recrystallized from water and from butanol, followed by extraction with ethyl ether. This procedure eliminated the minimum. Behenyl alcohol was prepared by reduction of behenic acid (from the Hormel Institute) with lithium aluminum hydride, followed by treatment with sodium hydroxide in methanol, two recrystallizations from acetone, and a fractional distillation under vacuum. Adol 18 (Archer-Daniels-Midland Co.) was fractionally distilled, and the middle cut was recrystallized from hexane to obtain 1-tetradecanol. Monsanto's 6-phenyldodecane was used as received.

Solubilization Procedure. Excess Orange OT was added either to detergent solutions of the correct concentration or to solutions between three and four times too concentrated, which were later diluted with water or with sodium chloride solutions. Agreement between solubilization data obtained from the side of supersaturation and those obtained by starting with the solid dye indicates that both represent equilibrium values. Impurities, when added, were measured out as solutions in acetone by means of a microburet or were added in bulk form and solubilized by warming the solutions, prior to the dye addition. The highest concentration of acetone tested, 0.6%, did not affect the solubilization limit nor the extinction coefficient of the dye. The highest acetone level actually employed was below 0.4%.

The solutions, protected from light and stored under nitrogen, were agitated on a jar-rolling mill for at least 4 days, followed by at least 1 week of storage at 25.0 ± 0.1 or $29.8 \pm 0.2^\circ$. The exception was sodium dodecyl sulfate, the solutions of which were agitated for only 2 days and equilibrated at 25° for 3. In the case of all four detergents, halving or quadrupling these times did not alter the amount of dye solubilized. Agitating the solutions on the jar-rolling mill caused agglomeration of suspended dye, including even the finely dispersed dye which had been precipitated by diluting concentrated detergent–dye mixtures. Excess dye was removed by filtration through a tightly packed plug of absorbent cotton,⁴ discarding the initial 50 cm³. Cotton was shown not to adsorb solubilized dye because refiltration of filtered solutions through fresh plugs did not lower the absorbancy. Removal of suspended dye was complete because raising the detergent concentration of filtered samples by adding solid detergent did not increase the absorbancy.

(6) J. W. McBain and R. C. Merrill, Jr., *Ind. Eng. Chem.*, **34**, 915 (1942).

(7) J. W. McBain and A. A. Green, *J. Am. Chem. Soc.*, **68**, 1731 (1946).

Concentrations of filtrates were rechecked by their solids contents.

Spectroscopic Measurements. The amount of solubilized dye was determined by measuring the maximum absorbancy around 500 $m\mu$. For dye solubilized in $C_{12}(EO)_{16}$, the absorption maximum was located at 495 $m\mu$, with a weak shoulder at higher wavelengths. For dye solubilized by the two anionic detergents, there were two overlapping absorption maxima in the spectrum, apparently at 499 and 521 $m\mu$, respectively. The former maximum was not much stronger than the latter, and the apparent shift from 495 to 499 $m\mu$ is probably due to overlapping by the 521- $m\mu$ maximum. The plateau at and above 600 $m\mu$ nearly coincided with the base line of the blank and was used as reference intensity (I_0). Every spectrum was taken in duplicate with a Perkin-Elmer 202 ultraviolet-visible spectrophotometer and with a Beckman DK-2 recording spectrophotometer, using quartz cells 0.5, 1.0, 5.0, and 10.0 cm long. Beer's law was obeyed at all absorbancies tested.

The absorbancy $A = \log(I_0/I)$ is the product of the molar extinction coefficient ϵ , molar concentration c_{OCT} , and path length L in centimeters. The molar extinction coefficient of Orange OT was determined by adding very small volumes of its acetone solutions to 2.00% solutions of $C_{12}(EO)_{16}$, 1.50% solutions of sodium dodecyl sulfate, and 2.50 and 3.00% solutions of sodium decane sulfonate. The value of ϵ in $C_{12}(EO)_{16}$ was identical with that in $C_{12}(EO)_{28}$, namely, $(1.740 \pm 0.007) \times 10^4$ l./mole cm.¹ Dye solubilized in the two anionic detergents had a somewhat higher molar extinction coefficient, probably owing to reinforcement of the 499- $m\mu$ maximum by the overlapping 521- $m\mu$ maximum. Eight absorbancy measurements of Orange OT dissolved in sodium dodecyl sulfate solutions at concentrations between 1.411 and 13.139 mg/l. gave a mean value of 1.994×10^4 l./mole cm for the molar extinction coefficient; the standard deviation of the mean was 0.011×10^4 , and the range of values was $\pm 0.040 \times 10^4$. Eight absorbancy measurements of the dye dissolved in sodium decane sulfonate solutions at concentrations between 1.390 and 37.076 mg/l. gave a mean value of 1.987×10^4 l./mole cm for ϵ ; the standard deviation of the mean was 0.009×10^4 , and the range of values was $\pm 0.065 \times 10^4$. Four dye solutions in each detergent were acidified with gaseous hydrogen chloride, and in three cases each, the dye in acetone was added to acidified detergent solutions; this did not affect the absorbancies. The two ϵ values determined in the two anionic detergents are identical within the accuracy of the measurements, since the difference between the two averages is less than 1 standard

deviation. The present ϵ values are in good agreement with those of Kolthoff² and Rigg,⁴ both measured in aqueous ethanol, but are lower than the ϵ value of Williams, Phillips, and Mysels, measured in acidified sodium dodecyl sulfate solutions,³ by exactly a factor of 10.

Additional Measurements. Sedimentation constants were determined in a Spinco Model E ultracentrifuge using a synthetic boundary cell, at the temperature of $26.3 \pm 0.1^\circ$ and a speed of 59,780 rpm. Pictures were taken at 16-min intervals. All schlieren patterns contained single, sharp peaks. Densities and viscosities were determined at $26.3 \pm 0.1^\circ$, the former with a 20-cm³ pycnometer, the latter with a 2-min Cannon-Fenske viscometer, neglecting the kinetic energy correction.

Turbidities were measured in a Brice-Phoenix photometer at 25.0 – 26.5° , with blue light at 436 $m\mu$ and a standard 40×40 mm semioctagonal cell. The photometer was calibrated with an opal-glass diffuser. Each solution was made up by weighing the detergent into a volumetric flask rather than by dilution. The solutions were filtered through an ultrafine sintered-glass filter into the cell. The refractive index increment was determined with a Brice-Phoenix differential refractometer at the same temperature and wavelength used in the light-scattering measurements.

Results and Discussion

Effect of Dye Solubilization on Micellar Molecular Weight. In order to ascertain whether solubilized dye changes the mmw, sedimentation velocity measurements were made on three solutions of $C_{12}(EO)_{28}$ without dye, three solutions equilibrated with excess Orange OT and filtered, and one solution half saturated with the dye.

Plots of the logarithm of r , the distance from the axis of rotation, vs. time t gave the values for the sedimentation constant s shown below, calculated according to

$$s = \frac{dr/dt}{\omega^2 r} = \frac{d \ln r/dt}{\omega^2} \quad (1)$$

where ω is the rotational speed (radians/sec).

Solutions of $C_{12}(EO)_{28}$ with concentrations of 0.498, 0.339, and 0.200% had sedimentation constants of 1.346, 1.394, and 1.516 S, respectively. Solutions containing 0.500, 0.350, and 0.197% $C_{12}(EO)_{28}$ which were saturated with Orange OT had s values of 1.356, 1.445, and 1.487 S, respectively. A solution of 0.409% $C_{12}(EO)_{28}$ which was half saturated with the dye had an s value of 1.452 S.

Table I: Critical Micelle Concentrations, Slopes of Concentration *vs.* Absorbancy Plots, and Micellar Molecular Weights

	Cmc, g/l.	b, ^a g/l.	Micellar molecular weights determined by			
			Dye solubilization	Light scattering	Ultra- centrifugation	Other methods
Nonionic detergents at 25°						
C ₁₂ (EO) ₂₈ (water)	0.1186 ^b	4.960	82,892 ± 1513	82,000 ± 2270	81,600 ± 5000	
C ₁₂ (EO) ₁₆ (water)	0.2205	3.589	62,112 ± 463	59,500 ± 1980		
Sodium decane sulfonate at 30°						
Water	10.66 ^c	3.484	69,293 ± 204	9,900 ^d		
0.10 M NaCl	5.364	3.553	70,584 ± 321			
Sodium dodecyl sulfate at 25°						
Water	2.324	1.851	36,879	11,400–20,500 ^e	16,700 ^e	7,210–23,650 ^e
0.03 M NaCl	0.918	1.793	35,740	20,765–21,700 ^e		28,840–29,417 ^f
0.10 M NaCl	0.410	1.907	37,954	21,918–24,600 ^e	21,918 ^g	31,724–32,301 ^f
0.40 M NaCl	0.1894	1.457	29,053	34,608–36,050 ^e	34,320 ^g	

^a Defined by eq 3. ^b Based on detergent concentrations below 4.0 g/l. ^c Based on detergent concentrations above 11.5 g/l. ^d From ref 13. Where no reference is given, values are from this work. ^e References listed in ref 15. ^f Discounting water of hydration; references listed in ref 5. ^g From ref 15.

Table II: Micellar Molecular Weight of C₁₂(EO)₂₈ from Absorbancy of Solutions Saturated with Orange OT at 25°

Detergent concn, g of C ₁₂ (EO) ₂₈ /l.	Absorbancy for 1.00-cm cell	Mmw
6.62	1.443	78,048
5.76	1.325	73,769
5.67	1.107	86,889
5.00	1.100	76,911
5.00 ^a	1.096	77,190
5.00 ^b	1.105	76,562
3.50	0.688	85,240
3.50 ^b	0.683	85,866
2.75	0.515	88,630
2.00	0.383	85,336
1.97	0.384	83,734
1.39	0.241	91,838
0.88	0.164	81,225
0.50	0.075	89,959
		Mean 82,892 ± 1513
0.058	0.000	

^a After a 3-month storage at 25°, with occasional shaking.
^b Made up by saturating a solution of 16 g of C₁₂(EO)₂₈/l. with dye and diluting with water. All other solutions were prepared by adding the dye to the detergent solutions of the final concentration.

Calculating *s*₀, the sedimentation constant at infinite dilution, by extrapolation according to⁸

$$s = s_0 / (1 + Kc) \quad (2)$$

gives the value of 1.643 ± 0.017 S for the solutions without dye and 1.598 ± 0.012 S for the saturated solutions. According to the Student *t* test, the difference

between the two *s*₀ values is not significant: The solubilized dye does not affect the micellar size of the nonionic detergent. Considering that the solubilized dye constitutes only 0.32% of the weight of the micelle which it saturates, this result is not surprising.

Critical Micelle Concentrations. Since little or no Orange OT is solubilized below the cmc,^{2,3} plots of absorbancy of detergent solutions saturated with the dye *vs.* detergent concentration intersect the detergent concentration axis at the cmc. In the case of sodium decane sulfonate in water, the plot was linear except that it curved somewhat toward the absorbancy axis at low concentrations. The cmc was determined by extrapolating the linear portion to zero absorbancy. This procedure has been shown to give the correct cmc value for sodium dodecyl sulfate in water.³ Dye solubilization below the cmc may indicate premicellization. For C₁₂(EO)₂₈, the plot was linear up to 4 g/l. and slightly curved at higher concentrations. The remaining systems gave straight lines over the whole range of detergent concentration examined. The equation of these straight lines can be represented by

$$c = \text{cmc} + bA \quad (3)$$

The constants, calculated by the method of least squares, are listed in Table I.

Among the systems listed in Table I, cmc values for the following are also reported in the literature: C₁₂(EO)₂₈,¹ sodium decane sulfonate in water,⁹ and

(8) H. K. Schachman, "Ultracentrifugation in Biochemistry," Academic Press Inc., New York, N. Y., 1959.

(9) H. B. Klevens, *J. Phys. Colloid Chem.*, **52**, 130 (1948).

sodium dodecyl sulfate in water and in 0.03 and 0.10 *M* NaCl solutions.³ All five published cmc values are in good agreement with their counterparts of Table I. In the case of sodium dodecyl sulfate solutions at the four levels of NaCl, there is a linear relation between the logarithm of the cmc and the logarithm of the concentration of Na⁺, as is commonly observed.⁵ The sole apparent incongruity is that the cmc of C₁₂(EO)₂₈ is half that of C₁₂(EO)₁₆, whereas it is well known that the cmc increases with increasing EO content. The incongruity probably results from a difference in the distribution of EO chain lengths, especially since the shortest chain components had been removed from C₁₂(EO)₁₆. Crook, *et al.*, have shown that pure, single-species, nonionic surfactants have about twice as large a cmc value as the normal-distribution surfactants of the same EO content and have ascribed the difference to the effect of the species of shortest EO chains in the latter.¹⁰

Micellar Molecular Weights from Amount of Solubilized Dye. The mmw can readily be calculated from the absorbancy of detergent solutions saturated with dye by making the following two assumptions:

(a) the solubilization ratio is one micelle per dye molecule; (b) the concentration of detergent not associated into micelles is constant and equal to the cmc. The results are shown in Tables II–V. According to eq 3, the mmw equals $bL\epsilon$. For C₁₂(EO)₂₈, this product, 85,808, is somewhat larger than the mean of Table II because the value of b was calculated only for concentrations below 4 g/l. The high precision of this method of determining mmw is shown by the fact that the standard deviation of the mean amounts to between only 0.3 and 1.8% of the mean. Light-scattering

Table III: Micellar Molecular Weight of C₁₂(EO)₁₆ from Absorbancy of Solutions Saturated with Orange OT at 25°

Detergent concn. g of C ₁₂ (EO) ₁₆ /l.	Absorbancy for 1.00-cm cell	Mmw
7.63	2.055	62,269
5.81 ^a	1.558	62,042
4.51	1.210	61,373
4.51 ^b	1.212	61,286
3.00	0.789	60,965
2.03	0.485	64,643
1.01	0.219	62,205
	Mean	62,112 ± 463
0.10	0.0000 ^c	
0.08 ^d	0.0000 ^c	
0.05 ^e	0.0000 ^c	
0.05	0.0000 ^c	
4.61 ^f	1.213	62,607
4.51 ^g	1.198	61,949
4.51 ^h	1.163	63,811

^a Prepared by diluting a 19.50 g/l. solution saturated with dye. ^b Stored 2 months at 25° before filtering. ^c Measured in 10.0-cm cells with instrumental setting of 90–100% transmittance expanded to full scale. ^d Made up by diluting a 1.01 g/l. solution containing excess dye. ^e Made up by diluting a 1.01 g/l. solution saturated with dye. ^f Also contained 2.0 g of acetone/l. ^g Also contained 0.0257 g of behenyl alcohol/l. and 2.1 g of acetone/l. ^h Also contained 0.0153 g of 6-phenyldodecane/l. and 0.7 g of acetone/l.

Table IV: Micellar Molecular Weight of Sodium Decane Sulfonate from Absorbancy of Solutions Saturated with Orange OT at 30°

Detergent concn. g/l.	Absorbancy for 1.0-cm cell	Mmw
	(1) In Water	
20.33	2.774	69,269
14.90	1.222	68,943
14.02	0.964	69,250
14.00 ^a	0.959	69,208
13.13	0.713	68,841
12.06 ^b	0.396	70,246
	Mean	69,293 ± 204
	Aggregation no.	284
11.16	0.1994	
10.34	0.0476	
10.08 ^b	0.0042 ^c	
9.810 ^b	0.0003 ^c	
9.641	0.0006 ^c	
6.313 ^b	0.0000 ^c	
13.00 ^d	0.853	54,507
	(2) In 0.10 <i>M</i> NaCl	
8.445	0.867	70,600
8.000	0.744	70,406
6.960	0.442	71,763
6.494	0.318	70,607
6.490 ^a	0.316	70,818
6.421 ^b	0.303	69,311
	Mean	70,584 ± 321
	Aggregation no.	289
4.108	0.0000 ^c	

^a Sample had a minimum in the surface tension–concentration curve. ^b Made up by saturating a detergent solution about 2 or 3 times more concentrated with Orange OT and then diluting. ^c Measured in 10.0-cm cells, with an instrumental setting of 90–100% transmittance expanded to full scale. ^d Also contained 0.084 g of 1-tetradecanol/l.

(10) E. H. Crook, D. B. Fordyce, and G. F. Trebbi, *J. Phys. Chem.*, **67**, 1987 (1963).

Table V: Micellar Molecular Weight of Sodium Dodecyl Sulfate from Absorbancy of Solutions Saturated with Orange OT at 25°

Sodium chloride concn, <i>M</i>	Detergent concn, g/l.	Absorbancy for 1.00-cm cell	Mmw
0	2.679	0.192	36,868
	2.760	0.235	36,996
	2.761 ^{a,b}	0.237	36,766
	2.940 ^c	0.333	36,886
	2.941 ^a	0.333	36,884
	Mean		36,879
	Aggregation no.		128
0.03	1.194	0.154	35,737
	1.410	0.276	35,549
	1.592	0.372	36,128
	2.157 ^c	0.695	35,547
	Mean		35,740
	Aggregation no.		124
0.10	0.650 ^a	0.126	37,980
	0.650	0.126	37,980
	0.900 ^a	0.258	37,870
	1.060 ^c	0.341	38,012
	Mean		37,954
	Aggregation no.		131
0.40	0.765 ^c	0.400	28,714
	1.045 ^a	0.579	29,480
	1.305	0.768	28,975
	1.810 ^{a,c}	1.113	29,041
	Mean		29,053
	Aggregation no.		101

^a Sample of highly purified detergent, without minimum in the surface tension-concentration curve. ^b The same absorbancy was obtained (1) when the solution was made by diluting one 4 times more concentrated and saturated with Orange OT, followed by 4-hr stirring and 40-hr equilibrating at 25°, and (2) when the solution was equilibrated for 10 days at 25°. ^c Prepared by diluting a more concentrated solution saturated with Orange OT.

measurements of solutions of the two nonionic detergents without dye gave an mmw of 82,000 ± 2270 for C₁₂(EO)₂₈ and 59,500 ± 1980 for C₁₂(EO)₁₆.

These values, calculated by extrapolating the Debye function¹¹ to zero micellar concentration, are in agreement with those determined by dye solubilization. The two Debye plots were linear in the range of concentrations covered, up to 7.6 × 10⁻³ g/cm³, and the slopes did not differ significantly from zero. The very small or zero value for the second virial coefficient arises from the compactness of the micelles, resulting in a small excluded volume, plus the lack of repulsion owing

to the absence of charge. There was no measurable dissymmetry.

The molecular radius of the hydrated C₁₂(EO)₂₈ micelle can be calculated from *s*₀ by the equation

$$R = \sqrt{\frac{9}{2} \frac{s_0 \eta}{(1/\bar{v} - \rho)}} \quad (4)$$

This is the form which the Svedberg equation takes for independent, spherical, uncharged particles, for which the diffusion constant is given by the Einstein-Sutherland equation and the frictional force by Stokes' law.⁸ The partial specific volume of the detergent, $\bar{v} = 0.9621$ cm³/g, was obtained from measured densities by the graphical method of intercepts. The value of *R* = 39 Å must be reduced by a factor of 1.24, since the diameters of micelles of nonionic detergents measured by light scattering are on the average about 24% smaller than those measured by sedimentation velocity, the difference being due to water of hydration.¹² A radius of 31.5 Å corresponds to an mmw of 81,600. This value is only a rough estimate, since a small change in the 1.24 factor introduces a large error in the mmw.

It is interesting to note that the presence of solubilized alcohol and hydrocarbon did not affect the solubilization of Orange OT nor the mmw.

Light-scattering values of sodium decane sulfonate solutions gave an mmw of 9900;¹³ the present value is 7 times larger. A possible source of error in the dye solubilization procedure is the assumption of unit solubilization ratio. However, solubilization ratios smaller than unity would increase the discrepancy: For example, if there were two molecules of Orange OT solubilized in each micelle, the mmw would be doubled. Thus, the present value represents the smallest mmw obtainable by dye solubilization, since solubilization ratios greater than 1 are extremely unlikely for highly purified detergents. Another reason for eliminating impurities as a cause of the discrepancy in mmw determined by light scattering and dye solubilization is that the solution of a less pure sample of sodium decane sulfonate solubilized the same amount of dye as the highly purified sample. Moreover, the addition of a relatively large amount of tetradecanol increased the amount of solubilized dye by only 21% (Table IV). This is probably due to a decrease in the cmc: a drop from 10.66 to 10.02 g/l. would account for the observed increase in solubiliza-

(11) P. Debye, *J. Phys. Colloid Chem.*, **53**, 1 (1949).

(12) M. J. Schick, S. M. Atlas, and F. R. Eirich, *J. Phys. Chem.*, **66**, 1326 (1962).

(13) H. V. Tartar and A. L. M. Lelong, *ibid.*, **59**, 1185 (1955).

tion. Alternative explanations are decreases by 21% in the solubilization ratio or in the mmw.

There is an apparent contradiction between the unit solubilization ratios observed in the present work even in the presence of small amounts of an added long-chain alcohol or hydrocarbon and the mostly larger solubilization ratios calculated from literature data. Two possible explanations come to mind. According to the first, many of the solubilization data reported in the literature were obtained with technical grade detergents which most likely contained considerably larger amounts of impurities than those added here to the pure detergents and probably of different structures as well. While the two impurities used here probably fit into the micellar palisade, one or more of the impurities contained in the technical grade detergents may only fit in the center of the micelle and preempt it, preventing it from solubilizing Orange OT. If one molecule of Orange OT saturates a micelle, it is quite possible that some of the impurities contained in technical grade detergents can do likewise. An alternative explanation is that the mmw's of the anionic detergents reported in the literature, which were determined by light scattering in the absence of added electrolyte, were too small (see below).

According to the *t* test, the 1.8% difference between the mean mmw's of sodium decane sulfonate in water and in 0.1 *N* NaCl solution listed in Table IV is significant. The solubility of the detergent in 0.1 *N* NaCl decreases rapidly as the temperature is decreased below 30°: around 24°, a large amount of acicular crystals separated. An observation of interest was that when the solution contained solubilized dye, the crystals were orange and the supernatant solution colorless.

The absorbancies of sodium dodecyl sulfate solutions saturated with Orange OT at the three lowest sodium chloride levels are in good agreement with the values of Williams, Phillips, and Mysels³ (see Figure 1). The mmw's vary little with the concentration of added salt between 0.0 and 0.1 *M* NaCl, just as was observed for sodium decane sulfonate. This effect was postulated by Hutchinson.¹⁴ The largest source of error in determining the mmw is probably the uncertainty in the cmc values. However, the mmw in 0.4 *M* NaCl is decidedly lower (see Table V). The considerable variation among the published mmw values, illustrated in Figure 8 of ref 15, makes a comparison of the aggregation numbers in Table V with those in the literature of doubtful value.

Conclusion

The method of determining the mmw of nonionic

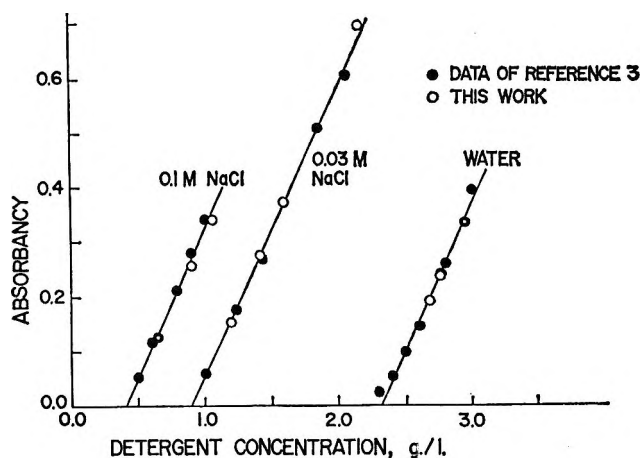


Figure 1. Absorbancies of solutions of sodium dodecyl sulfate saturated with Orange OT in water and 0.03 and 0.1 *M* NaCl.

and anionic detergents by dye solubilization involves only simple experimental techniques and equipment and has good precision. Since the method is not affected by electrical charges, it is theoretically much more simple than light scattering when applied to anionic detergents, and there is no need for the supporting electrolyte required by the sedimentation techniques; nor is there a need for assuming particle shape, which is required for determining mmw's by self-diffusion or conductivity. Small amounts of impurities normally occurring in not very thoroughly purified detergents, particularly long-chain alcohols present as unreacted starting materials or degradation products, do not affect the mmw determination by dye solubilization.

While the mmw's determined by light scattering and by the dye solubilization method are in excellent agreement in the case of the two nonionic detergents and agree reasonably well for sodium dodecyl sulfate in swamping electrolyte, there is a big gap in the case of the two anionic detergents in water (see Table I). It is in the case of highly charged particles in media of low ionic strength that molecular weight determination by light scattering is the least well understood.¹⁶ For instance, Debye plots for solutions of albumin,¹⁷ sodium polymethacrylate,¹⁸ and phosphotungstic¹⁹ and silicotungstic acids^{19,20} curved strongly downward

(14) E. Hutchinson, *J. Colloid Sci.*, **9**, 191 (1954).

(15) E. W. Anacker, R. M. Rush, and J. S. Johnson, *J. Phys. Chem.*, **68**, 81 (1964).

(16) A. Vrij and J. T. G. Overbeek, *J. Colloid Sci.*, **17**, 570 (1962).

(17) P. Doty and R. F. Steiner, *J. Chem. Phys.*, **20**, 85 (1952).

(18) A. Oth and P. Doty, *J. Phys. Chem.*, **56**, 43 (1952).

(19) M. Kerker, J. P. Kratochvil, R. H. Ottewill, and E. Matijevic, *ibid.*, **67**, 1097 (1963).

(20) M. J. Kronman and S. N. Timasheff, *ibid.*, **63**, 629 (1959).

at low concentrations in the absence of supporting electrolyte. Those systems which were also examined with electrolyte added, *viz.*, polymethacrylate and silicotungstate,^{16,20} yielded linear plots. In the latter case, the straight line intercepted the ordinate at the same point as the curved line obtained in the absence of swamping electrolyte.

Despite these effects, it is not easy to imagine that the mmw's derived from light scattering are too small by a factor of 2 or 7. On the other hand, as previously mentioned, an error in the dye solubilization method resulting from the solubilization of more than one dye molecule per micelle would give mmw's which are multiples of those listed here and hence would widen the gap. As is already evident from Anacker's compila-

tion of the mmw's of sodium dodecyl sulfate,¹⁵ a critical reexamination of the methods for determining mmw's is in order.

Acknowledgment. The author is indebted to Mr. J. J. Hutchison and Professor M. Goodman of the Polytechnic Institute of Brooklyn for determining the sedimentation constants, to Dr. A. H. Gilbert for preparing sodium decane sulfonate and behenyl alcohol, to Dr. E. D. Goddard for helpful discussions, to Mr. E. M. Mecheski for preparing sodium dodecyl sulfate and tetradecanol, to Dr. M. J. Schick for measuring turbidities, to the General Aniline and Film Corp. for one of the nonionic detergents, and to the Lever Brothers Co. for permission to publish this paper.

Interaction of the Tetraethanolammonium Ion with Water as Determined from Transport Properties

by D. Fennell Evans, G. P. Cunningham, and Robert L. Kay¹

Mellon Institute, Pittsburgh, Pennsylvania 15213 (Received April 4, 1966)

Precise conductance measurements are reported for tetraethanolammonium iodide, $(\text{EtOH})_4\text{NI}$, in water at 25° and for the bromide at 25 and 45°, as well as viscosity B coefficients from measurements on aqueous solutions at concentrations up to 0.1 M for the bromide at temperatures ranging from 0 to 65°. This substitution of a hydroxyl group for a terminal methyl group in the Pr_4N^+ ion is shown to result in the elimination of the effects that have been attributed to water structure enforcement around the side chains of the large tetraalkylammonium ions. This interpretation is shown to be consistent with existing conductance data for the $\text{Me}_2(\text{EtOH})_2\text{N}^+$ and the $\text{Me}_3(\text{EtOH})\text{N}^+$ ions and their correct alkyl analogs. The number of carbon atoms in the side chains is shown to be a poor criterion for comparison of various quaternary ammonium ions since water structure enforcement does not commence significantly until the chain reaches the size of a propyl group. The concentration dependence of the tetraethanolammonium salts is compared with that for the tetraalkylammonium salts.

Introduction

Recent conductance² and viscosity³ measurements for the large tetraalkylammonium ions at 10, 25, and 45° in aqueous solution have demonstrated that the transport behavior of these ions is influenced to a significant extent by the enforcement of water structure about their hydrocarbon chains. This structure has been attributed to the inert and hydrophobic nature of the hydrocarbon side chains.⁴ The explanation generally given for this phenomenon is that water molecules situated at the surface of these large ions will be oriented very little either by the ionic charge or the nonpolar side chains on its one side. Consequently, such water molecules can be oriented to a greater extent than normal by their nearest water molecule neighbors and can in effect be oriented into favorable positions for the formation of water cages about the inert side chains. Although the water in these cages will be exchanging very rapidly with bulk water, the net effect will be an increase in the size of the ions involved as well as an increase in the local viscosity about the ions. Both effects decrease the ionic mobility, the effect being greater the lower the temperature. At the same time, this explanation accounts for

the viscosity increase resulting from solution of these ions that is far greater than can be accounted for by their size alone.³ This viscosity increase is also very temperature dependent and disappears rapidly as the temperature increases.³

This explanation suggests that if the nonpolar hydrocarbon chains were made polar by substitution of a hydroxyl group in place of the terminal methyl group, the water structural effects causing the abnormal transport properties of these large ions should disappear. We have verified this hypothesis by investigating the temperature dependence of the transport properties of the tetraethanolammonium ion in aqueous solution. This conclusion is in conflict with those reported from measurements on the lower homologs of $(\text{EtOH})_4\text{N}^+$, namely, the $(\text{EtOH})_2\text{Me}_2\text{N}^+$ ⁵ and $(\text{EtOH})\text{Me}_3\text{N}^+$ ⁶

(1) To whom all correspondence is to be addressed.

(2) (a) D. F. Evans and R. L. Kay, *J. Phys. Chem.*, **70**, 366 (1966); (b) R. L. Kay and D. F. Evans, *ibid.*, **70**, 2325 (1966).

(3) R. L. Kay, T. Vituccio, C. Zawoycki, and D. F. Evans, *ibid.*, **70**, 2336 (1966).

(4) H. S. Frank and W. Y. Wen, *Discussions Faraday Soc.*, **24**, 133 (1957).

(5) J. Varimbi and R. M. Fuoss, *J. Phys. Chem.*, **64**, 1335 (1960).

(6) H. O. Spivey and F. M. Snell, *ibid.*, **68**, 2126 (1964).

ions. Both conclusions are based on a comparison of mobilities of the ethanol derivatives with the tetraalkylammonium ions. We have resolved the discrepancy by noting that such comparisons must be made with the correct tetraalkylammonium analog.

Wen and Saito⁷ have measured activity coefficients and partial molar volumes of $(\text{EtOH})_4\text{NBr}$ and $(\text{EtOH})_4\text{NF}$ in aqueous solution at 25° and have found that these thermodynamic properties are more normal in the case of these salts than was found for their tetraalkylammonium analogs. Also, Price⁸ has reported that the introduction of hydroxyl groups into the tetraalkylammonium ions reduced the heat of transport significantly, a direction in keeping with less rather than more order in the solution.

Experimental Section

All electrical equipment, cells, salt-cup dispensing device, and general techniques for the conductance measurements were the same as previously described.^{9,10} The modification required for the 45°^{2b} conductance determination and the method employed for weighing hygroscopic salts¹¹ have already been reported. The cell constant was determined at 25° and calculated for 45°, the change amounting to less than 0.01%.^{2b} The conductance baths were set at $25 \pm 0.003^\circ$ and $45 \pm 0.007^\circ$ with a calibrated platinum resistance thermometer.

The viscosity measurements were carried out using a suspended-level Ubbelohde-type viscometer with a flow time of 500 sec. No kinetic energy correction was found necessary at any temperature. The experimental techniques were the same as those previously described.³

Tetraethanolammonium bromide, $(\text{HOCH}_2)_4\text{NBr}$, was prepared by the method described by Wen and Saito⁷ with a number of modifications; 0.8 mole of 2-bromoethanol (Fisher Scientific Co.) was refluxed with 1.6 moles of triethanolamine (Fisher Scientific Co.) in 300 ml of methanol for 24 hr. This reaction gives approximately equal amounts of $(\text{EtOH})_4\text{NBr}$ and $(\text{EtOH})_3\text{NHBr}$, and it is the separation of these two products which presents the greatest difficulty in the synthesis of $(\text{EtOH})_4\text{NBr}$. The reaction mixture was titrated with concentrated aqueous hydrobromic acid to pH 3 to convert the remaining free amine to $(\text{EtOH})_3\text{NHBr}$. The resulting $(\text{EtOH})_3\text{NHBr}$ crystals were removed by filtration and the filtrate was taken to dryness by azeotroping off the last traces of water with ethanol under reduced pressure. The amine hydrobromide is only sparingly soluble in methanol, whereas $(\text{EtOH})_4\text{NBr}$ is exceedingly soluble at temperatures as low as -20° . This property permitted further separa-

tion of the mixture since only the hydrobromide precipitated on cooling a saturated methanol solution to -20° . The white, nonhygroscopic hydrobromide was detected by its sharp melting point of 187° .

Final purification of $(\text{EtOH})_4\text{NBr}$ was effected by dissolving the salt in the minimum volume of methanol and adding four volumes of absolute ethanol. White crystals precipitated on slow cooling with periodic shaking. This recrystallizing procedure was repeated 12 times. Recrystallization from absolute ethanol produced an oil which completely solidified even on slow cooling. Owing to its hygroscopic nature, all recrystallizations and manipulations of $(\text{EtOH})_4\text{NBr}$ were carried out in a drybox. The powdered salt was dried under vacuum at 56° for 15 hr. The purified compound melted at approximately 100° , with decomposition. In fact, this salt appeared to undergo decomposition readily at temperatures above 80° , and melting points taken on samples in evacuated sealed tubes gave the same results. Upon standing for 1 month, this salt showed some signs of decomposition, as indicated by the insoluble residue found when an old sample was dissolved in methanol. Our conductance results also confirmed this observation since measurements on month-old samples gave limiting conductances that were somewhat higher than those obtained using freshly prepared salt samples. However, the conductance parameters obtained from freshly recrystallized samples were shown to be independent of further recrystallization.

All attempts to obtain the $(\text{EtOH})_4\text{NBr}$ by titration of $(\text{EtOH})_4\text{NOH}$ (97.8%, RSA Corp., New York, N. Y.) gave a 90% yield of $(\text{EtOH})_3\text{NHBr}$, but we could detect no $(\text{EtOH})_4\text{NBr}$.

$(\text{EtOH})_4\text{NI}$ was prepared from the purified bromide by ion exchange. When all free amine had been removed from reagent grade anionic exchange resin in the hydroxyl form by repeated washing with water, the resin was converted to the iodide form with KI. One pass through a tenfold excess of resin converted $(\text{EtOH})_4\text{NBr}$ to the iodide. The only test performed on the final product to test for complete exchange was to note that the final product was not hygroscopic, whereas the bromide is extremely hygroscopic.

Conductivity grade water^{2a} was prepared by passing

(7) W. Y. Wen and S. Saito, *J. Phys. Chem.*, **69**, 3569 (1965).

(8) C. D. Price, Technical Report, Armed Services Technical Information Agency, AD 276280 (1961).

(9) J. L. Hawes and R. L. Kay, *J. Phys. Chem.*, **69**, 2420 (1965).

(10) D. F. Evans, C. Zawoyski, and R. L. Kay, *ibid.*, **69**, 3878 (1965).

(11) R. L. Kay, C. Zawoyski, and D. F. Evans, *ibid.*, **69**, 4208 (1965).

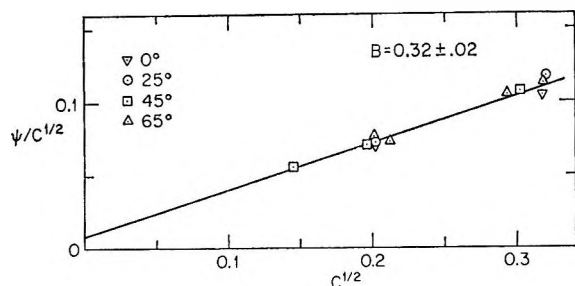


Figure 1. Plots of eq 1 for $(\text{EtOH})_4\text{NBr}$ in aqueous solution at various temperatures.

distilled water through a 4-ft mixed-bed ion-exchange column.

Results

The density increments for the volume concentrations and viscosity measurements were obtained by direct measurement on 0.06 M solutions. The θ value in the density equation, $d = d_0 + \theta\bar{m}$, where \bar{m} is the concentration in moles per kilogram of solution, was found to be 0.098 at 25 and 45° for the bromide and was assumed to be constant in the temperature range 0–65° used in the viscosity measurement. The value of θ was assumed to be 0.03 higher for the iodide in keeping with previous experience.^{2a}

The viscosity data for $(\text{EtOH})_4\text{NBr}$ are given in graphical form in Figure 1 and can be seen to conform to the Jones–Dole equation¹²

$$\psi/C^{1/2} = A + BC^{1/2} \quad (1)$$

where $\psi = (\eta/\eta_0) - 1$. The intercept $A = 0.008$ is identical with the value calculated from the Falkenhagen equation¹³ within the precision of the measurements. It can be seen that $B = 0.32 \pm 0.02$ is independent of temperature within the stated precision. The small amount of spread in the points in Figure 1 can be attributed almost entirely to the temperature dependence or the bromide ion that has been shown to have ionic B values³ that vary from -0.08 to -0.01 in the temperature range 0–65°, respectively.

The measured equivalent conductances and corresponding concentration in moles per liter are given in Table I along with κ_0 , the specific conductances of the solvent. Conductance parameters in Table II were obtained from the Fuoss–Onsager conductance equation¹⁴

$$\Lambda = \Lambda_0 - SC^{1/2} + EC \log C + (J - B\Lambda_0)C \quad (2)$$

using a least-square computer analysis.⁹ The values 0.8903, 0.5963, 78.38, and 71.51 were used for the viscosity in centipoise and dielectric constant of water at 25^{2a} and 45°,^{2b} respectively. The limiting ionic conduc-

Table I: Equivalent Conductances in Aqueous Solution

$10^3 C$	Λ	$10^3 C$	Λ	$10^3 C$	Λ
— $(\text{EtOH})_4\text{NBr}$, 25°—					
$10^7 \kappa_0 = 1.6$		$10^7 \kappa_0 = 1.9$		— $(\text{EtOH})_4\text{NBr}$, 45°—	
$10^7 \kappa_0 = 3.2$					
11.991	102.31	10.665	102.47	11.358	146.40
24.631	101.02	23.891	101.03	23.570	144.54
35.153	100.17	37.560	99.97	31.423	143.60
44.402	99.54	49.757	99.18	41.746	142.53
54.642	98.92	62.286	98.46	51.758	141.62
65.980	98.28	73.549	97.89	61.643	140.80
75.307	97.83	84.532	97.38	70.911	140.09
87.613	97.25	98.814	96.77	80.652	139.42
— $(\text{EtOH})_4\text{NI}$, 25°—					
$10^7 \kappa_0 = 1.3$		$10^7 \kappa_0 = 1.5$			
7.887	101.52	7.415	101.48		
17.570	100.23	17.489	100.20		
26.910	99.30	27.366	99.27		
36.716	98.49	36.063	98.57		
44.803	97.94	44.026	98.01		
53.101	97.39	52.889	97.44		
61.330	96.90	61.858	96.92		
69.680	96.44	71.445	96.41		

tances, calculated on the basis of $\lambda_0(\text{Br}^-)_{25^\circ} = 78.22$ and $\lambda_0(\text{I}^-)_{25^\circ} = 76.98$, are $\lambda_0[(\text{EtOH})_4\text{N}^+]_{25^\circ} = 27.07$ from the bromide and 26.87 from the iodide. Considering the problems of stability of these salts and the extreme hygroscopic nature of the bromide, this agreement is entirely acceptable. At the higher temperature, a $\lambda_0[(\text{EtOH})_4\text{N}^+]_{45^\circ} = 40.08$ is obtained from $\lambda_0(\text{Br}^-)_{45^\circ} = 110.69$.²

The δ parameter given in Table II for $(\text{EtOH})_4\text{NBr}$ at 25° is in good agreement with the values 1.6, 1.86, and 1.8 reported² for Pr_4NBr at 10, 25, and 45°, respectively, and the value at 45° of 2.41 is not too different. On the other hand, the average δ value for $(\text{EtOH})_4\text{NI}$ of 1.3 reported here is substantially higher than the 0.1, 0.3, and 0.4 obtained for Pr_4NI at 10, 25, and 45°, respectively.² In the case of Pr_4NI , the conductance data analyzed for a small amount of association. The same analyses of the data for $(\text{EtOH})_4\text{NI}$ detected a small amount of association in the first run but none in the second.

Discussion

In the absence of any change in the interaction with the solvent, replacement of a terminal methyl by a

(12) G. Jones and M. Dole, *J. Am. Chem. Soc.*, **51**, 2950 (1929).

(13) H. S. Harned and B. B. Owen, "The Physical Chemistry of Electrolytic Solutions," 3rd ed, Reinhold Publishing Corp., New York, N. Y., 1958, p 240.

(14) R. M. Fuoss and F. Accascina, "Electrolytic Conductance," Interscience Publishers, Inc., New York, N. Y., 1959.

Table II: Conductance Parameters in Aqueous Solution at 25 and 45°

	Temp, °C	Λ_0	d	σ_A	J
(EtOH) ₄ NBr	25	105.30 ± 0.006	1.91 ± 0.02	0.008	92.3
		105.27 ± 0.01	1.97 ± 0.03	0.01	95.4
(EtOH) ₄ NI	45	150.77 ± 0.01	2.41 ± 0.03	0.015	181.7
	25	103.92 ± 0.02	1.08 ± 0.08	0.03	44.4
		103.84 ± 0.005	1.48 ± 0.02	0.006	68.1

hydroxyl group is expected to result in little change in the size of a quaternary ammonium ion. Consequently, the alkyl analog of the (EtOH)₄N⁺ ion is the Pr₄N⁺ ion, and the two ions should have the same hydrodynamic properties if size is the only criterion. However, in aqueous solution at 25°, $\lambda_0 \eta_0$ (Pr₄N⁺) = 23.22, some 15% lower than the corresponding value for (EtOH)₄N⁺ as reported here. This mobility difference suggests that the enforcement of water structure around the hydrocarbon side chains detected^{2b} in the Pr₄N⁺ ion is absent in the case of the (EtOH)₄N⁺ ion, owing to the presence of the polar groups in the otherwise inert side chains. This conclusion is substantiated by the effect of temperature on the mobilities involved, as is shown in Figure 2. The $\lambda_0 \eta_0$ product for the (EtOH)₄N⁺ ion does not show an increase with temperature as do the larger quaternary ammonium ions around which water structure enforcement is prevalent.^{2b} In contrast to its alkyl analog, the Walden product for (EtOH)₄N⁺ shows a very slight decrease with temperature, a behavior much more characteristic of structure-breaking ions such as Me₄N⁺.^{2b} Further evidence that (EtOH)₄N⁺ does not enforce water structure in its immediate vicinity comes from the fact that its Walden product (0.241) for aqueous solution is almost identical with those for its alkyl analog in acetonitrile^{2a} (0.240), nitromethane¹⁵ (0.245), and methanol^{2a} (0.251), in which the hydrodynamic properties of the Pr₄N⁺ ion should be essentially unaffected by solvent interaction.

Further evidence that cages of water do not form around the side chains of the (EtOH)₄N⁺ ion can be obtained from the viscosity data. Viscosity B coefficients for (EtOH)₄NBr are compared with those for the tetraalkylammonium bromides³ at temperatures between 0 and 65° in Figure 3. The "melting" of such cages around the side chains of both the Pr₄N⁺ and Bu₄N⁺ ions is evident³ from the rapid decrease in B for the bromides of these ions with increased temperature. In contrast, the B coefficients for (EtOH)₄NBr are independent of temperature and much lower than those for Pr₄NBr. It is possible that, at temperatures high enough for the elimination of all water structural effects, the B coefficients for these two salts would be

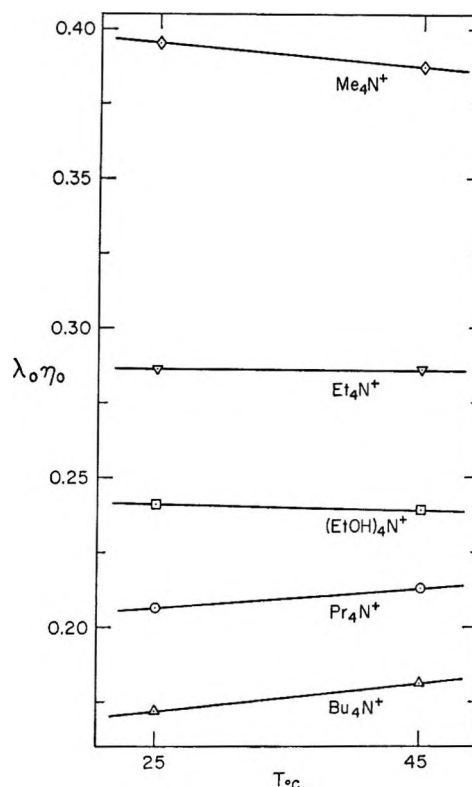


Figure 2. Temperature dependence of the Walden product for the (EtOH)₄N⁺ ion as compared to the tetraalkylammonium ions in aqueous solution.

the same as theory predicts for ions of the same size. Again, from viscosity measurements it would appear that the transport properties of the (EtOH)₄N⁺ ion are affected very little by interaction with water.

We conclude from these results that the substitution of an ethanol for a propyl group in a quaternary ammonium ion results in an increase in mobility in aqueous solution due to the disrupting effect of the polar group on the water-structure enforcement normally around a propyl group. This conclusion would appear to be in conflict with the results reported in previous investigations of this type of ion^{5,6} since the inclusion of an

(15) R. L. Kay, S. C. Blum, and H. I. Schiff, *J. Phys. Chem.*, **67**, 1223 (1963).

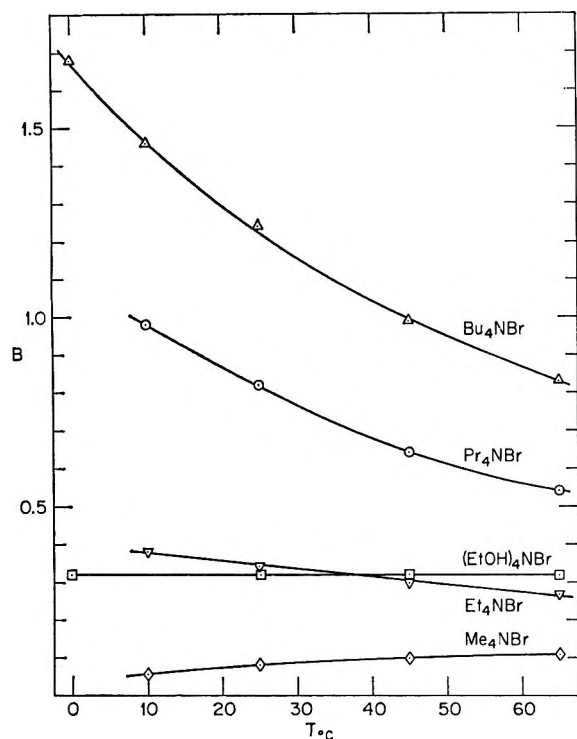


Figure 3. Temperature dependence of the viscosity B coefficients for $(\text{EtOH})_4\text{NBr}$ as compared to the tetraalkylammonium bromides.

ethanol group in a quaternary ammonium ion was claimed to have little or no effect on its mobility in aqueous solution. We have resolved this conflict by noting that the alkyl analogs used for comparison had the same number of carbon atoms but did not have the correct geometry. This can be seen in Figure 4 where the limiting conductances for a number of quaternary ammonium ions at 25° in aqueous solution are shown as a function of the number of carbon atoms in the side chains. The values used for the limiting conductances, after recalculation on the basis of eq 2, are given in Table III and were taken from sources already cited and from data quoted by Kraus and co-workers.¹⁶⁻¹⁸ The results of previous investigations^{5,6} of quaternary salts containing ethanol side chains were compared to a smooth curve passing through the points for the symmetrical R_4N^+ ion. Since the point for $\text{Me}_3(\text{EtOH})\text{N}^+$ was very close to this line and that for $\text{Me}_2(\text{EtOH})_2\text{N}^+$ was not too far removed from it, it was concluded that either the addition of an ethanol group affects the mobility to the same extent as a propyl group⁵ or, if the ethanol group was interacting with the water molecules in its vicinity, there were compensating factors that masked the effect on the mobility.⁶ Spivey and Snell⁶ attributed the low mobility of the Me_3PrN^+ ion, as compared to that for the sym-

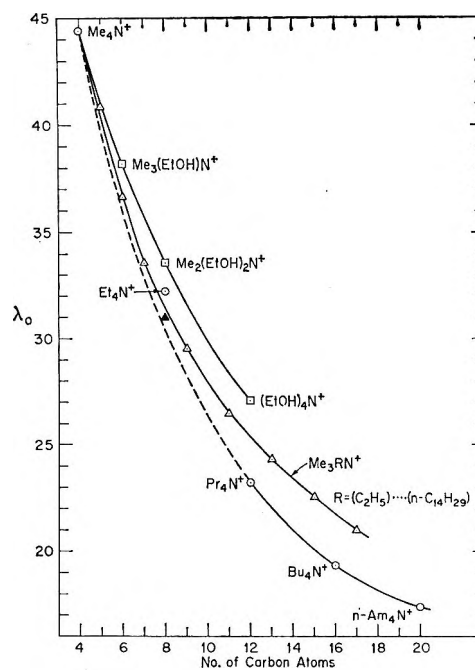


Figure 4. Limiting conductances for various quaternary ammonium ions in water at 25° as a function of the total number of carbon atoms or their equivalent in the side chains: \blacktriangle , predicted value for the $\text{Me}_2\text{Pr}_2\text{N}^+$ ion.

metrical quaternary cations, to its asymmetry. However, the $\text{Me}_3(\text{EtOH})\text{N}^+$ ion is equally as asymmetric and has a much higher mobility than the Me_3PrN^+ ion. Furthermore, $(\text{EtOH})_4\text{N}^+$ and Pr_4N^+ are both symmetric ions with equivalent numbers of carbon atoms, but the mobility of the latter is 15% lower. It would appear from these observations that symmetry, as well as number of carbon atoms, is not the deciding factor on which to base a comparison of the mobility for these large ions.

The mobilities of the ions given in Table III fall into three separate families depending on the number of side chains about which there is enforcement of water structure. We have used a different approach in order to compare the mobility of these large ions. The larger symmetrical tetraalkylammonium ions fall into one category, as shown by the line through the points for Pr_4N^+ , Bu_4N^+ , and $n\text{-Am}_4\text{N}^+$ in Figure 4. The Et_4N^+ ion, however, does not fit on the extension of this line to the Me_4N^+ ion owing to its inability to enforce water structure to the same extent per carbon atom as the ions containing larger side chains. This suggests that there is a critical size of hydrocarbon chain in a quater-

(16) H. M. Daggett, E. J. Bair, and C. A. Kraus, *J. Am. Chem. Soc.*, **73**, 799 (1951).

(17) M. J. McDowell and C. A. Kraus, *ibid.*, **73**, 2170 (1951).

(18) E. J. Bair and C. A. Kraus, *ibid.*, **73**, 1129 (1951).

Table III: Limiting Ionic Conductances for Aqueous Solutions at 25°^a

Ion	λ_0^+	Ref	Ion	Ion	Ref
Me ₄ N ⁺	44.42	1	Me ₃ EtN ⁺	40.86	5, 17
Et ₄ N ⁺	32.22	1	Me ₃ PrN ⁺	36.64	6
Pr ₄ N ⁺	23.22	1	Me ₃ BuN ⁺	33.54	17
Bu ₄ N ⁺	19.31	1	Me ₃ -hexyl-N ⁺	29.52	17
<i>n</i> -Am ₄ N ⁺	17.38	16	Me ₃ -octyl-N ⁺	26.49	17
			Me ₃ -decyl-N ⁺	24.30	17
Me ₃ (EtOH)N ⁺	38.21	5, 6	Me ₃ -dodecyl-N ⁺	22.40	17, 18
Me ₂ (EtOH) ₂ N ⁺	33.58	5	Me ₃ -tetradecyl-N ⁺	20.96	17
(EtOH) ₄ N ⁺	27.0	This work			

^a The cation limiting conductances are based on the following anion limiting conductances:² $\lambda_0(\text{Cl}^-) = 76.39$, $\lambda_0(\text{Br}^-) = 78.22$, $\lambda_0(\text{I}^-) = 76.98$, and $\lambda_0(\text{NO}_3^-) = 71.57$.

nary ammonium ion below which water structure enforcement drops off rapidly but above which such structure is cooperatively formed with relative ease. Thus, in these ions, the methyl and ethyl groups are poor structure markers, but the propyl group has excellent structure-making properties. Further evidence for this critical size and cooperative aspect can be seen in the ionic conductances for the trimethylalkylammonium ions, as shown in Figure 4. On the basis of number of carbon atoms, they fall on a separate and higher line than do the R₄N⁺ ions; that is, they act as ions with fewer carbon atoms. Thus, the three methyl groups are ineffective as structure markers and may well be reflecting some structure-breaking properties. This suggests, therefore, that the logical comparison for the Me₃(EtOH)N⁺ ion is the Me₃PrN⁺ ion and that the correct comparison for the Me₃(EtOH)₂N⁺ ion is not the Et₄N⁺ ion but rather the Me₂Pr₂N⁺ ion. A calculation shows that the increase in the limiting conductances for Me₃(EtOH)N⁺ and (EtOH)₄N⁺ over their correct alkyl analogs is $4.0 \pm 0.2\%$ per ethanol group. On this basis, the mobility to be expected for the Me₂Pr₂N⁺ ion is 31.0 or 8% lower than that for Me₂(EtOH)₂N⁺. This point is designated by a solid triangle in Figure 4 and, as expected for an ion with water structure enforcement about two side chains, it is between the lines for ions about which there is water enforcement about one side chain and about four side chains.

The obvious conclusion resulting from these data is that an ethanol group does not enforce water structure when substituted in a quaternary ammonium ion. On the other hand, ethanol itself, when added in small amounts to pure water, is known to enforce water structure,^{19,20} presumably by being hydrogen bonded into the water cages.²¹ However, there is no evidence that the ethanol groups in the (EtOH)₄N⁺ ion are incorporated into the "flickering clusters"⁴ of structured

water since a substantial decrease in mobility would result. No such decrease in mobility has been detected here on the basis of any realistic comparison. We conclude that the side chains of the (EtOH)₄N⁺ ion are not incorporated into the surrounding water structure.

In a previous investigation¹ of the tetraalkylammonium salts in aqueous solution, it was shown that the decrease of the conductance with concentration became greater the larger the anion and cation, contrary to the predictions of theory.¹⁴ The possibility of attributing the effect to ionic association and to changes in solvent structure due to overlap of ionic cospheres has been considered in some detail.² The same effect was observed by Skinner and Fuoss²² in their measurements on *i*-Am₃BuNBr in aqueous solution, but the effect is particularly evident in the iodides. However, the conductance of (EtOH)₄NI is about 0.5% greater at $C = 0.007 M$ than that which would be required for the same concentration dependence as Pr₄NI. This is a significant amount considering the agreement in λ_0^+ from the bromide and iodide. It indicates that (EtOH)₄NI acts more like Me₄NI than like Pr₄NI and suggests that the abnormally large decrease in conductance for Pr₄NI and Bu₄NI is due to water structure considerations. Opposed to this conclusion is the fact that sodium tetraphenylboride in aqueous solution has a normal concentration dependence²² although recent measurements²³ indicate that water structure enforcement around the aryl groups is about the same as that around a butyl group. These results indicate that all

(19) F. Franks, *Ann. N. Y. Acad. Sci.*, **125**, 277 (1965).

(20) R. L. Kay and T. Vituccio, to be published.

(21) A. D. Potts and D. W. Davidson, *J. Phys. Chem.*, **69**, 996 (1965).

(22) J. F. Skinner and R. M. Fuoss, *ibid.*, **68**, 1882 (1964).

(23) G. P. Cunningham, D. F. Evans, and R. L. Kay, to be published.

the significant factors affecting the concentration dependence of conductance in dilute solutions are not known at the present time.

Acknowledgment. This work was sponsored by the Office of Saline Water, U. S. Department of the Interior, under Contract No. 14-01-0001-359.

Lanthanum-Lanthanum Hydride Phase System¹

by D. T. Peterson and J. A. Straatmann

Contribution No. 1874 from the Institute for Atomic Research and Department of Metallurgy, Iowa State University, Ames, Iowa (Received April 5, 1966)

The phase relationships between lanthanum and lanthanum hydride have been determined. The addition of hydrogen increased the melting point and decreased the fcc-to-bcc transformation temperature of lanthanum to a eutectoid at 773° and 23.5 at. % hydrogen. The solubility of lanthanum hydride in fcc lanthanum ranged from 2.83 at. % at 375° to 21.3 at. % hydrogen at 773°. The enthalpy of solution was calculated to be 5.76 ± 0.17 kcal. Above 773° the solubility of lanthanum hydride in bcc lanthanum increases rapidly, and complete solubility occurs at temperatures above 960°. Hydrogen depressed the low-temperature transformation in lanthanum by 27°.

Introduction

The lanthanum-hydrogen system has been investigated by Mulford and Holley² by determining pressure-composition isotherms in the temperature range between 600 and 800°. They found a significant solubility of hydrogen in the metal which increased with increasing temperature while the lower hydrogen concentration limit of the hydride decreases with increasing temperature. Pressure-composition isotherms are limited to a small temperature range because the hydrogen dissociation pressure becomes either too small or too large to measure with reasonable accuracy. General relationships between the properties of metallic hydrides and their structure have been reviewed by Libowitz.³ The heat of formation of lanthanum hydride is -49.7 kcal/mole of H₂. The face-centered-cubic (fcc) fluorite structure of lanthanum hydride exhibits a composition range from below lanthanum dihydride to nearly lanthanum trihydride. Neutron diffraction studies indicate that the tetrahedral holes are filled by hydrogen first, and further absorption of hydrogen results in the filling of the octahedral holes

in the structure. The effect of hydrogen on the melting point and structural transformations of lanthanum metal has not been investigated. In order to determine these effects and more accurately establish the solubility limits over a wider range of temperatures, this system was investigated by differential thermal analysis, isothermal equilibration, X-ray diffraction, electrical resistivity, and dilatometer techniques.

The melting point and the allotropic transformation temperatures of pure lanthanum have been measured by a number of investigators. Love⁴ reports a low-temperature transformation from a hexagonal-close-packed (hcp) structure to an fcc structure at 310° and a transformation from the fcc structure to a body-

(1) This work was performed in the Ames Laboratory of the Atomic Energy Commission.

(2) R. N. R. Mulford and C. E. Holley, Jr., *J. Phys. Chem.*, **59**, 1222 (1955).

(3) G. G. Libowitz, "The Solid-State Chemistry of Binary Metal Hydrides," W. A. Benjamin, Inc., New York, N. Y., 1965.

(4) B. Love in "Metals Handbook," Vol. 1, American Society for Metals, Novolty, Ohio, 1961, pp 1230, 1231.

centered-cubic (bcc) structure at 862°. The bcc remains stable until the melting point of 917° is reached. These values for the high-temperature transformation and the melting temperature are in agreement with the results of other investigators. However, there is considerable disagreement about the low-temperature transition. There is disagreement as to the exact temperature or range of temperatures at which the transition occurs and as to the extent of the transformation. The prior history of the metal and its shape and size seem to influence the structure of the metal below this transformation temperature. The transformation has been studied by dilatometer,⁵ electrical resistivity,^{6,7} and X-ray diffraction techniques.^{8,9} The results of many of the investigators have been reviewed by Herrmann,¹⁰ and he reports the low-temperature phase to be an hcp structure with a double *c* axis.

Experimental Procedures

The lanthanum metal used in this study was prepared by the method developed by Spedding and Daane.^{11,12} The main impurities were: Ta, 1300 ppm; Pr, 300 ppm; Ce, 300 ppm; Nd, 200 ppm; O, 480 ppm; N, 104 ppm; and H, 16 ppm. The metal was stored under an argon atmosphere, and most of the handling was done in a glove box evacuated to less than 10 μ and filled with argon. The exposure of the metal to atmospheric moisture was kept at a minimum to prevent contamination. Pure hydrogen was obtained from the thermal decomposition of UH₃, which had been formed by reacting hydrogen with uranium turnings.

The transformation and melting temperatures were investigated by differential thermal analysis. The thermal analysis samples were prepared by placing approximately 20 g of lanthanum metal in a tantalum capsule 6 cm long and 1.9 cm in diameter. The bottom of the tantalum capsule contained a thermocouple well which was 1 cm long and 0.3 cm in diameter.

The capsule containing the sample was placed in a Vycor furnace tube, the system was evacuated, and the sample was heated to a temperature between 600 and 700°. The required amount of hydrogen was measured by filling the calibrated volume to the appropriate pressure. The hydrogen was then allowed to react with the lanthanum sample until it had been absorbed. By closing the stopcock in front of the furnace tube, the whole assembly could be transferred to a glove box filled with argon without exposing the sample to atmospheric moisture. A tantalum cap was welded on the thermal analysis capsule in the glove box. The samples were held under a static vacuum during

the thermal analysis so that any hydrogen evolved during the heating and cooling of the sample could be detected with a manometer. The pressure in the 250-ml volume of the apparatus was always less than 50 mm during the analysis of all the alloys with less than 30 at. % hydrogen. This amounted to a composition change of less than 0.1 at. % hydrogen for the thermal analysis specimens. At the high temperatures required to melt the high hydrogen alloys, higher hydrogen pressures were observed but the hydrogen gas evolved always represented a composition change of less than 1 at. % hydrogen in the specimen. A manual potentiometer which could be read to 0.1 mv was used to determine the temperature of the transformations.

To determine the solubility of lanthanum hydride in lanthanum metal, lanthanum specimens which had been equilibrated with lanthanum hydride at various temperatures were analyzed by hot vacuum extraction. The lanthanum specimens were 3 × 3 mm and 3 cm long. The specimens to be equilibrated at temperatures below 600° were first heated to a temperature between 600 and 700° for 15 min to break up any protective surface layer which could hinder the reaction of hydrogen with the sample to form a uniform hydride layer. Sufficient hydrogen was measured into the calibrated volume to constitute a 25% excess above that necessary to saturate the specimen at the temperature in question. The hydrogen was charged in increments because this procedure gave a hydride layer which was more uniform in thickness than if the hydrogen were all admitted at one time. The addition of hydrogen in increments also reduced the temperature fluctuation of the sample due to either the addition of the cool gas or the heat of reaction. The time that the samples were held at the equilibration temperature in order to ensure equilibrium varied from 2 hr at 960° to 40 hr at 259°. These times were estimated on the basis of the dimensions of the specimen and the dif-

(5) (a) M. Foex, *Compt. Rend.*, 217, 501 (1943); (b) F. Barson, S. Legvold, and F. H. Spedding, *Phys. Rev.*, 105, 418 (1957).

(6) F. M. Jaeger, J. A. Bottema, and E. Rosenbohn, *Rec. Trav. Chim.*, 57, 1137 (1938).

(7) N. R. James, S. Legvold, and F. H. Spedding, *Phys. Rev.*, 88, 1092 (1953).

(8) W. T. Ziegler, R. A. Young, and A. L. Floyd, *J. Am. Chem. Soc.*, 75, 1215 (1953).

(9) G. S. Anderson, Ph.D. Thesis, Iowa State University of Science and Technology, Ames, Iowa, 1957.

(10) K. W. Herrmann, Ph.D. Thesis, Iowa State University of Science and Technology, Ames, Iowa, 1955.

(11) F. H. Spedding and A. H. Daane, *J. Metals*, 6, 1131 (1954).

(12) F. H. Spedding and A. H. Daane, *ibid.*, 6, 504 (1954).

fusion coefficients of hydrogen in thorium¹³ to be at least 10 times as long as necessary to achieve 95% of the saturation value. After equilibration and cooling to room temperature, the furnace tube was transferred to a glove box. A portion of the specimen was polished and examined metallographically. In every sample, a layer of hydride phase was observed surrounding the saturated core, and the boundary between the two phases was distinct. The dark gray hydride layer was removed from the remainder of the specimen by filing and the saturated core was cut into samples for analysis. The lanthanum hydride layer surrounding the core was also analyzed from several specimens which had been especially prepared with a thicker hydride layer. The hydride layer was removed by pounding in a mortar and pestle, and the resulting chips of hydride were wrapped in tantalum foil so that they could be easily handled during the analysis. The samples were analyzed by hot vacuum extraction of the hydrogen at 950°. The samples were dropped into a quartz boat in the furnace tube to protect the furnace tube from the molten lanthanum. Six samples were analyzed from each equilibration specimen. The relative standard deviation of all the hydrogen analyses was 0.055. This figure is based on 87 separate analyses of hydrogen concentrations from 1 at. % hydrogen to 40 at. % hydrogen. The relative error in the hydrogen analysis was determined from the analyses of six samples from a specimen of known hydrogen concentration and was found to be +0.0068.

An X-ray diffraction powder pattern of lanthanum hydride was obtained with a Debye-Scherrer camera using nickel-filtered copper radiation. The X-ray sample was prepared by crushing lanthanum hydride in a mortar and pestle and passing the powder through a 200-mesh screen. The fine powder was transferred to a thin-walled capillary. The above operation was carried out in an argon-filled glove box, and the open end of the capillary was sealed with Apiezon wax before exposing it to the atmosphere. The sealed capillary was then heated to 250° to remove any distortion in the sample caused by the filing and crushing.

Bulk specimens of pure lanthanum and a 10 at. % hydrogen-lanthanum alloy were examined with a diffractometer to determine the effect of hydrogen on the crystal structure of lanthanum at room temperature. The 10 at. % hydrogen-lanthanum alloy was prepared at 700°, and the alloy was held at this temperature for 3 hr to ensure equilibrium. The pure lanthanum sample was also annealed at 700° for 3 hr, and both samples were furnace cooled from this temperature. A portion of the 10 at. % hydrogen-

lanthanum alloy was sealed in a quartz capsule under vacuum, reheated to 900° for 2 hr, and quenched in water. The three samples were then mounted in Bakelite, ground through 600-grit abrasive, and examined on the diffractometer. The samples were also examined after electropolishing in a solution of 6% perchloric acid-menthanol¹⁴ at a temperature of -76°. The diffractometer traces obtained with these different surface preparations were the same.

The effect of hydrogen on the low-temperature transformation from the hcp to the fcc structure was investigated by electrical resistivity and dilatometer measurements. The electrical resistivity samples were 2.5-mm diameter swaged lanthanum rods 12.5 mm long. A thermocouple to measure the temperature of the sample was attached by spotwelding as were tantalum leads to measure the voltage drop along the length of the rod. The dilatometer specimens were obtained from a 6.3-mm diameter machined lanthanum rod and were 25.4 mm long. An X-Y recording potentiometer was used to measure the temperature and the voltage drop or change in length of the samples.

Results and Discussion

The lanthanum-lanthanum hydride phase diagram is presented in Figure 1. The dotted lines indicate phase boundaries that were not definitely established in this study but were drawn from consideration of the thermodynamic rules that govern the construction of phase diagrams. The fcc to bcc transformation at 860° and the melting point at 918° found for pure lanthanum are in agreement with the values reported by Love.⁴ Differential thermal analysis revealed that the addition of hydrogen increased the melting point of lanthanum and decreased the fcc to bcc transformation temperature. The decrease in the transformation temperature continued down to 773° where the bcc lanthanum undergoes a eutectoid decomposition to fcc lanthanum plus lanthanum hydride. The eutectoid composition was 23.5 at. % hydrogen. The thermal arrest due to this eutectoid decomposition was found in alloys that contained up to 60 at. % hydrogen. The melting points were measured on samples up to the 40.3 at. % hydrogen alloy which melted at 1079°. The melting temperatures of specimens above this hydrogen composition could not be measured owing to the high dissociation pressure. The thermal analysis results shown on Figure 1 are from heating curves and were averaged from a number of analyses of each

(13) D. T. Peterson and D. G. Westlake, *J. Phys. Chem.*, **64**, 649 (1960).

(14) E. N. Hopkins, D. T. Peterson, and H. H. Baker, submitted to the 19th AEC Metallography Group Meeting, April 1965.

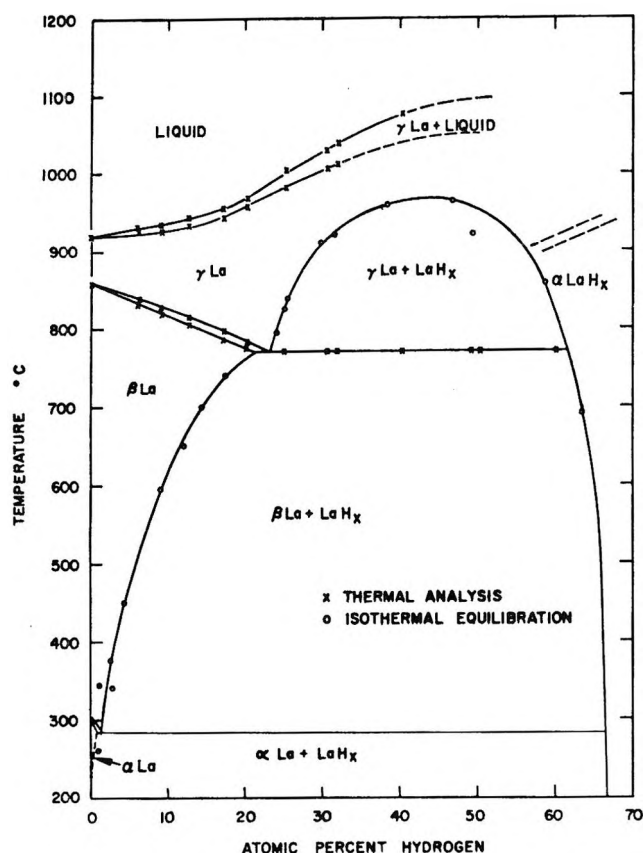


Figure 1. Lanthanum-lanthanum hydride phase diagram.

alloy. The usual heating and cooling rates were 5°/min, and changes in this rate had little effect on the transformation temperatures. The arrests on heating and on cooling always agreed within 4°. The low-temperature hcp to fcc transformation was not observed by thermal analysis in either the pure lanthanum or the lanthanum-hydrogen alloys. This was expected since the enthalpy of this transformation has been reported to be only 67 cal by Berg.¹⁵

The solubility limits of lanthanum hydride in lanthanum metal were determined by isothermal equilibration and the results are tabulated in Table I.

These solubility limits could not be detected by thermal analysis and could be checked only partially by metallography. The solubility of lanthanum hydride in fcc lanthanum ranged from 2.8 at. % hydrogen at 375° to 21.3 at. % hydrogen at 733°. The solubility of lanthanum hydride in lanthanum metal at 259° was found to be 1.1 at. % hydrogen. This value falls on the extension of the solubility curve for the fcc region but it is not certain whether the metal was in the cubic or hexagonal modification at this temperature. If it was in the hexagonal form, the lanthanum hydride solubility was not appreciably

Table I: Isothermal Equilibration Data

Temp. °C	At. % hydrogen		Temp. °C	At. % hydrogen	
	Metal phase	Hydride phase		Metal phase	Hydride phase
259	1.1		740	17.5	
340	2.9		795	24.2	
345	1.1		826	25.2	
375	2.8		840	25.5	
450	4.6		859		58.7
595	9.3		912	29.8	
652	12.0		922	31.8	49.5
692		63.6	960	39.6	46.3
700	14.5				

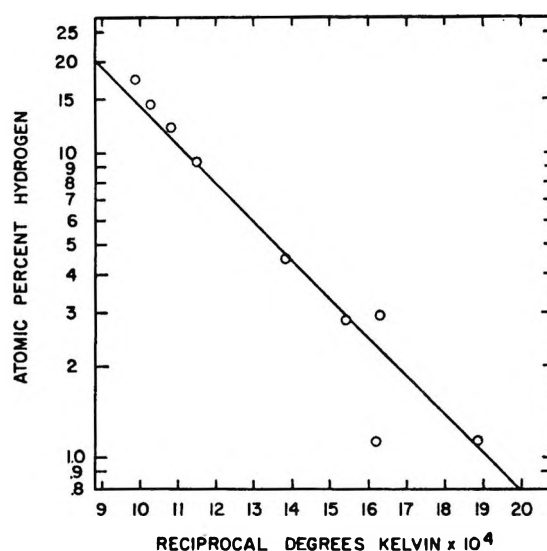


Figure 2. The solubility of lanthanum hydride in lanthanum as a function of temperature.

changed by the transformation. A plot of the logarithm of the solubility of lanthanum hydride in fcc lanthanum as a function of reciprocal temperature is shown in Figure 2. An analytical expression was fitted to the data by a least-squares method. This equation was that $\log C = -1260 \pm 30/T + 2.402 \pm 0.507$, where C is the at. % hydrogen. The enthalpy of solution calculated from this equation is $+5.76 \pm 0.17$ kcal.

Above 773° the solubility of lanthanum hydride in bcc lanthanum increased rapidly, and complete solubility occurs at temperatures above 960°. This rapid increase in the solubility of hydrogen in lanthanum metal along with a rapid decrease in the hydrogen concentration of the coexisting lanthanum hydride is

(15) J. R. Berg, Ph.D. Thesis, Iowa State University of Science and Technology, Ames, Iowa, 1961.

in agreement with the solubility limits found by Mulford and Holley.² This type of relationship has been observed in a number of metal-hydrogen systems.

Lanthanum hydride coexisting with lanthanum metal at room temperature was found by X-ray diffraction to have the fcc fluorite structure reported by Holley, Mulford, and Ellinger.¹⁶ The lattice constant was 5.669 Å which is in satisfactory agreement with the value of 5.667 Å reported by the above authors. This fcc hydride would not be expected to be able to form a continuous solid solution with the bcc lanthanum metal. Consequently a phase transition in lanthanum hydride has been postulated although no evidence for this transition was found in the thermal analyses. If the phase transition is at a high temperature, it would be very difficult to establish because of the high hydrogen dissociation pressure.

The crystal structure of pure lanthanum and lanthanum-hydrogen alloys at room temperature was investigated with an X-ray diffractometer using bulk samples. The pure lanthanum metal structure was found to be a mixture of fcc lanthanum and hcp lanthanum. The lanthanum-hydrogen alloy also contained both crystal forms of lanthanum but the fcc peaks were slightly stronger than in the pure metal. A sample of this alloy was quenched from a region where all the hydrogen was in solution and reexamined on the X-ray diffractometer. The results showed that both crystal forms of lanthanum were still present but the ratio of fcc lanthanum to hcp lanthanum had greatly increased. A slight increase of the diffraction angles was also found, and this indicated an increase in the lattice parameter of lanthanum apparently due to the retention of some hydrogen in solution.

The effect of hydrogen on the temperature of the hcp to fcc transformation was studied by dilatometer and electrical resistivity measurements. Figure 3 shows the expansion of pure lanthanum and a 3 at. % hydrogen-lanthanum alloy as a function of temperature. The hysteresis in the transformation temperature was found by both the dilatometer and electrical resistivity measurements. The results indicated that a slight excess of hydrogen over the solubility limit in this temperature range lowers the temperature of the hcp to fcc transformation. The transformation temperatures were not changed by variation in the heating and cooling rate. The transformation temperatures shown in Figure 1 are midpoint values of the transformation on heating. The pure lanthanum transformed at 324° and the addition of hydrogen apparently results in an eutectoid reaction of fcc lanthanum to hcp plus lanthanum hydride at 297°.

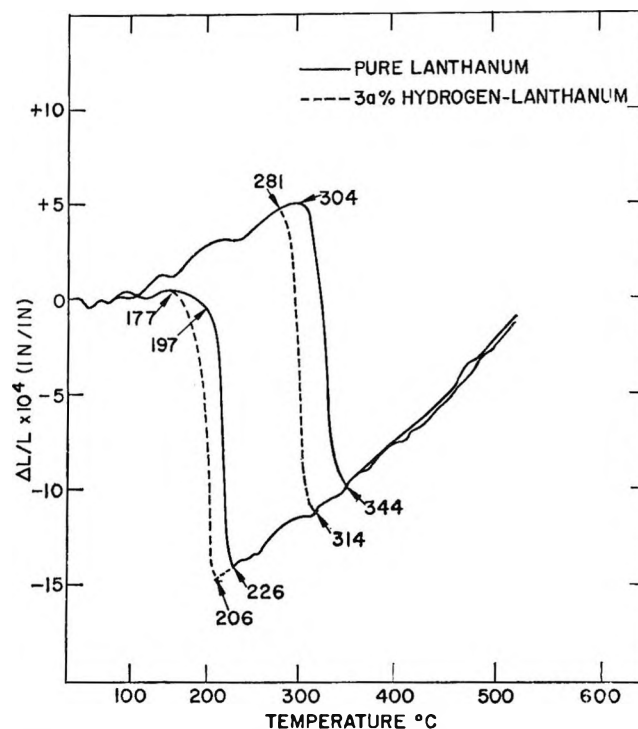


Figure 3. Relative changes in length vs. temperature.

Hydrogen has been found to be extensively soluble in lanthanum at elevated temperatures and to stabilize the bcc phase by raising the melting temperatures and also lowering the transition to fcc lanthanum. The increase in the melting temperature is similar to the effect of hydrogen in the alkaline earth metals. The lowering of the transition to the bcc form is analogous to the effect of hydrogen in zirconium and titanium but differs from the effect of hydrogen in calcium and strontium. The fcc to hexagonal phase transition in lanthanum is lowered slightly by hydrogen but the kinetics and completeness of the transformation are not affected. The interpretation of the influence of hydrogen on the phase transitions in the rare earth metals will probably not be possible until more of these systems have been studied.

Acknowledgments. The authors wish to express their appreciation to Mr. Ardis Johnson for the necessary welding, Mr. John Omohundro and Mr. David Dennison for their experimental assistance during the electrical resistivity and dilatometer measurements, and Mr. Earl Hopkins and Mr. Harlan Baker for their assistance in developing metallography techniques.

(16) C. E. Holley, Jr., R. N. R. Mulford, and F. H. Ellinger, *J. Phys. Chem.*, 59, 1226 (1955).

The Vapor Pressure and Enthalpy of Vaporization of Molten Mercuric Chloride to the Critical Point¹

by J. W. Johnson, W. J. Silva, and D. Cubicciotti

Stanford Research Institute, Menlo Park, California (Received April 11, 1966)

The vapor pressure of molten mercuric chloride has been measured by an inverted capillary technique from 573°K and 0.96 atm to 968°K and 111.6 atm. The data are fitted by the linear relation $\log P(\text{atm}) = 4.9929 - 2854.8/T^\circ\text{K}$ from 660 to 968°K with an average deviation of 0.9% for the 25 experimental points. Below 660°K, the experimental points fall below the linear relationship. A critical pressure of 113.7 ± 1.6 atm is predicted by the linear equation at a critical temperature of $972 \pm 2^\circ\text{K}$. The enthalpy of vaporization of molten mercuric chloride has been calculated from 700 to 970°K.

Introduction

An investigation of some of the properties of molten salts above the normal boiling point has been under way for some time in this laboratory. A previous paper² reported the critical temperature and coexistence curve of mercuric chloride. This report describes the measurement of the vapor pressure of mercuric chloride from the normal boiling point to the critical point.

Experimental Section

The semimicro boiling point method used in this study was the same as that employed in the determination of the vapor pressure of bismuth chloride.³ The apparatus has been described in detail elsewhere.⁴

The mercuric chloride was from the same preparation used in the determination of the coexistence curve and critical temperature. The analysis was 73.89% Hg and 26.13% Cl by weight, compared with the theoretical values of 73.88% Hg and 26.12% Cl.

Results and Discussion

The vapor pressure of molten mercuric chloride was determined at 35 points over a temperature range of 573 to 968°K and a pressure range of 0.96 to 111.6 atm. The experimental data are presented in Table I. The temperatures recorded were corrected for gradients between the position of the thermocouple and the liquid surface. These corrections ranged from 2 to 3° depending on the temperature. The listed pressures, up to 17 atm, were corrected by the addition of 0.02

atm for the static head of molten mercuric chloride. Vapor pressures above 17 atm are recorded to the nearest 0.1 atm and the correction was negligible.

Three runs were made using different samples of mercuric chloride as indicated in Table I. It was found that the experimental data could be fitted by the relation

$$\log P(\text{atm}) = 4.9929 - 2854.8/T^\circ\text{K} \quad (1)$$

from 660 to 968°K with an average deviation of 0.9% for the 25 experimental points. From 660 to 573°K the experimental points tend to fall below the straight line defined by eq 1. In that region the vapor pressure curve is in transition between the high-temperature linear form and the low-temperature Clausius-Clapeyron equation for low pressures, which includes curvature due to a ΔC_p term. Because there is no established theoretical form for the equation in the transition region, a smooth curve was drawn through the data on a large scale plot. Values taken from the curve are compared with the experimental points in the lower part of Table I in the temperature range 570 to 660°K. Values

(1) This work was made possible by the support of the Research Division of the U. S. Atomic Energy Commission under Contract No. AT(04-3)-106.

(2) J. W. Johnson, W. J. Silva, and D. Cubicciotti, *J. Phys. Chem.*, **70**, 1169 (1966).

(3) J. W. Johnson, W. J. Silva, and D. Cubicciotti, *ibid.*, **69**, 3916 (1965).

(4) W. J. Silva, J. W. Johnson, and D. Cubicciotti, *Rev. Sci. Instr.*, **36**, 1505 (1965).

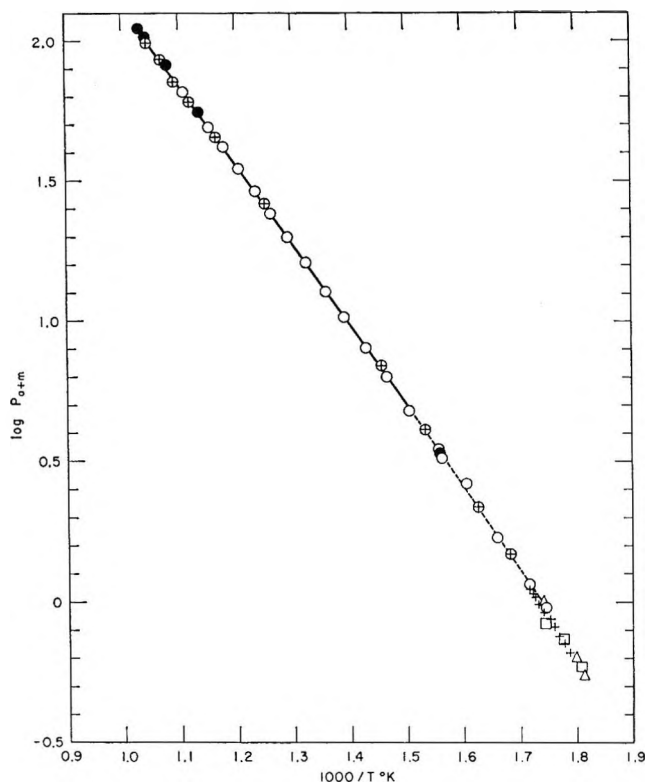


Figure 1. Vapor pressure of mercuric chloride: O, run no. 1; \oplus , run no. 2; \bullet , run no. 3, this work; +, Prideaux; \square , Wiedemann, *et al.*; \triangle , Johnson. Full line is calculated from eq 1; dashed curve represents smoothed curve through lower temperature data.

of the vapor pressure in that range, taken from the smoothed curve, are given in Table II for 10° intervals.

Figure 1 presents the experimental data on a $\log P$ vs. $1/T$ plot. The circles represent the data points obtained on three different samples. There is no evidence of a systematic deviation between the individual runs. The solid line drawn through the points in the high-pressure range was calculated from eq 1. The dashed line through the points in the low-pressure range represents the smoothed curve of the lower temperature data.

The critical pressure calculated from eq 1 is 113.7 ± 1.6 atm using the critical temperature of $972 \pm 2^\circ\text{K}$, reported previously,² for mercuric chloride.

The present work overlaps that of previous investigators Prideaux,⁵ Wiedemann, Stelzner, and Nederschulte,⁶ and Johnson⁷ over a very short range of pressure and temperature as is shown in Figure 1. The normal boiling point obtained in this work is 575.0°K , compared with the 577°K derived from the data of Prideaux⁶ and the 575.7°K reported by Johnson.⁷ Prideaux determined the vapor pressure of mercuric chloride in the temperature range of 560 to 582°K in great detail, reporting over 35 data points. Our pres-

Table I: Vapor Pressure Data for Molten Mercuric Chloride

Run no.	Obsd		Calcd, eq 1	
	Temp, $^\circ\text{K}$	Pressure, atm	Pressure, atm	Dev, %
	972 ± 2^a		113.7 ± 1.6^a	
3	967.7	111.6	110.4	-1.1
3	957.3	104.1	102.5	-1.5
2	955.5	99.3	101.4	2.1
2	932.9	85.7	85.7	0
3	924.1	83.0	80.1	-3.5
2	913.5	72.0	73.7	2.4
1	900.6	66.0	66.5	0.8
2	892.0	60.8	62.0	2.0
1	883.2	58.0	57.6	-0.7
3	878.4	56.0	55.3	-1.2
1	865.6	49.2	49.5	0.6
2	857.5	45.5	46.1	1.3
1	847.2	42.0	42.0	0
1	828.8	35.2	35.3	0.3
1	809.1	29.3	29.2	-0.3
2	798.5	26.3	26.2	-0.4
1	791.9	24.4	24.4	0
1	773.4	20.0	20.0	0
1	754.6	16.24	16.21	-0.2
1	735.3	12.88	12.89	0.1
1	718.3	10.45	10.43	-0.2
1	699.2	8.11	8.13	0.2
2	686.6	6.96	6.84	-1.7
1	681.7	6.40	6.38	-0.3
1	663.4	4.82	4.89	1.4

Av 0.9%

Smooth curve values

2	651.8	4.13	4.10	-0.7
1	642.7	3.51	3.55	1.1
3	641.1	3.41	3.45	1.2
1	639.4	3.27	3.36	2.8
1	622.8	2.65	2.54	-4.2 ^b
2	614.5	2.19	2.19	0
1	602.2	1.71	1.74	1.8
2	593.6	1.49	1.47	-1.3
1	582.6	1.17	1.18	0.8
1	573.0	0.96	0.96	0

Av 1.1%

^a Critical point. ^b Value omitted in curve-fitting and deviation calculation.

sures are about 5% higher than those of Prideaux. It will be recalled that Prideaux's liquid densities were

(5) E. B. R. Prideaux, *J. Chem. Soc.*, 97, 2032 (1910).

(6) E. Wiedemann, K. Stelzner, and G. Nederschulte, *Ber. Deut. Physik. Ges.*, 3, 161 (1905).

(7) F. M. G. Johnson, *J. Am. Chem. Soc.*, 33, 777 (1911).

Table II: Vapor Pressures of HgCl₂ from 570 to 660°K (from Smoothed Curve)

<i>T</i> , °K	<i>P</i> , atm	<i>T</i> , °K	<i>P</i> , atm
660	4.64	600	1.67
650	3.99	590	1.37
640	3.40	580	1.11
630	2.88	575.0 ^a	1.00
620	2.42	570	0.92
610	2.02		

^a Boiling point taken from the curve.

higher and melting point lower than those reported in ref 2. The work of Yosim and Mayer⁸ shows that Hg₂Cl₂ is soluble in the liquid and lowers the freezing point of HgCl₂ and presumably would lower the vapor pressure. Also, since the density of Hg₂Cl₂ is greater, we would expect it to increase the density of HgCl₂. These three types of measurement are all in accord in suggesting that there was an impurity of Hg₂Cl₂ in Prideaux's material.

There was no indication of thermal dissociation of HgCl₂ at the highest temperature reached in this study. The liquid phase remained transparent and colorless and no mercury deposit was observed in the parts of the apparatus maintained at room temperature. On this basis it is presumed that HgCl₂ does not dissociate at the critical temperature.

A comparison of the vapor pressure of HgCl₂ with other substances is made in Figure 2. There the log of reduced vapor pressure (vapor pressure divided by value at the critical temperature) is plotted *vs.* reciprocal of reduced temperature. The data for that figure were taken from Din's tables⁹ except that H₂O values were from Faxen¹⁰ and BiCl₃ from ref 3. The figure indicates that there is a degree of correlation between the relative positions of the vapor pressure curves and the polarity of the molecules of the substance. With increasing polarity, the pressure curve is lower in the figure. The curve for HgCl₂ falls intermediate between those for the substances having symmetrical nonpolar molecules (Ar, N₂, C₂H₆) and those having polar molecules (H₂O, BiCl₃). In fact, the curves for CO₂ and HgCl₂ fall very close together. Since these both have linear, quadrupolar molecules, this rough correlation of molecular structure with similarity of vapor pressure curve is borne out. The fact that NH₃ falls very close to HgCl₂ (and CO₂) presumably indicates that its (di-) polarity has the same net effect as the quadrupolarity of HgCl₂ and CO₂.

The enthalpy of vaporization of HgCl₂ may be cal-

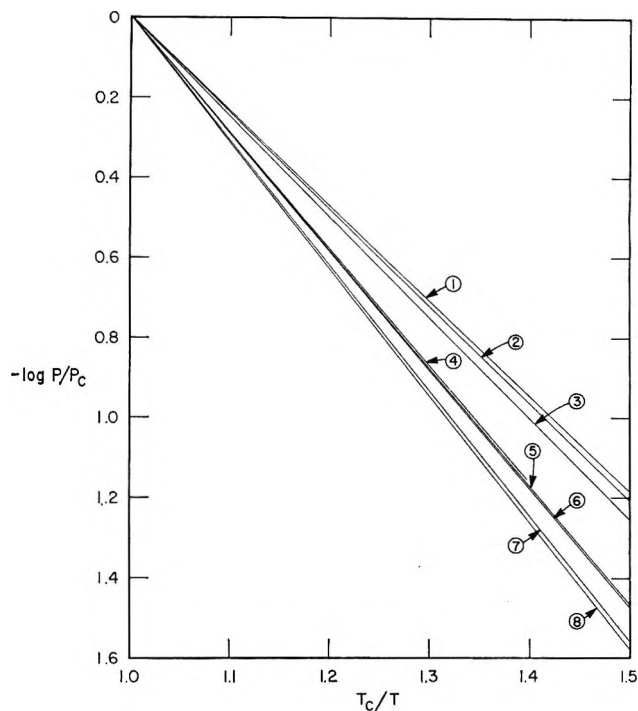


Figure 2. Reduced vapor pressure curves for several substances: 1, Ar; 2, N₂; 3, C₂H₆; 4, CO₂; 5, HgCl₂; 6, NH₃; 7, H₂O; 8, BiCl₃.

culated from the present data using the Clapeyron relation, which can be written

$$\Delta H_{\text{vap}} = \frac{T(V_g - V_l)(dp/dT)}{41,300}$$

where V_g and V_l are the orthobaric volumes of vapor and liquid, respectively, and (dp/dT) is the rate of change of vapor pressure with respect to temperature; the numerical factor converts the value to kilocalories per mole. The orthobaric volumes were calculated from the data of ref 2 and (dp/dT) from eq 1. The results of these calculations are shown in Table III.

Figure 3 shows the variation of the enthalpy of vaporization as a function of temperature. The circles represent the enthalpy of vaporization using the modified Guggenheim relation from ref 2 to calculate $V_g - V_l$ and (dp/dT) from eq 1. The values of the enthalpy of vaporization are reasonable above 750°K, but below this temperature the values are too high. This is probably due to an error in $(V_g - V_l)$ since the modified Guggenheim relation used in ref 2 fits the experimental

(8) S. J. Yosim and S. W. Mayer, *J. Phys. Chem.*, **64**, 909 (1960).

(9) F. Din, Ed., "Thermodynamic Functions of Gases," Vol. 1-3, Butterworth and Co. (Publishers) Ltd., London, 1962.

(10) O. H. Faxen, "Thermodynamic Tables in the Metric System for Water and Steam," Nordisk Rotogravyr, Stockholm, Sweden, 1953.

Table III: Vaporization Data for Mercuric Chloride

T , °K	P , atm	dp/dt , atm/deg	ΔV_{vap} , cc/mole	ΔH_{vap} , kcal/ mole
700	8.21	0.1102	6856	12.80
725	11.36	0.1420	4642	11.57
750	15.36	0.1795	3254	10.61
775	20.4	0.2231	2393	10.02
800	26.6	0.2732	1763	9.33
825	34.1	0.3292	1326	8.72
850	43.1	0.3922	1004	8.10
860	47.1	0.4187	897.0	7.82
870	51.5	0.4473	804.2	7.58
880	56.1	0.4763	717.9	7.28
890	61.0	0.5063	638.3	6.96
900	66.2	0.5373	565.2	6.62
910	71.7	0.5692	496.9	6.22
920	77.6	0.6028	433.0	5.81
930	83.8	0.6370	372.2	5.34
940	90.3	0.6719	312.7	4.78
950	97.2	0.7081	252.5	4.11
960	104.5	0.7455	187.4	3.25
970	112.2	0.7840	90.84	1.67
972 ^a	(113.7)	(0.7917)	(0)	(0)

^a Critical point.

densities with an average deviation of ± 0.008 g/cc. Therefore, the dashed line represents our estimate of the enthalpy of vaporization between 750 and 700°K. It is interesting to note that at 700°K the ideal vapor density and the vapor density calculated from the modified Guggenheim relation of ref 2 are identical, *i.e.*, 0.039 g/cc, while the vapor density corresponding to the enthalpy of vaporization indicated by the dashed line is 0.042 g/cc. With the high sensitivity to the vapor density in this region and the scatter of the experimental vapor densities,² it is not surprising that the enthalpy of vaporization cannot be calculated with precision below about 750°K.

Partington¹¹ has pointed out that there have been many empirical relations evolved between enthalpy of vaporization and temperature. Of these the relatively simple one of Winter modified by Bowden and Jones¹² was applied to the present case, namely

$$\Delta H_{\text{vap}} = l_0 \left(\frac{T_c - T}{T_c} \right)^n$$

in which l_0 and n are constants. A log-log plot of the data for HgCl_2 is shown in Figure 4. The results fall

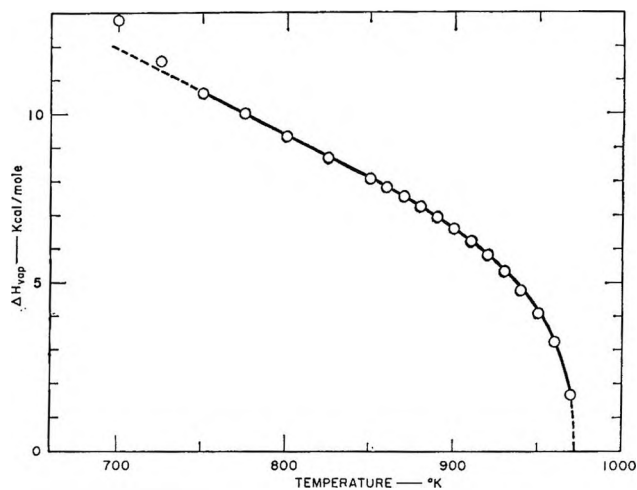


Figure 3. Enthalpy of vaporization of mercuric chloride: O, calculated from eq 3.

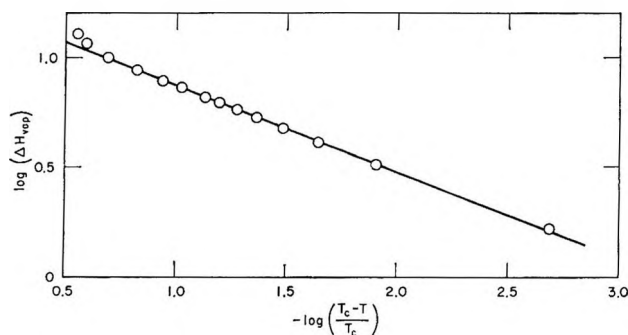


Figure 4. Enthalpy of vaporization *vs.* $(T_c - T)/T_c$ on log-log plot.

on a straight line from 2° to about 250° below the critical point, then deviate from the line. The values of the constants derived from the straight line drawn through the data are: $l_0 = 18.50$, $n = 0.394$. These can be compared with values given by Partington for several fluids. For n , his values range from 0.3 to 0.45 and average about 0.39 for nonassociated liquids. Values of l_0 for these same liquids depend on the molecular constitution much more than n and range from about 47 to SnCl_4 to about 155 for CO_2 . The low value for HgCl_2 , of course, reflects its relatively higher enthalpies of vaporization (or higher boiling point).

(11) J. R. Partington, "An Advanced Treatise on Physical Chemistry," Vol. II, Longmans, Green and Co., London, 1951, pp 319-324.

(12) W. J. Jones and S. T. Bowden, *Phil. Mag.*, 37, 480 (1946).

The Saturation Thermodynamic Functions for Mercuric Chloride

from 298°K to the Critical Point¹

by Daniel Cubicciotti, H. Eding, and J. W. Johnson

Stanford Research Institute, Menlo Park, California 94025 (Received April 29, 1966)

The saturation enthalpy increments above room temperature for HgCl_2 in its condensed phases were determined with a drop calorimeter to within 50° of the critical point. These were combined with previously determined enthalpies of vaporization to obtain values for the saturated vapor, and the data were extrapolated to the critical point. Saturation entropies for vapor and condensed phases were calculated from the enthalpies. The internal energy departures of the gas from ideal values were evaluated and compared with similar data for molecular fluids.

Introduction

The present report is a part of our study of the thermodynamic properties of inorganic liquids at elevated temperatures. Recent investigations of bismuth chloride²⁻⁴ are being followed by studies on mercuric chloride. The volume change on vaporization⁵ and the vapor pressure⁶ of HgCl_2 up to its critical point were determined previously in this laboratory, and the enthalpy and entropy of vaporization have been obtained from those results. In the present paper, we have determined the enthalpy increments (above the solid at 298°K) for the condensed phases under saturation conditions, and from them and the enthalpies of vaporization we have obtained values for the saturated vapor. The entropies and free energy functions for both the condensed and gas phases were calculated from the enthalpy increments and their temperature derivatives.

Measured Heat Increments

The same method was used for this work as reported in our BiCl_3 study:⁴ samples of HgCl_2 sealed in evacuated quartz glass ampoules were heated to various temperatures, some within 50° of the critical temperature, and dropped into a modified Parr calorimeter at room temperature. From the heat transferred to the calorimeter, the enthalpy of HgCl_2 in the condensed phases, under saturation conditions, was calculated.

The samples heated to the higher temperatures required heavy-walled glass ampoules to withstand

the vapor pressure of the HgCl_2 . As a result, a substantial fraction of the heat evolved came from the glass, and so the accuracy of those determinations was limited. To obtain more accurate data in the lower temperature range, where the vapor pressure was low enough, sealed platinum containers were used. The important details of the samples are listed in Table I.

Table I: Details of Samples Used

Sample no.	Container material	Wt of HgCl_2 , g	Wt of container, g	Internal vol. of ampoule, cc	Symbol used in Figures 1 and 2
A	Quartz glass	24.0608	6.8617	6.9181	⊙
B	Quartz glass	7.0609	6.4409	2.0891	⊖
C	Quartz glass	5.3083	6.0779	2.2132	⊕
D	Platinum	13.4660	7.7860	...	×

(1) This work was made possible by financial support from the Research Division of the U. S. Atomic Energy Commission under Contract No. AT(04-3)-106.

(2) J. W. Johnson and D. Cubicciotti, *J. Phys. Chem.*, **68**, 2235 (1964).

(3) J. W. Johnson, W. J. Silva, and D. Cubicciotti, *ibid.*, **69**, 3916 (1965).

(4) D. Cubicciotti, H. Eding, F. J. Keneshea, and J. W. Johnson, *ibid.*, **70**, 2389 (1966).

(5) J. W. Johnson, W. J. Silva, and D. Cubicciotti, *ibid.*, **70**, 1169 (1966).

(6) J. W. Johnson, W. J. Silva, and D. Cubicciotti, *ibid.*, **70**, 2985 (1966).

A small part of the heat liberated by the sample was due to condensation of HgCl_2 vapor. The amount of that heat for each drop was calculated from the known liquid and vapor densities and the volumes of the ampoules. For the calculation, the enthalpy of vaporization at the sample temperature was used instead of the more complicated calculation of integration over the range of temperatures for which condensation occurred. Since the total correction was small, the difference in methods of calculation was negligible. For determinations made below 700°K , the correction itself was negligible.

The heat liberated by the fused quartz containers, to be subtracted from the results for the total sample, was calculated from the equation given in ref 4. Values of the heat liberated by the platinum container were taken from the work of Kendall, Orr, and Hultgren.⁷

The mercuric chloride used was prepared as described in ref 5 and was filtered through sintered glass under vacuum into the quartz bulbs, which were sealed under vacuum. The platinum capsule was filled in air and the end was pinched closed and platinum-soldered.

The resultant heat increments for HgCl_2 in its condensed phases (*i.e.*, heat liberated when cooled from T to 298°K) are shown as data points in Figures 1 and 2. The more precise results obtained on the platinum capsule are shown on a larger scale in Figure 1.

The heat evolved by a sample in equilibrium with its vapor when cooled from T to 298°K is equal to the integral⁸

$$\int_{298}^T C_\sigma dT = \int_{298}^T T \left(\frac{\partial S}{\partial T} \right) dT$$

The temperature derivative of that quantity gives C_σ , the saturation heat capacity. The quantity C_σ is related to the saturation enthalpy by

$$\begin{aligned} \left(\frac{\partial H}{\partial T} \right)_\sigma &= C_\sigma + V \left(\frac{\partial P}{\partial T} \right)_\sigma \\ &= C_p + V \left[1 - \frac{T}{V} \left(\frac{\partial V}{\partial T} \right)_p \right] \left(\frac{\partial p}{\partial T} \right)_\sigma \end{aligned}$$

For temperatures at which the vapor pressure is less than a few atmospheres, the last term is negligible and drop calorimeter measurements give the enthalpy increments at constant (low) pressure as well as the saturation enthalpy increments. For pressures well above a few atmospheres (which occur above 700°K), the differences become significant, although small. Since we have no information about the compressibility of the liquid, we are not able to evaluate the constant pressure heat capacity or enthalpy increments, and so we can only evaluate the saturation quantities above

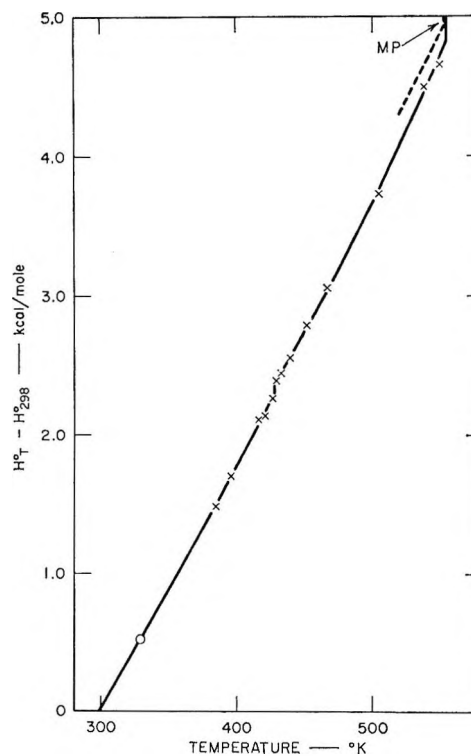


Figure 1. Standard enthalpy increments above 298°K for solid HgCl_2 . Crosses are data obtained in Pt capsule. Dashed line represents data of Topol and Ransom.¹⁰ Circle is data of Ewald.⁹ Full curves are calculated from eq 1 and 2.

700°K . Therefore, the treatment of the data is divided into two parts—one above and the other below 700°K .

Enthalpy Increments for Condensed Phases to 700°K

The results for the solid are best shown in Figure 1. The difference between the standard enthalpy (referring to the substance under constant pressure of 1 atm) and saturation enthalpy (referring to the substance under its own vapor pressure, which changes with temperature) is entirely negligible in these measurements. The enthalpy increments in Figure 1 are described as standard-state values, but they may equally be considered saturation values.

The data indicate that there is a small discontinuity in the curve at about 428°K . This effect seemed larger than could be accounted for on the basis of experimental scatter. In an attempt to resolve the

(7) W. B. Kendall, R. L. Orr, and R. Hultgren, *J. Chem. Eng. Data*, **7**, 516 (1962).

(8) For a discussion of thermodynamics under saturation conditions, see E. A. Guggenheim, "Thermodynamics," 3rd ed. North-Holland Publishing Co., Amsterdam, 1957, p 149, or J. S. Rowlinson, "Liquids and Liquid Mixtures," Academic Press, New York, N. Y., 1959, p 16 ff.

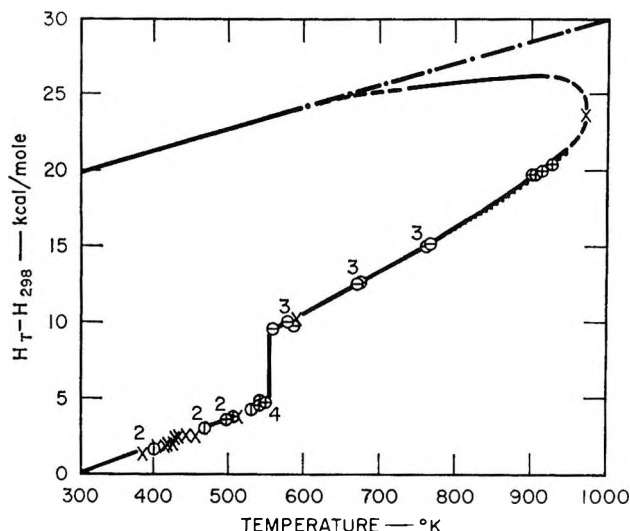


Figure 2. Saturation enthalpy increments referred to solid HgCl_2 at 298°K . Lower curves refer to condensed phases, upper curves to vapor. The various symbols for data points refer to the samples described in Table I. Numbers on curve give the number of indistinguishable circle points in each cluster. Dashed curves represent interpolated or extrapolated data; full curves are based on measured results. The dot-dash curve represents the vapor in the ideal standard state.

question, X-ray powder patterns were taken above and below the transition temperature; however, these indicated no difference in structure. Thus the discontinuity must be due to a change that is more subtle than a first-order transition and may represent a lambda point. The total heat effect for the transition was about 77 cal/mole.

Equations were derived to fit the data above and below the discontinuity. These were

$$H^\circ_T - H^\circ_{298} \text{ (cal/mole)} = 11.73T + 818 \times 10^{-5}T^2 - 4224 \quad (298 \text{ to } 428^\circ\text{K}) \quad (1)$$

$$H^\circ_T - H^\circ_{298} \text{ (cal/mole)} = -5.33T + 25.2 \times 10^{-3}T^2 + 36 \quad (428 \text{ to } 553.7^\circ\text{K}) \quad (2)$$

The full curves in Figure 2 represent these equations. The melting point of the material used in this work was $553.7 \pm 0.5^\circ\text{K}$.

There are two literature references of comparable data known to us. Ewald's⁹ results provide the point shown as a circle in Figure 1. It is in good agreement with our smoothed curve. Topol and Ransom¹⁰ report the enthalpy increment above 298°K for the solid at the melting point and a (constant) heat capacity

derived from enthalpy measurements just below the melting point. These were used to calculate the dashed line in Figure 1. Their enthalpy increments are about 120 cal/mole greater than ours at the melting point. For the liquid, their enthalpy increments are about 200 cal/mole greater than ours near the melting point. We have no good explanation for these differences, which are substantially larger than the comparable differences for BiCl_3 . It may be that the purity of their HgCl_2 was different from ours. Their melting point was low.

The enthalpy increments above 298° for the liquid are shown in Figure 2. The data were adequately fit by a straight line up to 700°K and beyond. Below 700°K , where the pressure does not exceed 8 atm, the slope of the line is equal within experimental error to C_p , the constant pressure (1 atm) heat capacity, and had a value of 28.1 ± 1.0 cal/mole deg. This value is in agreement with the 27.2 ± 1.1 found by Topol and Ransom.

The heat of fusion was derived by extrapolating the enthalpy curves for the solid and liquid to 553.7°K , the melting point of our material. The value obtained was 4.49 ± 0.1 kcal/mole. This is somewhat smaller than the value of Topol and Ransom.

The standard enthalpy increments calculated from our equations for the solid and from the straight line drawn through the liquid data are reported in Table II up to 700°K .

Σ -Plot Treatment of Vapor Pressure Data

The vapor pressure of HgCl_2 has been reported from room temperature to the critical point (972°K). Enthalpy increment data reported above, together with the comparable information for the gas obtained from molecular constant data, make it possible to carry out a careful Σ -plot treatment of the vaporization data over the range in which the low-pressure form of the Clausius-Clapeyron equation holds, namely from room temperature to somewhat above the boiling point. The Σ -plot method described in ref 11 was used for this purpose. Σ is defined as

$$-\Sigma' = R \ln p(\text{atm}) + \Delta \text{ fef incr}$$

in which

$$\Delta \text{ fef incr} = \text{fef}(\text{gas}, T) - \text{fef}(\text{gas}, 298) - \text{fef}(\text{condensed}, T) + \text{fef}(\text{condensed}, 298)$$

(9) R. Ewald, *Ann. Physik Chem.*, **44**, 1213 (1914).

(10) L. E. Topol and L. D. Ransom, *J. Phys. Chem.*, **64**, 1339 (1960); **65**, 2267 (1961).

(11) D. Cubicciotti, *ibid.*, **70**, 2410 (1966).

Table II: Thermodynamic Functions for HgCl₂ in Standard State Condensed Phases up to 700°K

T, °K	$H^\circ_T - H^\circ_{298},^a$ kcal/ mole	S°_T , eu	$-(G^\circ_T - H^\circ_{298})/T,^a$ eu	Vapor press., atm
298	...	34.93	34.93	1.63×10^{-7}
320	370	36.12	34.97	1.60×10^{-6}
340	710	37.16	35.07	2.31×10^{-5}
360	1,060	38.15	35.21	5.06×10^{-5}
380	1,415	39.12	35.39	2.12×10^{-4}
400	1,775	40.04	35.60	7.75×10^{-4}
420	2,145	40.94	35.83	2.47×10^{-3}
428	2,295	41.30	35.94	3.81×10^{-3}
428	2,370	41.48	35.94	
440	2,570	41.93	36.09	7.08×10^{-3}
460	2,920	42.70	36.36	1.84×10^{-2}
480	3,280	43.49	36.64	4.42×10^{-2}
500	3,670	44.28	36.93	9.93×10^{-2}
520	4,080	45.07	37.23	0.206
540	4,510	45.88	37.54	0.406
553.7 (s)	4,810	46.44	37.75	0.62
553.7 (l)	9,300	54.55	37.75	
560	9,480	54.86	37.94	0.72
580	10,040	55.85	38.54	1.12
600	10,600	56.80	39.14	1.67
620	11,160	57.72	39.72	2.39
640	11,720	58.62	40.30	3.33
660	12,280	59.48	40.67	4.55
680	12,850	60.32	41.42	6.08
700	13,410	61.13	41.98	7.87

^a The reference state for these values is the solid in its standard state at 298°K.

and f_{ef} represents the free energy function, namely $(G^\circ_T - H^\circ_{298})/T$. Values for f_{ef} incr for the condensed phases were calculated from the enthalpy data reported above by the methods of ref 12, while those for the gas were obtained from the data in the "JANAF Tables"¹³ (which had been calculated from molecular constant data).

The data given in the following literature references (with temperature range and method in parentheses) were included in the Σ -plot treatment: Prideaux¹⁴ (286 to 309°, boiling point method); Johnson, Silva, and Cubicciotti⁶ (300 to 695°, boiling point method); Niwa¹⁵ (45 to 70°, effusion); Ruf and Treadwell¹⁶ (11 to 59°, effusion); Johnson¹⁷ (152 to 302°, spiral gauge); Schmidt and Walter¹⁸ (100 to 180°, transpiration); and Stelzner, Niederschulte, and Wiedemann¹⁹ (60 to 300°, transpiration).

The data of Stock and Zimmermann²⁰ were not included in the treatment, since their values were so discordant with those of the above authors as to indicate a systematic error in their work. The Σ plot

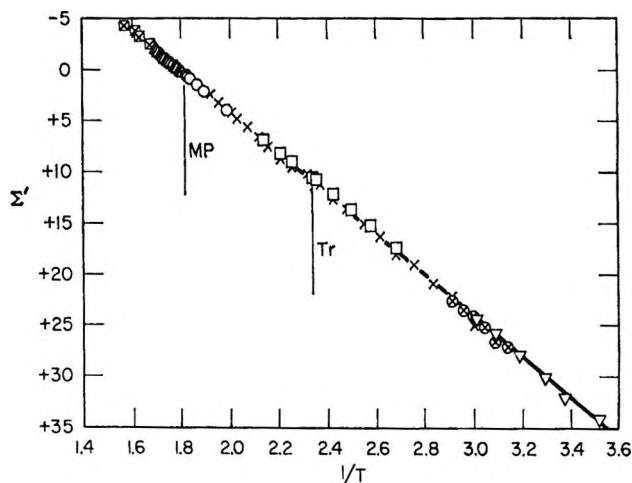


Figure 3. Σ plot for HgCl₂ vapor pressure data. Data points were from the following references: \boxtimes , Johnson, Silva, and Cubicciotti;⁶ Δ , Prideaux;¹⁴ \circ , Johnson;¹⁴ \times , Stelzner, Niederschulte, and Wiedemann;¹⁹ \square , Schmidt and Walter;¹⁸ \otimes , Niwa;¹⁵ and ∇ , Ruf and Treadwell.¹⁶

itself is shown in Figure 3. The data fell quite close to a straight line, and more than 90% of the 96 points fell between two straight lines defined by the $(\Sigma', 1/T)$ coordinates: $(-3.90, 1.6 \times 10^{-3})$ and $(36.18, 3.6 \times 10^{-3})$ for one line and $(-3.58, 1.6 \times 10^{-3})$ and $(35.58, 3.6 \times 10^{-3})$ for the other. The thermodynamic parameters for sublimation of HgCl₂ and their 90% confidence levels calculated from the data were $\Delta H^\circ_{298} = 19.85 \pm 0.20$ kcal/mole and $\Delta S^\circ_{298} = 35.5 \pm 0.8$ eu.

The enthalpy increments for the ideal gas, referred to the solid in its standard state at 298°K, were calculated from the enthalpy of sublimation at 298°K and the enthalpy increments for the ideal gas were calculated from molecular constant data and reported in the "JANAF Tables." These are shown as the full curve in the upper part of Figure 2 below 600°K and a dot-dash curve above 600°K. Below 600°K the vapor pressure is low enough so that the enthalpy of the ideal gas is essentially equal to that of the real gas.

(12) K. S. Pitzer and L. Brewer, "Thermodynamics," revision of book by G. N. Lewis and M. Randall, McGraw-Hill Book Co., Inc., New York, N. Y., 1961, p 166 ff.

(13) "JANAF Thermochemical Tables," The Dow Chemical Co., Midland, Mich., revised Dec 31, 1965.

(14) E. B. R. Prideaux, *J. Chem. Soc.*, **97**, 2032 (1910).

(15) K. Niwa, *J. Chem. Soc. Japan*, **57**, 1309 (1936).

(16) R. Ruf and W. D. Treadwell, *Helv. Chim. Acta*, **37**, 1941 (1954).

(17) F. M. G. Johnson, *J. Am. Chem. Soc.*, **33**, 777 (1911).

(18) G. C. Schmidt and R. Walter, *Ann. Physik*, **72**, 565 (1923).

(19) K. Stelzner, G. Niederschulte, and E. Wiedemann, *Ber. Deut. Phys. Ges.*, **3**, 159 (1905).

(20) A. Stock and W. Zimmermann, *Monatsh.*, **53-54**, 786 (1929).

The absolute entropy of solid HgCl_2 can be obtained from that of the gas and the above value for the sublimation entropy. For the gas the absolute entropy at 298°K has been reported in the "JANAF Tables" as 70.43 as calculated from observed molecular constants. Therefore, the absolute entropy of crystalline HgCl_2 at 298°K is 34.93 ± 0.8 eu. This quantity, together with the enthalpy data reported above, allows the calculation of the absolute entropies and the free energy functions for elevated temperatures. The values for these functions for HgCl_2 in its condensed phases up to 700°K are given in Table II.

The vapor pressure of HgCl_2 can readily be calculated from the evaporation parameters through the relation

$$\Sigma' = \frac{\Delta H_{298}^\circ}{T} - \Delta S_{298}^\circ = R \ln p(\text{atm}) - \Delta \text{fef incr}$$

Values calculated in this way are given in Table II. The boiling point obtained by interpolation was $575 \pm 0.5^\circ\text{K}$.

Enthalpy Increments from 700°K to Critical Point

As indicated above, the heat capacity derived from the drop calorimeter measurements on a sample in equilibrium with vapor is the saturation heat capacity, C_σ , and it is closely equal to the constant pressure heat capacity, C_p , as long as the vapor pressure is less than a few atmospheres. These conditions obtain below 700°K and the results below that temperature were used to calculate the standard state (1 atm) thermodynamic functions. At some temperature above 700°K, C_p and C_σ differ by the quantity $T(\partial V/\partial T)_p$, and since the expansivity of the liquid is unknown, we can only evaluate the thermodynamic functions under saturation conditions above that temperature. We have arbitrarily chosen 700°K as the temperature above which the two types of heat capacities are no longer considered equal.

The saturation enthalpy increments above 298°K for the liquid were obtained as follows. A smooth curve was drawn through the measured values of the heats evolved. This curve is shown as a dotted line (which merges at lower temperatures with the full curve representing the enthalpy increments) in Figure 2. The slope of that curve was taken as C_σ . The saturation enthalpy increments, $(H_T - H_{298}^\circ, s)_\sigma$, were calculated from 700 to 910°K in 10° increments by numerical integration of the equation

$$\left(\frac{\partial H}{\partial T}\right)_\sigma = C_\sigma + V\left(\frac{\partial P}{\partial T}\right)_\sigma$$

Values of $V(\partial P/\partial T)_\sigma$ were taken from our earlier measurements of the volume of the liquid and the vapor pressure. The resulting enthalpy increment curve for the liquid is shown as a full line.

For the critical point a value of $(H_T - H_{298}^\circ, s)_\sigma$, the saturation enthalpy referred to the solid in its standard state at 298°K, was estimated from the enthalpy increments below 910°K and data for other substances. To do this, a plot of reduced enthalpy increments for both liquid and vapor *vs.* reduced density was constructed²¹ for several substances: Ar, CO_2 , NH_3 , and H_2O . These formed a family of curves that were relatively close together for the liquid. Comparison of the data for HgCl_2 from about 850 to 910°K with the other substances led to a value of 23.8 kcal/mole for $(H_T - H_{298}^\circ, s)_\sigma$ at the critical point. This is shown as a cross at the apex of the curve in Figure 2.

The saturation enthalpy increments for the vapor from 700 to 910°K were calculated from those of the liquid and the enthalpies of vaporization reported earlier.⁶ A full curve is used to represent the values for the vapor in that region. This curve and the data for the liquid were extrapolated to the critical point in such a way that the difference between the curves was equal to the enthalpy of vaporization and so that the curves joined at the value estimated above for the critical point. These extrapolations are shown as dashed curves in Figure 2.

The saturation enthalpy curve for the vapor was extrapolated below 700°K so that the curve joined smoothly with that for the ideal vapor slightly above the boiling point.

Values for the saturation enthalpy increments of liquid and vapor from 700°K to the critical point are given in Table III with other thermodynamic data in that temperature range.

Entropies and Free Energy Functions above 700°K

The entropies of the liquid above 700°K under saturation conditions were calculated by integrating $C_\sigma d \ln T$ numerically at 10° intervals. The base point was the absolute entropy at 700°K as established above. The values of C_σ were taken from the slopes of the curves of measured heat evolved up to 910°K. Above 910°K, the slope of the extrapolated enthalpy curve was diminished by the quantity $V(\partial p/\partial T)_\sigma$ to obtain C_σ . The values of C_σ used, as well as the saturation entropies calculated for the liquid, are given in Table III.

Values for the saturation entropies for the vapor in the range 700 to 972°K were obtained by adding the

(21) Data for these substances were taken from F. Din, "Thermodynamic Functions of Gases," Vol. 1-3, Butterworth and Co. Ltd., London, 1961, 1962.

Table III: Thermodynamic Functions for HgCl₂ under Saturation Conditions to the Critical Point

T, °K	Liquid					Gas				
	$H_T - H^{298},^a$ kcal/mole	S_T , eu	$-(G_T - H^{298})/T,^a$ eu	C_p , eu	V , cc/mole	dP/dT , atm/deg	$H_T - H^{298},^a$ kcal/mole	S_T , eu	$-(G_T - H^{298})/T,^a$ eu	V , cc/mole
700	13.44	61.13	41.93	28.3	69.7	0.110	25.26	79.44	43.35	...
720	14.01	61.93	42.47	28.5	71.1	0.135	25.77	78.26	42.47	...
740	14.59	62.72	43.00	28.8	72.5	0.164	25.64	77.65	43.00	...
760	15.18	63.50	43.53	29	74.2	0.196	25.52	77.11	43.53	2940
780	15.78	64.26	44.03	30	75.9	0.233	25.65	76.91	43.03	2320
800	16.39	65.02	44.54	31	77.9	0.273	25.70	76.66	44.53	1840
820	17.02	65.8	45.0	31	80.2	0.317	25.81	76.4	44.9	1480
840	17.66	66.5	45.5	32	82.6	0.366	26.03	76.5	45.5	1210
860	18.31	67.3	46.0	33	85.6	0.418	26.12	76.4	46.0	980
880	19.00	68.1	46.5	35	88.9	0.475	26.27	76.3	46.4	807
900	19.7	68.8	46.9	37	93.1	0.536	26.3	76.2	47.0	658
920	20.5	69.7	47.4	39	98.5	0.601	26.3	76.0	47.4	532
940	21.3	70.6	47.9	41	106.1	0.670	26.1	75.6	47.8	419
960	22.4	71.7	48.4	68	120	0.744	24.6	75.1	48.4	307
972	23.8	73	48.5	...	140	...	23.8	73	48.5	140

(Critical point)

^a The reference state used for both liquid and vapor was the solid in its standard state at 298°K.

entropy of evaporation to the entropies of the liquid. The entropies of evaporation were calculated from the enthalpies of evaporation from ref 6 divided by temperature.

Below about 600°K the saturation entropies were calculated by subtracting $R \ln p$ (vapor pressure in atmospheres) from the standard entropies of the ideal

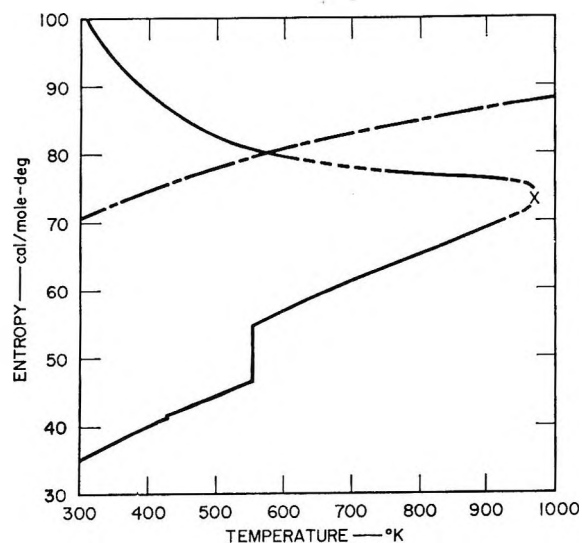


Figure 4. Absolute entropy for HgCl₂ vapor and condensed phases. Upper curves refer to liquid; lower to condensed phases. Dot-dash curve is entropy of ideal vapor in standard state. Full and dashed curves present the entropy under saturation conditions, the dashed portion representing interpolated and extrapolated regions.

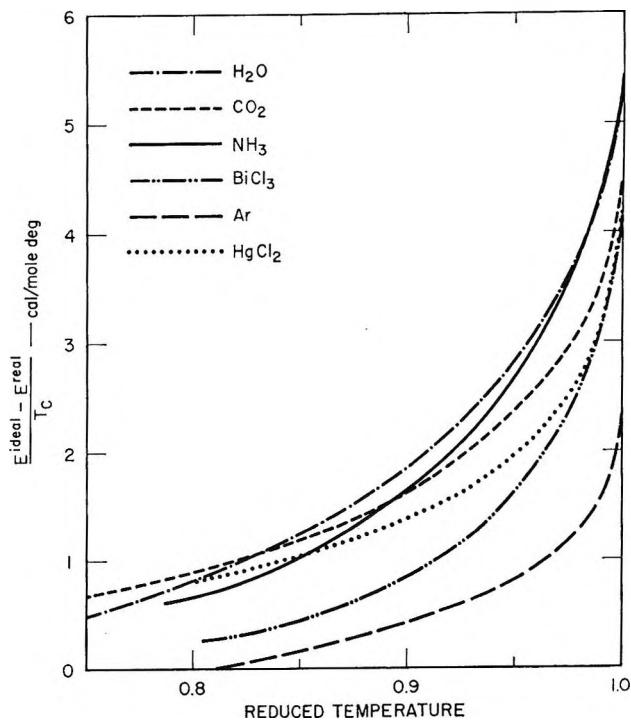


Figure 5. Energy departure from ideal gas values for several substances.

gas given in the "JANAF Tables." The results are shown as a full curve in Figure 4. Between 600 and 700°K, the two curves of saturation entropy for the vapor were smoothly joined by the dashed line shown.

Gas Imperfection Energy

The quantity $(E_T^{\text{ideal}} - E_T^{\text{real}})/T_c$ for the gas is a function that depends only on reduced properties of the gas and is a measure of the net attractive energy between the molecules. It was calculated for HgCl_2 by the same method that was used for BiCl_3 (see eq 4 of ref 4). The values obtained for $(E_T^{\text{ideal}} - E_T^{\text{real}})/T_c$ for HgCl_2 gas are shown as a function of reduced temperature compared to several other substances²¹ in Figure 5.

The curve for mercuric chloride is quite close to that for carbon dioxide. This is not surprising because of the similarity in their molecular structures—both are linear symmetrical molecules of point group $D_{\infty h}$. For both molecules the intermolecular interaction energy must arise primarily from quadrupole-quadrupole attractions. On the reduced basis of Figure 5, differences between interaction energies for molecules of the same type are suppressed, and only

qualitative differences between types of intermolecular potentials influence the relative shapes of the curves. Water and ammonia are seen, on this basis, to have similar shapes that are different from the form of the carbon dioxide and mercuric chloride curves. The curve for BiCl_3 has approximately the same shape as the H_2O and NH_3 curves but is displaced downward. Their similarity probably originates in the fact that these three molecules are dipolar. The displacement probably arises because H_2O and NH_3 are hydrogen bonded, while BiCl_3 is not. More detailed consideration of the relation between the nature of intermolecular potentials and plots of the type of Figure 5 should probably be made from statistical-thermodynamic considerations.

Acknowledgment. The X-ray search for a change in structure of solid HgCl_2 in the neighborhood of 428°K was performed by Dr. Malcolm Barlow. Mr. W. J. Silva performed some of the experimental work.

The Association of Bispyridinium Cations with Polycarboxylic Acids¹

by H. Morawetz and A. Y. Kandarian

Polymer Research Institute, Polytechnic Institute of Brooklyn, Brooklyn, New York (Received April 21, 1966)

The binding of α,ω -polymethylenebispyridinium bolaform cations to partially neutralized poly(acrylic acid), as well as isotactic and syndiotactic poly(methacrylic acid) was studied by a dialysis equilibrium technique. The variables explored included the concentration of polyions and bolions, the spacing of the charges on the bolions, the degree of ionization of the polymeric acid, and the concentration of added uni-univalent salt. The binding of Mg^{2+} by the polyions differs most strikingly from the binding of the bolions in its much lower sensitivity to the concentration of added uni-univalent electrolyte.

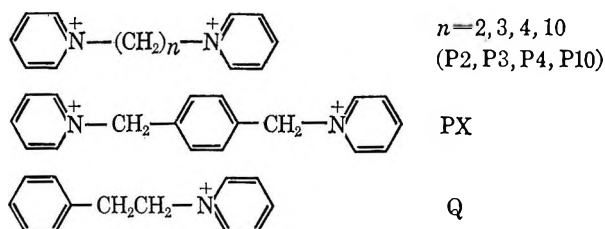
It is commonly observed that counterions in solutions of polyelectrolytes have unusually low activity coefficients. Several factors contribute to this effect. Part of the inactivation may be ascribed to long-range electrostatic forces which are, of course, particularly powerful in systems containing polyions with high charge densities. Another part is a consequence of ion-pair formation of counterions with ionized groups

carried by the polyion or the formation of complex ions, frequently considered together under the term of "site binding." These phenomena have been fully

(1) Abstracted from a doctoral dissertation submitted by A. Y. Kandarian to the Graduate School, Polytechnic Institute of Brooklyn, June 1964. We are grateful for a fellowship received by A. Y. Kandarian from the American Machine and Foundry Co. and for financial assistance of this work by Grant GM-05811 of the National Institutes of Health.

discussed,^{2,3} and Lyons and Kotin⁴ have recently considered the problem of how long-range electrostatic interactions and site binding may be differentiated from experimental data. Frequently, such a distinction cannot be made unambiguously, but a quantitative measure of site binding can be obtained for the interaction of transition metal cations with a polycarboxylic acid, where complex formation is evidenced by characteristic changes in the absorption spectrum⁵ and in the titration curve.^{5a,6} It can also be demonstrated by dialysis equilibrium measurements under conditions where a simple electrolyte, which does not participate in complex formation, is in large excess over the polyelectrolyte.^{5b}

In the present study we have used the dialysis equilibrium technique to determine the association of the doubly charged species P2, P3, P4, P10, and PX with partially ionized poly(acrylic acid) and with poly(methacrylic acid) samples of different stereoregularity.



Such species, in which two ionic charges are separated by several uncharged atoms have been designated as "bolaform ions"⁷ (or bolions), and it seems that their interaction with polyions has been investigated previously only by Ehrenpreis and his collaborators,⁸ who reported on the formation of insoluble complexes when certain bolaform cations were added to solutions of acidic polysaccharides. This work suggested that complex formation may depend critically on a correspondence of the spacing of the charges in the polyion and the bolaform counterion but changes in solubility are known to be a rather unreliable criterion of counterion binding by polyions.^{2,9} The present study employed, therefore, the dialysis equilibrium method to give an unambiguous measure of the extent of site-binding of bolaform counterions.

Experimental Section

Preparation of Bispyridinium Salts. The synthesis of the bispyridinium salts may be exemplified by the procedure used for 1,1'-ethylenebispyridinium bromide. Two grams of dry ethylene bromide was heated at 50° for 10 min with an excess of freshly distilled pyridine. The bispyridinium salt precipitated and was collected on a Büchner funnel. It was recrystallized twice from 95% ethanol and dried at 95° at a pressure of 2 mm.

The other salts were prepared in the same manner using the appropriate α,ω -dibromides. The melting points of the dibromides were: P2, 290° (lit.¹⁰ 295°); P3, 240° (lit.¹¹ 242.5°); P4, 237° (lit.^{11,12} 237–239°); P10, 196° (lit.¹¹ 196.5–198°); PX, 280° (lit.¹³ 281–282°). In addition, β -phenylethylpyridinium (Q) bromide was prepared to serve as a singly charged analog of P2. It had a melting point of 125° (lit.¹⁴ 125–126°). Bromine analyses for the six salts were (theoretical values in parentheses): 46.25% (46.18), 44.45% (44.38), 42.56% (42.72), 34.82% (34.91), 37.77% (37.88), and 30.04% (30.28).

Polymeric Acids. Freshly distilled acrylic acid was polymerized to a 30% conversion in butanone solution (15% by wt of monomer) at 60° using azobisisobutyronitrile initiator. The polymer was purified by extensive dialysis in bags of regenerated cellulose (Fisher Scientific Co.), until the dialyzate was neutral. It was then freeze dried for storage. Syndiotactic poly(methacrylic acid) (s-PMA) was prepared by irradiating a mixture of 15 ml of glacial methacrylic acid and 30 ml of dry methanol with 10 Mrads of γ rays from a Co⁶⁰ source at -78°. Isotactic poly(methacrylic acid) (i-PMA) was derived from poly(methyl methacrylate) prepared by *n*-butyllithium-catalyzed polymerization of methyl methacrylate in toluene solution at -78°. The poly(methyl methacrylate) was dissolved in cold 96% sulfuric acid and warmed for 30 min to 60°. After cooling, the solution was poured slowly into a 100-fold excess of water, precipitating the polymer, which was purified by washing and prolonged dialysis

- (2) H. Morawetz, *Fortschr. Hochpolymer. Forsch.*, **1**, 1 (1958).
- (3) S. A. Rice and M. Nagasawa, "Polyelectrolyte Solutions," Academic Press Inc., New York, N. Y., 1961, Chapters 5 and 9.
- (4) J. W. Lyons and L. Kotin, *J. Am. Chem. Soc.*, **87**, 1670 (1965).
- (5) (a) F. T. Wall and S. J. Gill, *J. Phys. Chem.*, **58**, 1128 (1954); (b) A. M. Kotliar and H. Morawetz, *J. Am. Chem. Soc.*, **77**, 3692 (1955); (c) H. Morawetz, *J. Polymer Sci.*, **17**, 442 (1955); (d) H. Morawetz and E. Sammak, *J. Phys. Chem.*, **61**, 1357 (1957).
- (6) (a) H. P. Gregor, L. B. Luttinger, and E. M. Loebl, *ibid.*, **59**, 34 (1955); (b) M. Mandel and J. C. Leyte, *J. Polymer Sci.*, **A2**, 2883, 3771 (1964).
- (7) O. V. Brody and R. M. Fuoss, *J. Phys. Chem.*, **60**, 156 (1956).
- (8) (a) S. Ehrenpreis and M. M. Fishman, *Biochem. Biophys. Acta*, **44**, 577 (1960); (b) S. Ehrenpreis and M. G. Kellock, *ibid.*, **45**, 525 (1960).
- (9) U. P. Straus, D. Woodside, and P. Wineman, *J. Phys. Chem.*, **61**, 1353 (1957).
- (10) J. A. Gautier and J. Renault, *Compt. Rend.*, **225**, 682 (1947).
- (11) J. L. Hartwell and M. A. Pogorelskin, *J. Am. Chem. Soc.*, **72**, 2040 (1950).
- (12) R. E. Lyle and J. J. Gardikes, *ibid.*, **77**, 1291 (1955).
- (13) F. Kohnke, *Ber.*, **71B**, 2583 (1938).
- (14) S. Sugawara and N. Sugimoto, *ibid.*, **72**, 977 (1939); F. Kohnke, *ibid.*, **72**, 2000 (1939); B. Riegel and H. Wittcoff, *J. Am. Chem. Soc.*, **68**, 1805 (1946).

(the un-ionized isotactic polymeric acid is insoluble in water). The completion of the hydrolytic process was checked by infrared spectroscopy of the neutralized polymeric acid, which showed no absorption at 1730 cm^{-1} .

The stereoregularity of the isotactic poly(methyl methacrylate) was characterized before hydrolysis by the high-resolution nmr method of Bovey and Tiers;¹⁵ it was found to contain 90% of isotactic triads. The syndiotactic poly(methacrylic acid) was methylated with diazomethane¹⁶ to obtain a sample suitable for nmr analysis. It was found to contain 85% of syndiotactic triads.

Determination of Dialysis Equilibria. Solutions were prepared containing partially neutralized polyacid with the desired concentrations of sodium bromide and the salt of a cation whose interaction with the polyanion was to be studied. This solution (10 ml) was placed inside a dialysis tube (Fisher Scientific Co. regenerated cellulose); the tube was looped and placed in a bottle with both ends of the tube hanging over the rim. The bottle contained 50 ml of a sodium bromide solution of the same concentration as the inside of the dialysis tube and the levels of the two solutions were essentially identical. The stoppered bottles were thermostated at $24 \pm 1^\circ$ and shaken once a day. About 4 days was required to attain equilibrium. The concentrations of the bispyridinium ions inside and outside the dialysis bag were determined by optical density measurements at $259\text{ m}\mu$, where the molar extinction coefficient was found to be 4700 per pyridinium residue. The concentration of the bolion in the dialysate was designated (Bol_f^{2+}) , equal to the concentration of the free bolions. The bound bolion concentration (Bol_b^{2+}) was obtained as the difference in the concentrations inside and outside the dialysis tube. The chemical stability of the bispyridinium salts was checked by keeping a solution of P2 for 192 hr at pH 10.2 and 25° . Since Hoffmann degradation with liberation of free pyridine would lead to a 60% reduction in the optical density, the absence of any change in the absorbance of the solution was taken as proof that degradation was negligible even in solutions much more basic than those employed in the dialysis experiments. Adsorption of the bispyridinium salts on the dialysis membrane was negligible and satisfactory material balances were obtained from concentrations determined inside and outside the dialysis tube.

In experiments in which the dialysis equilibrium of Mg^{2+} was investigated, the magnesium concentration was determined spectroscopically as the complex with eriochrome black T.¹⁷

Results and Discussion

Over the range of the experimental conditions studied, the ratio $r = (\text{Bol}_b^{2+})/(\text{Bol}_f^{2+})$ of bound free bolions was found to be independent of the stoichiometric bolion concentration. This is illustrated in Figure 1 for solutions containing P2 and half-neutralized poly(acrylic acid) (PAA, $\alpha = 0.5$) and would be expected as long as the concentration of the anionic sites attached to the polymer chains is in large excess over the concentration of the bolions. Similar series in which the PAA concentration was varied at a constant degree of neutralization of the polymeric acid showed that r is proportional to the concentration of the polyanions (see Table I), indicating that the chain molecules act as adsorption sites which are independent of each other. The dependence of r on the spacing of the cationic groups in the bolions is shown in Figure 2 for the binding to half-neutralized 0.02 N polyacids in the presence of 0.02 N NaBr. It is striking how the three polymeric acids differ from one another, with the isotactic PMA less efficient and the syndiotactic PMA more efficient than PAA in its binding of the bolaform counterions. Only with PAA does the binding clearly decrease with increasing separation of the charges of the bolions; with i-PMA the dependence on charge separation is very small and with s-PMA the affinity for the doubly charged cations actually increases slightly with increasing separation of their two charges. The behavior of PAA is the one to be expected on electrostatic grounds; with PMA it may be assumed that hydrophobic bonding is an additional factor and this would become more important as the length of the hydrocarbon chain between the two pyridinium residues

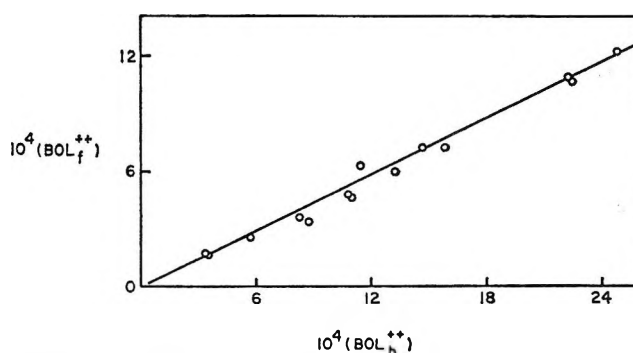


Figure 1. Equilibrium between bound and free P2 bolions in 0.01 N PAA at a degree of ionization $\alpha = 0.5$ and in the presence of 0.02 N NaBr.

(15) F. A. Bovey and G. V. D. Tiers, *J. Polymer Sci.*, **44**, 173 (1960).

(16) A. Katchalsky and H. Eisenberg, *ibid.*, **6**, 145 (1951).

(17) A. Young and T. R. Sweet, *Anal. Chem.*, **27**, 418 (1955).

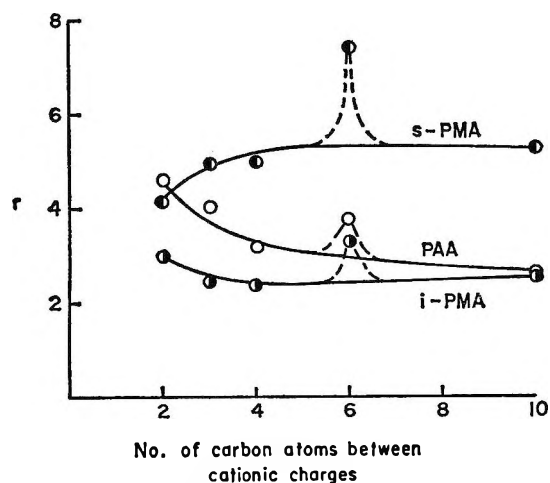


Figure 2. Dependence of the binding ratio r on the spacing of the cationic charges of bolions P2, P3, P4, PX, and P10. Polymeric acid concentration 0.02 N ; degree of ionization $\alpha = 0.5$; NaBr concentration 0.02 N .

is being extended. The dependence of the site-binding efficiency on the stereoisomerism of the chain is difficult to interpret. It should be noted, in any case, that the bolion PX, in which the spacing of the pyridinium residues is similar to that to be expected from 1,6-hexamethylenebispyridinium, is bound more tightly to all of the polyanions than expected on the basis of its charge separation. This may be accounted for by the rigidity of the PX structure, which reduces the loss of entropy when the two cationic centers are restrained to lie close to two ionized groups of the polyanions. The extent to which hydrophobic bonding contributes to the binding of PX may be assessed from results obtained with its singly charged analog Q. Under conditions comparable to those illustrated in Figure 2, the binding ratio r for Q is 0.38 with s-PMA and 0.26 with PAA.

It would be expected that an increase in the concentration of added sodium bromide would reduce the ex-

Table I: The Dependence of P2 Binding to Half-Neutralized PAA on the Normality of Carboxylate Groups Carried by the Polymer Acid (C_{Pa})

C_{NaBr}	C_{Pa}	r	r/C_{Pa}
0.02	0.02	8.03	401
0.02	0.01	4.58	458
0.02	0.005	2.27	454
0.04	0.02	3.29	164
0.04	0.01	1.55	155
0.04	0.005	0.80	160
0.06	0.02	1.02	51
0.06	0.01	0.80	80
0.06	0.005	0.40	80

tent of binding of the bispyridinium ions. The dependence of the binding ratio r on the total Na^+ concentration (from the neutralization of the polyacid and from the added salt) was found to be of a very simple form, with $r(Na^+)^2$ having a nearly constant value for any given polyacid, degree of neutralization, and bolion counterion. This generalization is illustrated in Table II on the binding of P2 and PX by the half-ionized polymeric acids. It suggests that the number of countercharges site-bound near the ionized groups of the polyion is independent of whether these charges belong to univalent ions or to bolions. The equilibrium of this process may, therefore, be represented by



We are representing here the bound sodium ion as $(Na_b^+)_2$ to emphasize that on binding of a bolion two Na^+ ions are released from site binding to the same macromolecule. We should note that in the process represented by eq 1 the charge of the polyion with the site-bound counterions remains unchanged. This conclusion is supported experimentally by the observation

Table II: Dependence of the Binding of P2 and PX by Half-Ionized 0.02 N Polymeric Acids on the Concentration of Na^+ Counterions

Bolion	Polymer	$(Na^+), N$	r	$10^4 r(Na^+)^2$	$10^4 r(Na_f^+)^2$
P2	PAA	0.03	4.58	41.2	28.6
		0.05	1.55	38.8	31.4
		0.07	0.80	39.2	33.8
P2	i-PMA	0.03	3.02	27.2	18.9
		0.05	0.88	22.0	17.8
		0.07	0.40	19.6	16.9
P2	s-PMA	0.03	4.15	37.4	25.9
		0.05	1.52	38.0	30.8
		0.07	0.73	35.8	30.8
PX	PAA	0.03	3.85	34.7	24.1
		0.05	1.32	33.0	26.7
		0.07	0.73	35.8	30.8
PX	i-PMA	0.03	3.34	30.1	20.9
		0.05	1.04	26.0	21.1
		0.07	0.53	26.0	22.4
PX	s-PMA	0.03	7.45	67.0	46.6
		0.05	3.03	75.7	61.2
		0.07	1.46	71.5	61.7

that addition of small amounts of bolion salts to partially ionized polycarboxylic acids does not lead to an appreciable drop of pH, as would be expected if bolion binding reduced the polyion charge and increased, in consequence, the acidity of the carboxyl groups. Since the number of Na^+ counterions bound to a polyanion appears to depend little on the concentration of

added uni-univalent electrolyte,¹⁸ r should be inversely proportional to $(Na_f^+)^2$, rather than the square of the total Na^+ concentration, and the last column of Table II lists values of $r(Na_f^+)^2$ based on the assumption that half of the charges carried by the half-ionized polymeric acids are associated with site-bound counterions.¹⁹ It may be noted that for a series involving P2 binding, $r(Na_f^+)^2$ varies within less than 20% for variations of r by factors between 5.7 and 7.5. For the binding of PX, a more nearly constant value is obtained for $r(Na^+)^2$.

The question now arises as to how the binding ratio depends on the density of anionic groups attached to the polyanion. We may divide the process represented in eq 1 into two stages as shown in Figure 3. In stage a, one end of the bolion is bound to a fixed charge of the polyion and a bound sodium ion is simultaneously released (not necessarily from the same site). The equilibrium of this stage should depend on the concentration of ionized groups attached to all of the polyions in the system, *i.e.*

$$(Bol^{2+b})'(Na_f^+)/ (Bol^{2+t})C_P\alpha = K_1 \quad (2)$$

where $(Bol^{2+b})'$ represents the concentration of bolions site-bound to a single polyion charge. However, once a bolion is attached at one end to a given polyion, the probability of step b depends only on conditions within the domain of that one polyion. The simplest assumption is to set the probability of step b proportional to the fraction α of ionized monomer residues. Since the second bolion charge has to compete with free sodium ions for the binding site, the equilibrium of this step should be of the form

$$(Bol^{2+b})''(Na_f^+)/ (Bol^{2+b})'\alpha = K_2 \quad (3)$$

where $(Bol^{2+b})''$ represents the concentration of doubly bound bolions. Assuming that substantially all bound bolions interact with two binding sites, the bolion binding ratio $r = (Bol^{2+b})/(Bol^{2+t})$ would be expected to depend on polyion concentration and ionization and on the concentration of free monovalent ions as predicted from

$$r = KC_P\alpha^2/(Na_f^+)^2 \quad (4)$$

The dependence of the binding ratio r on the degree of ionization α of the various polymeric acids was measured in a series of experiments in which the polymer concentration was varied inversely with α so as to keep the concentration of ionized carboxyl $C_P\alpha$ at a constant value. The results obtained in duplicate determinations of the dialysis equilibrium are listed in Table III. We may see that the behavior of the various systems investigated does not conform to the prediction

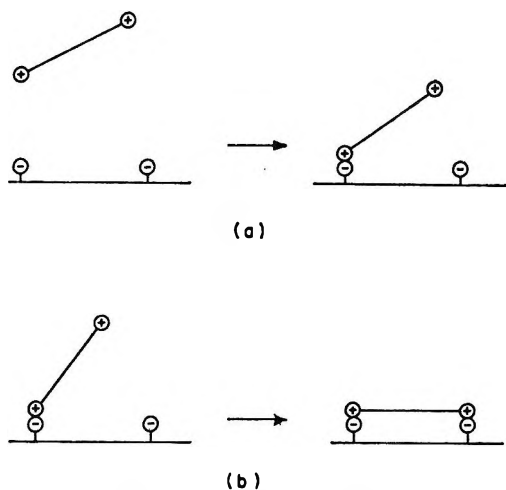


Figure 3. Schematic representation of the two stages in the binding of a bolion by a polyion.

of eq 4 but that the dependence of bolion binding on the degree of ionization of the polyion exhibits characteristic differences for the three polymeric acids. In the case of PAA, $r/C_P\alpha$ rises to a maximum at about $\alpha =$

Table III: Binding of P2 to Polymeric Acids as a Function of the Degree of Ionization of the Polyion

Polymeric acid	$10^2 C_P$	α	$r/C_P\alpha$		
			$(Na^+) = 0.03 N$	$(Na^+) = 0.05 N$	$(Na^+) = 0.07 N$
PAA	10.00	0.10	182 ± 2	106 ± 2	
	4.00	0.25	235 ± 13	92 ± 1	50 ± 1
	2.00	0.50	458 ± 9	154 ± 12	79 ± 2
	1.66	0.60	523 ± 37	179 ± 8	
	1.33	0.75	462 ± 9	143 ± 5	67 ± 5
i-PMA	4.00	0.25	125 ± 1	9 ± 1	3 ± 3
	2.00	0.50	303 ± 6	88 ± 0	40 ± 1
	1.33	0.75	360 ± 39	143 ± 5	59 ± 7
s-PMA	4.00	0.25	536 ± 9	223 ± 2	117 ± 4
	2.00	0.50	415 ± 16	151 ± 9	74 ± 1
	1.33	0.75	558 ± 7	172 ± 12	75 ± 5

0.6 and decreases somewhat at higher degrees of ionization. With i-PMA, the bolion is bound extremely weakly at $\alpha = 0.25$, particularly at the higher concentrations of simple electrolyte. This may be related to the low solvation of the polymer which is water insoluble in the un-ionized state. Finally, with s-PMA, $r/C_P\alpha$ changes little as the degree of ionization is changed, with possibly a slight tendency for $r/C_P\alpha$ to

(18) Z. Alexandrowicz, *J. Polymer Sci.*, **43**, 337 (1960); **56**, 115 (1962).

(19) J. R. Huizenga, P. F. Grieger, and F. T. Wall, *J. Am. Chem. Soc.*, **72**, 4228 (1950).

pass through a shallow minimum around $\alpha = 0.5$. We see then that (with the exception of i-PMA at low ionization) the bolion binding increases generally more slowly than in proportion to α^2 . The complicated behavior observed may reflect not only conformational transitions of the polymeric acids²⁰ but also the dependence of the binding of univalent counterions on the degree of ionization.

It is of interest to compare the binding of the bolaform cations discussed above with the chelation of a divalent cation such as Mg^{2+} . The characteristics of Mg^{2+} binding were found to have a surprisingly low sensitivity to the concentration of added sodium bromide. For instance, with 0.02 *N* half-ionized PAA, the binding ratio r was 13.6, 11.1, and 7.3 for concentrations of Na^+ counterions of 0.03, 0.05, and 0.07 *N*, respectively. The characteristic ratios $r/C_P\alpha$ for the binding of Mg^{2+} to isotactic and syndiotactic PMA at various degrees of ionization are listed in Table IV. It was found that $r/C_P\alpha$ remains constant for i-PMA as α is increased from 0.25 to 0.50, but drops off for $\alpha = 0.75$. For the syndiotactic polymer, $r/C_P\alpha$ is doubled as α rises from 0.25 to 0.50, but decreases again for $\alpha = 0.75$. At the higher degrees of ionization, the magnesium ion is bound much more strongly to the syndiotactic polyacid. It was pointed out previously that the affinity of i-PMA and s-PMA for Mg^{2+} is thus in an order opposite to that found for the affinity of these two polymers for Cu^{2+} .²¹ This specificity seems to indicate that neighboring carboxylate groups along the polymer chain,

with a well-defined mutual spatial relationship, are involved in chelate formation.

The relatively small dependence of the binding of Mg^{2+} by PAA on the concentration of simple electrolyte deserves some comment. The pH of half-neutralized 0.02 *N* PAA was found to be 5.9 and 5.5 in the presence of 0.02 and 0.06 *N* NaBr, respectively. Thus, the increase in the ionic strength leads to an increase of the apparent ionization constant of the polymeric acid by a factor of 2.5. It is well understood that this effect is a consequence of the reduction of the excess electrostatic free energy associated with the removal of a hydrogen ion away from the field of the polyanion.²² Since the Mg^{2+} ion bears a double charge, the association constant of this ion with half-ionized PAA might be expected to be reduced by a factor of $(2.5)^2 = 6.25$ as the NaBr concentration rises from 0.02 to 0.06 *N*. This prediction is not at all in accord with the experimental results, which gave a reduction of r by a factor of less than 2. We should note that the argument based on considerations of the electrostatic free energy assumes implicitly that the binding of an Mg^{2+} ion by PAA reduced the negative charge of the polyanion by 2 units. It neglects the possibility that binding of doubly charged cations may be accompanied by the release of site-bound univalent cations.²³ It is apparent that further progress in the understanding of chelation equilibria involving polyelectrolytes will require experimental evidence bearing on this point.

Acknowledgment. We are grateful to Professor E. M. Loebl for helpful discussions of this work.

Table IV: Binding of Mg^{2+} by Isotactic and Syndiotactic PMA in the Presence of 0.04 *N* NaBr

α	$10^2 C_P$	$r/C_P\alpha$	
		i-PMA	s-PMA
0.25	4.00	1370 \pm 100	1510 \pm 110
0.50	2.00	1360 \pm 60	3200 \pm 180
0.75	1.33	910 \pm 70	2350 \pm 350

(20) M. Nagasawa, T. Murase, and K. Kondo, *J. Phys. Chem.*, **69**, 4005 (1965); G. Barone, V. Crescenzi, and F. Quadrioglio, *Ric. Sci.* **35**, (II-A), 1069 (1965).

(21) J. J. O'Neill, E. M. Loebl, A. Y. Kandarian, and H. Morawetz, *J. Polymer Sci.*, **A3**, 4201 (1965).

(22) A. Katchalsky and S. Lifson, *ibid.*, **16**, 409 (1953).

(23) Under the experimental conditions used in this study, the number of hydrogen ions released as a consequence of Mg^{2+} binding is negligible compared to the number of Mg^{2+} ions bound.

NOTES

Nitrogen Adsorption on Iridium and Rhodium¹

by V. J. Mimeault and Robert S. Hansen

*Institute for Atomic Research and Department of Chemistry,
Iowa State University, Ames, Iowa (Received February 24, 1966)*

According to Bond,² nitrogen is not chemisorbed on group VIII-B metals. We have found this to be the case for iridium and rhodium by the absence of a pressure increase on heating a sample filament (Ir or Rh) dosed with nitrogen at 300°K. However, we have found some evidence that nitrogen adsorption does occur on iridium and rhodium if the nitrogen is thermally activated. The source of this thermal energy is the hot tungsten filaments present in conventional ionization gauges. This note is a summary of our findings.

The vacuum system and experimental procedure are described elsewhere.³ Nitrogen gas was leaked into the vacuum system until the steady-state pressure was 4×10^{-7} torr. On flashing the filament, either iridium or rhodium, the total pressure increase was measured with a Bayard-Alpert ionization gauge containing a thoriated tungsten filament operating at 0.4-ma emission, and the partial pressure increase was measured with a small bakeable mass spectrometer. The residual gases present in the background were less than 0.5% of the total nitrogen pressure. It was observed that under these conditions, no adsorption of nitrogen occurred as indicated by the absence of a pressure increase on flashing after dosing the filament for 15 min at 300°K. At this pressure (4×10^{-7} torr), enough molecules strike the surface to form a monolayer in ~ 6 sec (if the sticking probability is unity). Since the flash filament technique is capable of detecting 0.02 monolayer, the absence of a pressure increase on flashing implies that the amount of adsorption was negligible.

Nitrogen adsorption can be made to occur on iridium or rhodium if the tungsten filaments in the Nottingham ion gauge⁴ are operated at a temperature T_f greater than 2000°K. Since no direct line of sight exists between the tungsten filaments and the iridium or rhodium filament, a particle must make many collisions with the glass walls of the vacuum system in traveling from the tungsten filaments to the sample filament. The amount of nitrogen desorbed is proportional to the dosing interval for fixed T_f , and the proportionality constant increases strongly with T_f (Figure 1). The adsorbing iridium or rhodium filament was held at

300°K during dosing. A plot of the log of the amount of nitrogen desorbed for fixed dosing period (this amount is proportional to the adsorption rate constant) against $1/T_f$ is linear as shown in Figure 2. The slope of this plot corresponds to an activation energy of 58 kcal/mole, which is approximately one-fourth the dissociation energy of molecular nitrogen (226 kcal/mole).

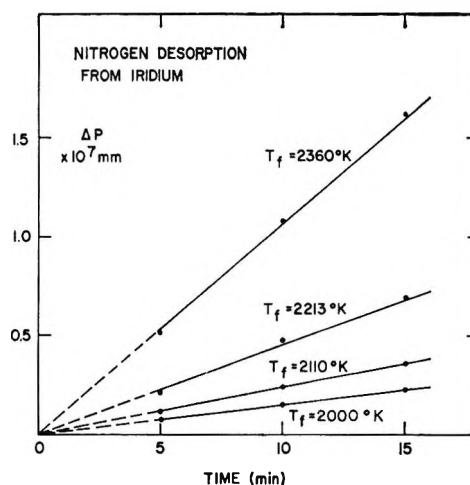


Figure 1. Desorption of nitrogen from iridium as a function of dosing time and temperature of the ion gauge filament.

During the long adsorption time, there was appreciable adsorption of CO from the ambient background impurities. The low-temperature (short time) mass 28 peak in Figure 3 is due to carbon monoxide, as is shown by the coincident peak in the mass 12 fragment. Figure 3 also shows that the high-temperature peak consists of $^{14}\text{N}_2$, $^{14}\text{N}^{15}\text{N}$, and $^{15}\text{N}_2$ in substantially statistical ratio although the dosing mixture contained only $^{14}\text{N}_2$ and $^{15}\text{N}_2$. Hence, substantially complete scrambling of isotopes has occurred in the adsorption-desorption process. This strongly indicates that the nitrogen has been adsorbed as independent atoms mobile on the surface at a temperature below the desorption temperature. The high desorption temperature ($\sim 1000^\circ\text{K}$) indicates strong binding of the nitrogen to the surface which is also consistent with atomic adsorption.

The adsorption of nitrogen on iridium and rhodium can be explained by a model based on the dissociation

(1) Work was performed at the Ames Laboratory of the U. S. Atomic Energy Commission. Contribution No. 186z.

(2) G. C. Bond, "Catalysis by Metals," Academic Press, New York, N. Y., 1962.

(3) V. J. Mimeault and R. S. Hansen, *J. Chem. Phys.*, in press.

(4) W. B. Nottingham, *Natl. Symp. Vacuum Technol. Trans.*, 1, 76 (1954).

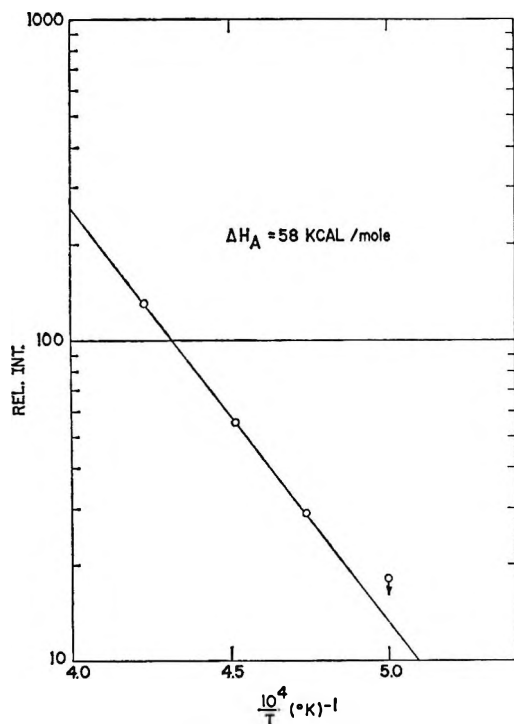


Figure 2. Dependence of the rate of adsorption of activated nitrogen on iridium on the temperature of the activating source.

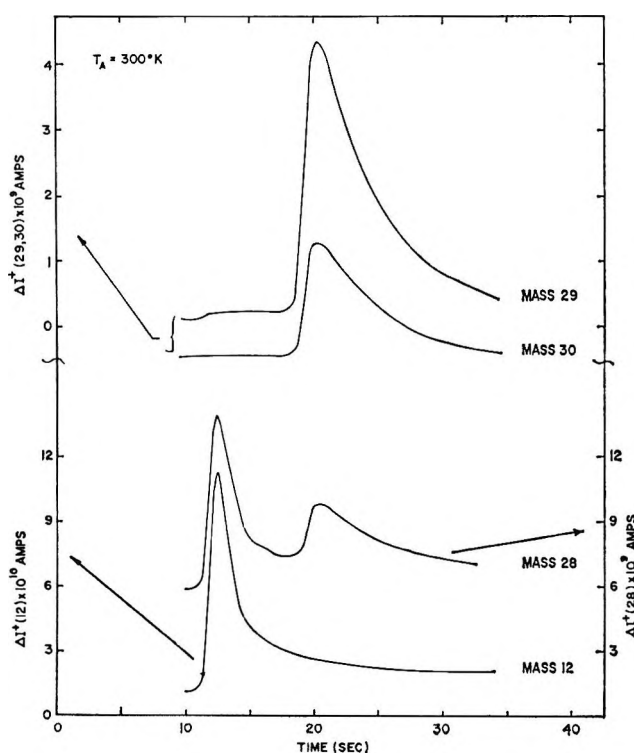
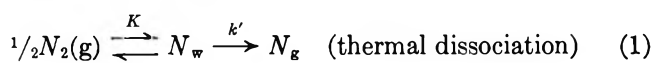


Figure 3. Desorption of nitrogen isotopes from rhodium dosed at 300°K with a mixture of $^{14}\text{N}_2$ and $^{16}\text{N}_2$. The curves are translated vertically for clarity. The arrows in each case relate the curve to the appropriate scale.

of molecular nitrogen on the hot tungsten filament, with the atomic nitrogen produced largely recombined catalytically on the glass walls so that a steady-state atomic nitrogen concentration is maintained by the balance of thermal dissociation and catalytic recombination. The rate of adsorption on the rhodium or iridium filament is then proportional to the steady-state concentration of atomic nitrogen. Let N_g , N_w , and N_G be the nitrogen atom concentrations (volume or surface as appropriate) in the gas phase and on the tungsten and glass surfaces, respectively, and let $N_2(\text{g})$ be the gas phase concentration of molecular nitrogen. The model is summarized in eq 1-3



plus the steady-state assumption that N_g is produced by reaction 1 and consumed by reactions 2 and 3 at the same rate.

The rate of production of atomic nitrogen due to the hot filament is

$$\left(\frac{dN_g}{dt}\right)_i = k'N_w = k'KP_{N_2}^{1/2} = kP_{N_2}^{1/2} = Ae^{-\Delta H_1^\ddagger/RT}P_{N_2}^{1/2} \quad (4)$$

where ΔH^\ddagger is the effective activation energy and A is the preexponential term for the over-all reaction 1; presuming the transition state for the second reaction is very nearly desorbed atomic nitrogen, as seems likely, $\Delta H_1^\ddagger = 113$ kcal, *i.e.*, half the dissociation energy of nitrogen.

From reactions 2 and 3 we obtain for the rate of recombination of atomic nitrogen on the glass

$$-\left(\frac{dN_g}{dt}\right)_G = k''N_G^2 = k''(K'N_g)^2 \quad (5)$$

For steady state, the production of atomic nitrogen according to eq 4 must be balanced by its consumption according to eq 5, *i.e.*

$$kP_{N_2}^{1/2} = k''(K'N_g)^2 \quad (6)$$

or

$$N_g = \left(\frac{k}{k''}\right)^{1/2} (K')^{-1}P_{N_2}^{1/4} \quad (7)$$

The rate of adsorption is assumed proportional to N_g . Of the rate constants on the right side of eq 7, only k changes as T_i is varied. The effective activation energy for atomic nitrogen adsorption should hence be half

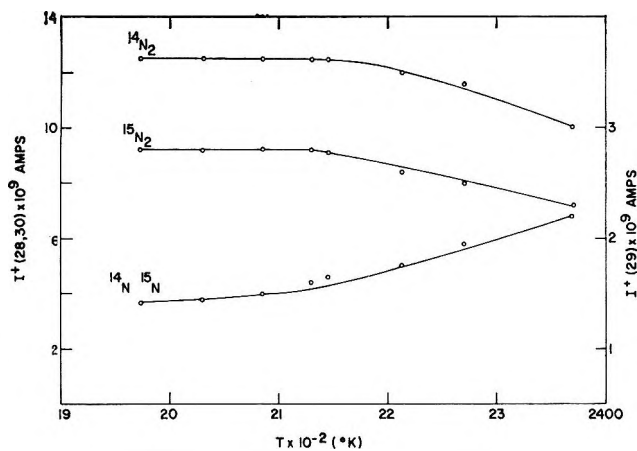


Figure 4. Equilibrium distribution of the nitrogen isotopes in the ambient of a flow system as a function of the temperature of the ion gauge filament.

that of k or 56.5 kcal, which compares well with the 58 kcal observed.

The ambient distribution of nitrogen isotopes is shown as a function of ion gauge filament temperature in Figure 4. The increase in $^{14}\text{N}^{15}\text{N}$ and decrease in $^{14}\text{N}_2$ and $^{15}\text{N}_2$ (the input gases) above 2100°K is apparent; part of the decrease is attributed to pumping by the glass walls.

Catalysis over Supported Metals. VI. The Application of Magnetic Studies in the Interpretation of the Catalytic Properties of Nickel

by J. L. Carter and J. H. Sinfelt

Esso Research and Engineering Company, Linden, New Jersey
(Received March 8, 1966)

In previously reported studies from this laboratory, it was shown that the catalytic activity of nickel for ethane hydrogenolysis varied markedly when the nickel was supported on different oxide carriers.^{1,2} From hydrogen chemisorption measurements it was concluded that the variations in nickel surface areas on the different supports were small compared to the variations in catalytic activity. In other words, the specific catalytic activity of the nickel varied with the support. It was also shown that the specific catalytic activity of nickel on a given support varied significantly with the nickel concentration. In the interpretation

of these results, it is important to consider factors such as differences in the crystallite size and reducibility of the nickel in the catalysts. Useful information of this type can be obtained from magnetic studies.³⁻⁸ Therefore, it was decided to obtain magnetic data on these particular catalysts, which include nickel supported on alumina, silica, and silica-alumina at concentrations of 1 and 10% nickel. In this report, the catalytic properties of these samples are considered in the light of the information obtained from the magnetic studies.

Experimental Section

Apparatus and Procedure. The Faraday method was used to determine the magnetic properties of the supported nickel catalysts. The apparatus is similar to others described in the literature.^{9,10} The sample, in a quartz bucket, was suspended from a Cahn electrobalance which was used to measure the force on the sample. A Varian 4-in. magnet with "constant gradient" pole pieces and a 2-in. gap provided magnetic fields up to 6500 gauss. The vacuum system was arranged so that samples could be reduced *in situ* in flowing hydrogen. Pressures of 10^{-6} torr were readily attainable in the apparatus. The standard procedure included reduction of the catalyst overnight at 370° in a hydrogen flow of 500 cc/min. The sample was then outgassed at the same temperature for 30 min. The magnetic measurements were made either *in vacuo* or in helium. If the measurements were made *in vacuo*, the approach to liquid nitrogen temperature was very slow, with a temperature of 85 to 90°K being the practical lower limit. In most cases a small amount of helium was added to facilitate the cooling to 80°K. The catalysts used in these studies have been described previously.^{1,2}

Results

Typical data on the effect of field strength on specific

- (1) W. F. Taylor, D. J. C. Yates, and J. H. Sinfelt, *J. Phys. Chem.*, **68**, 2962 (1964).
- (2) W. F. Taylor, J. H. Sinfelt, and D. J. C. Yates, *ibid.*, **69**, 3857 (1965).
- (3) P. W. Selwood in "Catalysis," Vol. I, Reinhold Publishing Corp., New York, N. Y., 1954, p 353.
- (4) P. W. Selwood, "Adsorption and Collective Paramagnetism," Academic Press Inc., New York, N. Y., 1962.
- (5) P. W. Selwood, T. R. Phillips, and S. Adler, *J. Am. Chem. Soc.*, **76**, 2281 (1954).
- (6) P. W. Selwood, S. Adler, and T. R. Phillips, *ibid.*, **77**, 1462 (1955).
- (7) P. W. Selwood, *ibid.*, **78**, 3893 (1956).
- (8) D. Reinen and P. W. Selwood, *J. Catalysis*, **2**, 109 (1963).
- (9) P. W. Selwood, "Magnetochemistry," 2nd ed, Interscience Publishers, Inc., New York, N. Y., 1956, pp 11-13.
- (10) P. E. Jacobson and P. W. Selwood, *J. Am. Chem. Soc.*, **76**, 2641 (1954).

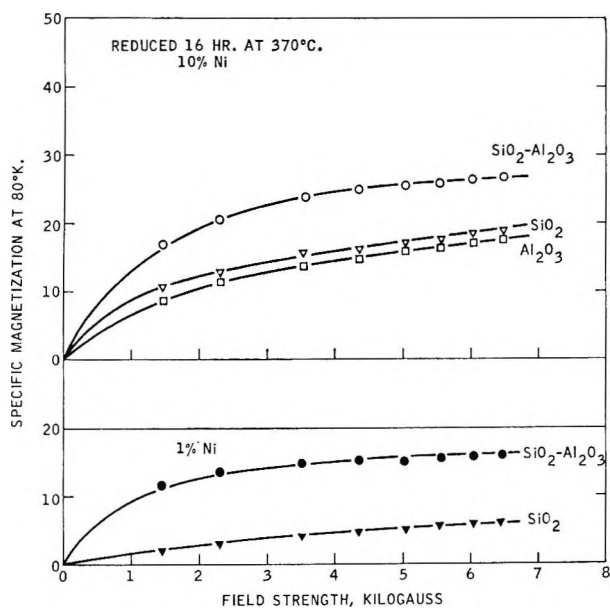


Figure 1. Specific magnetization of nickel on different supports.

magnetization at 80°K are given in Figures 1 and 2. In Figure 1, the data were obtained on the catalysts after reduction in hydrogen for 16 hr at 370°, followed by evacuation at 370°. The specific magnetization increases with increasing field strength and is higher when the nickel is supported on silica-alumina than when it is supported on alumina or silica. Furthermore, for a given support, the specific magnetization increases with increasing nickel concentration. It should be noted that the specific magnetization does not approach that of bulk nickel for any of the nickel catalysts shown. At 80°K, bulk nickel has a specific magnetization of 57.¹¹ In the interpretation of these results, two alternative explanations might be advanced: (a) the nickel catalysts are not fully reduced and the extent of reduction varies with the support and with nickel concentration, or (b) a significant fraction of the nickel crystallites is too small to exhibit ferromagnetism. To decide between the two alternative explanations, it is clearly necessary to do an experiment in which it is possible to separate the effects of reducibility and crystallite size. One way to do this is to heat the catalysts in a nonreducing atmosphere to induce growth of the metal crystallites. If such treatment increases the magnetization to a value approaching that of bulk nickel, then one can conclude that the catalyst was well reduced and that the low magnetization of the original catalyst sample was due to crystallite size effects.

To resolve this point, the samples were sintered under vacuum for 15 min at 800°, and magnetization

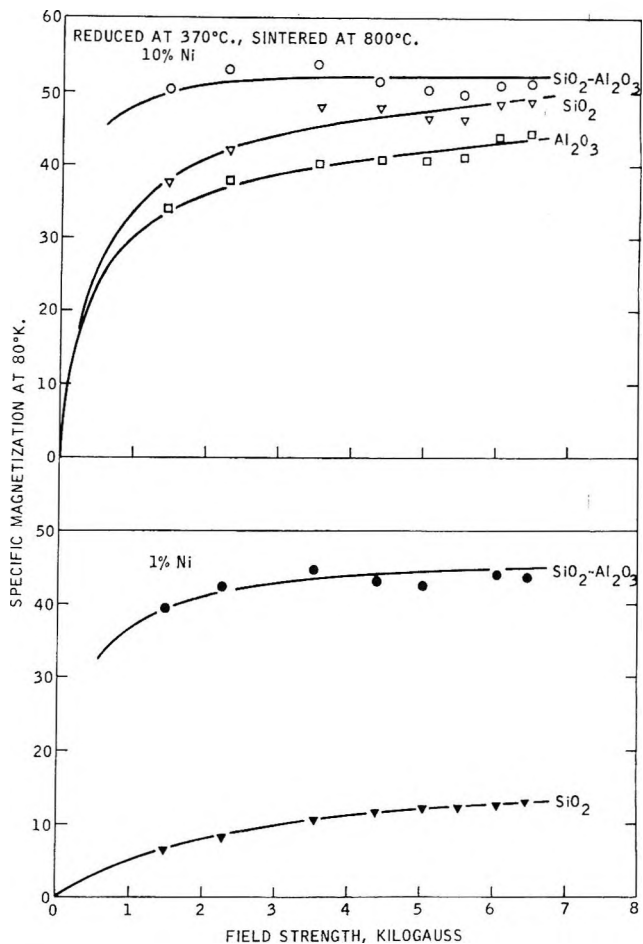


Figure 2. Effect of sintering on the specific magnetization of nickel on various supports. All samples were sintered under vacuum for 15 min at 800° after reduction in hydrogen at 370°.

data at 80°K were then obtained. The results are shown in Figure 2. There is clearly a large increase in magnetization upon sintering. The values for all of the 10% nickel catalysts and for the 1% Ni on SiO₂-Al₂O₃ catalyst approach the value for bulk nickel. The 1% nickel on SiO₂ is extremely difficult to sinter, however, and the magnetization is still far below that of bulk nickel. In a separate experiment the 1% Ni on SiO₂ catalyst was heated at a still higher temperature, 1000°, under vacuum, with the result that the specific magnetization increased to 35.7 at a field of 6450 gauss. In general, it is concluded that the nickel in these catalysts is well reduced after treatment with flowing hydrogen for 16 hr at 370°. The low magnetizations observed with the freshly reduced samples are attributed to crystallite size effects characteristic

(11) "American Institute of Physics Handbook," 2nd ed, McGraw-Hill Book Co., Inc., New York, N. Y., 1963, Section 5, p 170.

of highly dispersed metals. In the case of the 1% Ni on SiO₂ catalyst, the evidence is less convincing than for the other catalysts. However, a measurement on the freshly reduced, nonsintered sample, in which the sample container was surrounded by liquid helium, showed a much higher specific magnetization than was observed at 80°K. The estimated temperature of the sample was 38°K rather than 4.2°K, owing to poor heat-transfer conditions. The specific magnetization was 30.3 at a field of 6450 gauss, compared to a value of 6.2 at 80°K. A reasonable extrapolation of the data to 0°K would give a saturation magnetization close to that of bulk nickel. This further strengthens the conclusion that the nickel is well reduced and that the low magnetization at higher temperature is a consequence of the high degree of dispersion of the nickel.

A quantitative estimate of crystallite size can be obtained from the magnetic data by using an adaptation of a low-field approximation of the Langevin theory for the magnetization of an assembly of particles, as discussed by Selwood.¹² According to this theory, the average crystallite volume \bar{v}^2/\bar{v} is given by the relation

$$\frac{\bar{v}^2}{\bar{v}} = \frac{3kT}{I_{sp}H} \left(\frac{M}{M_s} \right) \quad (1)$$

where k is Boltzmann's constant, T is the absolute temperature, I_{sp} is the spontaneous magnetization, H is the field strength, and M/M_s is the ratio of the magnetization to the true saturation magnetization. The ratio M/M_s can be replaced by the corresponding ratio of specific magnetizations σ/σ_s . Assuming that the spontaneous magnetization of very small nickel crystallites is the same as that of bulk nickel (505 gauss at 80°K) and that σ_s is also the same as for bulk nickel (57.5), we can then calculate average crystallite volumes for the various catalysts from values of the quantity σ/H at sufficiently low fields. The crystallite size is then determined by taking the cube root of the volume so obtained. The quantity σ/H can be obtained from the initial slope of a plot of σ vs. H , since eq 1 applies at low fields where the magnetization is small compared to the saturation value. For the nonsintered samples after reduction and evacuation at 370°, crystallite sizes obtained from the magnetization curves in Figure 1 are summarized in Table I. The crystallite sizes are in the approximate range of 10–30 Å, and this is consistent with the observation that the crystallites are too small to be detected by X-ray diffraction line broadening (<40 Å). The crystallite sizes are larger on silica-alumina than on alumina or silica, and in the case of the 1% Ni on SiO₂ catalyst

the crystallites are much smaller than for the other samples. Although previous hydrogen chemisorption measurements² did not indicate an improvement in the dispersion of the nickel when the concentration of the nickel was decreased from 10 to 1%, the data on the

Table I: Summary of Data on Crystallite Size and Catalytic Activity of Nickel on Various Oxide Supports

Catalyst	Ni crystallite size, Å	Specific activity for ethane hydrogenolysis ^a
Ni on SiO ₂		
1% Ni	12	11
10% Ni	24	500
Ni on Al ₂ O ₃		
10% Ni	23	260
Ni on SiO ₂ -Al ₂ O ₃		
1% Ni	26	<0.08
10% Ni	29	9.5

^a Micromoles of ethane converted to methane per hour per square meter of nickel; conditions: 205°, ethane pressure 0.030 atm, hydrogen pressure 0.20 atm. For details of the catalytic studies, see ref 1 and 2.

magnetic properties of the nickel on silica catalysts leave little doubt that the nickel is dispersed more highly at the lower concentration. It is possible that the adsorption measurements on the low-concentration samples were not very accurate owing to the low amounts of hydrogen adsorbed.

Discussion

Previously reported results on ethane hydrogenolysis over the nickel catalysts are summarized in Table I for discussion purposes. In considering possible explanations for the differences in catalytic activity of nickel on the different supports, or as a function of nickel concentration, one might speculate that differences in the extent of reduction of the nickel could be responsible for the effect. However, the results of the present investigation indicate that the nickel on the various oxide supports is well reduced after treatment in flowing hydrogen for 16 hr at 370°, at least for the 10% nickel catalysts and for the 1% Ni on SiO₂-Al₂O₃. Since these reduction conditions were employed throughout, the variation in catalytic activity of the nickel on the various supports is not attributed to marked differences in the extent of reduction.

In pursuing an explanation for the effect of the support on the catalytic properties of nickel, it might be

(12) See ref 4, p 44.

suggested that the effect is associated with differences in the size of the nickel crystallites on the different supports. It is emphasized that such an explanation would require an influence of crystallite size over and above an effect on the extent of metal surface area, since the effect of the latter is accounted for in the determination of specific catalytic activity. Such an effect of crystallite size on specific activity may well exist and may account, in part, for the observed effect of the support. According to this line of reasoning, the higher catalytic activity and greater dispersion of nickel on silica or alumina as compared to silica-alumina indicate that the intrinsic catalytic activity is greater for the smaller crystallites. However, the catalytic data on the effect of nickel concentration indicate just the opposite, since increasing the nickel concentration increases crystallite size and activity correspondingly. Thus, one does not obtain a completely consistent explanation on the basis of crystallite size effects alone. The possibility of an optimum crystallite size for catalytic activity has been considered, but it would be difficult to establish such an effect from the available data.

The results of the present study indicate that the influence of the support on the catalytic properties of nickel is a more complex effect than one of gross differences in the reducibility of the metal or of crystallite size. The true nature of the effect remains to be seen. It is to be noted that the effect is particularly important at low metal concentrations.

van der Waals Volumes and Radii of Metals in Covalent Compounds

by A. Bondi

Shell Development Company, Emeryville, California
(Received April 19, 1966)

In an earlier paper,¹ an attempt was made to estimate van der Waals radii of metallic atoms. Additional consistent data could not be obtained from X-ray diffraction patterns of organometallic compounds. Yet, the increasing interest in organometallic compounds makes it desirable to correlate their properties within an existing body of property correlations. Hence, those van der Waals volumes of several compounds have been calculated which yield the correct number of external degrees of freedom ($3c$) per molecule when

linked with the known density and heat of vaporization data.¹

With most metal alkyl compounds, such as dimethyl cadmium, free rotation of the alkyl group around the metal-carbon bond can be assumed, so that, for example, for CdMe_2 $3c \approx 7$, etc. The van der Waals volume increments and radii of various metallic elements that are compatible with that requirement are listed in Table I. It is noteworthy that these V_w increments are of the same order as the electronic polarizability $[R]_\infty$ (and as the atomic volume of the element in its metallic state), a well-known result of classical physics for the case of conducting spheres.

Table I: van der Waals Volumes and Radii of Several Metals Derived from Metal Alkyl Data^a

Compd	E° , kcal/ mole	Θ_L , °K	$3c$	X	$V_w(X)$, cm ³ / mole	$r_w(X)$, Å	$[R]_\infty$, cm ³ / mole
ZnMe ₂	7.78	378	6.2	Zn	8.93	1.39	8.9
ZnEt ₂	10.10	445	6.9	Zn	8.93		
CdMe ₂	9.57	443	6.5	Cd	12.46	1.62	12.7
HgMe ₂	8.91	420	6.4	Hg	13.30	1.70	13.8
PbMe ₄	9.79	482	6.1	Pb	17.8		17.9

^a E° is the energy of vaporization at that temperature at which the ratio of molal volume to van der Waals volume (V/V_w) = 1.70. Θ_L is the characteristic temperature of liquid = $E^\circ/5cR$, determined experimentally as $1.535 \times$ (temperature (°K) at which $V/V_w = 1.80$). r_w is the van der Waals radius. V_w is the van der Waals volume. $[R]_\infty$ is the molar refractivity. References to the definitions and physical meaning of the first four items are given in ref 1.

The proximity of the V_w increments to $[R]_\infty$ is somewhat fortuitous because the increments were calculated for connection with carbon and would have been somewhat (but not very) different had they been calculated for combinations with other elements. The primary result of this investigation is the suggestion that the readily available Lorentz-Lorenz refractivity $[R]_\infty$ of metals² can be used as a starting point for the estimation of V_w and of r_w of metals in metal organic compounds.

Should the indicated relation be valid for metal atoms generally, it would mean that the electron density of metal atoms decreases far more steeply with distance outward from the point of maximum electron density³ than is the case with the atoms of

(1) A. Bondi, *J. Phys. Chem.*, **68**, 441 (1964).

(2) S. S. Batsanov, "Refractometry and Crystal Structure," Consultants Bureau, New York, N. Y., 1961.

(3) J. C. Slater, "Quantum Theory of Molecules and Solids," Vol. II, McGraw-Hill Book Co., Inc., New York, N. Y., 1965, p 106 ff.

nonmetallic elements. In view of the comparatively lower ionization potentials of the metallic elements, this is a rather unexpected result worthy of further investigation.

Studies on Solutions of High Dielectric Constant.

VIII. The Cationic Transport Numbers of Potassium Bromide in N-Methylformamide at Different Temperatures and Concentrations¹

by Ram Gopal and O. N. Bhatnagar²

Department of Chemistry, Lucknow University,
Lucknow, India (Received February 7, 1966)

In view of the lack of the transport number data of ions in N-methylformamide, it was considered desirable to extend the previous work^{3,4} on the determination of the transport numbers to solutions in N-methylformamide (NMF) in order to evaluate the limiting ionic mobilities from the existing electrolytic conductance data and also throw some light on the ion-solvent interaction in this solvent of very high dielectric constant (ϵ 182.4 at 25°).^{4a} With this aim in view, the cationic transport numbers of KBr in NMF, at different temperatures and concentrations, have been determined and are reported in the present communication.

Experimental Section

Potassium bromide was found to be an appropriate electrolyte on account of its appreciable solubility in NMF so that the transport numbers could be determined at the significantly different concentrations. The A.R. grade KBr was recrystallized from conductivity water, thoroughly dried in an electric oven at 110°, and was used for preparing the solutions.

The NMF of specific conductance 10^{-4} mho was dried over freshly ignited quicklime and distilled twice under reduced pressure. The process of drying, distilling, and collecting the middle fraction for redistillation was repeated until the conductance of the sample was reduced to about 10^{-6} mho. The sample of NMF thus obtained was kept in an amber bottle and stored in the dry nitrogen box. The sample was used for preparing the solutions soon afterward as the solvent appeared to be slightly more unstable than the other solvents of this family used earlier.^{3,4} However, the variation of conductance with time was found to be very little and was not expected to affect the results on

the transport numbers at ordinary temperatures. All of the solvent transfers were made in the dry nitrogen box.

The transport number cell was similar to that used in formamide³ and N-methylacetamide⁴ solutions. The cathode of the cell was a silver bromide electrode and was prepared as described elsewhere.⁴ The anode was a silver wire wound in the form of a spiral of about 4–5-mm diameter and 7–8 cm in length. The solution of any desired concentration was prepared in the manner described earlier and all possible precautions, given in detail in the previous communications,^{3,4} to keep away the atmospheric moisture while preparing the solutions and during the course of experiments, were taken. The experimental results are summarized in Table I.

Table I: Cationic Transport Numbers of Potassium Bromide in N-Methylformamide

Concn. <i>M</i>	Transport number, t_+			
	15°	25°	35°	45°
0.00	0.4945	0.5080	0.5210	0.5290 ^a
0.05	0.4909	0.5048	0.5184	0.5288
0.10	0.4881	0.5037	0.5169	0.5257
0.20	0.4804	0.4980	0.5119	0.5210
0.25	0.4765	0.4953	0.5097	0.5148
0.30	0.4723	0.4931	0.5084	0.5130

^a From the graph by interpolation.

From the transport numbers given in Table I, the limiting transport numbers, t_+^0 , of potassium ion at different temperatures were evaluated by using the Longworth procedure.⁵ The values of the various terms involved in calculating the Longworth function were as follows. Limiting equivalent conductivities of KBr at 15 and 25° were 36.51 and 43.69, as given by French and Glover,⁶ while those at 35 and 45° were 53.00 and 60.75 and were determined experimen-

(1) Work supported by the Council of Scientific and Industrial Research (India).

(2) CSIR Junior Research Fellow.

(3) R. Gopal and O. N. Bhatnagar, *J. Phys. Chem.*, **68**, 3892 (1964).

(4) R. Gopal and O. N. Bhatnagar, *ibid.*, **69**, 2382 (1965).

(4a) NOTE ADDED IN PROOF. G. P. Johari and P. H. Tewari [*ibid.*, **70**, 197 (1966)] have published the cationic transport numbers of KCl in formamide and in NMA without discussing and referring to the data given in ref 3 and 4. It is interesting to note that the "ever-vigilant" refereeing staff of the *Journal of Physical Chemistry* appears to have failed to draw the authors' attention to the already existing detailed investigations^{3,4} of such a recent publication.

(5) L. G. Longworth, *J. Am. Chem. Soc.*, **54**, 2741 (1932).

(6) C. M. French and K. H. Glover, *Trans. Faraday Soc.*, **51**, 1418 (1955).

tally by the usual procedure. The dielectric constants were ϵ_{15° 200.1, ϵ_{25° 182.4, ϵ_{35° 174.3, and ϵ_{45° 167.1 at the temperatures indicated and were those reported by Leader and Gormley.⁷ The values of viscosities at the different temperatures were $\eta_{15^\circ} = 0.0199$, $\eta_{25^\circ} = 0.0165$, $\eta_{35^\circ} = 0.0142$, and $\eta_{45^\circ} = 0.0123$ poise.^{6,8} The values of the limiting transport numbers, t_+ , of K^+ , at various temperatures, obtained from the plot of the Longworth function against concentration, are also given in Table I under the concentration heading 0.00 *M*.

Results and Discussion

As can be seen from Table I, the variations in the transport number, t_+ , of K ion in *N*-methylformamide are very much similar to those in formamide³ and in *N*-methylacetamide;⁴ *i.e.*, t_+ decreases with increase in concentration and increases with increase in temperature. The limiting transport number of potassium ion, *i.e.*, $t_{+(K^+)}$, increases from 0.4945 at 15° to 5290 at 45°. This behavior is opposite to that in aqueous solutions in which $t_{+(K^+)}$ decreases slightly with rise in temperature. Recently, Gill⁹ has reported similar behavior of the cationic transport number of KNO_3 in liquid ammonia in which $t_{+(K^+)}$ has been found to decrease with rise in temperature in the range -65 to -45°, although $t_{+(Na^+)}$, $t_{+(Li^+)}$, and $t_{+(NH_4^+)}$ increase with rise in temperature as $t_{+(K^+)}$ (KBr) does in *N*-methylformamide.

It may be noted that $t_{+(K^+)}$ increases beyond 0.5 with rise in temperature. This is a little unusual although such values of the transport number have been reported in the literature.¹⁰

Ionic Mobilities

The limiting cationic transport numbers at different temperatures can be used to calculate the ionic mobilities from the available electrolytic conductance data⁶ in this solvent and making use of the usual Kohlrausch law of the independent migration of ions. The ionic conductivities at infinite dilution of some ions thus obtained are given in Table II.

Since no ionic conductance data are available in the literature, it is not possible to verify the values given in Table II. However, they seem to be reasonable if they are compared with the corresponding values in formamide and in *N*-methylacetamide. Since the tetrahedral structure present in water is missing in these solvents, the structure-breaking effect of the larger ions like K^+ is also missing in these solvents and so all the ions behave normally. In view of the lack of sufficient and appropriate electrolytic, and hence the ionic, conductance data in this solvent, it is not possible

Table II: Mobilities of Some Ions in *N*-Methylformamide at Different Temperatures

Ion	Ionic mobility at			
	15°	25°	35°	45°
Na^+	17.59	21.56
K^+	18.05	22.13	27.62	32.15
Cs^+	19.90	24.39
$(C_2H_5)_4N^+$	21.52	26.20
Picrate ⁻	11.28	13.08
Cl^-	16.88	19.70
Br^-	18.46	21.56	25.38	28.60
I^-	19.38	22.76

to make a reasonable estimate of the solvation of ions as was done in *NMA*.⁴ This aspect will be examined later when the required data are available.

Acknowledgment. A grant from the Society of Sigma Xi and RESA Research Fund of the United States of America for the purchase of the solvents (*NMA*, *NMF*, and *NMP*) is very much appreciated.

(7) G. R. Leader and J. F. Gormley, *J. Am. Chem. Soc.*, **73**, 5731 (1951).

(8) R. Gopal and S. A. Rizvi, *J. Indian Chem. Soc.*, **43**, 179 (1966).

(9) J. B. Gill, *J. Chem. Soc.*, 5730 (1965).

(10) B. E. Conway, "Electrochemical Data," Elsevier Publishing Co., London, 1952, p 166.

Photooxidation of Perfluoroethyl Iodide and Perfluoro-*n*-propyl Iodide^{1a}

by Dana Marsh and Julian Hecklen^{1b}

Aerospace Corporation, El Segundo, California
(Received February 15, 1966)

In earlier reports, the oxidation of CF_3^2 and $CFCl_2^3$ radicals was examined. In the former case, the only carbon-containing product was CF_2O , whereas in the latter case only $CFCIO$ was found. In the presence of HI , the results were unchanged.

In this work, we extend the oxidation studies to C_2F_5 and *n*- C_3F_7 radicals in order to determine the products of reaction and the nature of the intermediates. In both cases, the major product is CF_2O .

(1) (a) This work was supported by the U. S. Air Force under Contract No. AF 04(695)-669. (b) To whom requests for reprints should be sent.

(2) J. Hecklen, *J. Phys. Chem.*, **70**, 112 (1966).

(3) D. G. Marsh and J. Hecklen, *ibid.*, **69**, 4410 (1965).

In the C_2F_5I system, it is produced with a quantum yield of about 2.0. CF_3CFO is also produced, but is only $1/40$ as important. With HI present, the oxidation is drastically modified, and the RO_2 intermediate must live at least 10^{-7} sec.

Experimental Section

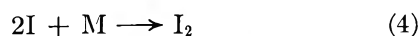
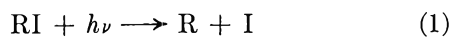
Perfluoroethyl iodide and perfluoro-*n*-propyl iodide were obtained from Peninsular ChemResearch, Inc. Gas chromatographic analysis showed no impurities in the C_2F_5I but one major impurity of about 7% in the *n*- C_3F_7I . The C_2F_5I was used after degassing at -196° , but the C_3F_7I was purified by trap-to-trap fractionation, and that fraction volatile at -63.5° but condensable at -126° used. In this way, the impurity level was reduced but not eliminated. Furthermore, the violet color of the impure material disappeared. Matheson research grade O_2 and anhydrous HI (degassed at -196°) were used.

Infrared analyses were performed *in situ* in a Perkin-Elmer Model 13 Universal spectrometer. A T-shaped cell was used, having 11.5-cm infrared and 10.7-cm ultraviolet path lengths. The ultraviolet light entered the stem of the T through a quartz window. The top of the T had sodium fluoride windows at each end and was situated in the infrared beam. Radiation was from a Hanovia-type SH, U-shaped mercury lamp and passed through a Corning 0-53 glass to remove wavelengths below 2800 Å before entering the cell. The effective radiation was primarily at 3130 Å with the line at 3020 Å also playing some role.

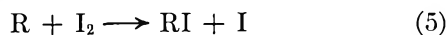
The ultraviolet absorption coefficients for HI, C_2F_5I , and C_3F_7I were determined at 3020 and 3130 Å on a Cary Model 15 spectrophotometer. For longer wavelengths (*i.e.*, 3340 Å and above) there was no absorption. Absolute quantum yields were measured by comparison with the CF_2O produced from photolysis of CF_3I-O_2 mixtures where $\Phi(CF_2O) = 1.0$.

Results and Discussion

The photolysis of C_2F_5I or C_3F_7I yields no products, even for extended exposures. As in all alkyl iodides, the indicated mechanism is



However, the I_2 is a powerful radical scavenger, and very quickly the reaction is inhibited by

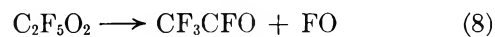
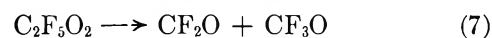
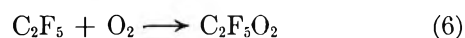


With $C_2F_5I-O_2$ mixtures, the products found were CF_2O , CF_3CFO , and SiF_4 . Iodine is also formed and perhaps F_2 or F_2O , though they would not be detected by infrared analysis. The rate of SiF_4 formation increases with exposure time, indicating secondary decomposition of some product. However, the CF_3CFO and CF_2O grow linearly with time; their quantum yields are listed in Table I. The C_2F_5I and O_2

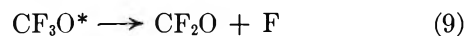
Table I: Photooxidation of C_2F_5I
($T = 25^\circ$, $I_0 = 35 \pm 5 \mu/min$)

(C_2F_5I) , mm	(O_2) , mm	$\Phi(CF_2O)$	$\Phi(CF_3CFO)$
11	10	2.1	0.072
10	300	2.0	0.054
31	10	1.4	0.040
28	33	2.7	0.072
28	265	1.6	0.035
100	10	1.7	0.069
102	127	2.1	0.051
100	300	1.9	0.043
315	10	...	0.056
300	315	2.2	0.024
300	362	4.8	0.069
		Av 2.0 ± 0.3	0.053 ± 0.013

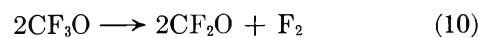
pressures were varied from 10 to 300 mm, but the quantum yields were unaffected. They are $\Phi(CF_2O) = 2.0$ and $\Phi(CF_3CFO) = 0.05$. The mechanism that most easily explains the results is



where k_7/k_8 is about 20. The CF_3O formed from (7) may have sufficient energy to decompose immediately

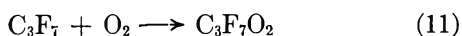


or it may form CF_2O by



With $C_3F_7I-O_2$ mixtures, the results are more difficult to interpret because of the presence of the impurity. The products observed were the same as in the $C_2F_5I-O_2$ photolysis. Initially, the unpurified C_3F_7I was irradiated and CF_2O was produced with a quantum yield of from 10 to 30. Purification of the C_3F_7I by fractionation reduced the impurity level considerably, but did not eliminate the impurities. Photolysis of mixtures of O_2 and the purified C_3F_7I showed the initial large $\Phi(CF_2O)$, but the rate of CF_2O produc-

tion rapidly dropped to a smaller constant value as the CF_2O approached about 1% of the $\text{C}_3\text{F}_7\text{I}$. Presumably, the initial reaction is similar to that for C_2F_5 radicals



In some manner, the $\text{C}_3\text{F}_7\text{O}_2$ radical must yield primarily CF_2O . How this occurs is not clear at all.

It is of interest to know whether the RO_2 radical has a measurable lifetime. To that end, we did a number of experiments with 5 to 40 mm of HI added. Two series of experiments were done, one with 280 mm of $\text{C}_2\text{F}_5\text{I}$ and 300 mm of O_2 , and the other with 100 mm of $\text{C}_3\text{F}_7\text{I}$ and 300 mm of O_2 . Hydrogen iodide had no effect at all on CF_3 or CFCl_2 oxidation.^{2,3} However, with C_2F_5 and C_3F_7 , very marked changes occurred in the oxidation. The results, the same for both series, showed no trend with HI pressure, thus indicating that the initially formed perfluoroalkyl radical was completely scavenged by O_2 .

The results can be summarized as follows. First, a red deposit was formed. Second, $\Phi(\text{CF}_2\text{O})$ was reduced at least 5- to 20-fold. Third, $\Phi(\text{CF}_3\text{CFO})$ may have increased to 0.13 to 0.30 for C_2F_5 radicals as based on the 9.05- μ band of CF_3CFO . The analysis is difficult because of the HI absorption in this region.

F

Fourth, the characteristic $\text{C}=\text{C}=\text{O}$ band at 5.31 μ was the most intense band and was formed at the same rate in all experiments with HI. The CF_3CFO can account for only 25 to 50% of the 5.31- μ band in the $\text{C}_3\text{F}_7\text{I}$ series, but perhaps all of it in the $\text{C}_2\text{F}_5\text{I}$ series. At least for the $\text{C}_3\text{F}_7\text{I}$ series, another product probably was formed. There can be no doubt that HI interferes with the oxidation. Consequently, the RO_2 radical must have a lifetime in excess of 10^{-7} sec.

Acknowledgment. The authors wish to thank Mrs. Barbara Peer for assistance with the manuscript.

Heats of Transport of the Rare Gases in a Rubber Membrane¹

by Mirion Y. Bearman and Richard J. Bearman

*Department of Chemistry, University of Kansas,
Lawrence, Kansas (Received February 21, 1966)*

Revised values for the heats of transport, Q^* , of the rare gases He, Ne, Ar, Kr, and Xe in rubber are presented. In the case of helium, it is shown that, within

experimental error, there is no pressure dependence of the heat of transport in the pressure range 25–65 cm. The apparent Q^* varies slightly with temperature difference across the membrane. Nevertheless, departures from linearity in the local phenomenological equations seem to be negligible even though the temperature gradients range up to 900°/in.

Revised Heats of Transport (Q^*)

In an earlier article, Bearman² reported the heats of transport (or "transfer"), Q^* , of the rare gases in a rubber membrane. His values were obtained from thermoosmosis experiments where, at steady state

$$\ln(p_{\text{H}}/p_{\text{C}})_{\infty} = -(Q^*/R)(1/T_{\text{C}} - 1/T_{\text{H}}) \quad (1)$$

Here, H and C refer to the hot and cold side, respectively, T is absolute temperature, p is pressure, and R is the gas constant. His measurements were subject to several errors of unknown magnitude arising chiefly from uncertainties in the pressure and temperature.

With the use of strain gauge pressure transducers and several thermocouple probes, we have constructed an improved apparatus, fully described elsewhere,^{3,4} in which the errors have been greatly lowered. In Table I, we present revised values for the heats of transport together with a comparison with the earlier results. The error estimates take into account the observed irreproducibility and also errors arising from temperature and pressure measurements. The irreproducibility is caused mostly by leakage, degassing, and adsorption in the system³ over the long course of the runs, which last days or sometimes weeks. A pure gum rubber membrane 0.0325 to 0.0350 cm in thickness was used for our measurements reported here.

Pressure and Temperature Difference Dependence of Q^*

Some additional measurements were made with helium. In Table II, we show that, within the experimental error, the heat of transport at constant mean temperature and temperature difference is independent of mean gas pressure in the system in the range from 25 to 65 cm. From this, we conclude that the He-He interactions in the membrane play little role

(1) This research was supported in its early stages by a grant from the National Science Foundation. We wish to make acknowledgment to the donors of the Petroleum Research Fund, administered by the American Chemical Society, for partial support of this research in its later phases.

(2) R. J. Bearman, *J. Phys. Chem.*, **61**, 708 (1957).

(3) M. Y. Bearman, Dissertation, University of Kansas, 1965. Available from University Microfilms, Ann Arbor, Mich.

(4) M. Y. Bearman and R. J. Bearman, *J. Appl. Polymer Sci.*, **10**, 773 (1966).

Table I

Gas	This work				Bearman			
	p_{mean} , cm	t_{mean} , °C	Δt , °C	Q^* , cal/mole	p_{mean} , cm	t_{mean} , °C	Δt , °C	Q^* , cal/mole
He	65-25	31.0	7.9	1375 ± 39	62.5	34.0	4	1130
Ne	65-45	31.4	7.3	1204 ± 37	45	34.5	4	900
Ar	53	30.7	7.7	-58 ± 11	62	34.5	4	-60
Kr	50	30.5	8.2	-275 ± 10	45	34.5	4	-170
Xe	46-26	30.5	8.7	-589 ± 18	40	34.5	4	-320

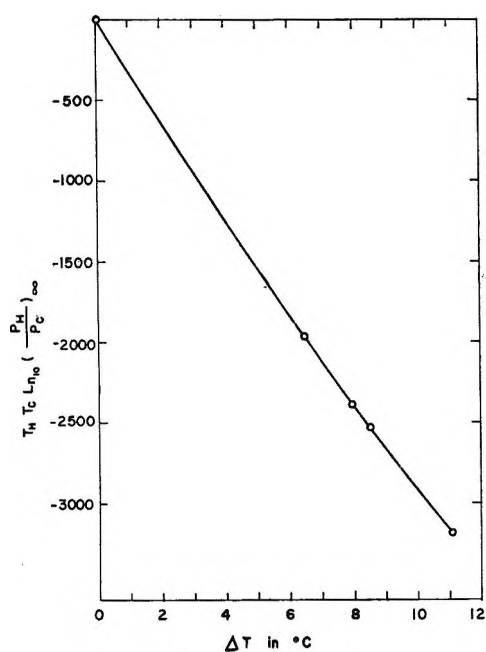


Figure 1.

in determining Q^* at these pressures, and that the gas is effectively at infinite dilution in the membrane.

In Figure 1, we plot, at constant mean temperature, $T_H T_C \log(p_H/p_C)_\infty$ vs. ΔT , the temperature difference across the membrane. We see that there is a perceptible departure from linearity in contradiction with eq 1 which predicts that the plot should be a straight line with slope proportional to Q^* . However, eq 1 is not entirely general. It is valid only when Q^* is independent of temperature and mole fraction of gas in the membrane. This can be seen, for example, from eq 13 of ref 2. If we assume that Q^* varies linearly with temperature and that the gas is at infinite dilution in the membrane, then it is not difficult to show that in place of eq 1, we have

$$T_H T_C \ln(p_H/p_C)_\infty = -R^{-1} \left(Q^* \Big|_T \Delta T + \frac{\partial Q^*}{\partial T} \Big|_T \frac{(\Delta T)^2}{2} \right) \quad (2)$$

where T is the arithmetic mean temperature. In this case, $T_H T_C \ln(p_H/p_C)_\infty$ vs. ΔT should be a parabola, which appears to be the shape of the curve in Figure 1. A parabolic least-squares fit of our data gives $Q^* = 1495$ cal/mole and $\partial Q^*/\partial T = -31.4$ cal/mole deg at the mean temperature of 31°. The heat is clearly of the proper magnitude and the temperature coefficient is not unreasonable,⁵ so that it appears eq 2 adequately accounts for the experimental results.

If eq 2 does correctly account for the temperature difference data, we may conclude that the usual local linear phenomenological equation for the flux of matter, J_1

$$J_1 = -TL_{11} \frac{\partial \mu_1/T}{\partial z} - \frac{L_{1U}}{T} \frac{\partial T}{\partial z} \quad (3)$$

in the notation of ref 2, is valid, provided we use values of the phenomenological coefficients, L_{11} and L_{1U} , appropriate to the state at each point of the membrane. The nonlinearity of $T_H T_C \ln(p_H/p_C)_\infty$ in ΔT is then caused solely by the variation of the transport coefficients across the membrane. Our experiments provide a fairly severe test of the linear phenomenological equation since the temperature gradients range up to 900°/in.

Evidently, the values for the heats of transport

Table II

Run	p_{mean} , cm	t_{mean} , °C	Δt , °C	Q^* , cal/mole	Length of run, min
27	64.8	31.2	8.0	1385	4190
40	54.5	31.2	7.6	1383	3255
1	51.8	30.6	8.3	1442	2720
3	51.6	30.9	8.2	1374	4190
30	34.9	30.9	8.0	1365	3420
32	34.9	31.1	7.9	1364	3465
31	25.2	31.0	8.0	1378	3525

(5) C. M. Crowe, *Trans. Faraday Soc.*, **53**, 692 (1957).

listed in Table I and calculated from eq 1 may be subject to systematic errors arising from the temperature dependence of Q^* . Thus, for precise work, our results must be accepted as effective values of Q^* valid at the quoted temperature difference and mean temperature.

The Methylene Blue–Ferrous Iron Reaction in a Two-Phase System¹

by D. Fraçkowiak and E. Rabinowitch

Department of Botany and Department of Physiology and Biophysics, University of Illinois, Urbana, Illinois
(Received February 25, 1966)

The photosynthetic apparatus of living plants separates from each other the probably highly unstable, intermediate oxidation and reduction products of the primary photochemical process and thus permits their conversion to (relatively) stable final products, carbohydrates and oxygen. This is probably accomplished by conveying these intermediates into different phases in the lamellar structure.² The failure to imitate *in vitro* the storage of light energy as chemical energy, achieved by plants in photosynthesis, may be due primarily to not providing such a separation mechanism. Mathai and Rabinowitch³ showed that an *in vitro* system can be constructed, in which the products of an oxidation–reduction reaction (that between thionine and ferrous ions), which runs in light against the gradient of chemical potential, are separated by distribution between water and ether in an emulsion. The light energy stored in this way can be liberated by permitting the two phases to mix again (*e.g.*, by adding methanol).

In continuing this work, Ghosh⁴ in this laboratory observed that separating is more effective if methylene blue is substituted for thionine; perhaps, more of the neutral species of the leuco dye is present in methylene blue than in thionine at the pH values used. (This species alone is likely to be involved in the extraction of the leuco dye into ether.)

The following experiments deal with the methylene blue–ferrous iron system. They provide some additional information concerning the effectiveness of the separation.

The reaction vessel used was a cylindrical Pyrex-glass vessel containing 30 ml of aqueous solution and 15 ml of ether (or another solvent immiscible with water). The approximate initial concentrations of methylene blue and FeSO_4 were of the order of 10^{-5} and 5×10^{-3}

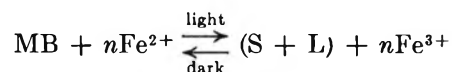
M , respectively. The mixture was stirred by bubbling through a stream of purified argon. No buffer was used; the pH was 3.5–4.

The light used for illumination was either white light from a 1000-w coiled filament incandescent lamp or the same light filtered through an interference filter (Balzer K-6) with maximum transmission of 650 $m\mu$ (near the peak of the methylene blue absorption band at 664 $m\mu$).

The experiments were made at room temperature maintained in a water bath.

Merck reagent grade methylene blue was used without purification. Chromatography on aluminum oxide and the test of Bergmann and O'Konski⁵ indicated that the dye was pure enough for our purpose. We tried out several combinations of immiscible solvents, but the most efficient separation of the photoproducts we were able to obtain took place in the system water + ethyl ether, already used in Mathai's work.

The reaction is



Here, MB is methylene blue, S, the semiquinone, and L, the leuco methylene blue; n is between 1 and 2, depending on relative amounts of S and L formed. From the work of Parker⁶ and the earlier work of Rabinowitch,⁷ it appears that in the photostationary state, partly reduced solutions of methylene blue contain only a small percentage of semiquinone, so that n is close to 2. The predominant ionic species (at the prevailing acid pH's) are monovalent positive ions of MB and monovalent (or divalent) positive ions of L. The neutral form of L, which we can assume to be the only one soluble in ether, is present only in minute amounts. This probably accounts for the slowness with which the leuco dye is extracted into ether. Further experiments on the effect of pH on the rate of extraction should clarify this point.

In the stationary state, the extent of extraction de-

(1) This research was supported by research grants from the National Science Foundation (GB 1946 and GB 3305) and from the Atomic Energy Commission [AT(11-1)-1502].

(2) E. Rabinowitch, paper presented at the Biophysical Society Meeting, Washington, D. C., 1962, Abstract FC3.

(3) K. G. Mathai and E. Rabinowitch, *J. Phys. Chem.*, **66**, 663 (1962).

(4) A. K. Ghosh, unpublished.

(5) K. Bergmann and C. T. O'Konski, *J. Phys. Chem.*, **67**, 2169 (1963).

(6) C. A. Parker in "Photochemistry in the Liquid and Solid States," L. J. Heidt, *et al.*, Ed., John Wiley and Sons Inc., New York, N. Y., 1960, p 48.

(7) E. Rabinowitch, *J. Chem. Phys.*, **8**, 551 (1940); see also L. F. Epstein, F. Karush, and E. Rabinowitch, *J. Opt. Soc. Am.*, **31**, 77 (1941).

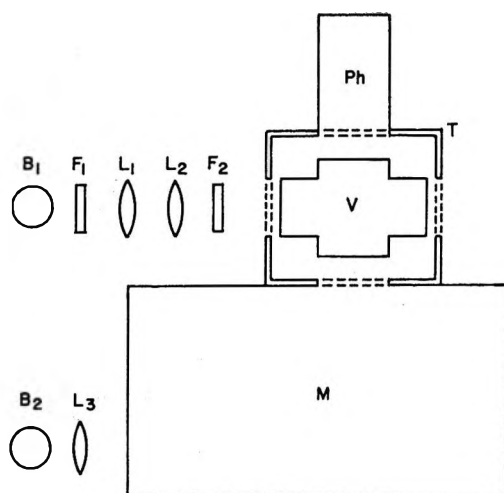


Figure 1. Apparatus used to study the bleaching of methylene blue by Fe^{2+} in light: B_1 , 1000-w tungsten filament lamp; F_1 , 2 cm thick water filter; L_1 , L_2 , L_3 , lenses; F_2 , Balzers broad-band interference filter (Type K-6), transmission peak at $650 \text{ m}\mu$; V , reaction vessel; Ph , photomultiplier (RCA 6217); T , water bath; M , Bausch and Lomb monochromator, 600 grooves/mm; B_2 , 6-v, 18-amp tungsten ribbon filament lamp.

depends on the partition coefficient of L between the two solvents. For small relative concentrations of L (*i.e.*, when only a small part of the dye is reduced), the amount extracted into ether is proportional to the total concentration of L .⁸ For a larger change of concentration (or for dimerized solutions), the amount of leuco dye extracted into ether ceases to be proportional to its concentration in water.

In a one-phase system, the stationary ratio $[\text{MB}]:[\text{L}]$ is established, in intense light, within a few seconds after the beginning of illumination.⁷ If the bleaching is measured (with the instrument shown in Figure 1) in the two-phase system, while the illumination is in progress (by reducing momentarily the stirring before each measurement), the bleaching of the aqueous phase is found to occur as rapidly as in the absence of ether. However, this fast process is superimposed by a much slower shift, caused by progressive extraction of the leuco dye into ether. This slow extraction is demonstrated by the following three experiments.

(1) *Change of Absorption in the Reoxidized Water Phase.* After a period of illumination, the gas flow is stopped and the two phases are allowed to separate. An aliquot of the water phase is transferred by a syringe from the photolytic vessel into a Bausch and Lomb spectrophotometer cuvette. During this operation, the dye in the aqueous phase is reoxidized by reaction of the leuco dye with Fe^{3+} , but because part of the leuco dye had been extracted into ether, the reoxidized

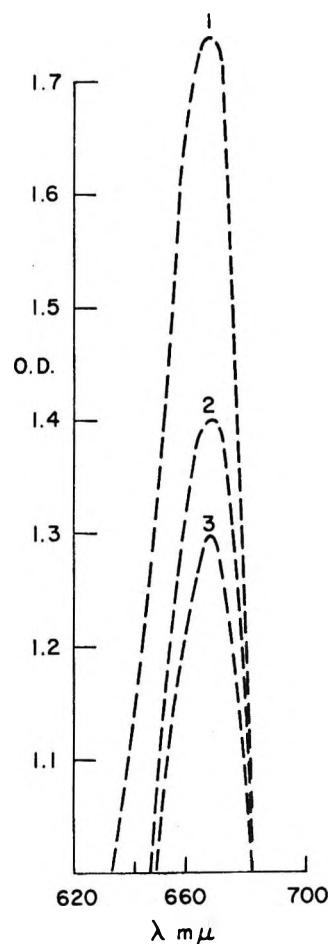


Figure 2. Absorption spectrum of the water phase after prolonged illumination: 1, $t = 0$; 2, $t = 50 \text{ min}$; 3, $t = 90 \text{ min}$.

aqueous solution contains less dye than it did before the illumination.

After this measurement of the absorption spectrum, the sample can be returned to the reaction vessel, the illumination resumed, and measurements repeated several times. The decrease of the absorption band area, shown in Figures 2 and 3, is proportional to the total time of illumination. This, of course, means that the illumination times used in these experiments were short compared to the time needed to reach a stationary distribution of the leuco dye between the two phases.

(2) *The Potential Difference between the Water and the Ether Phase.* For this measurement, a small volume (0.5 ml) of the ether phase was removed, after a certain illumination time, and placed in one half-cell of a galvanic cell, where it was mixed with 0.5 ml of methanol. A standard half-cell containing a $(\text{MB} + \text{FeSO}_4)$ solu-

(8) J. H. Hildebrand and R. L. Scott in "Solubility of Non-electrolytes," 3rd ed, Reinhold Publishing Corp., New York, N. Y., 1950, p 205.

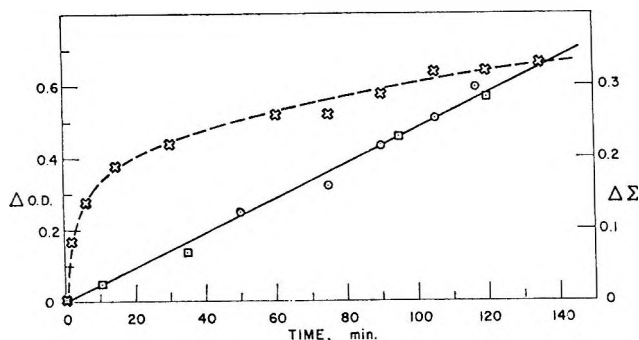


Figure 3. Changes of potential difference ($\Delta\epsilon$) between water and ether phases (crosses) and concomitant increase in absorption, ΔOD (integrated over the band) in water phase (circles); squares show the concomitant increase in absorption in reoxidized ether phase.

tion of known concentration was connected by an agar bridge saturated with KCl. Beckman platinum electrodes were used, and the difference of potential ($\Delta\epsilon$) between the half-cells was measured by a Leeds and Northrup universal pH indicator assembly. The results are shown in Figure 3 (crosses, scale at right). The curve indicates growing accumulation of the reduced dye in the ether phase.

(3) *Reoxidation of the Extracted Leuco Dye.* The separated ether phase was exposed to air after dilution by methanol (to prevent precipitation of MB). The increasing amount of MB found in this phase after prolonged illumination is shown in Figure 4. (Recoloration could be observed upon exposure to air also in methanol-free ether—although solid MB does not dissolve markedly in ether, and no MB is extracted into pure ether from an aqueous solution.)

These three sets of experiments indicate slowly growing extraction of the leuco form of MB into ether during prolonged illumination. The maximum amount extracted in some of our experiments, about 35% of the total dye present, seemed to be close to saturation. The whole process, bleaching and extraction, is fully reversible—at least, after a not excessively long illumination period. If both phases are mixed together again and the ether is permitted to evaporate, the absorption spectrum of the remaining aqueous solution is found to be the same as before the experiment.

With larger concentrations of MB ($\geq 5 \times 10^{-5} M$), the shape of the absorption curve changed during illumination. This must be attributed to the dimerization of the dye.⁹ Since the total concentration of MB in water was reduced by the extraction of a part of it (as leuco dye) into ether, the dimerization equilibrium must have been shifted.

These results confirm that a storage of photochemical energy can be achieved by dividing the photoproducts

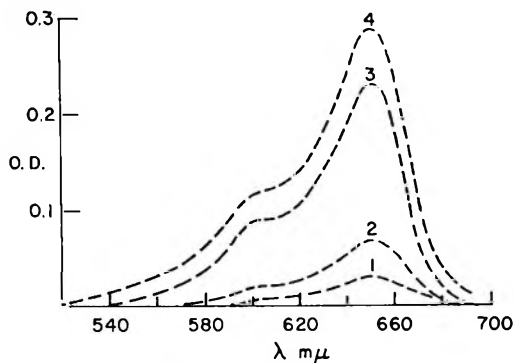


Figure 4. Absorption by reoxidized leuco dye in the ether phase after different times of illumination of the two-phase system: 1, 10 min; 2, 35 min; 3, 95 min; 4, 120 min.

between two phases in an inhomogeneous system. This could be considered as a model of the storage of photochemical energy in photosynthesis.²

Experiments should be made on the change in effectiveness of the separation of leuco methylene blue from illuminated solutions as function of concentration of the components, the pH, and the interface area between the two phases. (Competition between homogeneous recombination in the aqueous phase and the removal of the reduction product into another phase, preventing this recombination, must depend on the diffusion path between the locus of the primary reaction and the water-ether interface.) In order to reproduce better the situation in the living cell, one could prepare very thin layers—only a few molecules thick—alternately hydrophilic and hydrophobic, and study the separation process in such systems. Finally, one should try to find and use dyes in which a higher proportion of the leuco form is in the neutral state under the pH conditions used.

(9) E. Rabinowitch and L. F. Epstein, *J. Am. Chem. Soc.*, **63**, 69 (1941).

The First Ionization Potentials of Samarium, Europium, Gadolinium, Dysprosium, Holmium, Erbium, Thulium, and Ytterbium by the Electron-Impact Method

by K. F. Zmbov and J. L. Margrave

Department of Chemistry, Rice University, Houston, Texas
(Received April 1, 1966)

During a mass spectrometric study of gaseous equilibria involving rare earth subfluorides, it was possible

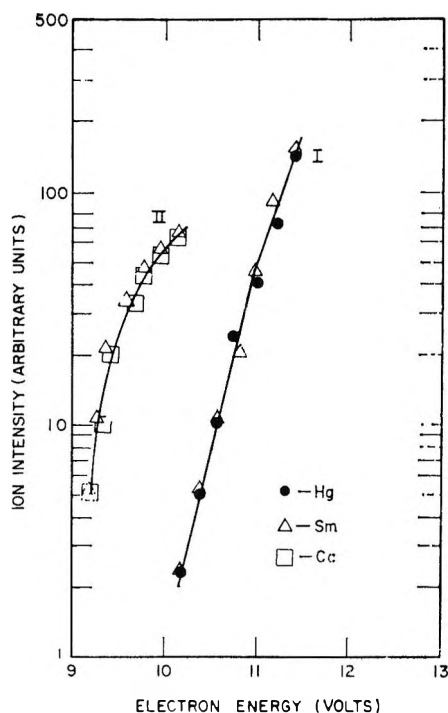


Figure 1. Ionization efficiency data for Sm^+ , Hg^+ , and Ca^+ using the semilog matching method. The Sm^+ scale must be shifted 4.87 and 0.65 eV to give the indicated matchings with Hg^+ and Ca^+ , respectively.

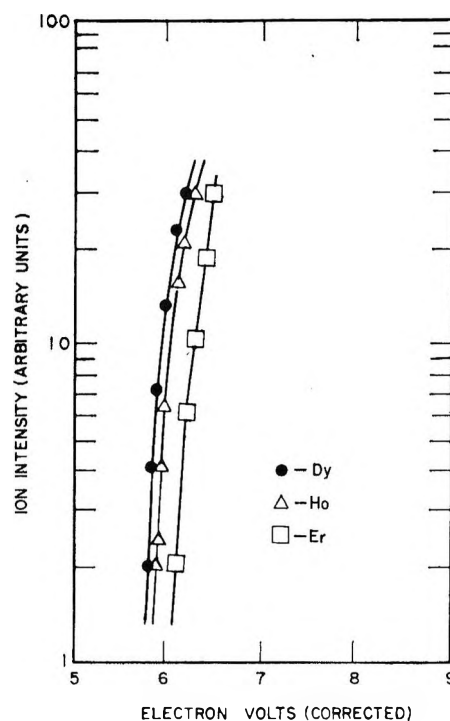


Figure 2. Ionization efficiency curves for Dy^+ , Ho^+ , and Er^+ ions.

Table I: Ionization Potentials of Rare Earth Atoms by Different Methods

Element	Ionization potential, eV	Method	Ref
Sm	(5.6) ^a	Optical spectroscopy	6
	5.70 ± 0.02	Surface ionization	7
	5.56 ± 0.10	Electron impact	This work
Eu	(5.67)	Optical spectroscopy	6
	5.68 ± 0.03	Surface ionization	7
	5.61 ± 0.10	Electron impact	This work
Gd	(6.16)	Optical spectroscopy	6
	5.98 ± 0.10	Electron impact	This work
Dy	(6.8)	Optical spectroscopy	6
	5.80 ± 0.02	Surface ionization	7
	5.8 ± 0.10	Electron impact	This work
Ho	6.19 ± 0.02	Surface ionization	7
	5.85 ± 0.10	Electron impact	This work
Er	6.08 ± 0.03	Surface ionization	8
	6.11 ± 0.10	Electron impact	This work
Tm	6.15 ± 0.03	Surface ionization	7
	5.87 ± 0.10	Electron impact	This work
Yb	(6.2)	Optical spectroscopy	6
	5.90 ± 0.10	Electron impact	This work

^a All values in parentheses indicate estimates.

to measure the ionization potentials of Sm, Eu, Gd, Dy, Ho, Er, Tm, and Yb atoms by the electron-impact

method. The experiments were carried out with a magnetic mass spectrometer described previously.¹ Optical spectra of rare earth atoms are complex and incompletely interpreted.²

Gaseous rare earth atoms were produced either by heating the metal in a tantalum Knudsen cell or by reduction of the various trifluorides and CaF_2 with Gd or Ho in the same cell. As a typical example, the ionization efficiency curve of Sm^+ is compared with that of Hg^+ ion from the background in Figure 1, curve I, or with Ca^+ from CaF_2 reduction in Figure 1, curve II, by using the semilog matching method,³ which consists of measuring the voltage shift required to match the initial portion of the ionization efficiency curve of the rare earth ion with that of the reference ion.

With the known ionization potentials of Hg (10.43 eV)^{2,4} and that of Ca (6.11 eV),^{2,5} one obtains 5.56 ± 0.10 eV for the ionization potential of Sm. This compares

(1) G. D. Blue, J. W. Green, R. G. Bautista, and J. L. Margrave, *J. Phys. Chem.*, **67**, 877 (1963).

(2) (a) For example, C. E. Moore, National Bureau of Standards Circular 467, Vol. I-III, U. S. Government Printing Office, Washington, D. C., 1949, 1952, and 1958, has not yet issued a volume on rare earth spectra. (b) J. Sugar and J. Reader, *J. Opt. Soc. Am.*, **55**, 1286 (1965).

(3) S. N. Foner and R. L. Hudson, *J. Chem. Phys.*, **36**, 2681 (1962).

(4) (a) W. B. Nottingham, *Phys. Rev.*, **55**, 203 (1939); (b) R. E. Fox, *J. Chem. Phys.*, **35**, 1379 (1961).

(5) J. C. Boyce, *Rev. Mod. Phys.*, **13**, 1 (1941).

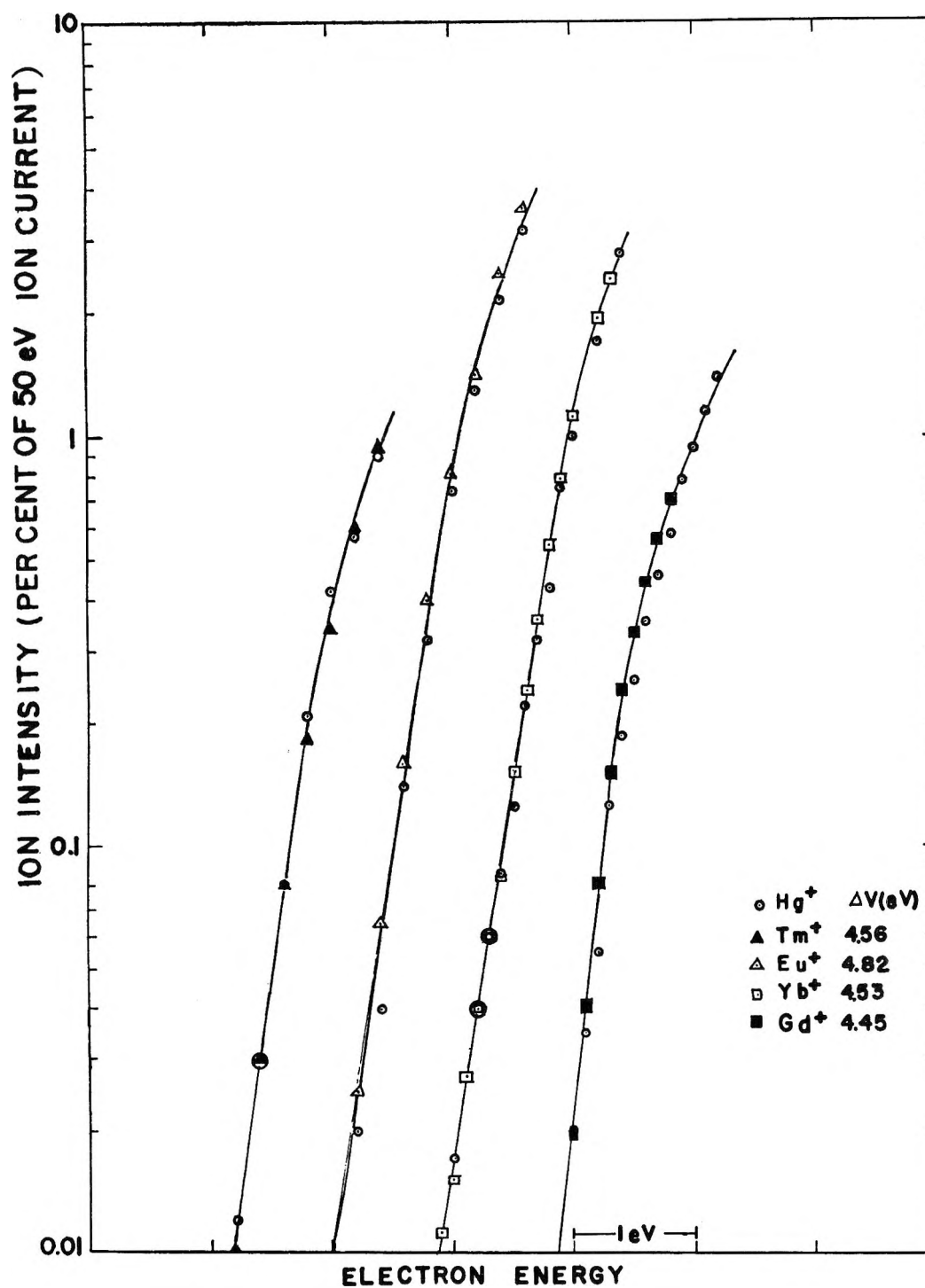


Figure 3. Ionization efficiency curves for Tm⁺, Eu⁺, Yb⁺, and Gd⁺ with Hg⁺ as a reference.

well with the estimated spectroscopic value of 5.6 eV⁶ and the recently published surface ionization data, 5.70 eV.⁷ Direct studies of Gd atoms sublimed from a Ta Knudsen cell yielded 5.98 ± 0.10 eV as the ionization potential of Gd.

Eu, Dy, Ho, Er, Tm, and Yb atoms were produced

by heating a mixture of the corresponding trifluorides with Gd metal in the tantalum Knudsen cell. Ioni-

(6) W. E. Forsythe, "Smithsonian Physical Tables," 9th revised ed. Publication 4169, Smithsonian Institution, Washington, D. C., 1954.

(7) N. I. Alekseev and D. L. Kaminskii, *Zh. Tekhn. Fiz.*, **34**, 1521 (1964).

zation efficiency curves on a semilog plot are shown for Dy, Ho, and Er in Figure 2 and for Eu, Gd, Tm, and Yb in Figure 3. The electron-voltage scale was calibrated by the vanishing-current method, using the background mercury as a standard. This method yielded 6.11 ± 0.1 ev for the ionization potential of Er, in excellent agreement with recently published data⁸ obtained by the surface ionization method (6.08 ± 0.03 ev). By using the Er value as a standard, one obtains I.P.(Dy) = 5.78 ± 0.1 ev and I.P.(Ho) = 5.85 ± 0.1 ev, and the use of the Ho value as a standard, along with Hg, yields the ionization potentials of Eu, Tm, and Yb.

Table I summarizes values for the ionization potentials obtained by the different methods. It appears that the general rule

$$I(M)/I(M^+) = 0.50 \pm 0.01$$

holds for the rare earth atoms based on these data and those of Sugar and Reader.^{2b}

Acknowledgment. This work was supported by the U. S. Atomic Energy Commission under Contract AT-(40-1)-2907.

(8) N. I. Ionov and M. A. Mitsev, *Zh. Eksperim. i Teor. Fiz.*, **38**, 1350 (1960).

COMMUNICATIONS TO THE EDITOR

Comments on the Paper "Solubility of Hydrogen in Potassium Hydroxide and Sulfuric Acid; Salting-out and Hydration"

by P. Ruetschi and R. F. Amlie

Sir: Recently,¹ Conway, Desnoyers, and Smith developed a detailed theory of salting-out of nonelectrolytes by simple salts and polymeric ions and showed that substantial improvements on previous continuous-distribution theories^{2,3} could be made by regarding the salting-out as arising from effects in two distinguishable regions near the ion: (i) that due to the loss of normal solvent function of the water molecules attached to the ion in the primary hydration shell⁴ of radius r_h , where appreciable dielectric saturation occurs; and (ii) that due to the more continuous distribution of solvent and nonelectrolyte in the region of solution beyond the hydration radius, r_h , arising^{2,3,6} from the different size and polarization of the nonelectrolyte and solvent water molecules in the field of the ion.

From the periphery of the ion of radius a to r_h , the dielectric constant is quite low (ca. 2-6) and most nonelectrolytes (except those more polar than water and of comparable size) will virtually be completely salted-out.¹

We wish to point out that in a paper recently published by Ruetschi and Amlie,⁵ a type of approach very similar to that which we published previously¹ has

evidently been made independently and a relation for the salting-out involving two integrands from a to r_h and r_h to R (cf. ref 1, 6) or ∞ is given as in our earlier paper.¹ A two-region model has also been used by Glueckauf⁷ in the interpretation of ionic dielectric decrements where a step-function for the dielectric constant was used with the discontinuity at r_h . While Ruetschi and Amlie⁵ based their calculations of the contribution arising from the nonelectrolyte-solvent distribution between r_h and R (or ∞) on Debye's theory² in terms of dielectric decrements (which are not always experimentally available), we preferred to extend Debye's theory to obtain the salting-out constants in terms of the more readily available partial molal volumes and dipole moments of the nonelectrolytes. In doing so, it was possible to show that an equation such as ours (or the similar one now given by the above authors) can account for the observed salting-out of a number of combinations of simple salts and simple nonelectrolytes.

(1) B. E. Conway, J. E. Desnoyers, and A. C. Smith, *Phil. Trans. Roy. Soc. (London)*, **A256**, 389 (1964).

(2) P. Debye and J. McAulay, *Physik. Z.*, **26**, 22 (1925); P. Debye, *Z. Physik. Chem.*, **130**, 55 (1927).

(3) J. A. V. Butler, *J. Phys. Chem.*, **33**, 1015 (1929); *Proc. Roy. Soc. (London)*, **A122**, 399 (1929).

(4) J. O'M Bockris, *Quart. Rev. (London)*, **3**, 173 (1949).

(5) J. O'M. Bockris, J. Bowler-Reed, and J. A. Kitchener, *Trans. Faraday Soc.*, **47**, 184 (1951).

(6) P. Ruetschi and R. F. Amlie, *J. Phys. Chem.*, **70**, 718 (1966).

(7) E. Glueckauf, *Trans. Faraday Soc.*, **60**, 1637 (1964).

We agree with the above authors that salting-out data can in principle be used to obtain V_h , the volume of the hydrated ions. However, it must be pointed out that the corresponding radii cannot be obtained from the spherical model since, near the ions, the solvent cannot be considered dimensionless compared with the size of the hydrated ions and part of the free space between the molecules is included in the experimentally determined V_h , as pointed out in ref 1 and by Glueckauf.⁸ In order to take the dead-space effect into account, we have shown^{1,9} that a term proportional to the surface area (*cf.* ref 8) of the hydrated ion should be added to the equation for the sphere and, if V_h is expressed in milliliters and r_h in angstroms, the equation

$$V_h = 2.51r_h^3 + 3.15r_h^2$$

results and was shown^{1,9} to account reasonably well for the relation between the radii and volumes of ions in water. With this relation, the mean radii of hydrated K^+ and OH^- are between 3.55 and 3.6 Å, values which are in better agreement with those obtained by Nightingale¹⁰ from mobility data.

(8) E. Glueckauf, *Trans. Faraday Soc.*, **61**, 914 (1965); **60**, 572 (1964).

(9) B. E. Conway, R. E. Verrall, and J. E. Desnoyers, *Z. Physik. Chem.*, **230**, 157 (1965).

(10) E. R. Nightingale, *J. Phys. Chem.*, **63**, 1381 (1959).

DEPARTMENT OF CHEMISTRY
UNIVERSITY OF SHERBROOKE
SHERBROOKE, QUEBEC, CANADA

J. E. DESNOYERS

DEPARTMENT OF CHEMISTRY
UNIVERSITY OF OTTAWA
OTTAWA, ONTARIO, CANADA

B. E. CONWAY

RECEIVED JUNE 15, 1966

Ultrasonic Study of the Helix-Coil Transition in Poly-L-lysine¹

Sir: In the neighborhood of room temperature and at pH less than 8, polylysine in aqueous solution exists in the random-coil form. As the pH is increased, there is a gradual transition proceeding presumably through a series of states involving alternating helical and coiled segments along a single chain until, at pH 12, the transition from coil to helix is essentially complete.²

In the absence of significant dispersion, the frequency dependence of the excess ultrasonic attenuation, α , due to a single process with relaxation time τ , may be expressed as shown in eq 1.

$$\frac{\alpha}{f^2} = \frac{C\tau}{1 + 4\pi^2 f^2 \tau^2} \quad (1)$$

For a simple reaction of the form $A \rightleftharpoons B$ in dilute aqueous solution, where C_p and C_v are very nearly equal and the temperature fluctuations associated with the passage of the sound wave may be neglected, $C = 2\pi^2 \rho c [x_a x_b / (x_a + x_b)] [(\Delta V)^2 / \bar{V} RT]$, where ρ is the density, c the velocity of sound, x_a and x_b the mole fractions of species A and B, ΔV the volume change (per mole) for $A \rightarrow B$, and \bar{V} the molar volume of the solvent.³ Thus, in favorable cases it should be possible to deduce a relaxation time and the volume change for the helix-coil transition from ultrasonic attenuation.

We have determined the optical rotation and the frequency dependence of ultrasonic velocity and attenuation as a function of pH and ionic strength in aqueous solutions of poly-L-lysine of weight-average molecular weight 86,300 (about 675 residues/chain). The attenuation at 35.8° in 0.6 M NaCl with the total polymer concentration of 20 g/l. is given in Figure 1, and the values of C and τ obtained by a least-square fit of the data to eq 1 (solid lines in Figure 1) are recorded in Table I as are the volume changes deduced from the observed values of C . The average velocity of sound at 35.8° is 1.561×10^5 cm/sec with the change in velocity between 1 and 50 Mc less than 0.2%. The fraction (f_H) of polymer present in the helical form was deduced from measurement of the optical rotation between pH 4 and 12.

Table I

pH	$10^8 C$, sec cm ⁻¹	$10^8 \tau$, sec	ΔV , cm ³ /mole	f_H	$\frac{10^4 x_a x_b}{x_a + x_b}$
9.60	8.82	3.39	6.2	0.146	3.49
9.22	6.90	3.21	7.6	0.068	1.77
7.20	2.27	5.66		<0.03	<0.81

Burke, Hammes, and Lewis⁴ have investigated the excess acoustic absorption in solutions of poly-L-glutamic acid in dioxane-water mixtures attributing the observed attenuation to perturbation of the solva-

(1) Support by the National Institute of Health and the A. P. Sloan Foundation.

(2) J. Applequist and P. Doty, "International Symposium on Polyamino Acids, Polypeptides, and Proteins," M. Stahmann, Ed., University of Wisconsin Press, Madison, Wis., 1961.

(3) K. Herzfeld and T. Litovitz, "Absorption and Dispersion of Ultrasonic Waves," Academic Press Inc., New York, N. Y., 1959, p 150.

(4) J. Burke, G. Hammes, and T. Lewis, *J. Chem. Phys.*, **42**, 3520 (1965).

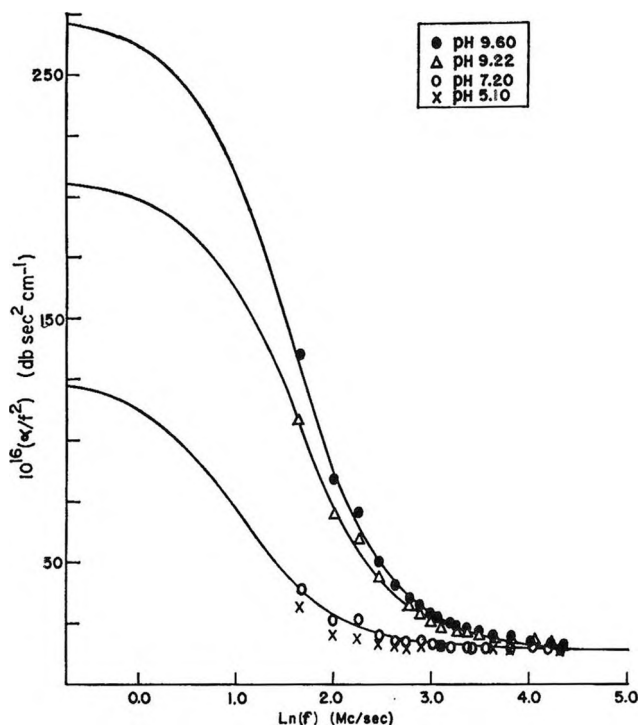


Figure 1. Ultrasonic absorption as a function of frequency in 0.156 *M* (moles of monomer/liter) poly-L-lysine solutions in 0.6 *M* NaCl at 35.8° and various values of the pH. Solid lines are least-square fits to the single relaxation equation. The classical value of α/f^2 is 13.95×10^{-16} db sec² cm⁻¹, in good agreement with the value for water interpolated from the data of Herzfeld (see ref 3, p 358).

tion equilibrium. There is no absolute assurance that similar phenomena are not involved in our results; indeed the volume change calculated is rather close to that estimated by Cohn and Edsall⁵ for the solvation of a singly ionized group. However, the dependence of *C* on the pH, much more pronounced than that observed by Burke, Hammes, and Lewis, and in particular the virtually negligible excess absorption at low pH would argue against such an interpretation. The observed variation of *C* with f_H is consistent with the notion that absorption due to perturbation of the helix-coil equilibrium is being observed.

Our data do not show a significant increase in the relaxation time when f_H is increased as predicted by Schwarz.⁶ However, we are restricted to rather low values of f_H by solubility limitations and such behavior cannot be ruled out. When attempts were made to analyze our data in terms of a Davidson-Cole⁷ distribution of relaxation times, somewhat surprisingly, values of β close to 1 resulted indicating a satisfactory fit in terms of a single relaxation. In summary, the excess acoustic absorption in polylysine solution may be

adequately described by a single process with a relaxation time $3-6 \times 10^{-8}$ sec and an associated volume change of 6-8 cm³/mole of monomer. The dependence of the absorption on pH is consistent with the notion that the process is the helix-coil transition.

(5) E. J. Cohn and J. T. Edsall, "Proteins, Amino Acids and Peptides as Ions and Dipolar Ions," Reinhold Publishing Corp., New York, N. Y., 1943.

(6) G. Schwarz, *J. Mol. Biol.*, **11**, 64 (1965).

(7) D. W. Davidson and R. H. Cole, *J. Chem. Phys.*, **19**, 1484 (1951).

DEPARTMENT OF CHEMISTRY
UNIVERSITY OF WASHINGTON
SEATTLE, WASHINGTON 98105

R. C. PARKER
K. APPLIGATE
L. J. SLUTSKY

RECEIVED JUNE 16, 1966

Geminate Recombination in Photochemistry: A First-Order Process¹

Sir: The dependence of *G* values and quantum yields on solute concentration in radiation chemistry^{2,3} and photochemistry⁴⁻⁶ has been theoretically interpreted by the use of diffusion kinetics. A recent critical review of the pertinent literature in radiation chemistry led the author⁷ to induce an alternative model: "excited water," either an electronically excited state or the H₃O-OH radical pair which undergoes geminate recombination by a first-order process, is precursor of intraspur hydrogen in the radiolysis of water.

Woods⁸ recently published very important results in the photochemistry of iron(II) in 1 *M* sulfuric acid. The dependence of $\Phi(\text{Fe}^{\text{III}})$ and $\Phi(\text{As}^{\text{III}})$ on arsenic acid concentration is identical both with the dependence of intraspur hydrogen *G* values on solute concentration⁷ and with the dependence of geminate recombination on solute concentration deduced by Noyes⁵ in that solute concentrations must exceed 0.01 *M* for significant effects. However, Woods⁸ concluded that the effect of arsenic acid was not due to inhibition of geminate

(1) Research sponsored by the U. S. Atomic Energy Commission under contract with Union Carbide Corp.

(2) A. Samuel and J. L. Magee, *J. Chem. Phys.*, **21**, 1080 (1953).

(3) A. Kuppermann in "The Chemical and Biological Actions of Radiations," Vol. 5, M. Haissinsky, Ed., Academic Press Inc., New York, N. Y., 1961.

(4) J. C. Roy, R. R. Williams, and W. H. Hamill, *J. Am. Chem. Soc.*, **76**, 3274 (1954).

(5) R. M. Noyes, *ibid.*, **77**, 2042 (1955).

(6) L. J. Monchik, *J. Chem. Phys.*, **24**, 381 (1956).

(7) T. J. Sworski, *J. Am. Chem. Soc.*, **86**, 5034 (1964); *Advances in Chemistry Series*, No. 50, American Chemical Society, Washington, D. C., 1965, p 263.

(8) R. Woods, *J. Phys. Chem.*, **70**, 1446 (1966).

recombination since $\Phi(\text{Fe}^{\text{III}})$ and $\Phi(\text{As}^{\text{III}})$ are not linearly related to the square root of arsenic acid concentration.

The dependence of $\Delta\Phi(\text{Fe}^{\text{III}})$ and $\Phi(\text{As}^{\text{III}})$ on arsenic acid concentration is quantitatively given by

$$1/\Delta\Phi(\text{Fe}^{\text{III}}) = (0.645 \pm 0.068) + 0.297/[\text{As}^{\text{V}}] \quad (\text{I})$$

$$1/\Phi(\text{As}^{\text{III}}) = (1.007 \pm 0.083) + 0.493/[\text{As}^{\text{V}}] \quad (\text{II})$$

with constants and standard deviations determined by the method of least squares. $\Delta\Phi(\text{Fe}^{\text{III}})$ is the increase in $\Phi(\text{Fe}^{\text{III}})$ induced by arsenic acid.

Equations I and II are consistent with a reaction mechanism based on the following assumptions: (1) light absorption yields "excited ferrous ion" which disappears by a first-order process with rate constant of $1/\tau$; (2) arsenic acid reacts only with $\text{Fe}^{\text{II}*}$ with rate constant of k to yield arsenic(IV) which oxidizes iron(II); and (3) the quantum yield for the process which yields iron(III) in the absence of arsenic acid is reduced by a factor equal to the fraction of $\text{Fe}^{\text{II}*}$ which reacts with arsenic acid. This reaction mechanism yields eq I' and II'

$$1/\Delta\Phi(\text{Fe}^{\text{III}}) = (1 + 1/\tau k[\text{As}^{\text{V}}])/1.777\Phi(\text{Fe}^{\text{II}*}) \quad (\text{I}')$$

$$1/\Delta\Phi(\text{As}^{\text{III}}) = (1 + 1/\tau k[\text{As}^{\text{V}}])/\Phi(\text{Fe}^{\text{II}*}) \quad (\text{II}')$$

Equations I' and II' become identical with the equations of Woods⁸ with the following substitutions: $\tau k = \epsilon_2 K/\epsilon_1$ and $\Phi(\text{Fe}^{\text{II}*}) = A_2' = (A_2 - A_1)/1.777$. Thus, the two alternative models give the same dependence of $\Phi(\text{Fe}^{\text{III}})$ and $\Phi(\text{As}^{\text{III}})$ on arsenic acid concentration.

Equations I and II yield values for $\Phi(\text{Fe}^{\text{II}*})$ of 0.87 and 0.99, respectively, equal within standard deviations and consistent with $\Phi(\text{Fe}^{\text{II}*}) = 1$. They also yield values of 2.04 and 2.17, respectively, for τk . Assuming reaction of arsenic acid with $\text{Fe}^{\text{II}*}$ is diffusion controlled, τ is 10^{-9} to 10^{-10} sec. There is, therefore, similarity between H_2O^* and $\text{Fe}^{\text{II}*}$. $\text{Fe}^{\text{II}*}$ may be an electronically excited state or may be either the $\text{Fe}^{\text{III}}\text{-e}_{\text{aq}}^-$, $\text{Fe}^{\text{III}}\text{-H}$, or $\text{Fe}^{\text{III}}\text{-H}_3\text{O}$ radical pair which undergoes geminate recombination by a first-order process.

Other recent studies⁹⁻¹² in the photochemistry of aqueous solutions indicate that inhibition of geminate recombination is sensibly complete with solute concentrations about 0.01 *M*. From this apparent contradiction, we may conclude that secondary recombination is inhibited by 0.01 *M* solute while reaction of solute with $\text{Fe}^{\text{II}*}$ inhibits primary recombination. If this be true, it is of great significance in the radiation chemistry of water since decrease of interspur hydrogen

could be attributed to inhibition of secondary recombination while decrease of intraspur hydrogen could be attributed to inhibition of primary recombination.

(9) J. Jortner, M. Ottolenghi, and G. Stein, *J. Phys. Chem.*, **68**, 247 (1964).

(10) F. S. Dainton and S. R. Logan, *Proc. Roy. Soc. (London)*, **A287**, 281 (1965).

(11) F. S. Dainton and P. Fowles, *ibid.*, **A287**, 312 (1965).

(12) P. L. Airy and F. S. Dainton, *ibid.*, **A292**, 340 (1966).

CHEMISTRY DIVISION
OAK RIDGE NATIONAL LABORATORY
OAK RIDGE, TENNESSEE 37831

T. J. SWORSKI

RECEIVED JUNE 28, 1966

Reactivity of Electron-Donor-Acceptor Complexes. III. Hydrogen Exchange between Acetylene and Organic Electron-Donor-Acceptor Complexes

Sir: In previous papers^{1,2} we have studied the reactivity of electron-donor-acceptor (EDA) complexes. It was found that the reactivity of such compounds as phthalocyanines and aromatic hydrocarbons increased remarkably when they were brought into contact with sodium, an electron donor, by forming EDA complexes. Accordingly, the exchange reaction of hydrogen between acetylene (or molecular hydrogen) and the complexes takes place at room temperatures, while it does not proceed in the absence of electron donor even at 200°. In this report phenothiazine is employed as an organic electron donor, and the reactivity of the EDA complexes formed with various organic electron acceptors is studied.

Phenothiazine was purified by repeated recrystallization and sublimation. A film was evaporated on the surface of a glass vessel under vacuum, to which various electron acceptors such as 2,3-dicyanoquinone, tetracyanoquinodimethane (TCNQ), pyromellitic dianhydride, 1,3,5-trinitrobenzene, *p*-chloranil, and 2,3-dicyano-5,6-dichloroquinone were sublimed, which resulted in deep green, red-violet, green-black, gray-green, dark green, and deep green complexes, respectively.

The hydrogen exchange reaction between the complexes and acetylene was studied in the temperature range between 25 and 140° under an acetylene pressure

(1) M. Ichikawa, M. Soma, T. Onishi, and K. Tamaru, *J. Phys. Chem.*, **70**, 2069 (1966).

(2) M. Ichikawa, M. Soma, T. Onishi, and K. Tamaru, *J. Catalysis*, accepted for publication.

of 15 cm in a closed circulating system. The exchange reaction proceeded reversibly in the following manner over the dicyanoquinone-phenothiazine complex



where HZ represents the EDA complex. When an equimolar mixture of C_2D_2 and C_2H_2 was employed, the over-all reaction to form C_2HD from C_2D_2 and C_2H_2 could be observed over the complex. The three components in the gas— C_2H_2 , C_2HD , and C_2D_2 —were analyzed quantitatively by infrared spectroscopy. A series of measurements was also carried out by introducing C_2D_2 only onto the complex surface. An activation energy of approximately 10 kcal/mole is observed for both exchange processes. Comparison of the rates of the two exchange reactions, $\text{C}_2\text{H}_2 + \text{C}_2\text{D}_2 = 2\text{C}_2\text{HD}$ and $\text{C}_2\text{D}_2 + \text{HZ} = \text{C}_2\text{HD} + \text{DZ}$, revealed that the former reaction proceeds *via* steps 1 and 2.

In the case of the TCNQ-phenothiazine complex, the reaction proceeded initially for a short time and then stopped at room temperatures, while a considerable amount of C_2HD was evolved at temperatures near 75° . No reaction took place over the pyromellitic dianhydride- and trinitrobenzene-phenothiazine complexes, probably because they are comparatively weak electron acceptors. Dicyanodichloroquinone and *p*-chloranil, on the other hand, are strong electron acceptors, but no reaction proceeded over their complexes with phenothiazine, presumably because they contain no hydrogen in their molecules.

The exchange reaction proceeds neither on the phenothiazine nor on those electron acceptors alone even at temperatures as high as 120° , which leads to the conclusion that the formation of EDA complex resulted in a marked reactivity in the case of dicyanoquinone-phenothiazine complex.

The film of the dicyanoquinone-phenothiazine complex was also prepared from the mixed solution in tetrahydrofuran. The rate of the exchange reaction over the film was of the same order of magnitude with that over the evaporated complex film. The irradiation by ultraviolet light showed no effect on the exchange rate within experimental error. The hydrogen exchange reaction for molecular hydrogen instead of acetylene did not proceed over the complex at 130° . However, it is interesting to note that the isomerization of *cis*-2-butene proceeded slowly at 120° to *trans*-2-butene, but not to 1-butene, over the dichlorodicyanoquinone- and dicyanoquinone-phenothiazine complexes.

The pure calcium carbide employed in the preparation of deuterioacetylene was prepared by Dr. N. Torikai of the Yokohama National University from pure calcium oxide and ashless carbon, for which the authors' thanks are due.

DEPARTMENT OF CHEMISTRY
THE UNIVERSITY OF TOKYO
HONGO, BUNKYO-KU
TOKYO, JAPAN

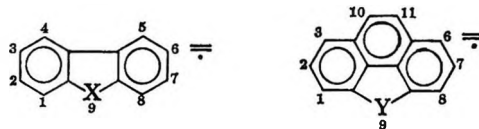
MASARU ICHIKAWA
MITSUYUKI SOMA
TAKAHARU ONISHI
KENZI TAMARU

RECEIVED JUNE 30, 1966

Electron Spin Resonance of Hydrocarbon Dianion Radicals

Sir: We wish to report on the electron spin resonance of fluorene, 9-phenylfluorene, benzofluorenes, 4,5-methylenephenanthrene, carbazole, and 4,5-imino-phenanthrene dianion radicals and the correlation of the observed hyperfine splitting with calculated spin densities.¹

The observed coupling constants are given in Table I according to the following numbering system



The assignment of coupling constants has been verified by methyl substitution in the case of fluorene and carbazole (1- and 2-methylfluorene and 2-methylcarbazole give spectra consistent with methyl substitution at high spin density positions). A plot of

(1) Dianion radicals were prepared by initial reaction of the hydrocarbon with potassium in tetrahydrofuran to form the carbanion or nitranion which on further reduction produced the dianion radical (E. G. Janzen and J. G. Pacifci, *J. Am. Chem. Soc.*, **87**, 5504 (1965)). Evidence for the structure of the radicals is: (a) The visible absorption maxima for the carbanion (T. E. Hogen-Esch and J. Smid, *ibid.*, **88**, 307 (1966); A. Streitwieser, Jr., J. I. Brauman, J. H. Hammons, and A. H. Pudjaatmaka, *ibid.*, **87**, 384 (1965); E. C. Steiner and J. M. Gilbert, *ibid.*, **87**, 382 (1965)) decrease in intensity and new bands appear at the point where the first esr signal can be detected. The increase in esr signal is accompanied by an increase in the new bands and a decrease in the carbanion bands. (b) Hyperfine coupling can be detected from two metal ions (*e.g.*, $A_{\text{Na}^+} = 0.85$ gauss in 2,3-benzofluorene dianion radical). (c) The g values are 0.00025 larger than for monoanion radicals of comparable structure (B. G. Segal, M. Kaplan, and G. K. Fraenkel, *J. Chem. Phys.*, **43**, 4191 (1965)). (d) Line broadening from reversible electron transfer with carbanion can be observed. (e) Electron transfer to naphthalene occurs. (f) It is known that two equivalents of potassium can be added to fluorene readily without carbon-carbon bond cleavage or rearrangement (G. W. H. Sherf and R. K. Brown, *Can. J. Chem.*, **38**, 697, 2450 (1960); **39**, 799 (1961)). All experiments were performed using vacuum line techniques and high surface alkali metal mirrors. A Varian 4502 epr spectrometer was used for esr measurements.

coupling constant as a function of spin density using McLachlan spin densities gives a reasonably good linear relationship with slope = 23.² The observed coupling constants correlate better with McLachlan spin densities than with spin densities calculated from simple HMO theory. On the basis of the esr spectra of five dianion radicals, two of which contain nitrogen in the framework of the aromatic ring, we conclude that McConnell's approximate equation for relating observed proton coupling constants with calculated spin densities on the attached carbon

$$A^H = Q_{CH}^H \rho_{CH} \quad (1)$$

can be applied to dianion radicals with $Q_{CH}^H \simeq 23$. The accuracy of this value will undoubtedly improve as the spectra of more dianion radicals are obtained.

Theory predicts and esr spectra substantiate that very little spin density resides at carbon-9 of fluorene and 4,5-methylenephenanthrene dianion radicals. The smallest proton splitting in fluorene dianion radical is due to three approximately equivalent hydrogens. One of these hydrogens can be assigned to carbon-9 since this coupling is absent in 9-phenylfluorene. The latter has very little spin density located in the phenyl ring and no splitting from phenyl hydrogens is resolved.

Nitrogen coupling in aromatic heterocyclic radical anions is proportional to the spin density located on the nitrogen atom and neighboring carbon atoms³

$$A^N = Q_N^N \rho_N + \sum_i Q_{C_i-N}^N \rho_{C_i} \quad (2)$$

Carbazole dianion radical shows no nitrogen coupling. The calculated spin densities agree well with this observation since not only is the spin density on nitrogen essentially zero but the spin densities on neighboring carbon atoms bonded to nitrogen are also zero (0.007 and -0.0003 for ρ_N and ρ_C , respectively, McLachlan calculations, $\lambda = 1.20$, $\alpha = 1.5$). For 4,5-iminophenanthrene dianion radical, the 0.60-gauss nitrogen splitting observed is in good agreement with

0.58 gauss predicted from eq 2 if $Q_N^N = 30.9$ and $Q_{C-N}^N = -2.0^4$ ($\rho_N = -0.013$, $\rho_C = 0.0432$, McLachlan calculations, $\lambda = 1.20$, $\alpha = 1.5$).

It is of interest to note that the spin densities and esr coupling constants of 4,5-methylenephenanthrene dianion radical are very similar to phenanthrene monanion radical. Similarly, 1,2-, 2,3-, and 3,4-benzo-fluorene dianion radicals can be described as substituted naphthalene anion radicals.

Acknowledgment. This work was supported by funds provided through the Director of General Research of the University of Georgia.

(2) This value is in good agreement with the esr of cycloheptatrienide dianion radical: N. L. Bauld and M. S. Brown, *J. Am. Chem. Soc.*, **87**, 4390 (1965).

(3) E. T. Strom, G. A. Russell, and R. Konaka, *J. Chem. Phys.*, **42**, 2033 (1965), and references therein.

(4) E. W. Stone and A. H. Maki, *ibid.*, **39**, 1635 (1963).

DEPARTMENT OF CHEMISTRY
THE UNIVERSITY OF GEORGIA
ATHENS, GEORGIA

EDWARD G. JANZEN
J. GRADY PACIFICI
JOHN L. GERLOCK

RECEIVED JULY 1, 1966

Pulse Radiolysis of the Aqueous Nitrate System. Formation of NO₃ in Concentrated Solutions and the Mechanism of "Direct Action"¹

Sir: Although unusual effects in the radiolysis of concentrated nitrate solution have long been recognized^{2a} and substantiated in later work^{2b} which ascribed them to "direct action" (*i.e.*, to energy absorbed directly by the solute), nothing was known about the mechanism of the primary processes and secondary reactions leading to the over-all chemistry. Accordingly, advantage has been taken of the recently developed technique of pulse radiolysis³ to investigate this problem.

A 14-15-Mev electron beam from the ANL linear accelerator was used with pulses from 0.4 to 3 μ sec and beam currents of 40-160 ma; the detection technique used was kinetic absorption spectroscopy.³ For 4 M NaNO₃ the characteristic structured spectrum of

Table I: Hyperfine Coupling Constants of Dianion Radicals

Dianion radical	Position					
	1,8	2,7	3,6	4,5	9	10,11
X = $\overset{\cdot\cdot}{C}H$	3.05	3.05	0.35	4.53	0.35	
X = $\overset{\cdot\cdot}{C}-C_6H_5$	2.76	3.98	0.59	3.98		
X = $\overset{\cdot\cdot}{N}$	2.48	4.10	0.59	4.10	<0.10	
Y = $\overset{\cdot\cdot}{C}H$	3.02	0.53	3.02		0.36	4.96
Y = $\overset{\cdot\cdot}{N}$	3.00	0.51	3.00		0.60	5.08

(1) Based on work performed under the auspices of the U. S. Atomic Energy Commission.

(2) (a) T. J. Sworski, *J. Am. Chem. Soc.*, **77**, 4689 (1955); (b) H. A. Mahlman, *J. Phys. Chem.*, **67**, 1466 (1963).

(3) L. M. Dorfman and M. S. Matheson, *Progr. Reaction Kinetics*, **3**, 239 (1965).

Figure 1 was obtained showing peaks of 670, 640, and 600 m μ , clearly very similar to the gas phase spectrum of NO₃.⁴ The possibility of this transient being NO₃²⁻ may be discounted as the spectrum is practically unchanged in 6 M HNO₃ (Figure 1) and agrees with that obtained by flash photolysis of cerium(IV) in the same medium.⁵

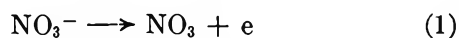
This transient absorption, which decays by a first-order process ($t_{1/2} = 40 \mu\text{sec}$) is not found in 10⁻² M NaNO₃ but is produced in increasing amounts as the concentration of NO₃⁻ is increased from 0.5 M up to the practical limit of 8 M. Over this range a considerable amount of energy is deposited in the nitrate, and in order to determine the origin of the NO₃, the absorbance per pulse, A , has been treated according to the equation

$$\frac{A}{f_{\text{H}_2\text{O}}} = A_{\text{H}_2\text{O}} + \frac{f_{\text{NO}_3^-}}{f_{\text{H}_2\text{O}}} A_{\text{NO}_3^-}$$

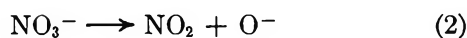
which has been set up by arbitrarily assuming that NO₃ may originate as a result of energy deposited either in the water or in the nitrate ($f_{\text{H}_2\text{O}}$ and $f_{\text{NO}_3^-}$ are the fractions of energy absorbed in water and nitrate, respectively, and the A 's are the respective coefficients). Reference to Figure 2 shows that in fact $A_{\text{H}_2\text{O}} = 0$; *i.e.*, all of the NO₃ is a transient characteristic of the reactions involved in "direct action." This result clearly makes unnecessary any discussion of excitation effects⁶ and energy transfer⁷ from solvent (water) to solute (NO₃⁻).

However, NO₃ is not the primary species formed by "direct action." This is shown by: (1) under certain conditions the kinetic curves give indications of a rise time, though this could not be clearly resolved; (2) formation of NO₃ can be completely eliminated by the prior addition of NO₂⁻ and methanol in concentrations not greatly affecting the decay of NO₃.

It may be concluded then that NO₃ has a radical precursor and thus is not formed as a result of the ionization process



As alternative primary processes the dissociation reactions



in which O⁻ and O are the NO₃ precursors, may be considered. Although the previous finding that $A_{\text{H}_2\text{O}} = 0$ indicates that OH radicals readily available from the radiolysis of water are ineffective in leading to NO₃ formation and hence are not the precursors of NO₃, additional dif-

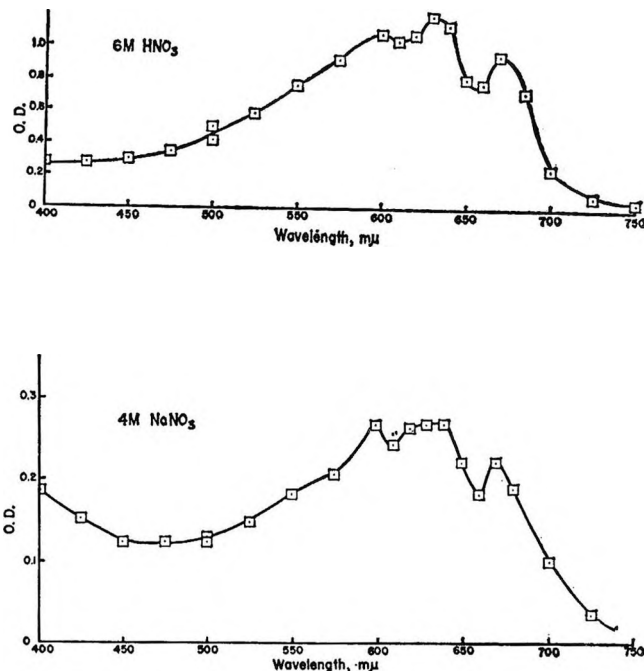


Figure 1. Absorption spectra of transient produced in 4 M NaNO₃ and 6 M HNO₃.

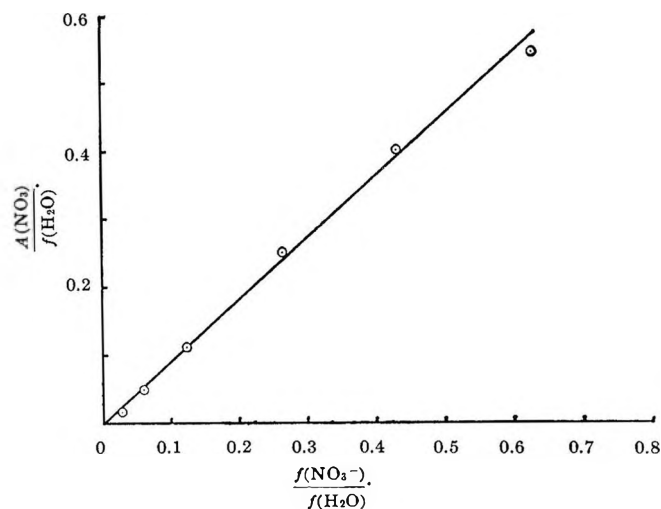


Figure 2. Dependence of NO₃ formation on fractional energy deposition.

(4) E. J. Jones and O. R. Wulf, *J. Chem. Phys.*, **5**, 873 (1937); G. Schott and N. Davidson, *J. Am. Chem. Soc.*, **80**, 1841 (1958); D. A. Ramsey, *Proc. Colloq. Spectros. Intern.*, **10th**, Univ. Maryland, 1962, 583 (1963).

(5) T. W. Martin, A. Henshall, and R. C. Gross, *J. Am. Chem. Soc.*, **85**, 113 (1963).

(6) M. A. Proskurnin and V. A. Sharpatyi, *Russ. J. Phys. Chem.*, **34**, 1009 (1960).

(7) J. Bednar and S. Lukac, *Coll. Czech. Chem. Commun.*, **29**, 341 (1964).

ferentiating evidence on this point has been obtained by competition kinetic studies for the precursor. Thus, experiments with NO_2^- and methanol give $k(\text{X} + \text{NO}_2^-)/k(\text{X} + \text{MeOH}) = 400$ where X represents the precursor. However, it is known that if X is OH (O^-), then this rate constant should be ~ 5 .⁸ Hence, it is concluded that reaction 2 does not represent the primary process of "direct action"; it is suggested that this primary process may be reaction 3.

To summarize, NO_3 radical has been detected in the radiolysis of concentrated nitrate solutions. It is characteristic of the "direct effect" but is not a primary species. This indicates strongly that excitation is an important primary process in the "direct effect."

A fuller account of these results and others will be presented later in conjunction with work currently in progress on the γ radiolysis of these solutions.

Acknowledgments. This work was carried out by the author at Argonne National Laboratory while on leave of absence from the Puerto Rico Nuclear Center. Thanks are due to Dr. J. R. Bugher, Director, PRNC, and Dr. E. J. Hart, Argonne National Laboratory, for facilitating and encouraging these arrangements.

(8) G. E. Adams and J. W. Boag, *Proc. Chem. Soc.*, 112 (1964); J. K. Thomas, *Trans. Faraday Soc.*, 61, 702 (1965).

RADIATION CENTER AND
CHEMISTRY DEPARTMENT
OREGON STATE UNIVERSITY
CORVALLIS, OREGON 97331

MALCOLM DANIELS

RECEIVED JULY 5, 1966

The Magnetic Susceptibility of Palladium Hydride

Sir: The linear decrease of the paramagnetic susceptibility of palladium as it absorbs hydrogen is well known.¹ The portion of the density of states curve to the right of the Fermi level is usually drawn to indicate that palladium lacks about 0.55 electron to fill the d level. It has been suggested² that hydrogen donates its electron to fill this d level so that when the spins are paired, the substance should become diamagnetic. This latter is observed experimentally but at a composition variously reported but close to $\text{PdH}_{0.66}$ rather than at $\text{PdH}_{0.55}$. If the above explanation is correct, it should be possible to obtain a linear increase in susceptibility as hydrogen is removed from $\text{PdH}_{\sim 0.66}$. This was attempted³ by a high-voltage method for extracting hydrogen without heating the sample and it was claimed that all the hydrogen could be removed

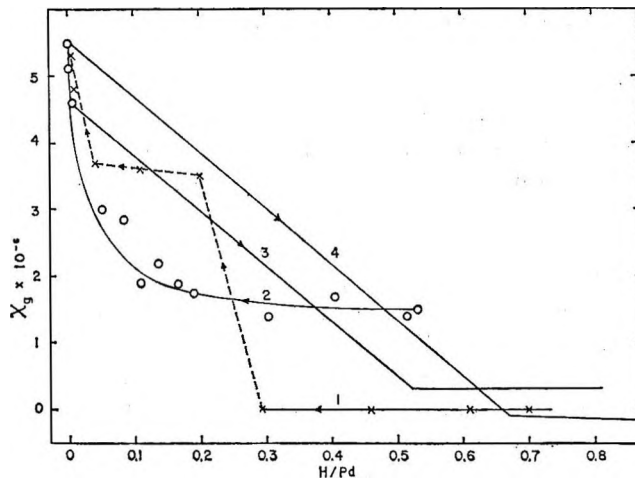


Figure 1. The effect of absorption and desorption of hydrogen on the paramagnetic susceptibility of palladium.

without any change in the magnetic susceptibility. These results were not confirmed by Lewis, *et al.*,⁴ using an electrolytic method for removing hydrogen but were partially confirmed in this laboratory⁵ using the high-voltage method.

In the present series of experiments diamagnetic and slightly paramagnetic samples of palladium hydride were prepared from very fine ($0.80\text{-}\mu$) palladium metal powder, by alternately heating and cooling the metal in pure hydrogen (obtained by evolution from UH_3), at a temperature which never exceeded 200° above which the powder sinters. These samples evolved hydrogen at room temperature when the hydrogen pressure above them fell below 18 mm. The magnetic susceptibility of samples of palladium hydride was continuously compared to that of a standard (Mohr's salt), while small measured quantities of hydrogen were removed from the sample, in an apparatus which has been described previously.⁶ The results are shown in Figure 1. Curves 1 and 2 show that it is possible to remove a large fraction of the hydrogen from diamagnetic palladium hydride and from palladium hydride which is slightly paramagnetic owing to an initial lower hydrogen content, without changing the susceptibility (χ_g). Curves 3 and 4 for the absorption of hydrogen by palladium are taken from Smith.¹ It thus appears

(1) D. P. Smith, "Hydrogen in Metals," University of Chicago Press, Chicago, Ill., 1947.

(2) N. F. Mott, *Advan. Phys.* 13, 325 (1964).

(3) A. Michel and M. Gallissot, *Compt. Rend.*, 208, 434 (1939).

(4) J. C. Barton, F. A. Lewis, and I. Woodward, *Trans. Faraday Soc.*, 59, 1201 (1963).

(5) T. R. P. Gibb, Jr., to be submitted.

(6) W. A. Norder, *Rev. Sci. Instr.*, 31, 849 (1960).

that the band theory explanation is not tenable for the desorption of hydrogen from palladium hydride and it may be that lattice expansion plays a more important role than was formerly thought. Further experimental and theoretical work is in progress.

Acknowledgment. The authors are indebted to the U. S. Atomic Energy Commission for financial support for this work.

DEPARTMENT OF CHEMISTRY
TUFTS UNIVERSITY
MEDFORD, MASSACHUSETTS

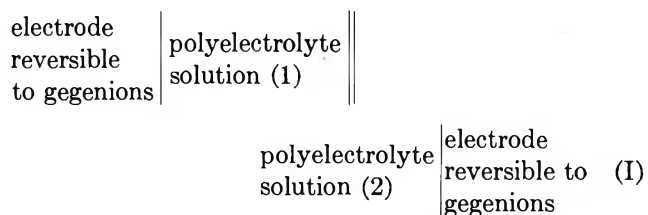
THOMAS R. P. GIBB, JR.
J. MACMILLAN
R. J. ROY

RECEIVED JULY 18, 1966

On the Validity of Single-Ion Activity in Polyelectrolyte Solution

Sir: As is well known, the liquid-junction potential problem was a focus of earlier studies in the physical chemistry of electrolyte solutions.¹ Some theoretical formulas have been derived for the potential and have been believed to be fairly satisfactory. This success has furnished a basis for the determination of the single-ion activities (including pH) in electrolyte solutions, which have no unique and rigorous thermodynamic meanings.¹ Though the electrochemical study has been gradually extended to polymeric electrolytes, the liquid-junction problem has usually been regarded as already solved approximately on the basis of the earlier work mentioned above. The main purpose of the present communication is to caution against the validity of this interpretation in highly charged polyelectrolyte solutions, using MacInnes' way of reasoning.²

Consider the following concentration cell with transference



The thermodynamic consideration gives for the liquid-junction potential E_1

$$E_1 = \frac{1 + \alpha}{\alpha} \frac{RT}{F} t_{2p} \ln \frac{a_2}{a_1} - \frac{RT}{F} \ln \frac{(a_{2g})_2}{(a_{2g})_1} \quad (1)$$

where α and t_{2p} are the effective valency and the transference number (assumed to be concentration independent) of the macroions, a is the mean activity of the

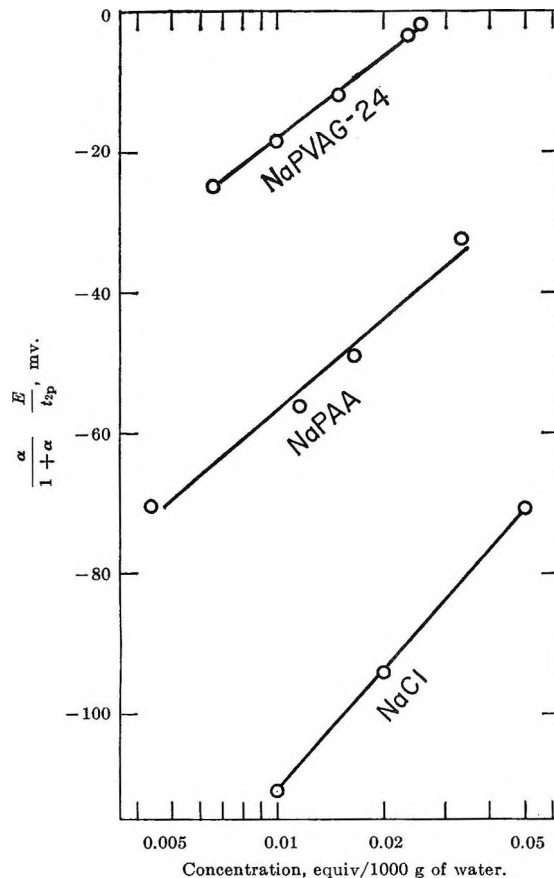


Figure 1. Test of equation for liquid-junction potential.

polyelectrolyte, a_{2g} is the single-ion activity of the gegenions, R , T , and F have the usual meanings, and the subscripts 1 and 2 refer to the two solutions forming the junction. The emf of cell I, E , is known to be given by

$$E = \frac{1 + \alpha}{\alpha} \frac{RT}{F} t_{2p} \ln \frac{a_2}{a_1} \quad (2)$$

If we denote the sum of the electrode potentials by E_e , we have

$$E_e = E - E_1 \quad (3)$$

By making tentatively the further approximation of

$$\frac{(a_{2g})_2}{(a_{2g})_1} = \frac{a_2}{a_1} \quad (4)$$

(1) See, for example, D. A. MacInnes, "The Principles of Electrochemistry," Reinhold Publishing Corp., New York, N. Y., 1939, Chapter 13; S. Glasstone, "An Introduction to Electrochemistry," D. Van Nostrand Co., Inc., New York, N. Y., 1962, Chapter 6; R. G. Bates, "Determination of pH, Theory and Practice," John Wiley and Sons, Inc., New York, N. Y., 1964, Chapter 3. The relevant references are given in these books.

(2) See Chapter 13 of MacInnes' work or Chapter 6 of Glasstone's work cited in ref 1.

we have

$$E_1 = \left[\frac{(1 + \alpha)t_p}{\alpha} - 1 \right] \frac{RT}{F} \ln \frac{a_2}{a_1} \quad (5)$$

and

$$E_e = \frac{\alpha}{1 + \alpha} \frac{E}{t_p} \quad (6)$$

For sufficiently dilute solutions, in which E_e is independent of the nature of the macroions, if the right-hand side is constant for various polyelectrolytes having the same sort of gegenions, eq 5 is correct. Figure 1 gives a test for the reliability of this equation. The experimental data were taken from our previous measurements of the *mean* activities of a sodium polyacrylate (NaPAA),^{3,4} a sodium salt of polyvinyl alcohol partially acetalized with glyoxylic acid (NaPVAG),⁵ and sodium chloride.⁴ For these electrolytes and in the concentration range under consideration, t_p and α were found to be independent of concentration.³⁻⁵ Figure 1 tells us that a linearity holds between E_e and concentration (on a log scale) with slopes of 56, 43, and 39, for NaCl, NaPAA, and NaPVAG, respectively. These differences in slope values imply the incorrectness of eq 5 which was obtained by assuming eq 4.

In previous work, the *mean* activity of polyelectrolytes was measured electrochemically⁴⁻⁶ and isopiestically,⁷ and simultaneously the single-ion activity of gegenions was also measured by the conventionally used electrochemical method.⁴⁻⁶ This method essentially depends on the validity of eq 4. Our results show,

however, that eq 4 does not hold for polyelectrolyte solutions and does hold, though approximately, for low molecular weight electrolyte solutions. Therefore, there exists an inconsistency between the assumption and result as far as the polyelectrolyte solutions are concerned. Thus we may say that the liquid-junction potential problem still remains unsolved for these solutions. This conclusion arouses strong suspicions pertaining to the validity of the single-ion activity determinations in polyelectrolyte solutions. We believe that various interpretations obtained from potentiometric titrations of polyelectrolytes including biologically important ones should be evaluated more carefully than in the case of low molecular weight electrolytes.

Acknowledgment. The authors gratefully acknowledge the encouragement and discussion received from Professor I. Sakurada.

(3) T. Okubo, Y. Nishizaki, and N. Ise, *J. Phys. Chem.*, **69**, 3690 (1965).

(4) N. Ise and T. Okubo, *ibid.*, **69**, 4102 (1965).

(5) N. Ise and T. Okubo, *ibid.*, **70**, 1930 (1966).

(6) N. Ise and T. Okubo, *ibid.*, **70**, 2400 (1966).

(7) N. Ise and T. Okubo, to be published. In this work the *mean* activity values determined electrochemically (ref 4, 5, and 6) were examined by the isopiestic vapor pressure measurements and excellent agreement was obtained.

DEPARTMENT OF POLYMER CHEMISTRY
KYOTO UNIVERSITY
KYOTO, JAPAN

NORIO ISE
TSUNEO OKUBO

RECEIVED JULY 21, 1966